

**DEPARTMENT OF  
CIVIL & ENVIRONMENTAL  
ENGINEERING**

**DRAFT VERSION**

**Natural Attenuation of Hydrocarbon and  
Trichloroethylene Vapors in the Subsurface  
Environment at Plattsburgh Air Force Base**

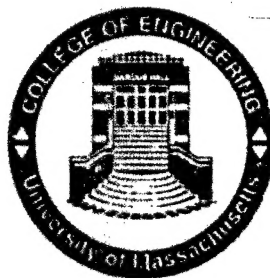
By

Ostendorf, D.W., Lutenegger, A.J., Ergas, S.J.  
Hinlein, E.S., Suchana, R.J., Tehrany, J.P., Reyes, P.O., Glass, R.C., Charkow, B.,  
Meyer, M.M., Kelley, S.P., and Mitchell, T.J.

Report of Research Conducted for  
Air Force Center for Environmental Excellence  
Brooks Air Force Base  
Contract No. F41624-95-C-8012

26/3/97

**DISTRIBUTION STATEMENT A**  
Approved for Public Release  
Distribution Unlimited



20010330 076

**COLLEGE OF ENGINEERING  
UNIVERSITY OF MASSACHUSETTS**



**DEPARTMENT OF THE AIR FORCE**  
**HEADQUARTERS AIR FORCE CENTER FOR ENVIRONMENTAL EXCELLENCE**  
**BROOKS AIR FORCE BASE TEXAS**

22 March, 2001

MEMORANDUM FOR : Defense Technical Information Center  
Attn: DTIC-OMI (Input Support Branch)  
Suite 0944  
8725 John J. Kingman Road  
Ft. Belvoir, VA 22060-6218

FROM: HQ AFCEE/ERT  
3207 North Road  
Brooks AFB TX 78235-5363

SUBJECT: Documents for input into DTIC

Enclosed are documents for input into DTIC. These documents do not net to be returned to us. Attached is a listing of the documents. For all these documents, distribution is unlimited. If you need additional informatio please call me at DSN 240-2597, (210) 536-2597

Thank you,  
Laura Pena  
HQAFCEE/ERT  
Technology Transfer Division  
(210) 536-2597, dsn 240-2597  
(210) 536-4330 fax  
[laura.pena@hqafcee.brooks.af.mil](mailto:laura.pena@hqafcee.brooks.af.mil)



HQAFCEE/ERT Documents, 21 March, 2001

1. Final: Demonstration of Phytoremediation of Chlorinated Solvents at facility 1381  
Cape Canaveral Air Station, June 1998
2. Draft Version Natural Attenuation of Hydrocarbon and Trichloroethylene Vapors in  
the Subsurface Environment at Plattsburgh Air Force Base, March 26, 1997

**NATURAL ATTENUATION OF HYDROCARBON AND  
TRICHLOROETHYLENE VAPORS IN THE SUBSURFACE ENVIRONMENT  
AT PLATTSBURGH AIR FORCE BASE**

**DRAFT VERSION-FINAL REPORT**

by

David W. Ostendorf (Associate Professor), Alan J. Lutenegger (Professor)  
Sarina J. Ergas (Assistant Professor)  
Erich S. Hinlein, Russell J. Suchana, J. Pierre Tehrany, Paul O. Reyes  
Rebecca C. Glass, Benjamin Charkhow, Michelle M. Meyer  
Shawn P. Kelley and Travis J. Mitchell (Research Assistants)

Report of Research Conducted for  
Air Force Center for Environmental Excellence  
Brooks Air Force Base  
Contract No. F41624-95-C-8012

Civil and Environmental Engineering Department  
University of Massachusetts at Amherst

26 March 1997

**DISTRIBUTION STATEMENT A**  
Approved for Public Release  
Distribution Unlimited

## EXECUTIVE SUMMARY

The Civil and Environmental Engineering Department of the University of Massachusetts at Amherst (UMASS) was contracted by the United States Air Force Center for Environmental Excellence (AFCEE) to conduct field research from 19 September 1995 to 30 September 1996 under Contract No. F41624-95-C-8012 "Surface Emissions from Jet Fuel Bioventing at Plattsburgh AFB". The work focused on bioventing of residual JP4 jet fuel and chlorinated solvents in the unsaturated zone and capillary fringe beneath Fire Training Area FT-002 at the Air Force Base in Plattsburgh, NY. **UMASS tested the hypothesis that natural attenuation processes, stimulated by injected air, reduce emissions of hydrocarbons and trichloroethylene vapors to acceptable air quality standards at the site.** Drs. David W. Ostendorf, Alan J. Lutenege, and Sarina J. Ergas were the UMASS Principal Investigators, while Patrick Haas served as AFCEE Technical Representative for the contract. This report describes the one year effort.

The contract was performed in four tasks: unsaturated zone characterization, soil gas and solid core sampling, maximum assimilative capacity testing, and emissions testing. UMASS completed this work through detailed subtasks:

### Unsaturated Zone Characterization

- Grain size distributions were measured at 108 depths from three boreholes. We determined moisture content profiles 785 samples from 24 boreholes completed during drilling trips on 9-13 October 1995, 30 November-1 December 1995, 5-7 June 1996, and 19-22 August 1996.
- We installed two thermocoupled arrays and measured soil temperature on 17 field sampling trips from 13 October 1995 to 19 December 1996, generating a data base of 377 observations.
- Stainless steel soil vapor probes were deployed in three boreholes on 11-13 October 1995 to determine ambient soil gas oxygen, total hydrocarbon, and carbon dioxide partial pressures across the unsaturated zone. Portable soil meters and a Tedlar bag sampling system were used to analyze the data from 38 depths in two of the boreholes, while a downhole oxygen sensor corroborated the profiles at 14 depths in the third borehole.
- We analyzed a separate phase sampled bailed from a recovery well by Base engineers to determine the composition of the residual JP4 jet fuel solvent liquid. A Hewlett Packard G1800A gas chromatograph with a mass spectrometer detector (GCD) was used to identify 84 alkanes, aromatics, and chlorinated hydrocarbons in the sample.
- UMASS personnel surveyed the plan location and mean sea level elevation of all probe profiles, clusters, arrays, and boreholes, for insertion into an AUTOCAD file for the project. Coordinates for all sample points are cited in Table 3.1.

### Soil Gas and Solid Core Sampling

- We constructed 26 stainless steel soil gas tubing clusters to document the fate and transport of vapors through the unsaturated zone. One cluster was a control positioned well outside underlying LNAPL. The clusters were multidepth, so that 45 depths were sampled.

- The soil gas tubing clusters were sampled with portable analyzers and field installed Hewlett Packard 5890 gas chromatographs equipped with flame ionization (FID) and electron capture (ECD) detectors. We sampled soil gas oxygen, carbon dioxide, total hydrocarbons, and trichloroethylene partial pressures in Tedlar bag samples from the clusters on 17 field trips from 26 October 1995 to 19 December 1996, generating 2,083 observations.
- The vertical distribution of separate phase contamination was estimated from gas chromatographic IFD analysis of methylene chloride extracts from 785 solid core samples from 24 boreholes sampled on 9-13 October 1995, 30 November-1 December 1995, 5-7 June 1996, and 19-22 August 1996.
- The headspace of the samples was analyzed in a nitrogen glove box on line, to direct sampling efforts and delineate the contaminated interval.
- Separate phase trichloroethylene content was determined at 66 depths in six of the boreholes, using the GCD.

### **Maximum Assimilative Capacity Testing**

- A soil venting system was installed in the center of the test area on 1 December 1995. The soil venting system injected heated air at a metered rate of 1 cfm into the capillary fringe, and included a helium tracer injection system. The soil was vented from 18 January 1996 to 9 August 1996, and a helium tracer was injected continuously from 7 February to 7 March 1996.
- We measured vented helium in 31 of the stainless steel tubing cluster sampling points on 13 February and 21 February 1996 to document the pneumatics of the soil venting. A field installed Hewlett Packard 5890 gas chromatograph with thermal conductivity detector (TCD) was used to measure the helium in Tedlar bag samples.
- An air sparging system was built in the center of the test area on 1 December 1995 as well. The air sparging system injected heated air 1.2 m below the water table from 9 August to 5 September 1996 and from 24 October to 19 December 1996. A helium tracer was injected continuously from 24 October to 24 November 1996.
- We measured helium in 35 of the stainless steel tubing cluster sampling points on 7 November and 29 November 1996, using the TCD gas chromatograph.
- A finite element model with supplemental analytical subroutines was used to model the stainless steel tubing cluster and vapor probe data. The model was tested with the helium tracer data, followed by soil gas data calibrations to determine the maximum assimilative capacity of the unsaturated zone for hydrocarbon and trichloroethylene vapor degradation. Air and total porosities were input from the moisture content data, and soil temperature was modeled with a constant diffusivity analysis.

### **Emissions Testing**

- We installed two near surface arrays to measure helium and TCE profiles through the root zone. The arrays were of stainless steel construction, with a low sample volume facilitating sampling on 5 cm vertical spacing. Fourteen depths were established at each array.
- We analyzed helium and trichloroethylene soil gas concentrations on 20 November 1996 using field installed gas chromatographs with TCD and ECD detectors.

- We measured soil gas oxygen, total hydrocarbons, carbon dioxide, and trichloroethylene partial pressures near the capillary fringe using a soil vapor probe during air sparging. Eighty one depths were sampled in seven boreholes on 21-22 August 1996, using portable meters and a field installed FID equipped gas chromatograph.
- The near surface array data were input to an analytical model of soil gas transport through the root zone. The helium data calibrated the pneumatics, while the TCE data were used to calibrate the capacity of the root zone to assimilate TCE vapors.
- A surface isolation flux chamber was designed, built, and deployed, to verify low levels of emissions from the site area.

## Conclusions

This extensive field sampling, laboratory analysis, and mathematical modeling efforts tests the hypothesis with the following result: **natural attenuation processes reduce emissions of hydrocarbon and trichloroethylene vapors to acceptable air quality standards at the site.** We support this general conclusion with particular results:

- **A significant mass of separate phase petroleum persists in and immediately below the capillary fringe.** We found total petroleum hydrocarbon levels as high as 26,400 mg TPH/kg dry soil (borehole 12AS), with contaminated intervals ranging from 1.1 to 2.54 m in extent (Table 5.6). The distribution is unimodal, and is reasonably described by capillary scaling theory (Figure 5.7). A significant fraction of the LNAPL is residually bound to the soil (as much as 7,000 mg TPH/kg dry soil). The separate phase is well correlated with the headspace concentrations.
- **Separate phase trichloroethylene occurs at levels as high as 59 mg TCE/kg dry soil immediately below the capillary fringe (Table 5.7).** The ratio of separate phase TCE to total LNAPL in 95 samples is 0.0025, yielding a separate phase mole fraction of 0.00222 and a saturated TCE vapor pressure of 170 ppm.
- **Soil gas oxygen and carbon dioxide concentrations suggest a maximum assimilative capacity of  $1.4 \times 10^{-6} \text{ s}^{-1}$  under ambient conditions near the capillary fringe (Equation 5.39b).** This capacity is based on high, stoichiometrically coupled fluxes of oxygen entering and carbon dioxide leaving the fringe by ambient diffusion.
- **Soil gas oxygen and carbon dioxide concentrations suggest that soil venting increases the maximum assimilative capacity near the capillary fringe to  $3.2 \times 10^{-5} \text{ s}^{-1}$  (Equation 5.67).** This capacity is based on a comparison of soil gas concentrations in study area with those observed at the control cluster.
- **We see little evidence of hydrocarbons or of hydrocarbon degradation in the unsaturated zone, although trichloroethylene exists at significant levels.** The finite element code, calibrated with tubing cluster data, suggests that trichloroethylene comprises a disproportionately high fraction of the hydrocarbon vapors found in the stainless steel tubing clusters under ambient, soil venting (Equation 5.53b), or air sparging (Equation 5.56b) conditions. The observed TCE concentrations are consistent with the saturated vapor pressure implied by Raoult's law, while the hydrocarbon pressures are two orders of magnitude lower than values expected in the absence of degradation. **These findings,**

together with the observed fluxes of oxygen and carbon dioxide, support the hypothesis that JP4 hydrocarbon vapors degrade aerobically near the capillary fringe.

- **Trichloroethylene vapors degrade in the root zone, at a maximum assimilative capacity of  $2.0 \times 10^{-6} \text{ s}^{-1}$  (Equation 5.59).** This conclusion reflects calibration of quasi steady vertical transport models for abiotic helium (Equation 5.58) and first order decaying trichloroethylene (Equation 4.57) with replicated near surface array data (Tables 5.46, 5.47 and Figure 5.25). These data were gathered late in the study period, after seven months of soil venting and two months of air sparging.
- **No detectable trichloroethylene was emitted to the atmosphere.** We base this conclusion on a computed flux rate of  $0.11 \text{ } \mu\text{g}/\text{m}^2\text{-min}$  (Equation 5.69b), confirmed by emissions testing at the site using the flux chamber.

## ACKNOWLEDGMENTS

This study was funded as Contract No. F41624-95-C-8012 "Surface Emissions from Jet Fuel Bioventing at Plattsburgh AFB", an agreement between the Air Force Center for Environmental Excellence and the Civil and Environmental Engineering Department of the University of Massachusetts at Amherst. The Principal Investigators acknowledge and appreciate the logistical support provided by the Base Realignment and Closure team at Plattsburgh AFB. This invaluable assistance included temporary laboratory space for gas chromatography and field sampling, as well as AUTOCAD and report availability.

The views, opinions, and findings contained in this report are those of the Authors and do not necessarily reflect the official view or policy of the AFCEE. This report does not constitute an Air Force standard, specification, or regulation.

## TABLE OF CONTENTS

EXECUTIVE SUMMARY.....	ii
ACKNOWLEDGMENTS.....	vi
TABLE OF CONTENTS.....	vii
LIST OF FIGURES.....	x
LIST OF TABLES.....	xii
LIST OF NOTATION.....	xvi
1 INTRODUCTION.....	1
2 SITE DESCRIPTION AND BACKGROUND.....	3
2.1 Site Description.....	3
2.1.1 Site History and Hydrogeology.....	3
2.1.2 Soil Gas Data and LNAPL Composition.....	10
2.2 Assimilative Capacity of the Vadose Zone.....	11
2.2.1 Hydrocarbon Vapor Degradation.....	11
2.2.2 Trichloroethylene Degradation.....	12
2.3 Soil Vapor Remediation Alternatives.....	17
2.3.1 Soil Vapor Extraction.....	18
2.3.2 In Situ Bioventing.....	19
2.3.3 Effects of Environmental Variables.....	22
2.3.4 Air Sparging.....	26
2.4 Soil Gas Models.....	27
3 METHODS AND MATERIALS.....	30
3.1 Soil Temperature, Grain Size Distribution, and Moisture Content.....	30
3.1.1 Soil Temperature.....	30
3.1.2 Grain Size Distribution.....	30
3.1.3 Soil Moisture.....	36
3.2 Separate Phase Petroleum Content in Solid Core Samples.....	38
3.2.1 Field Sampling.....	39
3.2.2 Soil Core Extrusion.....	39
3.2.3 Headspace Determination and Subsampling.....	41
3.2.4 Separate Phase Petroleum Extraction.....	44
3.2.5 Gas Chromatographic Analysis of Solid Core Extracts.....	47
3.2.6 Separate Phase Petroleum Calibration Standard.....	48
3.2.7 Method Detection Limit and Field Spikes.....	49



<b>3.3 GCD Analyses and TCE Content.....</b>	<b>52</b>
3.3.1 GCD Protocol for TCE Analyses.....	52
3.3.2 GCD Analysis of Total Hydrocarbons.....	54
<b>3.4 Soil Gas Sampling.....</b>	<b>57</b>
3.4.1 Overview of Soil Gas Sampling Technology.....	57
3.4.2 Vapor Probes.....	59
3.4.3 Stainless Steel Tubing Clusters and Near Surface Arrays.....	61
3.4.4 Soil Venting and Air Sparging Systems.....	67
3.4.5 Soil Gas Sample Dilution and Portable Meters.....	69
<b>3.5 Gas Chromatographic Analysis of Soil Gas Samples.....</b>	<b>71</b>
3.5.1 Flame Ionization Detector.....	71
3.5.2 Electron Capture Detector.....	73
3.5.3 Thermal Conductivity Detector.....	75
<b>3.6 Surface Isolation Flux Chamber.....</b>	<b>77</b>
 <b>4 MATHEMATICAL ANALYSIS.....</b>	 <b>80</b>
<b>4.1 Soil Temperature.....</b>	<b>80</b>
<b>4.2 Vertical Distribution of LNAPL.....</b>	<b>80</b>
4.2.1 Overview of LNAPL Distribution in the Capillary Fringe.....	80
4.2.2 Free Liquid Retention.....	81
4.2.3 LNAPL Entrapment.....	84
<b>4.3 Analytical Soil Gas Transport Models.....</b>	<b>87</b>
4.3.1 Model Overview.....	87
4.3.2 Pneumatics.....	88
4.3.3 Steady Ambient Diffusion and Reaction.....	89
4.3.4 Steady Advection and Diffusion.....	90
4.3.5 Unsteady Spherical Advection.....	91
<b>4.4 Finite Element Soil Gas Transport Model.....</b>	<b>92</b>
4.4.1 Soil Gas Diffusivity Estimation.....	92
4.4.2 Finite Element Model Formulation.....	92
4.4.3 Simulations and Sensitivity.....	100
<b>4.5 Boundary Flux Models.....</b>	<b>103</b>
4.5.1 Trichloroethylene Vapor Transport through the Root Zone.....	103
4.5.2 Vapor Transport near the Capillary Fringe.....	104
 <b>5 RESULTS.....</b>	 <b>105</b>
<b>5.1 Soil Temperature, Grain Size Distribution, and Moisture Content.....</b>	<b>105</b>
5.1.1 Soil Temperature.....	105
5.1.2 Grain Size Distribution.....	107
5.1.3 Moisture Content and Porosity.....	116
<b>5.2 Solid Core Sampling Results.....</b>	<b>123</b>
5.2.1 Calibration of LNAPL Profile Model.....	123
5.2.2 LNAPL Results.....	130

5.2.3	Separate Phase Trichloroethylene Profiles.....	137
<b>5.3</b>	<b>Soil Vapor Concentrations.....</b>	<b>143</b>
5.3.1	Ambient Soil Vapor Calibrations.....	143
5.3.2	Ambient Assimilative Capacity for Total Hydrocarbon Vapors.....	168
5.3.3	Helium Tracer Tests for Soil Venting and Air Sparging.....	173
5.3.4	Soil Venting and Air Sparging of Total Hydrocarbons.....	177
<b>5.4</b>	<b>Trichloroethylene Vapor Concentrations.....</b>	<b>182</b>
5.4.1	Trichloroethylene venting and sparging data.....	182
5.4.2	Trichloroethylene degradation in the root zone.....	190
<b>5.5</b>	<b>Total Hydrocarbon Assimilation Capacity Estimates and Surface Emissions.....</b>	<b>193</b>
5.5.1	Oxygen and Carbon Dioxide Concentration for Soil Venting.....	193
5.5.2	Assimilation Capacity for Total Hydrocarbons by Soil Venting.....	195
5.5.3	Surface Emissions.....	195
<b>6</b>	<b>SUMMARY AND CONCLUSIONS.....</b>	<b>197</b>
<b>6.1</b>	<b>Summary of Work.....</b>	<b>197</b>
6.1.1	Unsaturated Zone Characterization.....	197
6.1.2	Soil Gas and Solid Core Sampling.....	197
6.1.3	Maximum Assimilative Capacity Testing.....	198
6.1.4	Emissions Testing.....	198
<b>6.2</b>	<b>Conclusions.....</b>	<b>199</b>
	<b>APPENDIX I BOREHOLE LOGS.....</b>	<b>201</b>
	<b>APPENDIX II TUBING CLUSTER DETAILS.....</b>	<b>235</b>
	<b>APPENDIX III GRAIN SIZE DATA.....</b>	<b>267</b>
	<b>APPENDIX IV SOLID CORE SAMPLING ANALYSES.....</b>	<b>281</b>
	<b>APPENDIX V COMPUTER PROGRAM LISTINGS.....</b>	<b>304</b>
	<b>APPENDIX VI GCD OUTPUT FOR SEPARATE PHASE ANALYSIS.....</b>	<b>324</b>
	<b>APPENDIX VII EMISSIONS ISOLATION FLUX CHAMBER.....</b>	<b>337</b>

## LIST OF FIGURES

2.1 Site Plan: Plattsburgh Air Force Runway and Fire Training Area FT-002.....	4
2.2 Soil Gas Sampling Locations.....	7
2.3 Trichloroethylene Molecule.....	12
2.4 Anaerobic Dehalogenation of Trichloroethylene.....	14
2.5 Cometabolism of Trichloroethylene.....	15
3.1 Site Plan.....	31
3.2 Core Barrel Extruder.....	37
3.3 Replicate Soil Moisture and LNAPL Contents for Serum Bottle Samples.....	38
3.4 Field Glovebox for Solid Core Sampling.....	40
3.5 Separate Phase Petroleum Content vs Mason Jar Headspace for Typical Plattsburgh Boreholes.....	42
3.6 Separate Phase Petroleum Content vs Mason Jar Headspace.....	43
3.7 Typical FID Chromatogram for LNAPL Standard.....	45
3.8 Typical FID Chromatogram for LNAPL Extract.....	46
3.9 Standard Calibration Curve for 1995 October LNAPL Analyses.....	49
3.10 Method Detection Limit Study for LNAPL Analyses.....	50
3.11 Typical GCD Chromatogram of JP4 Jet Fuel Extract.....	52
3.12 GCD Calibration Curve for TCE.....	53
3.13 Stainless Steel Vapor Sampling Probe.....	58
3.14 Soil Gas Sampling System.....	60
3.15 Downhole Soil Gas Oxygen Sensor in Stainless Steel Probe.....	61
3.16 Downhole Sensed and Surface Sensed Soil Gas Oxygen Partial Pressure.....	62
3.17 Stainless Steel Tubing Cluster Details.....	63
3.18 Near Surface Array Construction Details .....	64
3.19 Soil Venting System.....	65
3.20 Air Sparging System.....	66
3.21 Tedlar Bag Dilution System.....	67
3.22 Typical FID Chromatograms for Soil Gas.....	72
3.23 Method Detection Limit Study for TCE by FID.....	73
3.24 Typical ECD Chromatograms for Soil Gas.....	74
3.25 Method Detection Limit Study for TCE by ECD.....	75
3.26 Typical TCD Chromatograms for Soil Gas.....	76
3.27 Surface Isolation Flux Chamber.....	78
3.28 Method Detection Limit for Trichloroethylene Flux.....	79
4.1 Typical Soil Temperature Profiles.....	81
4.2 Definition Sketch for Three Phase Fluid Distribution in Soil.....	83
4.3 Conceptual Diagram of Hysteretical Trapping of LNAPL.....	85
4.4 Domain for Finite Element Model.....	94
4.5 Element Interactions.....	96
4.6 Master Element.....	97

4.7 Steady State Analytical and Transient Finite Element Hydrocarbon Vapor Profiles.....	101
4.8 Steady State Analytical and Transient Finite Element Helium Vapor Profiles.....	102
5.1 Observed and Calibrated Soil Temperature.....	109
5.2 Typical Grain Size Distribution Data (Symbols) and Calibration (Curve), Uniformity Coefficient U as a Function of van Genuchten (1980) Uniformity Exponent.....	112
5.3 Grain Size Calibration Parameters in Boreholes SPK1, SPK2, and 12AY.....	117
5.4 Observed Moisture Content in Solid Core Boreholes.....	118
5.5 Total Porosity, Based on Hand Auger Tests and Saturated Soil Samples.....	122
5.6 Observed Total Petroleum Hydrocarbon Content in Solid Core Boreholes.....	124
5.7 Observed and Calibrated Total and LNAPL Saturations.....	131
5.8 Observed Separate Phase Trichloroethylene Content in Solid Core Boreholes.....	139
5.9 Ratio of Separate Phase Trichloroethylene to Total Petroleum Hydrocarbons in Solid Core Samples.....	142
5.10 Observed and Calibrated Ambient Soil Gas Oxygen and Carbon Dioxide in Clusters 12AN, 12AT, and 12AX.....	154
5.11 Observed and Calibrated Ambient Soil Gas Total Hydrocarbons in Clusters 12AN, 12AT, and 12AX.....	156
5.12 Observed and Calibrated Ambient Soil Gas Oxygen and Carbon Dioxide in VP1, VP2, and VP3.....	160
5.13 Observed and Calibrated Ambient Soil Gas Total Hydrocarbon in VP1 and VP3.....	162
5.14 Observed and Calibrated Ambient Soil Gas Oxygen and Carbon Dioxide in 12AA-12AM, 12AO-12AR, 12AU-12AW, 12AZ, and 12BA 26 October 1995-16 January 1996.....	164
5.15 Observed and Calibrated Ambient Soil Gas Total Hydrocarbons in 12AA-12AM, 12AO- 12AR, 12AU-12AW, 12AZ, and 12BA 26 October 1995-16 January 1996.....	166
5.16 Observed and Predicted Helium Concentrations for Soil Venting.....	175
5.17 Observed and Predicted Helium Concentrations for Air Sparging.....	176
5.18 Observed and Calibrated Total Hydrocarbon Concentrations in Vapor Probe Boreholes..	177
5.19 Observed and Calibrated Hydrocarbon Concentrations for Air Sparging.....	180
5.20 Vertical Hydrocarbon Flux Estimates by Vapor Probe Profiles and Stainless Steel Tubing Clusters.....	181
5.21 Observed and Calibrated Hydrocarbon Concentrations for Soil Venting.....	183
5.22 Observed and Calibrated Trichloroethylene Concentrations for Soil Venting.....	185
5.23 Observed and Calibrated Trichloroethylene Concentrations in Vapor Probe Boreholes....	186
5.24 Observed and Calibrated Trichloroethylene Concentrations for Air Sparging.....	189
5.25 Observed and Calibrated Helium and TCE Vapor Concentrations in Near Surface Arrays.....	192
5.26 Spatial Averaged Oxygen and Carbon Dioxide Partial Pressures for Soil Venting.....	194

## LIST OF TABLES

2.1 Soil Gas Data.....	6
2.2 Solid Core Analyses from Borehole 84D.....	9
2.3 Base Grid and Mean Sea Level Coordinates of Base Engineering Sampling Points.....	10
2.4 Semiquantitative GC/MS Estimate of LNAPL Composition.....	11
2.5 Mechanisms for Biodegradation of Selected Chlorinated Compounds.....	13
2.6 Comparison of Oxygen Levels in Various Carriers.....	19
3.1 Base Grid and Mean Sea Level Coordinates of UMASS Sampling Points.....	32
3.2 Soil Moisture and LNAPL Borehole Dates and Depth Intervals.....	36
3.3 LNAPL Standard Concentrations for Solid Core Analyses.....	48
3.4 LNAPL Field Spike Recoveries.....	51
3.5 GCD Identification of Compounds in Separate Phase Sample.....	55
3.6 Soil Venting and Air Sparging Test Program.....	69
4.1 Master Element Interactions.....	98
4.2 Sensitivity Study of Soil Gas Transport.....	102
5.1 Soil Temperature Data.....	106
5.2 Thermal Profile Parameters.....	108
5.3 van Genuchten (1980) Grain Size Calibration Parameters.....	113
5.4 van Genuchten (1980) Grain Size Calibration Parameters Borehole 12AY.....	115
5.5 Borehole Averaged M and Calculated Air Porosities.....	123
5.6 LNAPL Profile Parameters and Calibration Results.....	129
5.7 LNAPL and TCE Content in Borehole 12AS.....	138
5.8 LNAPL and TCE Content in Borehole 12AV.....	140
5.9 LNAPL and TCE Content in Borehole 12BB.....	140
5.10 LNAPL and TCE Content in Borehole 12BF.....	141
5.11 LNAPL and TCE Content in Borehole 12BI.....	141
5.12 LNAPL and TCE Content in Borehole 12BO.....	141
5.13 Soil Gas Constituents in Tubing Clusters 26 October 1995.....	144
5.14 Soil Gas Constituents in Tubing Clusters 16 November 1995.....	145
5.15 Soil Gas Constituents in Tubing Clusters 16 January 1996.....	146
5.16 Soil Gas Constituents in Tubing Clusters 7 February 1996.....	147
5.17 Soil Gas Constituents in Tubing Clusters 13 February 1996.....	148
5.18 Soil Gas Constituents in Tubing Clusters 7 March 1996.....	149
5.19 Soil Gas Constituents in Tubing Clusters 17 March 1996.....	150
5.20 Soil Gas Constituents in Tubing Clusters 4 April 1996.....	151
5.21 Soil Gas Constituents in Tubing Clusters 5 May 1996.....	152
5.22 Soil Gas Constituents in Tubing Clusters 15 June 1996.....	153
5.23 Soil Gas Constituents in Tubing Clusters 15 July 1996.....	155
5.24 Soil Gas Trichloroethylene in Tubing Clusters 9 August 1996.....	157
5.25 Soil Gas Constituents in Tubing Clusters 20 August 1996.....	158
5.26 Soil Gas Constituents in Tubing Clusters 13 October 1996.....	159

5.27	Soil Gas Constituents in Tubing Clusters 7 November 1996.....	161
5.28	Soil Gas Constituents in Tubing Clusters 21 November 1996.....	163
5.29	Soil Gas Constituents in Tubing Clusters 19 December 1996.....	165
5.30	Helium Tracer Pressures in Tubing Clusters.....	167
5.31	Soil Gas Constituents in Vapor Probe VP1.....	168
5.32	Soil Gas Constituents in Vapor Probe VP2.....	169
5.33	Soil Gas Constituents in Vapor Probe VP3.....	169
5.34	Soil Gas Constituents in Vapor Probe 12BC.....	170
5.35	Soil Gas Constituents in Vapor Probe 12BE.....	170
5.36	Soil Gas Constituents in Vapor Probe 12BH.....	171
5.37	Soil Gas Constituents in Vapor Probe 12BJ.....	171
5.38	Soil Gas Constituents in Vapor Probe 12BK.....	172
5.39	Soil Gas Constituents in Vapor Probe 12BM.....	172
5.40	Soil Gas Constituents in Vapor Probe 12BN.....	173
5.41	Total Hydrocarbon Profile Calibration near Capillary Fringe.....	179
5.42	Soil Venting of Total Hydrocarbons-Calibration Results.....	182
5.43	Soil Venting of Trichloroethylene-Calibration Results.....	184
5.44	Trichloroethylene Vapor Profile Calibration near Capillary Fringe.....	188
5.45	Helium and Trichloroethylene Soil Gas Concentrations in NAW.....	190
5.46	Helium and Trichloroethylene Soil Gas Concentrations in NAE.....	191
5.47	Near Surface Array Calibration Results.....	193
5.48	Surface Emissions Measurements 1 December 1996.....	196

## LIST OF NOTATION

Symbol	Meaning	Units
$b$	Depth below ground surface	m
$b_F$	Depth to capillary fringe	m
$b_L$	Depth to LNAPL table	m
$b_{LMAX}$	Depth to maximum LNAPL saturation	m
$b_M$	Depth to onset of free LNAPL contamination	m
$b_{MMIN}$	Minimum depth to water table	m
$b_R$	Root zone thickness	m
$b_W$	Depth to water table	m
$b_{WMAX}$	Maximum depth to water table	m
$b_{WMIN}$	Minimum depth to water table	m
$C$	Concentration of gaseous $CO_2$	$kg/m^3$ soil gas
$C_S$	Steady carbon dioxide concentration	$kg/m^3$ soil gas
$C_{EXT}$	Extract LNAPL concentration	$kg/m^3$ solution
$C_{TCE}$	TCE concentration in extract	$kg/m^3$
$D$	Dimensionless grain size	
$D_C$	Carbon dioxide diffusivity in soil	$m^2$ total/s
$D_{CS}$	Steady carbon dioxide diffusivity	$m^2/s$
$D_G$	Hydrocarbon vapor diffusivity in soil	$m^2/s$
$D_{GS}$	Steady $D_G$	$m^2/s$
$D_{HS}$	Steady helium diffusivity	$m^2/s$
$D_{REF}$	Reference vapor diffusivity	$m^2/s$
$D_T$	Thermal diffusivity	$m^2/s$
$D_X$	Oxygen diffusivity in soil	$m^2$ total/s
$D_{XS}$	Steady oxygen diffusivity	$m^2/s$
$d$	Grain size	mm
$d_M$	Mean grain size	mm
$F$	Cumulative density function	
$F_{GSPARGE}$	Spherical sparged G flux	kg/s
$F_{IK}$	Prior time step array	$m^3/s$
$F_{FINE}$	Fine fraction	
$f_F$	Full $F_{IK}$ element	$m^3/s$
$F_{YSPARGE}$	Spherical sparged Y flux	kg/s
$G_E$	G at radius of influence	$kg/m^3$ soil gas
$G_F$	G on source nodes	$kg/m^3$ soil gas
$G_J$	Nodal G value	$kg/m^3$ soil gas
$G_K$	Prior G value	$kg/m^3$ soil gas
$G_O$	Ambient source hydrocarbon concentration	$kg/m^3$ soil gas
$G_S$	Steady G profile	$kg/m^3$ soil gas
$G_{SAT}$	Saturated G	$kg/m^3$ soil gas
$g$	Gravitational acceleration	$m/s^2$
$H$	Helium concentration	$kg/m^3$ soil gas

$H_F$	Helium source concentration	kg/m <sup>3</sup> soil gas
$H_{INJ}$	Helium concentration in injection line	kg/m <sup>3</sup> soil gas
$H_P$	Predicted helium concentration	kg/m <sup>3</sup> soil gas
IN	Calibration curve intercept	
$J_C$	Flux of CO <sub>2</sub> in the unsaturated zone	kg/total m <sup>2</sup> -s
$J_{GF}$	Flux of G entering unsaturated zone	kg/total m <sup>2</sup> -s
$J_X$	Flux of O <sub>2</sub> in the unsaturated zone	kg/total m <sup>2</sup> -s
$J_{XO}$	Oxygen flux into ground	μg O <sub>2</sub> /total m <sup>2</sup> -s
$J_{YO}$	TCE flux entering root zone	kg/total m <sup>2</sup> -s
$K_{IJ}$	Transport array	m <sup>3</sup> /s
$k_{ABCD}$	Master element interaction	
M	Soil moisture content	kg moisture/kg dry soil
MDL	Method detection limit	
$m_C$	Molar mass of CO <sub>2</sub>	kg/mole
$m_G$	Molar mass of total hydrocarbons	kg/mole
$m_H$	Molar mass of helium	kg/mole
$m_{REF}$	Reference molar mass	kg/mole
$m_X$	Molar mass of O <sub>2</sub>	kg/mole
$m_Y$	Molar mass of trichloroethylene	kg/mole
N	Number of sample points	
$N_D$	Number of grains in volume	
$N_P$	Number of pores in volume	
n	Total soil porosity	m <sup>3</sup> pores/m <sup>3</sup> total
P	Method precision	
$p_C$	Carbon dioxide vapor pressure	Pa
$p_G$	Total hydrocarbon vapor pressure	Pa
$p_H$	Helium vapor pressure	Pa
$p_W$	Water pressure	Pa
$p_{WM}$	Water pressure at $b_M$	Pa
$p_X$	Oxygen vapor pressure	Pa
$p_Y$	Trichloroethylene vapor pressure	Pa
$p_{YMDL}$	MDL for TCE vapor pressure	Pa
$p_{YPURE}$	$p_{YSAT}$ above pure TCE liquid	Pa
$p_{YSAT}$	Saturated TCE vapor pressure	Pa
Q	Volumetric soil gas discharge	m <sup>3</sup> /s
$R_U$	Universal gas constant	Pa-m <sup>3</sup> soil gas/mole-°K
RF	Gas chromatograph response factor	1/area unit
r	Radial distance from well centerline	m
r'	Spherical distance from source	m
$r'_F$	Spherical source radius	m
$r_M$	Mean pore radius	m
$r_P$	Radius to measuring point	m
S	Effective total saturation	
$S_L$	Total LNAPL saturation	



$S_{LMAX}$	Maximum LNAPL saturation	
$S_{LF}$	Free LNAPL saturation	
$S_{LR}$	Residual LNAPL saturation	
$S_{LRMAX}$	Maximum residual LNAPL saturation	
$S_W$	Effective water saturation	
$S_{WMAX}$	Maximum water saturation	
$S_{WMIN}$	Minimum water saturation	
$s_G$	Soil grain specific gravity	
$T$	LNAPL content	mg LNAPL/kg dry soil
$T_{TCE}$	TCE content	mg TCE/kg dry soil
$T_{MAX}$	Maximum LNAPL content	mg LNAPL/kg dry soil
$T_{TCEMAX}$	Maximum TCE content	mg TCE/kg dry soil
$t$	Time	s
$t_{ADV}$	Advective residence time	s
$t_{DIF}$	Diffusive penetration time	s
$U$	Weighting function	
$U'$	Uniformity coefficient	
$v$	Radial specific discharge component	m/s
$v_R'$	Spherical specific discharge component	m/s
$w$	Vertical specific discharge component	m/s
$w_O$	w at the ground surface	m/s
$X$	Concentration of gaseous $O_2$	kg/m <sup>3</sup> soil gas
$X_O$	Atmospheric $O_2$ concentration	kg/m <sup>3</sup> soil gas
$X_S$	Steady oxygen concentration	kg/m <sup>3</sup> soil gas
$x_{INJ}$	Injection point north coordinate	feet
$Y$	Concentration of trichloroethylene vapor	kg/m <sup>3</sup> soil gas
$Y_{INJ}$	Injected TCE concentration	kg/m <sup>3</sup> soil gas
$Y_{PURE}$	$Y_{SAT}$ for pure phase TCE	kg/m <sup>3</sup> soil gas
$Y_{SAT}$	Saturated TCE vapor concentration	kg/m <sup>3</sup> soil gas
$y_{INJ}$	Injection point east coordinate	m
$z$	Distance above the ground surface	m
$z_O$	Depth to virtual origin	m
$\alpha_D$	van Genuchten (1980) grain size uniformity exponent	
$\alpha_P$	van Genuchten (1980) pore size uniformity exponent	
$\beta_L$	Scaling factor for LNAPL retention	1/m
$\beta_W$	Scaling factor for water retention	1/m
$\chi_{TCE}$	TCE mole fraction in separate phase	mole/total moles
$\Delta$	Amplitude of water table fluctuation	m
$\delta_C$	Carbon dioxide model error	
$\delta_D$	Grain size model error	
$\delta_{DM}$	Mean model error for grain size	
$\delta_G$	Total hydrocarbon vapor model error	

$\delta_{GM}$	Mean hydrocarbon vapor model error	
$\delta_H$	Helium model error	mg/m <sup>3</sup>
$\delta_{HM}$	Mean helium model error	mg/m <sup>3</sup>
$\delta_{SM}$	Mean saturation model error	
$\delta_T$	Temperature model error	
$\delta_{TM}$	Mean model error for temperature	
$\delta_X$	Oxygen model error	
$\delta_{XCM}$	Mean model error for oxygen and CO <sub>2</sub>	
$\delta_Y$	Trichloroethylene model error	mg/m <sup>3</sup>
$\delta_{YM}$	Mean TCE model error	mg/m <sup>3</sup>
$\epsilon$	Thickness of free LNAPL contamination in soil	m
$\lambda$	Hydrocarbon vapor decay constant	s <sup>-1</sup>
$\lambda_F$	Hydrocarbon decay constant in capillary fringe	s <sup>-1</sup>
$\lambda_{TCE}$	TCE first order decay constant	s <sup>-1</sup>
$\lambda'$	Pseudodecay constant	s <sup>-1</sup>
$\phi_I$	Galerkin basis function	
$\gamma$	Hysteretical trapping factor	
$\gamma_C$	Stoichiometric ratio, CO <sub>2</sub> to hydrocarbons	
$\gamma_X$	Stoichiometric ratio, oxygen to hydrocarbons	
$\phi$	Temperature phase shift	radians
$\theta$	Air porosity	m <sup>3</sup> soil gas/m <sup>3</sup> total
$\theta_F$	Irreducible volumetric moisture content	
$\theta_{LF}$	Free LNAPL content	
$\theta_{LR}$	Residual LNAPL content	
$\theta_W$	Water porosity	m <sup>3</sup> water/m <sup>3</sup> total
$\rho$	Water density	kg/m <sup>3</sup>
$\rho_B$	Dry soil bulk density	kg dry soil/m <sup>3</sup> total
$\rho_L$	LNAPL density	kg/m <sup>3</sup>
$\sigma_{LA}$	LNAPL-air surface tension	kg/s <sup>2</sup>
$\sigma_{CM}$	Error standard deviation for oxygen and CO <sub>2</sub>	
$\sigma_S$	Error standard deviation for saturation	
$\sigma_D$	Error standard deviation for grain size	
$\sigma_G$	Error standard deviation for hydrocarbons	
$\sigma_{GC}$	MDL standard deviation	
$\sigma_H$	Error standard deviation for helium	mg/m <sup>3</sup>
$\sigma_T$	Error standard deviation for temperature	
$\sigma_{WA}$	Water-air surface tension	kg/s <sup>2</sup>
$\sigma_{WL}$	Water-LNAPL surface tension	kg/s <sup>2</sup>
$\sigma_X$	Error standard deviation for O <sub>2</sub>	kg O <sub>2</sub> /m <sup>3</sup> soil gas
$\sigma_Y$	Error standard deviation for TCE	mg/m <sup>3</sup>
$\tau$	Soil gas temperature	°K
$\tau_M$	Temperature fluctuation amplitude	°K

$\tau_{\infty}$	Averaged soil gas temperature	$^{\circ}\text{K}$
$\omega$	Annual frequency	rad/s
$\zeta$	Thickness of capillary fringe	m

## 1 INTRODUCTION

The Civil and Environmental Engineering Department of the University of Massachusetts at Amherst (UMASS) was contracted by the United States Air Force Center for Environmental Excellence (AFCEE) to conduct field research from 19 September 1995 to 30 September 1996 under Contract No. F41624-95-C-8012 "Surface Emissions from Jet Fuel Bioventing at Plattsburgh AFB". The work focused on bioventing of residual JP4 jet fuel and chlorinated solvents in the unsaturated zone and capillary fringe beneath Fire Training Area FT-002 at the Air Force Base in Plattsburgh, NY. **UMASS tested the hypothesis that natural attenuation processes, stimulated by injected air, reduce emissions of hydrocarbons and trichloroethylene vapors to acceptable air quality standards at the site.**

The Contract research team is comprised of:

**Principal Investigator**-Dr. David W. Ostendorf, Associate Professor, Environmental Engineering Program, Civil and Environmental Engineering Department, University of Massachusetts at Amherst

**Principal Investigator**-Dr. Alan J. Lutenegger, Professor, Geotechnical Engineering Program, Civil and Environmental Engineering Department, University of Massachusetts at Amherst

**Principal Investigator**-Dr. Sarina J. Ergas, Assistant Professor, Environmental Engineering Program, Civil and Environmental Engineering Department, University of Massachusetts at Amherst

**AFCEE Technical Representative**-Patrick Haas, Technology Transfer Division, Air Force Center for Environmental Research

**Base Liaison**-Brady Baker, Civil Engineering, Base Realignment and Closure Division, Plattsburgh Air Force Base

**Research Assistant**-Erich S. Hinlein, Doctoral Candidate, Environmental Engineering Program, Civil and Environmental Engineering Department, University of Massachusetts at Amherst

**Research Assistant**-Russell J. Suchana, Masters Candidate, Environmental Engineering Program, Civil and Environmental Engineering Department, University of Massachusetts at Amherst

**Research Assistant**-J. Pierre Tehrany, Masters Candidate, Environmental Engineering Program, Civil and Environmental Engineering Department, University of Massachusetts at Amherst

**Research Assistant**-Paul O. Reyes, Environmental Engineering Program, Civil and Environmental Engineering Department, University of Massachusetts at Amherst

**Research Assistant**-Benjamin Charkhow, Environmental Engineering Program, Civil and Environmental Engineering Department, University of Massachusetts at Amherst

**Research Assistant**-Michelle M. Meyer, Environmental Engineering Program, Civil and Environmental Engineering Department, University of Massachusetts at Amherst

**Research Assistant**-Shawn P. Kelley, Masters Candidate, Geotechnical Engineering Program, Civil and Environmental Engineering Department, University of Massachusetts at Amherst

**Research Assistant**-Travis J. Mitchell, Masters Candidate, Geotechnical Engineering Program, Civil and Environmental Engineering Department, University of Massachusetts at Amherst

**Section 2** of this Final Report briefly summarizes existing site assessment and remedial efforts by Base engineers, along with an account of the FT-002 area history. Background information on natural attenuation of trichloroethylene and hydrocarbon vapors and engineered systems is also included in this Section. **Section 3** discusses the methods and materials of the UMASS study in detail. Soil temperature, grain size, and moisture content methods are explained first, followed by an account of separate phase sampling, extraction, and analysis by FID gas chromatography. We present corresponding methodology for separate phase TCE measurement next, featuring a gas chromatograph with mass spectrometer. Soil gas sampling protocol is addressed next, including the design and installation of vapor probes, stainless steel tubing clusters, and near surface array. The soil gas oxygen, total hydrocarbon, carbon dioxide, TCE, and helium partial pressures from Tedlar bag samples from these points are analyzed with portable meters and gas chromatographs equipped with FID, ECD, and TCD detectors. The Section concludes with a description of the surface isolation flux chamber used to check surface emissions.

**Section 4** features mathematical model derivations for soil temperature, LNAPL distribution, and soil gas fate and transport. The latter models include a finite element code with analytical subroutines for near surface fluxes. The results of the one year project are summarized in **Section 5**, including data, tests, and calibrations for:

- Soil temperature
- Grain size distribution
- Moisture content profiles
- Total separate phase hydrocarbon and TCE profiles
- Ambient, soil venting, and air sparging soil gas data
- Oxygen and carbon dioxide based estimates of aerobic degradation capacity
- Helium tracer tests for soil venting and air sparging
- TCE and total hydrocarbon transport by venting and sparging
- Root zone assimilation of trichloroethylene vapors
- Surface emissions

Some conclusions are drawn from the results of this work in **Section 6**. Raw data and references are appended to the report.

## 2 SITE DESCRIPTION AND BACKGROUND

### 2 Site Description

#### 2.1.1 Site History and Hydrogeology

The site of the bioventing study is the former Fire Training Area denoted as FT-002 at Plattsburgh Air Force Base, Plattsburgh, New York (Figure 2.1). The Air Force Base is located in northeastern New York State, 26 miles south of the Canadian border. Bound on the east by Lake Champlain, the north by the City of Plattsburgh, and the west and south by the Town of Plattsburgh, the current Base configuration was developed in 1954. The Base covers 4795 acres, including the old military installation, housing facilities, flightline, and support areas [Parsons Engineering Science (1995)].

Fire training area FT-002 lies between 248 and 270 feet above mean sea level. Most original features of the site were altered during development of the runway and flightline in 1954. Two rivers, the Saranac and the Salmon, lie to the north and south of the base, respectively. Lake Champlain is located to the east of the base. The flow of ground water at the site is to the southeast. No surface water bodies exist at the site and ground water lies at approximately 35 feet below ground surface. There are four units that underlie site FT-002. Medium to fine grained sand extends from the surface to approximately 90 feet below ground surface. Silty sand exists at the bottom of the sand layer. A 7-foot thick clay layer exists on the eastern side of the site. A 30 to 40 foot thick clay/till layer exists at approximately 80 to 105 feet below ground surface. The clay layer is underlain by limestone bedrock at approximately 120 feet below ground surface.

Three distinct ground water units exist below the site. A shallow unconfined aquifer is present at approximately 35 feet below ground surface. A series of aquitards and aquicludes exists within the network of clay lenses and glacial till. The third unit is a confined bedrock aquifer. The average ground water gradient at the site is 0.010 ft/ft. Ground water fluctuations of about 4-5 feet occur due to seasonal variations. In situ, hydraulic conductivity measurements at the site ranged from 0.059 to 90.7 ft/day, with the average determined to be 11.6 ft/day. Relationships between in situ values and those determined through empirical grain size data (8.49 to 84.9 ft/day) agreed well with these values. Effective porosity at the site has been assumed to be 0.30 by Base engineers.

The study area is located in the northeast corner of the Base, 150 m west of the runway and 150 m east of the western boundary. It is also bordered on the north by domestic waste/spent munitions landfill LF-023 and to the south by domestic waste landfill LF-022. Fire training area FT-002 was used to train fire fighting personnel from the mid to late 1950's until the facility was closed in May 1989. The pits were unlined until 1980 when two of the pits, designated 1 and 2, were modified with cement stabilized soil liners. Pits 1 and 4 had been removed from service at this point. Previous investigations have indicated that four unlined fire pits existed at the site and were filled with off-spec JP-4 jet fuel mixed with waste oil, solvents, and other miscellaneous chemicals before being set on fire as training exercises. Soil and ground water beneath the pits

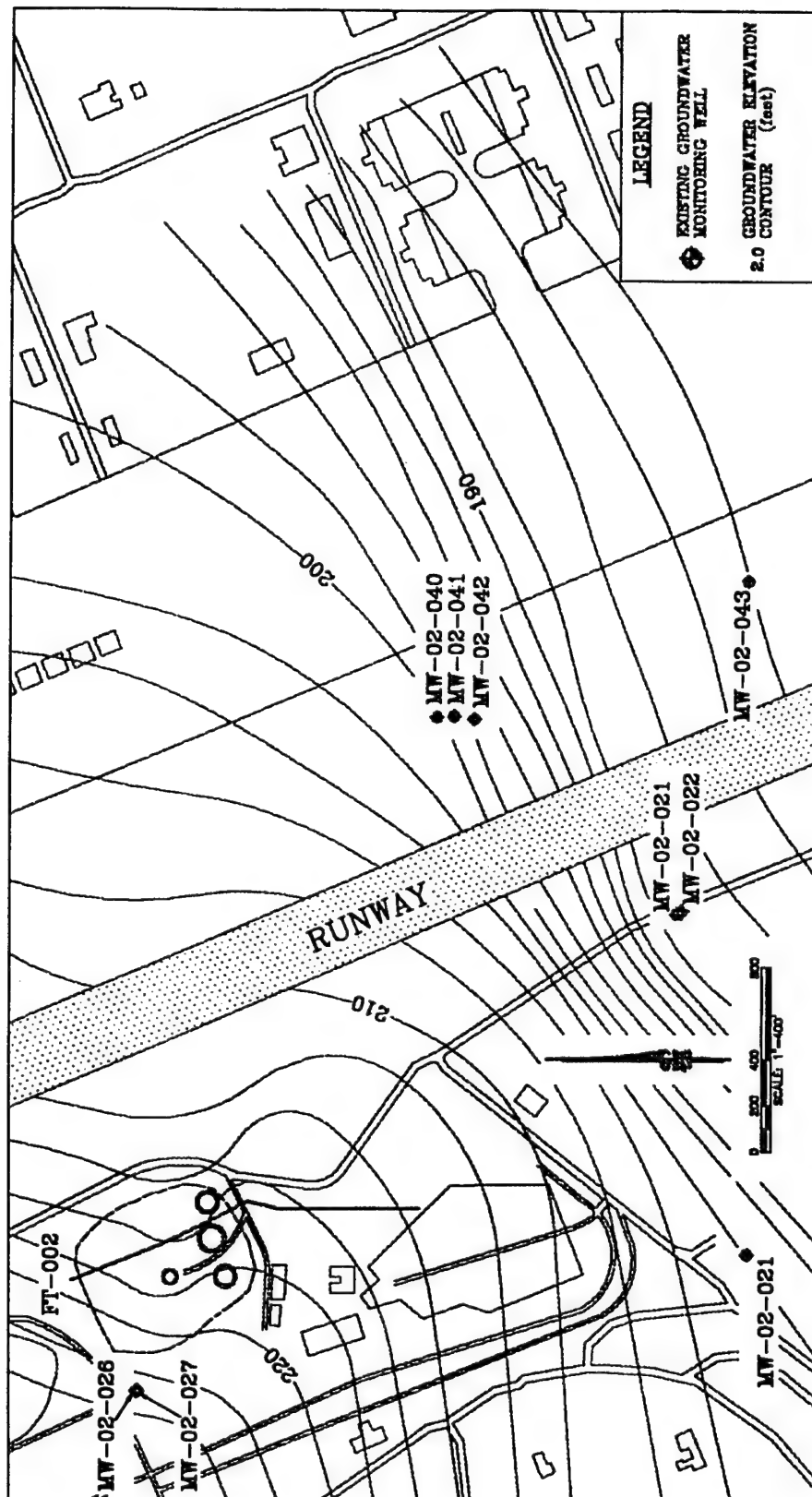


Figure 2.1a Site Plan: Plattsburgh Air Force Base Runway

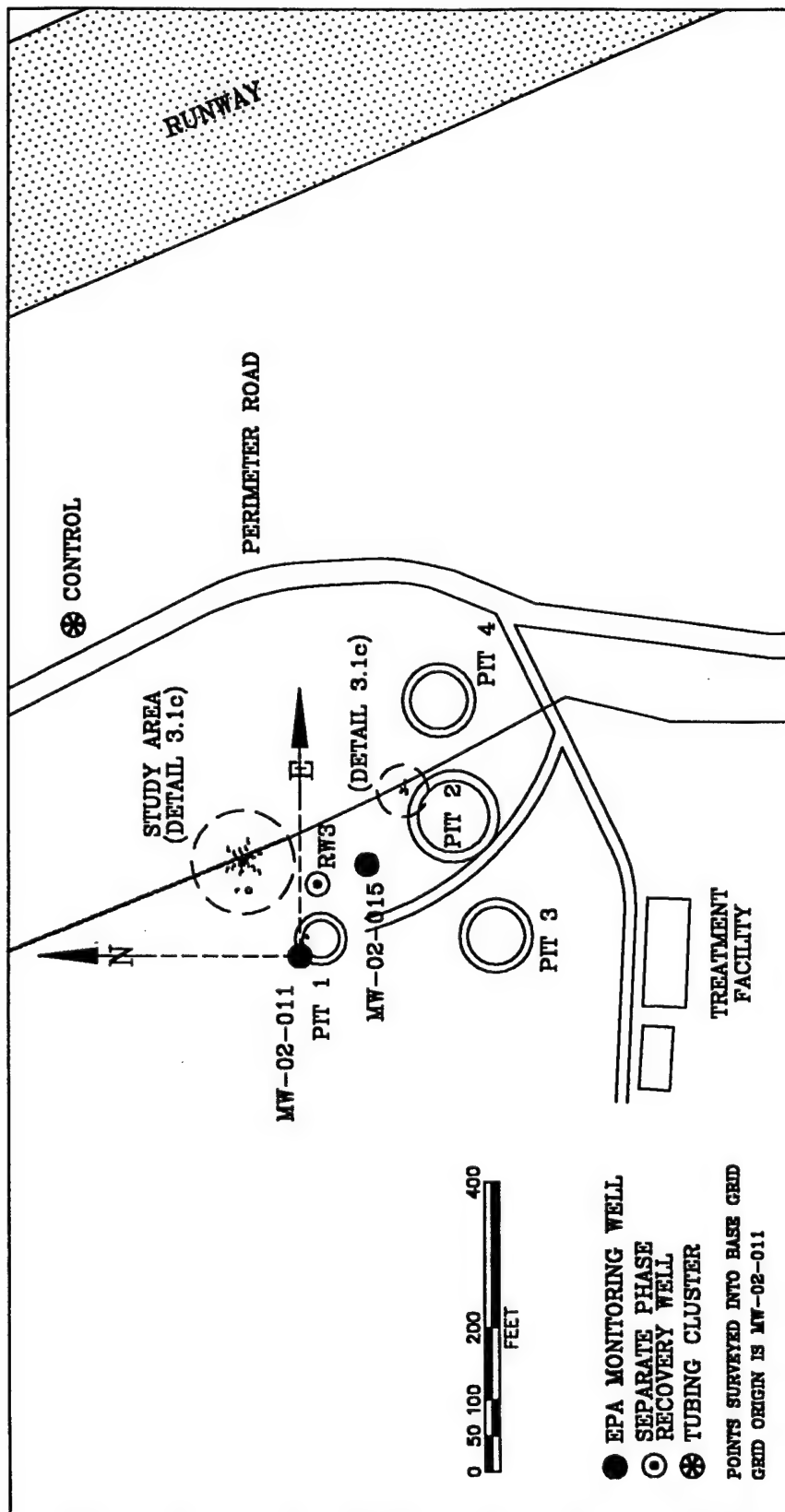


Figure 2.1b Site Plan: Fire Training Area FT-002



**TABLE 2.1 SOIL GAS DATA MAY 1994 [PARSONS ENGINEERING SCIENCE (1995)]**

Designatio	Depth, ft	p <sub>X</sub> , %	p <sub>C</sub> , %	P <sub>METHANE</sub> , %	p <sub>G</sub> , ppm	p <sub>Y</sub> <sup>b</sup>
12PTR1N	7.0	18.8	1.1	<0.1	320	0
12PTR1N	16.0	17.3	1.8	<0.1	180	0
12PTR1N	25.0	13.7	3.3	<0.1	260	0
12PTR1N	34.0	0.0	10.4	0.6	1000	3
14PTR2S	7.0	2.5	8.7	22.1	4700	5
14PTR2S	16.0	0.0	11.0	24.2	>4000	6
14PTR2S	25.0	0.0	11.3	38.7	*	7
14PTR2S	34.0	0.0	11.4	63.0	*	5
30PTR3S	7.0	13.0	4.9	<0.1	490	0
30PTR3S	16.0	8.6	7.3	<0.1	360	0
30PTR3S	25.0	4.9	8.6	<0.1	320	0
30PTR3S	34.0	0.0	11.2	<0.1	850	0
40PTR2N	7.0	15.8	3.4	<0.1	100	0
40PTR2N	16.0	12.5	5.3	<0.1	150	0
40PTR2N	25.0	1.8	10.4	4.1	2000	0
40PTR2N	34.0	0.0	11.3	66.3	6000	3
44PTR2N	7.0	18.0	1.0	<0.1	290	0
44PTR2N	16.0	14.5	2.7	<0.1	285	0
44PTR2N	25.0	7.3	6.3	<0.1	320	0/+1
44PTR2N	34.0	4.6	7.8	<0.1	330	3
48PTR4N	7.0	17.7	1.3	<0.1	270	0
48PTR4N	16.0	16.5	2.1	<0.1	300	0
48PTR4N	25.0	2.1	8.7	<0.1	750	0
48PTR4N	34.0	0.0	10.2	28.7	3000	3

<sup>a</sup>by volume as hexane.

<sup>b</sup>relative sniffer measure.

has been contaminated due to vertical and lateral migration of the chemicals that escaped being burned. During training exercises, the pits were typically saturated with water before the addition of from 75-100 gallons of fuel. Prior to the 1980's, a maximum of 2,000 gallons of fuel was dumped into the pits and ignited weekly [Radian (1985)].

Numerous site investigations have been conducted in order to characterize site FT-002 [Parsons ES (1995)]. Radian (1985) conducted a preliminary site assessment. E.C. Jordan Co. (1989a, 1990, 1989b, 1991a, 1991b) conducted a site inspection, a Phase I remedial

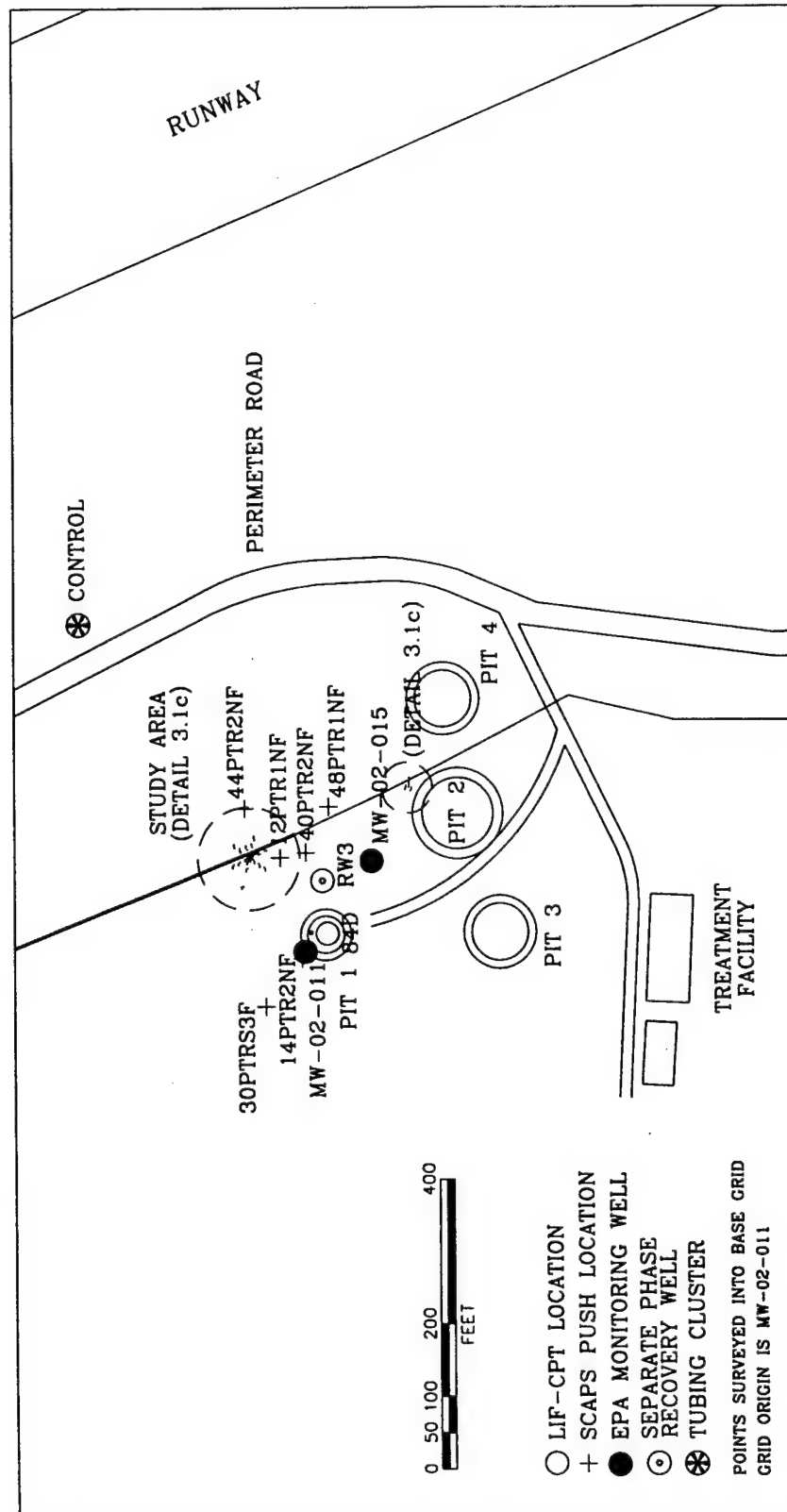


Figure 2.2 Soil Gas Sampling Locations [Parsons Engineering Science (1995)]

investigation, two free product recovery pilot tests, and a drainage flow study. ABB Environmental, Inc (1992) conducted a soil remediation investigation and, together with URS Consultants, Inc. (1993) a Phase II ground water remedial investigation.. In addition, URS Consultants, Inc. (1993) completed a Phase II feasibility study report for the site. The Parsons (1995) data were collected in part by researchers from the United States Environmental Protection Agency (USEPA) Robert S. Kerr Environmental Research Laboratory (RSKERL). This data was combined with that collected under the Installation Restoration Program to determine if natural attenuation mechanisms would eliminate ground water as a pathway for exposure. The site is on the National Priorities List (NPL) under the USEPA's Superfund program. In addition, site FT-002 was selected as a field scale bioventing test site under the Air Force Center for Environmental Excellence (AFCEE) Bioventing Test Initiative.

Previous investigations at the site have included: soil gas surveys, a magnetometer survey, ground penetrating radar, seismic refraction, terrain conductivity, laboratory clay testing, grain size analysis, standard hollow stem auger soil sampling, and a cone penetrometer survey. As part of the latest Parsons-ES effort [Parsons ES (1995)], several investigative techniques were used to further characterize the site. Soil profiling was conducted at the site using tip resistance, friction ratio, pore pressure values, and Laser Induced Fluorescence (LIF) in an instrumented Cone Penetrometer Testing tool and 5-foot and 2-foot Mostep soil samplers. Soil gas data were collected during the penetrometer pushes. Ground water samples were collected at the site using a cone penetrometer tool with a modified discrete sampler, a Geoprobe water sampler, monitoring wells installed in boreholes, and a HydroPunch sampler. Several aquifer tests were conducted including pump, slug, and rising head tests.

A dual pump LNAPL recovery system was installed at the site in 1993 consisting of four recovery wells, a ground water treatment building, and a product storage building. While initial recoveries were good (30-65 gallons product/day), recovery rates since have dramatically dropped. In 1993 and 1994, bioventing wells and associated vapor monitoring points were installed near each of the four fire training pits [Engineering Science (1993a)]. Initial tests conducted indicated that oxygen depleted conditions existed at the site and that the addition of oxygen would most likely stimulate aerobic biological fuel degradation. An extended, 1 year bioventing test was conducted at Pit 3 with encouraging results. However, at the time of the Parsons Engineering Science (1995) report, the New York State Department of Environmental Conservation (NYSDEC) had not approved the bioventing plan for the other three pits.

Parsons Engineering Science (1995) conducted a limited air sparging test at site FT-002 in May 1994 to assess the feasibility of using sparging technology to remove chlorinated solvents from the ground water. A sparge point was installed along with five ground water monitoring points radially located between 3 and 20 feet away from the sparge point. Air was injected at 15 PSI with a flow rate of 80 SCFH for 6 days. Water samples were collected every other day and were analyzed for TCE, cis-DCE, trans-DCE, and vinyl chloride. Contaminant levels at all sampling points decreased by an average of 15% by the end of the test. Points containing ground water with the highest contaminant concentrations experienced the greatest decrease in concentration as a result of the sparge test.

**TABLE 2.2 SOLID CORE ANALYSIS FROM BOREHOLE 84D DECEMBER 1993  
[PARSONS ENGINEERING SCIENCE (1995)]**

Depth, ft	T, mg/kg <sup>a</sup>	T <sub>TCE</sub> , mg/kg <sup>b</sup>	Depth, ft	T, mg/kg	T <sub>TCE</sub> , mg/kg
3-3.5	BLQ <sup>c</sup>	NS <sup>d</sup>	17-17.5	5400	ND <sup>e</sup>
3.5-4	BLQ	NS	17.5-18	4480	BLQ
4-4.5	BLQ	NS	18-18.5	4230	BLQ
4.5-5	BLQ	NS	18.5-19	3450	BLQ
5-5.5	BLQ	NS	19-19.5	3030	BLQ
5.5-6	BLQ	NS	19.5-20	2880	BLQ
6-6.5	176	NS	20-20.5	2360	BLQ
7-7.5	BLQ	NS	20.5-21	1150	ND
7.5-8	BLQ	NS	21-21.5	1790	BLQ
8-8.5	BLQ	NS	21.5-22	2340	BLQ
8.5-9	BLQ	NS	22-22.5	2220	BLQ
9-9.5	BLQ	NS	22.5-23	3240	BLQ
9.5-10	BLQ	NS	23.5-24	194	ND
10-10.5	BLQ	NS	35-35.5	112	BLQ
10.5-11	BLQ	NS	35.5-36	99	ND
11-11.5	BLQ	NS	36-36.5	3380	5.06
11.5-12	BLQ	NS	36.5-37	4780	17.4
12-12.5	BLQ	NS	37-37.5	7570	57.2
12.5-13	BLQ	NS	37.5-38	10100	169
13-13.5	BLQ	NS	38-38.5	18800	210
13.5-14	BLQ	NS	38.5-39	39400	615
14-14.5	BLQ	ND	39-39.5	75300	931
14.5-15	BLQ	ND	39.5-40	125000	1280
15-15.5	94	ND	40-40.5	120000	1130
15.5-16	4120	BLQ	40.5-41	78700	876
16-16.5	2080	BLQ	41-41.5	19400	314
16.5-17	5180	BLQ	44-44.3	BLQ	ND

<sup>a</sup>Total petroleum hydrocarbon mass/mass dry soil.

<sup>b</sup>Trichloroethylene mass/mass dry soil.

<sup>c</sup>Below quantitation limit.

<sup>d</sup>Not sampled.

<sup>e</sup>Not detected.

Parsons Engineering Science (1995) report a wealth data describing the composition of contaminated soil gas, soil, and separate phase petroleum LNAPL from numerous sampling points. Data relevant to the UMASS study are included here. Figure 2.2 displays the location of the Parsons Engineering Science (1995) sampling points. We modify the reported coordinates to reflect a datum at monitoring well MW-02-011, and list them in Table 2.3.

**TABLE 2.3 BASE GRID AND MEAN SEA LEVEL COORDINATES OF BASE  
ENGINEERING SAMPLING POINTS**

<b>Designation</b>	<b>Data</b>	<b>North, ft</b>	<b>East, ft</b>	<b>Elevation, ft<sup>a</sup></b>
<b>MW-02-011</b>	Grid origin	0.00	0.00	260.35
<b>RW3</b>	Separate phase sample	97.93	-23.88	255.58
<b>84D</b>	LNAPL profile	24.90	-30.86	260.00
<b>12PTR1N</b>	Soil gas profile	129.14	35.07	255.90
<b>14PTR2N</b>	Soil gas profile	-9.67	4.19	260.00
<b>30PTRS3</b>	Soil gas profile	-75.87	55.51	262.50
<b>40PTR2N</b>	Soil gas profile	136.30	-0.70	255.74
<b>44PTR1N</b>	Soil gas profile	197.14	84.12	254.50
<b>48PTR1N</b>	Soil gas profile	199.19	-32.88	253.50

<sup>a</sup>Elevation is estimated.

#### 2.1.2 Soil Gas and LNAPL Composition

Parsons Engineering Science (1995) used a Geoprobe cone penetrometer to collect soil gas samples from 24 depths in six boreholes adjacent to the site area (12PTR1N, 14PTR2S, 30PTR3S, 40PTR2N, 44PTR2N, and 48PTR4N). The boreholes are sketched in Figure 2.2, with coordinates included in Table 2.3, referred to monitoring well MW-02-011 as the grid datum. Oxygen  $p_X$ , total hydrocarbon  $p_G$ , and carbon dioxide  $p_C$  partial pressures were measured with portable hydrocarbon meters, along with methane  $p_{\text{METHANE}}$  and trichloroethylene  $p_Y$  levels. Elevated total hydrocarbon and carbon dioxide concentrations were found throughout the fire training area, with highest values near the capillary fringe. The soil gas is oxygenated, though at decreasing levels near the fringe, in all boreholes except 14PTR2. This latter profile lies in Pit 1, which experienced contaminated liquid infiltration during fire training operations. Trichloroethylene vapors were detected near the capillary fringe in 12PTR1, 40PTR2, 44PTR2, and 48PTR4. Trichloroethylene was not sensed in 30PTR3, but was found at all depths in the Pit 1 borehole.

Parsons Engineering Science (1995) present a vertical profile of solid core analyses as well, which we cite in Table 2.2. The soil was sampled continuously from borehole 84D, whose location is shown in Figure 2.2 and coordinates are listed in Table 2.3. The borehole is positioned inside Pit 1. Separate phase petroleum was found over an interval from 4.7 to 12.6 m below the ground surface, with a maximum reported total hydrocarbon contamination  $T_{\text{MAX}}$  of 125,000 mg/kg. Separate phase trichloroethylene was found over the 11.0 to 12.6 m interval, with a maximum reported  $T_{\text{TCEMAX}}$  value of 1,130 mg/kg. The ratio of TCE to total petroleum hydrocarbons in the separate phase ranged from 0.0015 to 0.0156 with an average of 0.0105. Parsons Engineering Science (1995) report LNAPL compounds in a free product sample bailed from recovery well MW-02-015 in December 1993. Table 2.4 lists the results of a semiquantitative gas chromatograph/mass spectrometer analysis of the LNAPL.

**TABLE 2.4 SEMIQUANTITATIVE GC/MS ESTIMATE OF LNAPL COMPOSITION  
DECEMBER 1993 FREE PRODUCT SAMPLE FROM MW-002-011  
[PARSONS ENGINEERING SCIENCE (1995)]**

Compound	Conc., ppm	Mass, %	Compound	Conc., ppm	Mass, %
Benzene	1,400	0.83	Dodecane	11,100	6.59
Toluene	8,970	5.32	Heptane	1,170	0.70
Ethylbenzene	5,440	3.23	Hexane	4,090	2.43
m Xylene	13,700	8.13	Napthalene	1,370	0.81
o Xylene	4,570	2.71	Nonane	15,300	9.10
p Xylene	4,920	2.92	Octane	14,600	8.67
1,2,3 trimethylbenzene	3,560	2.11	Pentadecane	2,980	1.77
1,2,4 trimethylbenzene	6,960	4.13	Tetradecane	5,490	3.26
1,3,5 trimethylbenzene	4,110	2.44	Trichloroethylene	16,400	9.74
1 methylnapthalene	1,400	0.83	Tridecane	9,320	5.53
2 methylnapthalene	1,990	1.18	Undecane	12,000	7.12
Decane	17,600	10.5			

Trichloroethylene is reported as 9.10% by mass of the measured concentrations, which is an order of magnitude higher than the reported  $T_{TCE}/T$  ratios found in the solid core analyses of Table 2.2.

## 2.2 Assimilative Capacity of the Vadose Zone

### 2.2.1 Hydrocarbon Vapor Degradation

The assimilative capacity of the vadose zone may be attributed to microorganisms residing in residual soil moisture. These aerobic organisms create carbon dioxide and consume hydrocarbon vapors and oxygen, so that soil gas sampling is commonly used to assess the natural attenuation potential of the vadose zone [AFCEE (1994)]. The ability of the vadose zone microbes to degrade petroleum hydrocarbon vapors is well documented in the field and laboratory. Kampbell et al. (1987) measure the ex situ treatment efficiency of a biofilter to degrade propane vapors, while Ostendorf and Kampbell (1991) present an account of natural diffusive attenuation of aviation gasoline vapors in the unsaturated zone. Bioventing [AAEE (1994)] and air sparging [Hinchee (1994)] are treatment alternatives that exploit the assimilative capacity of the vadose zone for volatile hydrocarbons. We discuss these remedial measures in more detail in subsequent Sections.

### 2.2.2 Trichloroethylene Degradation

Bourg et al. (1992) present a list of the most common chlorinated contaminants found in the subsurface in order of likely occurrence:

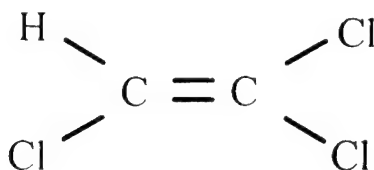


**Figure 2.3 Trichloroethylene Molecule**

- Trichloroethylene
- Tetrachloroethylene
- 1,1,1-Trichloroethane
- Dichloroethene
- Dichloroethane
- Carbon Tetrachloride
- Vinyl chloride
- Dichloromethane

The list suggests that trichloroethylene is the most common chlorinated hydrocarbon compound likely to be found in the subsurface. Trichloroethylene is a colorless, volatile, chlorinated compound containing two carbon atoms, three chlorine atoms and one hydrogen atom (Figure 2.3). The following are some properties of TCE

- |                      |                           |
|----------------------|---------------------------|
| • Molecular Weight   | 131.4 g/mol,              |
| • Specific Gravity   | 1.46                      |
| • Solubility         | 1100 mg/L,                |
| • Vapor Pressure     | 58 mm Hg @ 20°C.          |
| • Henry's Law Const. | 0.39 dimensionless @ 25°C |

Contrary to most chlorinated compounds, hydrocarbon compounds are in a reduced state and energy can be gained through chemical oxidation. Thus, hydrocarbon compounds such as gasoline, other fuel oils, and their distillates are particularly amenable to aerobic biodegradation [Ostendorf and Kampbell (1991), Hickey (1995a), Kerfoot (1990)]. On the other hand, halogenated compounds are already in an oxidized state and reduction is the energetically favored process. While many studies have focused on the biodegradation of hydrocarbon compounds, only recently has there been a focus on the biodegradation of chlorinated compounds. There is still a great deal to be learned regarding the biological processes that occur with various chlorinated compounds in the subsurface environment but there are several processes that are generally accepted as occurring. Table 2.5 lists these mechanisms.

Many TCE degradation mechanisms are anaerobic. A number of studies [Vogel and McCarty (1985), Freedman and Gosset (1989)] have shown that tetrachloroethylene (PCE) can be transformed to TCE, dichloroethylene (DCE), vinyl chloride (VC), and partially to ethylene

**TABLE 2.5 MECHANISMS FOR BIODEGRADATION OF SELECTED  
CHLORINATED COMPOUNDS**

Oxygen	Substrate	Carbon Tetrachloride	Tetrachloro- ethylene	Trichloro- ethylene	Trichloro- ethane
Aerobic	Primary	no	no	no	no
Aerobic	Cometabolite	no	no	yes	maybe
Anaerobic	Primary	no	maybe	maybe	no
Anaerobic	Cometablite	yes	yes	yes	yes

(ETH) under methanogenic conditions by the process of reductive dehalogenation. The addition of an electron donor (methanol) is required to sustain the process with the rate limiting step being the transformation of VC to ETH. Pavlostathis and Zhuang (1991) demonstrate the reductive dechlorination of TCE by sulfate reducing bacteria, via the pathway shown in Figure 2.4.

While anaerobic degradation of TCE has been well researched, direct aerobic metabolism has yet to be documented. Thus far, the only cases of aerobic metabolism of TCE have been through cometabolism. Cometabolism is the biological transformation of a compound by a system of enzymes only while in the presence of, or immediately after it is exposed to, a cosubstrate. A cosubstrate is a compound which allows a system of enzymes to transform a compound that is not transformed in the absence of a cosubstrate. A cosubstrate can be an enzyme or an electron donor. Cometabolic degradation of TCE by methanotrophic bacteria has been well documented in batch and column studies [Lanzarone and McCarty (1990), Speitel and Closmann (1991), Wilson and Wilson (1985), Alvarez-Cohen et al. (1992)] and saturated zone field experiments [Semprini et al. (1991)]. Under natural conditions without contamination, indigenous, methanotrophic bacteria utilize methane as an electron donor and oxidize it to ethanol. This is accomplished using the bacterially produced enzyme, methane monooxygenase (MMO) as a catalyst. Due to a lack of substrate specificity, the MMO enzyme will attack the TCE molecule as well. During the process of TCE utilization, the MMO enzyme inserts an oxygen atom across the double bond of the TCE molecule forming an epoxide. The epoxide is then mineralized through hydrolysis to CO<sub>2</sub> and H<sub>2</sub>O (Figure 2.4). While MMO will degrade TCE as it will methane, no energy is gained from the reaction. For the organisms to flourish, they require methane, and will degrade TCE as an aside. This cometabolic phenomenon can be exploited to treat TCE contamination in-situ. Several previous studies have shown that the addition of methane and oxygen into the subsurface can stimulate the growth of organisms that produce MMO [Lanzarone and McCarty (1990), Alvarez-Cohen et al. (1992), Speitel and Closmann (1991)]. While methane is typically the substrate that allows for the production of MMO, it has also been shown that MMO producing organisms can be grown with methanol as a substrate [Fitch et al. (1996)]. When attempting to stimulate the cometabolism of TCE through use of MMO, one must design a system to properly balance the available methane or other substrate to the organism population. If an oversupply of methane is provided, the organisms will choose to degrade methane only and not degrade TCE. This is competitive inhibition and it has been shown to occur in aquifers between methane and TCE [Semprini et al. (1991)]. On the other hand, without enough methane, because the organisms gain no energy from TCE



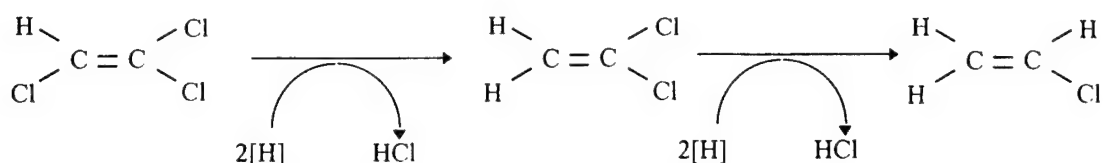


**Figure 2.4 Anaerobic Dehalogenation of Trichloroethylene**

degradation, the bacteria population will not thrive, therefore a careful balance must be achieved between methane and TCE concentrations. Wilson and Wilson (1984) show through column studies that TCE can be degraded cometabolically using a mixture of natural gas and air. The natural gas consisted of 77% methane, 10% ethane, 7% propane, 2.4% *n*-butane, 1% *iso*-butane, 1.5% pentanes, and 0.7% hexanes. Using radiolabeled TCE, the authors determine that, in columns exposed to the gas/air mixture, 99% of the radiolabeled carbon was recovered as CO<sub>2</sub>. Wilcox et al. (1995) also induce biodegradation of TCE using propane.

Lanzarone and McCarty (1990) study the methanotrophic degradation of TCE and 1,2-DCA in column experiments. Radiolabeled TCE and 1,2-DCA were introduced into columns filled with saturated sandy aquifer materials. Dissolved propane and methane was tested at several concentrations. It was found that no TCE degradation occurred with propane and when methane was added at levels of 4.5 mg/L and above. An optimal dissolved methane concentration of 1.5 mg/L led to TCE degradation. Alternating high and low methane levels also led to TCE metabolism. The addition of nutrients did not have any noticeable effect on degradation rates. Speitel and Cloosmann (1991) studied degradation rates of TCE, 1,2-DCE and chloroform in unsaturated soil batch experiments. The authors exposed soil to a methane/air atmosphere. Results showed that 1,2-DCE degraded fastest followed by TCE and then chloroform. Degradation rates were based only on removal of the parent compound.

In addition to methane utilizing bacteria, it has also been demonstrated that bacteria capable of aerobically degrading certain aromatic hydrocarbon compounds such as toluene [Fan and Scow (1993), Landa et al. (1994), Malachowsky et al. (1994), Mars et al. (1996), Leahy et al. (1996)] and phenol [Hopkins et al. (1993), Hecht et al. (1995)] can cometabolically degrade trichloroethylene. The enzyme toluene dioxygenase (TDO) has been strongly implicated in the cometabolic degradation of TCE in the presence of toluene [Nelson et al. (1988), Li and Wackett (1992)] as well as toluene monooxygenase [Luu et al. (1995)]. Fan and Scow (1993) studied cometabolism of TCE with toluene in unsaturated soils by indigenous microorganisms. Experiments studying the effects of TCE and toluene concentrations on TCE and toluene degrading bacteria populations were carried out by Mu and Scow (1994). Degradation of TCE by a hybrid ring dioxygenase is presented by Furukawa et al. (1994).

There are additional factors required for metabolism whether aerobic or anaerobic. A nitrogen source is one of the primary nutrients required for biological growth. However, the addition of nitrogen is not usually required. Previous work has indicated that methane oxidizing

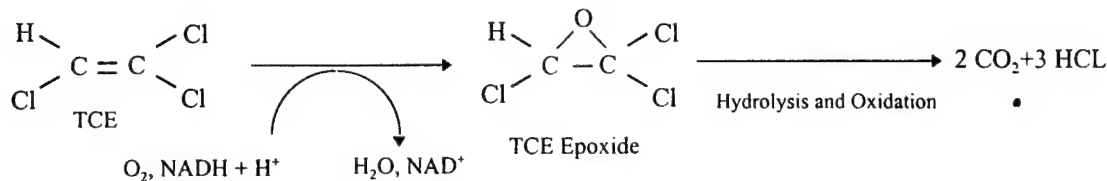


**Figure 2.5 Cometabolism of Trichloroethylene**

bacteria, when supplied with molecular nitrogen, are able to oxidize TCE as efficiently as cells supplied with ammonia ( $\text{NH}_4^+$ ) and nitrate ( $\text{NO}_3^-$ ) [Chu et al. (1995)]. In addition, Lanzarone and McCarty, 1990 found that the addition of nitrogen and phosphorous compounds in aerobic column studies did not conclusively effect degradation rates. Enzein et al. (1994) present a study in which a methanotrophic fluidized bed is used to create a combination aerobic and anaerobic environment. While TCE can be degraded anaerobically and aerobically, PCE can not and requires anaerobic conditions. Under strictly anaerobic conditions, VC and DCE tend to build up as by-products of TCE degradation. This combination aerobic/anaerobic environment allowed for the degradation of PCE and its daughter products (TCE, DCE, and VC).

Recent studies indicate that the root zone and rhizosphere offer increased potential for microbial degradation of toxic compounds. The root zone is the upper area of the soil containing the roots of the plants growing at the surface. The rhizosphere is the interface where plant roots come into contact with the surrounding soil. There are two schools of thought regarding possible mechanisms for the enhanced degradation ability of the root zone/rhizosphere [Anderson and Walton (1995)]. The first is that plant roots release compounds that aid in overall microbial growth allowing for an increased microbial population density. The second is that the plant roots exude compounds that are analogs to anthropogenic contaminants. Thus, organisms are present and acclimated which are capable of degrading contaminants. A study utilizing radiolabeled TCE along with vegetated and non vegetated soil from a TCE contaminated site yielded promising results. Vegetated soils with both acclimated and non acclimated plant species showed a marked increase in their ability to transform TCE to  $\text{CO}_2$ . There was additional uptake of [ $^{14}\text{C}$ ] in plant tissues which appeared to be specific to plant species and water uptake rate [Anderson and Walton (1995)]. Boyle and Shan (1995) conducted laboratory studies on the biodegradation capacity of rhizosphere and non rhizosphere soils with four compounds: phenol, 2,4-Dichlorophenol (2,4-DCP), 2,4-Dichlorophenoxyacetic acid (2,4-D), and 2,4,5-Trichlorophenoxyacetic acid (2,4,5-T). Results showed that rhizosphere soils played a key role in the mineralization of the more recalcitrant compounds (2,4-D and 2,4,5-T) but little or no difference was seen in degradation rates between the two types of soils for phenol and 2,4-DCP.

### 2.3 Soil Vapor Remediation Alternatives

There are many remediation schemes for treating contamination in the subsurface. The most common can be grouped into three categories: ground water pump and treat, soil

excavation, and soil venting/vapor extraction systems, the category in which bioventing is placed. Early attempts to remediate sites with hydrocarbon contamination involved ground water pump and treat technology. Ground water was extracted from the subsurface through a network of recovery wells or trenches, treated, and then reinjected, land applied, or sent to a water treatment facility. As more advanced attempts to treat ground water evolved, dual pump or skimmer pump recovery systems were used. In these systems, one pump operated as a ground water depression pump and a second pump or passive element acted to remove any floating separate phase product that accumulated on the water surface as a result of the ground water depression.

Because the residual phase can serve as a constant source of contamination, it becomes all but impossible, despite great magnitudes of ground water being pumped to the surface, to remediate a site to low levels of contaminant concentration. Ground water samples collected within a recovery well appear to be clean but, in fact, if the flow is stopped and the ground water is allowed to come to equilibrium with the surrounding contaminated soils, contaminant levels will rise again to near initial levels. What must be addressed are the residual trapped hydrocarbon compounds that are serving as the source. Pump and treat strategies are effective at removing the bulk, mobile separate phase from the subsurface and also a portion of the contaminated ground water. However, pump and treat technologies generally are not sufficient to remove the majority of a typical subsurface hydrocarbon spill. A large portion of the spill typically remains in an immobile, discontinuous phase within the soil pores both above and below the water table. The immobile NAPL phase serves as a continuous hydrocarbon source to the surrounding ground water.

### 2.3.1 Soil Vapor Extraction

Several different strategies are typically implemented to address the residual phase,. Soil vapor extraction (SVE) or in situ air stripping is one strategy that is in wide use. The principles of this technique are as follows. A vent well is installed so that it is screened through or near the interval of soil contamination. A blower is connected at the surface to the end of the well and a vacuum is induced on the well. Soil gas, including gaseous contaminants, is pulled to the surface where it is generally treated before being released to the atmosphere. When the gas is withdrawn from the subsurface, a pressure void exists in the vadose zone such that atmospheric air from the surface is drawn down to replace it. This constant flow of air strips volatile contaminants from the subsurface and brings them to the surface where the air stream can be treated.

To be amenable to SVE, a site must contain substances that are volatile enough to be stripped by this technique. Substances must partition from the separate phase or dissolved phase into the gaseous phase at a rate that makes treatment by this method possible in a reasonable amount of time. High vapor pressure and low solubility are desired characteristics (Rathfelder et al., 1995). Secondly, the site soils must be permeable enough to allow the SVE system to move air through the area of contamination. While SVE is an effective, proven technique for the in situ treatment of contaminated vadose zone soils, it does have several drawbacks. Spills of fuel oils such as diesel and heating oil contain fractions of heavier, less volatile compounds. Constituents such as naphthalene, phenanthrene, and other PAHs have relatively low vapor

pressure constants and therefore volatilize very slowly. The slow volatilization means that the process is severely rate limited with respect to these compounds. These heavier compounds therefore, can not be effectively treated by SVE. Another drawback to SVE is that the compounds that are stripped from the subsurface and brought to the surface often must be treated to meet regulatory emissions levels. Often the cost of treating the off gas exceeds that of construction and operation of the SVE system.

Whether planned or not, during the SVE process more than just air stripping of volatile compounds occurs. When soil gas is withdrawn from the subsurface, air from the atmosphere flows in to replace it. The points where air enters the ground vary based on withdrawal rate and site geology, but at some point the withdrawn gas volume is replaced. Atmospheric air contains 20.9% oxygen by volume. Generally, in an area of high hydrocarbon contamination, soil gas oxygen levels are greatly depleted when compared to atmospheric oxygen levels.

At most hydrocarbon spill sites there are bacteria present in the subsurface that are capable of degrading many of the hydrocarbon compounds that exist there. The most efficient of these bacteria are aerobic due to the fact that using  $O_2$  as an electron acceptor yields more energy for the bacteria than alternative acceptors such as nitrate, sulfate, or iron. In order to function, the bacteria require four things: an electron donor, electron acceptor, a carbon source, and water. In addition, several trace nutrients are required. The hydrocarbon compounds provide the electron donor and the carbon source. Assuming adequate moisture is present along with necessary micronutrients, the requirement that is lacking is typically oxygen. Thus the bacteria are hindered from further growth by a lack of  $O_2$ . By increasing the levels of  $O_2$  in the subsurface, a corresponding increase in bioactivity and resultant depletion of hydrocarbon compounds by mineralization will occur. SVE, by pulling oxygen rich gas from the subsurface, inadvertently stimulates biological growth. The results of increased biological activity have been seen at SVE sites [Gomes-Lahoz et al. (1994)]. Bioventing exploits this aspect of soil vapor extraction.

### 2.3.2 In Situ Bioventing

The technique of in situ bioventing has become an accepted practice for remediating soils contaminated with hydrocarbon compounds. Bioventing is an effort to enhance the indigenous microbial population's hydrocarbon degrading capability by supplying electron acceptor, usually in the form of atmospheric  $O_2$ . In many ways, a bioventing system operates with the same basic equipment and under the same principles as SVE. A bioventing system maximizes microbial degradation of contaminant compounds while minimizing withdrawal of contaminants to the ground surface where they would require additional treatment. Advantages of bioventing over SVE and other methods include the fact that heavy compounds such as diesel and heavy heating oils can be effectively treated in-situ [Downey et al. (1995), Leeson et al. (1993), Bulman et al. (1993), Dupont (1993), Long (1992)]. These heavy compounds can not otherwise be brought to the surface economically for treatment.

In order for bioventing to work successfully, sufficient water must be present to permit the transfer of enzymes necessary for biodegradation. Nutrients such as orthophosphate and

ammonium nitrogen are sometimes added at the surface along with moisture addition to optimize biodegradation [Long (1992)].

The following list, adapted from Long (1992), presents parameters that should be known prior to implementation of a bioventing system:

#### **Contaminants**

- Compounds Present Above Action Levels for Treatment
- Volatility
- Solubility
- Aerobic Degradability

#### **Site**

- Permeability
- Vacuum/ Pressure Requirements
- Air Flow Paths
- Water Table Elevation
- Ability to Lower Water Table

#### **Regulatory**

- Permits and Regulations that Apply to Installation of a Bioventing System
- Levels of Government Involved
- Level of Government at which Permits will be Written

Relatively few bioventing field demonstrations have been reported in the literature with most involving JP4 jet fuel, JP5 jet fuel, diesel, and gasoline [Lee and Swindoll (1993)]. The most active bioventing program has been instituted by the United States Air Force. Laboratory treatability studies were conducted at more than a dozen sites. Over half were contaminated with light hydrocarbon compounds such as gasoline, diesel and light to medium weight crude oil. Most sites experienced high removals in the area of 90%. Heavier fuel oil sites experienced less effective treatment. Sites that contained chlorinated solvents such as dichloromethane, tetrachloromethane, chloroform and carbon tetrachloride experienced reductions in these also but this was mostly due to venting with similar effluent concentrations as venting alone. The authors note limited aerobic degradation of these compounds without a cometabolic substrate.

Part of the reason bioventing is effective is that it uses as an electron acceptor. Table 2.6, adapted from Dupont, 1993 presents the number of pounds of carrier required to yield one pound of oxygen for various carrier solutions. It can be seen that 110,000 grams of water saturated with air is required to provide 1 gram of O<sub>2</sub> while the same requirement can be provided with only 4.5 grams of air. As an example, assuming an O<sub>2</sub> requirement of 3gm O<sub>2</sub> per gram of hydrocarbons, a 1,000 gallon fuel spill weighing 7,000 lbs. would require 21,000 lbs. of O<sub>2</sub>. If air saturated

**TABLE 2.6 COMPARISON OF OXYGEN LEVELS IN VARIOUS CARRIERS**

Carrier Solution	g Carrier/g O <sub>2</sub>
WATER SATURATED W/AIR	110,000
WATER SATURATED W/O <sub>2</sub>	22,000
H <sub>2</sub> O <sub>2</sub> SOLUTION @ 500 mg/l	2,000
AIR	4.5

H<sub>2</sub>O was used, one would need 2,310,000,000 gallons to provide adequate O<sub>2</sub> to remediate the area assuming 100% efficiency. In addition to being a prohibitively large quantity of water to deliver, this much water added to the soil of a relatively small site would greatly reduce soil permeability. While hydrogen peroxide provides more O<sub>2</sub> per gram than oxygen saturated water, initial tests conducted at Eglin AFB, FL using H<sub>2</sub>O<sub>2</sub> and nutrients by Hinchee and Ong (1992) showed low reductions of hydrocarbon levels due to poor distribution of H<sub>2</sub>O<sub>2</sub> and in addition, a breakdown of H<sub>2</sub>O<sub>2</sub>. On the other hand, by using air which contains 20.9% O<sub>2</sub> by volume, large quantities of O<sub>2</sub> can be efficiently delivered to the subsurface efficiently without a reduction in permeability. Alternatively, research by Gates and Siegrist (1995) appears to indicate that H<sub>2</sub>O<sub>2</sub> is a viable alternative for use where clay soils are contaminated with trichloroethylene.

Bioventing involves supplying oxygen usually in the form of air to the organisms in the subsurface. In the case of a single vent well, air can be withdrawn from an extraction well causing air from the ground surface to be drawn down replacing withdrawn soil gas. In the case of a multiple well installation, inlet wells can be used to allow air to flow directly to deep areas of contamination. As an alternative to withdrawing vapor from the subsurface, air can be forced in under positive pressure. This provides the highest oxygen levels where the air injection well is screened. Bioventing is enhanced by lower air rates and longer flow paths. Bioventing can operate in a vacuum mode, much like SVE, where soil gas is extracted from the subsurface or alternatively, bioventing can be operated in a pressure mode where atmospheric air is forced into the subsurface under positive pressure. In the vacuum configuration, air containing O<sub>2</sub> enters the subsurface from the ground surface ideally over the entire area of influence covered by the collection/extraction well. Air is pulled downward and radially inward towards the collection/extraction well. In the positive pressure mode, O<sub>2</sub> enters the subsurface through the injection well and flows radially outward.

An interesting application of bioventing is the use of passive bioventing [Nilson et al. (1991), Wilson et al. (1989), Zwick et al. (1994), Weeks (1979), Pirkle et al. (1992)]. Passive bioventing involves using changes in barometric pressure to cause either soil gas to flow out of, or ambient air to flow into, the subsurface. Passive bioventing is an applicable technology when the required pressure gradient can be periodically generated and when rapid cleanup times are not a priority.



The advantages and disadvantages of utilizing vacuum or pressure systems for bioventing are as follows. The vacuum, or negative pressure, configuration provides one or more central, concentrated points where soil gas can be collected. This makes collection of gas for treatment, if required, much simpler than if soil gas emanating from a positive pressure system requires capture and collection. In the case of a positive pressure system, collection could take the form of a ground sealing device such as a tarp with a collection device attached. With a negative pressure system, gas is being withdrawn from a contaminated area, where there will almost always be volatile contaminants in the gas stream that will either be difficult to degrade or have not had enough time to degrade while in the subsurface. These contaminants will usually require some sort of off gas treatment prior to release to the atmosphere which can be costly.

In addition, a vacuum withdrawal system poses the disadvantage of possibly producing ground water upwelling in the area of the vent well if it is placed too close to the water table [Johnson (1990b)]. This is particularly unadvantageous because, in most cases, the area to be biovented lies just above the water table. When ground water rises and fills the soil pore spaces, O<sub>2</sub> can not reach the degrader organisms and bioventing becomes impractical. A way to solve this problem is to pump the ground water table down, but this requires the installation of additional ground water withdrawal wells.

A positive pressure system does not produce a concentrated contaminant gas stream. Instead, as a response to blowing additional gas into the subsurface, soil gas will be forced to the ground surface in order to reach a pressure equilibrium. Thus, soil gas will be emanating from the soil surface all around within the area of influence of the injection well or wells. This makes gas collection difficult and is often a reason for implementing the vacuum method. However, if the injection system is operated properly, soil gas that is traveling to the surface will have already undergone biotransformation and contaminants will not be emitted at levels above those which have been determined to be unacceptable by regulatory agencies. If operated in this mode, with proper area monitoring, there are no off gases to treat and the overall system operating costs are less.

Prior to implementing a subsurface remediation scheme, it is often advantageous to use a tracer material in order to better understand the hydraulics or pneumatics of an area that is often difficult if not impossible to characterize by other methods. Effective tracers have the properties of being long lived, non reactive, not degradable, non toxic, while being measurable at useful concentrations. Tracers such as Cl<sup>-</sup> have been used to characterize saturated media for some time. The unsaturated zone can be characterized using gaseous compounds such as sulfur hexafluoride [Wilson and Mackay (1993)] or helium. Sulfur hexafluoride (SF<sub>6</sub>) is readily available and detectable as it is commonly used in the HVAC industry. Helium is also available and has the advantage of diffusing faster in the subsurface due it relatively small molecular size as compared to SF<sub>6</sub>.

### 2.3.3 Effects of Environmental Variables

There are several compound related properties that must be taken into account to operate a bioventing system properly, many of which are important to SVE also. Of primary importance

to bioventing and not to SVE is the biodegradability of the compound. If indigenous microorganisms cannot degrade the compound, then supplying additional electron acceptor will not aid in the degradation process. Certain compounds are aerobically directly degradable while others require additional substrate be present for the microorganisms and can only be degraded aerobically through cometabolism. Additional properties include volatility, solubility, the sorption characteristics of a particular compound, and finally toxicity.

The volatility of a compound determines what flow rates will be required, the number and placement of bioventing wells as well as the overall pneumatic design. A more volatile compound may be swept by the air stream to areas with additional moisture, surfaces, and organisms. This will speed the degradation process allowing, for example, a drop of a compound to be spread out and degraded simultaneously over a large surface area as opposed to degradation merely occurring at the droplet surface. While volatility is an extremely positive property with regard to SVE, a compound with a high volatility may make efficient bioventing difficult if the volatile compound is carried to the surface before it can be properly degraded. Less volatile compounds will generally require a more effective oxygen distribution network due to the fact that they will stay in an area as opposed to migrating through the subsurface.

Solubility of a compound must be taken into account. If a compound is highly soluble, it will remain trapped within moisture droplets where conditions are not conducive to aerobic degradation. In addition, mass transport within water is several orders of magnitude slower than in a gas. Compounds can only slowly pass through water to the water/gas interface to be degraded. Transport through a water film can often be the rate limiting step during soil venting of hydrocarbon compounds and TCE [Grathwohl (1993)]. While not typically a concern, because of the requirement for living microorganisms, the contaminant level in the vadose zone must be kept below toxic limits. In addition, there cannot be other compounds present in the soil at levels toxic to the degrader organisms.

There are also several soil and site properties which must be within certain ranges for a bioventing system to be effective. Because bioventing requires a thriving microorganism population, it is essential that conditions be as conducive to growth and degradation as possible. Like all living organisms, degrading bacteria require water, an energy and carbon source, trace nutrients, and favorable environmental conditions. Bioventing has been successfully shown to be effective in soils with moisture contents in the range of from 2 to 25% [Downey et al. (1995)]. Fan and Scow (1993) reported moisture levels below 5% inhibited degradation while levels in the 15-30% range yielded good results. The lower moisture limit is based on the fact that the organisms need some moisture to function and hence survive. The upper moisture limit is driven by a reduction in soil permeability. If high levels of moisture are present in a soil, air filled porosity is greatly reduced and pathways for air flow are subsequently reduced. Without air flow pathways,  $O_2$  can not reach the microorganism population. Experiments conducted by McCarthy and Johnson (1985) showed that the effective diffusion coefficient of TCE in soil columns wetted from field capacity to saturation changed by three orders of magnitude from  $1 \times 10^{-6} \text{ m}^2/\text{s}$  to  $1 \times 10^{-9} \text{ m}^2/\text{s}$ .



Soil permeability is function of grain size distribution and air filled porosity. The intrinsic permeability and the air filled porosity alone control permeability which is not a function of the type of liquid filling the pore space [Stylianou and DeVantier (1995)]. Site permeability assessments with respect to ground water flow have been conducted for decades. More recently, permeability estimates for soil gas flow have been determined using the same and modified ground water flow equations. Johnson et al. (1990b) developed simple models to predict vapor flow rate, vapor flow path, contaminant distribution, and contaminant composition during soil venting operations

Soil temperature is a critical parameter when assessing the feasibility of implementing bioventing at a site. Temperature affects both the viscosity and density of gases but this is negligible over the temperature ranges common in the subsurface [Johnson et al. (1990a)]. However, although less important for bioventing than SVE, the key parameter of vapor pressure increases by a factor of 3 to 4 for every 10°C rise in temperature [Rathfelder et al. (1995)]. Leeson et al. (1993) present a study on bioventing in cold climates. The focus is a JP4 jet fuel spill site at Eielson AFB, Alaska. A bioventing system was designed to operate in a positive pressure mode. To adequately heat the soil as outdoor temperatures dropped, hot water had to be added. Additional water brought additional moisture which lowered soil permeability and made air flow in the soil more difficult. This translated into a decreased supply of O<sub>2</sub> to the microorganisms and thus a decrease in bioactivity. Thus, a balance had to be maintained between supplying enough O<sub>2</sub> and keeping the site warm enough.

In addition to temperature and moisture levels, trace nutrient concentrations must be adequate to support a thriving population of bacteria. Macro and micro nutrients essential for the production of cell materials must be present in the appropriate ratios. A typical macronutrient C:N:P ratio of 100:10:1 is usually adequate. From the literature, it appears that at most bioventing sites, there is not a shortage of such nutrients. Several studies [Dupont (1993), Downey et al. (1995), Hickey (1995b)] have shown that the addition of nutrients, typically nitrogen and phosphorous, did not increase microbial numbers or bioactivity indicating that, at most sites, nutrients are available in adequate quantities. However, there have been some studies conducted [Bulman et al. (1993)] where these nutrients were apparently limiting because, subsequent to nutrient addition, there was a noted rise in microbial numbers and bioactivity. Chu and Alvarez-Cohen (1996) studied the effects of various nitrogen sources on TCE degradation by methane oxidizing bacteria. Results indicated that nitrogen fixing cells exhibited the highest TCE transformation capacity, thus addition of alternative nitrogen sources was not required. Significant degradation of hydrocarbon compounds has been measured in soils with TKN values less than 20 mg/kg soil and P levels less than 3 mg/kg soil [Bulman et al. (1993)]. In addition, research conducted at Tyndall AFB suggests that there is a recycling of nutrients and that there are nitrogen fixing bacteria present [Downey et al. (1995)]. A survey of the literature by Rathfelder et al. (1995) indicated inconclusive results regarding the need for nutrient addition.

One of the only ways to determine if a site is suitable for bioventing is to conduct field tests. A bioactivity test should be conducted to determine if there is an active microbial degrader population present at the area of contamination. In addition, a permeability test should be conducted to determine if the site's pneumatic parameters will allow air and thus O<sub>2</sub> to be

transported to the organisms. The use of in situ respiration tests has become an accepted method for determination of bioactivity potential [Hinchee and Ong (1992), Leeson et al. (1993), Dupont (1993)]. The typical in situ respiration test requires that the site be prepared with an air injection well and several gas monitoring points installed near the injection well. To conduct the test, initial background levels of O<sub>2</sub> and CO<sub>2</sub> are measured at the various monitoring points. Typically, oxygen is measured by discrete sampling with subsequent analysis [Hinchee and Ong (1992)] but can also be measured using more innovative techniques such as in situ oxygen sensors [Li (1995)]. Air is forced into the subsurface through the injection well in an effort to raise the soil gas O<sub>2</sub> levels to ambient (20.9%) levels. Once this has been achieved, air injection ceases and the monitoring points are periodically measured for O<sub>2</sub> and CO<sub>2</sub> levels. Alternatively, Hickey (1995b) used a vapor extraction system to bring O<sub>2</sub> and CO<sub>2</sub> levels in a contaminated area to levels equivalent to biologically less active areas. If there is a viable aerobic degrader community present, the level of O<sub>2</sub> will decrease and the level of CO<sub>2</sub> will rise as the result of aerobic respiration. The test is typically ends when O<sub>2</sub> levels become depleted to less than 5% by volume. When conducting in situ tests it is imperative that background levels of O<sub>2</sub> and CO<sub>2</sub> be measured to accurately determine utilization and production rates due to hydrocarbon degrader metabolism.

Hinchee and Ong (1992) outline a rapid in situ respiration test for quantifying biodegradation rates for hydrocarbons in soil. The paper describes a test to assess whether bioventing is a viable alternative for remediation of petroleum hydrocarbon contaminated soils. The test involves ventilating the soil and then turning off the vent system while monitoring O<sub>2</sub> and CO<sub>2</sub> levels in the surrounding the ventilation point. The paper focuses on 8 contaminated sites with differing geological and climatic conditions. Most of the sites were contaminated with petroleum products (fuels) with two of the sites contaminated with PAHs. The estimated biodegradation rates based on O<sub>2</sub> utilization were generally more reliable than those based on CO<sub>2</sub> production because CO<sub>2</sub> tends to be converted to carbonate in alkaline soils. In addition, CO<sub>2</sub> might not be a good indicator of microbial activity because not all O<sub>2</sub> utilized is converted to CO<sub>2</sub>. Results from the 8 sites indicated that O<sub>2</sub> utilization rates were generally .02-.99 %/hour and biodegradation rates ranged from 0.4 to 19 mg/kg/day.

Leeson et al. (1993) conducted in-situ respiration tests at Eilson AFB in Alaska. Air was introduced into the vadose zone and was subsequently shut off. O<sub>2</sub> and CO<sub>2</sub> were monitored over time at various sampling points. As is typical during aerobic respirometry, O<sub>2</sub> was consumed and CO<sub>2</sub> was produced. Experiments were terminated when O<sub>2</sub> concentrations reached 5% or after about 1 week, whichever came first. A test was conducted in October and yielded good results while an additional test was conducted in January which showed microbial activity was less. Hinchee et al. (1992) present a bioventing study that took place at Hill AFB, Utah. In situ respiration tests confirmed that microbial activity was indeed present, leading to the production of CO<sub>2</sub>. Isotope ratios of <sup>13</sup>C/<sup>12</sup>C in soil gas were measured to confirm that the CO<sub>2</sub> source was indeed microbially generated. However, at the end of the study it was determined that the majority of fuel was removed through the physical process of volatilization while approximately 15 to 25% of the fuel was degraded in situ.

Permeability tests are typically conducted by injecting or withdrawing air from a central well and measuring changes in pressure with time in wells spaced away from the center. Alternatively, a tracer gas can be injected into a central well and tracer gas concentration measurements with time can be obtained. Permeability estimates can then be calculated using the same equations used for soil permeability estimates related to groundwater flow.

#### 2.3.4 Air Sparging

Often, in areas with reasonably shallow water tables, if contamination is present in the unsaturated zone it is also present in the ground water. While bioventing directly treats the unsaturated zone, it only indirectly treats the ground water because no air flow occurs in saturated media. The major process occurring to treat the ground water is equilibrium shifting and partitioning to the gaseous phase. This can be a gradual process with ground water acting as a slow, continuous source. Because of this, the technique of air sparging is often used to more rapidly remove compounds from the ground water into the soil gas [Long (1992)], thus enhancing bioventing.

Air sparging is, in effect, air stripping of the ground water. The process is implemented by installing sparge points below the water table. Sparge points are typically narrow bore wells which are screened over a short interval below the water table. Air is forced in under pressure into the sparge point with the bubbles exiting the screened portion of the well, stripping contaminants from the ground water and releasing them into the vadose zone. An excellent, practical paper on air sparging is presented by Brown (1993). An additional approach that presents more contaminated media to the bioventing system is lowering the water table to increase the treatable unsaturated zone [Long (1992)].

### 2.4 Soil Gas Models

We review the current mathematical modeling efforts in the area of contaminant fate and transport within the subsurface. Models surveyed included all phases of subsurface contamination; NAPL, dissolved and gaseous. Some of them represent modeling efforts alone while others include laboratory experiments for calibration and/or verification.

Mathematical models can be divided into two groups: analytical models and numerical models. Rathfelder et al. (1995) present an excellent overview of the current status of modeling in the areas of SVE and bioventing. Analytical models [Pantazidou and Sitar (1993), Wood and Ginn (1995), Chrysikopoulos (1995), Shan (1995), Baehr and Baker (1995), Hatfield and Stauffer (1993), Jin et al. (1994), Zaidel and Russo (1994), Dietsch and Smith (1995), Batterman et al. (1995), Gierke et al. (1992)] solve the equations through the application of integration techniques such as integral tables, integration by parts, fourier transforms and other convolution techniques. Analytical models tend to be simpler in nature than numerical models, involving fewer parameters and/or dimensions. Numerical models [Kaluarachchi and Islam (1995), Unger et al. (1995), Van Geel and Sykes (1994), Roberts and Wilson (1993)] are iterative in nature and are almost exclusively solved through the use of a computer. Numerical models are typically

divided into two categories: finite difference and finite element. Numerical models tend to be more complex and due to this complexity, usually require a more detailed data base.

Modeling has been used successfully to predict the transport of NAPL in both saturated [Chrysikopoulos (1995), Hatfield (1993), Unger (1995)] and unsaturated [Pantazidou and Sitar (1993), Sleep and Sykes (1989, 1993), Falta et al. (1993)] porous media. Contaminant vapor generation [Roberts and Wilson (1993)], fate and transport [Ostendorf and Kampbell (1991)] along with the effects of contaminant and media [Batterman et al. (1995)] properties can be predicted. Some models are complex, allowing for the study the reaction of gases such as O<sub>2</sub>, CO<sub>2</sub>, N<sub>2</sub> along with any number of hydrocarbons [Baehr and Baker (1995)]. Other models focus on one contaminant [Chrysikopoulos (1995)] incorporating gas advection, diffusion, liquid to gas transfer, partitioning and sorption of subsurface movement of organic vapors [Gierke et al. (1992)]. The importance of models incorporating multiphase multicontaminant transport is growing in light of the numerous compounds present at sites and their differing properties [Russell (1995)].

The modeling of technologies such as soil vapor extraction [Baehr et al. (1989), Wilson et al. (1994), Beckett and Huntley (1994)] and bioventing [Mohr and Merz (1995)] allows for ballpark feasibility determinations and the possible elimination of unneeded pilot testing in the event of a negative result. On the other hand, a positive result typically requires pilot tests. Biological activity in the subsurface can also be modeled. Examples include the coupling of biodegradation and transport of contaminant vapors [Ostendorf and Kampbell (1991), Jin (1994)], the prediction of metabolic lag due to acclimation and removal of food source [Wood and Ginn (1995)] and cometabolic biodegradation of halogenated compounds [Alvarez-Cohen and McCarty (1991)]. Efforts to increase the efficiency of existing technologies such as the introduction of heated air for vapor extraction [Kaluarachchi and Islam (1995)] or surfactant addition to aid in pump and treat remediation [Deitsch and Smith (1995)] can be predicted through modeling efforts. Models predict air permeability based on simple field tests [Shan (1995)] and couple vacuum extraction with air sparging for use in predicting DNAPL treatment rates [Unger et al. (1995)].

While general transport models incorporate many properties of both the contaminant and media in their equations, others focus on specific properties such as the impact of soil gas humidity on TCE vapor transport [Batterman et al. (1995)]. Sleep and Sykes (1989, 1993) model TCE concentrations numerically, coupling both the aqueous and vapor phases. Density driven flow of organic compounds in the unsaturated zone has also been modeled [Falta et al. (1989)].

### 3 METHODS AND MATERIALS

The field data base includes data taken from boreholes, stainless steel tubing clusters, vapor probes, and thermocouple arrays distributed across the study area. Figure 3.1 displays the plan location of the various sample points, which were surveyed into the Plattsburgh Air Force Base grid by UMASS personnel using a Topcon 5 sec Total Station (Northeast Supply Co., East Longmeadow, MA). Table 3.1 lists north, east, and vertical coordinates of the UMASS sampling array, relative to mean sea level and a Base monitoring well (MW-02-011).

#### 3.1 Soil Temperature, Grain Size Distribution, and Moisture Content

##### 3.1.1 Soil Temperature

Soil temperature influences the soil gas diffusivity and the ideal gas law in the soil gas transport model, and affects biodegradation rates as well. We installed thermocouple arrays in boreholes SPK1 on 12 October 1995 and 12AT on 2 December 1995. Figure 3.1 displays the location of the two arrays, which consist of thermocouple leads (Omega Engineering Inc., Stamford, CT) attached to 1.91 cm rigid PVC casing deployed through hollow stem augers. The thermocouples are staggered at 0.3 m intervals to a depth of 3 m in borehole SPK1, then spaced a 1.5 m intervals to a depth of 10.7 m. The 12AT array features 0.6 m spacing to a depth of 3 m, then 1.5 m spacing to the 9.1 m depth. We read the leads with an Omega HH 73K1 handheld digital thermometer on 17 sampling trips from 13 October 1995 to 19 December 1996, generating a data base of 377 observations.

##### 3.1.2 Grain Size Distribution

Particle size distributions and soil moisture content were observed in order to confirm our assumption of a homogenous, well drained unsaturated zone with constant air porosity. Soil samples were obtained from boreholes SPK1, SPK2, and 12AY using the Standard Penetration Test and a two inch OD split spoon sampler in accordance with ASTM (1992a) protocol. The split spoon soil samples were measured for recovery and immediately placed into "zip-lock" plastic bags to retain the natural moisture content. In the laboratory, the bagged samples were weighed and an average weight from ten clean dry bags was subtracted to obtain the moist soil weight. The split spoon samples were analyzed for grain size distribution [ASTM (1992b)]. The soil, after being oven dried for 24 hours, was placed into a mortar and a rubber-covered pestle to break up the aggregations of soil particles. The following nest of U.S. Standard Sieves was used in the analysis:

- US Standard 3/8 inch (9.54 mm)
- US Standard No. 4 (4.76 mm)
- US Standard No. 10 (2.00 mm)
- US Standard No. 20 (0.840 mm)
- US Standard No. 40 (0.420 mm)
- US Standard No. 60 (0.250 mm)
- US Standard No. 80 (0.185 mm)





**TABLE 3.1 BASE GRID AND MEAN SEA LEVEL COORDINATES OF UMASS  
SAMPLING POINTS**

<b>Designation</b>	<b>Data</b>	<b>North, ft</b>	<b>East, ft</b>	<b>Elevation, ft</b>
<b>MW-02-011</b>	Grid origin	0.00	0.00	260.35
<b>RW3</b>	Separate phase sample	97.93	-23.88	255.58
<b>12AA</b>	Tubing cluster	129.66	77.49	256.26
<b>12AB</b>	Tubing cluster	127.37	72.53	256.37
<b>12AC</b>	Tubing cluster	128.36	81.92	256.54
<b>12AD</b>	Tubing cluster	123.62	90.75	256.41
<b>12AE</b>	Tubing cluster	115.21	80.39	256.70
<b>12AF</b>	Tubing cluster	90.52	86.04	257.32
<b>12AG</b>	Tubing cluster	120.19	99.09	256.46
<b>12AH</b>	Tubing cluster	132.03	73.06	256.30
<b>12AI</b>	Tubing cluster	134.85	62.82	256.22
<b>12AJ</b>	Tubing cluster	139.42	53.90	255.90
<b>12AK</b>	Tubing cluster	122.14	65.21	256.48
<b>12AL</b>	Tubing cluster	116.77	57.07	256.55
<b>12AM</b>	Tubing cluster	125.38	78.79	256.53
<b>12AN</b>	Tubing cluster	221.85	-147.63	250.24
<b>12AO</b>	Tubing cluster	154.31	70.96	255.61
<b>12AP</b>	Tubing cluster	141.01	81.08	256.04
<b>12AQ</b>	Tubing cluster	143.27	98.24	255.47
<b>12AR</b>	Tubing cluster	137.47	90.07	255.60
<b>12AS</b>	LANPL profile	133.08	69.02	256.29
<b>12AT</b>	Tubing cluster	223.64	-139.90	250.18
<b>12AU</b>	Tubing cluster	122.44	76.11	256.53
<b>12AV</b>	Tubing cluster	129.67	70.28	256.36
<b>12AW</b>	Tubing cluster	126.89	85.69	256.32
<b>12AX</b>	Tubing cluster	230.27	-153.47	249.97
<b>12AY</b>	Grain size distribution	145.82	58.92	255.46
<b>12AZ</b>	Tubing cluster	142.74	77.64	254.18
<b>12BA</b>	Tubing cluster	138.43	85.83	255.86
<b>12BB</b>	TCE profile	123.21	68.83	256.48
<b>12BC</b>	Vapor probe	120.71	70.03	256.45
<b>12BD</b>	Intact core sleeves	116.27	70.48	256.47
<b>12BE</b>	Vapor probe	121.66	77.75	256.52
<b>12BF</b>	TCE profile	120.75	83.74	256.61
<b>12BG</b>	Intact core sleeves	117.38	78.05	256.65
<b>12BGMC</b>	moisture content determination	121.67	79.40	256.53
<b>12BH</b>	Vapor probe	138.96	84.05	255.73
<b>12BI</b>	TCE profile	142.03	88.13	255.55
<b>12BJ</b>	Vapor probe	145.28	92.01	255.35
<b>12BK</b>	Vapor probe	116.83	65.99	256.60

**TABLE 3.1 (Continued) BASE GRID AND MEAN SEA LEVEL COORDINATES OF  
UMASS SAMPLING POINTS**

<b>Designation</b>	<b>Data</b>	<b>North, ft</b>	<b>East, ft</b>	<b>Elevation, ft</b>
<b>12BM</b>	Vapor probe	127.59	67.54	256.45
<b>12BN</b>	Vapor probe	117.40	87.79	256.57
<b>12BO</b>	TCE profile	133.52	95.23	255.78
<b>NA1</b>	50 cm tubing cluster, west	109.95	61.89	256.63
<b>NA2</b>	25 cm tubing cluster, west	113.49	61.31	256.57
<b>NAW</b>	Near surface array, west	112.25	63.90	256.70
<b>NA3</b>	50 cm tubing cluster, east	153.80	78.03	255.68
<b>NA4</b>	25 cm tubing cluster, east	154.82	81.51	255.47
<b>NAE</b>	Near surface array, east	152.38	80.97	255.53
<b>VENT1</b>	Vent well	130.74	74.58	256.25
<b>VENT2</b>	Vent well	129.29	79.32	256.30
<b>SPARGE1</b>	Sparge well	127.71	76.13	256.30
<b>CONT</b>	Control	452.62	313.21	244.12
<b>SPK1</b>	Thermocouple array	144.78	73.74	255.92
<b>SPK2</b>	Grain size distribution	106.44	82.40	257.01
<b>SPK 3</b>	Grain size distribution	98.64	84.18	257.01
<b>VP1</b>	Vapor probe	131.15	78.39	256.26
<b>VP2</b>	Vapor probe	129.66	77.17	256.26
<b>VP3</b>	Vapor probe	114.57	102.99	256.26

- US Standard No. 100 (0.149 mm)
- US Standard No. 200 (0.074 mm)
- Pan

We placed the soil was placed into the sieves, covered the nest and shook it by hand for 30 seconds to allow all the finer soil to pass the 3/8 inch sieve. The 3/8 inch sieve was inspected visually for small particles retained on the sieve, and any smaller particles were assisted by hand through the 3/8 inch sieve. The 3/8 inch sieve was then removed from the nest (because of limited room in the mechanical shaker) and its contents weighed in a tared porcelain bowl. The rest of the sieves were covered and placed onto the mechanical shaker for six minutes. The 3/8 in. sieve was then removed from the top of the nest, and its contents removed by using a small round brush to clean all the soil out and into a tared porcelain bowl. The soil weight retained was recorded and the process continued down the nest of sieves and into the pan.

Figure 3.1 displays the location of boreholes SPK1, SPK2, and 12AY. We measured particle size distributions in 0.3 or 0.5 m intervals down to the water table in each borehole:



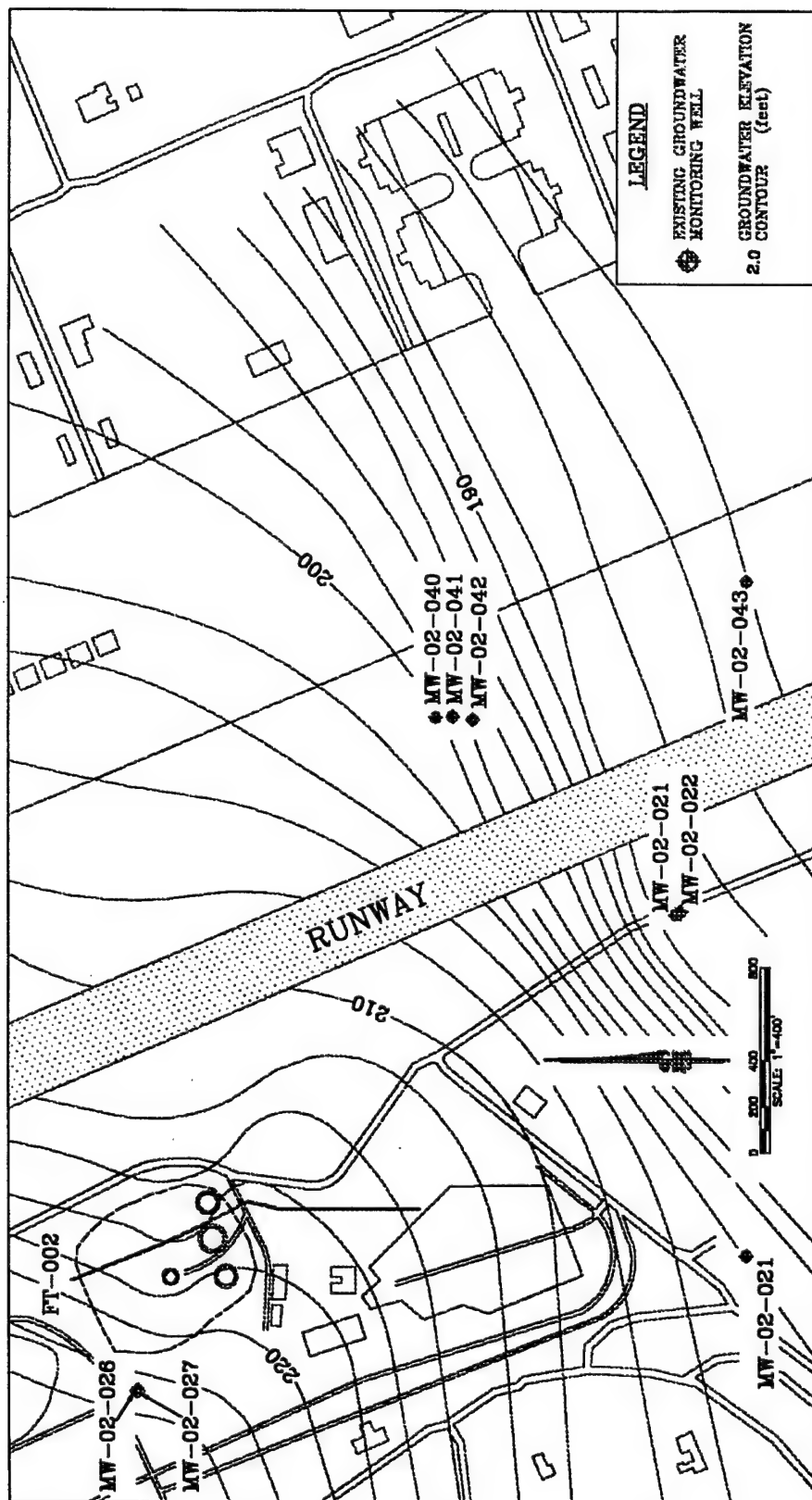


Figure 3.1a Site Plan: Plattsburgh Air Force Base Runway

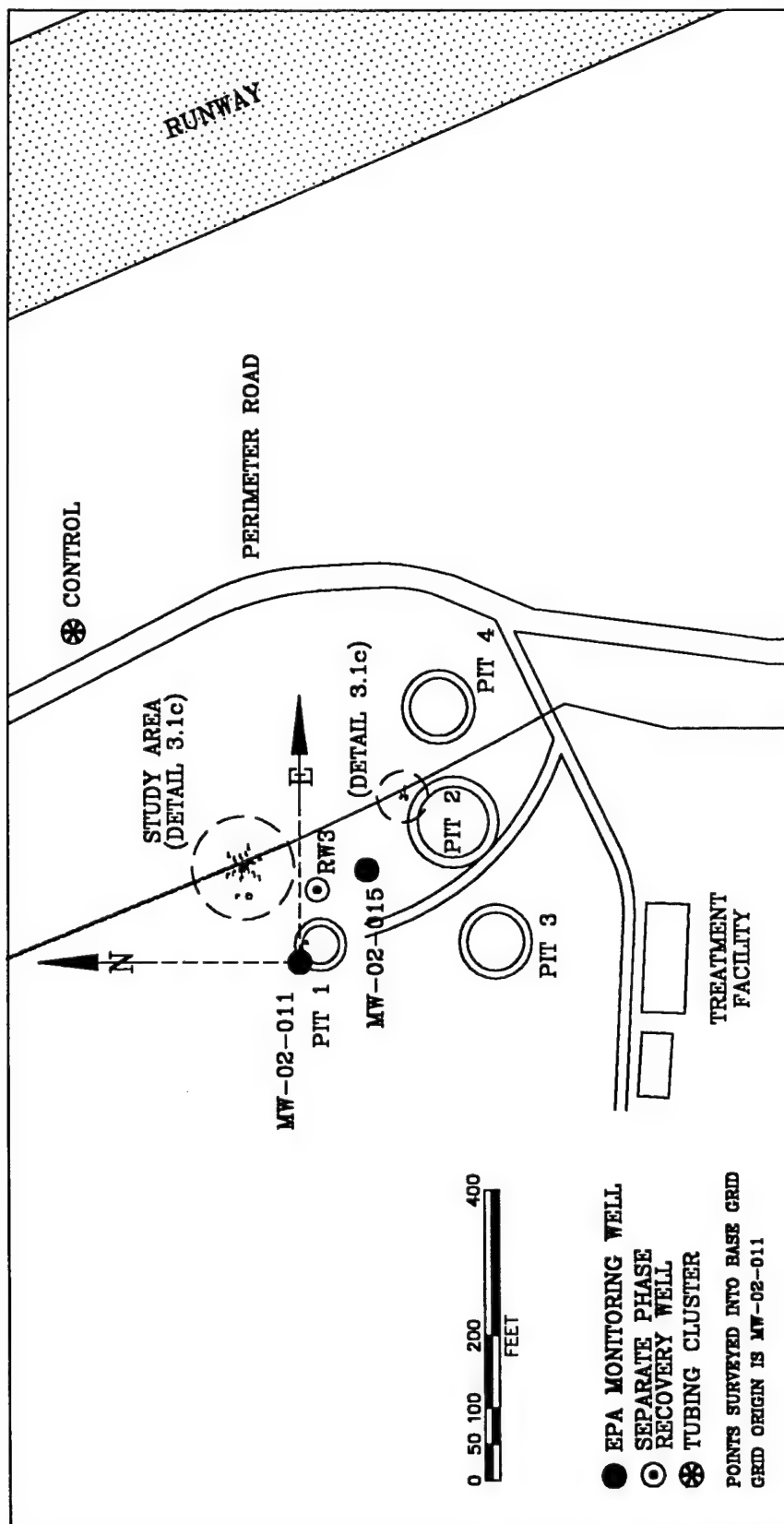


Figure 3.1b Site Plan: Fire Training Area FT-002

**TABLE 3.2 SOIL MOISTURE AND LNAPL BOREHOLE DATES AND DEPTH INTERVALS<sup>a</sup>**

<b>Borehole</b>	<b>Date</b>	<b>Core Barrel Diameter</b>	<b>Number of samples</b>	<b>Interval, m below surface</b>
12AA	9Oct95	3 inches	34	0.2-15.2
12AB	9Oct95	3 inches	6	10.8-14.1
12AD	10Oct95	3 inches	25	0.1-14.1
12AG	10Oct95	3 inches	27	0.1-14.0
12AK	11Oct95	3 inches	32	0.1-14.2
12AM	12Oct95	3 inches	22	10.7-14.2
12AP	12Oct95	3 inches	17	10.8-13.6
12AR	13Oct95	3 inches	21	10.7-14.2
12AS	2Dec95	3 inches	63	10.7-15.1
12AT	1Dec95	3 inches	60	7.6-11.9
12AU	5Jun96	3 inches	22	11.7-14.9
12AV	5Jun96	3 inches	35	10.7-14.9
12AW	5Jun96	3 inches	33	10.7-14.7
12AX	6Jun96	3 inches	27	1.6-11.0
12AY	6Jun96	2 inches	18	11.0-13.5
12AZ	7Jun96	3 inches	46	10.7-16.1
12BA	7Jun96	3 inches	35	10.8-16.1
12BB	19Aug96	3 inches	34	0.1-14.5
12BF	20Aug96	2 inches	33	10.7-14.4
12BI	21Aug96	2 inches	25	11.3-14.2
12BO	22Aug96	2 inches	22	11.1-14.1
VENT1	30Nov95	3 inches	49	10.7-12.9
VENT2	30Nov95	3 inches	29	10.7-13.0
SPARGE1	1Dec95	3 inches	70	10.7-14.9

<sup>a</sup>Twenty gm samples stored in serum bottles. Borehole logs are in Appendix I.

- Borehole SPK1 - 33 depths
- Borehole SPK2 - 25 depths
- Borehole 12AY - 50 depths

### 3.1.3 Soil Moisture

We observed a series of soil moisture profiles through the unsaturated zone and capillary fringe as part of the separate phase petroleum profile sampling at Plattsburgh. Table 3.2 lists the dates, depth intervals, and number of sampling points comprising the moisture (and LNAPL) data base. Logs for these boreholes are listed in Appendix I. Ten mL disposable syringe barrels (Becton Dickinson) were used to withdraw 10 gm samples from the pared face of a core barrel extruded in the field. Figure 3.2 displays the extruder, which consists of a 6.2 cm diameter piston with a 1.1 m stroke, driven hydraulically by a 4 horsepower Honda gasoline power

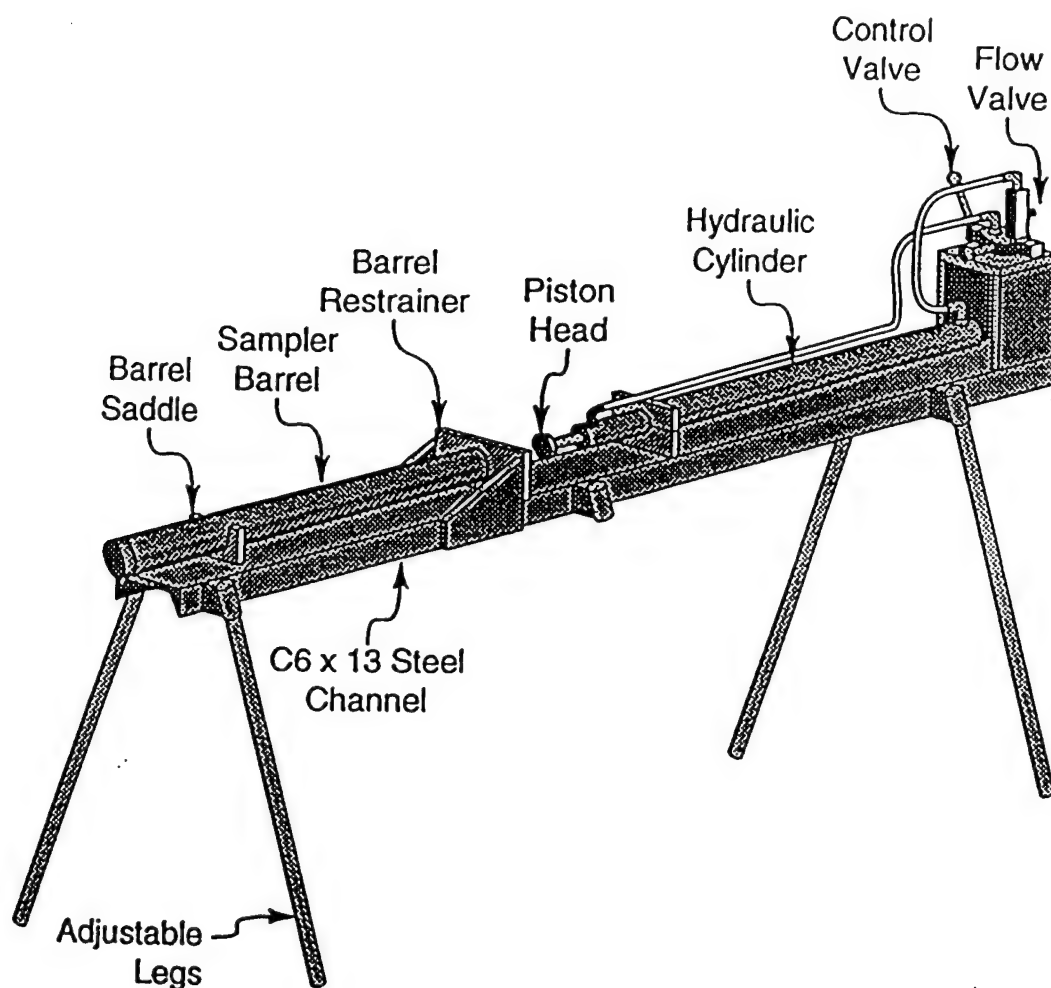
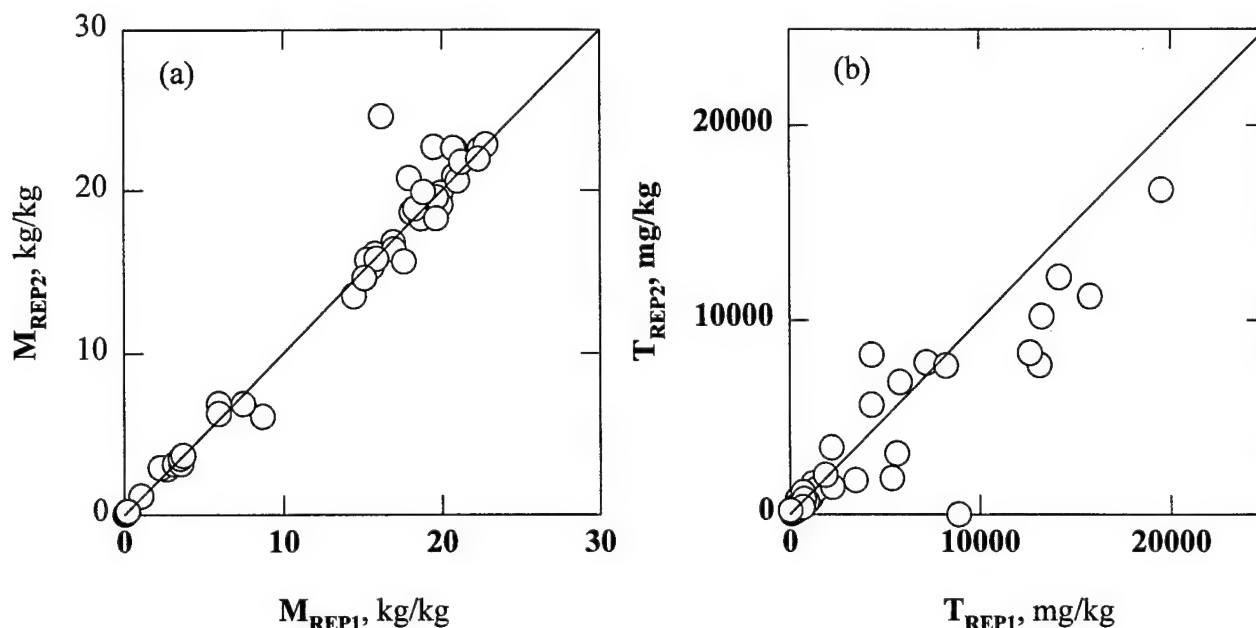


**Figure 3.2 Core Barrel Extruder**

generator. We control the extruder with a 3 position detente style valve with flow control. The piston is mounted on a C6 x 13 steel channel, equipped with adjustable iron pipe legs and a steel barrel saddle. The upper end of the core barrel is threaded into a threaded gusset barrel restrainer that provides a reaction force to the extruding friction.

The moist samples were stored in preweighed, dried, 20 mL serum bottles with Teflon septa and plastic screwcaps for subsequent gravimetric determination of soil moisture content [ASTM (1992c)]. Data are reported as mass based moisture content  $M$

$$M = \frac{\text{mass} \cdot \text{moisture} \cdot \text{volume}}{\text{dry} \cdot \text{soil} \cdot \text{mass}} \quad (3.1)$$



Note: Symbols are data, while straight line is perfect precision

**Figure 3.3 Replicate Soil Moisture (a) and LNAPL (b) Contents for Serum Bottle Samples**

Replicate soil moisture samples were obtained in order to assess the method precision  $P$  defined by

$$P = \frac{2|\text{replicate1} - \text{replicate2}|}{(\text{replicate1} + \text{replicate2})} \quad (3.2)$$

Figure 3.3a displays 57 moisture replicates taken over the course of field sampling--the average  $P$  of 6% suggests excellent precision in spite of the relatively small soil mass required for vertically resolved sampling in a core barrel.

### 3.2 Separate Phase Petroleum Content in Solid Core Samples

The determination of the separate phase petroleum content of solid core samples features field sampling, laboratory extraction, and gas chromatographic analysis. The field sampling protocol follows the pioneering work of the Robert S. Kerr Environmental Research Laboratory of the US Environmental Protection Agency [Leach et al. (1988)], and the gas chromatography is a modification of RS Kerr methodology for the analysis of light hydrocarbons [Vandegrift and Kampbell (1988)]. The EPA field and laboratory methods have been demonstrated by the Environmental Engineering Program laboratory of the University of Massachusetts at Amherst

on a peer reviewed [Ostendorf et al. (1991)], EPA audited [Ostendorf et al. (1992)] research project with the RS Kerr Laboratory.

### 3.2.1 Field Sampling

The initial step in obtaining a contaminated soil sample is removal of a soil core from the subsurface. After a prospective sampling location was determined, a steam cleaned, 17 cm outer diameter hollow stem auger was driven by a Central Mine and Equipment Company (CME) 75 drilling rig adjacent to the initial sampling depth. As the augers were driven down, a weighted plug was inserted into the 8.3 cm inner diameter annulus to prevent soil from entering into the hollow portion of the augers. Upon reaching sampling depth, the plug was removed and a 0.46 m long, 7.6 cm OD, soil sampler was inserted into the hollow stem auger. The barrel assembly consisted of four parts:

- A 7.6 cm OD cutting shoe which threaded onto the bottom end of the barrel and cut into the underlying, undisturbed soil
- A plastic soil retainer which fit between the cutting shoe and the barrel and prevented the loss of sample when the barrel was removed from to the surface
- A barrel which contained the soil core after collection
- A drive head which threaded onto the top end of the barrel, connecting it to the drive rods

The core barrel, positioned at the sampling depth, was then percussively driven into the underlying soil by a 140 lb automatic hammer with a 76 cm drop. This type of hammer is typically used to run a Standard Penetration Test (SPT) for foundation design, but for this project, hammer blows were counted in order to empirically determine changes in site stratigraphy. Measurements were taken on the portion of the drive rods above the surface, so that the sampler was only driven the 18 inch length of its body. Once this occurred, the sampler was hydraulically lifted to the surface, unscrewed from the driving apparatus, and sent to the next stage of the sampling process. As the sampler with the soil core was at the next stage, a freshly steam cleaned barrel was attached to the drive rods and the whole process began again. This rapid type of soil core acquisition allowed for both continuous or incremental sample collection.

### 3.2.2 Soil Core Extrusion

The full sampling tube was extruded into a nitrogen filled glove box in accordance with USEPA aseptic field sampling protocol [Leach et al. (1988)]. We first measured sample recovery in the tube, then mounted it horizontally on a hydraulic extruder designed by the University of Massachusetts Geotechnical Engineering Department (Figure 3.2). The cutting shoe was loosened and this end of the sampler was inserted into a nitrogen filled glovebox through a neoprene iris (Figure 3.4). A 6.2 cm piston was then hydraulically pushed into the opening of the sampler opposite the glovebox. Once the shoe and retainer were removed inside, the piston incrementally pushed the soil core into the aseptic sampling environment. This type of soil removal system is intended to minimize sample disturbance.

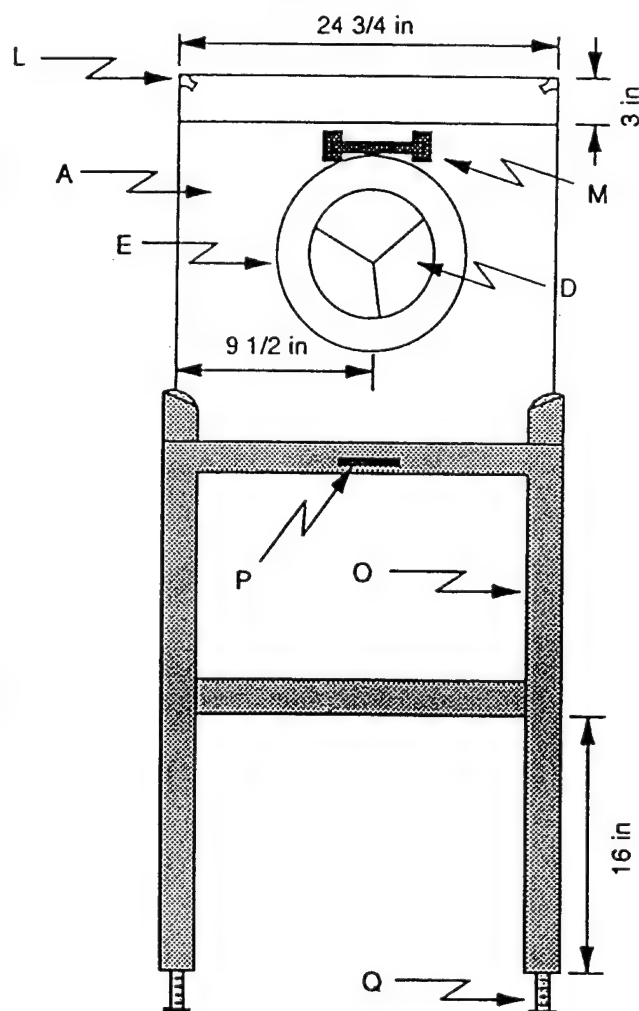
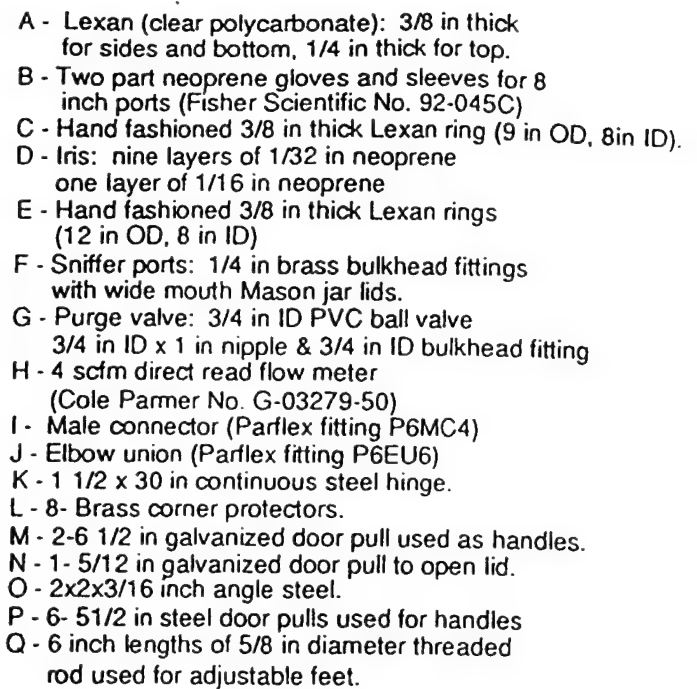


**Figure 3.4 Field Glovebox for Solid Core Sampling**

The glovebox, modeled after a United States Environmental Protection Agency (USEPA) prototype, was designed and built by the University of Massachusetts Environmental Engineering Program. It is constructed of clear Lexan sheets with dimensions of 92x59x64 cm, as shown in Figure 3.4. Other features include two pairs of neoprene access gloves, an iris for inserting soil samplers, a flow meter for regulating nitrogen flow into the box, a nitrogen purge valve, and a headspace sampling port. The glovebox rests in a vertically adjustable stand to facilitate establishment of a level sample plane. The glovebox was purged prior to sampling with prepure grade nitrogen (Merriam-Graves; West Springfield, MA) at a flow rate of 5 ft<sup>3</sup>/min for 5 minutes. Once sampling commences, the flow was reduced to 0.5 ft<sup>3</sup>/min. Nitrogen was passed into the glovebox to establish a positive pressure inside the sampling area, thereby excluding contaminated surface air. If biological samples are taken, either nitrogen or synthetic air can be used depending on the type of microbiological study being performed.

Wide mouth, 1 quart, Mason jars (Alltrista Corporation; Muncie, IN) were used as sample collection vessels for the extruded soil cores. These jars were autoclaved and labeled prior to each trip and packed numerically, 24 at a time, into the glovebox before the nitrogen was turned on. The standard size Mason jar was filled 2/3 full with approximately 15 cm of soil core. Sampling in this manner allowed for three sampling points per core. Smaller volume jars (pints and half pints) were used for more resolved vertical separate phase profiles. The extruded section of soil core was introduced into the Mason jar using a trowel that was wiped clean with Kimwipes between samples. Accurate field logging, linking borehole ID to depth to jar ID was essential at this step of the sampling procedure.

### 3.2.3 Headspace Determination and Subsampling

We measured the total hydrocarbon vapor pressure in the Mason jar headspace to estimate the degree of volatility of the separate phase product residing in the soil, and thus guide the acquisition of solid core samples. The glovebox was equipped with a Mason jar lid with Swagelok penetrations, globe valve, and a Teflon transfer line to the Bacharach TLV sniffer to facilitate headspace sampling. We screwed the filled jar into the lid, opened the globe valve, and pulled headspace into the TLV sniffer. It took approximately 30 seconds for the meter to measure the headspace of the jar. The in-line globe valve was then closed, the meter allowed to rezero, and the Mason jar recapped and set aside for further processing.

The headspace hydrocarbon vapor partial pressure ( $p_G$ ) correlates positively with separate phase petroleum content (T) for solid core samples from the contaminated capillary fringe. Figure 3.5 displays the Mason jar headspace for four typical contaminated boreholes--headspaces as high as 6,000 ppm correlated with soil as contaminated with as much as 26,000 mg petroleum/kg dry soil. This finding is consistent with other field results, as summarized in Figure 3.6 [Ostendorf et al. (1996)]. We compare headspace correlation for weathered LNAPL contaminated soils from three field sites:

- Figure 3.6a - Gasoline/diesel fuel (high volatility)
- Figure 3.6b - Fuel oil (low volatility)



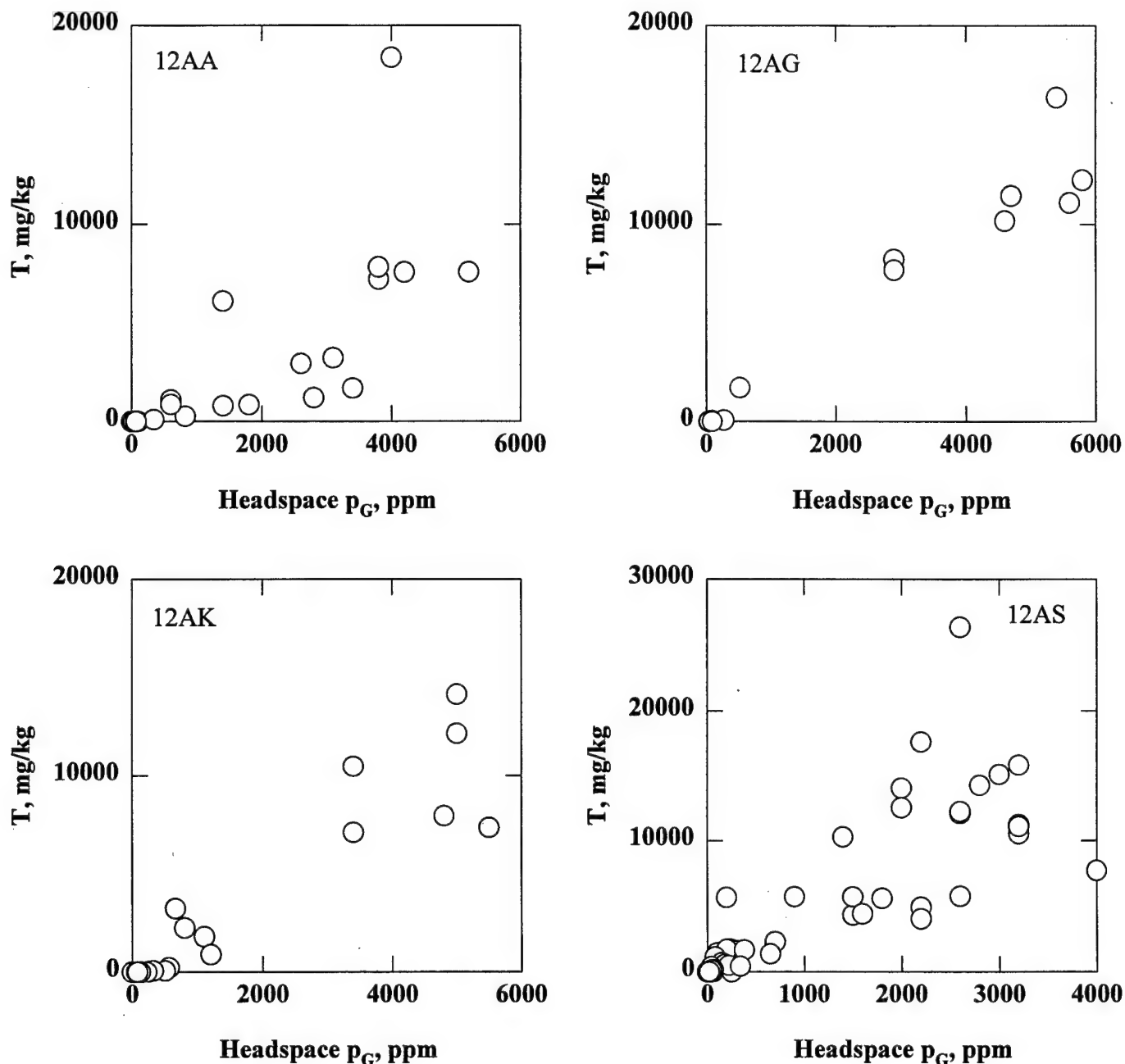


**Figure 3.5 Separate Phase Petroleum Content (T) vs Mason Jar Headspace ( $p_G$ ) for Typical Plattsburgh Boreholes**

- Figure 3.6c - Aviation gasoline (highest volatility)

The weathered separate phase aviation gasoline yields the highest headspace pressures, T values less than 5,000 mg/kg exhibit  $p_G$  levels in excess of 10,000 ppm into the Mason jar headspace. Weathered JP-4 and the gasoline/diesel fuel mixture yield a weaker (but still readily detectable)

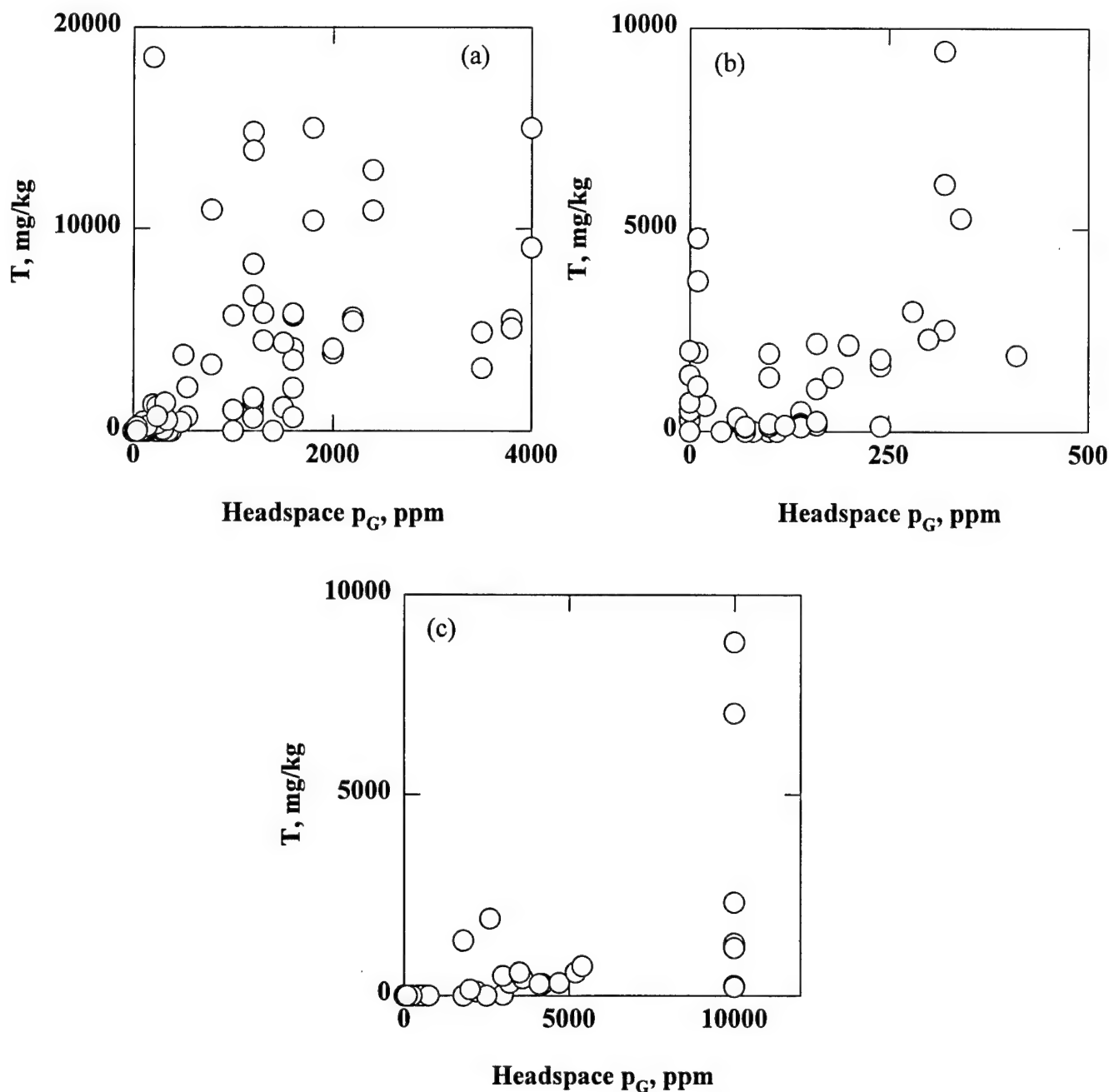


**Figure 3.6 Separate Phase Petroleum Content (T) vs Mason Jar Headspace ( $p_G$ ): (a) Gasoline/Diesel Fuel, (b) Fuel Oil, (c) Aviation Gasoline [Ostendorf et al. (1996)]**

headspace, as indicated by Figures 3.5 and 3.6a. The fuel oil generates a very weak response by virtue of its low volatility. Indeed, Figure 3.6b suggests that a number of Mason jars containing several gms fuel oil/kg dry soil do not exhibit any headspace hydrocarbon vapor pressures at all.

We began to subsample in the field upon completion of drilling for the day. core barrel extrusion for each day in the afternoon of the samplined once the core barrel acquisition step

was complete and all of the soil had been sampled into respective jars. This step began by loading the glovebox with the following items:

- Twenty four Mason jars containing contaminated soil samples that were collected that day.
- A rack of 50 cleaned, autoclaved, and labeled 20 mL EPA vials (Kimble; Owens, IL) with Teflon coated silicone septa for separate phase analysis. Each vial was prefilled in the laboratory with 3 mL of GC Resolve Methylene Chloride ( $\text{CH}_2\text{Cl}_2$ ) (Fisher Scientific; Pittsburgh, PA) and 5 mL of organic free water and weighed to determine its presampling mass.
- A rack of 50 cleaned and labeled 20 mL EPA vials (Kimble; Owens, IL) with Teflon coated silicone septa for moisture content analysis.
- Cleaned and autoclaved 10 cc syringe barrels with removed tips (Becton Dickinson Corporation; Franklin Lakes, NJ).

The glove box was again purged and filled with nitrogen, as in the extrusion step. When this was complete, an approximate 15 g sample was taken from each jar using a 10 cc syringe barrel and deposited into a respective subsampling vial filled with methylene chloride and water. The threads of the vial were then wiped clean, the cap tightened, and the vial replaced in the rack. Using the same 10 cc syringe barrel, a 30 g soil sample was deposited into a corresponding moisture content vial. To prevent cross contamination, a new syringe barrel was used for each new jar. Careful records needed to be taken down throughout this phase of the sampling because it was simple to mix up the jar ID and vial ID within the confines of the glovebox. After subsampling was complete, the filled methylene chloride and moisture content vials were packed with ice in coolers for transportation back to the UMASS Environmental Engineering Lab, where they were stored at 4°C in sample refrigerators until the laboratory extraction and analysis steps. The sample jars were also brought back to UMASS and stored in a well ventilated area for future soil grain size analysis.

Since the sampling jars contain approximately 15 cm of soil core, the separate phase and moisture content profiles possess a data point every 15 cm of depth. Therefore, the four steps involved in this field sampling protocol produce a relatively precise representation of the subsurface in a short sampling period.

### 3.2.4 Separate Phase Petroleum Extraction

The extraction process commenced once the field samples are transported to the laboratory. First, the subsampling vials were weighed in order to calculate the wet mass of the soil sample. The difference between the pre and post sampling masses provided this value. They were then horizontally shaken on a modified shaker table (Eberbach Corporation; Ann Arbor, MI) for 20 minutes. This step allowed the solvent to penetrate into the pores of the soil, causing continuous separate phase and any trapped petroleum ganglia to dissolve into it. Effective agitation allowed the small 3 mL volume of solvent to extract the contamination efficiently.

After shaking, the vials were each centrifuged at 3000 rpm for 1 minute in a International

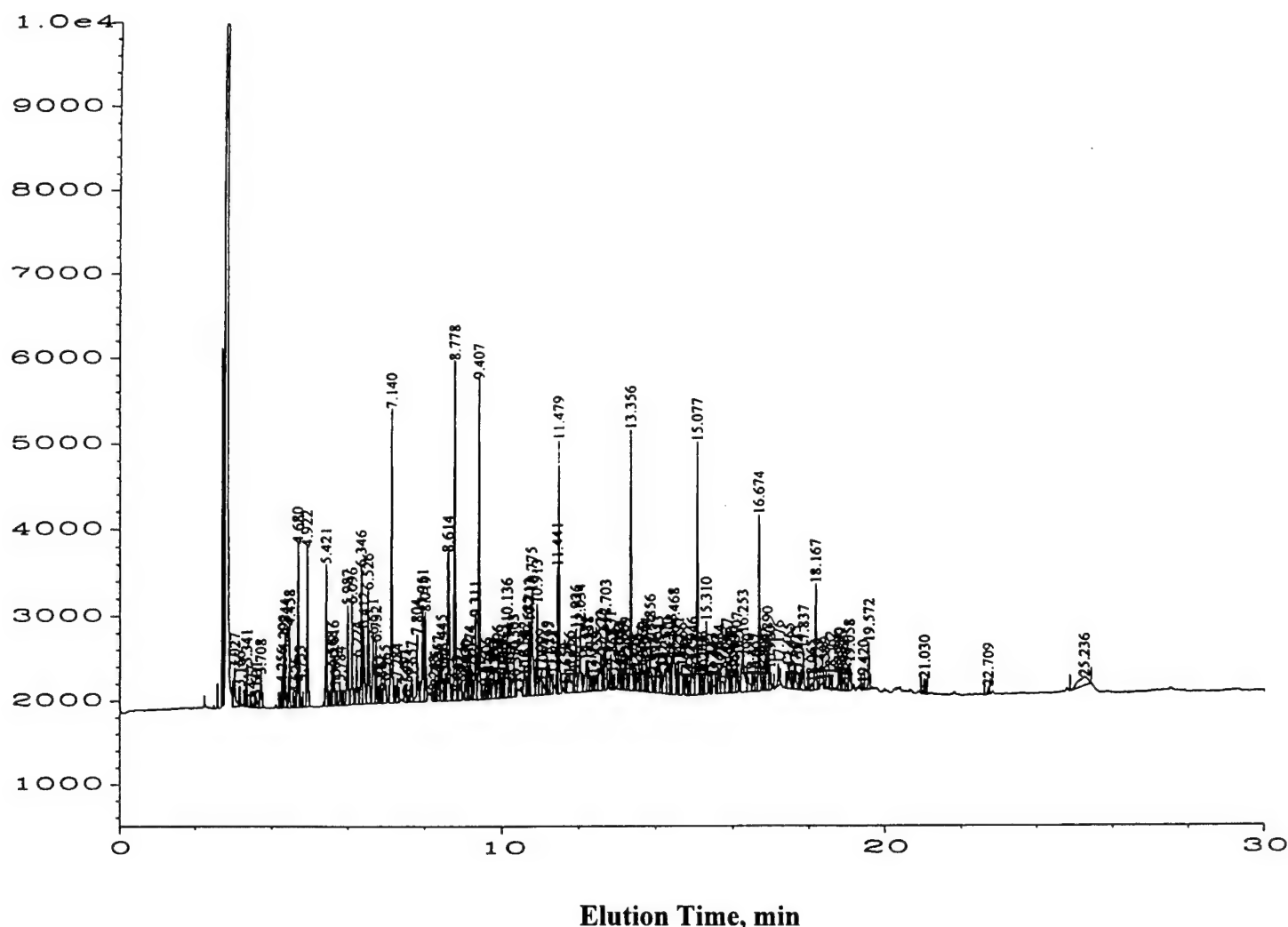
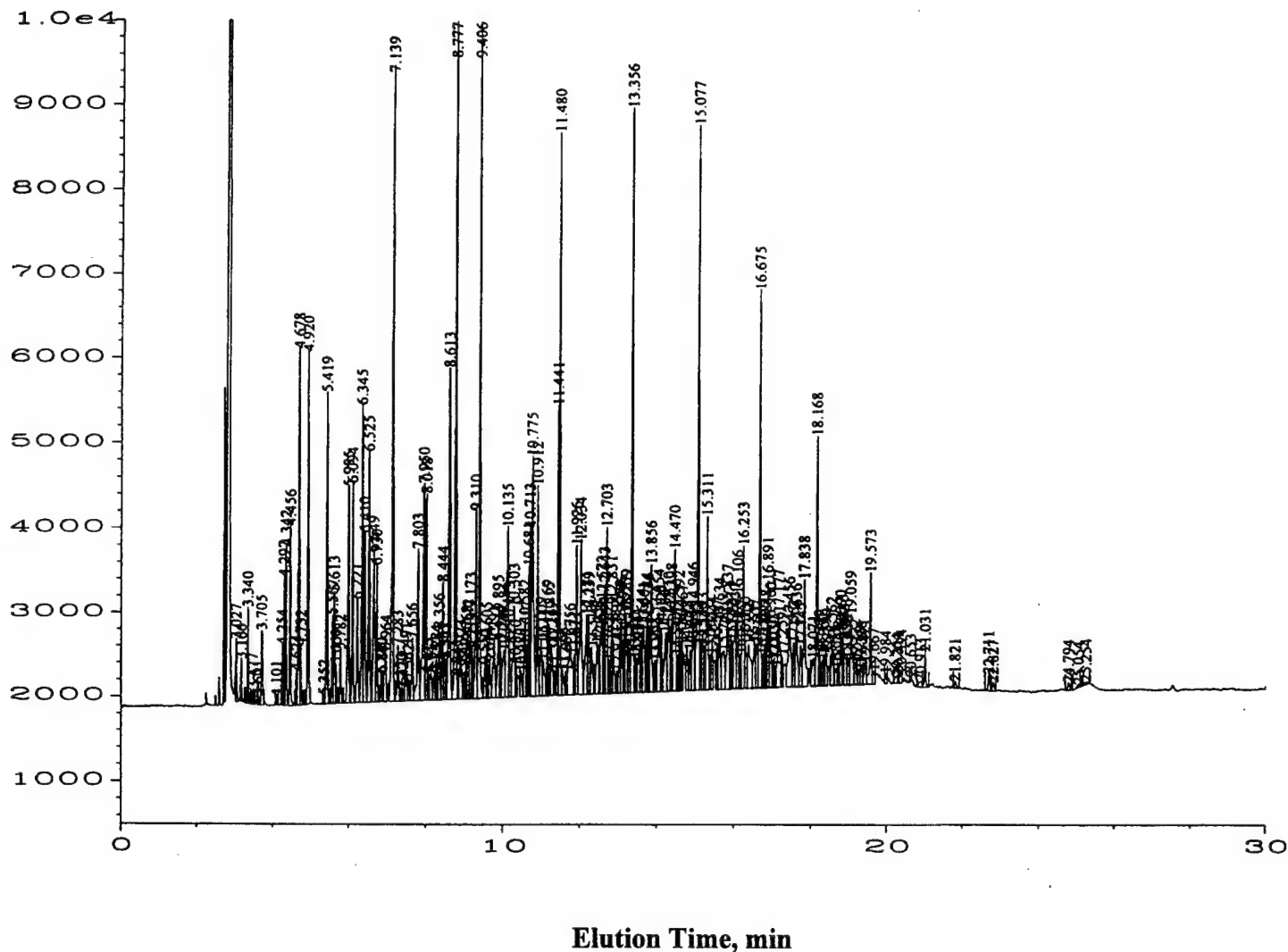


**Figure 3.7 Typical FID Chromatogram for LNAPL Standard**

Equipment Corporation CI2 centrifuge (International Equipment Corporation; Boston, MA). This process separated the soil, water and methylene chloride with dissolved hydrocarbons into three different density layers. In some cases where silty soil layers were encountered, the vials need to be manually tapped so that the isolated bubbles of solvent coalesced into one large lens. A degree of skill was necessary on the part of the analyst when extracting from fine grained soils. Once the solvent with dissolved hydrocarbons was separated from the other media found in the vial, a 3 cc syringe with a 5.1 cm, 21 gauge, bevel tipped needle (Becton Dickinson Corporation; Franklin Lakes, NJ) punctured the vial's septa. After probing for the solvent lens with the needle, the material was withdrawn from the vial using the syringe. Typically, a 1 to 3 mL sample was obtained during this step.

Any remaining water was extracted from the sample by passing it through a glass pipette (Fisher Scientific; Pittsburgh, PA), filled with 10-60 mesh, anhydrous sodium sulfate ( $\text{Na}_2\text{SO}_4$ ) (Fisher Scientific; Pittsburgh, PA), and glass wool (Supelco; Bellefonte, PA) caps. The water in



### 3.2.5 Gas Chromatographic Analysis of Solid Core Extracts

We used an HP 5890 Series II gas chromatograph for nearly all of the separate phase petroleum content determinations (Hewlett Packard; Wilmington, DE). It possesses an HP automatic liquid sampling system consisting of a controller, an injector module and a tray module, with data acquisition by an HP Series II Chemstation software package. All hardware settings and data manipulation activities are also controlled through this program.

The gas chromatograph is outfitted with a flame ionization detector (FID) connected to an HP-5 capillary column (Hewlett Packard; Wilmington, DE). The column has a length of 30 meters, an inner diameter of 0.32 mm, and a 0.25  $\mu\text{m}$  thick, methyl silicone stationary phase with 5% phenol. Zero grade nitrogen (Merriam-Graves; Springfield, MA) is used as a carrier gas, detector makeup gas, and septum purge gas. The carrier gas flow through the column is set at 2.0 mL/min by an electronic pressure control system, while makeup gas and septum purge flows are set at 28 mL/min and 3 mL/min respectively. The nitrogen flow entering the injector is split 100 to 1 prior to entrance into the capillary column. Control of the auxiliary gas flows is monitored by two external regulators which limited the pressure of the zero grade air (Merriam-Graves; Springfield, MA) entering the machine to 37 psi (314 mL/min) and the zero grade hydrogen (Merriam-Graves; Springfield, MA) to 18 psi (36 mL/min). Finally, all of the gases are cleansed of moisture upon entering the gc by scrubbers (Hewlett Packard; Wilmington, DE) placed in-line with each stream. Oxygen is also removed from the nitrogen flow by an oxygen scrubber positioned in series with the flow's moisture scrubber. The 29.5 minute gc temperature program varied oven temperature from 35°C for the first three minutes of the run, to an increasing rate of 10°C/min for 16.5 minutes, to a final temperature of 200°C for 10 minutes. Injector and detector temperatures were set at 300°C and 325°C respectively. This program provided the best total petroleum hydrocarbon results for the types of product found at the study site. All of the hydrocarbon constituents eluted within the desired analysis time period without any build up in the column.

A two  $\mu\text{L}$  sample of refined methylene chloride ( $\text{CH}_2\text{Cl}_2$ ) and dissolved hydrocarbon was injected into the split mode injector using a 10  $\mu\text{L}$  HP autosampler syringe (Hewlett Packard; Wilmington, DE). The ability of the device to split the sample enabled sample mass to be injected into the gc without fear of column clogging or detector overload. The syringe was autocleaned after each run by rinsing it with  $\text{CH}_2\text{Cl}_2$  and discharging the rinse fluid into a waste container. This solvent wash was changed after every 24 hours of analysis to prevent contamination. A new HP predrilled injector septa (Hewlett Packard; Wilmington, DE) was installed after every 75 to 100 gc injections. The underside of the septa was protected by the 3 mL septum purge flow of nitrogen which prevented petroleum products from building up, thereby alleviating random desorption into the carrier gas stream.

All analog output from the gas chromatograph was stored as digital data in a data file set up by the Chemstation software program. This fluctuating data was then integrated in the data analysis section of the program, yielding a chromatogram with tabulated peak information. The

**TABLE 3.3 LNAPL STANDARD CONCENTRATIONS FOR SOLID CORE ANALYSES  
OCTOBER 1995 ANALYSES**

Standard ID ( $\mu$ l Sep Phase)	Concentration <sup>a</sup>	FID Area <sup>b</sup>
100	111.11	4425363
50	52.63	2149720
10	10.10	423793
5	5.03	173056
1	1.00	22827
0.5	0.50	8424

<sup>a</sup> $\mu$ L separate phase/mL methylene chloride.

<sup>b</sup>excludes the methylene chloride solvent peak.

integration abilities of the machine are quite varied and were easily manipulated to suit the needs of the research. This analysis utilized a simple integration method which did not include the area under the solvent peak into the total chromatographic area calculation. Results of the data analysis were then stored in both digital and hardcopy format. Figures 3.7 and 3.8 show typical chromatograms for an LNAPL standard and an LNAPL sample extract, respectively. The chromatograms contain numerous peaks, indicating a blend of one hundred or more petroleum hydrocarbons in the separate phase JP4 jet fuel spill.

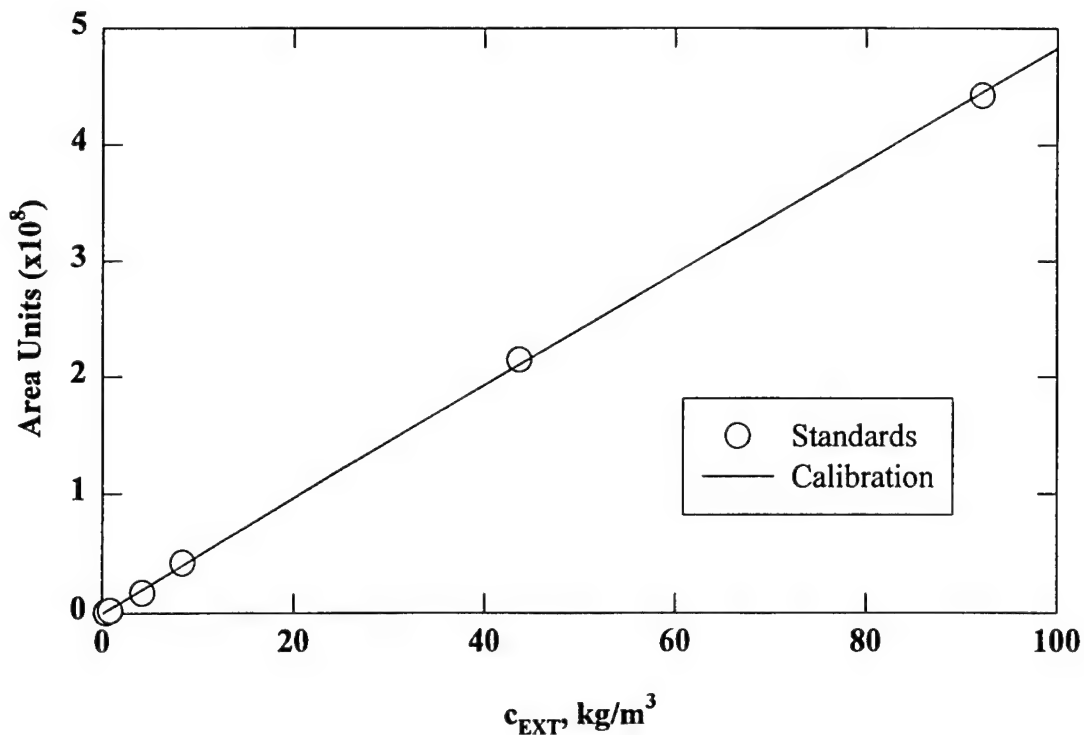
### 3.2.6 Separate Phase Petroleum Calibration Standard

We collected a separate phase sample from a separate phase recovery well RW3 on 28 June 1995 to serve as a separate phase total petroleum hydrocarbon standard for the four batches of Plattsburgh soil core samples. The well is adjacent to the UMASS study area, as shown in Figure 3.1. The sample was contained in a 20 mL EPA vial with Teflon coated silicone septa, wrapped in Parafilm and stored in an explosion proof refrigerator at 4°C in order to preserve the integrity of the standard. Six methylene chloride/LNAPL standard solutions of varying concentrations were injected into the gas chromatograph, generating a separate phase LNAPL calibration curve for each batch of samples. Table 3.3 and Figure 3.9 present the standard injections and FID responses for the October 1995 analyses. The response factor RF and intercept IN of the calibration curve convert total chromatographic area (excluding the methylene chloride solvent area) to extract concentration  $c_{EXT}$ .

$$c_{EXT} = \rho_L [RF(\text{area} \cdot \text{units}) + IN] \quad (\rho_L = 830 \text{ kg/m}^3) \quad (3.3a)$$

$$c_{EXT} = \frac{\text{kg} \cdot \text{LNAPL}}{\text{m}^3 \cdot \text{extract}} \quad (3.3b)$$

The JP4 jet fuel liquid density  $\rho_L$  cited in Equation 3a was measured by weighing a known



$$RF = 2.50 \times 10^{-8} \text{ area units}^{-1}$$

$$IN = 9.53 \times 10^{-5}$$

**Figure 3.9 Standard Calibration Curve for 1995 October LNAPL Analyses**

volume of RW3 product on a Mettler H54 analytical balance (Mettler; Hightstown, NJ). The LNAPL content  $T$  of the solid core samples is computed from the known extract concentration

$$T = \frac{\text{mass} \cdot \text{LNAPL}}{\text{mass} \cdot \text{dry} \cdot \text{soil}} \quad (3.4a)$$

$$T = \frac{c_{EXT} V_{EXT}}{M_{DRY}} \quad (V_{EXT} = 3\text{mL}) \quad (3.4b)$$

with measured dry soil mass  $M_{DRY}$  and methylene chloride extract volume  $V_{EXT}$ .

### 3.2.7 Method Detection Limit and Field Spikes

The method detection limit (MDL) was determined for LNAPL analyses, with the results summarized in Figure 3.10. Seven low strength injections of 0.03% separate phase standard



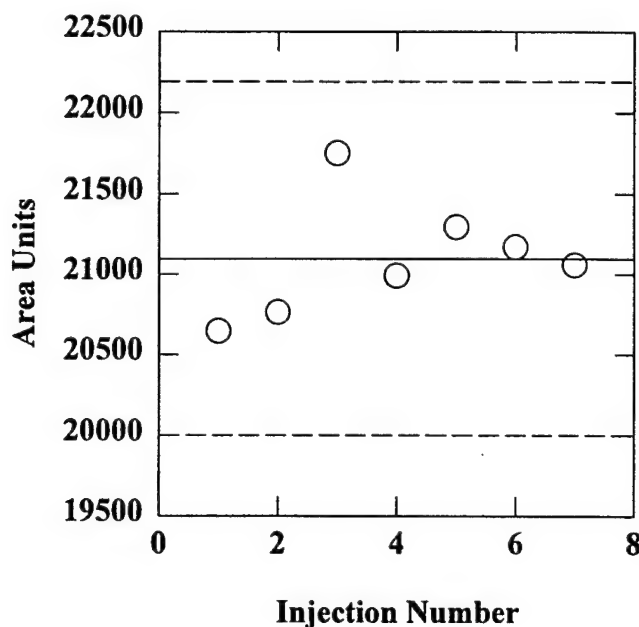


**Figure 3.10 Method Detection Limit Study for LNAPL Analyses**

were injected successively into the gas chromatograph, and the MDL was computed in accordance with [Taylor (1987)]

$$\delta_{MDL} = \frac{1}{N} \sum_N \text{area} \cdot \text{units} \quad (N \text{ samples}) \quad (3.5a)$$

$$\sigma_{MDL} = \sqrt{\frac{1}{N} \sum_N \text{area} \cdot \text{units}^2 - \delta_{MDL}^2} \quad (3.5b)$$

We measured a sample mean of 21,096 and a standard deviation about the mean of 365 area units. The latter corresponds to a method detection limit MDL of

$$MDL = 3\sigma_{MDL} \quad (3.6a)$$

$$MDL = 1095 \text{area} \cdot \text{units} \quad (3.6b)$$

$$T_{MDL} = 1 \frac{\text{mg}}{\text{kg}} \quad (3.6c)$$

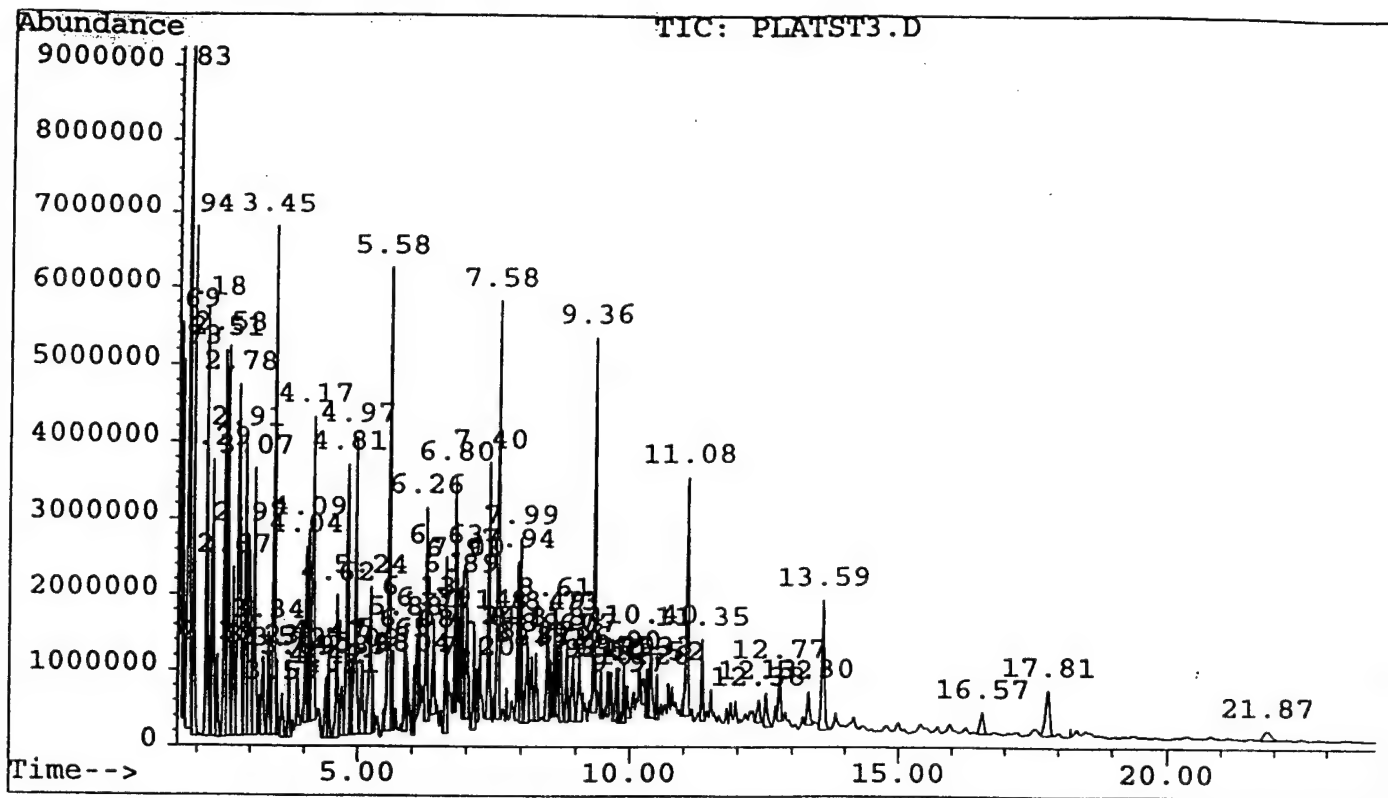
The separate phase method detection limit  $T_{MDL}$  cited in Equation 3.6c is based on a representative dry soil mass of 0.02 kg. It is four orders of magnitude smaller than the maximum observed LNAPL concentration, so that the gc/FID methodology is quite accurate.

**TABLE 3.4 LNAPL FIELD SPIKE RECOVERIES**

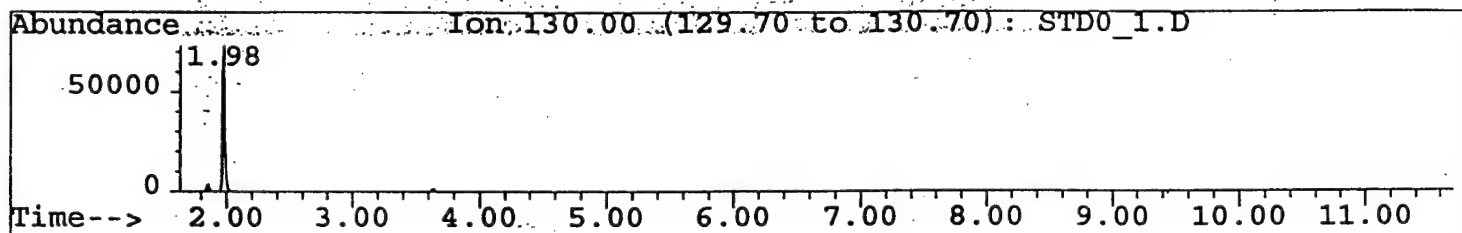
<b>Dates</b>	<b>Spike Volume, <math>\mu</math>L</b>	<b>Recovery, %</b>	<b>Dates</b>	<b>Spike Volume, <math>\mu</math>L</b>	<b>Recovery, %</b>
<b>9-13Oct95</b>	50	105	<b>5-7Jun96</b>	50	73
	100	117		100	105
	150	107		200	111
	200	100		50	104
	50	114		100	106
	100	98		200	114
	150	109			
	200	99			
<b>30Nov-Dec95</b>	50	109	<b>20-22Aug96</b>	100	113
	100	84		60	106
	150	93		50	102
	200	92		30	101
	50	108		20	94
	100	112		10	84
	150	109		5	65

We also ran replicate injections of the same extract as part of the quality assurance program associated with LNAPL profiling. Replicate injection precision, defined by Eq. 3.2, is 6% for the October 1995 samples and 4% for the December 1995 samples: the gas chromatograph is very precise. Figure 3.3b lists sample results for 37 replicates, consisting of LNAPL determinations in soil subsamples withdrawn by syringe barrel from the same (quart sized) Mason jar. A precision of 39% is exhibited by these replicates, reflecting the scatter inherent in field sampling from a 15 cm interval of the borehole. Much of the scatter is attributable to a few anomalous replicates. The outlier at the bottom of Figure 3.3 exhibits a P of 200% for example, and the average precision would be 34% without it. We note that the method would likely be more precise (smaller P) for smaller Mason jars and larger subsample masses, but the logistics of LNAPL profiling of many boreholes precluded this.

Field spiking is a QA/QC technique that monitors the extraction protocol and sample transportation/storage conditions. We spiked blank field samples of known mass and moisture content with 20  $\mu$ L of methylene chloride standard solutions of 0.04% strength in the field during drilling operations. After injection, the spike was stored, transported, extracted, and analyzed in identical fashion to the other field samples. The spike recovery is the ratio of the observed T to the original T. Table 3.4 summarizes the average separate phase petroleum spike recovery for the four trips. The recoveries for the four ranged from 65 to 114% in magnitude with an average value of 101% and a standard deviation of 12%. The high recovery and low standard of deviation indicates that the extraction and storage protocol for the samples was very effective. It also infers that the LNAPL, as well as, the soil types from each site, were well suited for the solvent extraction process implemented in this project.



**Ion Chromatograph for Separate Phase Extract**



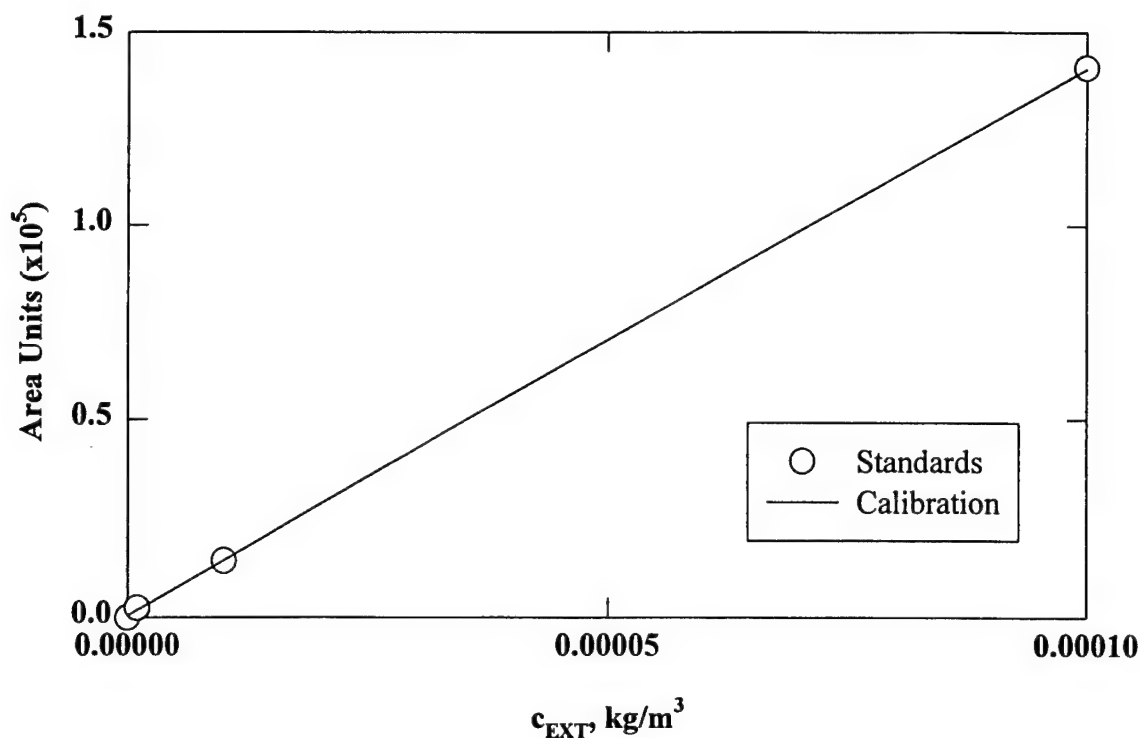
**Scan for Trichloroethylene (Mass/Charge Ratio 129.70 to 130.70, 1.98 min Retention Time)**

**Figure 3.11 Typical GCD Chromatogram of JP4 Jet Fuel Extract**

### 3.3 GCD Analyses and TCE Content

#### 3.3.1 GCD Protocol for TCE Analyses

We measured the separate phase trichloroethylene content  $T_{TCE}$  in methylene chloride extracts from 6 of the solid core boreholes discussed in Section 3.2. We withdrew 2.0  $\mu$ l of extract from the target vials with a 10  $\mu$ l Hamilton Gastight syringe (RN 1701) equipped with a Chaney adaptor and a 26 gage stainless steel needle with beveled tip. The extract was injected into a Hewlett Packard G1800A Gas Chromatograph with mass spectrometer detector (GCD).



$RF = 7.14 \times 10^{-10} \text{ kg/m}^3\text{-area unit}$   
 $IN = 3.58 \times 10^{-7} \text{ kg/m}^3$

**Figure 3.12 GCD Calibration Curve for TCE**

The split/splitless injector temperature was 250°C and a split ratio of 20 to 1 was used, with 1 ml/min zero grade helium used as a carrier gas. The sample was carried into an oven held at 40°C for 4 min, then ramped at 10°C/min to 150°C. The oven was equipped with a 0.32 mm ID, DB5 capillary column 30 m long, featuring a 0.25  $\mu\text{m}$  thick film with crosslinked 5% phenylmethylsiloxane. The mass spectrometer detector was heated to 280°C and scanned over a mass to charge ratio range of 10 to 425. Figure 3.11 displays a typical separate phase extract GCD chromatogram. Appendix VI lists a typical GCD chromatogram for a separate phase extract.

Trichloroethylene was identified by a comparison of observed ionization spectra with Hewlett Packard library spectra, then confirmed by analysis of standard injections of the chlorinated organic. The TCE coelutes with heptane, so that a scan through a mass charge ratio of 130 is used to isolate the compound. A set of separate phase TCE standards was injected into the instrument to develop a calibration curve and response factor similar to Equations 3.3. Figure 3.12 displays a typical calibration curve. The resulting equation for the extract TCE concentration  $c_{TCE}$  is

$$c_{TCE} = RF(\text{area} \cdot \text{units}) - IN \quad (3.7)$$

### 3.3.2 GCD Analysis of Total Hydrocarbons

We also used the GCD to identify major constituents of the separate phase JP4 jet fuel. We analyzed free product sampled from recovery well RW3 (Figure 3.1b) by Base engineers on 28 June 1995. Table 3.5 lists 84 compounds identified by library search. The primary separate phase petroleum constituents identified by the GCD are branched alkanes:

- (4.99% by area) 2,2 dimethylhexane
- (4.01% by area) octane
- (4.01% by area) nonane
- (3.79% by area) 2 methylheptane
- (2.91% by area) methylcyclohexane
- (2.87% by area) decane
- (2.57% by area) 2 methyloctane
- (2.57% by area) 1,1,3 trimethylcyclohexane

Aromatic compounds comprise 12.9% of the total separate phase hydrocarbons, distinguished by the following primary constituents:

- (1.67% by area) 1 ethyl 3 methylbenzene
- (1.67% by area) 1,3,5 trimethylbenzene
- (1.16% by area) propylbenzene
- (1.14% by area) 1,2,4 trimethylbenzene

Nineteen compound identities were confirmed by analyzing a GCD standard. This standard consists of a group of alkanes and aromatics distributed over a range of retention times

- (1.69 min) 2,3 dimethylpentane
- (1.94 min) trichloroethylene
- (1.94 min) heptane
- (2.78 min) 2 methylheptane
- (3.45 min) octane
- (3.59 min) tetrachloroethylene
- (4.17 min) 1,1,3 trimethylcyclohexane
- (4.71 min) ethylbenzene
- (4.81 min) 2 methyloctane
- (5.58 min) nonane
- (6.26 min) 3,6 dimethyloctane
- (6.93 min) 1,2,3 trimethylbenzene
- (7.40 min) 1,3,5 trimethylbenzene
- (7.58 min) decane
- (8.73 min) 2 methyldecane
- (9.36 min) undecane

**TABLE 3.5 GCD IDENTIFICATION OF COMPOUNDS IN SEPARATE PHASE**

Retention Time, min	Area %	SAMPLE Compound	Match, %	Confirmed
1.69	1.83	2,3-Dimethylpentane	87	Yes
1.73	1.72	3-Methylhexane	87	
1.83	4.99	2,2-Dimethylhexane	78	
1.94	3.14 <sup>a</sup>	Trichloroethylene	Ion scan	Yes
1.94	3.14 <sup>a</sup>	Heptane	93	Yes
2.18	2.91	Methylcyclohexane	96	Yes
2.29	2.07	3,4-Dimethylhexane	78	
2.39	0.52	1,2,4-Trimethylcyclopentane	78	
2.51	3	2,3,4-Trimethylpentane	90	
2.58	2.79	2,3,3-Trimethylpentane	90	
2.67	1.41	2,3-Dimethylhexane	78	
2.78	3.79	2-Methylheptane	95	
2.91	2.39	3-Methylheptane	95	
2.97	1.91	cis-1,3-Dimethylcyclohexane	95	
3.23	0.73	cis-1-Ethyl-2-methylcyclopentane	93	
3.34	0.76	1,3-Dimethyl-transcyclohexane	94	
3.45	4.1	Octane	90	
3.5	0.43	1,3-Dimethyl-cis-cyclohexane	95	
3.59	0.37	Tetrachloroethylene	99	
3.72	0.53	2,3,5-Trimethylhexane	90	
3.89	0.38	2,4-Dimethylheptane	91	Yes
4.04	1.48	2,6-Dimethylheptane	94	
4.09	1.23	Ethylcyclohexane	90	
4.17	2.57	1,1,3-Trimethylcyclohexane	50	
4.42	0.59	1-Nonene	43	
4.47	0.58	1,3,5-Trimethylcyclohexane	91	
4.62	1.15	2,3-Dimethylheptane	86	
4.71	0.47	Ethylbenzene	91	
4.81	2.57	2-Methyloctane	91	
4.89	0.43	p-Xylene	97	
4.97	2.46	3-Methyloctane	87	Yes
5.24	1.68	1-Ethyl-3-methylcyclohexane	81	
5.28	0.33	1-Ethyl-4-methyltranscyclohexane	83	
5.58	4.01	Nonane	87	
5.65	0.41	1-Bromo-3-methylcyclohexane	64	
5.88	0.83	Bicyclo[3.3.1]nonane	76	
6.04	0.45	1-Methylethylbenzene	93	
6.08	0.47	2-Ethyl-1-decanol	59	
6.13	0.55	1-Methylethylcyclohexane	91	
6.26	1.43	3,6-Dimethyloctane	90	
6.39	0.78	3-Ethyl-2-methylheptane	72	

**TABLE 3.5 (Continued) GCD IDENTIFICATION OF COMPOUNDS IN  
SEPARATE PHASE SAMPLE**

Retention Time, min	Area %	Compound	Match, %	Confirmed
6.63	1.16	Propylbenzene	83	
6.8	1.67	1-Ethyl-3-methylbenzene	93	
6.89	0.56	2-Methylnonane	91	
6.93	0.82	1,2,3-Trimethylbenzene	95	Yes
7	0.96	3-Methylnonane	70	
7.14	0.67	1-Ethyl-2-methylbenzene	94	
7.2	0.31	1-Methyl-3-propylcyclohexane	72	
7.24	0.32	1-Methyl-4-(1-methylethyl)-cyclohexane	45	
7.4	1.67	1,3,5-Trimethylbenzene	94	Yes
7.58	2.87	Decane	97	Yes
7.94	1.14	1,2,4-Trimethylbenzene	94	
7.99	1.21	4-Methyldecane	94	
8.11	0.73	Butylcyclohexane	93	
8.19	0.69	3-Methyldecane	70	
8.27	0.53	3-Methyldecane	87	
8.49	0.85	1-Methyl-3-propylbenzene	90	
8.53	0.46	1-Methyl-2-propylbenzene	92	
8.61	0.52	5-Methyldecane	70	
8.67	0.41	4-Methyldecane	97	
8.73	0.75	2-Methyldecane	93	Yes
8.84	0.47	3-Methyldecane	97	
8.96	0.62	4-Ethyl-1,2-dimethylbenzene	91	
9.07	0.75	1,2,3,4-Tetramethylbenzene	83	
9.36	2.39	Undecane	96	Yes
9.47	0.28	Decahydro-2-methylnaphthalene	90	
9.6	0.34	1-Methyl-4-(1-methylethyl)-benzene	91	
9.75	0.36	Decahydro-2-methylnaphthalene	90	
9.79	0.31	3,8-Dimethylundecane	83	
9.9	0.34	n-Amylcyclohexane	90	
9.97	0.25	Pentylcyclopentane	38	
10.26	0.26	3,6-Dimethyldecane	52	
10.33	0.29	4-Methylundecane	58	
10.4	0.6	2-Methylundecane	95	
10.52	0.28	3-Methylundecane	78	
11.08	1.91	Dodecane	95	Yes
11.35	0.62	2,6-Dimethylundecane	96	
12.38	0.28	4-Methyldodecane	95	
12.52	0.41	2-Methyldodecane	72	
12.77	0.42	4,6-Dimethyldodecane	83	
13.3	0.37	2-Methylnaphthalene	94	



**TABLE 3.5 (Continued) GCD IDENTIFICATION OF COMPOUNDS IN SEPARATE PHASE SAMPLE**

Retention Time, min	Area %	Compound	Match, %	Confirmed
13.59	1.55	Tridecane	97	Yes
16.57	0.35	2,6,11-Trimethyldodecane	86	
17.81	0.86	Tetradecane	91	Yes

<sup>a</sup>Heptane and trichloroethylene coelute, TCE content is by ion scan.

These 19 compounds (plus toluene) were combined into a methylene chloride solution, with an individual constituent concentration of 10 mg/L. Once prepared, the pure standard was serially diluted to produce 0.1, 0.01, and 0.001 mg/L liquid standards.

### 3.4 Soil Gas Sampling

#### 3.4.1 Overview of Soil Gas Sampling Technology

Soil gas sampling has proven to be a useful means of delineating the areal extent of gasoline [Deyo et al. (1993)], diesel fuel [Downey et al. (1991)], heating oil [Folkes et al. (1987)], and other light petroleum distillate spills beneath the ground surface. These immiscible hydrocarbons are lighter than water and so spread out over the water table. Evaporation is a preferential transport mechanism because the contaminants are volatile, giving rise to elevated concentrations of hydrocarbon vapors in the soil gas above the separate phase hydrocarbons. Thus, soil gas surveys may be used to delineate the separate phase source of petroleum contamination.

Soil gas sampling works best in dry, coarse grained soils with low organic carbon content [Marrin et al. (1988)]. Infiltrating water, perched water tables, low permeability lenses, barometric pressure fluctuations, lower soil temperatures, and biodegradation can all significantly reduce hydrocarbon vapor concentrations with increasing distance from the separate phase source. The infiltrating water, barometric pressure, and soil temperature effects are transient and can introduce seasonal or diurnal variations in gaseous contamination [Deyo et al. (1993), Van Vliet et al. (1993)], so that frequent sampling from a permanent soil gas monitoring point is needed for a quantitative measure of contamination. Aerobic biodegradation of hydrocarbon vapors consumes oxygen [Ostendorf and Kampbell (1991)] and generates carbon dioxide [Kerfoot et al. (1988)], while anaerobic degradation creates methane gas [Marrin (1991)]. The correlation of these constituents with an inert tracer gas is often used to assess the biodegradation potential of petroleum spills in the subsurface environment [Miller et al. (1991), Kittel et al. (1993)].

A suite of increasingly sophisticated technologies is available for the sampling and analysis of soil gas. Probes as simple as a 1.3 cm diameter stainless steel tube tipped with a loose carriage bolt [Kampbell et al. (1990)] or a drive point [Deyo et al. (1993)] have been deployed successfully in the field, as have more elaborate 2.0 cm diameter stainless steel systems

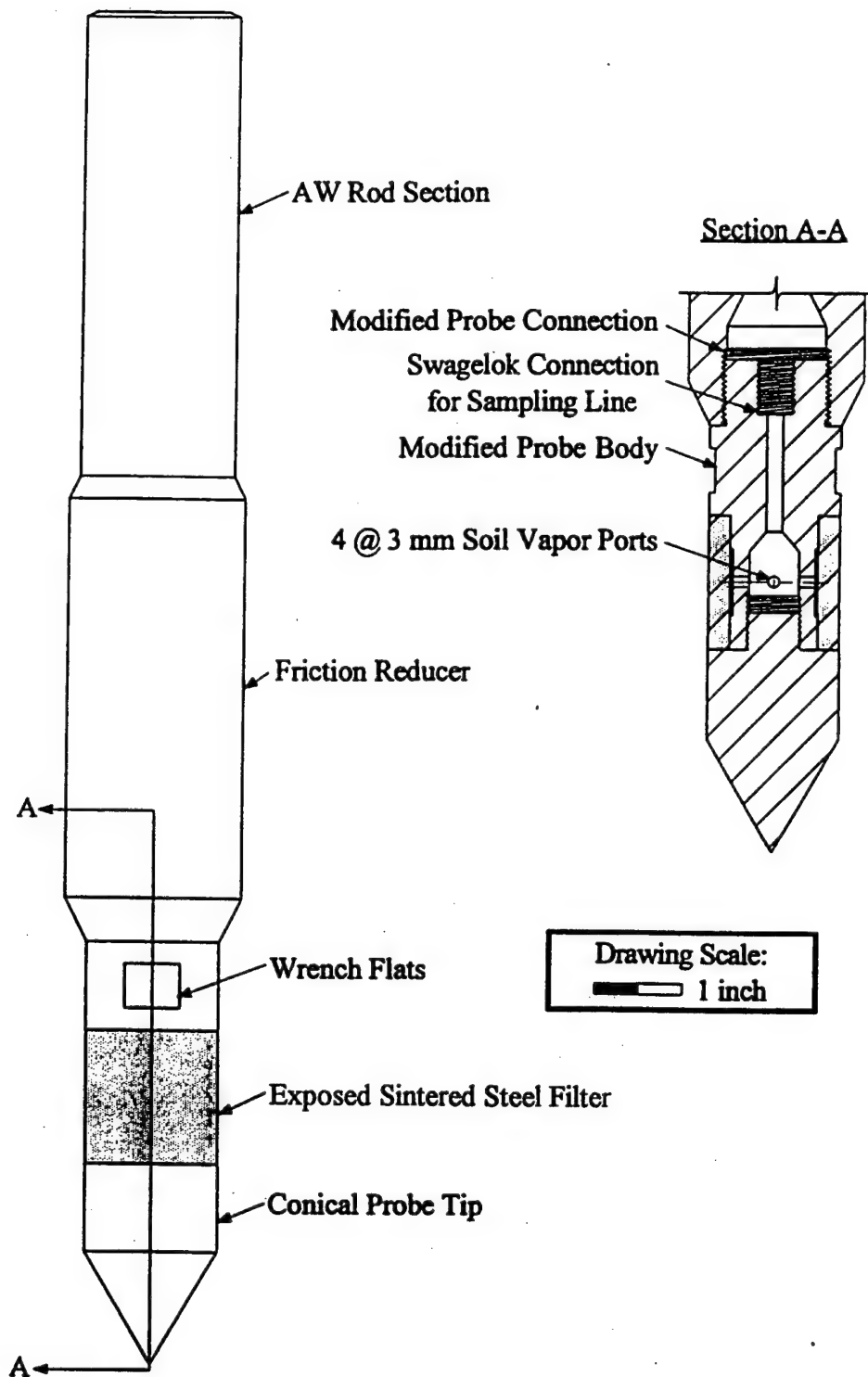


**Figure 3.13 Stainless Steel Vapor Sampling Probe**

with side ports [Kerfoot (1987)], or retractable shields [Christy and Spradlin (1992)]. The driving force may be a manual or handheld electric hammer [Kampbell et al. (1990), Kerfoot (1987)], truck mounted piston [Tillman and Leonard (1993)], or a drill rig mounted hammer [Ostendorf et al. (1995c)], depending on the type of soil and sampling depth. Shields or filter elements may be required for finer grained soils to prevent clogging of ports. Soil gas is pulled from the probes through stainless steel or flexible tubing to the ground surface by manual

[Kerfoot (1987)] or electric vacuum sampling pumps, where it can be trapped for subsequent laboratory analysis [Moyer et al. (1994)], subsampled by syringes [Kerfoot (1987)], or directly fed into field meters [Kampbell et al. (1990)]. In the latter regard, organic vapor analyzers with built in vacuum pumps and catalytic combustion chambers are used to measure total hydrocarbon vapor pressures, while potentiometric cells and infrared absorption sensors also see widespread use for the detection of oxygen and carbon dioxide content, respectively. Tedlar bag dilution may be needed for field meter readings of highly contaminated soil gas [Robbins et al. (1990)]. Petroleum distillates are blends of many hydrocarbon compounds with varying saturated vapor pressures, solubilities, and biodegradation potentials [Potter (1989)], and a catalytic combustion chamber does not differentiate constituents. Soil gas is consequently analyzed by direct injection or trap desorption into portable or mobile gas chromatographs to elucidate its hydrocarbon composition.

### 3.4.2 Vapor Probes

We used soil vapor probes to map the vertical distribution of soil gas constituents in the following boreholes:

- VP1-11 October 1995, 0.6 to 11.6 m depth, hydrocarbons, oxygen, and carbon dioxide
- VP2-11 October 1995, 0.61 to 7.9 m depth, oxygen
- VP3-13 October 1995, 0.3 to 6.1 m depth, hydrocarbons, oxygen, and carbon dioxide
- 12BC-21 August 1996, 10.1 to 11.3 m depth, hydrocarbons, oxygen, CO<sub>2</sub>, and TCE
- 12BE-21 August 1996, 9.5 to 11.4 m depth, hydrocarbons, oxygen, CO<sub>2</sub>, and TCE
- 12BH-21 August 1996, 9.3 to 11.0 m depth, hydrocarbons, oxygen, CO<sub>2</sub>, and TCE
- 12BJ-21 August 1996, 9.3 to 11.0 m depth, hydrocarbons, oxygen, CO<sub>2</sub>, and TCE
- 12BK-22 August 1996, 9.3 to 11.1 m depth, hydrocarbons, oxygen, CO<sub>2</sub>, and TCE
- 12BM-22 August 1996, 9.3 to 11.1 m depth, hydrocarbons, oxygen, CO<sub>2</sub>, and TCE
- 12BN-22 August 1996, 9.3 to 11.0 m depth, hydrocarbons, oxygen, CO<sub>2</sub>, and TCE

Table 3.1 and Figure 3.1 locate the vapor probe boreholes.

Two different probes were designed, fabricated, and deployed by UMASS personnel on field trips in October 1995 and August 1996. Nearly all of the data were obtained with a 3.81 cm diameter stainless steel vapor sampling probe sketched in Figure 3.13, and used at other hydrocarbon spill sites [Ostendorf et al. (1995a)]. The probe is equipped with a 5.1 cm friction reducer and a sintered 40  $\mu$ m stainless steel filter element, flush mounted and exposed to the soil. The probe is driven through hollow stem augers into undisturbed soil by a 140 pound SPT rig mounted safety hammer with a 0.76 m drop height. The probe admits soil gas through four 3.18 mm diameter ports to a plenum connected to 1.6 mm ID nalgene tubing routed to the surface through the annulus of AW drill rods. The thin tubing minimizes purging requirements, and was coupled to the surface sampling system with stainless steel 6.4 mm Swagelok fittings. A generator (Honda EX1000) powered, Cole Parmer Model 7530-40 single head diaphragm vacuum pump equipped with a water trap, vacuum gauge, and Cole Parmer 0-5 L adjustable flow meter pulled gas to the ground surface at a rate of 2 L/min. We purged one L of soil gas from the

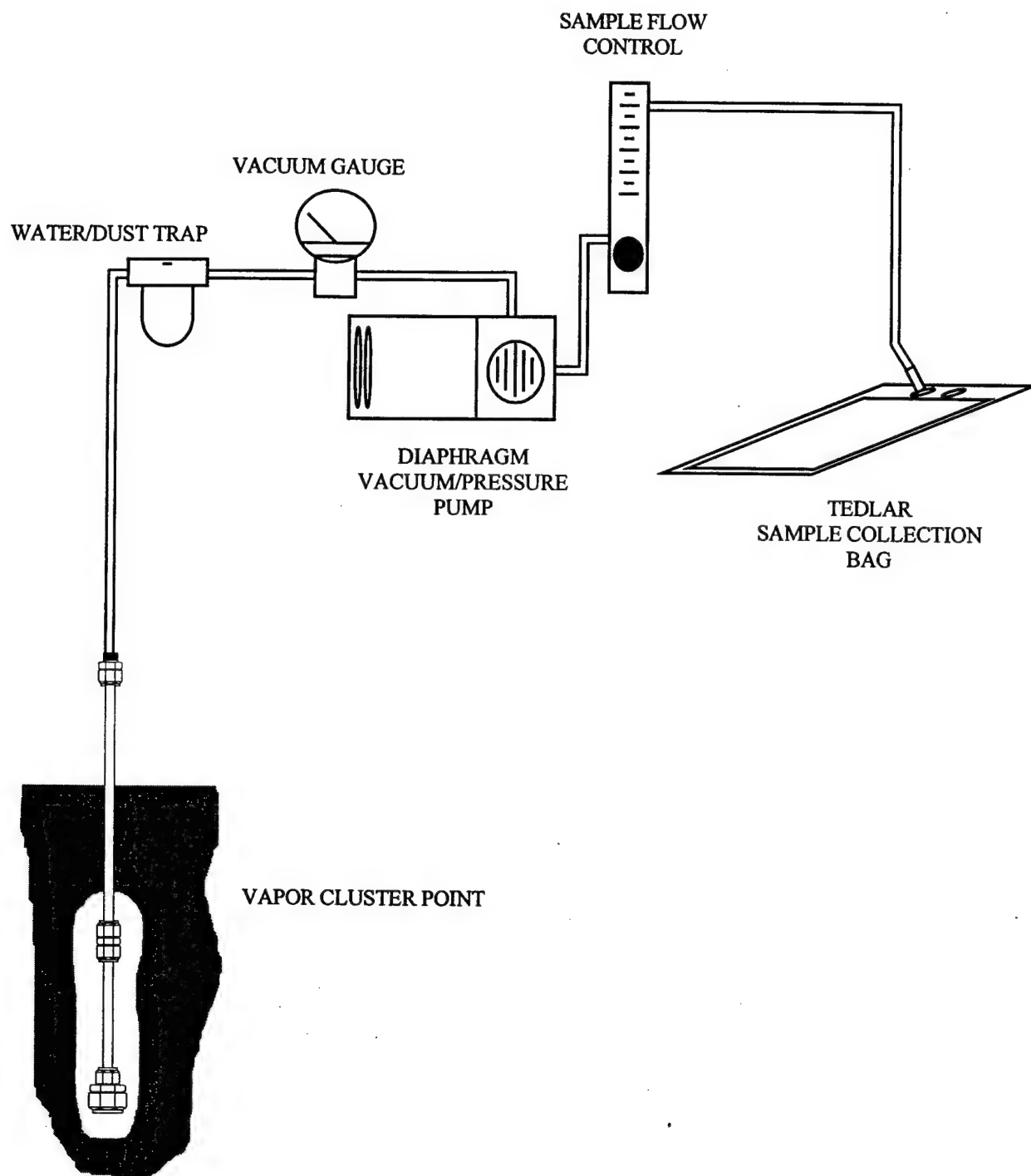


**Figure 3.14 Soil Gas Sampling System**

system before filling 2 L of sample into evacuated, nitrogen rinsed, 3 L Tedlar bags (SKC Company, Eight Four, PA). Figure 3.14 displays the soil gas sampling equipment, which is used for vapor probes and stainless steel tubing clusters.

Borehole VP2 was sampled with a GC Industries (Freeport, CA) model GC 33-200 potentiometric oxygen sensor mounted in the plenum of the stainless steel vapor probe sketched

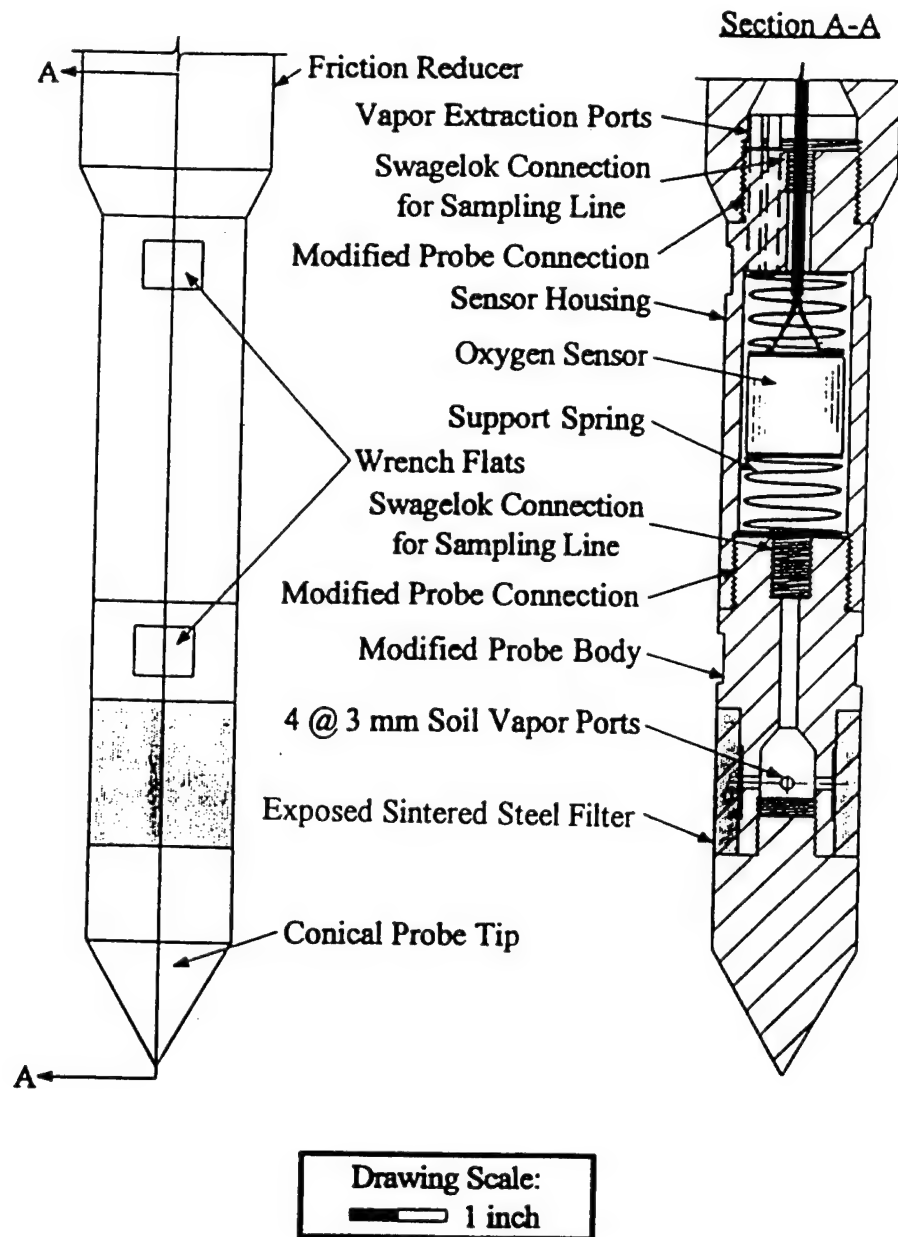


**Figure 3.15 Downhole Soil Gas Oxygen Sensor in Stainless Steel Probe**

in Figure 3.15. The sensor housing is isolated from hammer shocks by support springs, and sends a signal up a lead through the AW rod annulus. The lead is tied to nalgene tubing, which is itself connected to the vacuum pump used to draw soil gas into the plenum for downhole sensing. Since the analysis is downhole, no purging is needed. Figure 3.16 compares the downhole sensed oxygen in borehole VP2 with soil gas oxygen observed in Tedlar bag samples from borehole VP1 using a Bacharach model 302 oxygen meter. The data agree, with an average precision of 8% (as defined by Equation 3.2).

### 3.4.3 Stainless Steel Tubing Clusters and Near Surface Arrays

Soil gas constituents were also measured using a series of stainless steel tubing clusters placed in 26 boreholes throughout the study area. Table 3.1 and Figure 3.1 locate the clusters,

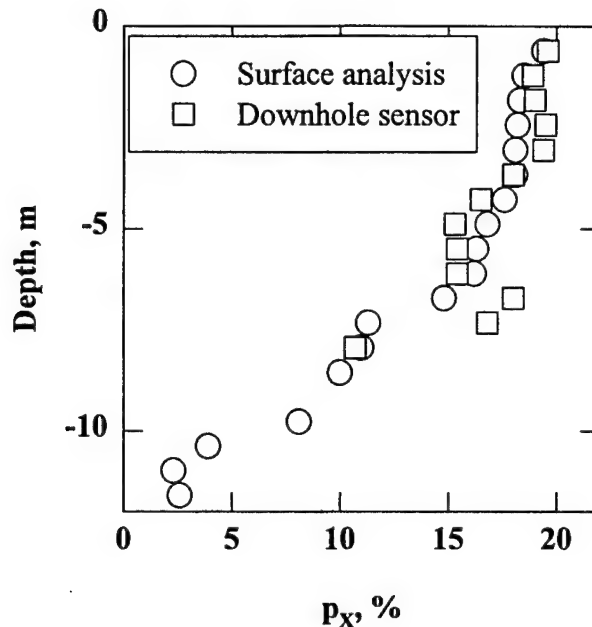


**Figure 3.16 Downhole Sensed (Squares, VP2) and Surface Sensed (Circles, VP1) Soil Gas Oxygen Partial Pressure  $p_X$**

while Appendix II details their construction. The stainless steel soil gas points were installed at depths ranging from 0.9 to 11 meters below grade. Each soil gas point consisted of an inlet section, a riser, and a sampling connection, as shown in Figure 3.17. The inlet section, where soil gas enters the point, consisted of a Swagelok 1/4" to 1/2" union (Swagelok, Salon, OH) with a 1/2" diameter x 1/16" thick sintered stainless steel disk with 100 micron pores (Mott Metallurgical, Farmington, CT) installed in the 1/2" end of the union. The disk was secured by the 1/2" nut supplied with the union. The riser section consisted of the appropriate length of 1/4" OD x 3/16" ID stainless steel tubing attached to the 1/4" end of the union. Swagelok unions (1/4" x 1/4") were used in conjunction with the 1/4" OD stainless steel riser to install points at depths of over six feet. To form a sampling connection, 1/4" to 1/4" unions were used with one end attached to the riser and a Swagelok 1/4" female cap used to seal the top of the point when not in use. Single or multiple cluster points installed at the same location were completed by housing the surface sampling connections in 0.2 m diameter steel and cast iron road boxes (Boart-Longyear, Stone Mountain, GA) with removeable watertight caps fastened with three hexagonal bolts and set into a concrete pad.

We installed the soil gas cluster points by augering to the lowest sampling depth with 0.17 m OD hollow stem augers driven by a CME-75 drill rig. After reaching the appropriate depth, with the augers left in place, a 0.15 m sandpack layer (Morie Gravel) was placed and a cluster point was lowered down the hole. An additional 0.15 m of sand was then placed, followed by a 0.6 m thick bentonite pellet seal (Bentoseal). After all cluster points for a given hole were installed, the remainder of each hole was filled with a bentonite grout (Bentoseal). A tremie pipe was used to facilitate installation of the grout mix. Augers were periodically

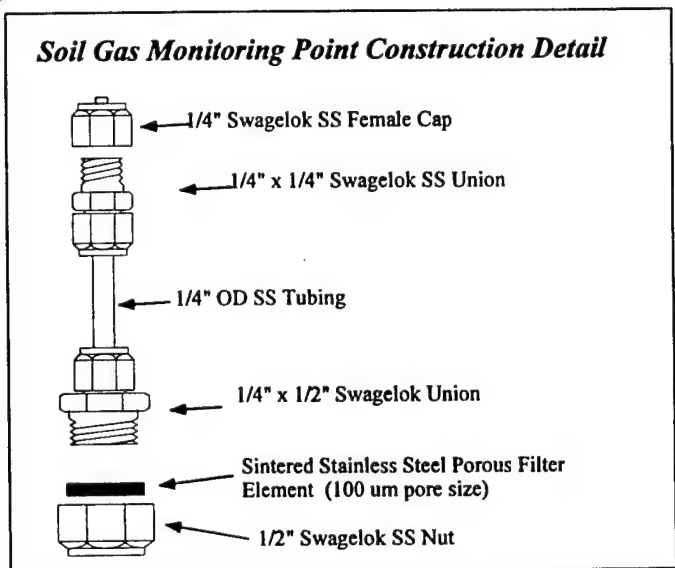
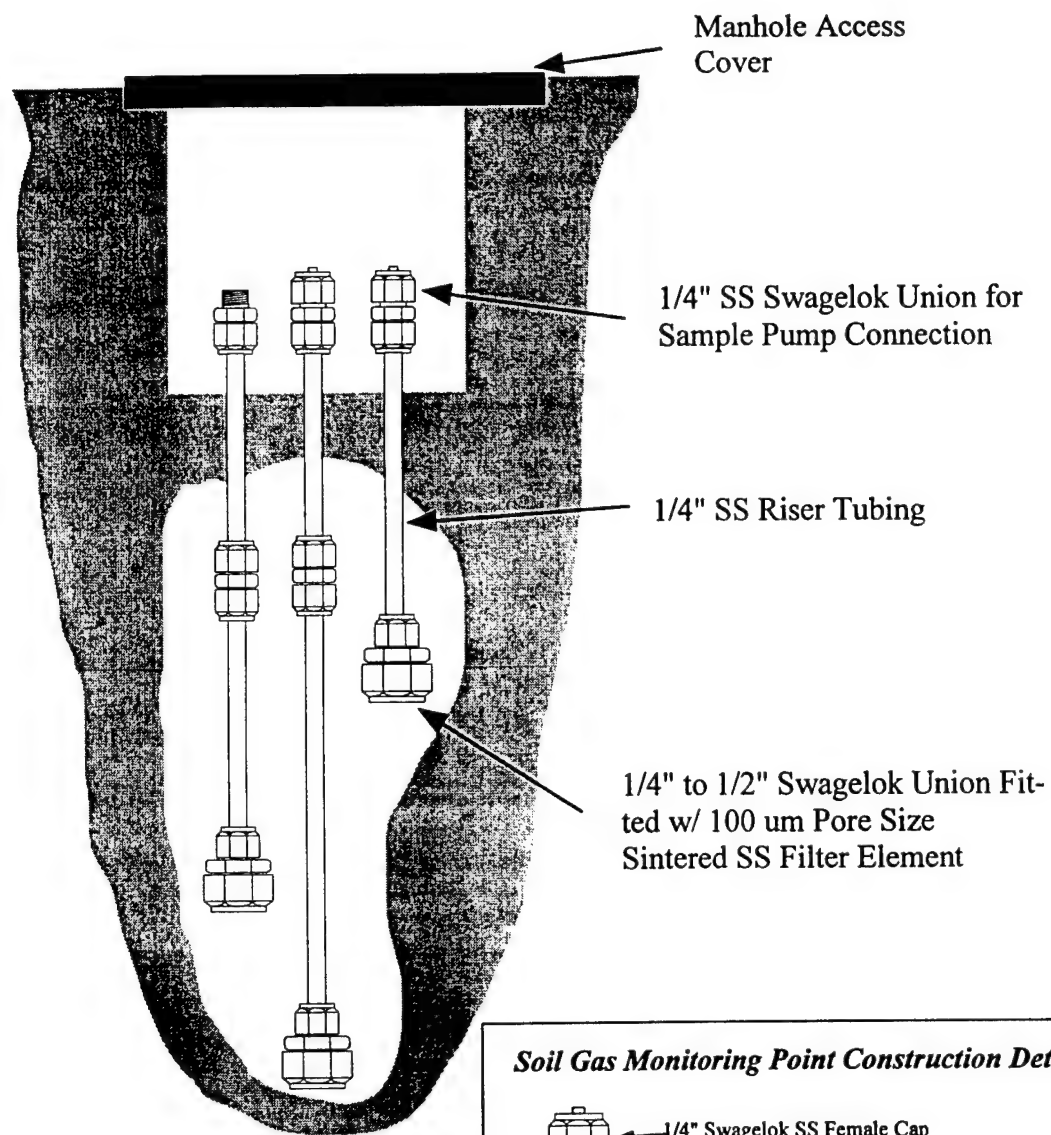


**Figure 3.17 Stainless Steel Tubing Cluster Details**

retracted so as to keep the hole open and to allow for proper placement of filter and sealing materials.



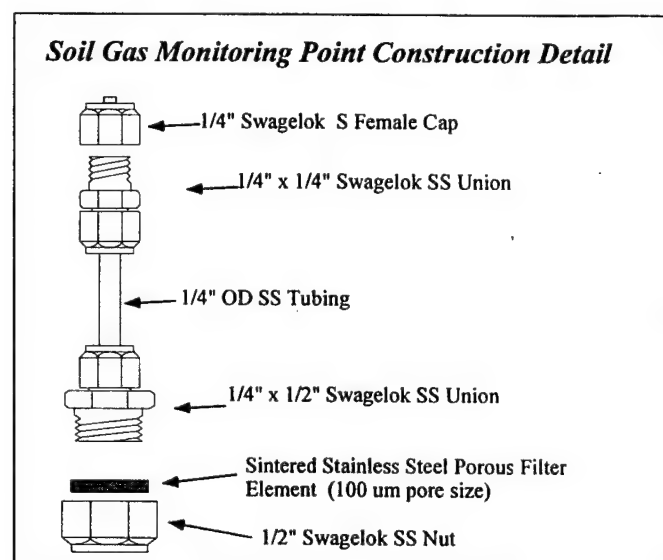
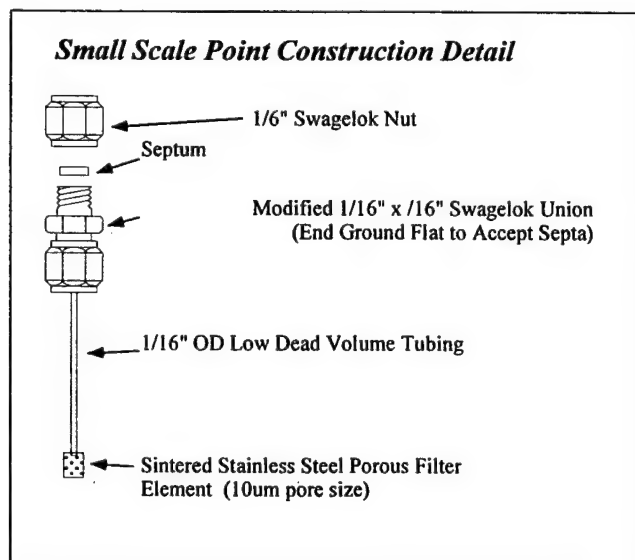
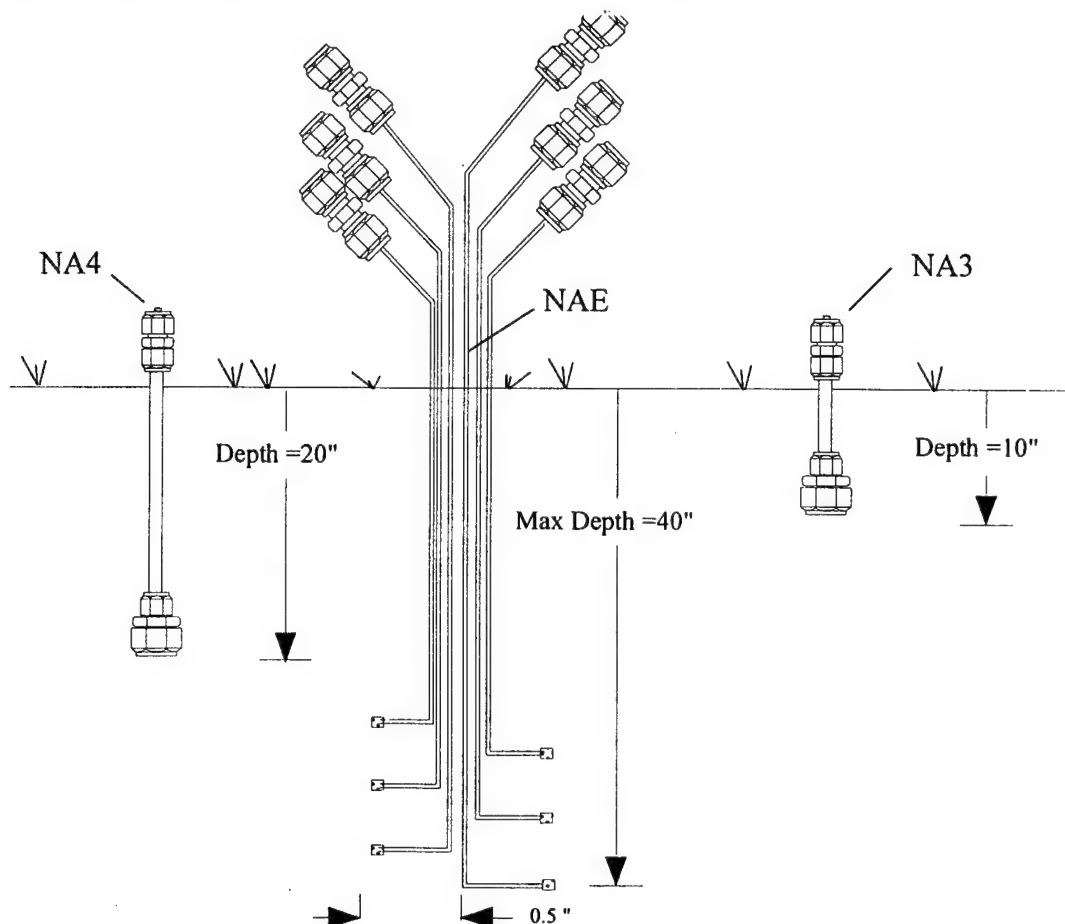


**Figure 3.18 Near Surface Array Construction Details**

Four stainless steel near surface arrays were constructed to resolve the vertical soil gas profile through the root zone of the site area at locations NAE and NAW, as shown in Figure 3.1. The small scale points (Figure 3.18) are constructed of the appropriate length of 1/16 inch diameter by 0.01 inch ID low dead volume tubing (Valco, Houston, TX) pressed into a 1/8 inch x 1/8 inch sintered stainless steel cup with a 10 mm pore size (Mott Metallurgical, Farmington,

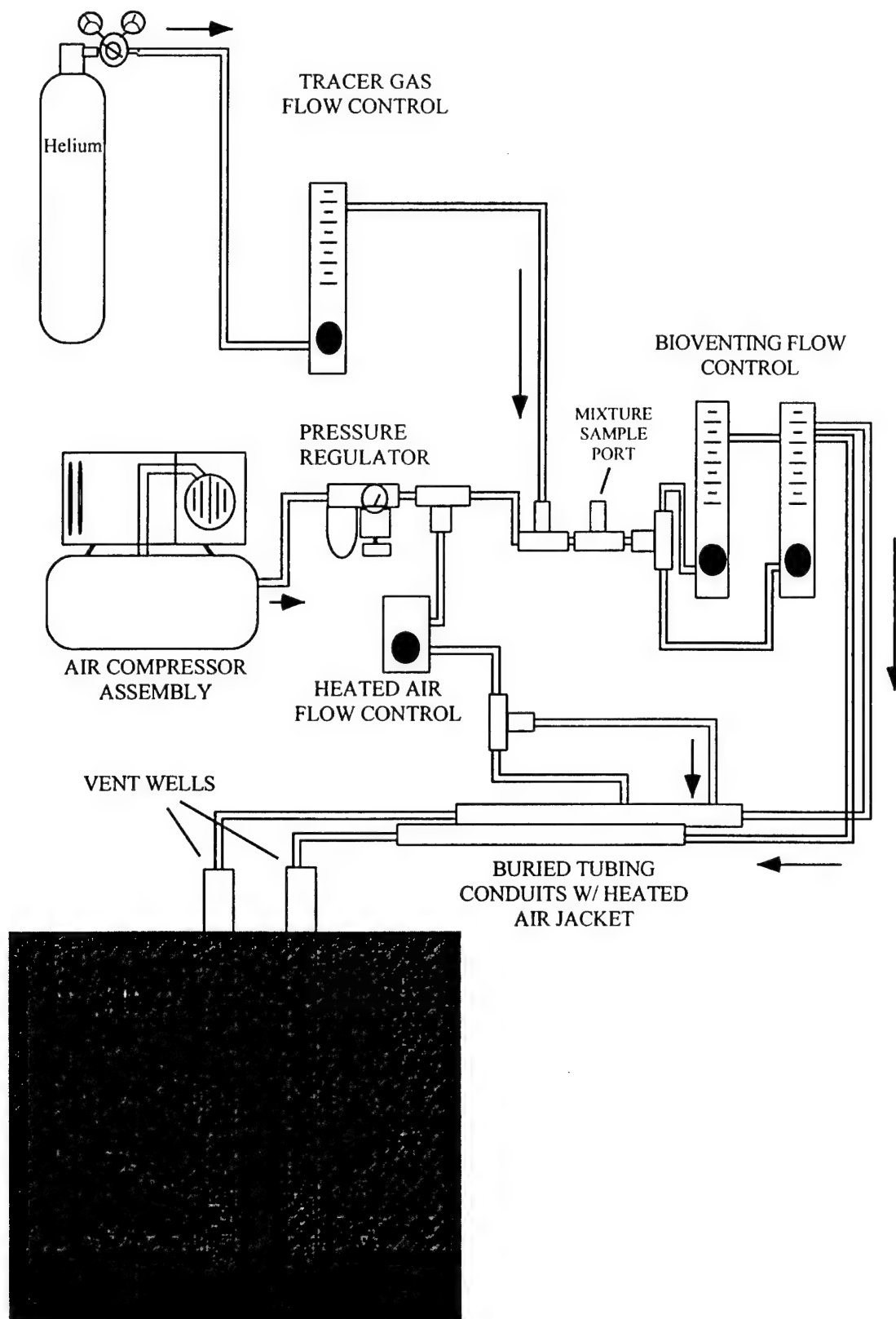


**Figure 3.19 Soil Venting System**

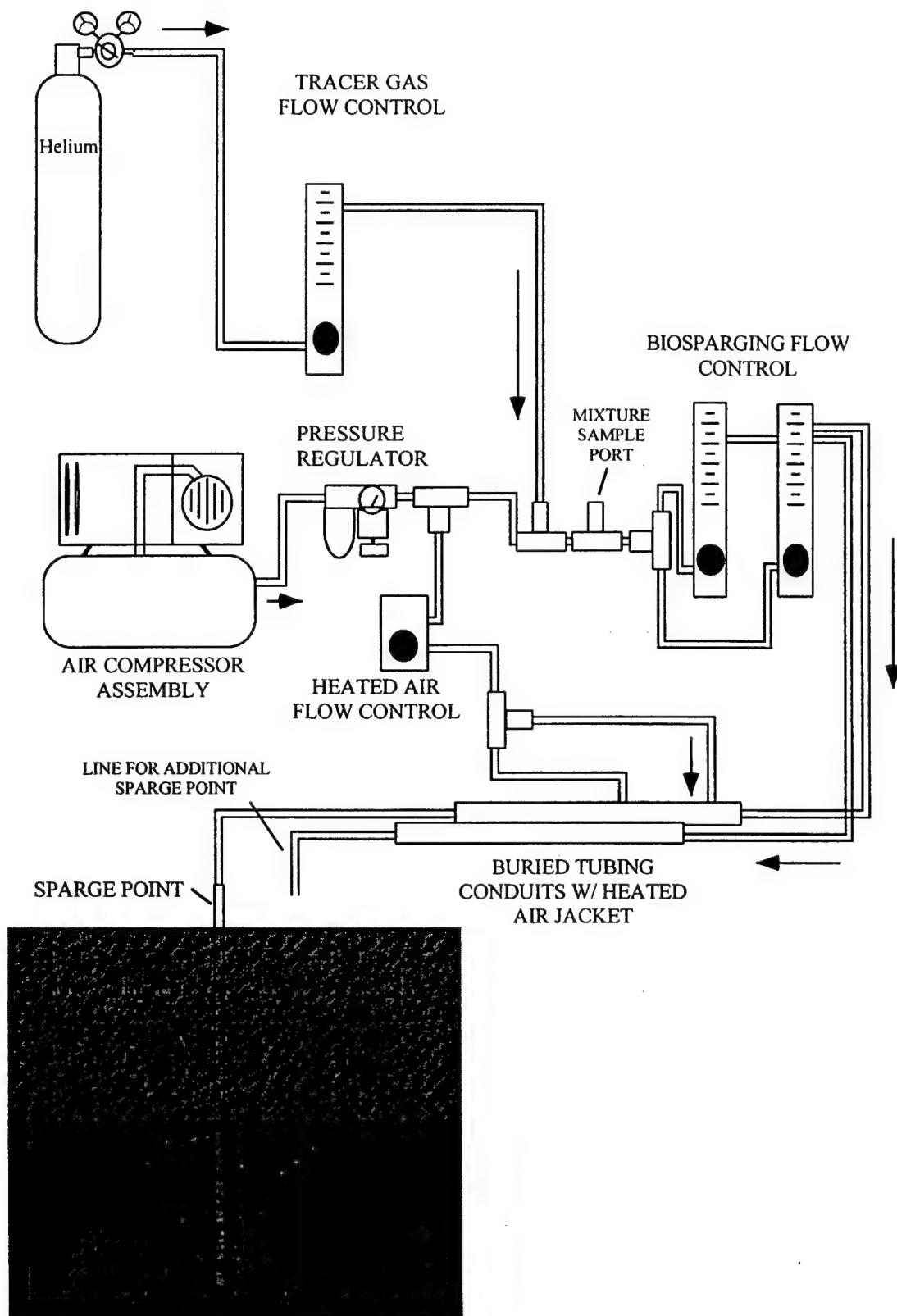


**Figure 3.20 Air Sparging System**

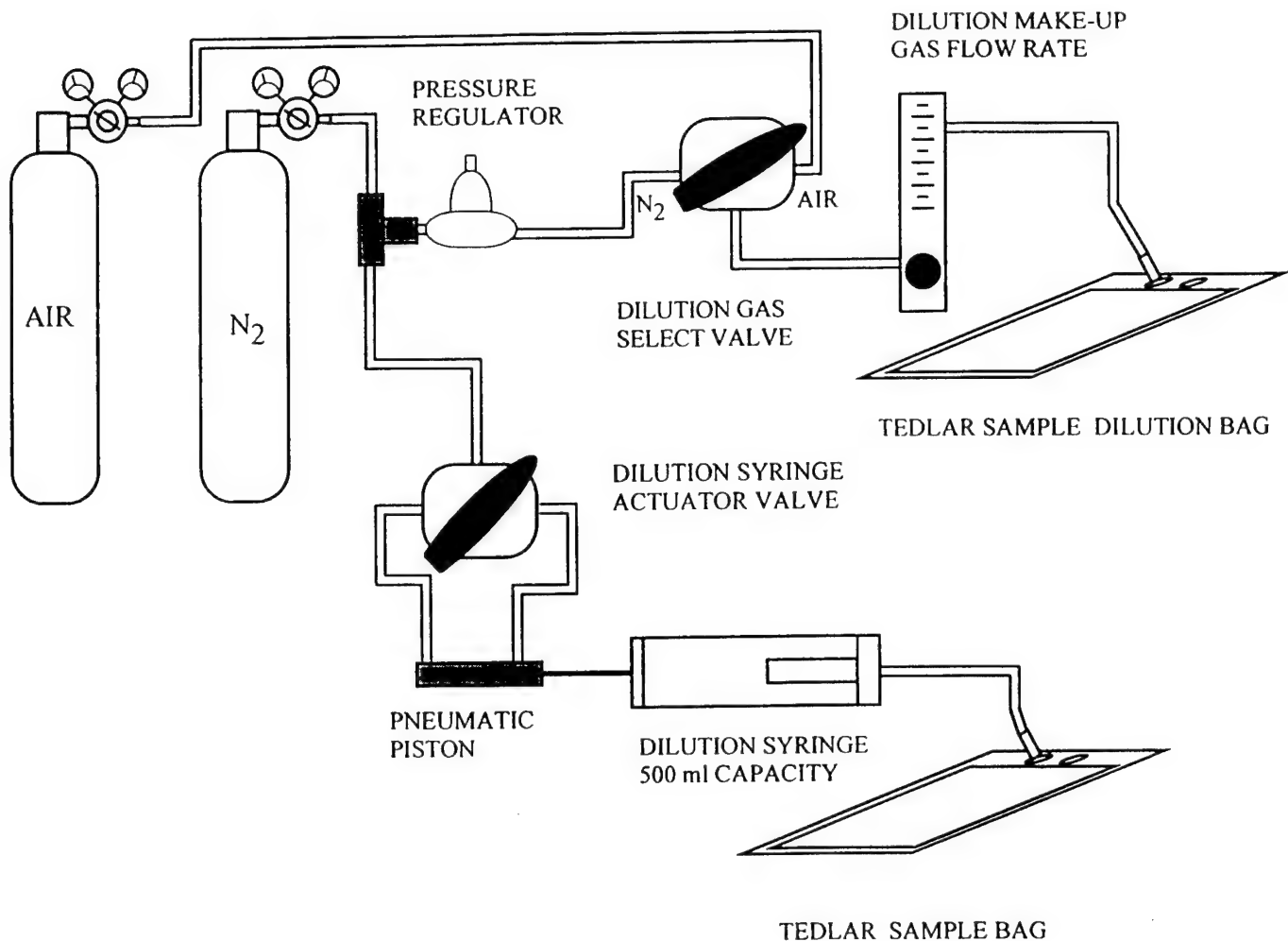


**Figure 3.21 Tedlar Bag Dilution System**

CT) A modified 1/16" to 1/16" stainless steel union (Swagelok, Solon, OH) was mounted at the other end which was fitted with a 5 mm GR-2 septa supplied by Supelco, Inc., Bellafonte, PA. We collected soil gas samples from each small scale near surface sample point using a Hamilton 250  $\mu$ L gastight syringe for on site analysis in a gas chromatograph. Prior to sample collection, 100  $\mu$ L of gas was purged from each point followed by a 250  $\mu$ L sample for direct injection and analysis by GC/ECD.

#### 3.4.4 Soil Venting and Air Sparging Systems

Air was vented to the capillary fringe through two vent wells in boreholes VENT1 and VENT2. Figure 3.1 and Table 3.1 locate the vent wells, whose construction details are sketched in Appendix II. The two vent wells were installed using 0.2 m ID, 0.31 m OD hollow stem augers. Each well consisted of a 1.5 m section of 0.5 mm slotted, PVC well screen with a flush threaded cap at the bottom and 3-inch diameter flush thread PVC riser to the surface (Diedrich Drilling, Inc., LaPorte, IN). The vent wells were installed using six inches of sandpack (Morie

beneath the well point, 1.8 m of sandpack to 0.31 m above the well screen, a 3.1 m bentonite seal above this, and 3.1 m of grout above the bentonite. The remainder of the borehole was filled with native materials. At the surface, the wells were protected by 0.31 m diameter manholes (Boart-Longyear, Stone Mountain, GA). Each vent well was installed with a 1.5 meter screened interval based at 12.8 m below grade. The screens extended 0.76 m below the water table, and 0.76 m above the water table at the time of construction.

Air flow was supplied to the vent wells via 6.4 mm OD by 4.8 mm ID nylon tubing (Cole Parmer, Vernon Hills, IL) buried approximately 0.31 m below grade within a .02 m diameter PVC conduit surrounded by 0.013 m thick pipe insulation. Air lines entered the vent well manholes below grade through an access hole cut into the buried steel manhole skirts (Figure 3.19). The air lines were fitted to the 0.08 m diameter vent wells using 0.08 m to 0.05 m rubber couplings fitted with custom made 0.05 m to 1/4-inch NPT adapters. A total air injection rate Q of 28 L/min was conveyed to the vadose zone via the vent wells

$$Q = 4.67 \times 10^{-4} \frac{\text{m}^3}{\text{s}} \quad (\text{venting}) \quad (3.8)$$

A 1.2 x 1.2 x 1.2 m, wooden, fully insulated, pump shed was constructed and installed at the site to house the compressor, flow meters and valves. A Model 4H series 100 PSI, 3.5 CFM open flow, 230 VAC, oilless piston, compressor (Gast, Benton Harbor, MI) was used to provide air flow. Air from the pump flowed into a 0.2 m<sup>3</sup> pancake type pressure ballast tank (Grainger, Lincolnshire IL) equipped with an automatic shutoff switch (Grainger). A combination line regulator and water trap (Grainger) was installed in the air line before reaching the manifold board. A 750/1000W ceramic heater (Toastermaster, Boonville, MO) was installed in the shed to maintain proper operating temperatures and to preheat ambient injection air.

Access to all controls and gauges was provided on a hinged manifold board. The manifold board was designed to be operated as two separate sections. Each section contained a tracer gas inlet port (Swagelok, Salon, OH) a mixture sampling port (Swagelok), a tee (Swagelok) into two flow meters with flow control valves, and two 0-15 PSI outlet pressure gauges (Cole Parmer, Vernon Hills, IL). Initially, the manifold board was set up to supply air to the two vent wells at flow rates of 14 L/min. in each well. The other two flow controlled outlets were used to blow warmed air into the 3/4" buried conduits containing the air supply lines to the vent wells in order to keep the air in the supply lines from condensing and freezing during winter operation.

Air was sparged into the subsurface below the water table through SPARGE1, a 2.0 cm diameter PVC injection pipe with a 0.5 mm slotted screen section 20 cm long. The screen was installed 1.2 m below the water table, set in a Morie sand pack with bentonite pellet and slurry seals, as delineated in Appendix II. Other well details are similar to VENT1 and VENT2.

A helium injection system was incorporated into both venting and sparging systems to facilitate tracer tests during system operation. Zero grade helium (Merriam Graves, Plattsburgh,

**TABLE 3.6 SOIL VENTING AND AIR SPARGING TEST PROGRAM**

	<b>Soil Venting</b>	<b>Air Sparging</b>
Start of air flow	18 January 1996	9 August 1996
End of air flow	9 August 1996	5 September 1996
Restart air flow	Not applicable	24 October 1996
Finish air flow	Not applicable	19 December 1996
Start tracer test	7 February 1996	24 October 1996
End tracer test	7 March 1996	24 November 1996
$H_{INF}$	2,022 ppm <sup>a</sup>	5,900 ppm <sup>a</sup>
Round 1 sampling	13 February 1996	7 November 1996
Round 2 sampling	21 February 1996	20 November 1996

<sup>a</sup>by volume.

NY) was fed into the injection air flow at a nominal flow rate of 100 mL/min through a Swagelok stainless steel union during four week periods in February and November 1996. Injection concentrations  $H_{INF}$  were measured in the discharge line with the results cited in Table 3.6, which also lists the venting and sparging periods, and the corresponding helium injection periods.

#### 3.4.5 Soil Gas Sample Dilution and Portable Meters

There are several occasions when gas samples require dilution prior to or during analysis. One example is during hydrocarbon analysis. Often, when analyzing gas samples at petroleum contaminated sites, the samples contain high hydrocarbon concentrations and at the same time, low oxygen concentrations. One type of meter used for hydrocarbon analysis (the type used in the majority of field hydrocarbon analysis during this project) uses a catalytic combustion sensor which requires an oxygen level of at least 5% to provide an accurate hydrocarbon reading. Oxygen levels at petroleum contaminated sites near areas of heavy microbial activity can decrease to levels below 1%. Without the addition of oxygen, the hydrocarbon analysis meter will provide a reading that is too low due to the limited combustion that can take place in the sensor. To alleviate this problem, if a sample is analyzed and the oxygen concentration is below 5%, the sample is diluted by a factor of ten with zero grade air thus providing additional oxygen. The meter analysis is then reconducted and the hydrocarbon concentration is corrected for the tenfold dilution. Dilution can also be required when the concentration of a certain component of a soil gas mixture is present at concentrations that exceed the useable range of the instrument chosen for analysis. As an example, this can occur when carbon dioxide concentrations are in excess of 1% for one of the field meters to be used in this study (PMI-300) or when the total hydrocarbon concentrations are in excess of 10,000 ppm when using the Bacharach TLV meter.

Dilution of Tedlar bags for field analysis was conducted using the field dilution system (Figure 3.21). The field dilution system consists of a 500 mL gastight gas sampling syringe (Supelco, Bellafonte, PA), a pneumatic piston drive unit to actuate the syringe (Herbach and Rademan, Bristol, PA), a 5 L/min flow meter (Cole Parmer, Niles, IL), a 4 way valve to control the pneumatic piston (Swagelok, Salon, OH), a pressure regulator (Herbach and Rademan), and a

3-way air/nitrogen select valve (Swagelok), along with various hoses and fittings. Operation of the dilution apparatus is straightforward. The sample bag requiring dilution is attached to the 500 ml syringe intake/outlet line via a 1/8 inch to 3/16 inch union. The 4-way valve is turned causing the pneumatic piston to pull back the syringe plunger. Stops are installed so that a 200 ml sample is withdrawn from the sample bag. A clean bag is then attached to the dilution gas outlet to receive either air or nitrogen as the dilution gas depending on the type of dilution required. A volume of 1.8 liters (for a 10x dilution) of dilution gas is pumped into the additional bag. Once the bag has received 1.8 liters, it is then attached to the outlet tube on the syringe. The 200 ml sample collected from the original bag is then pumped into the dilution bag for a total volume of 2 liters. The 4-way valve and pneumatic piston are used to drive the syringe plunger as with the original sample withdrawal. The new bag is now ready to be analyzed but with a hydrocarbon or CO<sub>2</sub> concentration that is one tenth of the original value.

Oxygen, carbon dioxide, and total hydrocarbon soil gas concentrations in the field were measured using a series of handheld, battery operated instruments. Four meters were used for the bulk of the analyses:

- Total hydrocarbon pressure (p<sub>G</sub>)-Bacharach TLV meter (Bacharach, Inc., Pittsburgh, PA)
- Oxygen pressure (p<sub>X</sub>) Bacharach Model 302 Sniffer (Bacharach, Inc., Pittsburgh, PA)
- Carbon dioxide pressure (p<sub>C</sub>) PMI-300 CO<sub>2</sub> analyzer (CEA Instruments, Inc., Emerson, NJ)

The Bacharach TLV Sniffer incorporates an "active" catalytic coated resistance element which oxidizes combustible gases as they enter the sensor. The heat produced by the oxidation process increases the resistance of the element proportional to the concentration of oxidizable material in the gas. An identical reference element without a catalytic coating is present along with the catalytic element in a wheatstone bridge configuration to compensate for ambient temperature changes and aging effects. A small internal bellows type sample pump draws sample gas into the sampling chamber at a flow rate of 2 L/min. The analog output meter operates with three scales: 0-100 ppm, 0-1,000 ppm, and 0-10,000 ppm. Calibration is performed by supplying hexane gas at a concentration of 500 PPM to the meter inlet and adjusting as per the owners manual operating instructions (Bacharach, 1990).

The Bacharach Model 302 Sniffer is a combination oxygen and combustible gas meter. Combustible gas concentrations are reported as percent of the lower explosive limit (% L.E.L) using the same sensing element as is in the Bacharach TLV unit. The oxygen portion of the unit consists of an electrochemical potentiometric cell capable of measuring O<sub>2</sub> concentrations in the range of 0-25%. The oxygen portion of the unit is calibrated to atmospheric concentrations (20.9%). Oxygen and combustible gas values are displayed on an LCD readout at the top of the unit. For this research, only the oxygen portion of the unit will be used. The TLV unit discussed above was used for combustible gas (hydrocarbon vapor) analysis.

The PMI-300 CO<sub>2</sub> meter is capable of measuring CO<sub>2</sub> concentrations in gas samples with a range of 0-100%. The method of detection is infrared absorbence. The functional portion of the unit consists of a glass cell through which the sample is pumped incorporating an infrared source, filter, and detector unit. The concentration of carbon dioxide in the cell contents is



proportional to the amount of infrared light absorbed. This signal is then conditioned, compared with a reference cell, and displayed on a 4 digit front mounted LCD readout. Controls for zero and full span are provided on the front. The unit is calibrated with a 99.8% CO<sub>2</sub> calibration gas (Scott Specialty Gas, Plumsteadville, PA). An adjustable flow rate sample pump draws the sample into the infrared absorbance cell.

### 3.5 Gas Chromatographic Analysis of Soil Gas Samples

Two Hewlett Packard Model 5890 laboratory gas chromatographs complete with PC-based data acquisition systems were brought to the field site for soil gas analysis. One gas chromatograph was equipped with two detectors: an electron capture detector (ECD), and a thermal conductivity detector (TCD), while the other had a flame ionization detector (FID). We used the FID to measure trichloroethylene in the tubing clusters and vapor probes, while the more sensitive ECD was reserved for near surface area samples with lower concentrations. Helium tracers were measured with the TCD. We describe the chromatography below.

#### 3.5.1 Flame Ionization Detector

We withdrew a 250  $\mu$ L sample from the Tedlar bag using a Hamilton Gastight 250  $\mu$ L syringe equipped with a 26 gauge, bevelled tip needle. The FID gc was run with the following settings

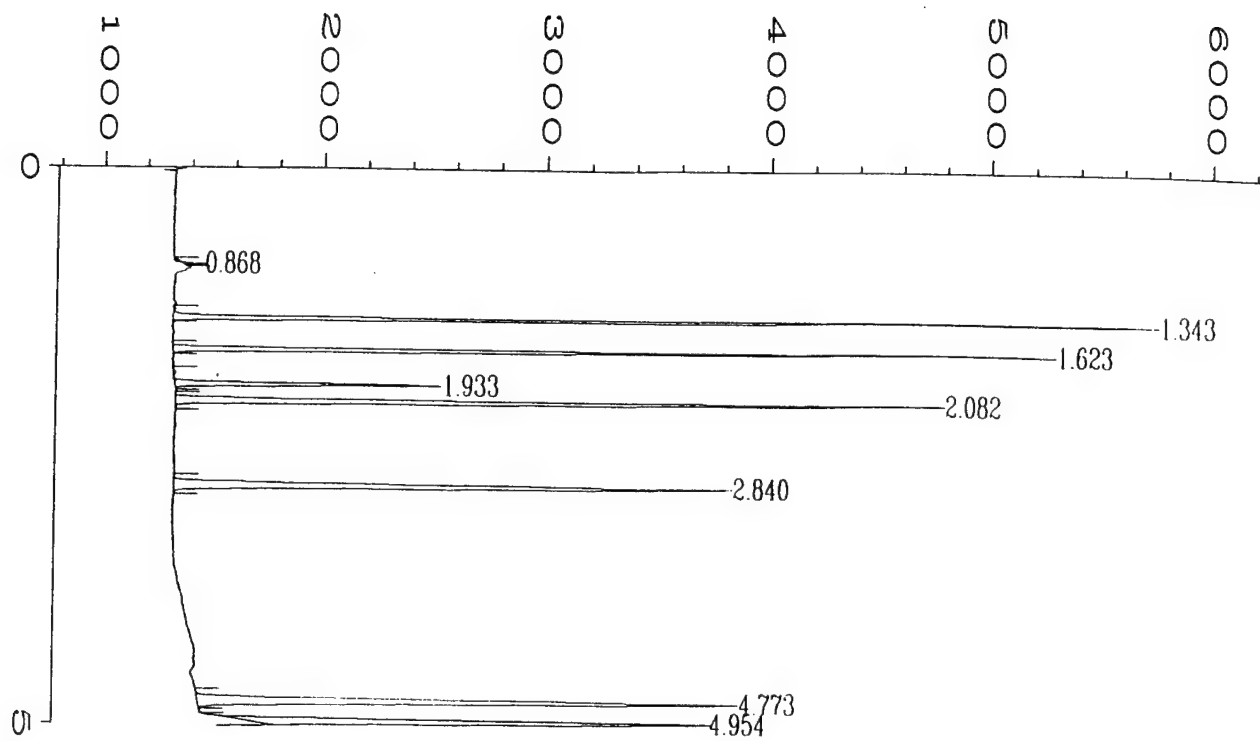
- Injector-20 to 1 split ratio, 250°K temperature, 2 mL/min zero grade N<sub>2</sub> carrier gas
- Capillary column-HP5 0.32mm diameter, 30 m length, 25  $\mu$ m film thickness (crosslinked 5% PH ME siloxane)
- Oven temperature-35°C for 3 min, 10°C/min to 70°C
- Detector-Temperature of 300°C, makeup gas flow rate of 20 mL/min

The data were captured with Hewlett Packard ChemStation software on a computerized data acquisition system.

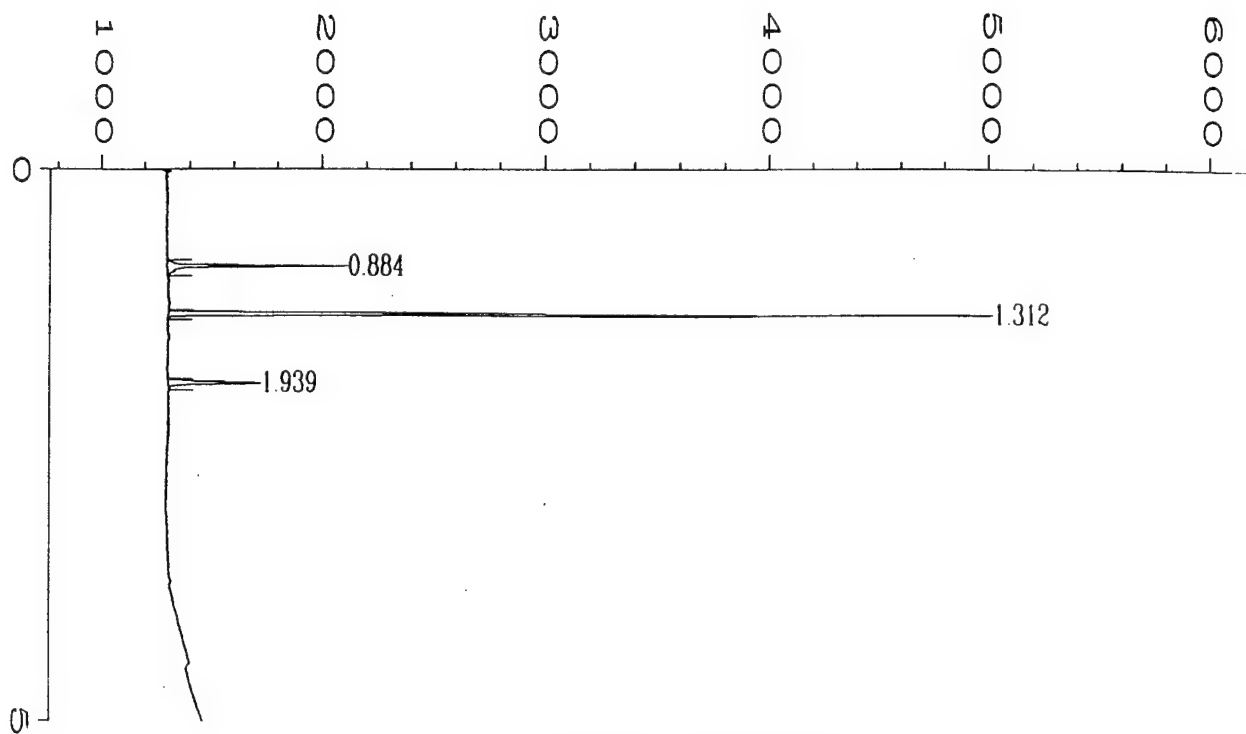
A synthetic gas standard (Scott Specialty Gases, South Plainfield, NJ) was used to calibrate the FID. The standard is comprised of a blend of 10 ppm partial pressures of seven compounds in nitrogen:

- hexane (1.343 minute retention time)
- benzene (1.623 minute retention time)
- trichloroethylene (1.933 minute retention time)
- heptane (2.082 minute retention time)
- toluene (2.840 minute retention time)
- ethylbenzene (4.773 minute retention time)
- m xylene (4.954 minute retention time)

Figure 3.22 displays typical chromatograms for the standard, and a soil gas sample.



Standard Chromatogram



Sample Chromatogram

Figure 3.22 Typical FID Chromatograms for Soil Gas

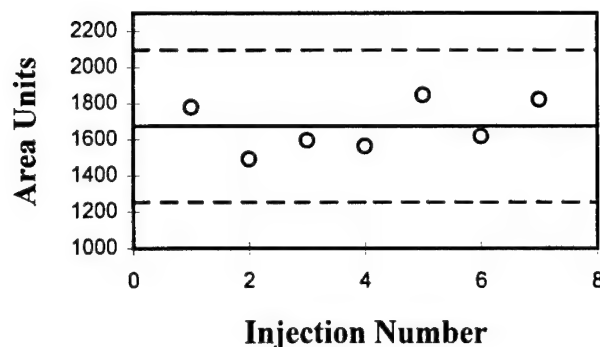


**Figure 3.23 Method Detection Limit Study for TCE by FID**

We ran a method detection limit (MDL) study by injecting seven replicate 10 ppm TCE soil gas samples into the gas chromatograph, with the results shown in Figure 3.23. Equations 3.5 and 3.6 are used to compute the MDL for trichloroethylene by FID analysis:

$$p_{YMDL} = 2.6\text{ppm} \quad (\text{FID}) \quad (3.9)$$

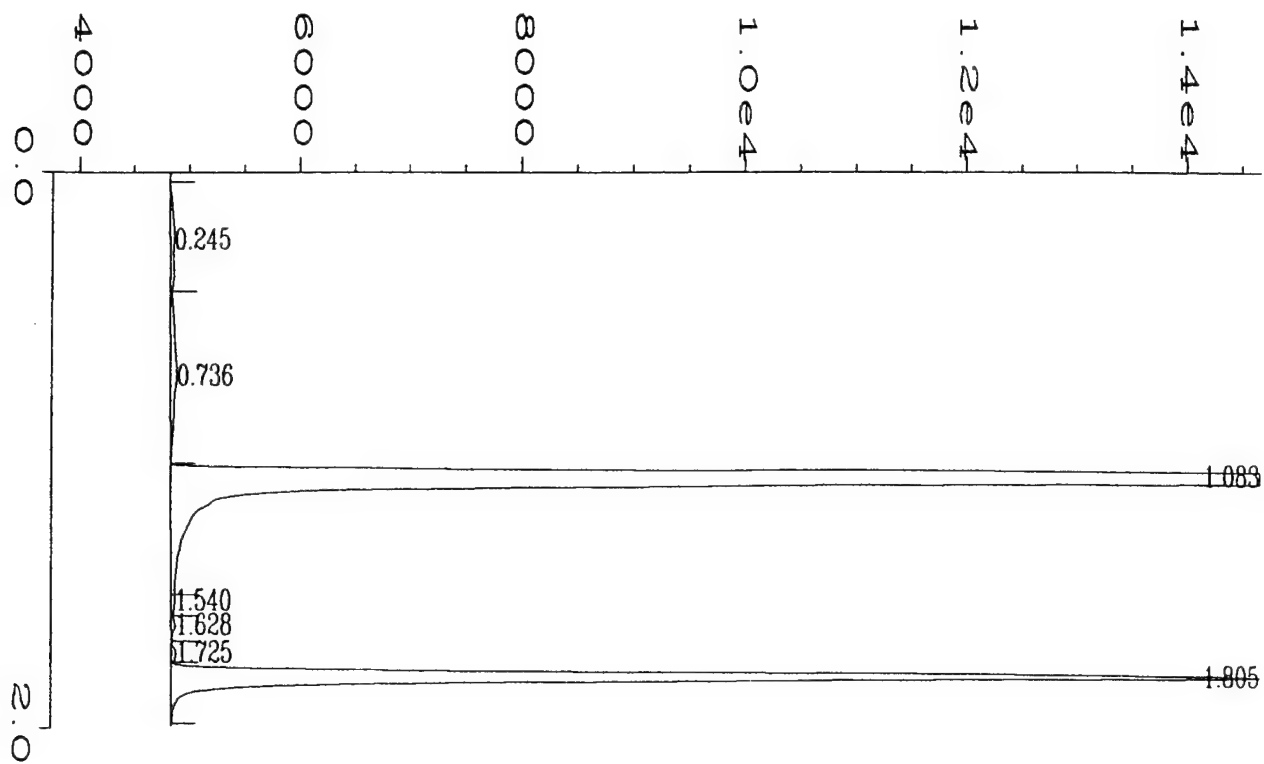
This precision is sufficient for observations in the tubing clusters and vapor probes. Concentrations diminish near the surface due to the atmospheric boundary condition however, so that a more sensitive detector is needed for the near surface array samples. This is provided by the ECD.

### 3.5.2 Electron Capture Detector

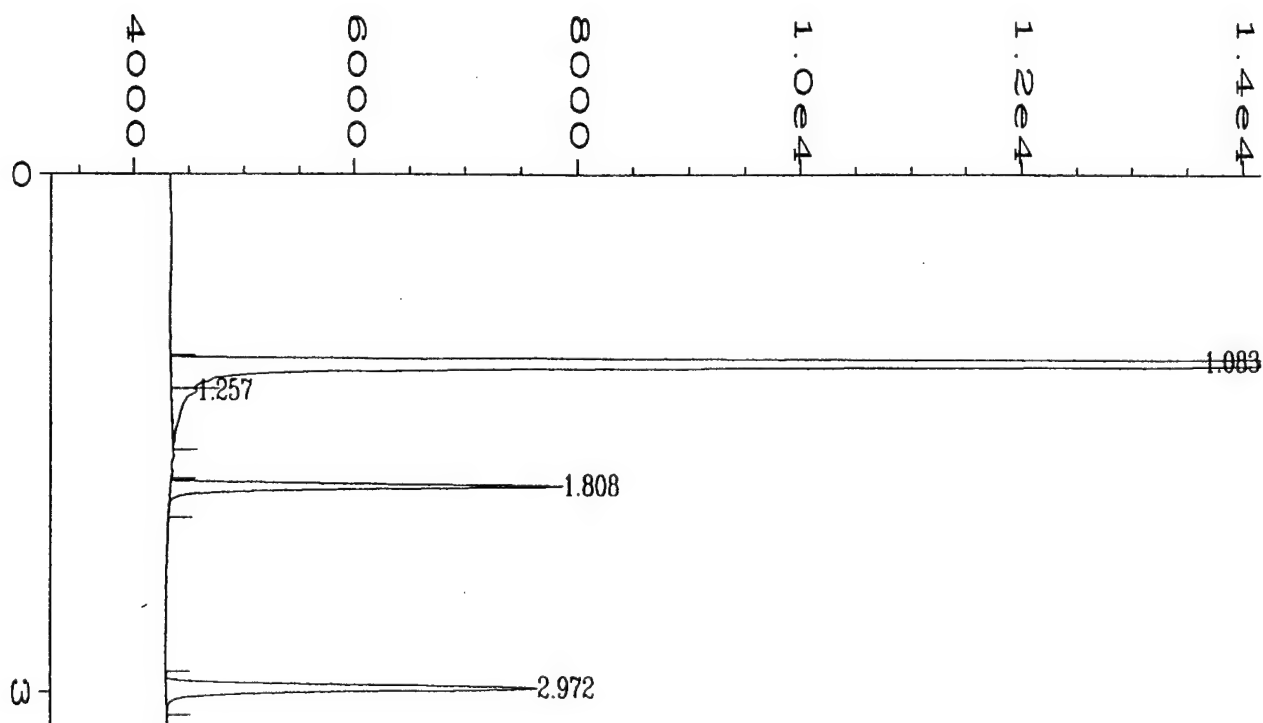
A 250  $\mu\text{L}$  soil gas sample is injected into the gas chromatograph with the ECD, maintained at the following settings:

- Injector-20 to 1 split ratio, 200°C temperature, 2 mL/min zero grade  $\text{N}_2$  carrier gas
- Capillary column-HP1 0.25mm diameter, 30 m length, 25  $\mu\text{m}$  film thickness (crosslinked 1% PH ME siloxane)
- Oven temperature-35°C for 3 min, 10°C/min to 70°C
- Detector-Temperature of 250°C, makeup gas flow rate of 20 mL/min

The data were captured with Hewlett Packard ChemStation software on a computerized data acquisition system. A 100 ppb TCE standard was prepared by serial dilution of the FID standard in Tedlar bags. Figure 3.24 displays standard and sample chromatograms generated by the ECD.



Standard Chromatogram



Sample Chromatogram

Figure 3.24 Typical ECD Chromatograms for Soil Gas

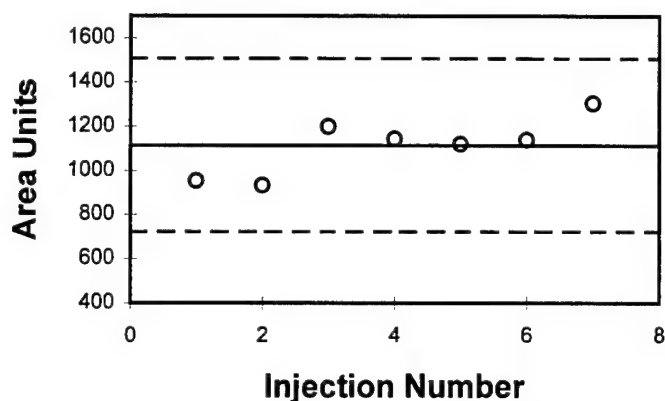


**Figure 3.25 Method Detection Limit Study for TCE by ECD**

TCE elutes at a retention time of 1.805 minutes. Figure 3.25 displays a method detection limit study for trichloroethylene vapors by ECD methodology. Seven replicate 1 ppm injections were run through the chromatograph, yielding an MDL of

$$P_{YMDL} = 3\text{ppb} \quad (\text{ECD}) \quad (3.10)$$

The highly precise MDL is suitable for near surface array analysis, which features TCE pressures ranging from 1 to 1,000 ppb.

### 3.5.3 Thermal Conductivity Detector

Helium was sensed by a Hewlett Packard 5890 gas chromatograph equipped with a packed column and a thermal conductivity detector in accordance with the following program:

- Injector-splitless, 200°K temperature, 25 mL/min zero grade N<sub>2</sub> carrier gas
- Packed column-HP5 31 mm OD, 2 m length, 60/80 mesh molecular sieve
- Oven temperature-Isothermal at 50°C
- Detector-Temperature of 150°C

Helium standards were prepared by serial dilution of Tedlar bag samples, using successive 10 mL injections of pure helium (Merriam Graves, Plattsburgh, NY). Figure 3.26 shows typical standard and sample chromatograms for helium, which elutes at 0.359 minutes. We ran a method detection limit study for helium, as shown in Figure 3.27. The resulting MDL is

$$P_{HMDL} = 23\text{ppm} \quad (\text{TCD}) \quad (3.10)$$

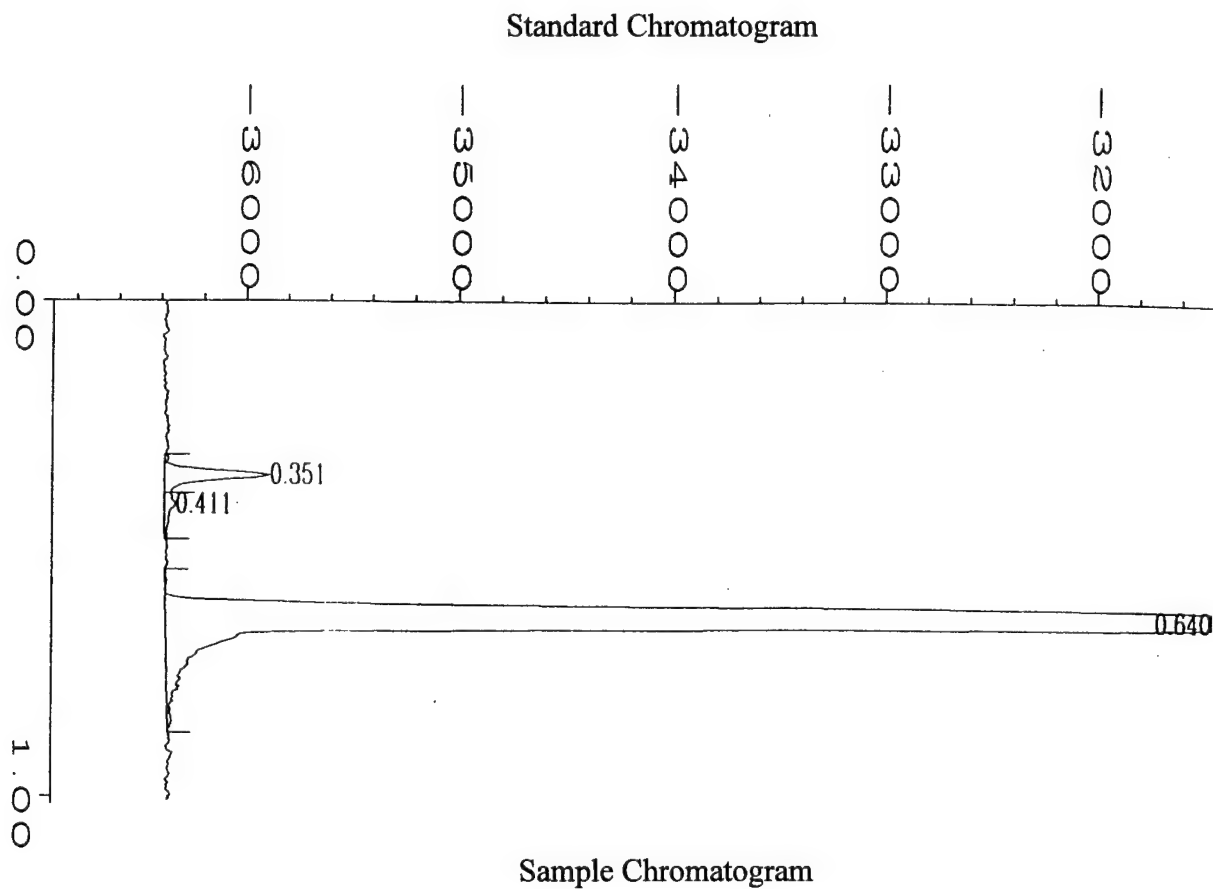
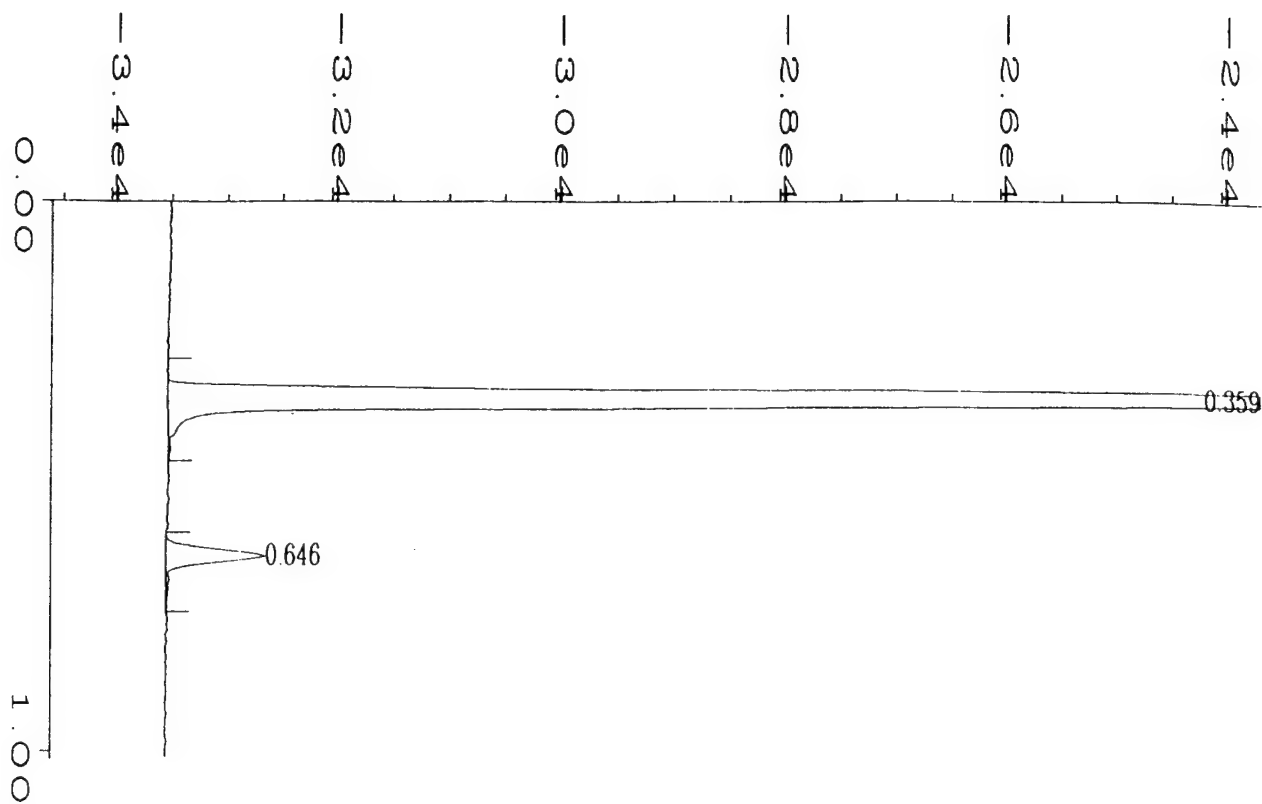


**Figure 3.26 Typical TCD Chromatograms for Soil Gas**

### 3.6 Surface Isolation Flux Chamber

When conducting mass balance calculations on contaminant mass and monitoring emissions for regulatory reasons, it is often necessary to measure the efflux of contaminants from the ground surface to the atmosphere. There are several effective tools for measuring soil gas flux at the ground surface for the determination of contaminant impacts on ambient air. Surface flux measurements can also monitor the effectiveness of remedial actions such as containment barriers. Existing flux measurement equipment includes: the emissions isolation flux chamber, vent sampling, concentration profiles and transect methods. Transect and concentration profile methods require much instrumentation, are labor and time intensive, and are affected by varying site conditions such as temperature. Vent sampling is relatively simple but may not provide values representative of the area [Batterman et al. (1992)]. For these reasons, the flux chamber method is preferred for characterizing soil gas. However, there are still some disadvantages to isolation flux chamber use. Much equipment is required, including a compressed air supply, power, and flow balancing equipment. In addition the flux is only measured over a relatively small area, typically 0.1-0.3 m<sup>3</sup> and over a relatively short and possibly non representative time period. Inherent heterogeneities at most sites require that to properly characterize a site, many points must be sampled, ideally simultaneously.

Batterman et al. (1992) describe an inexpensive, simple to install, and easy to analyze surface flux sampling system. The sampler consists of three major components: an inverted, open ended canister, an activated carbon layer installed at the top of the canister, and an absorbent badge. The carbon produces a gradient which simulates the vapors being swept away at the ground surface. The sampler is installed by pushing it a short way into the ground surface. After a predetermined period of time the canister is then retrieved. The absorbent badge is removed and compounds are extracted. Another stationary passive sampler method is described by Gomes et al. (1994). The PETREX method is a passive soil gas measurement technique combining stationary activated carbon coated filaments with high resolution GC/MS analysis thus making it capable of detecting and identifying over 9,000 VOC's and SVOC's. Detection limits for this method are generally in the ug/m<sup>3</sup> range.

We designed and built a surface isolation flux chamber to measure emissions from the site area. Figure 3.27 displays the device, which is a modification of an Environmental Protection Agency design [Dupont (1987)], comprised of a stainless steel cylinder 18 cm high, with a 41 cm internal diameter. We welded a 51 cm outer diameter aluminum flange to the top of the cylinder to receive a Gore tex gasket and an acrylic dome. Five stainless steel ports are provided through the base of the chamber:

- temperature access port
- pressure gage port
- sweep gas inlet port
- sweep gas outlet port
- reserve port

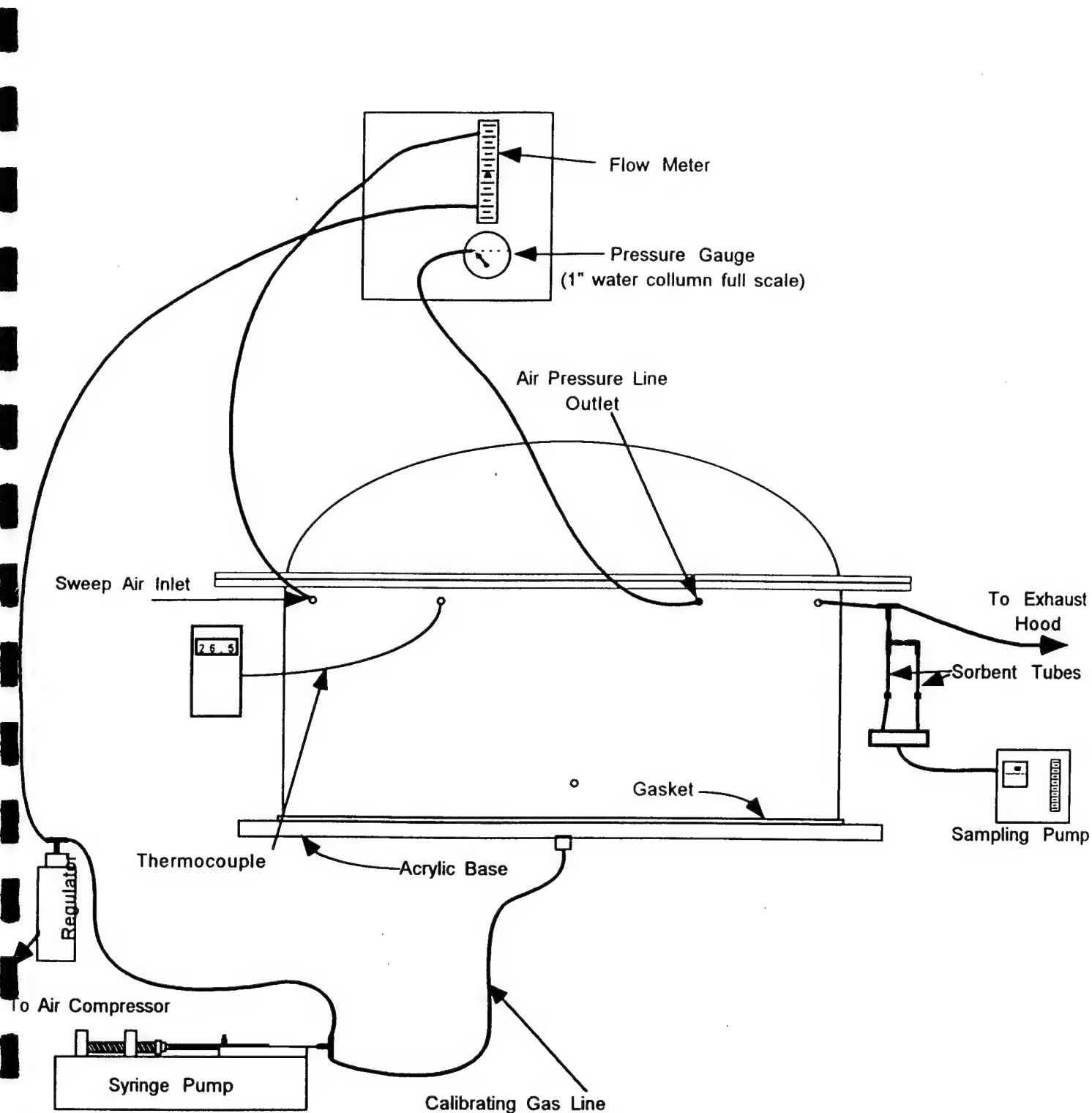


**Figure 3.27 Surface Isolation Flux Chamber**

Temperature was monitored with K type thermocouples (Omega, Stamford, CT), while magnehelic pressure gages were used to measure gas pressure. The chamber headspace was swept with regulated, metered (Aalborg Instruments and Controls, Monsey, NY), zero grade nitrogen gas (Merriam Graves, Plattsburgh, NY). Fine control was exerted by SKC 224



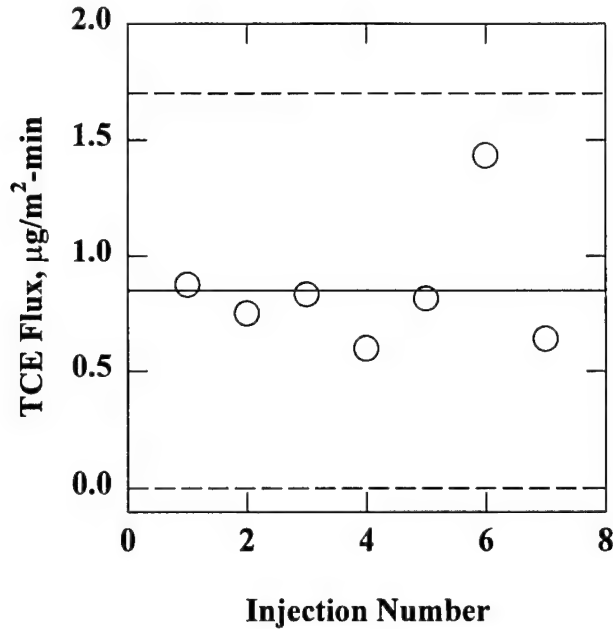


**Figure 3.28 Method Detection Limit Study for Trichloroethylene Flux**

sampling pumps (Eighty Four, PA) on the inlet and exhaust sample lines, which were of 6.3 mm diameter, Teflon construction with stainless steel Swagelok coupling. The exhaust sample line was equipped with a sampling port, for syringe withdrawal and gas chromatographic injection. A Hewlett Packard 5890 gas chromatograph with ECD was used to analyze the tetrachloroethylene concentrations, using the protocol stated in Section 3.5.2. Tehrany et al. (1996) use chemostatic analysis to relate the observed headspace concentration  $Y_{\text{HEAD}}$  to the flux  $J_{\text{YO}}$  emitted to the atmosphere

$$J_{\text{YO}} = \frac{(Q_{\text{SWEEP}} + w_{\text{O}}A_{\text{HEAD}})Y_{\text{HEAD}}}{A_{\text{HEAD}}} \quad (3.12)$$

with sweep flow  $Q_{\text{SWEEP}}$  and headspace area  $A_{\text{HEAD}}$ .

We conducted a method detection limit study for trichloroethylene flux in the laboratory by replicate injections of a 5.5 ppb standard, with the results summarized in Figure 3.28. The emissions protocol yielded a flux MDL of

$$J_{\text{YMDL}} = 0.87 \frac{\mu\text{g}}{\text{m}^2 - \text{min}} \quad (\text{ECD}) \quad (3.13)$$

## 4 MATHEMATICAL ANALYSIS

### 4.1 Soil Temperature

Seasonally varying surface temperature also imparts an annual frequency  $\omega$  to the soil temperature  $\tau$ , which is governed by a thermal diffusion equation [Carslaw and Jaeger (1973)]

$$\frac{\partial \tau}{\partial t} - D_T \frac{\partial^2 \tau}{\partial z^2} = 0 \quad (4.1a)$$

$$\tau = \tau_{\infty} \quad (z = -\infty) \quad (4.1b)$$

$$\tau = \tau_M \sin(\omega t + \phi) \quad (z = 0) \quad (4.1c)$$

with time  $t$ , elevation  $z$  above the ground surface, phase shift  $\phi$ , thermal diffusivity  $D_T$ , mean temperature  $\tau_{\infty}$ , and seasonal amplitude  $\tau_M$ .

A separation of variables technique is adopted [Rainville and Bedient (1969)] in view of the periodicity of the boundary condition 4.1c, leading to the following solution

$$\tau = \tau_{\infty} + \tau_M \exp\left(z \sqrt{\frac{\omega}{2D_T}}\right) \sin\left(\omega t + z \sqrt{\frac{\omega}{2D_T}} + \phi\right) \quad (4.2)$$

Figure 4.1 displays typical temperature profiles for different values of the dimensionless depth

$z \sqrt{\frac{\omega}{D_T}}$ , based on the following parameter values:

- Average temperature  $\tau_{\infty} = 10^\circ\text{C}$
- Amplitude of temperature variation  $\tau_M = 15^\circ\text{C}$
- Phase shift  $\phi = 0$

The soil insulation delays the temperature fluctuation and reduces its amplitude with increasing depth.

### 4.2 Vertical Distribution of LNAPL

#### 4.2.1 Overview of LNAPL Distribution in the Capillary Fringe

We model the vertical distribution of free and residual light nonaqueous phase liquid (LNAPL) through the capillary fringe. The LNAPL is immiscible with and less dense than water, so that infiltrating JP4 jet fuel from the fire training pit source spreads out over the water table, subject to retention in the overlying capillary fringe under the action of surface tension

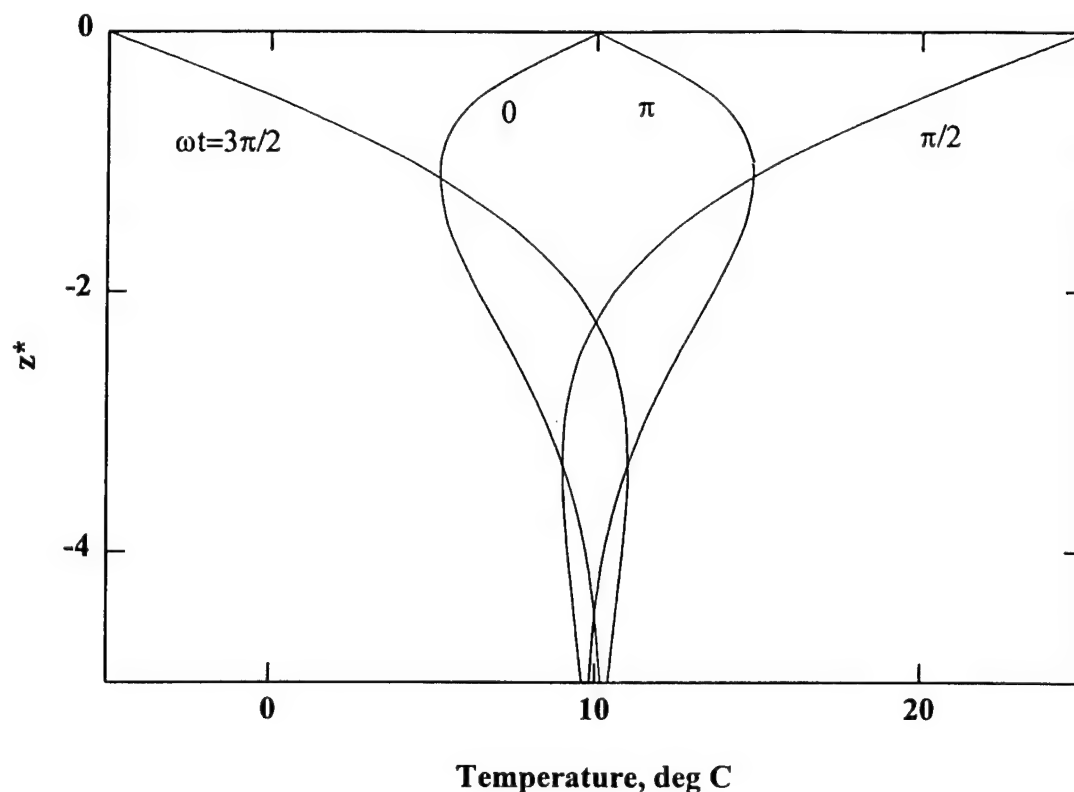


**Figure 4.1 Typical Soil Temperature Profiles**

[Schwille (1967), Pinder and Abriola (1986)]. The initial spreading of immiscible contaminants through the subsurface as a continuous phase is considered in numerous mathematical [Abriola and Pinder (1985), Corapcioglu and Baehr (1987), Sleep and Sykes (1989)] and laboratory [Schwille (1988), Reibel et al. (1990)] investigations. The dynamic models are complemented by static matrix pressure-saturation characteristic curves for continuous LNAPL-air-water systems, and substantial advances have been achieved in the prediction [Lenhard and Parker (1987,1990)] and laboratory measurement [Lenhard and Parker (1988)] of the necessary constitutive relations. The occurrence and distribution of a discontinuous residual nonaqueous phase liquid has received a degree of theoretical [Parker and Lenhard (1987)] and laboratory study [Wilson and Conrad (1984), Hoag and Marley (1986), Kia and Abdul (1990), Conrad et al. (1992)] comparable to its continuous counterpart.

#### 4.2.2 Free Liquid Retention

A three phase saturation case common to most LNAPL spills exists at Plattsburgh. The usual wetting progression of water-LNAPL-air is in force when free LNAPL is present, and the subsurface is comprised of initially water wet soil, so that water fills all the small pores to an irreducible volumetric water content  $\theta_F$ . The water is assumed to be continuous over the entire

spatial domain with an apparent [Parker and Lenhard (1987)] effective water saturation  $S_w$  that includes the residual LNAPL content  $\theta_{LR}$  trapped inside the water

$$S_w = \frac{\theta_w + \theta_{LR} - \theta_F}{n - \theta_F} \quad (4.3a)$$

$$\theta_{LR} = \frac{\text{volume} \cdot \text{residual} \cdot \text{LNAPL}}{\text{total} \cdot \text{volume}} \quad (4.3b)$$

The total saturation  $S$  includes the LNAPL content, free ( $\theta_{LF}$ ) and residual

$$S = \frac{\theta_w + \theta_{LF} + \theta_{LR} - \theta_F}{n - \theta_F} \quad (4.4a)$$

$$S_{LF} = S - S_w \quad (4.4b)$$

The free LNAPL saturation  $S_{LF}$  follows from Eqs. 4.3a and 4.4a.

A van Genuchten (1980) pore size distribution describes all free liquid phases, with scaling factors reflecting capillary pressures and surface tensions across controlling interfaces in accordance with Parker and Lenhard (1987). The total saturation is governed by the LNAPL/air interfacial tension  $\sigma_{LA}$  and the LNAPL matric pressure in the region where free LNAPL is present [Lenhard and Parker (1990)]

$$S = \{1 + [\beta_L (b_L - b)]^{\alpha_p}\}^{1/\alpha_p - 1} \quad (b_L > b > b_M) \quad (4.5a)$$

$$S = 1 \quad (b > b_L) \quad (4.5b)$$

with depth  $b$  below the ground surface and free LNAPL extending from  $b_M$  to the "LNAPL table" at depth  $b_L$  below the ground surface, as sketched in Figure 4.2. The latter parameter marks the surface of free product in a monitoring well.

The pore size uniformity exponent appearing in Equation 4.5 is  $\alpha_p$  and the LNAPL scaling factor  $\beta_L$  is related to the mean pore radius  $r_M$  by the capillary equation [Streeter and Wylie (1979)] for presumed circular pores and a small contact angle

$$\beta_L = \frac{\rho_L g r_M}{2\sigma_{LA}} \quad (4.6a)$$

$$\sigma_{WA} = \sigma_{LA} + \sigma_{WL} \quad (4.6b)$$

with aviation gasoline density  $\rho_L$  and gravitational acceleration  $g$ . The water/air surface tension  $\sigma_{WA}$  is equal to the sum of the water/LNAPL tension  $\sigma_{WL}$  and so long as dissolved hydrocarbons do not appreciably alter the interfacial chemistry of the water [Lenhard and Parker (1990)].

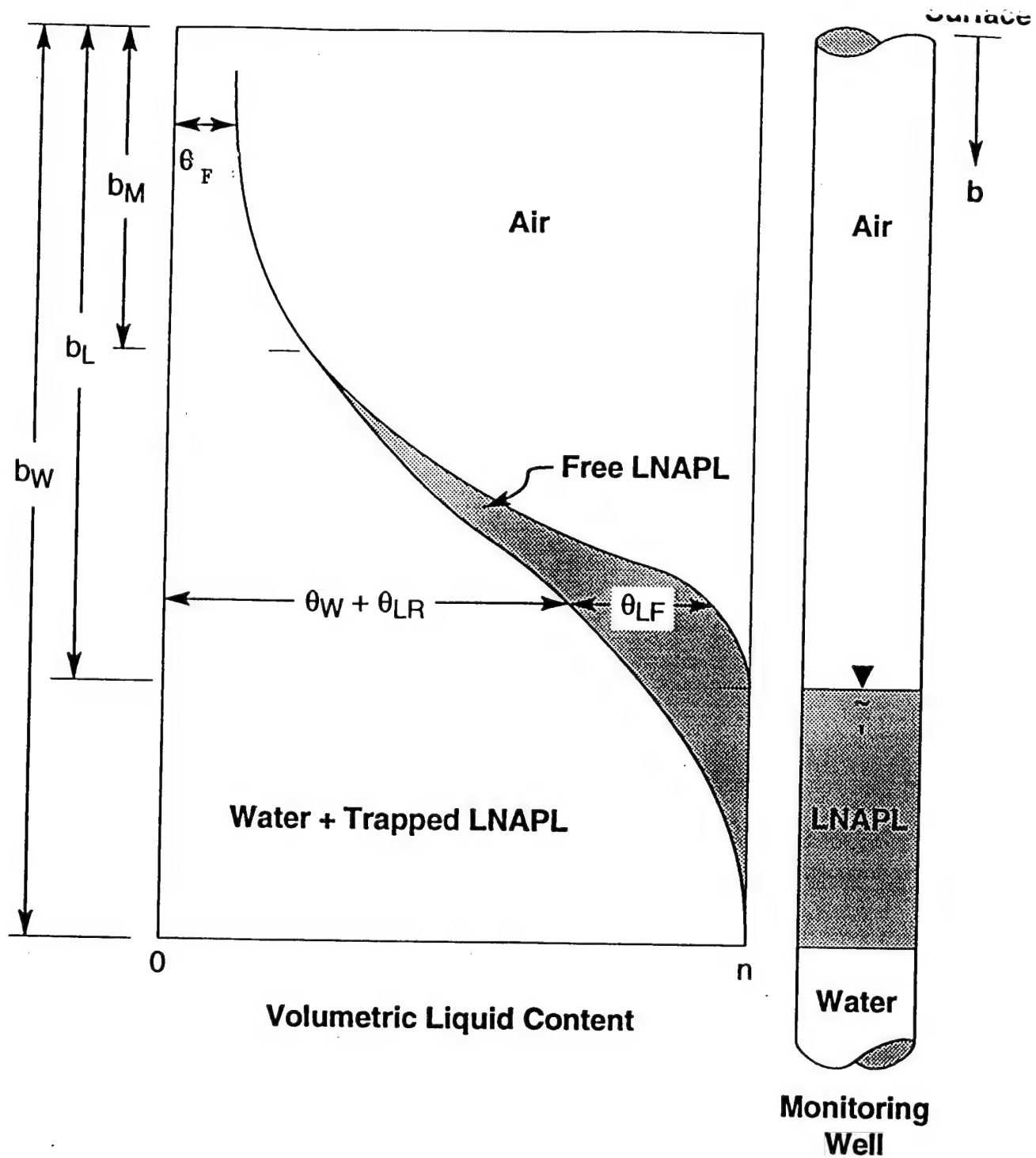


**Figure 4.2 Definition Sketch for Three Phase Fluid Distribution in Soil**

The apparent effective water saturation is scaled by the LNAPL/water surface tension in the presence of free oil, with a capillary pressure differential across the interface of the two fluids

$$S_w = \{1 + [\beta_w(b_w - b)]^{\alpha_p}\}^{1/\alpha_p - 1} \quad (b_w > b > b_M) \quad (4.7a)$$

$$S_w = 1 \quad (b > b_w) \quad (4.7b)$$

with distance to the water table  $b_w$  delineating the thickness  $(b_w - b_L)$  of free product in a monitoring well. The scaling factor  $\beta_w$  is given by Lenhard and Parker (1990) as

$$\beta_w = \beta_L \frac{(\frac{\rho}{\rho_L} - 1)\sigma_{LA}}{\sigma_{WL}} \quad (4.8)$$

with water density  $\rho$ . The free LNAPL persists until the depth  $b_M$ , determined by setting  $S_w$  and  $S$  equal in Equations 4.5a and 4.7a with the result

$$b_M = \frac{\beta_L b_L - \beta_w b_w}{\beta_L - \beta_w} \quad (4.9a)$$

$$p_{WM} = \rho g \varepsilon - \rho_L g (b_w - b_L) \quad (4.9b)$$

$$\varepsilon = b_w - b_M \quad (4.9c)$$

Lenhard and Parker (1990) demonstrate that the water matrix pressure  $p_{WM}$  at this depth is equal to the value cited in Equation 4.9b. The distance  $b_w - b_M$  corresponds to the free LNAPL contaminated soil interval  $\varepsilon$ .

The total saturation and water saturation are coincident above  $b_M$  as suggested by Figure 4.2, and are governed by the water/air tension and the water matrix pressure  $p_w$ . We impose a continuous  $p_w$  constraint at  $b_M$  and deduce an expression for the apparent effective water saturation in the shallower region from Equations 4.6a and 4.9b

$$p_w = p_{WM} + \rho g (b_M - b) \quad (4.10a)$$

$$S_w = (1 + \{ \frac{\beta_L \sigma_{LA}}{\sigma_{WA}} [b_L - b_w + \frac{\rho}{\rho_L} (b_w - b)] \}^{\alpha_p})^{1/\alpha_p - 1} (b_M > b) \quad (4.10b)$$

Equations 4.7a and 4.10b match at  $b_M$  by virtue of Equations 4.8 and 4.9a, ensuring a continuous water saturation profile as well.

The free water and free LNAPL profiles reflect the positions of the LNAPL and water tables at the time of sampling, in contrast to the trapped LNAPL, which is a function of historical fluctuations of these parameters.

#### 4.2.3 LNAPL Entrapment

The residual LNAPL is thought to be the result of hysteretical trapping of JP4 jet fuel as it falls and rises through the water wet soil over a fluctuating water table. The residual LNAPL

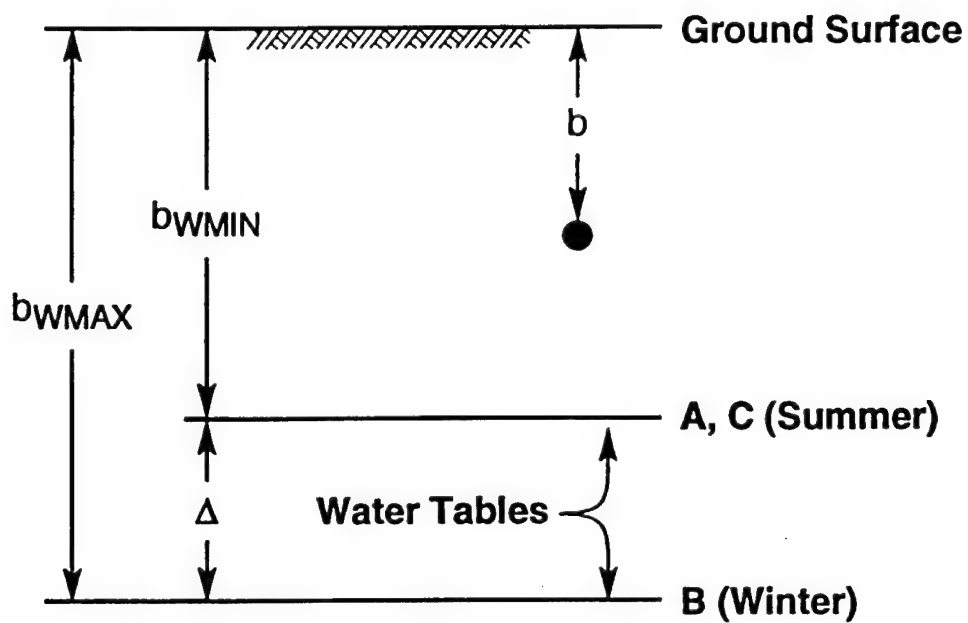
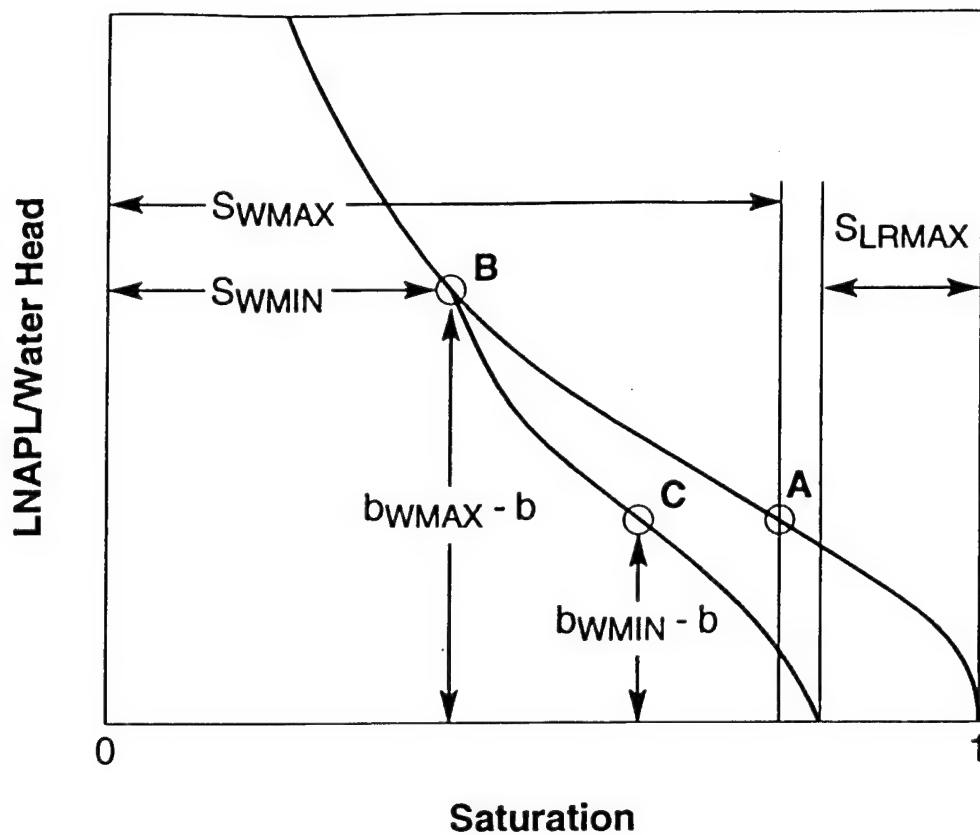


Figure 4.3 Conceptual Diagram of Hysteretical Trapping of LNAPL

saturation  $S_{LR}$  reflects the fraction of the drainable pore space that is filled by discontinuous masses of JP4 jet fuel left behind by the process

$$S_{LR} = \frac{\theta_{LR}}{n - \theta_F} \quad (4.11)$$

Parker and Lenhard (1987) suggest that the residual product distribution is governed by the position of the LNAPL/water interface, as tracked by the water saturation and LNAPL/water capillary pressure differential.

Figure 4.3 shows the concept. Available sites at a given depth  $b$  drain as the water table drops during the fall months along path AB to its maximum depth  $b_{WMAX}$  in the winter at Plattsburgh. The minimum water saturation  $S_{WMIN}$  at this reversal point [Parker and Lenhard (1987)] is specified by Equation 4.7a, since free LNAPL is present

$$S_{WMIN} = \{1 + [\beta_w (b_{WMAX} - b)]^{\alpha_p}\}^{1/\alpha_p - 1} \quad (4.12a)$$

$$S_{WMAX} = \{1 + [\beta_w (b_{WMIN} - b)]^{\alpha_p}\}^{1/\alpha_p - 1} \quad (4.12b)$$

$$b_{WMAX} = b_{WMIN} + \Delta \quad (4.12c)$$

Some of the free LNAPL is trapped during spring imbibition as the water table rises along a drier moisture characteristic towards a summer minimum depth  $b_{WMIN}$ , defined by the fluctuation amplitude  $\Delta$ . The minimum water table depth yields a maximum water saturation  $S_{WMAX}$  (Equation 4.12b) at the given  $b$  value. The hysteretical wetting process yields a maximum trapped LNAPL saturation  $S_{LRMAX}$  if the water table rises past the depth  $b$  under consideration, as described by Parker and Lenhard (1987)

$$S_{LRMAX} = \frac{1 - S_{WMIN}}{1 + \gamma(1 - S_{WMIN})} \quad (4.13)$$

with the hysteretical factor  $\gamma$  geometrically defined by the primary drainage and imbibition curves. In the absence of detailed field data describing the primary moisture characteristics,  $\gamma$  is calibrated in this study from observed maximum residual saturation data at the site.

Those elevations higher than the minimum water table depth attained during trapping experience occluded masses less than the maximum, in accordance with Parker and Lenhard's (1987) empirical relationship

$$S_{LR} = S_{LRMAX} \left(1 - \frac{1 - S_{WMAX}}{1 - S_{WMIN}}\right) \quad (b < b_{WMIN}) \quad (4.14a)$$

$$S_{LR} = S_{LRMAX} \quad (b_{WMIN} < b < b_{WMAX}) \quad (4.14b)$$



$$S_{LR} = 0 \quad (b_{WMAX} < b) \quad (4.14c)$$

$$S_{LR} = 0 \quad (b < b_{MR}) \quad (4.14d)$$

Equation 4.12c reflects our concern with an LNAPL, which floats on the heavier water, and so is not present below the water table. Free LNAPL must exist at a given location in order for trapping to occur, so that occluded product does not exist above the minimum free product depth  $b_{MMIN}$ .

### 4.3 Analytical Soil Gas Transport Models

#### 4.3.1 Model Overview

We model the transport of soil gas constituents between the top of the capillary fringe at  $z$  equals  $-b_F$  to the ground surface at  $z$  equals 0. Oxygen, helium, carbon dioxide, total hydrocarbon, and trichloroethylene vapor concentrations are considered, as defined by  $X$ ,  $H$ ,  $C$ ,  $G$ , and  $Y$

$$C = \frac{\text{mass} \cdot \text{CO}_2}{\text{volume} \cdot \text{soil} \cdot \text{gas}} \quad (m_C = 0.044 \text{ kg/mole}) \quad (4.15a)$$

$$G = \frac{\text{mass} \cdot \text{total} \cdot \text{hydrocarbon} \cdot \text{vapors}}{\text{volume} \cdot \text{soil} \cdot \text{gas}} \quad (m_G = 0.114 \text{ kg/mole}) \quad (4.15b)$$

$$H = \frac{\text{mass} \cdot \text{He}}{\text{volume} \cdot \text{soil} \cdot \text{gas}} \quad (m_H = 0.004 \text{ kg/mole}) \quad (4.15c)$$

$$X = \frac{\text{mass} \cdot \text{O}_2}{\text{volume} \cdot \text{soil} \cdot \text{gas}} \quad (m_X = 0.032 \text{ kg/mole}) \quad (4.15d)$$

$$Y = \frac{\text{mass} \cdot \text{TCE}}{\text{volume} \cdot \text{soil} \cdot \text{gas}} \quad (m_Y = 0.130 \text{ kg/mole}) \quad (4.15e)$$

The molar masses  $m$  cited in Equation 4.15 reflect the chemical composition of the vapor--the assumed JP4 jet fuel value corresponds to the molecular weight of volatile alkanes and aromatics.

We consider steady pneumatics and transient gaseous contamination in vertical and cylindrical coordinates. The air porosity is assumed to be uniform, so that the effect of infiltration on the flow of air and contaminants is neglected. Advection and gaseous diffusion are included in the transport model, along with stoichiometrically coupled, first order vapor

reaction rates for oxygen, carbon dioxide, and total hydrocarbons. Trichloroethylene reactions are considered, but on a decoupled basis, since total hydrocarbons are taken as the primary substrate of biodegradation. Helium is used as an abiotic tracer in the modeling efforts, and no reactions disturb its transport. Adsorption is neglected, on the premise of low organics and sandy soil in a moist climate.

#### 4.3.2 Pneumatics

We consider the steady airflow induced by soil venting near the capillary fringe or air sparging at a point below the water table. The volumetric soil gas discharge  $Q$  is taken as a constant in either case, neglecting transience and the effect of temperature on air density

$$Q = \text{const} \quad (\text{no boundary}) \quad (4.16a)$$

$$Q = 0 \quad (\text{ambient}) \quad (4.16b)$$

This discharge is assumed to be injected into the subsurface at the capillary fringe edge  $b_F$  below the ground surface, and the air flows spherically away from this point in the  $r'$  direction

$$v_{R'} = \frac{Q}{2\pi r'^2} \quad (\text{spherical direction}) \quad (4.17)$$

We note that the spherical specific discharge  $v_{R'}$  varies inversely with distance  $r'$  from the source. The discharge proceeds through a hemisphere in the unsaturated zone. This solution ignores the presence of the ground surface.

Our capillary fringe and ground surface boundaries are in the  $z$  plane however, so that a cylindrical coordinate system must be adopted, with radial distance  $r$  from the injection point and vertical distance  $b_F + z$ . These coordinates and the specific discharge components  $v$  and  $w$  are related to their spherical counterparts by

$$v = v_{R'} \frac{r}{r'} \quad (\text{radial}) \quad (4.18a)$$

$$w = v_{R'} \frac{b_F + z}{r'} \quad (\text{vertical}) \quad (4.18b)$$

$$r'^2 = r^2 + (b_F + z)^2 \quad (4.18c)$$

Equations 4.17 and 4.18 specify the spatial variation of the cylindrical specific discharge components in cylindrical coordinates in the absence of a surface boundary. We superimpose an image sink a distance  $b_F$  above the ground to simulate the zero head boundary, with the result

$$v = \frac{Qr}{2\pi} \left\{ \frac{1}{[r^2 + (b_F + z)^2]^{3/2}} - \frac{1}{[r^2 + (b_F - z)^2]^{3/2}} \right\} \quad (\text{with boundary}) \quad (4.19a)$$

$$w = \frac{Q}{2\pi} \left\{ \frac{b_F + z}{[r^2 + (b_F + z)^2]^{3/2}} + \frac{b_F - z}{[r^2 + (b_F - z)^2]^{3/2}} \right\} \quad (\text{with boundary}) \quad (4.19b)$$

### 4.3.3 Steady Ambient Diffusion and Reaction

Transport simplifies considerably in the absence of airflow and transience, since we have a one dimensional balance of gaseous diffusion and reaction in this case. We write the transport equation and boundary conditions for steady total hydrocarbon concentration  $G_S$

$$D_{GS} \frac{d^2 G_S}{dz^2} = \lambda G_S \quad (\text{ambient}) \quad (4.20a)$$

$$G_S = 0 \quad (z=0) \quad (4.20b)$$

$$G_S = G_F \quad (z=-b_F) \quad (4.20c)$$

with steady total hydrocarbon diffusivity  $D_{GS}$ , first order total hydrocarbon degradation rate  $\lambda$ , constant concentration  $G_O$  at the origin, and a zero surface condition maintained by rapid atmospheric diffusion. The solution to this homogeneous, linear second order differential equation with constant coefficients is straightforward [Rainville and Bedient (1969)]

$$G_S = G_F \frac{\sinh\left(-z\sqrt{\frac{\lambda}{D_{GS}}}\right)}{\sinh\left(b_F\sqrt{\frac{\lambda}{D_{GS}}}\right)} \quad (\text{ambient}) \quad (4.21)$$

We assume that aerobic biodegradation degrades total hydrocarbons and oxygen to carbon dioxide and water vapor in accordance with



$$\gamma_X = 3.22 \frac{\text{kg} \cdot \text{oxygen}}{\text{kg} \cdot \text{LNAPL}} \quad (4.22b)$$

$$\gamma_C = 2.70 \frac{\text{kg} \cdot \text{carbon} \cdot \text{dioxide}}{\text{kg} \cdot \text{LNAPL}} \quad (4.22c)$$

Oxygen is assumed to diffuse downward from its atmospheric value  $X_O$  at the origin. We adopt a (negative) flux  $-J_{XO}$  as a second boundary condition, hence

$$D_{XS} \frac{d^2 X_S}{dz^2} = \gamma_X \lambda X_S \quad (\text{ambient}) \quad (4.23a)$$

$$X_S = X_O \quad (z=0) \quad (4.23b)$$

$$-\theta D_{XS} \frac{dX}{dz} = -J_{XO} \quad (z=0) \quad (4.23c)$$

with steady oxygen concentration  $X_S$  and diffusivity  $D_{XS}$ . The solution to the ambient oxygen transport equation is similar to its hydrocarbon counterpart

$$X_S = X_O \cosh\left(z \sqrt{\frac{\gamma_X \lambda}{D_{XS}}}\right) + \frac{J_{XO}}{\theta \sqrt{\gamma_X \lambda D_{XS}}} \sinh\left(z \sqrt{\frac{\gamma_X \lambda}{D_{XS}}}\right) \quad (4.24)$$

Biodegradation generates carbon dioxide in the subsurface, and it diffuses upward towards a swept boundary condition. The exit flux is taken as stoichiometrically proportional to the oxygen flux consumed in the aerobic degradation process [Ostendorf et al. (1997a)]. The resulting ambient carbon dioxide transport equation is

$$-D_{CS} \frac{d^2 C_S}{dz^2} = \gamma_C \lambda C_S \quad (\text{ambient}) \quad (4.25a)$$

$$C_S = 0 \quad (z=0) \quad (4.25b)$$

$$-\theta D_{CS} \frac{dC_S}{dz} = J_{XO} \frac{\gamma_C}{\gamma_X} \quad (z=0) \quad (4.25c)$$

with steady carbon dioxide concentration  $C_S$  and diffusivity  $D_{CS}$ . The solution is given by

$$C_S = \frac{\gamma_C J_{XO}}{\gamma_X \theta \sqrt{\gamma_C \lambda D_{CS}}} \sin\left(-z \sqrt{\frac{\gamma_C \lambda}{D_{CS}}}\right) \quad (4.27)$$

Equations 4.21, 4.24, and 4.27 constitute a stoichiometrically coupled system of steady state soil gas profiles describing aerobic transport in the unsaturated zone.

#### 4.3.4 Steady Advection and Diffusion

Helium is injected at a constant rate  $QH_{\text{INJ}}$  in a series of field tracer experiments, with injection line concentration  $H_{\text{INJ}}$ . The transport approaches a steady balance of advection and diffusion in spherical coordinates

$$2\pi r'^2 (v_{R'} H_S - \theta D_{\text{HS}} \frac{dH_S}{dr'}) = QH_{\text{INJ}} \quad (\text{steady}) \quad (4.28a)$$

$$H_S = 0 \quad (r' = \infty) \quad (4.28b)$$

with steady helium concentration  $H_S$  and diffusivity  $D_{\text{HS}}$ . We invoke steady pneumatics (Equation 4.17) and derive a general solution to this nonhomogeneous, linear, first order differential equation with variable coefficients [Rainville and Bedient (1969)]

$$H_S = H_{\text{INJ}} [1 - \exp(\frac{-Q}{2\pi\theta D_{\text{HS}} r'})] \quad (\text{steady}) \quad (4.29a)$$

$$H_S = H_{\text{INJ}} \quad (r' = 0) \quad (4.29b)$$

The steady helium concentration approaches  $H_{\text{INF}}$  at a given radius as  $Q$  increases and advection dominates.

#### 4.3.5 Unsteady Spherical Advection

The unsteady spherical transport of helium is a balance of storage and advection

$$2\pi r'^2 \theta \frac{\partial H}{\partial t} + \frac{\partial}{\partial r'} (2\pi r'^2 v_{R'} H) = 0 \quad (4.30)$$

This can be solved with the method of characteristics. The helium concentration is constant in a frame of reference traveling with the air molecules at speed  $v_{R'}/\theta$  away from the injection point. Equation 4.30 becomes

$$\frac{dH}{dt} = 0 \quad (4.31a)$$

$$\frac{dr'_{\text{FRONT}}}{dt} = \frac{v_{R'}}{\theta} \quad (4.31b)$$

$$\frac{dr'_{\text{FRONT}}}{dt} = \frac{Q}{2\pi r'^2_{\text{FRONT}} \theta} \quad (4.31c)$$

The front position  $r'_{\text{FRONT}}$  establishes the arrival of the source concentration  $H_F$  with time from the start of injection. We integrate Equation 4.31 and find

$$H = H_F \quad (r' < r'_{\text{FRONT}}) \quad (4.32a)$$

$$H = 0 \quad (r'_{\text{FRONT}} < r') \quad (4.32b)$$

$$r_{\text{FRONT}} = \left( \frac{3Qt}{2\pi\theta} \right)^{1/3} \quad (4.32c)$$

We use the analytical models to check the accuracy of the finite element soil gas transport model.

#### 4.4 Finite Element Soil Gas Transport Model

##### 4.4.1 Soil Gas Diffusivity Estimation

Millington's (1959) classical gaseous diffusion model is used to characterize the instantaneous hydrocarbon diffusivity  $D_G$  in terms of a free air reference value  $D_{\text{REF}}$

$$D_G = D_{\text{REF}} \left( \frac{\tau}{\tau_{\infty}} \right)^{7/4} \sqrt{\frac{m_{\text{REF}}}{m_G}} \frac{\theta^{7/3}}{n^2} \quad (4.33a)$$

$$D_{\text{REF}} = 1.90 \times 10^{-5} \frac{\text{m}^2}{\text{s}} \quad (\text{O}_2 \text{ at } 282.14^\circ\text{K}) \quad (4.33b)$$

The reference diffusivity is based on a literature value for oxygen [Weast (1967)], adjusted to the site averaged temperature at Plattsburgh. The temperature and molar mass adjustments are summarized by Reid et al. (1987)--heavy, cold gas molecules diffuse more slowly than light, warm molecules. Molar mass adjustments in Equation 4.30 yield the oxygen and carbon dioxide instantaneous diffusivities.

Equations 4.2 and 4.33a suggest that the seasonal temperature fluctuation imparts a small, depth dependence to the diffusivity. The steady state diffusivities used in ambient profiling incorporate porosity and molecular mass influences but not temperature, since the latter factor is averaged out

$$D_{\text{GS}} = D_{\text{REF}} \sqrt{\frac{m_{\text{REF}}}{m_G}} \frac{\theta^{7/3}}{n^2} \quad (4.34)$$

The steady diffusivities for oxygen ( $D_{\text{XS}}$ ), carbon dioxide ( $D_{\text{CS}}$ ), and helium ( $D_{\text{HS}}$ ) appearing in Equations 4.24, 4.27, and 4.29 follow by substituting the molar mass for oxygen and carbon dioxide into Equation 4.34.

##### 4.4.2 Finite Element Model Formulation

We model air sparging or soil venting from a point source as a transient transport process in cylindrical coordinates, featuring storage, advection, gaseous diffusion, and first order decay. The transport equation for total hydrocarbons is given by

$$\theta \frac{\partial G}{\partial t} + \frac{1}{r} \frac{\partial (vrG)}{\partial r} + \frac{\partial (wG)}{\partial z} - \frac{1}{r} \frac{\partial}{\partial r} (r\theta D_G \frac{\partial G}{\partial r}) - \frac{\partial}{\partial z} (\theta D_G \frac{\partial G}{\partial z}) = -\lambda \theta G \quad (4.35a)$$

$$\frac{\partial}{\partial r} (vrG - r\theta D_G \frac{\partial G}{\partial r}) = 0 \quad (r=0) \quad (4.35b)$$

The no flux boundary condition is imposed on the radial axis, since the source is presumed to lie on the bottom boundary of the domain. The soil gas diffusivity is allowed to vary in the transient domain as well, due to tempature dependence. We use a finite difference approximation to the temporal derivative, predicated on a known prior concentration  $G_K$  and a time step  $\Delta t$

$$\frac{\partial G}{\partial t} \cong \frac{G - G_K}{\Delta t} \quad (4.36a)$$

$$\frac{1}{r} \frac{\partial (vrG)}{\partial r} + \frac{\partial (wG)}{\partial z} - \frac{1}{r} \frac{\partial}{\partial r} (r\theta D_G \frac{\partial G}{\partial r}) - \frac{\partial}{\partial z} (\theta D_G \frac{\partial G}{\partial z}) + \lambda' \theta G = \frac{\theta G_K}{\Delta t} \quad (4.36b)$$

$$\lambda' = \lambda + \frac{1}{\Delta t} \quad (4.36c)$$

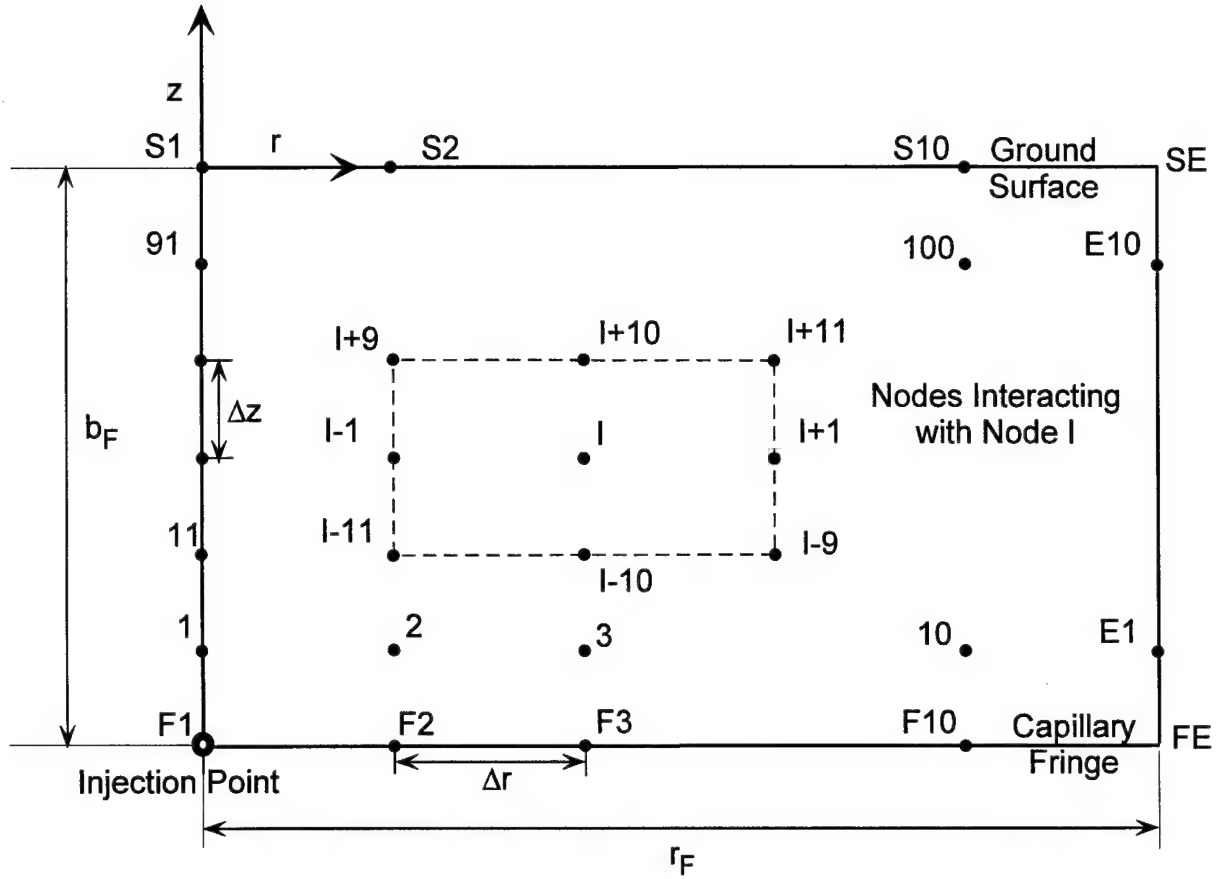
Equation 4.36 is the differential formulation of the transport problem.

We move to a variational formulation by multiplying the transport equation by a weighting function  $U(z,r)$ , then integrating over the spatial domain [Becker et al. (1981)]. In the latter regard our air flow extends from the top of the capillary fringe at  $z$  equals  $-b_F$  out to a radius of influence  $r_F$  (Figure 4.4)

$$\int_{-b_F}^0 \int_0^{r_F} \left\{ U \frac{\partial}{\partial r} [rvG - \frac{\partial}{\partial r} (r\theta D_G \frac{\partial G}{\partial r})] \right\} dr dz + \int_0^{r_F} \int_{-b_F}^0 \left\{ U \frac{\partial}{\partial z} [wG - \frac{\partial}{\partial z} (\theta D_G \frac{\partial G}{\partial z}) + \lambda' \theta G] \right\} dz dr = \int_0^{r_F} \int_{-b_F}^0 \frac{\theta U G_K}{\Delta t} dz dr \quad (4.37a)$$

$$U = 0 \quad (z=0, z=-b_F, r=r_F) \quad (4.37b)$$

The weighting function is zero on the bottom, top, and outside boundaries of the domain, while the radial flux vanishes at  $r$  equals zero. We may accordingly integrate by parts and thereby reduce the order of Equation 4.37a



Note: 100 equispaced nodes in  $r, z$  plane.

**Figure 4.4 Domain for Finite Element Model**

$$\int_0^{r_F} \int_{-b_F}^0 \left\{ \theta D_G \left( \frac{\partial U}{\partial r} \frac{\partial G}{\partial r} + \frac{\partial U}{\partial z} \frac{\partial G}{\partial z} \right) - G \left( v \frac{\partial U}{\partial r} + w \frac{\partial U}{\partial z} \right) + \lambda' \theta U G \right\} dz dr = \int_0^{r_F} \int_{-z_F}^0 \frac{\theta U G_K}{\Delta t} dz dr \quad (4.38)$$

Equation 4.38 is the variational statement of the transport problem.

Galerkin basis functions  $\phi_I$  [Becker et al. (1981)] lead to a finite element formulation. We assume that the weighting function, present, and past concentration may all be expressed as series of basis functions

$$U = \sum_N \phi_I \quad (4.39a)$$

$$G = \sum_N G_J \phi_J \quad (4.39b)$$

$$G_K = \sum_N G_K \phi_K \quad (4.39c)$$



We discretize our domain with a 10 by 10 grid of nodes at locations  $r_I, z_I$ , as indicated by Figure 4.4. The nodes are numbered sequentially outwards and are equispaced at increments  $\Delta r, \Delta z$ , so that adjacent nodes are specified by

$$r_{I+1} - r_I = \Delta r \quad (4.40a)$$

$$z_{I+10} - z_I = \Delta z \quad (4.40b)$$

The basis functions are pyramids that equal unity on the nodes and vanish elsewhere, so that  $G_J$  and  $G_K$  are the concentrations (present and past) on the nodes

$$\phi_I = \left(\frac{r_{I+1} - r}{\Delta r}\right) \left(\frac{z_{I+10} - z}{\Delta z}\right) \quad (r_I < r < r_{I+1}, z_I < z < z_{I+1}) \quad (4.41a)$$

$$\phi_I = \left(\frac{r - r_{I-1}}{\Delta r}\right) \left(\frac{z_{I+10} - z}{\Delta z}\right) \quad (r_{I-1} < r < r_I, z_I < z < z_{I+1}) \quad (4.41b)$$

$$\phi_I = \left(\frac{r - r_{I-1}}{\Delta r}\right) \left(\frac{z - z_{I-10}}{\Delta z}\right) \quad (r_{I-1} < r < r_I, z_{I-10} < z < z_I) \quad (4.41c)$$

$$\phi_I = \left(\frac{r_{I+1} - r}{\Delta r}\right) \left(\frac{z - z_{I-10}}{\Delta z}\right) \quad (r_I < r < r_{I+1}, z_{I-10} < z < z_I) \quad (4.41d)$$

We note that all the terms in the transport equation contain basis function product terms that are nonzero only when the weighting node (I subscript) is within one node of the concentration nodes (J or K). Figure 4.5 displays the logic of the basis function interaction.

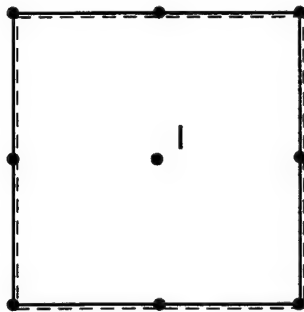
We proceed to the finite element model formulation by substituting Equation 4.39 into 4.38 and integrating term by term

$$\sum_J K_{IJ} G_J = \sum_K F_{IK} G_K + \sum \text{Boundary} \quad (I=1 \text{ to } N) \quad (4.42)$$

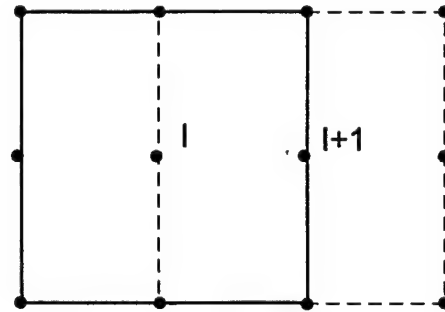
with transport and prior time step arrays  $K_{IJ}$  and  $F_{IK}$  approximated by

$$K_{IJ} = \int_{\eta-1}^{\eta+1} r \int_{z_{I-10}}^{z_{I+10}} [\theta D_{GI} \left( \frac{\partial \phi_I}{\partial r} \frac{\partial \phi_J}{\partial r} + \frac{\partial \phi_I}{\partial z} \frac{\partial \phi_J}{\partial z} \right) - v \phi_J \frac{\partial \phi_I}{\partial r} - w \phi_J \frac{\partial \phi_I}{\partial z} + \lambda' \theta \phi_I \phi_J] dz dr \quad (4.43a)$$

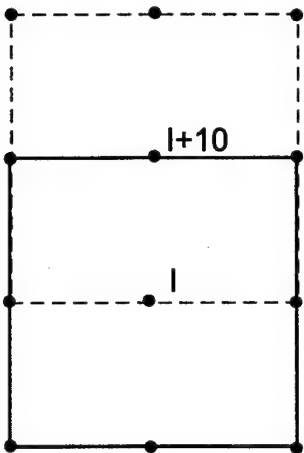
$$F_{IK} = \theta \int_{\eta-1}^{\eta+1} r \int_{z_{I-10}}^{z_{I+10}} \frac{1}{\Delta t} \phi_I \phi_K dz dr \quad (4.43b)$$



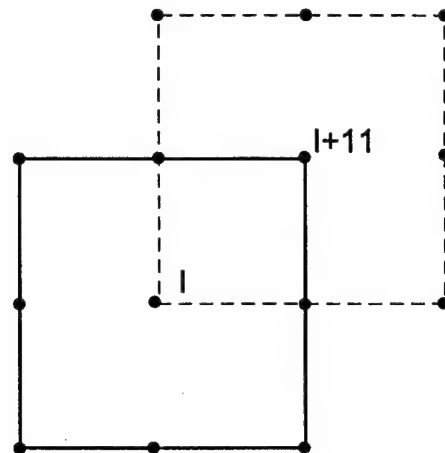
**Full Interaction ( $K_{II}$ )**



**Radial Interaction ( $K_{II+1}$ )**



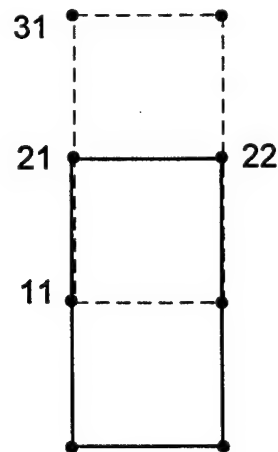
**Vertical Interaction ( $K_{II+10}$ )**



**Diagonal Interaction ( $K_{II+11}$ )**



**Full Boundary Interaction ( $K_{11,11}$ )**



**Vertical Boundary Interaction ( $K_{11,21}$ )**

**Figure 4.5 Element Interactions**

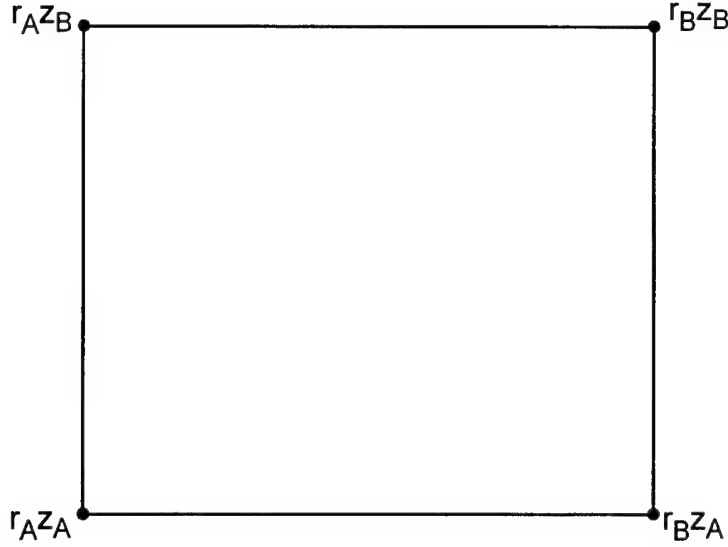


**Figure 4.6 Master Element**

The integrals in Equation 4.43 are nonzero only for similar or adjacent pairs of interacting nodes. We use the master element shown in Figure 4.6 to evaluate the contribution (e.g.,  $\Delta k_{AABB}$ ) of adjacent nodes ( $r_A, z_A$  and  $r_B, z_B$ ) to the  $K_{IJ}$  (and  $F_{IK}$ ) arrays. Basis functions may be centered on each corner of the element:

$$\phi_I = \left(\frac{r_B - r}{\Delta r}\right)\left(\frac{z_B - z}{\Delta z}\right) \quad (\text{corner AA}) \quad (4.44a)$$

$$\phi_I = \left(\frac{r - r_A}{\Delta r}\right)\left(\frac{z_B - z}{\Delta z}\right) \quad (\text{corner BA}) \quad (4.44b)$$

$$\phi_I = \left(\frac{r_B - r}{\Delta r}\right)\left(\frac{z - z_A}{\Delta z}\right) \quad (\text{corner AB}) \quad (4.44c)$$

$$\phi_I = \left(\frac{r - r_A}{\Delta r}\right)\left(\frac{z - z_A}{\Delta z}\right) \quad (\text{corner BB}) \quad (4.44d)$$

A similar set of equations is written for  $\phi_J$  (or  $\phi_K$ ), inserted into Equation 4.43, and integrated over the master element domain to generate  $\Delta k$ 's (and  $\Delta f$ 's)

$$\Delta k = \int_{r_A}^{r_B} \int_{z_A}^{z_B} [\theta D_{GI} \left( \frac{\partial \phi_I}{\partial r} \frac{\partial \phi_J}{\partial r} + \frac{\partial \phi_I}{\partial z} \frac{\partial \phi_J}{\partial z} \right) - v \phi_J \frac{\partial \phi_I}{\partial r} - w \phi_J \frac{\partial \phi_I}{\partial z} + \lambda' \theta \phi_I \phi_J] dz dr \quad (4.45a)$$

TABLE 4.1 MASTER ELEMENT INTERACTIONS

Contribution	$r_A$	$z_A$	Contribution	$r_A$	$z_A$
$\Delta k_{AAAA}$	$r_I$	$z_I$	$\Delta k_{ABAA}$	$r_I$	$z_I - \Delta z$
$\Delta k_{BBBB}$	$r_I - \Delta r$	$z_I - \Delta z$	$\Delta k_{BBBA}$	$r_I - \Delta r$	$z_I - \Delta z$
$\Delta k_{ABAB}$	$r_I$	$z_I - \Delta z$	$\Delta k_{BBAA}$	$r_I - \Delta r$	$z_I - \Delta z$
$\Delta k_{BABA}$	$r_I - \Delta r$	$z_I$	$\Delta k_{ABBA}$	$r_I$	$z_I - \Delta z$
$\Delta k_{AABA}$	$r_I$	$z_I$	$\Delta k_{BAAB}$	$r_I - \Delta r$	$z_I$
$\Delta k_{ABBB}$	$r_I$	$z_I - \Delta z$	$\Delta k_{AABB}$	$r_I$	$z_I$
$\Delta k_{BAAA}$	$r_I - \Delta r$	$z_I$	$\Delta k_{BABB}$	$r_I - \Delta r$	$z_I$
$\Delta k_{BBAB}$	$r_I - \Delta r$	$z_I - \Delta z$	$\Delta k_{AAAB}$	$r_I$	$z_I$

$$F_{IK} = \theta \int_{\eta-1}^{\eta+1} r \int_{z_I-10}^{z_I+10} \frac{1}{\Delta t} \phi_I \phi_K dz dr \quad (4.45b)$$

Table 4.1 lists the sixteen possible interactions on the master element, along with the location of the AA corner with respect to the nodal coordinates. We use six point Gauss quadrature [Abramowitz and Stegun (1972)] to approximate the master element integrals, then combine them to generate the interior array elements

$$K_{II} = \Delta k_{AAAA} + \Delta k_{BBBB} + \Delta k_{ABAB} + \Delta k_{BABA} \quad (\text{full interaction}) \quad (4.46a)$$

$$K_{II+1} = \Delta k_{AABA} + \Delta k_{ABBB} \quad (\text{right}) \quad (4.46b)$$

$$K_{II-1} = \Delta k_{BAAA} + \Delta k_{BBAB} \quad (\text{left}) \quad (4.46c)$$

$$K_{II+10} = \Delta k_{AAAB} + \Delta k_{BABB} \quad (\text{up}) \quad (4.46d)$$

$$K_{II-10} = \Delta k_{BBBA} + \Delta k_{ABAA} \quad (\text{down}) \quad (4.46e)$$

$$K_{II+11} = \Delta k_{AABB} \quad (\text{up, right}) \quad (4.46f)$$

$$K_{II+9} = \Delta k_{BAAB} \quad (\text{up, left}) \quad (4.46g)$$

$$K_{II-9} = \Delta k_{ABBA} \quad (\text{down, right}) \quad (4.46h)$$

$$K_{II-11} = \Delta k_{BBAA} \quad (\text{down, left}) \quad (4.46i)$$

We define nonzero  $\phi_I$  basis functions on no flux boundaries, so that partial interaction occurs on the  $r$  equals zero axis. This gives rise to partial array elements, since the basis functions do not extend beyond the boundary

$$K_{II} = \Delta k_{AAAA} + \Delta k_{ABAB} \quad (I=1,11,\dots,91) \quad (4.47a)$$

$$K_{II+10} = \Delta k_{AAAB} \quad (4.47b)$$

$$K_{II-10} = \Delta k_{ABAA} \quad (4.47c)$$

A similar set of equations determines  $F_{IK}$ . There is no radial interaction between nodes at different elevations in the unsaturated zone (Figure 4.4)

$$K_{II+1} = K_{I+II} = F_{II+1} = F_{I+II} = 0 \quad (I=10,20,30,\dots,90) \quad (4.48)$$

We define boundary nodes on the top, bottom, and outside boundaries of our domain, where the weighting function must vanish and the concentration is known

$$\phi_I = 0; K_{IJ} = F_{IK} = 0 \quad (\text{boundaries}) \quad (4.49a)$$

$$G = G_{INJ} \quad (I=F1) \quad (4.49b)$$

$$G_I = G_O \quad (I=F2,F3,\dots,F10,FE) \quad (4.49c)$$

$$G_I = G_E \quad (I=E1,E2,\dots,E10) \quad (4.49d)$$

$$G_I = 0 \quad (I=S1,S2,\dots,S10,SE) \quad (4.49e)$$

The injection concentration is centered on node F1, while Equation 4.21 specifies the outside (ambient) boundary nodal concentrations  $G_E$  on nodes E1-E10. The remaining nodes on the ground surface are pure, while the ambient  $G_O$  concentration exists on the capillary fringe away from the source.

The known boundary concentration terms comprise the boundary vector  $\Sigma \text{Boundary}$  on the right hand side of Equation 4.42. The bottom boundary requires downward interaction with the source and bottom nodes

$$\Sigma \text{Boundary} = G_{INJ}(F_{IF1} - K_{IF1}) + G_{F2}(F_{2F1} - K_{2F1}) \quad (I=1) \quad (4.50a)$$

$$\Sigma \text{Boundary} = G_{FI-1}(F_{IFI-1} - K_{FI-1}) + G_{FI}(F_{IFI} - K_{IFI}) + G_{FI+1}(F_{IF+1} - K_{IF+1}) \quad (I=2..9) \quad (4.50b)$$

$$\begin{aligned} \Sigma \text{Boundary} = & G_{F9}(F_{10F9} - K_{10F9}) + G_{F10}(F_{10F10} - K_{10F10}) + G_{FE}(F_{10FE} - K_{10FE}) \\ & + G_{E1}(F_{10E1} - K_{10E1}) + G_{E2}(F_{10E2} - K_{10E2}) \quad (I=10) \end{aligned} \quad (4.50c)$$

The corner node 10 interacts with nodes on the bottom and outside boundaries, with outside concentration  $G_E$  specified by Equation 4.21. The remaining outside nodes are given by

$$\Sigma \text{ Boundary} = G_{EI-1}(F_{IEI-1} - K_{IEI-1}) + G_{EI}(F_{IEI} - K_{IEI}) + G_{EI+1}(F_{IEI+1} - K_{IEI+1}) \quad (I=20,30..90) \quad (4.51)$$

The surface boundary contributions are listed for completeness, although most terms are zero

$$\Sigma \text{ Boundary} = (0)[(F_{9IS1} - K_{9IS1}) + (F_{9IS2} - K_{9IS2})] \quad (I=91) \quad (4.52a)$$

$$\Sigma \text{ Boundary} = (0)[(F_{ISI-1} - K_{ISI-1}) + (F_{ISI} - K_{ISI}) + (F_{ISI+1} - K_{ISI+1})] \quad (I=92,93..99) \quad (4.52b)$$

$$\begin{aligned} \Sigma \text{ Boundary} = (0)[(F_{100S9} - K_{100S9}) + (F_{100S10} - K_{100S10}) + (F_{100SE} - K_{100SE})] + \\ + G_{E10}(F_{100E10} - K_{100E10}) + G_{E9}(F_{100E9} - K_{100E9}) \quad (I=100) \end{aligned} \quad (4.52c)$$

Equation 4.42 represents 100 simultaneous equations for 100 unknown nodal concentrations. We use Gauss elimination to generate  $G_j$  for each time step, starting with a known initial condition

$$G = G_K \quad (t=0) \quad (4.53)$$

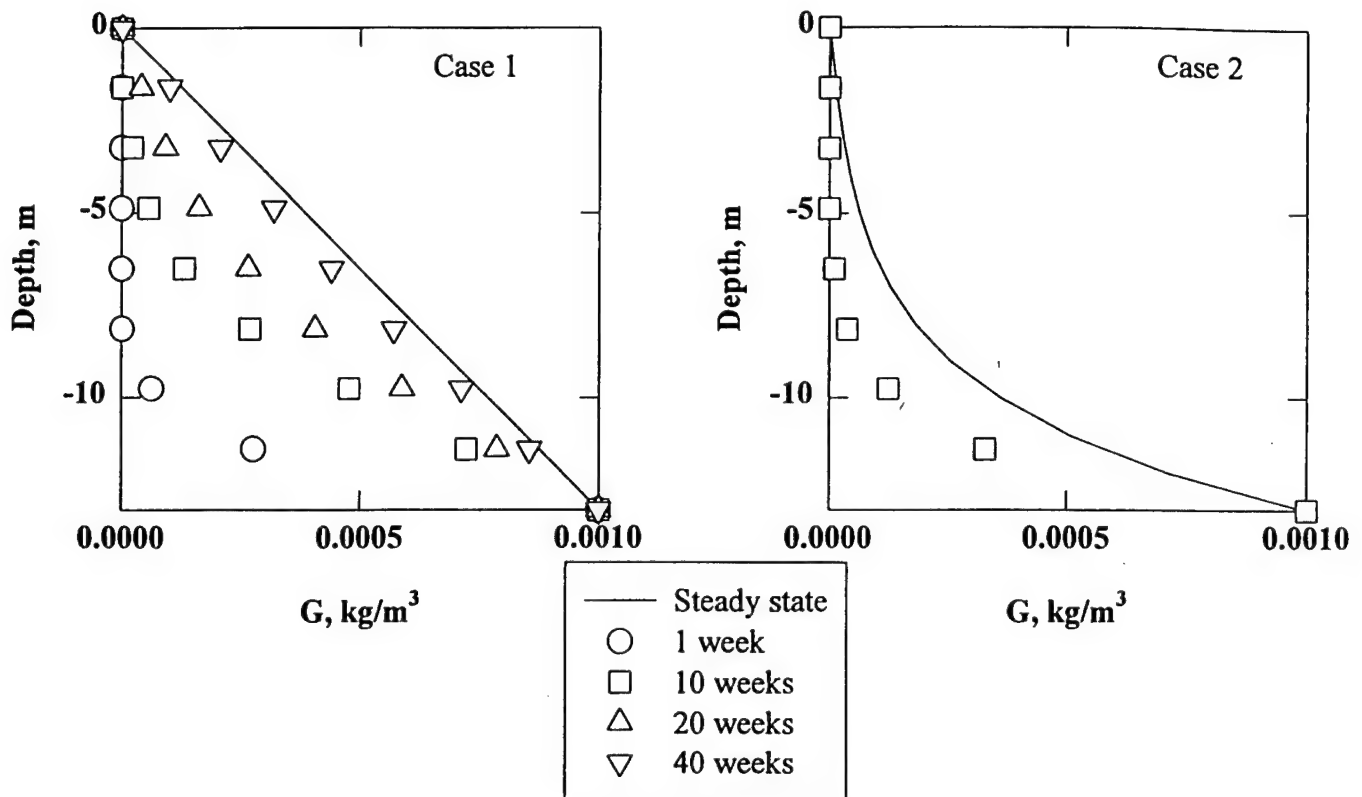
#### 4.4.3 Simulations and Sensitivity

Table 4.2 lists four simulations used to check the model accuracy as well as its sensitivity to transport parameter values. We note the following common values in the simulations:

##### Common Parameter Values for Simulations

- Initial condition  $G_K=0$
- Air porosity  $\theta = 0.288$
- Time step  $\Delta t=1$  week
- Temperature fluctuation  $\tau_M=12^\circ\text{K}$
- Average temperature  $\tau_\infty=282^\circ\text{K}$
- Phase  $\phi=0$  rad
- Thermal diffusivity  $D_T=1.74 \times 10^{-6} \text{ m}^2/\text{s}$

Cases 1 and 2 represent one dimensional diffusion of total hydrocarbon vapors from the fringe to the ground surface. Case 1 constitutes conservative transport. Since the initial condition is a pure unsaturated zone, this case also illustrates the diffusive response time  $t_{DIF}$  of the vadose zone. Figure 4.7 displays the analytical (Equation 4.21) and numerical profiles at various times. The transient profile approaches the steady, linear profile after about 40 weeks of gaseous diffusion, a slow response time reflective of the deep unsaturated zone assumed in the simulation. These results are confirmed by an order of magnitude estimate of the diffusive penetration time  $t_{DIF}$



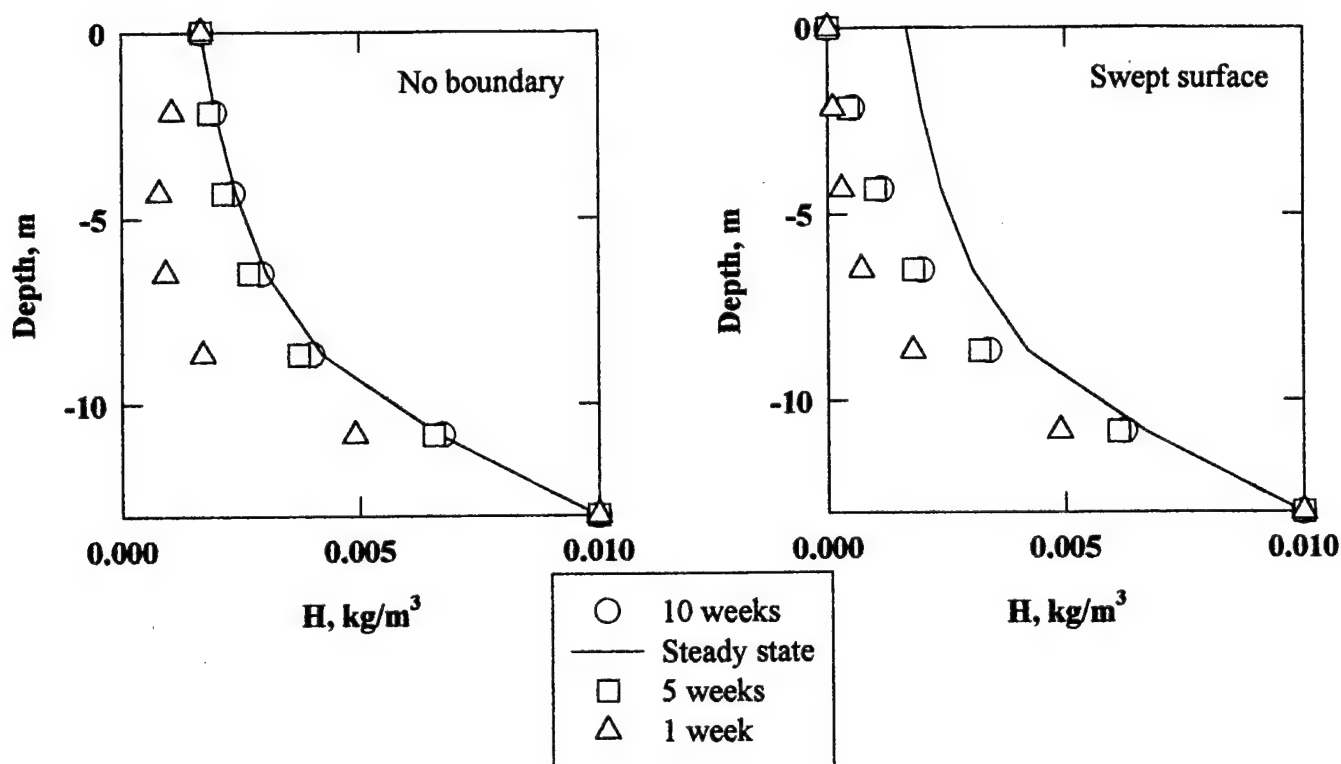
Note: Profiles computed at  $r=4.28$  m

**Figure 4.7 Steady State Analytical (Solid Curve) and Transient Finite Element (Symbols) Hydrocarbon Vapor Profiles**

$$t_{DIF} \approx \frac{b_F^2}{D_{GS}} \quad (4.54)$$

Case 2 demonstrates the role of reactions, which lower the unsaturated zone concentrations below the conservative values. Concentrations do not persist over the entire depth of the unsaturated zone under strongly reactive conditions, and the profile is nonlinear. With the unsaturated zone thickness of order 10 m and the hydrocarbon diffusivity of order  $5 \times 10^{-6} \text{ m}^2/\text{s}$  in magnitude, Eq. 4.54 suggests that vapors will diffuse to the ground surface about 30 weeks after evaporation from the capillary fringe. We include a listing of the QBASIC compute code used to simulate the no advection case in Appendix V.

Cases 3 and 4 examine the role of helium advection. A no flow boundary condition is imposed on the capillary fringe, and helium is injected at a constant rate and concentration in the lower inside node of the domain (Figure 4.4). Case 3 simulates an infinite domain (as a check on



Note: Profiles computed at  $r=0$  m

Figure 4.8 Steady State Analytical (Solid Curve) and Transient Finite Element (Symbols) Helium Vapor Profiles

TABLE 4.2 SENSITIVITY STUDY OF SOIL GAS TRANSPORT

Parameter	Case 1	Case 2	Case 3	Case 4
Contaminant	Hydrocarbons	Hydrocarbons	Helium	Helium
$\lambda, s^{-1}$	0	$5 \times 10^{-7}$	0	0
$Q, m^3/s$	0	0	0.0001	0.0001
$D_S, m^2/s$	$(D_{GS}) 4.37 \times 10^{-6}$	$(D_{GS}) 4.37 \times 10^{-6}$	$(D_{HS}) 2.33 \times 10^{-5}$	$(D_{HS}) 2.33 \times 10^{-5}$
$c_O, kg/m^3$	$(G_O) 0.001$	$(G_O) 0.001$	No flux	No flux
$c_F, kg/m^3$	0	0	$(H_{INF}) 0.01$	$(H_{INF}) 0.01$
$b_F, m$	13	13	No boundary	13
$r_E, m$	15	15	No boundary	25

the numerical model) by setting the surface and outside boundary node concentrations equal to steady state values (Equation 4.29a). Concentrations return to their steady values within a 10 weeks period for case 3, in accordance with an advective time scale (residence time)  $t_{ADV}$  computed in accordance with



$$t_{ADV} \approx \frac{4\pi\theta b_F^3}{3Q} \quad (4.55)$$

The finite element model accurately simulates the analytical model. Case 4 illustrates the effect of a swept surface on helium transport. The atmosphere increases the concentration gradient and the diffusive flux as a consequence, lowering soil gas concentrations throughout the unsaturated zone.

The advective diffusive finite element transport model computer code is listed in Appendix V.

#### 4.5 Boundary Flux Models

The near surface array and the vapor probes provide resolved vertical soil gas concentration profiles through the root zone and capillary fringe, respectively. We derive quasi steady, vertical transport models near these two boundaries to supplement the finite element code.

##### 4.5.1 Trichloroethylene Vapor Transport through the Root Zone

We model trichloroethylene vapor transport through the root zone as a quasi steady, one dimensional balance of advection, diffusion, and first order decay

$$w_O \frac{dY}{dz} - \theta D_Y \frac{d^2Y}{dz^2} = -\theta \lambda_{TCE} Y \quad (\text{near surface}) \quad (4.56a)$$

$$Y = 0 \quad (z=0) \quad (4.56b)$$

$$Y = Y_O \quad (z=-b_R) \quad (4.56c)$$

with constant near surface vertical specific discharge  $w_O$ , and first order TCE degradation rate  $\lambda_{TCE}$ . The trichloroethylene concentration approaching the root zone  $Y_O$ , and the root zone thickness is  $b_R$ .

The solution to this second order, linear, homogeneous, ordinary differential equation with constant coefficients is given by [Rainville and Bedient (1969)]

$$Y = Y_O \exp\left[\frac{w_O(z + b_R)}{2\theta D_Y}\right] \left[ \frac{\sinh\left(-\frac{w_O z}{2\theta D_Y} \sqrt{1 + \frac{4\lambda_{TCE}\theta^2 D_Y}{w_O^2}}\right)}{\sinh\left(\frac{w_O b_R}{2\theta D_Y} \sqrt{1 + \frac{4\lambda_{TCE}\theta^2 D_Y}{w_O^2}}\right)} \right] \quad (4.57)$$

#### 4.5.2 Vapor Transport near the Capillary Fringe

The transport of soil gas constituents immediately above the capillary fringe is dominated by vertical concentration gradients. We ignore reactions and radial and temporal variability, so that total hydrocarbons are described by a constant flux layer governing equation

$$w_F G - \theta D_G \frac{dG}{dz} = J_{GF} \quad (\text{near fringe}) \quad (4.58a)$$

$$G = G_F \quad (z = -b_F) \quad (4.58b)$$

with characteristic vertical specific discharge  $w_F$ , hydrocarbon concentration  $G_F$  on the capillary fringe boundary, and hydrocarbon flux  $J_{GF}$  entering the fringe. The simple solution is

$$G = \frac{J_{GF}}{w_F} + \left(G_F - \frac{J_{GF}}{w_F}\right) \exp\left[\frac{w_F(z + b_F)}{\theta D_G}\right] \quad (\text{near fringe}) \quad (4.59)$$

## 5 RESULTS

### 5.1 Soil Temperature, Grain Size Distribution, and Moisture Content

#### 5.1.1 Soil Temperature

Table 5.1 lists soil temperatures observed in the thermocouple arrays in boreholes SPK and 12AT from October 1995 to December 1996. A sinusoidal temporal variation is evident, with a phase shift and a dampened amplitude with depth. Indeed, soil insulation reduces the amplitude of the seasonal temperature fluctuation from 14 °K at the ground surface to 1.2 °K at a depth of 10 m. The time of maximum temperature at the 10 m depth lags the surface occurrence by 2.4 rads, or 139 days.

We calibrate the theory of Section 4.1 with these data, based on the following adopted parameter values:

$$\omega = 1.99 \times 10^{-7} \frac{\text{rad}}{\text{s}} \quad (\text{annual frequency}) \quad (5.1a)$$

$$\tau_{\infty} = 282.14^{\circ} \text{K} \quad (\text{average temperature}) \quad (5.1b)$$

$$\phi = 2.1 \text{ rad} \quad (\text{phase shift}) \quad (5.1c)$$

$$\text{temporal origin} = 1 \text{ September } 95 \quad (5.1d)$$

We optimize the thermal error mean  $\delta_{TM}$  and standard deviation  $\sigma_T$  by a nested Fibonacci search [Beveridge and Schechter (1979)] for thermal diffusivity and seasonal disturbance amplitude, with the error statistics defined by [Benjamin and Cornell (1970)]

$$\delta_T = \frac{\tau(\text{measured}) - \tau(\text{predicted})}{\tau_{\infty}} \quad (5.2a)$$

$$\delta_{TM} = \frac{1}{N} \sum_N \delta_T \quad (5.2b)$$

$$\sigma_T = \sqrt{\frac{1}{N} \sum_N \delta_T^2 - \delta_{TM}^2} \quad (5.2c)$$

Figure 5.1 displays the observed and calibrated temperature profiles resulting from the search, which results in the the following parameter values:

$$D_T = 1.74 \times 10^{-6} \frac{\text{m}^2}{\text{s}} \quad (5.3a)$$

**TABLE 5.1 SOIL TEMPERATURE DATA<sup>a</sup>**

Depth, m	13Oct95	2Nov95	18Nov95	2Dec95	17Jan96	7Feb96	1Mar96
SPK1-0.3	13.7	6.8	1.8	-0.1	-0.2	-5.6	-4.5
0.60	13.8	8.2	3.6	1.2	0.7	-2.9	-1.9
0.90	14.1	10.2	5.8	3.4	1.8	-0.1	-1.2
1.20	14.4	11.4	7.4	4.9	2.6	1.0	-0.5
1.50	14.5	12.1	8.4	6.1	3.2	1.7	0.0
1.80	14.7	12.4	9.3	6.8	3.7	2.3	0.5
2.10	14.7	12.9	10.2	7.9	4.7	3.1	1.3
2.40	14.8	13.2	10.8	8.7	5.3	3.6	2.1
2.70	14.7	13.2	11.3	9.4	6.0	4.2	2.6
3.00	14.4	13.3	11.6	10.0	6.6	4.7	3.2
4.60	13.3	12.7	12.1	11.3	8.5	6.9	5.7
6.10	11.6	11.2	11.1	11.1	9.6	8.2	7.3
7.60	10.4	9.7	9.9	10.3	9.6	8.7	8.1
9.10	9.6	8.9	9.2	9.6	9.3	8.6	8.2
10.7	9.3	8.3	8.5	9.1	8.7	8.0	8.0
12AT-0.6	NS <sup>b</sup>	NS	NS	0.9	0.4	-4.2	-3.4
1.20	NS	NS	NS	3.3	1.3	-0.3	-2.3
1.80	NS	NS	NS	5.7	2.8	1.6	-0.7
2.40	NS	NS	NS	7.7	4.6	3.1	1.1
3.00	NS	NS	NS	9.2	6.2	4.3	2.1
4.60	NS	NS	NS	10.7	8.3	6.6	4.5
6.10	NS	NS	NS	11.0	9.9	8.3	6.5
7.60	NS	NS	NS	10.4	10.2	9.2	7.7
9.10	NS	NS	NS	9.5	9.8	9.4	8.3

<sup>a</sup>deg C.

<sup>b</sup>Not sampled.

$$\tau_M = 14.0^\circ \text{K} \quad (5.3b)$$

The fit is excellent, as evidenced by an error standard deviation of 0.5%. The insulating effect of the soil is evident in the figure--soil temperature fluctuations are damped and delayed with increasing depth in the soil.

Table 5.2 compares the Plattsburgh thermal profile parameters with values from two sites in eastern Massachusetts [Ostendorf et al. (1995c, 1997b)]. All three profiles have a surface temperature equal to the average value at the end of April, reflecting Spring warming in the northern hemisphere. The Massachusetts average temperatures are nearly 2 °K warmer than the Plattsburgh average, due to their more southerly location. We also note that the proximity of the

TABLE 5.1 (Continued) SOIL TEMPERATURE DATA<sup>a</sup>

Depth, m	21Mar96	4Apr96	5May96	20Jun96	9Aug96	21Aug96	17Oct96
SPK1-0.3	NS <sup>b</sup>	2.9	11.0	22.3	27.5	29.9	14.0
0.60	-0.8	2.0	9.8	19.4	20.9	21.9	11.6
0.90	-1.3	0.4	8.1	17.0	19.0	20.4	12.8
1.20	0.6	0.0	6.9	15.1	17.5	19.6	13.7
1.50	0.2	0.1	6.2	13.7	16.4	18.9	14.3
1.80	1.9	0.3	6.0	12.7	15.7	18.3	14.7
2.10	3.0	0.6	5.6	11.6	14.7	17.6	14.8
2.40	3.4	1.0	5.2	10.6	13.7	16.6	15.1
2.70	3.9	1.7	5.1	9.7	12.9	16.1	15.1
3.00	4.3	2.2	4.9	8.8	12.3	15.3	14.9
4.60	6.4	4.4	5.4	6.9	9.5	12.5	13.7
6.10	8.5	6.1	6.8	6.5	7.7	10.4	11.9
7.60	9.2	7.3	7.9	7.0	7.0	9.3	10.5
9.10	9.2	7.7	8.4	7.5	6.9	8.8	14.1
10.7	9.0	7.7	8.6	7.8	6.9	6.9	9.3
12AT-0.6	-0.6	2.9	10.0	20.0	21.6	21.4	14.1
1.20	0.0	1.9	7.9	17.1	19.0	19.7	12.4
1.80	1.2	1.8	6.3	14.2	16.6	18.2	13.8
2.40	2.4	2.4	5.3	11.6	14.6	16.8	14.6
3.00	3.1	3.3	4.9	9.8	13.1	15.4	15.1
4.60	5.6	5.5	5.0	7.9	10.4	12.6	14.3
6.10	8.0	7.3	6.3	7.2	8.6	10.2	12.9
7.60	9.3	8.6	7.9	7.6	7.9	9.1	11.4
9.10	9.3	9.1	8.9	8.4	7.9	8.7	10.4

<sup>a</sup>deg C.

<sup>b</sup>Not sampled.

ocean moderates the fluctuation amplitude at the coastal sites, so that the Plattsburgh  $\tau$  is higher than the Massachusetts values. The calibrated thermal diffusivity for Plattsburgh is comparable to the sandy site value at Plymouth, and somewhat larger than the silty sand  $D_T$  for Boston. This finding is consistent with Hillel (1982), who notes that finer grained soils tend to have lower thermal diffusivities.

We substitute Equations 5.1 and 5.3 into Equation 4.2 in order to estimate temperature effects on gas concentration (through the ideal gas law) and gaseous diffusivity in the analysis of gas transport, once the moisture and grain size data have been presented.

### 5.1.2 Grain Size Distribution

**TABLE 5.1 (Continued) SOIL TEMPERATURE DATA<sup>a</sup>**

Depth, m	7Nov96	20Nov96	19Dec96	Depth, m	7Nov96	20Nov96	19Dec96
SPK1-0.3	14.1	8.7	3.0	7.60	10.7	12.1	11.0
0.60	11.0	5.2	4.0	9.10	9.8	11.1	10.0
0.90	9.1	7.4	2.0	10.7	9.2	10.4	9.0
1.20	13.6	9.1	5.0	12AT-0.6	NS <sup>b</sup>	NS	NS
1.50	11.2	10.1	6.0	13.7	9.1	6.1	4.3
1.80	11.6	11.0	6.0	12.7	11.1	8.8	5.9
2.10	12.2	11.9	7.0	11.6	12.2	10.6	7.6
2.40	12.7	12.5	8.0	10.6	12.9	11.7	8.8
2.70	12.9	12.9	9.0	9.7	13.4	12.7	10.9
3.00	13.1	13.3	9.0	8.8	12.8	12.8	11.9
4.60	13.1	13.7	11.0	11.5	9.5	12.2	12.0
6.10	11.9	13.2	11.0	10.5	7.7	10.7	11.3

<sup>a</sup>deg C.

<sup>b</sup>Not sampled.

**TABLE 5.2 THERMAL PROFILE PARAMETERS**

Reference	Location	Zero Date	Soil Type	D <sub>T</sub> , m <sup>2</sup> /s	τ <sub>M</sub> , °K	τ <sub>∞</sub> , °K
This site	Plattsburgh	30 April	Sand	1.73x10 <sup>-6</sup>	14.0	282.1
Ostendorf et al. (1995c)	Lexington, MA	3 May	Silty sand	1.11x10 <sup>-6</sup>	10.8	284.0
Ostendorf et al. (1997b)	Plymouth, MA	21 April	Sand	1.46x10 <sup>-6</sup>	12.7	283.6

We focus our efforts on the unsaturated zone, which consists of uniform coarse sand. A van Genuchten (1980) grain size distribution is fit to grain size data from 111 split spoon samples in boreholes SPK1, SPK2, and 12AY (Figure 3.1)

$$F(D) = (1 + D^{-\alpha_D})^{\frac{1}{\alpha_D} - 1} \quad (\alpha_D > 1) \quad (5.4a)$$

$$D = \frac{d}{d_M} \quad (5.4b)$$

with cumulative density function  $F(D)$ , dimensionless grain size  $D$ , dimensional grain size  $d$ , mean grain size  $d_M$ , and grain size uniformity exponent  $\alpha_D$ . The mean grain size and the uniformity exponent are varied to minimize the error mean  $\delta_{DM}$  and standard deviation  $\sigma_D$  by a nested Fibonacci search, with error statistics defined by

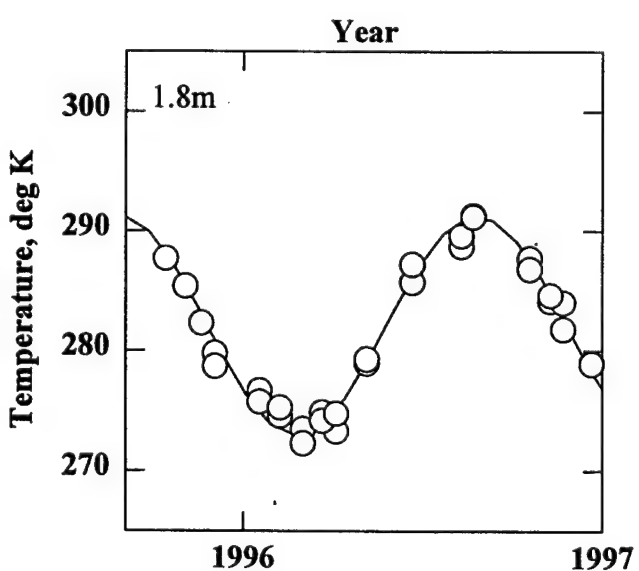
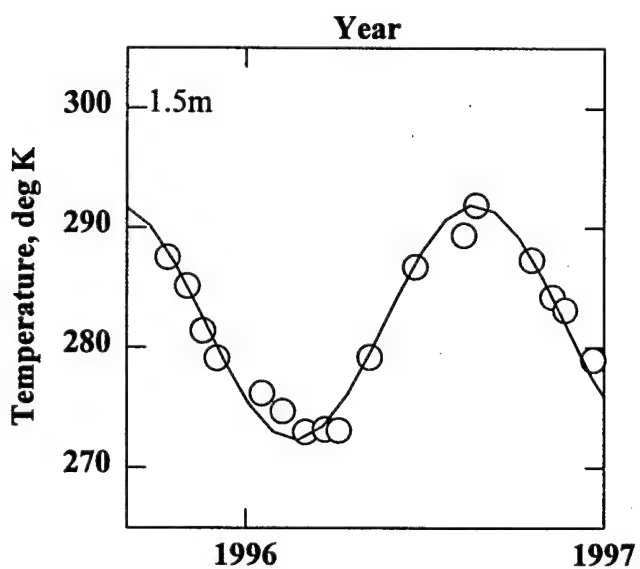
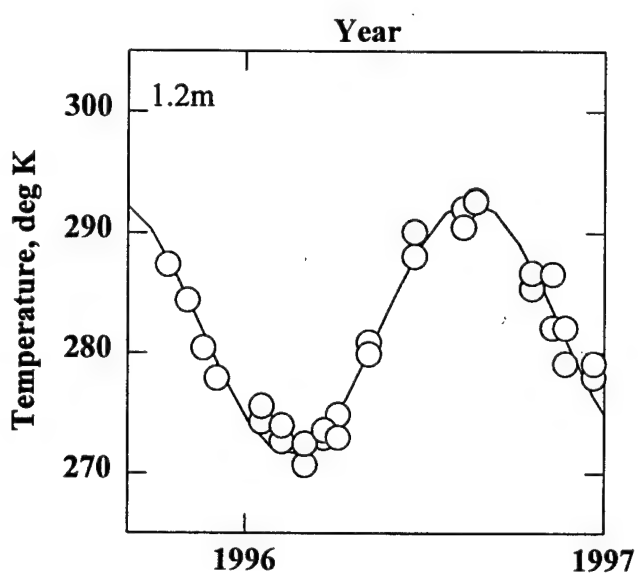
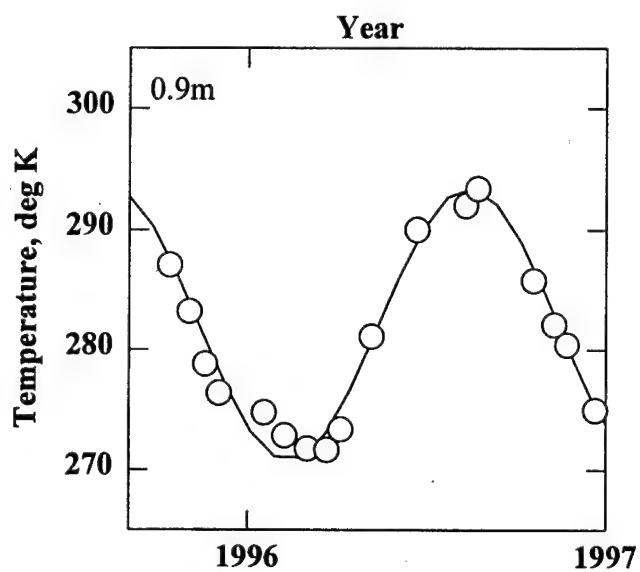
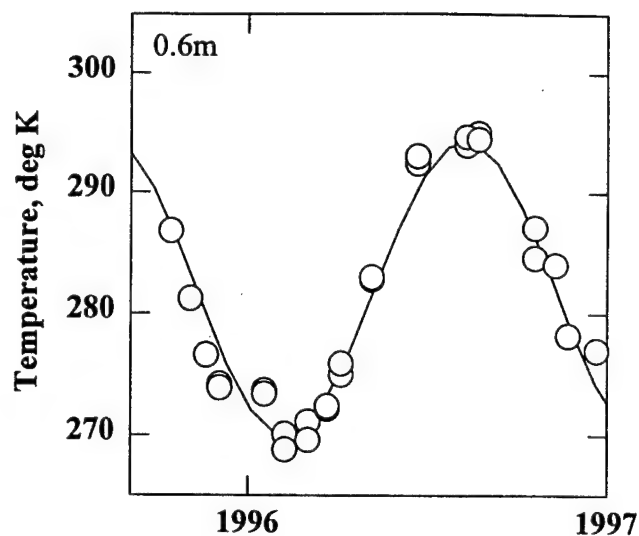
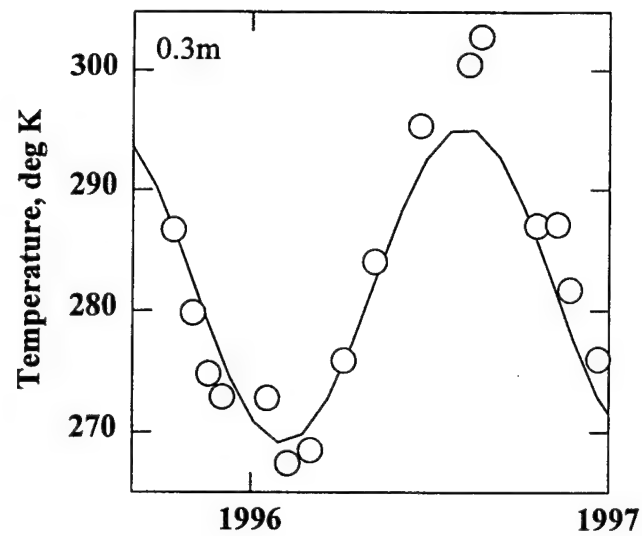


Figure 5.1 Observed (Symbols) and Calibrated (Curves) Soil Temperature

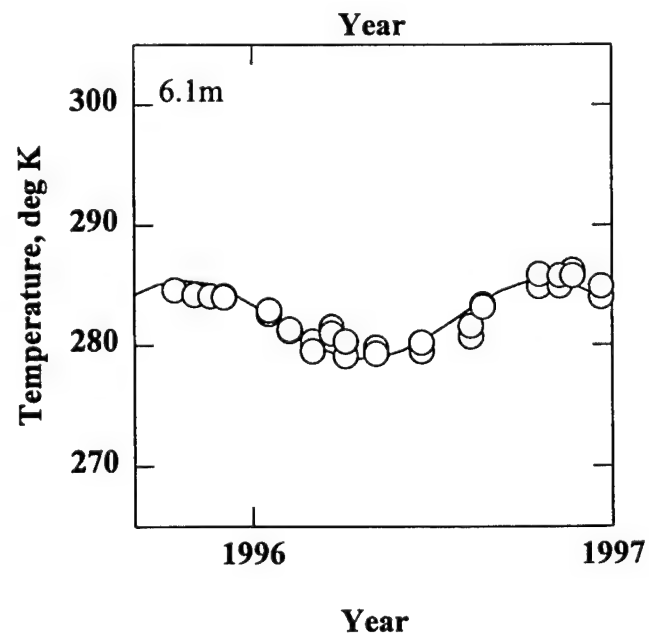
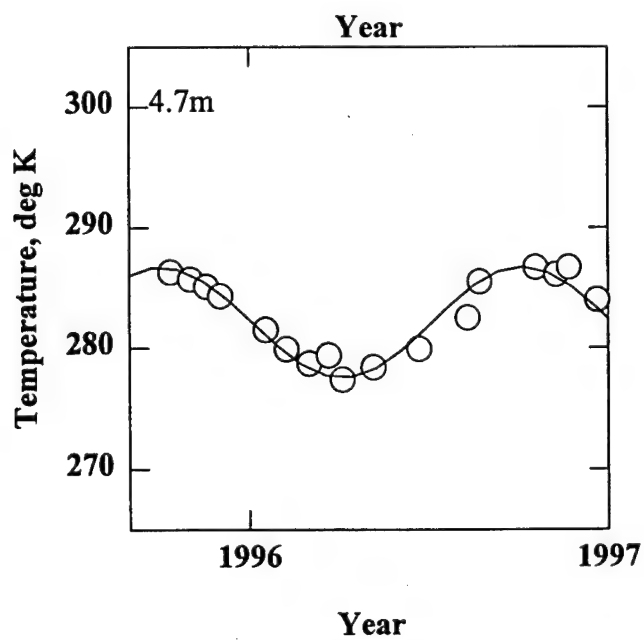
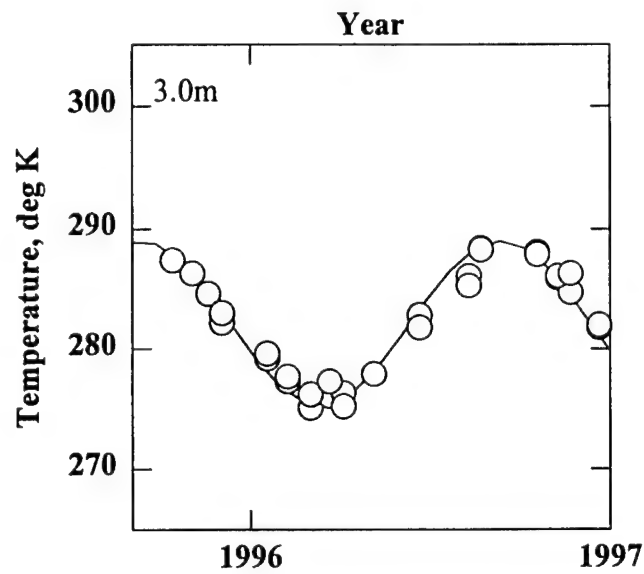
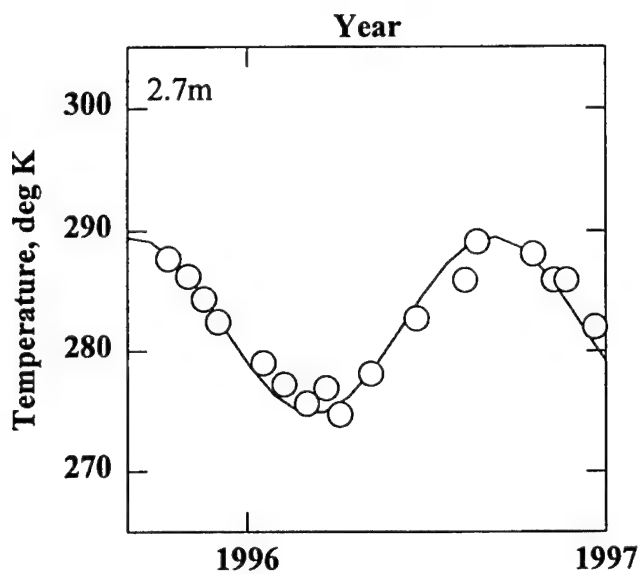
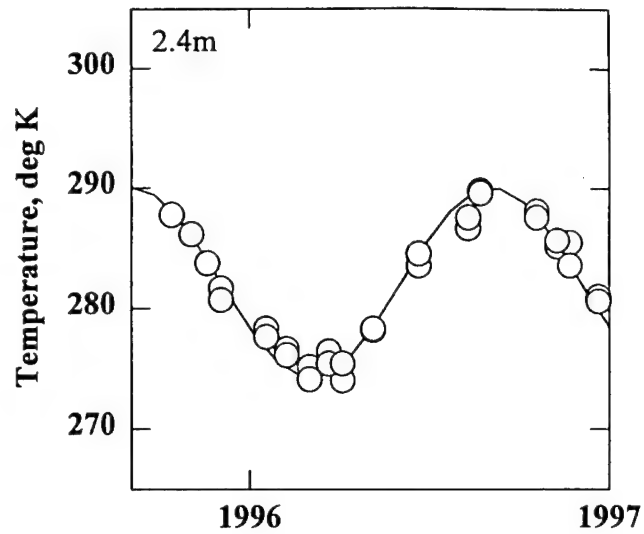
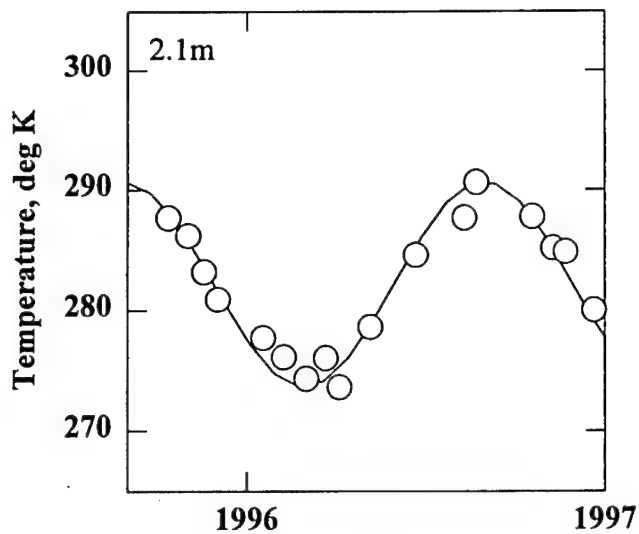
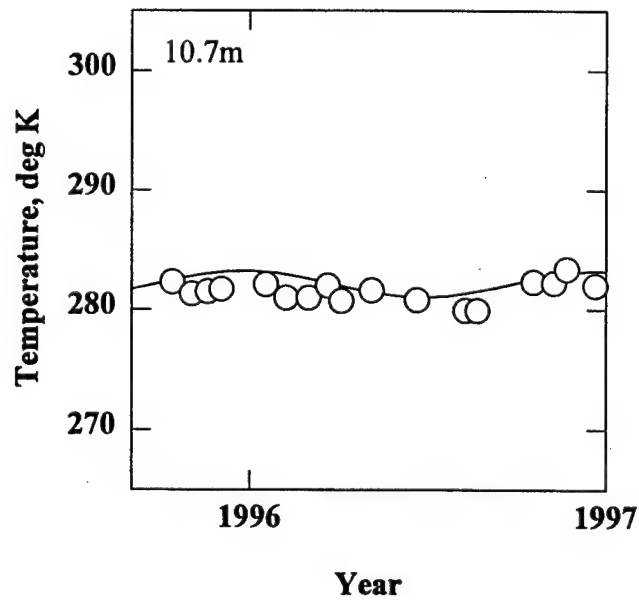
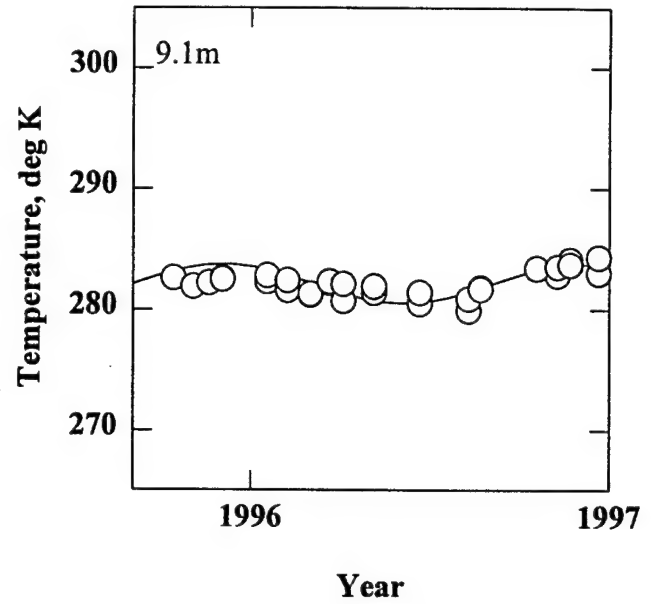
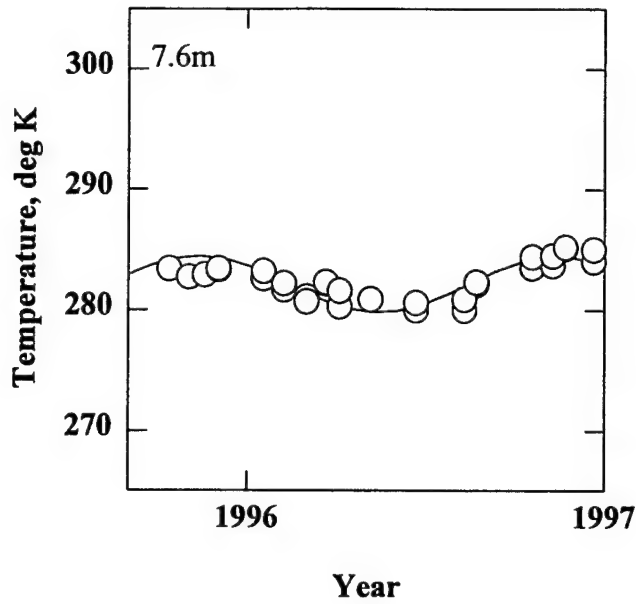


Figure 5.1 (Continued) Observed (Symbols) and Calibrated (Curves) Soil Temperature





**Figure 5.1 (Continued) Observed (Symbols) and Calibrated (Curves) Soil Temperature**

$$\delta_D = F(D)\text{measured} - F(D)\text{calibrated} \quad (5.5a)$$

$$\delta_{DM} = \frac{1}{N} \sum_N \delta_D \quad (5.5b)$$

$$\sigma_D = \sqrt{\frac{1}{N} \sum_N \delta_D^2 - \delta_{DM}^2} \quad (5.5c)$$

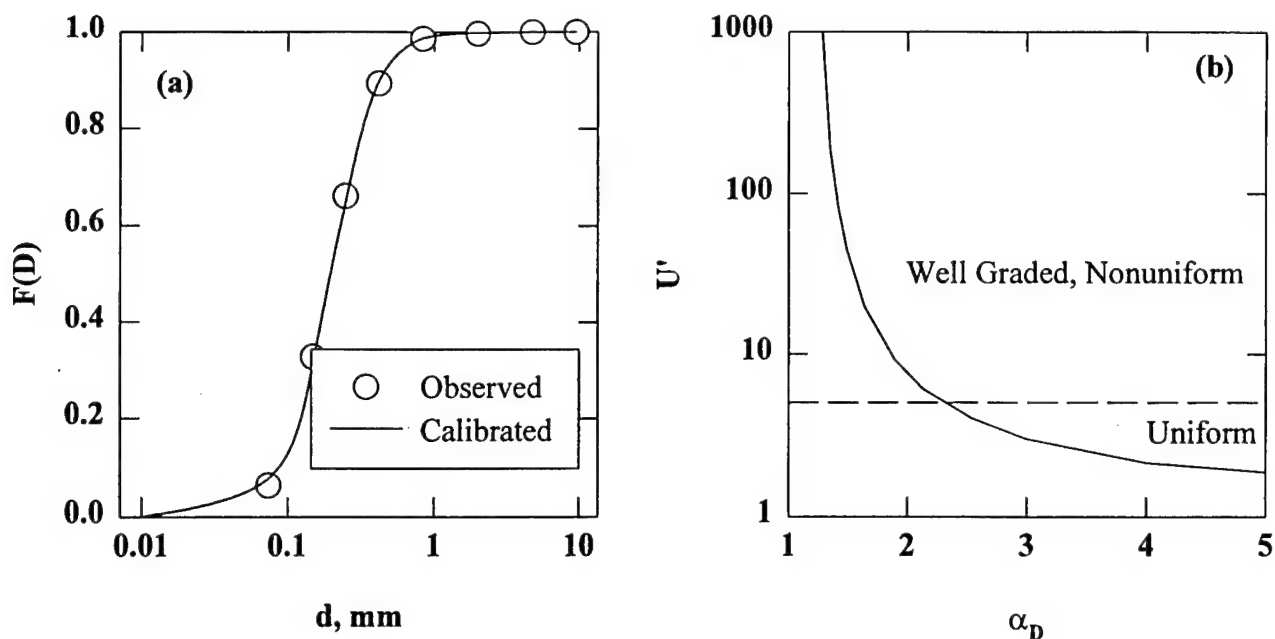


**Figure 5.2 (a) Typical Grain Size Distribution Data (Symbols) and Calibration (Curve), (b) Uniformity Coefficient  $U$  as a Function of van Genuchten (1980) Uniformity Exponent**

Typical calibration results at a particular depth are shown in Figure 5.2a (borehole SPK2, 4.34 m depth). The soil at this location is a medium sand ( $d_M=0.24$  mm) with a high uniformity exponent ( $\alpha_D=3.16$ ). In the latter regard, nearly all of the grain sizes are within one order of magnitude in size. Tables 5.3 and 5.4 list the individual calibrations for the depths in each borehole. Figure 5.3a displays the optimal uniformity exponents, which vary from 2.05 to 6.15 in borehole SPK1, 2.22 to 5.00 in borehole SPK2, and 1.56 to 5.58 in borehole 12AY, indicative of highly uniform material. Uniformity coefficients  $U'$  are also computed as a conventional measure of particle sorting [Holtz and Kovacs (1981)]

$$U' = \frac{d_{60}}{d_{10}} \quad (5.6a)$$

$$d = d_N \quad [F(D)=N/100] \quad (5.6b)$$

$$U' = \left[ \frac{(0.1)^{\frac{\alpha_D}{1-\alpha_D}} - 1}{(0.6)^{\frac{\alpha_D}{1-\alpha_D}} - 1} \right]^{\frac{1}{\alpha_D}} \quad (5.6c)$$

Equation 5.6c, which follows from Equations 5.4a and 5.6a, suggests that  $\alpha_D$  and  $U$  are inversely related, as indicated by Figure 5.2b. Uniform (poorly graded) soils have  $U$  values less than 5 in

**TABLE 5.3 VAN GENUCHTEN (1980) GRAIN SIZE CALIBRATION PARAMETERS  
BOREHOLE SPK1**

Depth, m	$d_M$ , mm	$\alpha_D$	$\sigma_D$ , %	U'	F <sub>FINE</sub> , %
0.23	0.47	3.47	3.1	2.5	4
0.69	0.79	2.65	4.5	3.6	3
1.14	0.92	2.43	7.6	4.3	3
1.60	1.59	2.05	5.7	6.8	3
2.06	0.57	3.41	1.9	2.5	1
2.52	0.56	3.21	3.7	2.7	2
2.97	0.55	3.19	1.4	2.7	2
3.43	0.58	2.92	1.8	3.1	3
3.89	0.38	2.69	1.1	3.6	8
4.34	0.42	2.75	0.7	3.4	6
4.80	0.31	2.15	1.2	5.9	17
5.26	0.28	3.06	1.1	2.9	6
5.72	0.21	3.63	3.0	2.4	7
6.17	0.16	3.44	1.7	2.5	14
6.63	0.15	6.15	5.6	1.6	15
7.09	0.23	4.07	2.5	2.1	7
7.55	0.23	4.49	2.4	1.9	5
8.00	0.16	2.93	1.6	3.1	22
8.46	0.14	4.13	1.5	2.1	12
8.92	0.19	4.10	2.1	2.1	8
9.37	0.26	3.17	3.7	2.8	10
9.83	0.39	4.51	1.2	1.9	2
10.3	0.42	4.25	1.3	2.0	3
11.2	0.37	4.78	0.9	1.9	2
11.7	0.46	3.45	2.0	2.5	5
12.1	0.46	4.85	0.5	1.8	1
12.6	0.46	4.85	0.4	1.8	1
13.0	0.41	4.54	0.8	1.9	1
13.5	0.40	4.77	2.0	1.9	2
13.9	0.38	4.70	1.0	1.9	2
14.4	0.38	3.84	2.1	2.2	4
14.9	0.39	4.67	1.0	1.9	2
15.3	0.42	4.38	0.7	2.0	1

magnitude. The U' values listed in Tables 5.2-5.4 suggest that this is the case at Plattsburgh.

Figure 5.3b displays optimal mean grain sizes for the three boreholes. The mean grain size varies from 0.14 to 1.59 mm in borehole SPK1, with an average value of 0.43 mm, corresponding to medium sand. The grain size decreases slightly with depth, a trend that is

**TABLE 5.3 (Continued) VAN GENUCHTEN (1980) GRAIN SIZE CALIBRATION  
PARAMETERS BOREHOLE SPK2**

Depth, m	$d_M$ , mm	$\alpha_D$	$\sigma_D$ , %	U'	$F_{FINE}$ , %
0.23	0.48	2.97	2.0	3.0	4
0.69	0.63	2.37	3.4	4.6	3
1.14	0.57	3.07	1.1	2.9	3
1.60	0.47	2.75	1.4	3.4	5
2.06	0.49	2.72	0.4	3.5	4
2.52	0.44	2.65	1.2	3.6	4
2.97	0.36	2.22	2.8	5.4	9
3.43	0.28	2.65	4.1	3.6	4
3.89	0.28	4.84	0.6	1.8	1
4.34	0.24	3.16	0.8	2.8	6
4.80	0.24	4.04	0.9	2.1	3
5.26	0.16	4.83	1.2	1.8	7
5.72	0.14	3.48	0.8	2.5	18
6.17	0.13	3.65	1.1	2.3	20
6.63	0.19	3.92	0.5	2.2	7
7.09	0.26	4.88	1.4	1.8	2
7.55	0.12	3.86	1.3	2.2	22
8.00	0.16	3.37	2.6	2.6	18
8.46	0.14	4.15	0.7	2.1	13
8.92	0.22	4.20	1.2	2.1	4
9.37	0.23	3.75	1.9	2.3	7
9.83	0.43	4.01	0.8	2.1	2
10.3	0.42	4.84	1.1	1.8	2
10.8	0.63	3.20	3.2	2.7	2
12.1	0.43	5.00	0.6	1.8	0

replicated in SPK2 and 12AY. The mean grain size ranges from 0.12 to 0.63 mm in borehole SPK2, with an average value of 0.33 mm. Borehole 12AY exhibits a  $d_M$  varying from 0.12 to 2.12 m in size, with an average value of 0.50 mm. We average all the data to characterize the soil in the site area as a highly uniform, medium sand

$$d_M = 0.441\text{mm} \quad (5.7a)$$

$$\alpha_D = 3.68 \quad (5.7b)$$

The observed fine fractions  $F_{FINE}$  are also listed in Tables 5.2-5.4, where

$$F = F_{FINE} \quad (d=0.074 \text{ mm}) \quad (5.8)$$

**TABLE 5.4 VAN GENUCHTEN (1980) GRAIN SIZE CALIBRATION PARAMETERS  
BOREHOLE 12AY**

Depth, m	$d_M$ , mm	$\alpha_D$	$\sigma_D$ , %	U	$F_{FINE}$ , %
0.15	0.76	2.44	6.4	4.3	3
0.46	0.61	2.46	2.4	4.2	4
0.76	0.64	2.44	3.5	4.3	4
1.07	0.77	2.54	4.9	4.0	3
1.37	0.62	3.01	4.5	3.0	3
1.68	1.73	2.06	10.6	6.7	2
1.98	2.12	1.98	7.4	7.7	2
2.29	0.60	2.70	4.9	3.5	2
2.59	1.82	2.02	8.5	7.2	3
2.90	1.87	1.56	14.6	29	5
3.20	0.38	4.04	1.0	2.1	2
3.51	0.48	3.39	0.9	2.5	3
3.81	0.49	3.07	0.9	2.9	4
4.11	0.61	3.08	0.9	2.9	2
4.42	0.45	3.34	0.9	2.6	3
4.72	0.39	3.85	0.7	2.2	2
5.03	0.34	3.25	2.1	2.7	6
5.33	0.17	2.43	0.9	4.3	27
5.64	0.34	3.81	2.8	2.2	2
5.94	0.18	3.81	1.5	2.2	7
6.25	0.18	3.89	1.4	2.2	8
6.55	0.15	3.77	1.7	2.3	11
6.86	0.14	3.20	1.7	2.7	20
7.16	0.17	5.58	3.4	1.7	7
7.47	0.22	4.97	2.2	1.8	5
7.77	0.21	3.50	1.7	2.5	9
8.38	0.12	2.67	3.2	3.6	30
8.69	0.13	3.38	0.9	2.6	23
8.99	0.18	3.67	1.8	2.3	12
9.30	0.21	4.22	2.3	2.0	5
9.60	0.24	3.69	2.9	2.3	8
9.91	0.45	4.06	0.7	2.11	2
10.2	0.45	4.04	1.3	2.1	3
10.5	0.46	3.54	1.3	2.4	3
10.8	0.61	3.35	5.7	2.6	2
11.1	0.42	3.10	1.4	2.9	5
11.2	0.39	4.57	1.7	1.9	3
11.5	0.37	4.23	1.2	2.0	3
11.7	0.37	4.06	2.3	2.1	5
11.8	0.38	4.87	0.9	1.8	2

**TABLE 5.4 (Continued) VAN GENUCHTEN (1980) GRAIN SIZE CALIBRATION  
PARAMETERS BOREHOLE 12AY**

Depth, m	d <sub>M</sub> , mm	α <sub>D</sub>	σ <sub>D</sub> , %	U'	F <sub>FINE</sub> , %
12.0	0.43	4.74	0.8	1.9	1
12.1	0.44	5.07	0.3	1.8	1
12.2	0.41	4.86	1.0	1.8	1
12.4	0.42	4.15	1.3	2.1	3
12.6	0.43	4.67	0.4	1.9	1
12.8	0.38	4.89	0.7	1.8	1
13.0	0.37	4.83	1.0	1.8	2
13.2	0.38	4.90	0.6	1.8	1
13.4	0.36	4.98	0.6	1.8	1
13.6	0.36	4.70	0.9	1.9	2

The fine fractions are also sketched in Figure 5.3c. The sand is generally clean above the 5 m depth and below the 10 m depth, with an appreciable fine fraction in between. In the latter regard, we observe F<sub>FINE</sub> values as high as 22% in the 5-10 m interval in boreholes SPK1 and SPK2. The fine fraction is as high as 30% at the 8.38 m depth in borehole 12AY.

We list the raw grain size data in Appendix III.

### 5.1.3 Moisture Content and Porosity

Figure 5.4 displays the mass based moisture content M observed in conjunction with solid core sampling from 24 boreholes throughout the study area. We can infer the volumetric based moisture content θ<sub>w</sub> from M when the porosity n is known

$$\theta_w = (1 - n)s_G M \quad (s_G=2.65) \quad (5.9a)$$

$$\theta_w = \frac{\text{moisture} \cdot \text{volume}}{\text{total} \cdot \text{volume}} \quad (5.9b)$$

$$n = \frac{\text{void} \cdot \text{volume}}{\text{total} \cdot \text{volume}} \quad (5.9c)$$

with soil specific gravity s<sub>G</sub>. We estimate the total porosity n from measured values of the soil moisture content of saturated soil samples

$$n = \left( \frac{1}{s_G M} + 1 \right)^{-1} \quad (M \text{ saturated}) \quad (5.10)$$

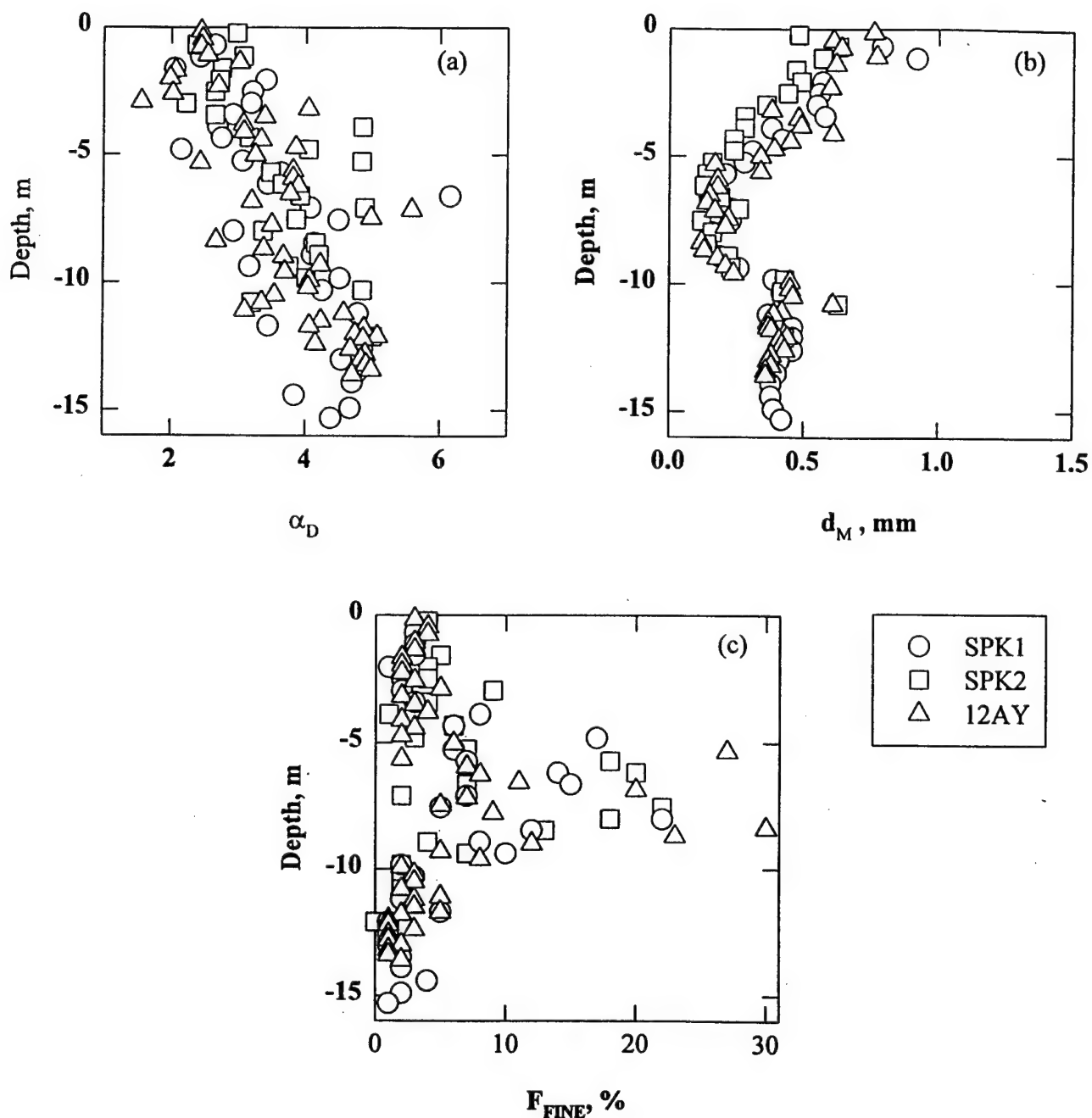
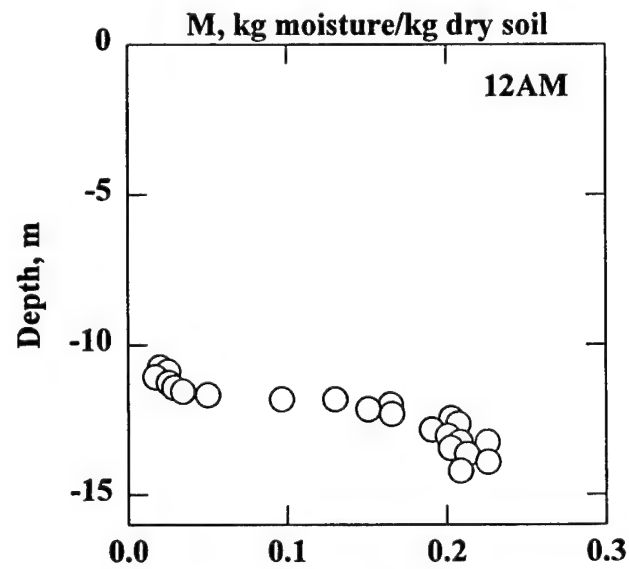
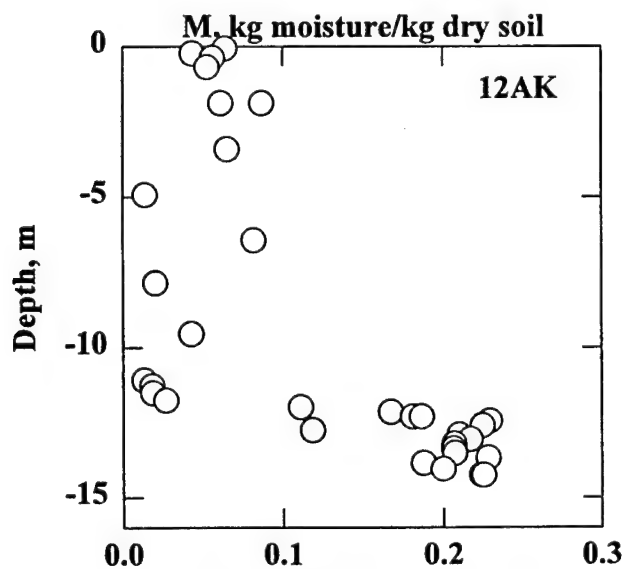
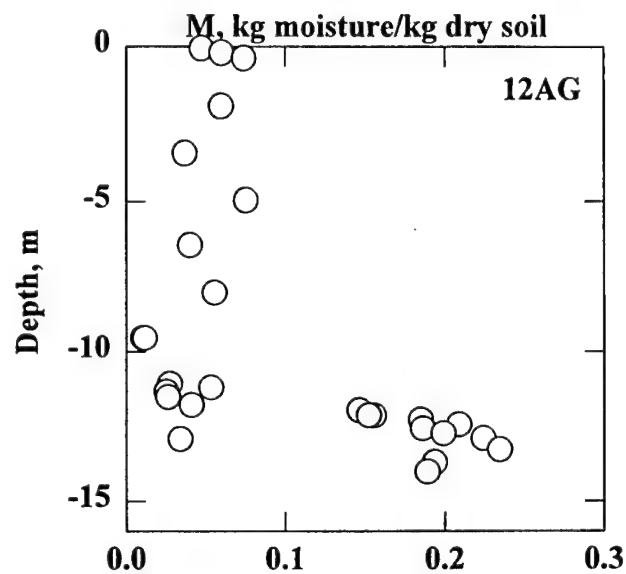
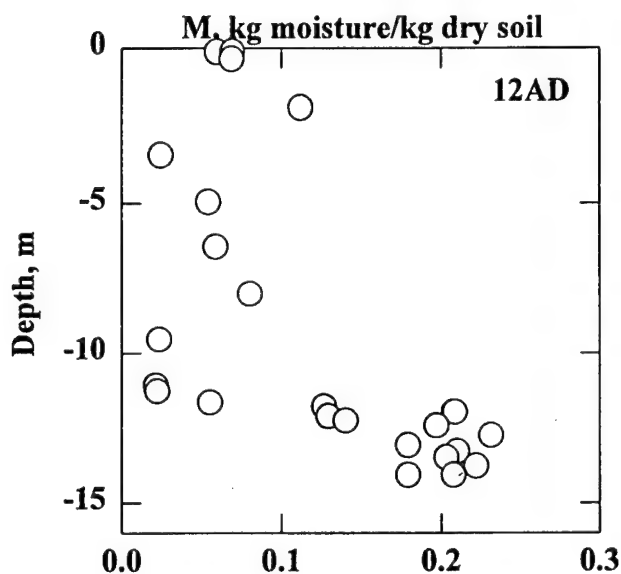
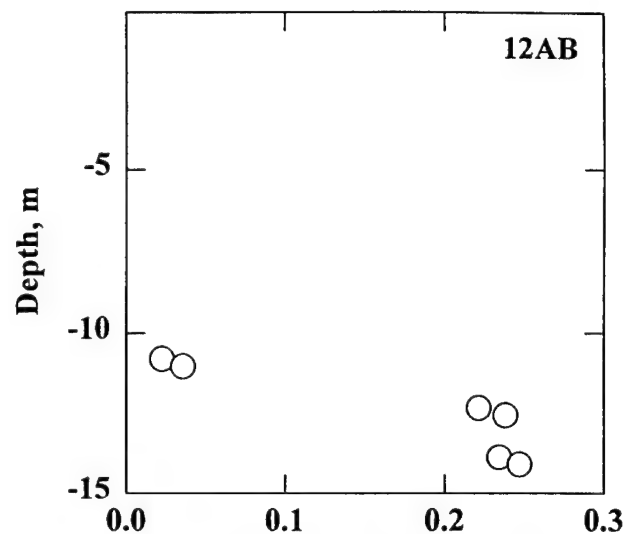
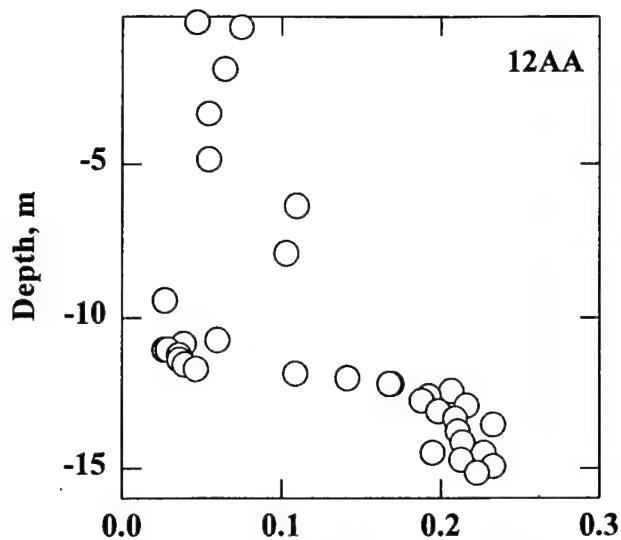


**Figure 5.3 Grain Size Calibration Parameters in Boreholes SPK1, SPK2, and 12AY: (a) van Genuchten (1980) Uniformity Exponent, (b) Mean Grain Size, (c) Fine Fraction**

We average saturated moisture contents observed in 323 samples taken below the water table from the 24 soil borings shown on Figure 5.4 with the following results

$$M = 0.209 \frac{\text{kg} \cdot \text{moisture}}{\text{kg} \cdot \text{dry} \cdot \text{soil}} \quad (\text{saturated}) \quad (5.11a)$$

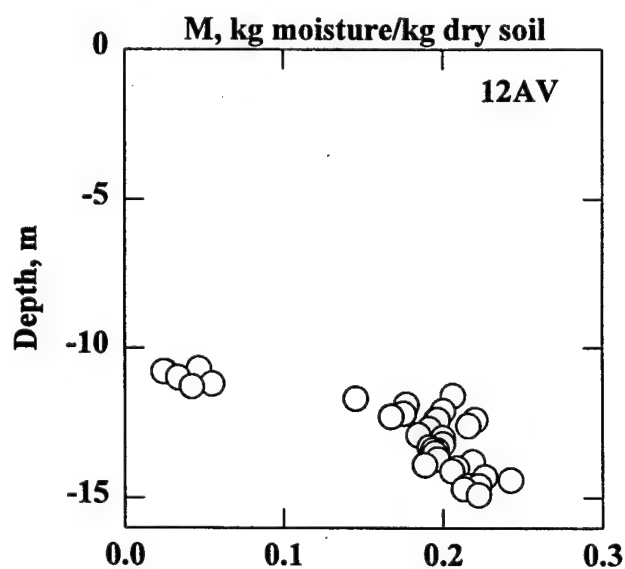
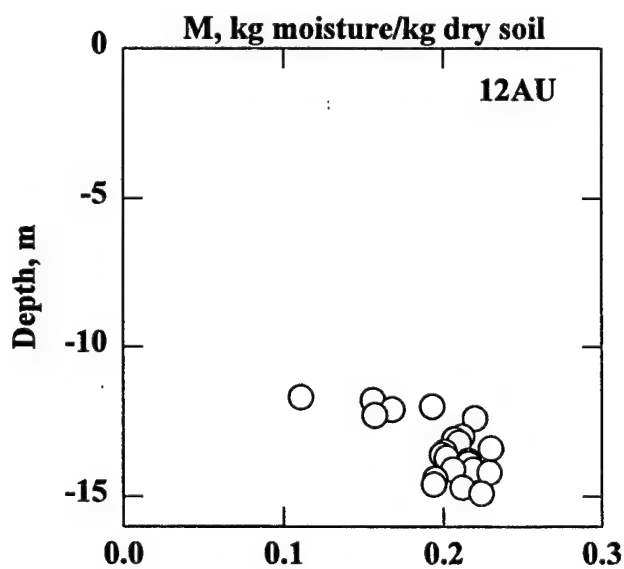
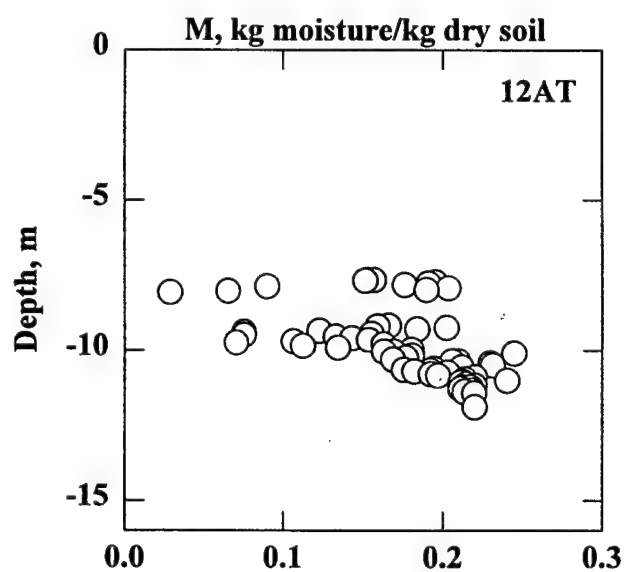
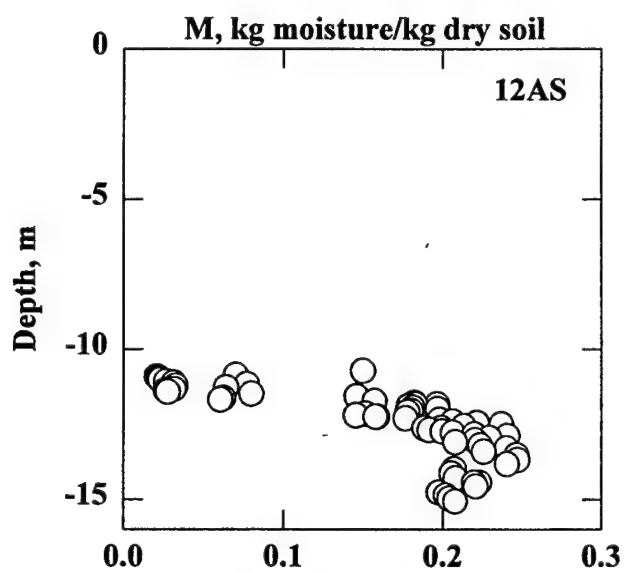
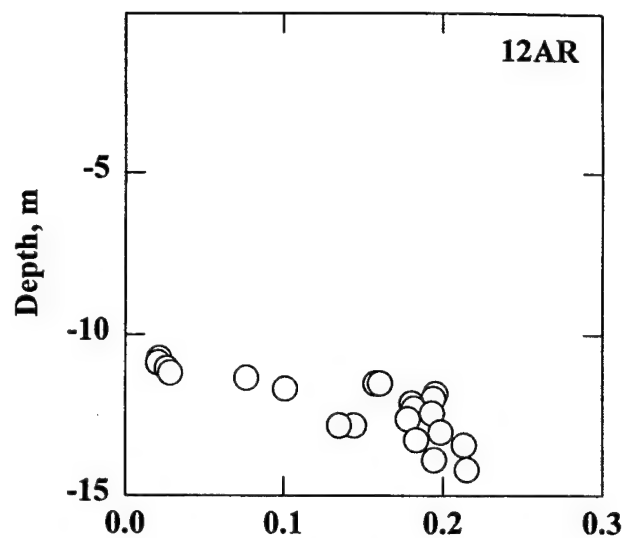
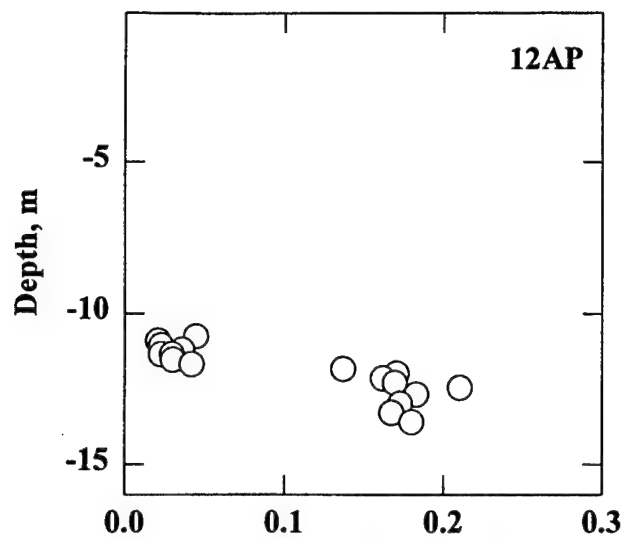


M, kg moisture/kg dry soil

M, kg moisture/kg dry soil

Figure 5.4 Observed Moisture Content in Solid Core Boreholes

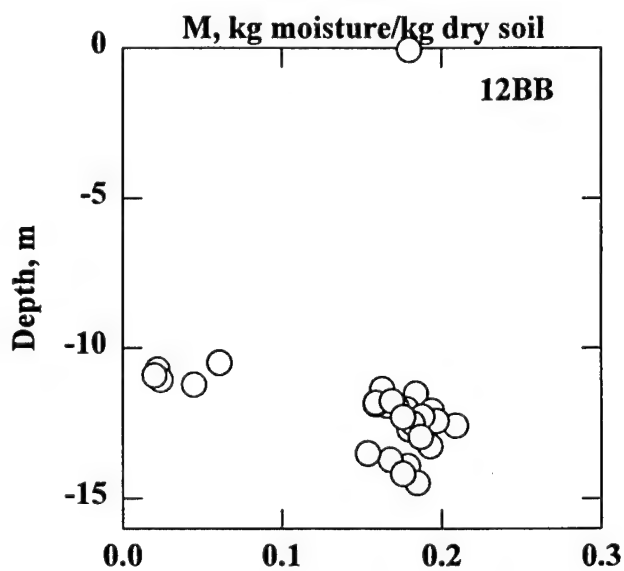
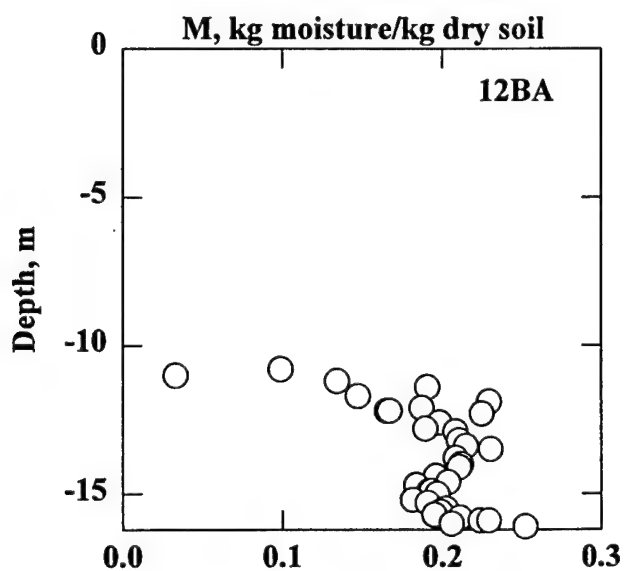
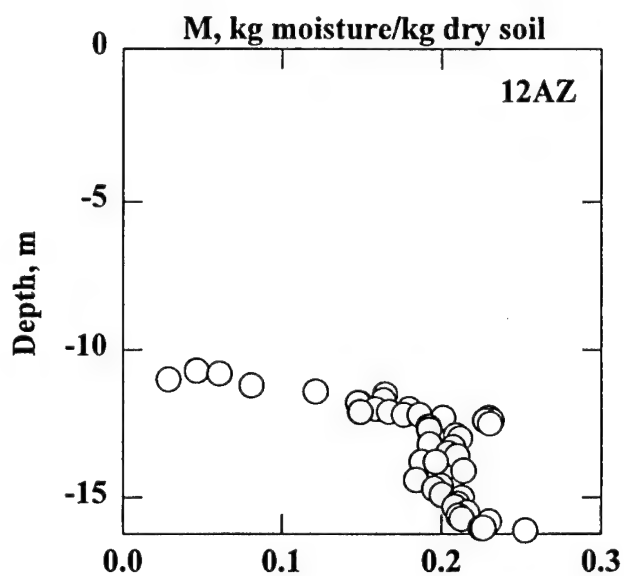
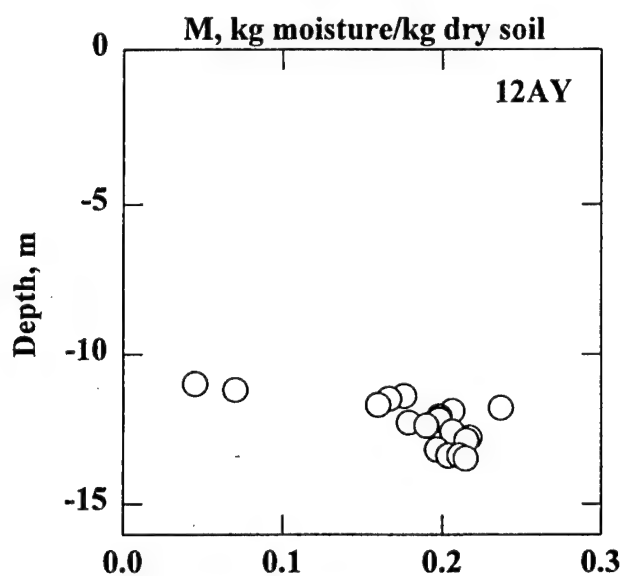
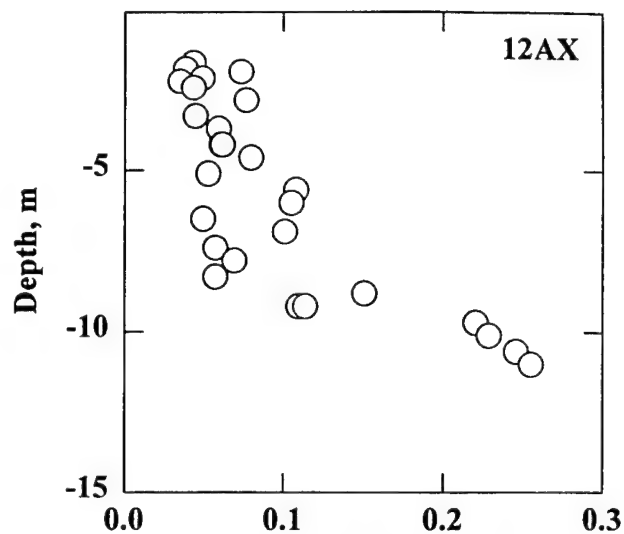
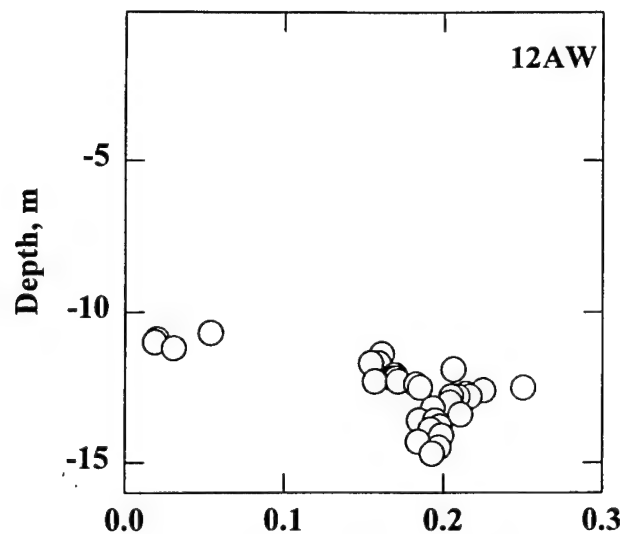




M, kg moisture/kg dry soil

M, kg moisture/kg dry soil

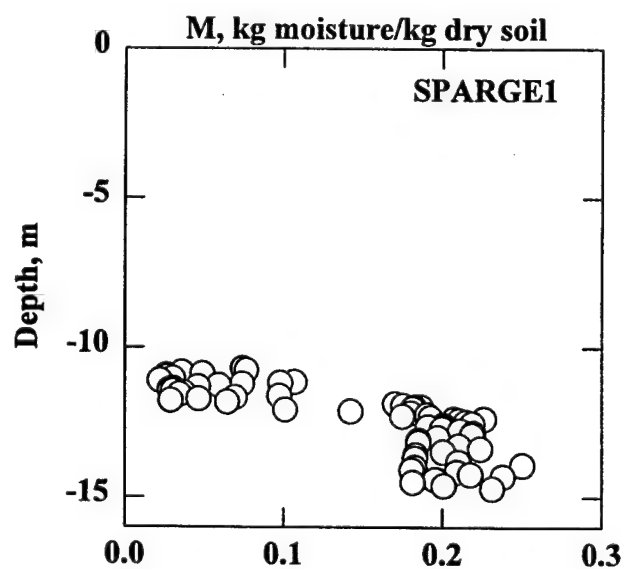
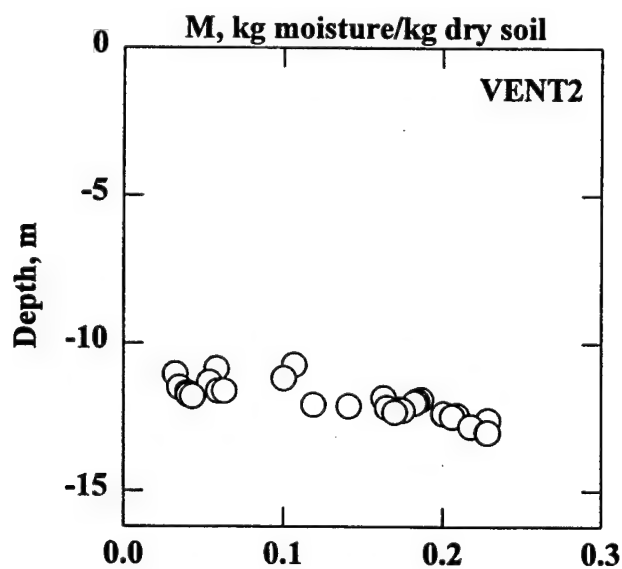
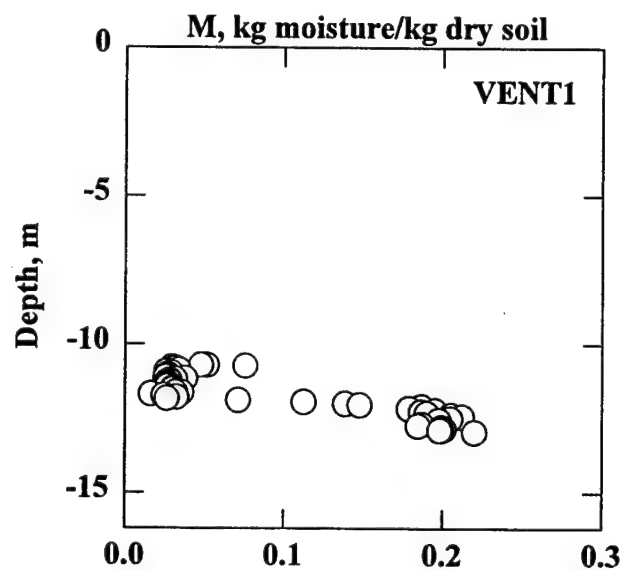
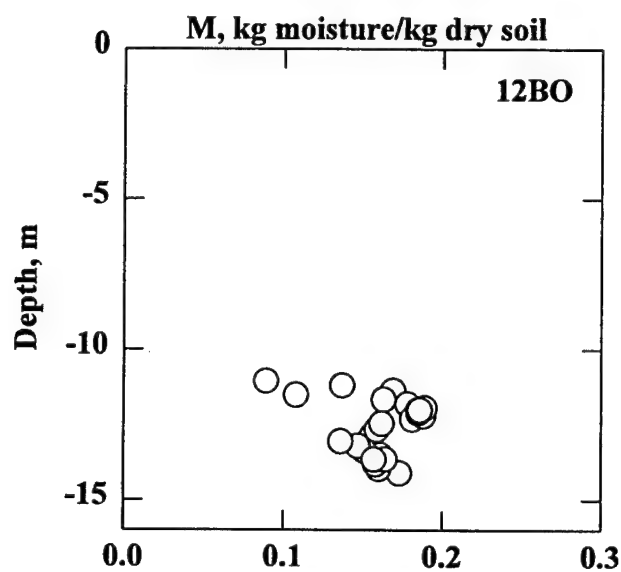
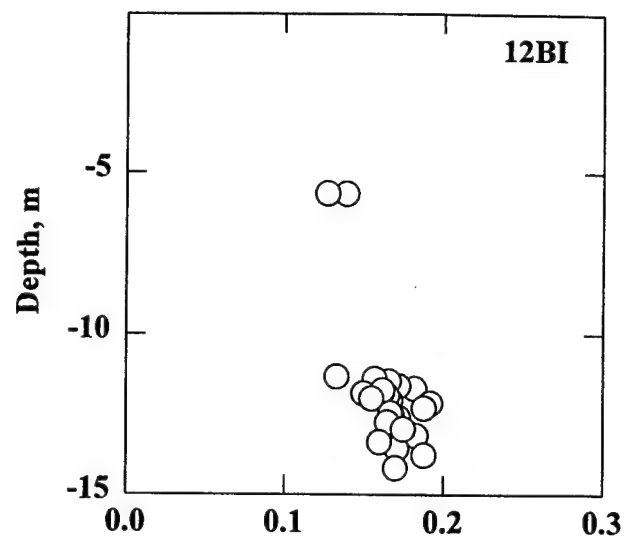
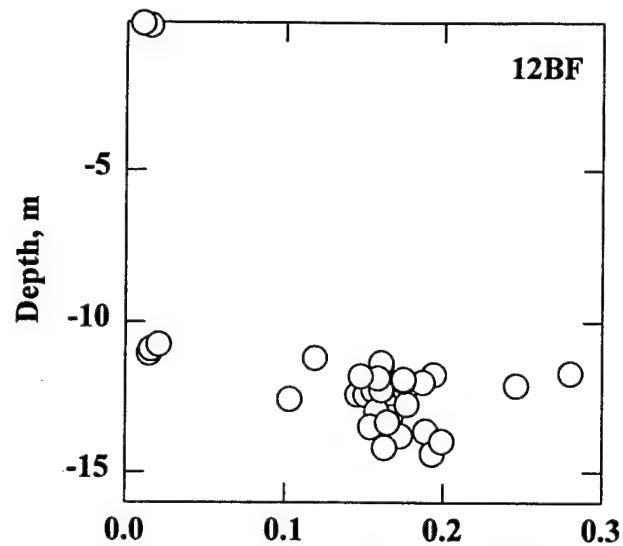
Figure 5.4 (Continued) Observed Moisture Content in Solid Core Boreholes



M, kg moisture/kg dry soil

M, kg moisture/kg dry soil

Figure 5.4 (Continued) Observed Moisture Content in Solid Core Boreholes



M, kg moisture/kg dry soil

M, kg moisture/kg dry soil

Figure 5.4 (Continued) Observed Moisture Content in Solid Core Boreholes

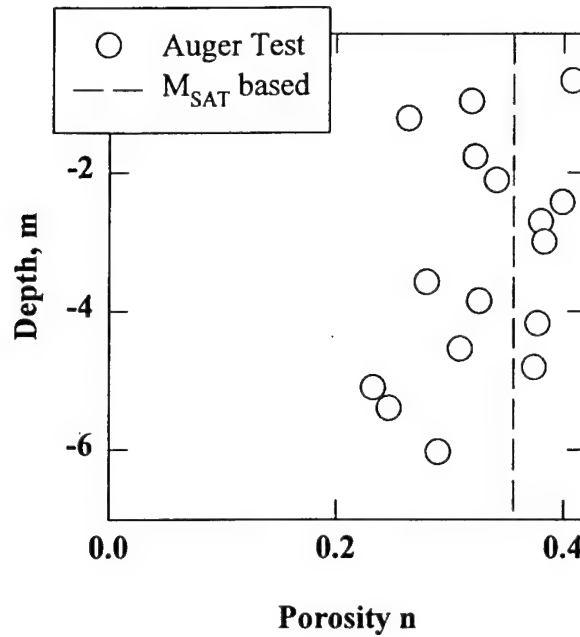


**Figure 5.5 Total Porosity, Based on Hand Auger Tests and Saturated Soil Samples**

$$n = 0.356 \quad (5.11b)$$

The coefficient of variation of the saturated soil samples is 0.19, corresponding to a reasonably precise estimate of the quantity.

Equation 5.11b compares favorably with the independent porosity estimates inferred from the hand auger data from borehole 12XX. Figure 5.5 plots 16 values observed by weighing known volumes of soil from the borehole--their average of 0.335 is close to the  $M_{SAT}$  based value of 0.356.

The total porosity value and moisture content specify the air porosity  $\theta$  in accordance with

$$\theta = n - \theta_w \quad (5.12a)$$

$$\theta = n - (1 - n)s_G M \quad (5.12b)$$

$$\theta = \frac{\text{air} \cdot \text{volume}}{\text{total} \cdot \text{volume}} \quad (5.12c)$$

**TABLE 5.5 BOREHOLE AVERAGED M AND CALCULATED AIR POROSITIES**

Borehole	Interval, m	Samples	Date	M	$\theta^a$
12AA	0.2-11.7	16	9Oct95	0.053	0.265
12AB	10.8-11.0	2	9Oct95	0.030	0.305
12AD	0.1-11.7	12	10Oct95	0.054	0.263
12AG	0.1-11.8	15	10Oct95	0.043	0.282
12AK	0.1-11.7	15	11Oct95	0.044	0.281
12AM	10.7-11.5	6	12Oct95	0.025	0.313
12AP	10.8-11.7	8	12Oct95	0.031	0.303
12AR	10.7-11.2	4	13Oct95	0.024	0.315
12AS	10.7-11.4	13	1Dec95	0.046	0.277
12AV	10.7-11.3	6	5Jun96	0.038	0.291
12AW	10.7-11.2	4	5Jun96	0.031	0.303
12AX	1.6-8.3	20	6Jun96	0.063	0.248
12AY	11.0-11.2	2	6Jun96	0.057	0.259
12AZ	10.7-11.0	3	7Jun96	0.045	0.279
12BB	10.5-11.2	5	19Aug96	0.034	0.298
12BF	0.0-11.1	5	21Aug96	0.015	0.330

<sup>a</sup>Computed using Equation 5.12b, based on porosity of 0.356.

We compute borehole averaged air porosities for the unsaturated zone by substituting moisture content data of Figure 5.4 into Equation 5.12b, with the results summarized in Table 5.5. The air porosity varies from 0.25 to 0.33, with a site averaged value given by

$$\theta = 0.288 \quad (5.13)$$

The air porosity and total porosity estimates of Equations 5.11b and 5.13 are used in gaseous transport modeling.

## 5.2 Solid Core Sampling Results

Figure 5.6 displays the total petroleum hydrocarbon content observed in 26 boreholes drilled over the study period. We calibrate the vertical LNAPL distribution model presented in Section 4.2, then assess the separate phase trichloroethylene content determined in selected profiles. The raw data are included in Appendix IV.

### 5.2.1 Calibration of LNAPL Profile Model

Equations 4.4 and 4.11 relate the mass based total petroleum hydrocarbon observations to the volume based free and residual LNAPL saturation  $S_L$  used in our model

$$S_L = S - S_w + S_{LF} \quad (5.14a)$$

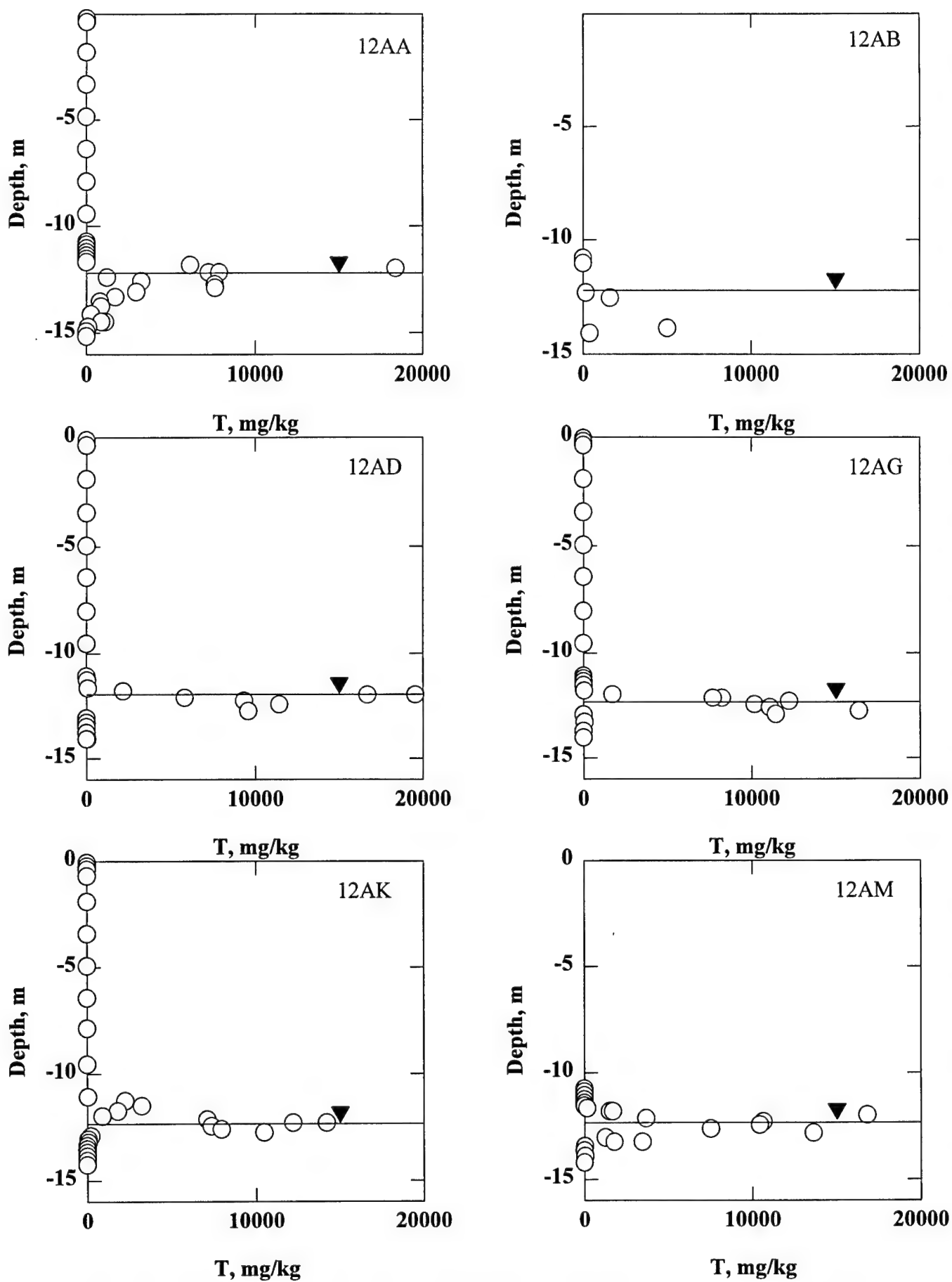


Figure 5.6 Observed Total Petroleum Hydrocarbon Content in Solid Core Boreholes

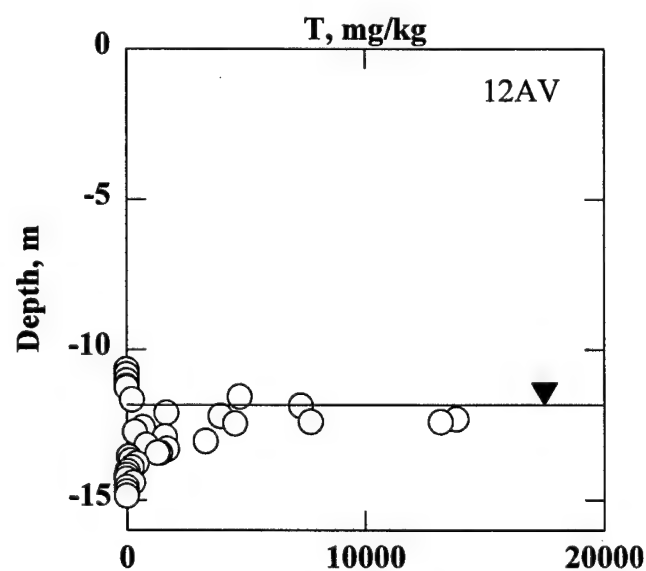
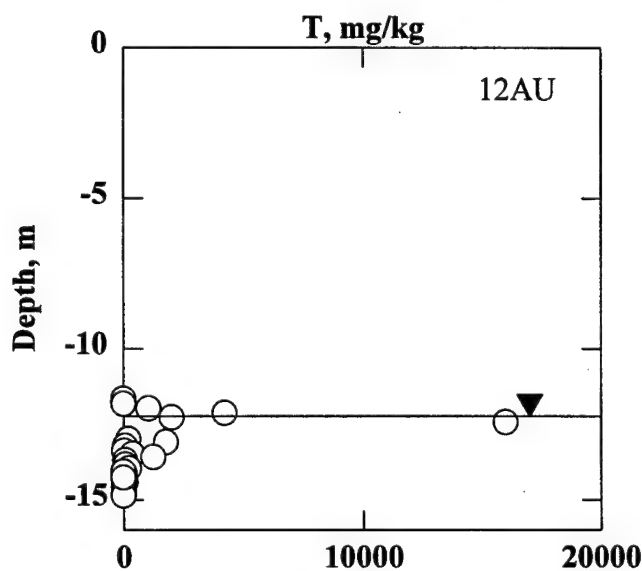
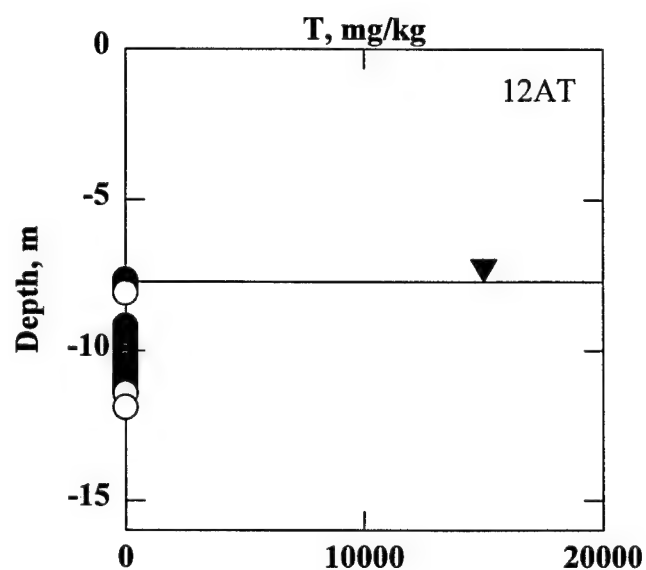
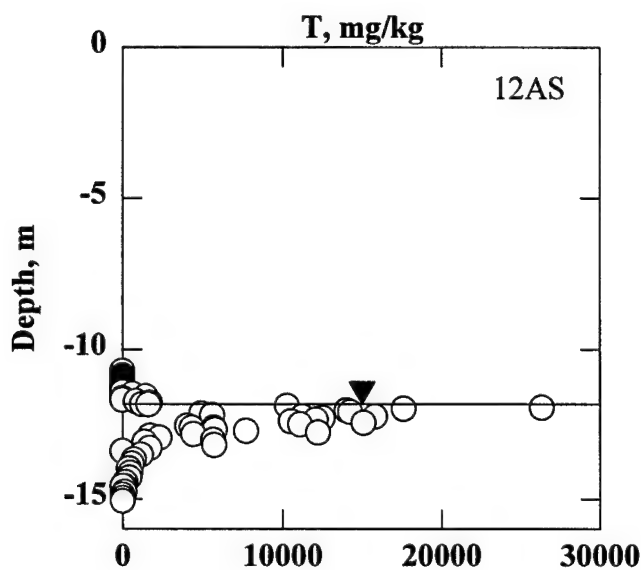
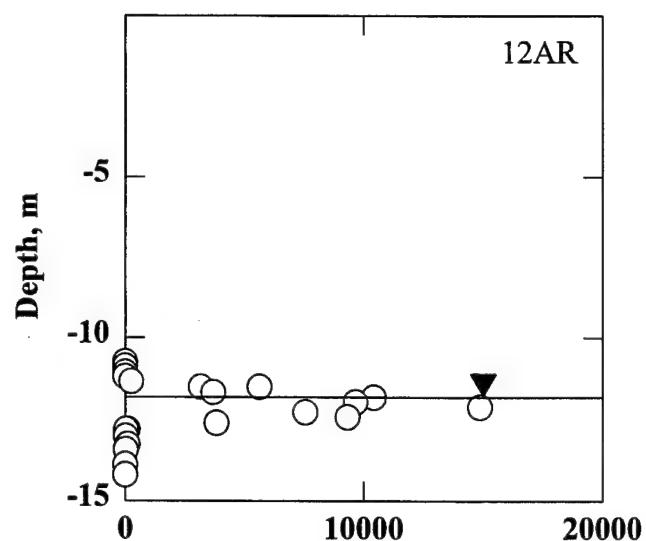
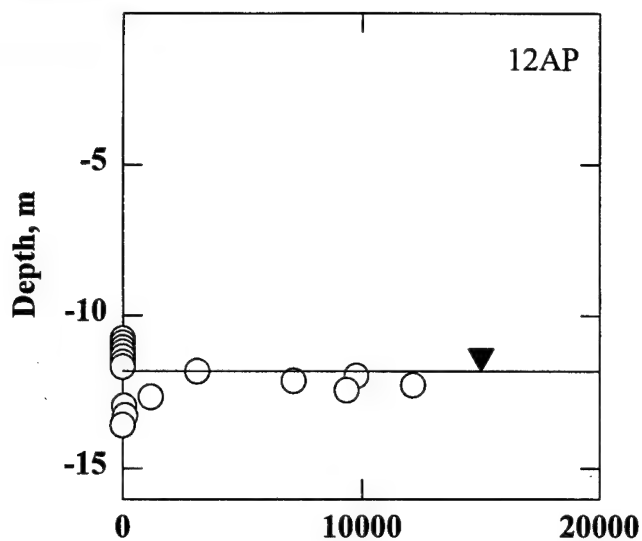


Figure 5.6 (Continued) Observed Total Petroleum Hydrocarbon Content in Solid Core Boreholes

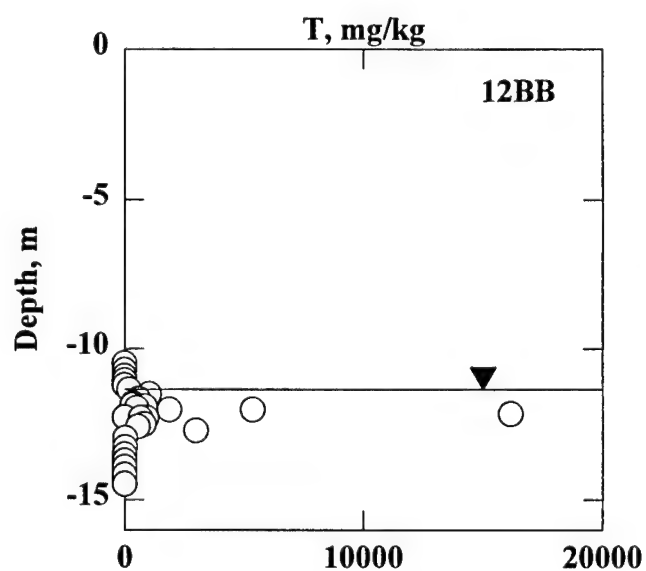
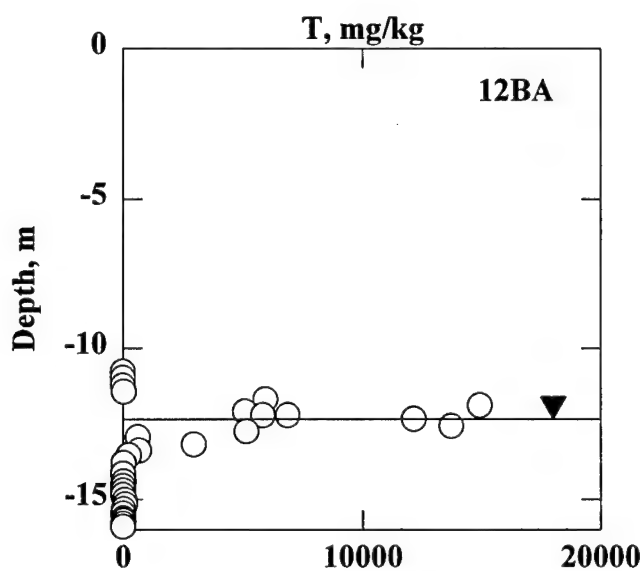
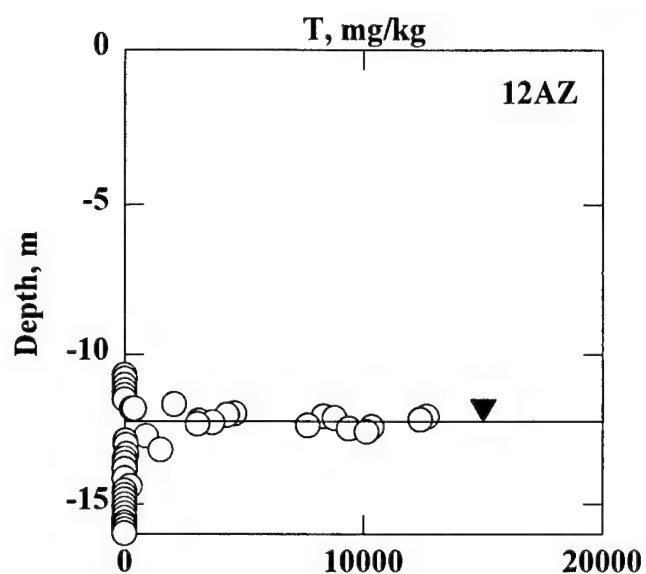
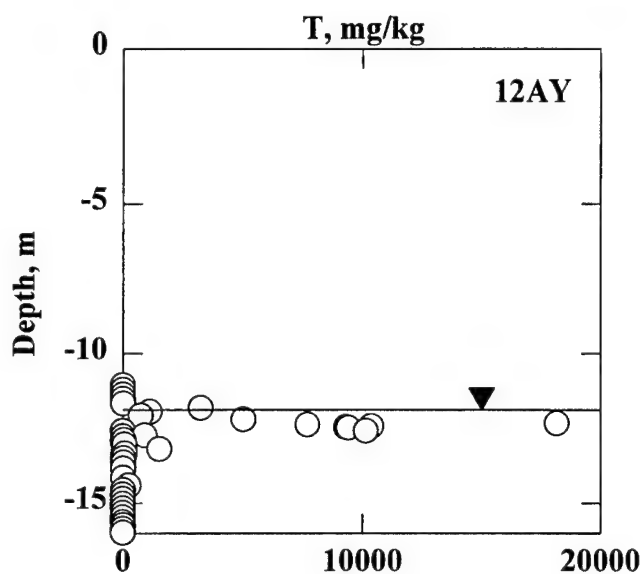
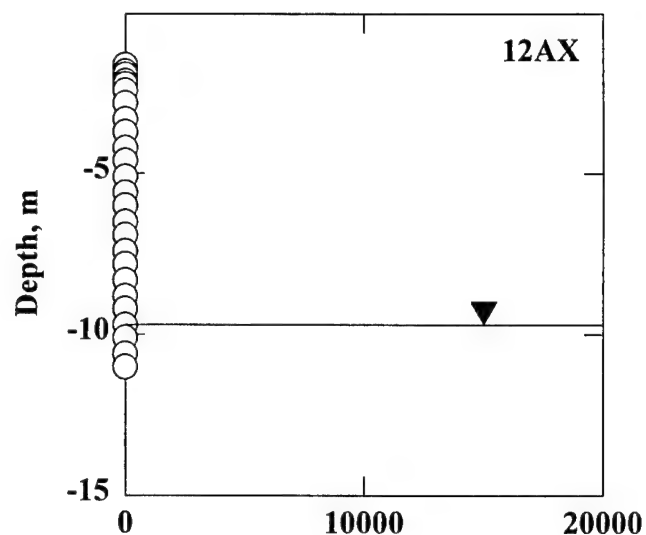
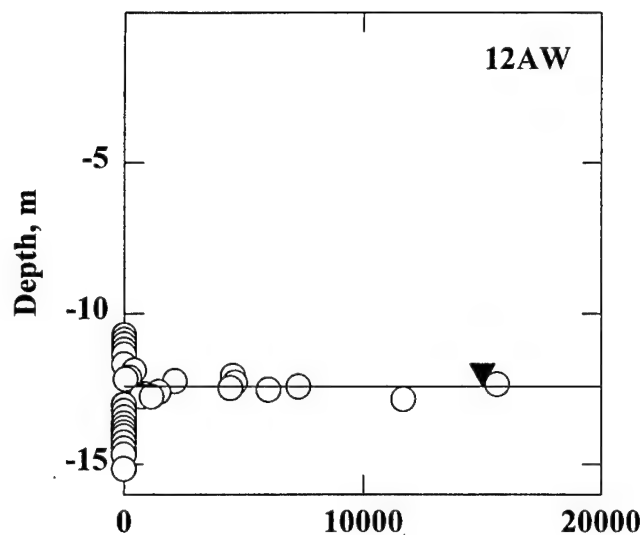


Figure 5.6 (Continued) Observed Total Petroleum Hydrocarbon Content in Solid Core Boreholes



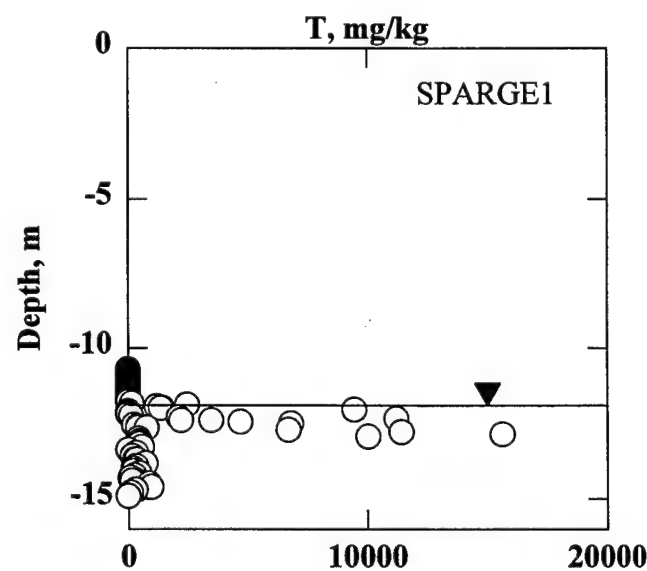
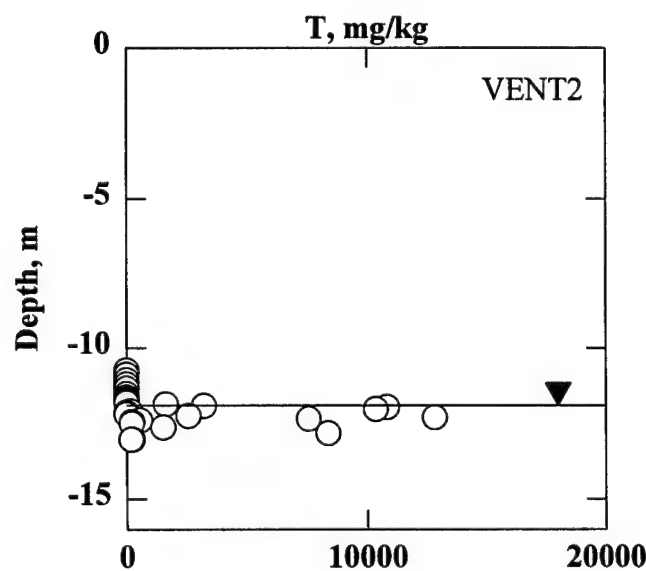
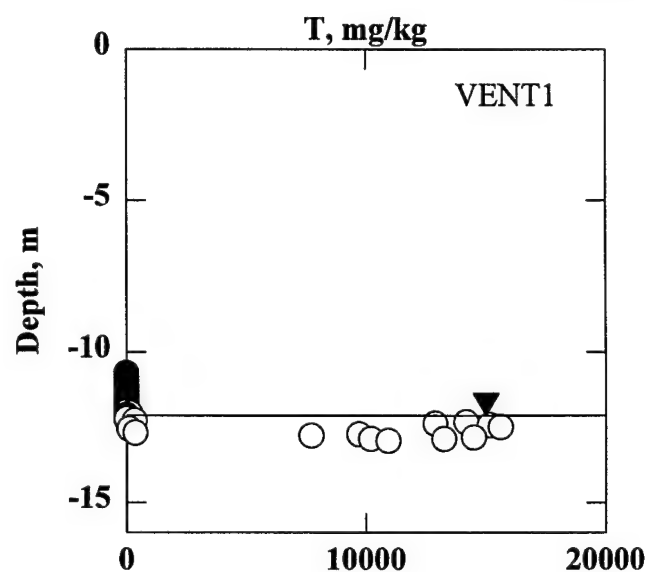
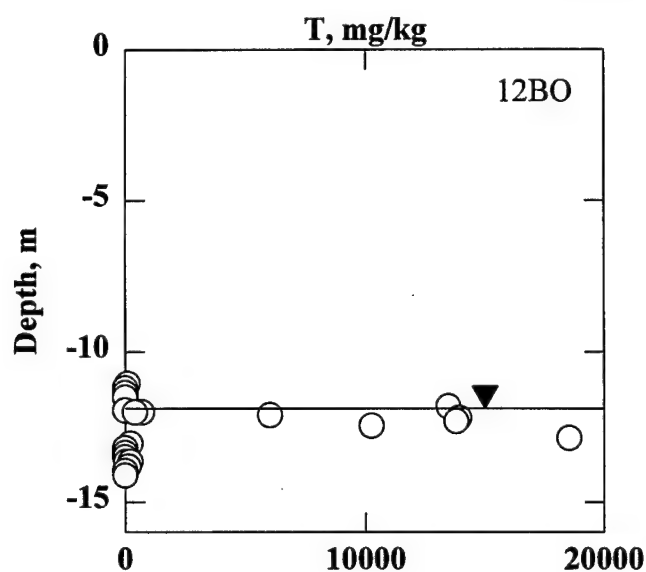
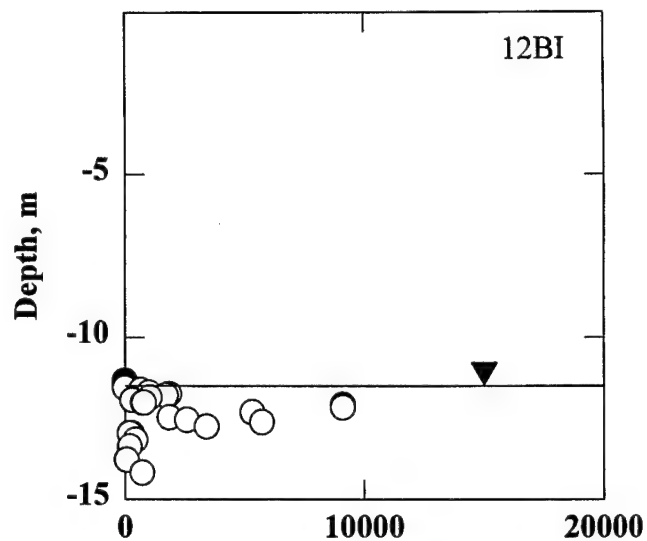
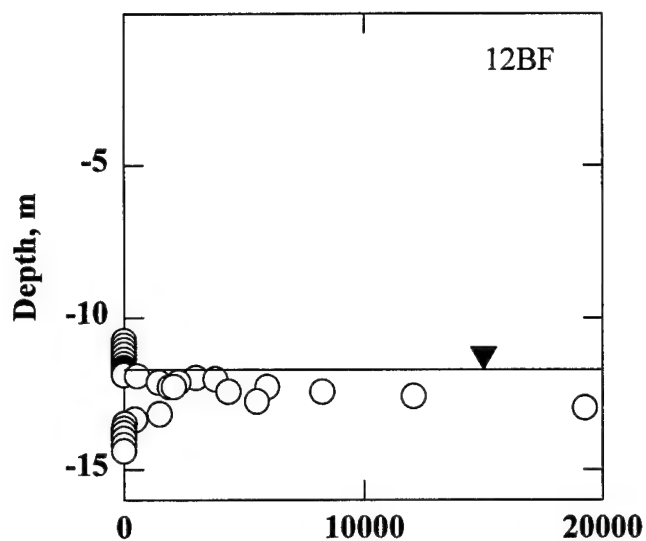
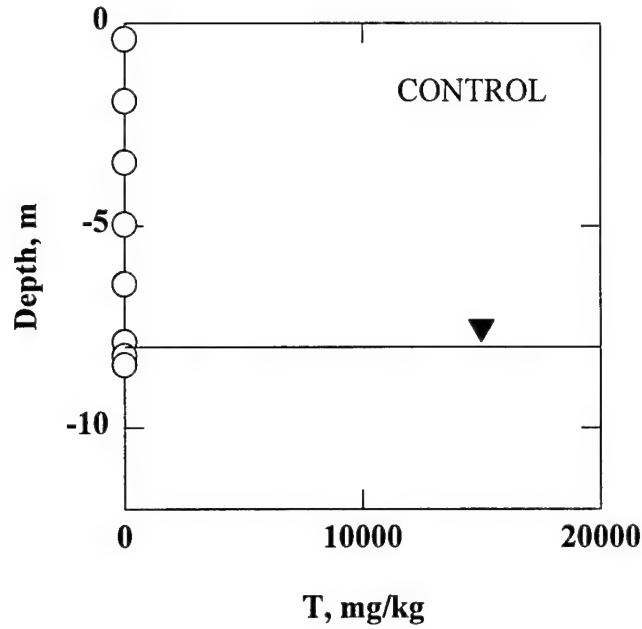


Figure 5.6 (Continued) Observed Total Petroleum Hydrocarbon Content in Solid Core Boreholes



**Figure 5.6 (Continued) Observed Total Petroleum Hydrocarbon Content in Solid Core Boreholes**

$$S_L = \frac{\rho_B T}{\rho_L (n - \theta_F)} \quad (5.14b)$$

$$S_L = S_{LF} + S_{LR} \quad (5.14c)$$

We obtained a sample of separate phase liquid from a monitoring well near the site area and determined the LNAPL density gravimetrically

$$\rho_L = 830 \frac{\text{kg}}{\text{m}^3} \quad (5.15)$$

while literature values are adopted for surface tensions

$$\sigma_{WA} = 0.074 \frac{\text{N}}{\text{m}} \quad [\text{Streeter and Wylie (1979)}] \quad (5.16a)$$

$$\sigma_{LA} = 0.023 \frac{\text{N}}{\text{m}} \quad [\text{Lenhard and Parker (1990)}] \quad (5.16b)$$

**TABLE 5.6 LNAPL PROFILE PARAMETERS AND CALIBRATION RESULTS**

Borehole	$\epsilon, \text{m}^a$	$T_{\text{MAX}}, \text{mg/kg}^a$	$\alpha_P$	$\beta_L, \text{m}^{-1}$	$\delta_{\text{SM}}, \%$	$\sigma_S, \%$
12AA	1.65	18,400	6.82	10.0	0.0	15.9
12AD	1.82	19,500	4.84	19.8	0.0	25.6
12AG	1.81	16,400	2.05	5.65	6.2	21.0
12AK	1.98	14,200	6.81	7.05	0.0	20.4
12AM	1.95	16,800	4.40	15.2	0.0	16.3
12AP	1.45	12,100	6.96	7.05	11.9	20.2
12AR	2.09	14,900	3.18	7.22	0.0	25.9
12AS	2.54	26,400	4.03	9.78	0.0	21.5
12AV	2.22	13,800	3.12	7.39	0.0	27.5
12AW	1.43	15,600	3.04	7.05	0.0	28.9
12AY	1.10	18,200	1.76	7.05	7.0	25.9
12AZ	2.72	12,700	3.32	7.05	0.0	24.5
12BA	2.11	14,900	2.05	7.77	0.3	17.2
12BB	2.03	16,200	3.40	7.16	0.1	33.0
12BF	1.80	19,300	3.04	7.04	29.3	43.5
12BO	1.62	13,900	1.67	3.34	0.5	29.6
VENT2	1.32	12,800	3.85	7.05	0.0	28.2
SPARGE1	2.05	15,600	5.38	5.06	0.0	31.0

<sup>a</sup>Observed.

$$\sigma_{\text{WL}} = 0.051 \frac{\text{N}}{\text{m}} \quad [\text{Lenhard and Parker (1990)}] \quad (5.16\text{c})$$

Groundwater level data cited by the Base engineers [ABB (1993)] suggest a water table fluctuation of

$$\Delta = 1.0\text{m} \quad (5.17)$$

in the vicinity of the study area. The core data support a hysteretical trapping factor of 20, which leads to an estimate of the maximum trapped LNAPL by virtue of Eq. 4.13

$$\gamma = 20 \quad (5.18\text{a})$$

$$S_{\text{LRMAX}} \cong 0.050 \quad (\gamma \gg 1) \quad (5.18\text{b})$$

We complete the specification of common profile parameters by estimating the irreducible moisture content and the dry soil bulk density. The smallest M value in Table 5.5 (0.015), corresponding to dry conditions, is substituted into Eq. 5.9a to derive a value for  $\theta_F$

$$\theta_F = 0.026 \quad (5.19)$$

The total porosity estimate (Eq. 5.11b) implies a  $\rho_B$  value

$$\rho_B = s_G(1 - n)\rho \quad (s_G=2.65) \quad (5.20a)$$

$$\rho_B = 1,710 \frac{\text{kg}}{\text{m}^3} \quad (5.20b)$$

The model calibration requires that total and LNAPL saturation data determine the error statistics, since both are described by the same pore size distribution. A nested Fibonacci search is run through the  $S$  and  $S_L$  data for each borehole, to establish minimal saturation error mean  $\delta_{SM}$  and standard deviation  $\sigma_S$ . The statistics are defined by the two data sets

$$\delta_{SM} = \frac{1}{2N} \sum [S(\text{observed}) - S(\text{predicted}) + \frac{S_L(\text{observed}) - S_L(\text{predicted})}{0.2}] \quad (5.21a)$$

$$\sigma_S = \sqrt{\frac{1}{2N} \sum \{ [S(\text{observed}) - S(\text{predicted})]^2 + [\frac{S_L(\text{observed}) - S_L(\text{predicted})}{0.2}]^2 - \delta_{SM}^2 \}} \quad (5.21b)$$

The use of a typical maximum observed LNAPL saturation (0.20) to normalize the LNAPL error contribution places equal weight on the total and LNAPL saturation in determining the error statistics, since  $S$  has a maximum value of unity. We optimize the pore size uniformity to zero the mean error and the scaling factor  $\beta_L$  (hence, the mean pore radius) to minimize  $\sigma_S$  for each borehole.

We use an approximate peak concentration matching relation to enforce a relation between the van Genuchten (1980) pore size parameters ( $\alpha_p, \beta_L$ ) and the LNAPL and water table depths ( $b_L, b_w$ ) for the free LNAPL profiles. The maximum observed LNAPL saturation  $S_{LMAX}$  and its depth  $b_{LMAX}$  are set equal to their observed values, based on data cited in Table 5.6. The matching relations are derived by Ostendorf et al. (1993)

$$b_w = \left\{ \frac{S_{LMAX} - S_{LRMAX}}{(1 - \frac{1}{\alpha_p})[1 - (\frac{\beta_w}{\beta_L})^{\frac{\alpha_p}{\alpha_p-1}}]} \right\}^{\frac{1}{\alpha_p}} \left( \frac{1}{\beta_w} \right) + b_{LMAX} \quad (5.22a)$$

$$b_L = (b_w - b_{LMAX}) \left( \frac{\beta_w}{\beta_L} \right)^{\frac{\alpha_p}{\alpha_p-1}} + b_{LMAX} \quad (5.22b)$$

## 5.2.2 LNAPL Results

Figure 5.7 and Table 5.6 summarize the LNAPL calibration results for 18 solid core profiles. The pore size uniformity exponent varies between 1.67 and 6.96, while the LNAPL

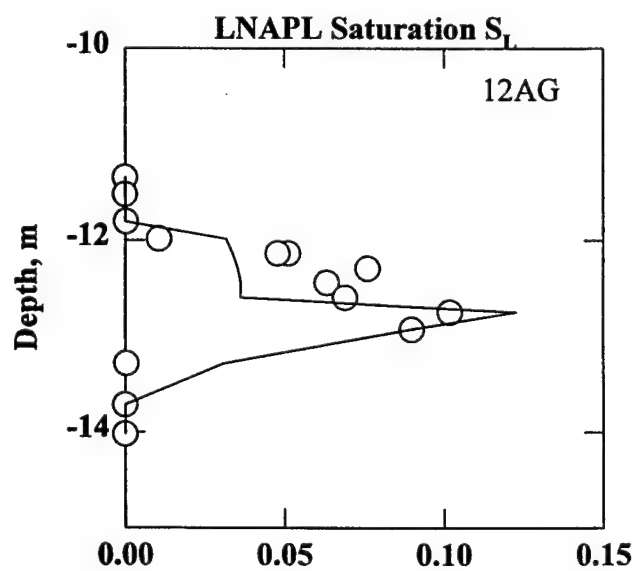
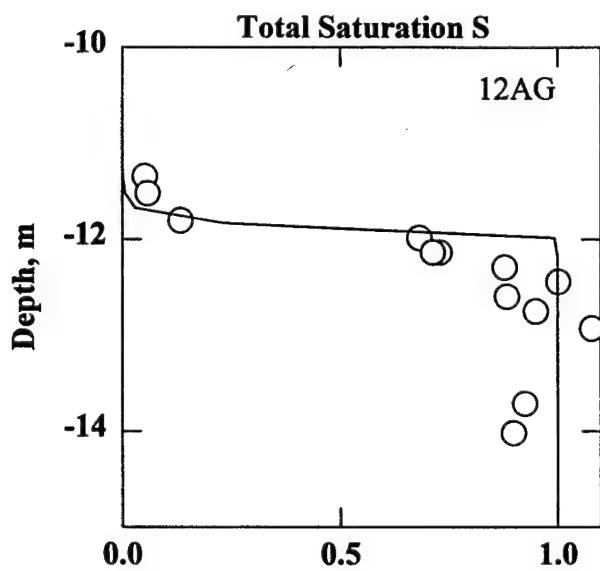
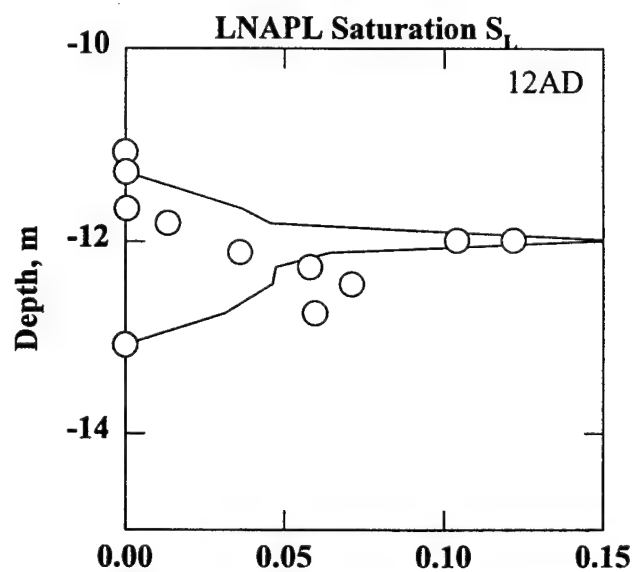
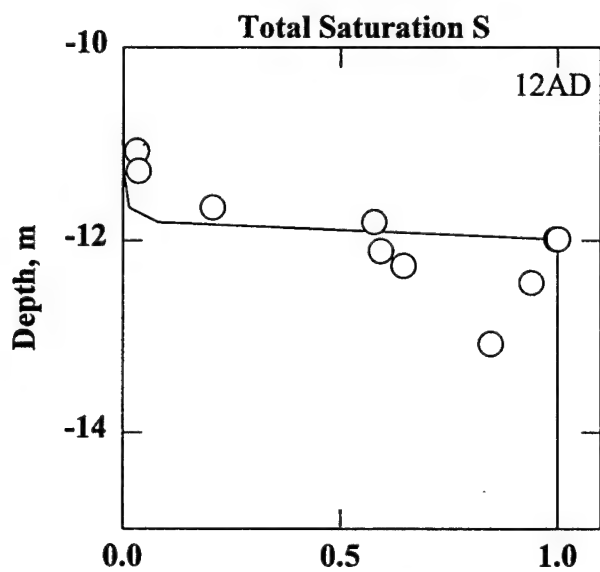
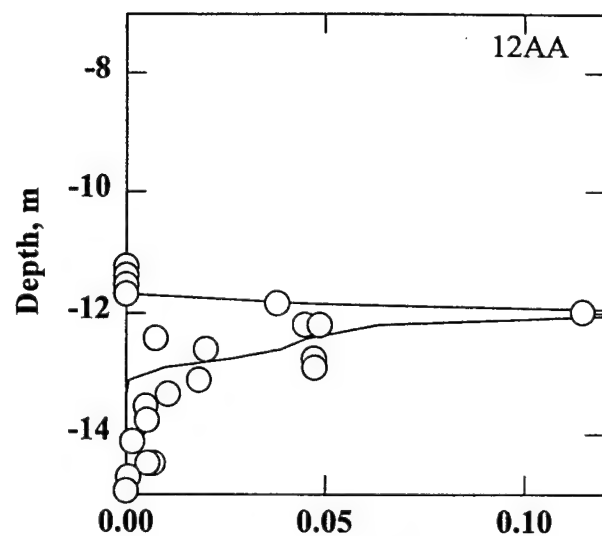
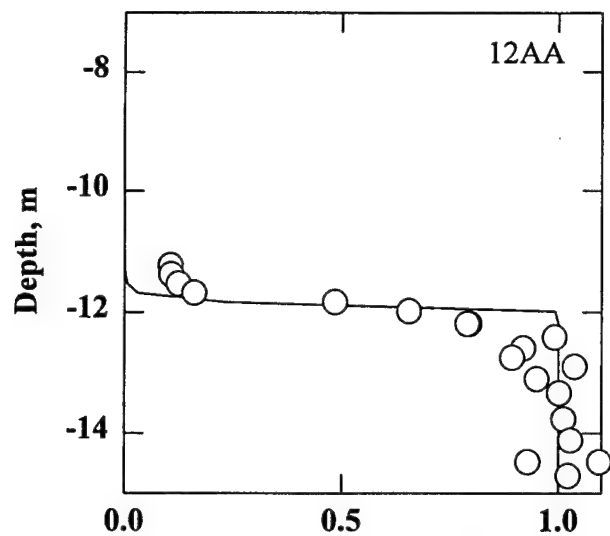


Figure 5.7 Observed (Symbols) and Calibrated Total and LNAPL Saturations

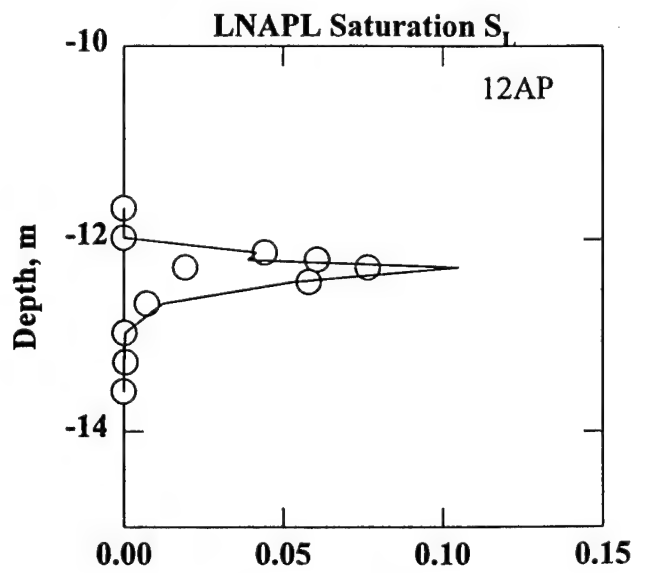
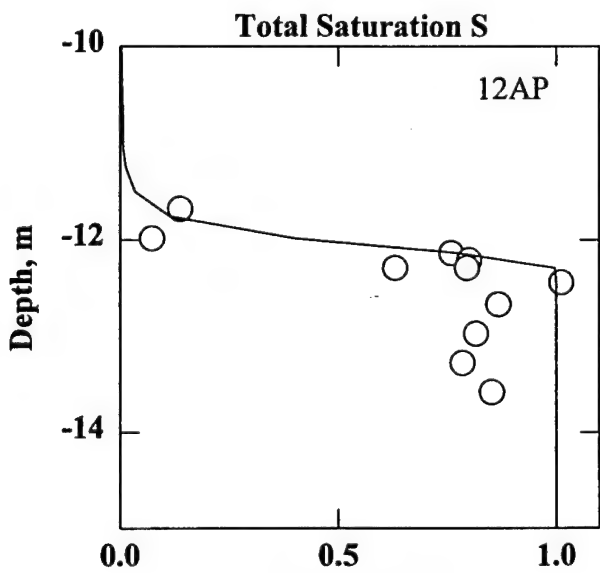
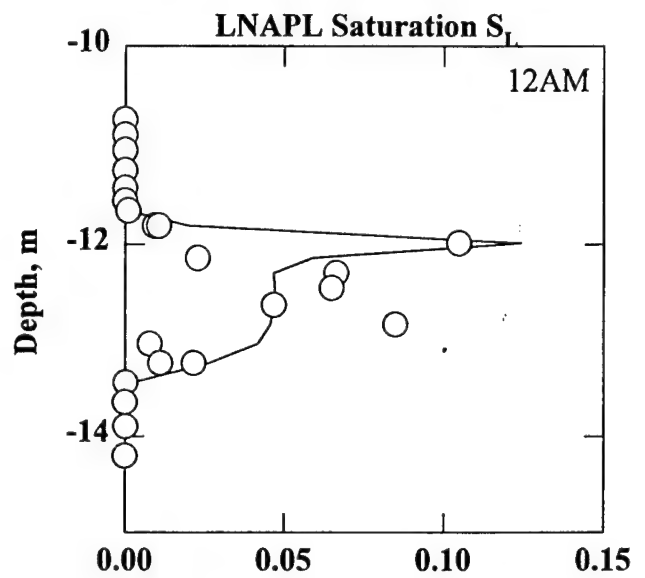
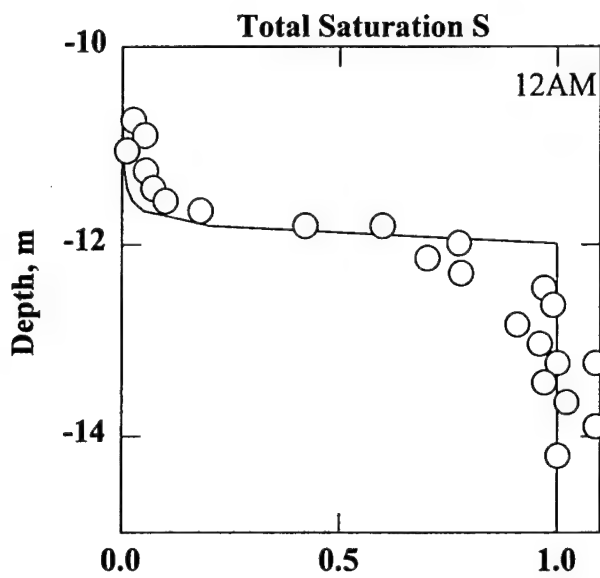
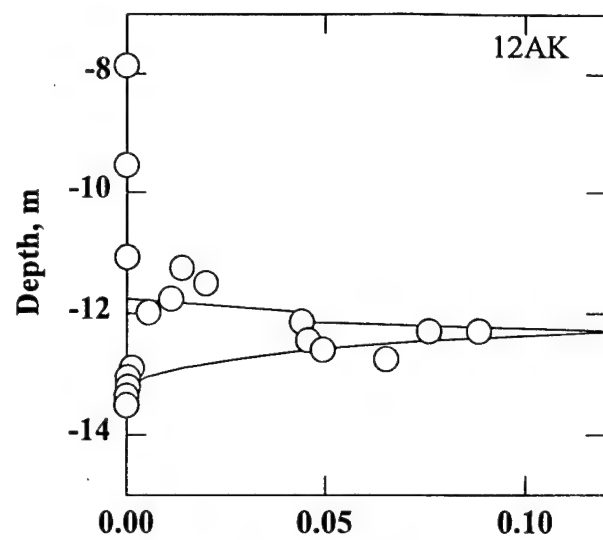
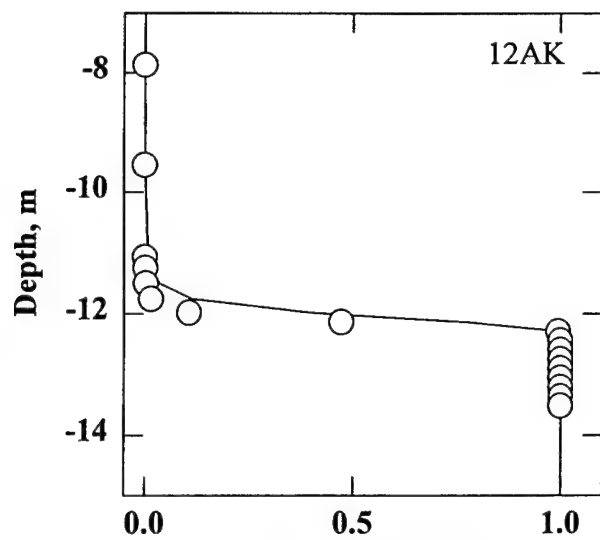
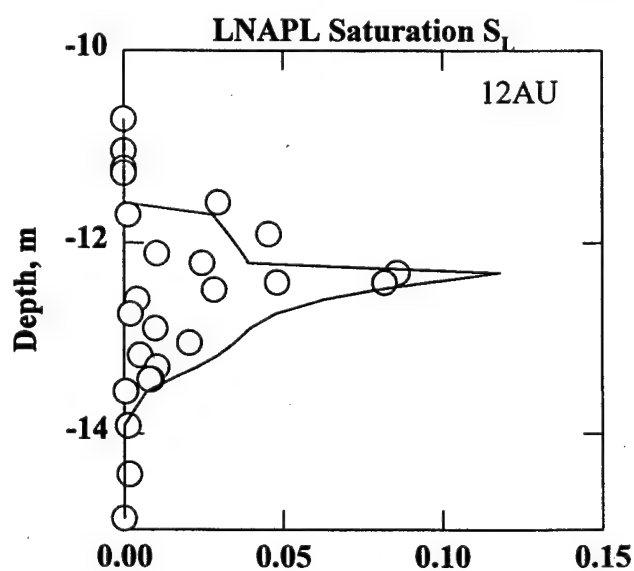
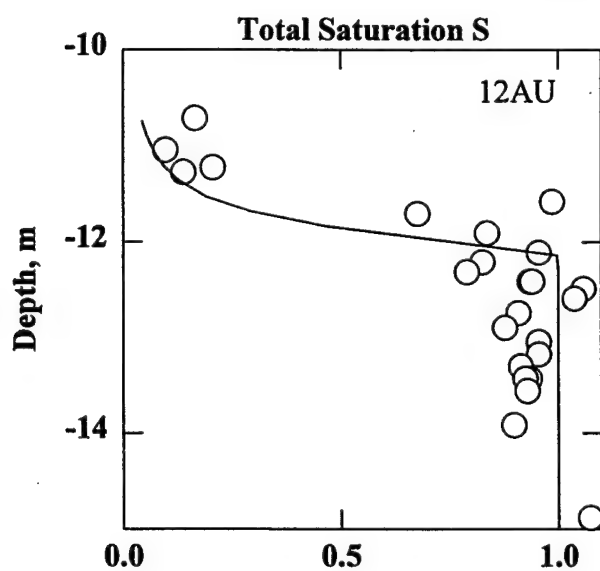
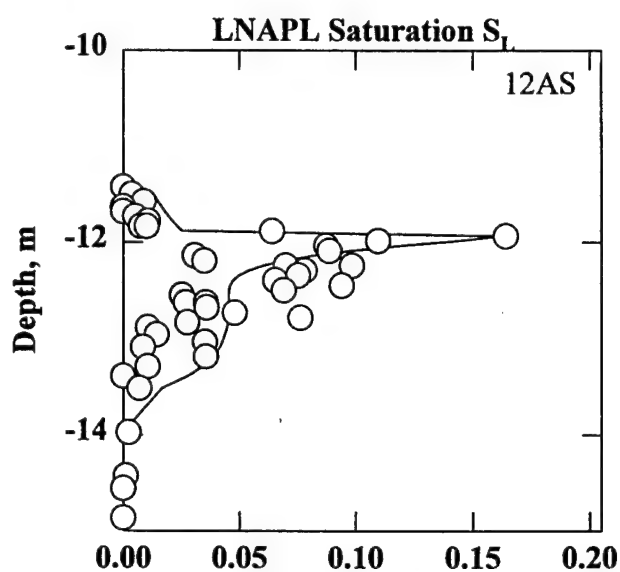
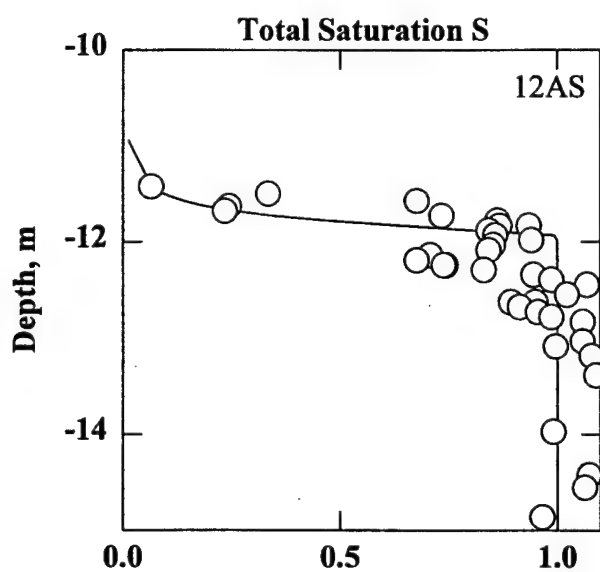
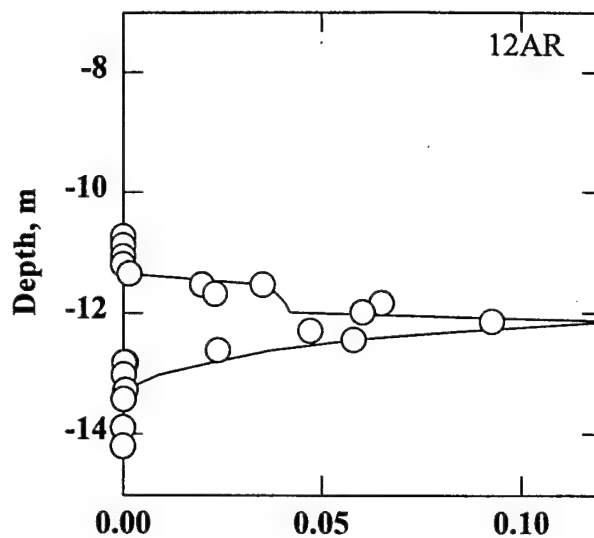
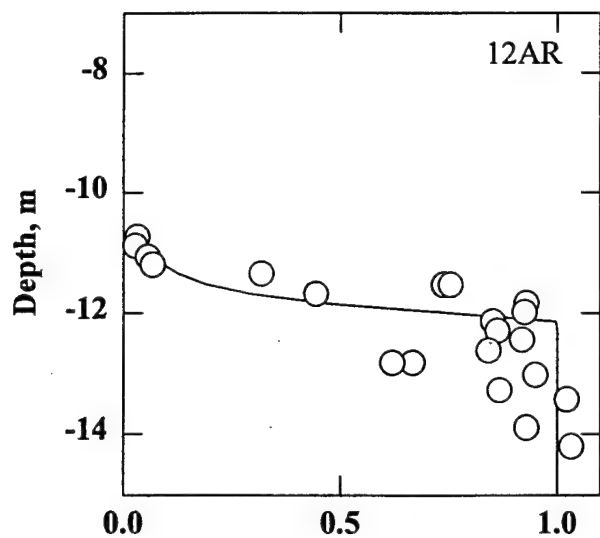


Figure 5.7 (Continued) Observed (Symbols) and Calibrated Total and LNAPL Saturations



Total Saturation  $S$

LNAPL Saturation  $S_L$

Figure 5.7 (Continued) Observed (Symbols) and Calibrated Total and LNAPL Saturations

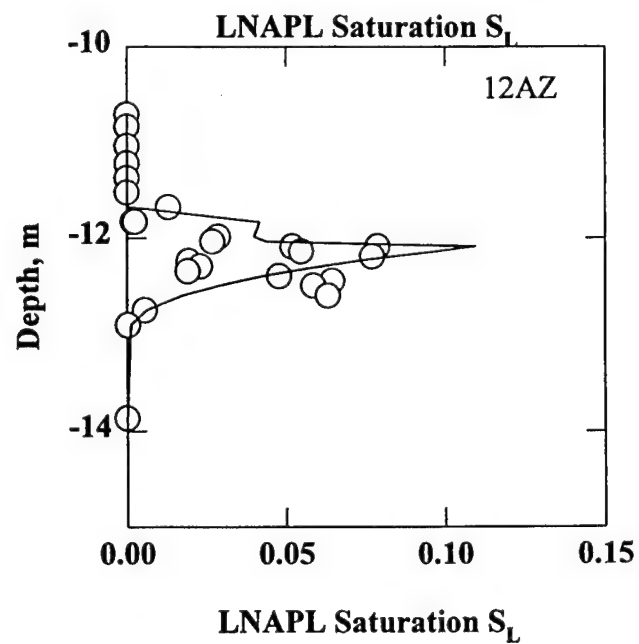
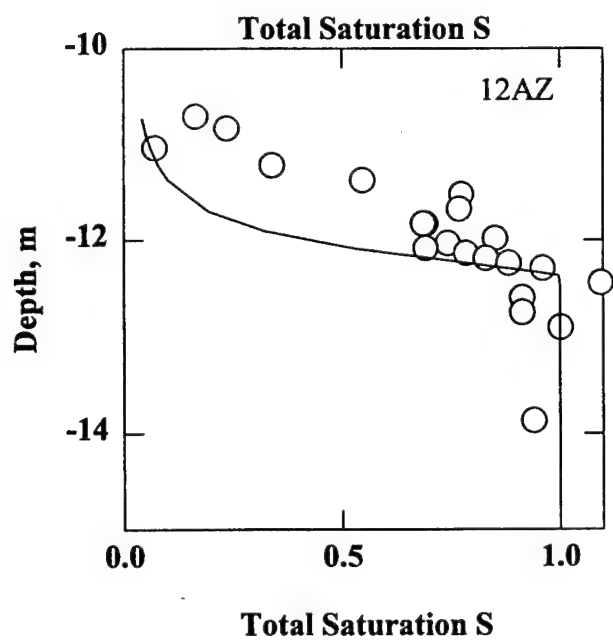
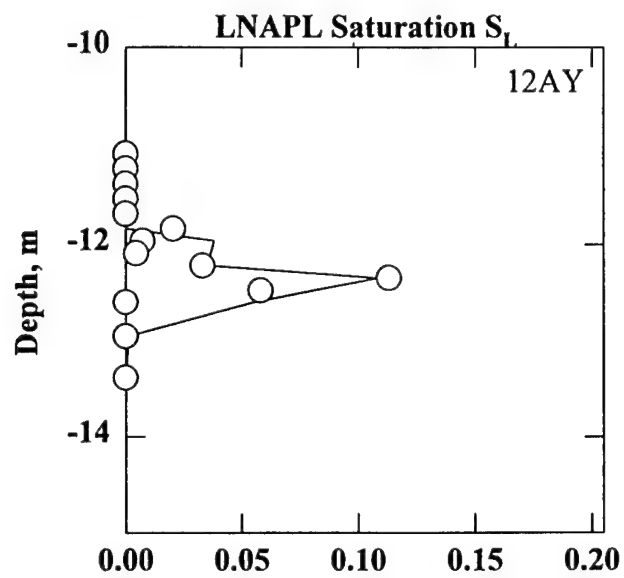
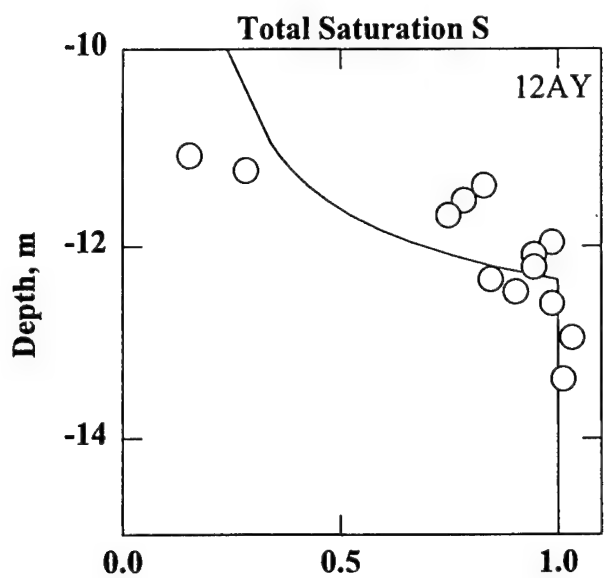
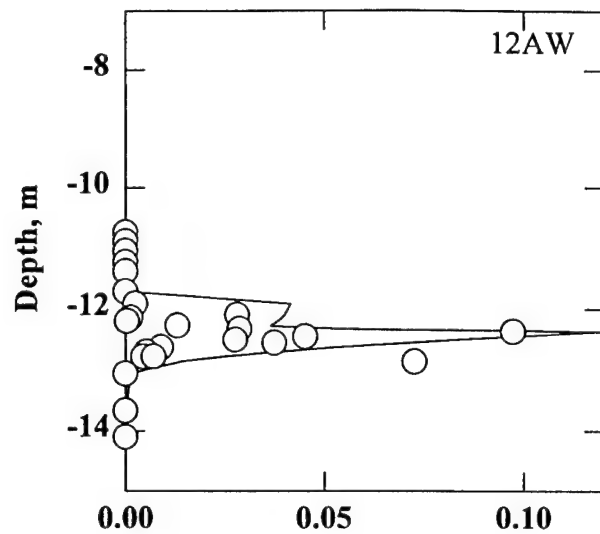
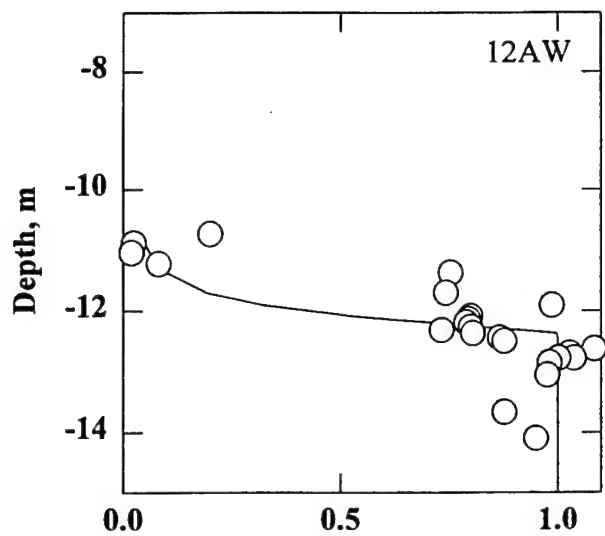


Figure 5.7 (Continued) Observed (Symbols) and Calibrated Total and LNAPL Saturations



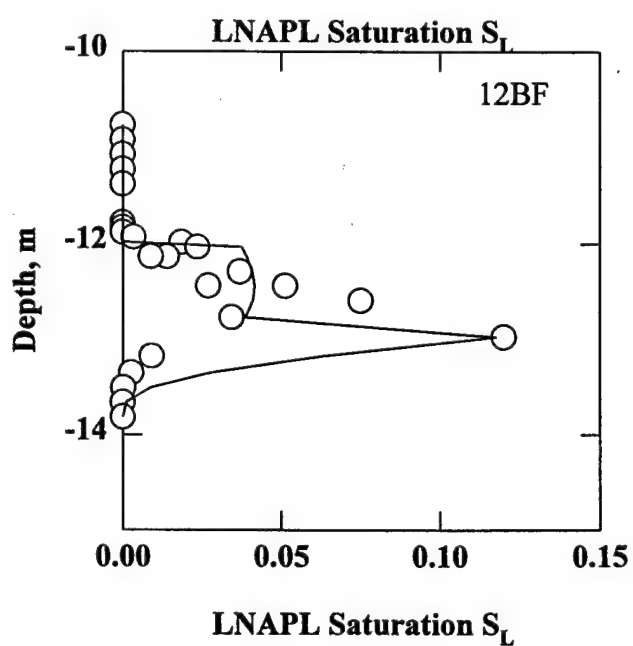
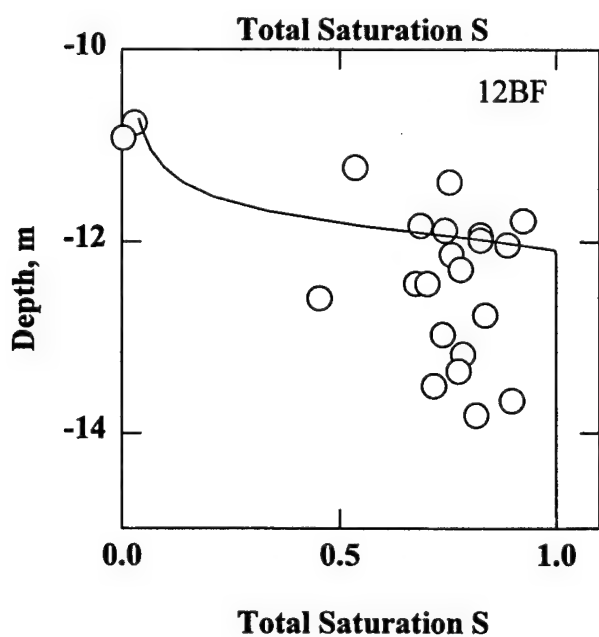
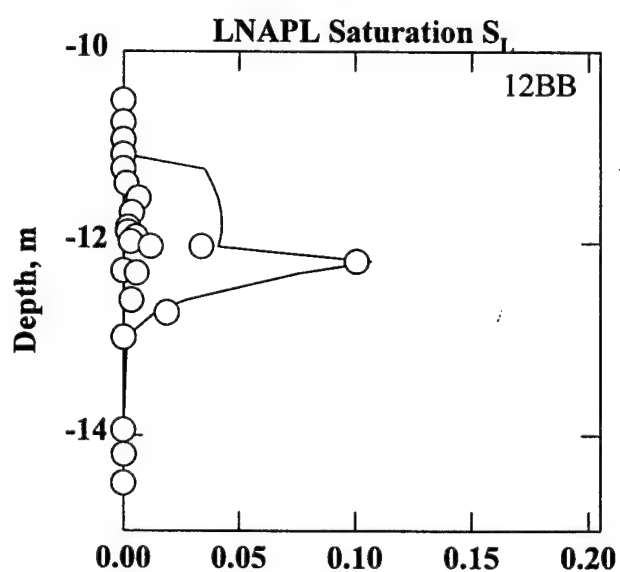
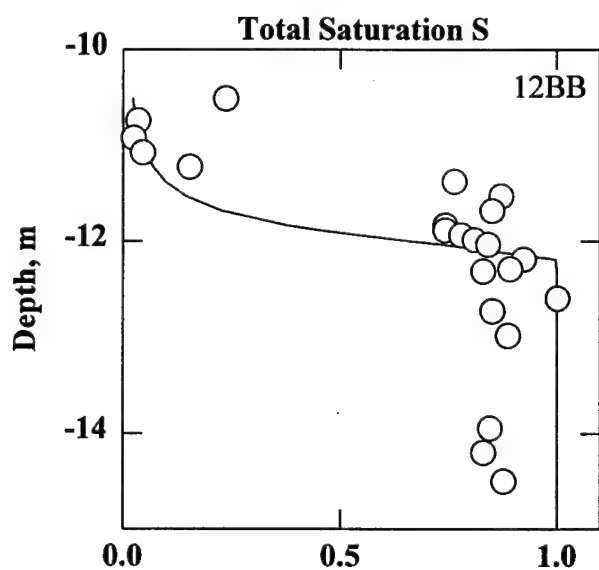
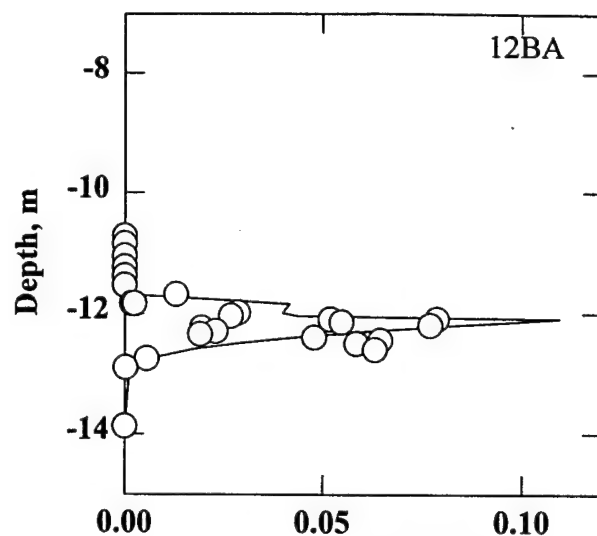
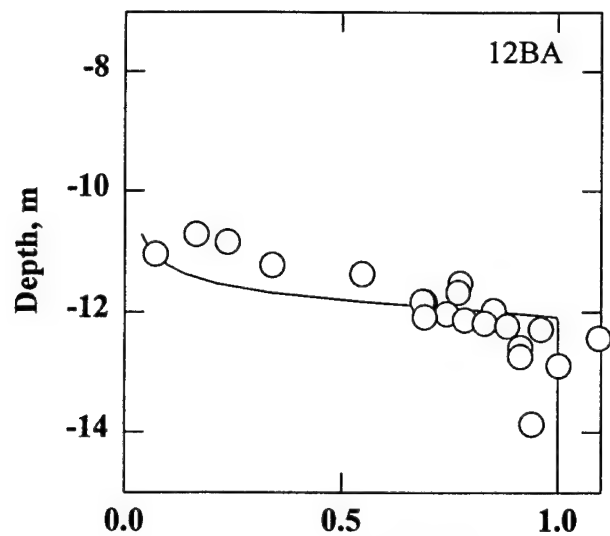
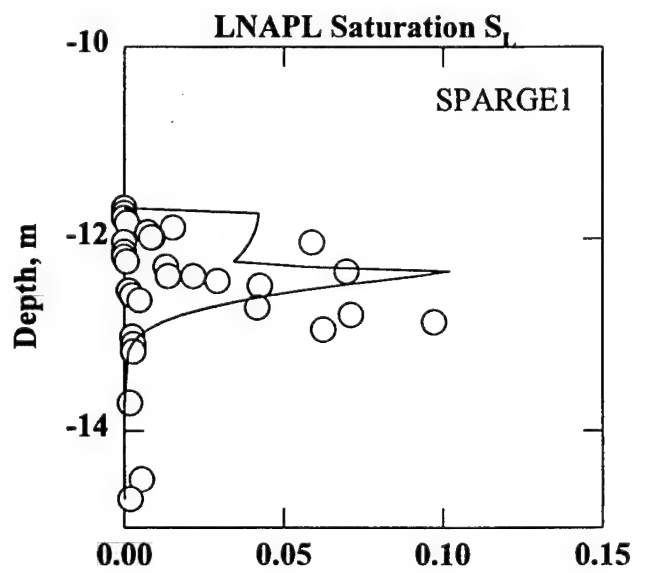
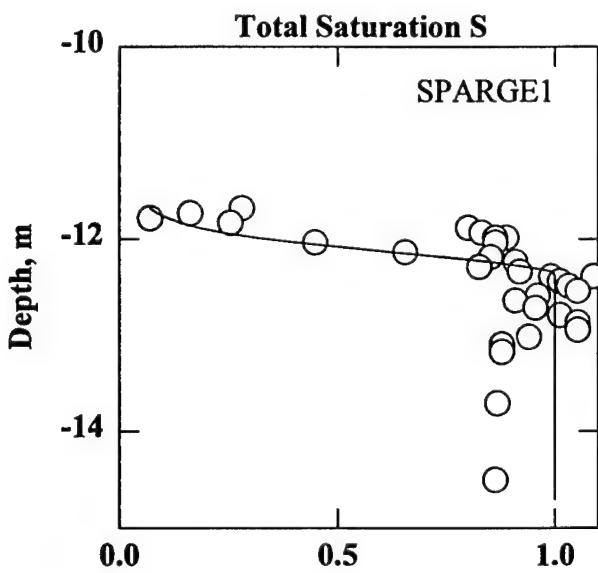
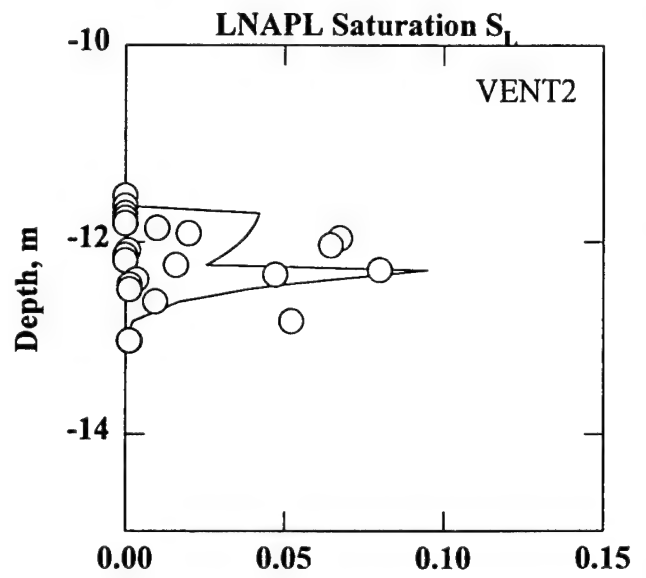
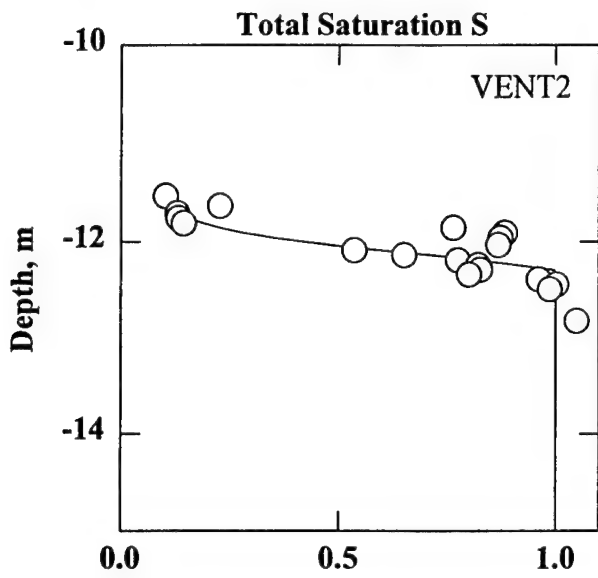
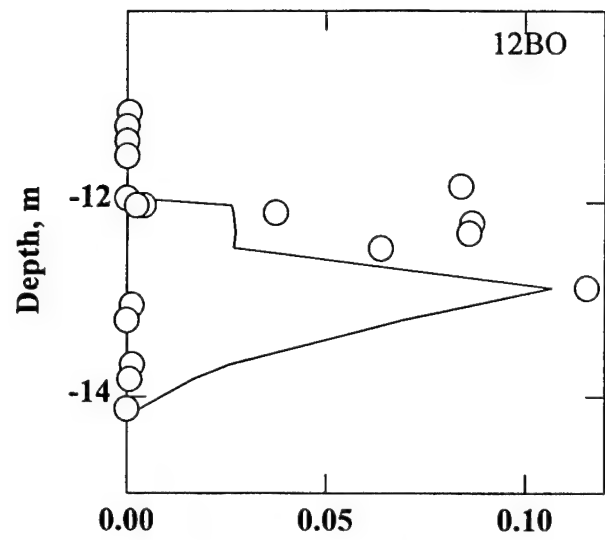
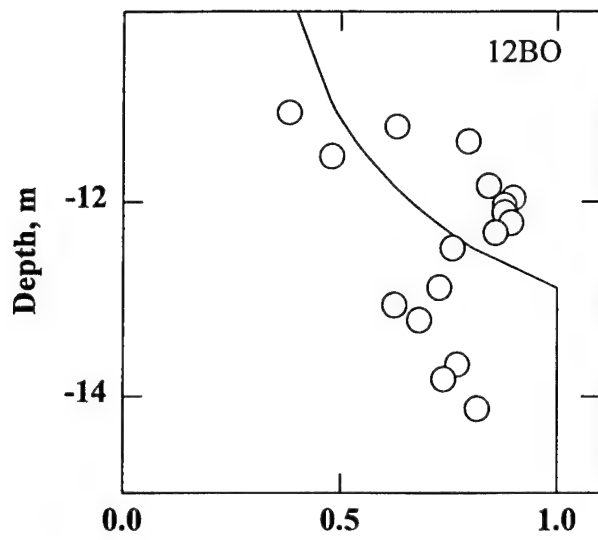


Figure 5.7 (Continued) Observed (Symbols) and Calibrated Total and LNAPL Saturations



Total Saturation S

LNAPL Saturation  $S_L$

Figure 5.7 (Continued) Observed (Symbols) and Calibrated Total and LNAPL Saturations

scaling factor ranges from 3.34 to 19.8 m<sup>-1</sup> in magnitude. The average values of the 18 calibrations is

$$\alpha_p = 3.87 \quad (5.23a)$$

$$\beta_L = 8.21 \quad (5.23b)$$

$$r_M = 0.046 \text{ mm} \quad (5.23c)$$

The average pore radius implied by Equation 5.23b follows from Equations 4.6a and 5.16b, and is used to model the distribution of both water and separate phase JP4 jet fuel. The average pore size uniformity exponent is remarkably close to its grain size counterpart ( $\alpha_D$ ) of 3.68 (Equation 5.7b). The correspondence of these independently calibrated exponents is physically plausible, since the grain size distribution determines the distribution of the pore spaces between the solids in a porous medium.

We deduce a relation between the mean pore radius and the mean grain size by approximating the numbers  $N_p$  and  $N_D$  of pores and grains in a representative soil volume

$$\frac{N_p \left( \frac{4\pi r_M^3}{3} \right)}{N_D \left( \frac{\pi d_M^3}{6} \right)} = \frac{n}{1-n} \quad (5.24)$$

The numerator of Equation 5.24 is proportional to the pore volume while the denominator is proportional to the solid grain volume. We equate the surface area of the pores to the surface area of the grains in the representative volume in deriving a second equation for the  $N_p$  to  $N_D$  ratio with the result

$$N_D \pi d_M^2 = N_p 4\pi r_M^2 \quad (5.25a)$$

$$r_M = d_M \frac{n}{2(1-n)} \quad (d_M = 0.441 \text{ mm}) \quad (5.25b)$$

The  $d_M$  listed in Equation 5.23b is the average of the Table 5.3 values, and implies a pore size radius of 0.12 mm. This is somewhat larger than Equation 5.23c, but still within an order of magnitude of the moisture based calibrated value.

### 5.2.3 Separate Phase Trichloroethylene Profiles

We observed trichloroethylene in the LNAPL extract chromatograms for boreholes 12AS, 12AV, 12BB, 12BF, 12BI, and 12BO. Tables 5.7-5.12 list the separate phase TCE

**TABLE 5.7 LNAPL AND TCE CONTENT IN BOREHOLE 12AS**

<b>Depth, m</b>	<b>T<sub>TCE</sub>, mg/kg</b>	<b>T, mg/kg</b>	<b>T<sub>TCE</sub>/T</b>	<b>Depth, m</b>	<b>T<sub>TCE</sub>, mg/kg</b>	<b>T, mg/kg</b>	<b>T<sub>TCE</sub>/T</b>
11.49	0.18	602	0.00030	12.49	11.91	11086	0.00108
11.49	0.21	602	0.00036	12.54	7.23	4032	0.00179
11.73	0.56	824	0.00068	12.61	0.00	5689	0
11.78	1.00	1703	0.00059	12.61	7.31	4311	0.00170
11.78	1.08	1703	0.00063	12.67	3.74	5739	0.00065
11.83	1.08	1220	0.00088	12.72	20.10	7697	0.00261
11.83	1.11	1618	0.00068	12.77	10.01	12228	0.00082
11.88	25.23	10284	0.00245	12.82	1.37	4414	0.00031
11.93	58.60	26335	0.00223	12.88	0.30	1694	0.00028
11.98	37.72	17593	0.00214	12.94	0.34	2285	0.00015
12.04	29.70	14021	0.00212	13.02	5.83	5644	0.00103
12.04	29.26	14021	0.00209	13.08	4.66	1360	0.00343
12.09	35.73	14241	0.00251	13.18	10.04	5701	0.00176
12.14	11.49	4917	0.00234	13.28	0.93	1678	0.00056
12.19	10.74	5586	0.00192	13.51	0.49	1129	0.00044
12.19	9.64	5586	0.00173	13.66	0.46	688	0.00067
12.24	42.77	15796	0.00271	13.82	0.29	572	0.00051
12.24	31.37	11226	0.00279	13.97	0.04	383	0.00010
12.29	0.00	12536	0	14.12	0.11	458	0.00023
12.34	26.24	12087	0.00217	14.27	0.17	418	0.00040
12.39	21.48	10514	0.00204	14.43	0.05	153	0.00035
12.44	0.00	15078	0				

concentrations T<sub>TCE</sub> along with the total LNAPL content in the profiles. We observed the following maximum (T<sub>TCEMAX</sub>) levels in the six boreholes:

- borehole 12AS-T<sub>TCEMAX</sub>=58.6 mg/kg
- borehole 12AV-T<sub>TCEMAX</sub>=47.3 mg/kg
- borehole 12BB-T<sub>TCEMAX</sub>=24.5 mg/kg
- borehole 12BF-T<sub>TCEMAX</sub>=47.0 mg/kg
- borehole 12BI-T<sub>TCEMAX</sub>=21.2 mg/kg
- borehole 12BO-T<sub>TCEMAX</sub>=113 mg/kg

Figure 5.8 displays the separate phase TCE profiles, which exhibit a vertical structure similar to their total LNAPL counterparts in Figure 5.7. The TCE maxima occur near the water table and coincide with the T<sub>MAX</sub> depths.

The ratio of separate phase trichloroethylene to total LNAPL is also cited in Tables 5.7-5.12, and is plotted a function of depth in Figure 5.9. Trichloroethylene is less than 2% of the total LNAPL (by mass), with an average value for 95 samples of

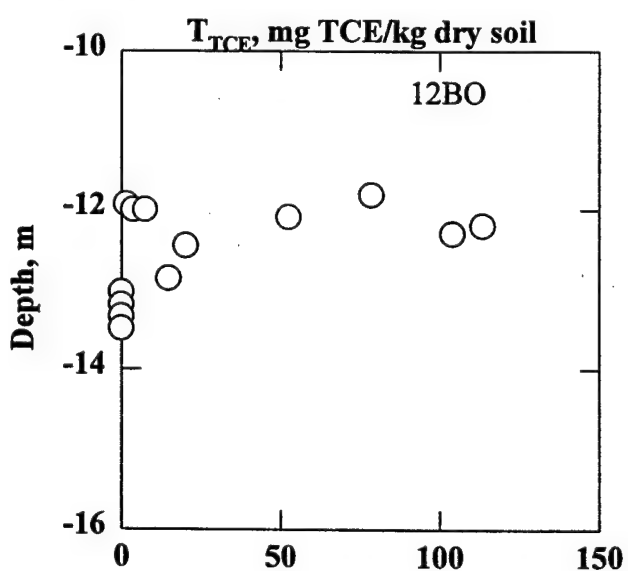
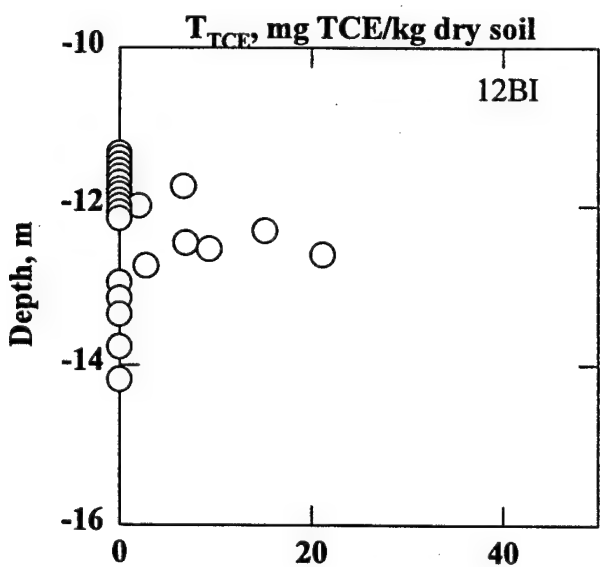
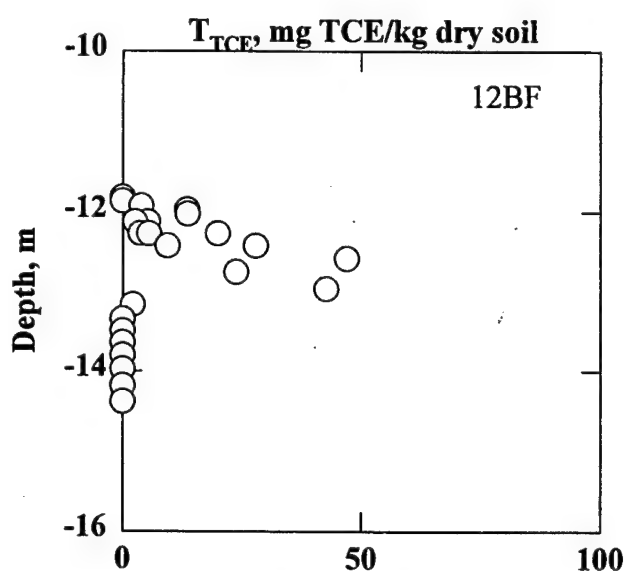
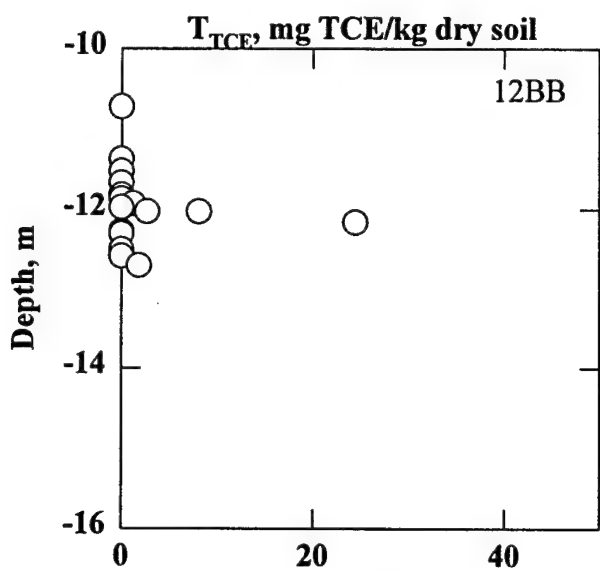
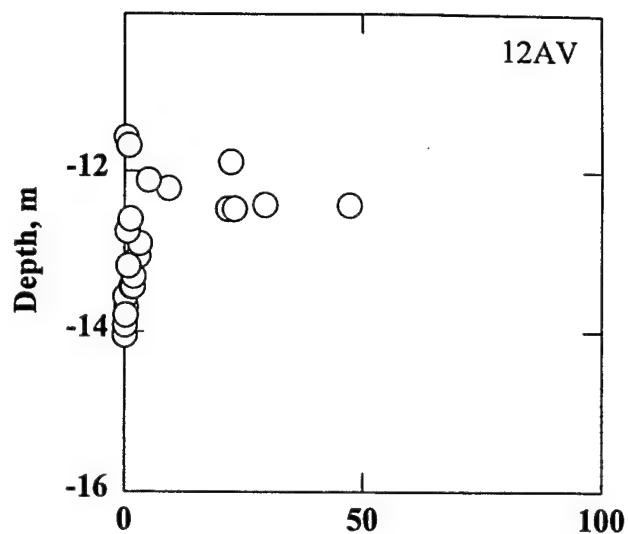
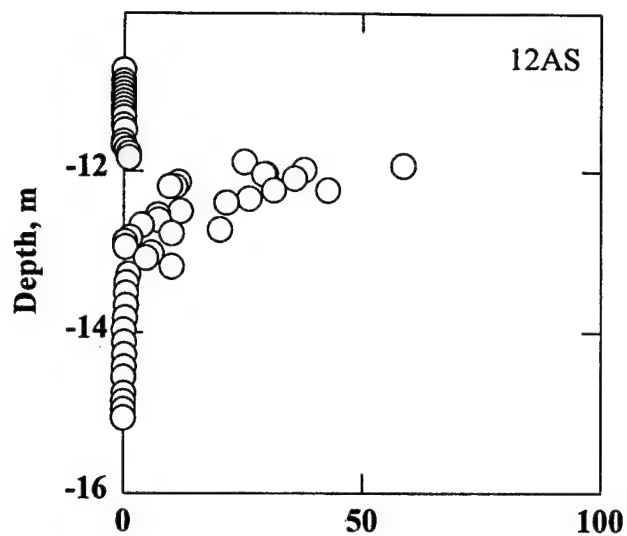


Figure 5.8 Observed Separate Phase Trichloroethylene Content in Solid Core Boreholes

**TABLE 5.8 LNAPL AND TCE CONTENT IN BOREHOLE 12AV**

Depth, m	T <sub>TCE</sub> , mg/kg	T, mg/kg	T <sub>TCE</sub> /T	Depth, m	T <sub>TCE</sub> , mg/kg	T, mg/kg	T <sub>TCE</sub> /T
11.68	1	231	0.00433	13.05	2.99	3312	0.00090
11.88	22.4	7324	0.00306	13.18	0.9	816	0.00110
12.11	5.09	1669	0.00305	13.31	1.98	1691	0.00117
12.21	9.34	3947	0.00237	13.44	1.54	1394	0.00111
12.42	29.64	7732	0.00383	13.44	1.79	1394	0.00128
12.42	47.28	13156	0.00359	13.44	1.84	1293	0.00142
12.47	21.8	4558	0.00478	13.56	0.24	89	0.00267
12.47	23.19	4558	0.00509	13.69	0.37	161	0.00230
12.60	1.34	679	0.00197	13.79	0.36	412	0.00087
12.75	0.7	340	0.00206	13.92	0.17	210	0.00081
12.90	3.3	1594	0.00207				

**TABLE 5.9 LNAPL AND TCE CONTENT IN BOREHOLE 12BB**

Depth, m	T <sub>TCE</sub> , mg/kg	T, mg/kg	T <sub>TCE</sub> /T	Depth, m	T <sub>TCE</sub> , mg/kg	T, mg/kg	T <sub>TCE</sub> /T
11.36	0.00	185	0.00000	12.16	24.46	16164	0.00151
11.51	0.00	1039	0.00000	12.30	0.00	912	0.00000
11.66	0.00	582	0.00000	12.30	0.00	669	0.00000
11.81	0.00	343	0.00000	12.50	0.00	809	0.00000
11.86	0.00	316	0.00000	12.58	0.00	553	0.00000
11.92	1.21	850	0.00142	12.70	1.83	3000	0.00061
11.97	0.00	498	0.00000	12.96	0.00	17	0.00000
12.02	2.68	5388	0.00050	12.96	0.00	16	0.00000
12.02	8.07	1877	0.00430	13.26	0.00	21	0.00000

$$\frac{T_{TCE}}{T} = 0.00253 \quad (5.26a)$$

$$\chi_{TCE} = \frac{T_{TCE}}{T} \frac{m_G}{m_Y} \quad (5.26b)$$

$$\chi_{TCE} = 0.00222 \quad (\text{separate phase}) \quad (5.26c)$$

The molar masses for TCE and total hydrocarbons cited in Equation 4.15 convert this mass fraction to the separate phase mole fraction  $\chi_{TCE}$  in Equation 5.26c. The separate phase mole fraction is important because it specifies the saturated TCE vapor concentration  $Y_{SAT}$  by virtue of

**TABLE 5.10 LNAPL AND TCE CONTENT IN BOREHOLE 12BF**

Depth, m	T <sub>TCE</sub> , mg/kg	T, mg/kg	T <sub>TCE</sub> /T	Depth, m	T <sub>TCE</sub> , mg/kg	T, mg/kg	T <sub>TCE</sub> /T
11.92	3.90	535	0.00729	12.42	9.43	4328	0.00218
11.97	13.50	2970	0.00455	12.42	27.90	8242	0.00339
12.02	13.57	3778	0.00359	12.58	47.01	12061	0.00390
12.12	5.30	2241	0.00236	12.75	23.80	5516	0.00432
12.12	2.61	1429	0.00182	12.96	42.64	19253	0.00221
12.27	19.89	1882	0.01057	13.16	2.11	1471	0.00144
12.27	3.71	5944	0.00062	13.34	0.00	443	0.00000
12.27	5.52	2054	0.00269				

**TABLE 5.11 LNAPL AND TCE CONTENT IN BOREHOLE 12BI**

Depth, m	T <sub>TCE</sub> , mg/kg	T, mg/kg	T <sub>TCE</sub> /T	Depth, m	T <sub>TCE</sub> , mg/kg	T, mg/kg	T <sub>TCE</sub> /T
11.62	0.00	666	0.00000	12.46	6.91	1867	0.00370
11.70	0.00	994	0.00000	12.54	9.34	2592	0.00360
11.75	6.68	1853	0.00361	12.61	21.19	5748	0.00369
11.79	0.00	1727	0.00000	12.75	2.78	3416	0.00081
11.85	0.00	1035	0.00000	12.96	0.00	288	0.00000
11.93	0.00	298	0.00000	12.96	0.00	199	0.00000
12.00	2.06	745	0.00277	13.16	0.00	435	0.00000
12.00	0.00	805	0.00000	13.36	0.00	192	0.00000
12.08	0.00	9119	0.00000	13.77	0.00	84	0.00000
12.16	0.00	9123	0.00000	14.18	0.00	719	0.00000
12.31	15.16	5350	0.00283				

**TABLE 5.12 LNAPL AND TCE CONTENT IN BOREHOLE 12BO**

Depth, m	T <sub>TCE</sub> , mg/kg	T, mg/kg	T <sub>TCE</sub> /T	Depth, m	T <sub>TCE</sub> , mg/kg	T, mg/kg	T <sub>TCE</sub> /T
11.81	78.62	13457	0.00584	12.30	104.00	13800	0.00754
12.00	3.66	681	0.00537	12.45	20.17	10247	0.00197
12.00	7.40	385	0.01922	12.86	14.80	18536	0.00080
12.09	52.54	6001	0.00876	13.03	0.00	204	0.00000
12.20	113.36	13907	0.00815				

Raoult's law [Eastman (1975)]

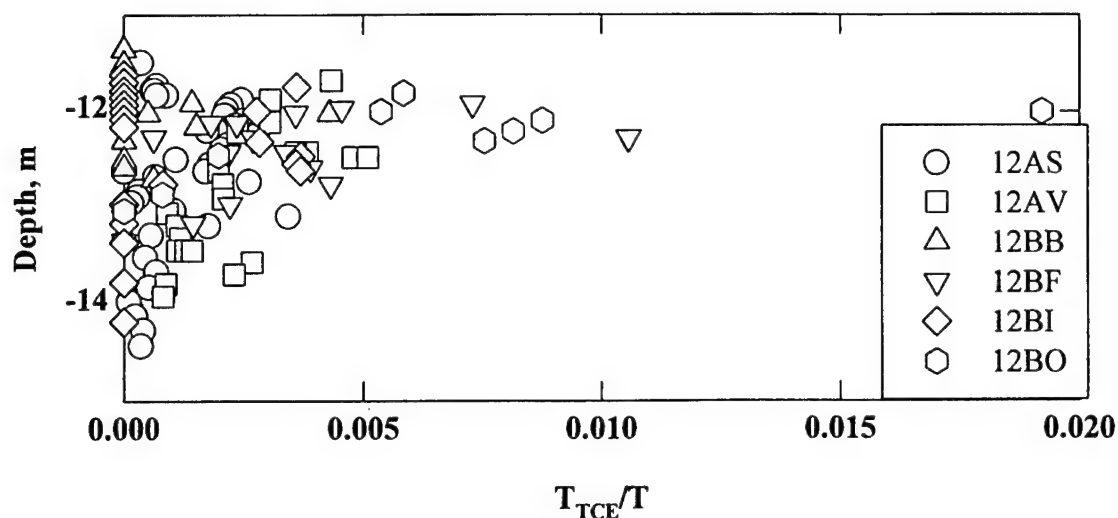


**Figure 5.9 Ratio of Separate Phase Trichloroethylene to Total Petroleum Hydrocarbons in Solid Core Samples**

$$Y_{\text{SAT}} = Y_{\text{PURE}} \chi_{\text{TCE}} \quad (5.27a)$$

$$Y_{\text{PURE}} = 0.422 \frac{\text{kg}}{\text{m}^3} \quad (293^\circ\text{K}) \quad (5.27b)$$

The ideal gas law [Eastman (1975)] is used to compute the saturated vapor concentration above pure trichloroethylene  $Y_{\text{PURE}}$  from the saturated pressure value  $p_{\text{YPURE}}$  cited by Mackay and Shiu (1981)

$$Y_{\text{PURE}} = \frac{p_{\text{YPURE}} m_{\text{TCE}}}{R_U T} \quad (5.28a)$$

$$R_U = 8.31 \frac{\text{mole} \cdot \text{m}^3}{^\circ\text{K} \cdot \text{Pa}} \quad (5.28b)$$

$$p_{\text{YPURE}} = 7.86 \times 10^3 \text{ Pa} \quad (293^\circ\text{K}) \quad (5.28c)$$

Equations 5.27 and 5.28 yield estimates of the (293°K) saturated TCE vapor pressure and concentration in the separate phase contaminated soil at Plattsburgh

$$Y_{\text{SAT}} \approx 9.39 \times 10^{-4} \frac{\text{kg}}{\text{m}^3} \quad (5.29a)$$



$$p_{\text{YSAT}} \approx 17.4\text{Pa}$$

$$(p_{\text{YSAT}} \approx 174 \text{ ppm})$$

$$(5.29b)$$

### 5.3 Soil Vapor Concentrations

#### 5.3.1 Ambient Soil Vapor Calibrations

Tables 5.13-5.29 list the total hydrocarbon, oxygen, carbon dioxide, and trichloroethylene vapor pressure data observed in the soil gas tubing clusters by UMASS researchers. The helium tracer test data are summarized in Table 5.30, while the soil vapor probe data are presented in Tables 5.31-5.40. We distinguish ambient, venting, and sparging data bases, depending on the presence of air injection at or below the capillary fringe:

##### Ambient data base

- Clusters 12AN, 12AT, and 12AX: All dates
- Clusters 12AA-12AM, 12AO-12AR, 12AU-12AW, 12AZ, and 12BA: 26Oct95 through 16Jan96
- Vapor probes VP1, VP2, and VP3

##### Soil venting data base

- Clusters 12AA-12AM, 12AO-12AR, 12AU-12AW, 12AZ, and 12BA: 17Jan96 through 15Jul96

##### Air sparging data base

- Clusters 12AA-12AM, 12AO-12AR, 12AU-12AW, 12AZ, and 12BA: 20Aug96 through 19Dec96
- Vapor probes 12BC, 12BE, 12BH, 12BJ, 12BK, 12BM, and 12BN

We calibrate the coupled, first order, steady state, ambient oxygen and carbon dioxide models (Equation 4.27) with the data from clusters 12AN, 12AT, and 12AX with the results summarized in Figure 5.10. We adopt zero  $\text{CO}_2$  and an atmospheric oxygen value  $X_0$  of  $0.288 \text{ kg/m}^3$  (20.9% by volume at  $282^\circ\text{K}$ ) as surface boundary conditions. A Fibonacci search through the combined data sets minimizes the error mean  $\delta_{\text{XCM}}$  and standard deviation  $\sigma_{\text{XC}}$  defined by

$$\delta_X = \frac{X(\text{measured}) - X(\text{predicted})}{X(\text{predicted})} \quad (5.30a)$$

$$\delta_C = \frac{C(\text{measured}) - C(\text{predicted})}{C(\text{predicted})} \quad (5.30b)$$

$$\delta_{\text{XCM}} = \frac{1}{2N} \sum_N (\delta_X + \delta_C) \quad (5.30c)$$

$$\sigma_{\text{XC}} = \sqrt{\frac{1}{2N} \sum_N (\delta_X^2 + \delta_C^2) - \delta_{\text{XCM}}^2} \quad (5.30d)$$

**TABLE 5.13 SOIL GAS CONSTITUENTS IN TUBING CLUSTERS  
26 OCTOBER 1995**

<b>Sample ID</b>	<b>Depth, m</b>	<b>p<sub>G</sub>, ppm<sup>a</sup></b>	<b>p<sub>X</sub>, %<sup>a</sup></b>	<b>p<sub>C</sub>, %<sup>a</sup></b>
12AA	7.3	230	9.8	7.9
12AB	0.9	60	18.4	2.2
	4.6	110	15.4	4.6
12AC	1.8	60	18.6	2.1
	5.5	100	15.5	3.3
12AD	3.7	60	17.3	2.1
	7.3	180	9.8	5.9
12AE	1.8	40	18.5	2.2
	5.3	80	15.7	4.3
12AF	1.8	30	19.0	1.5
	5.0	60	15.7	3.7
12AG	0.9	40	19.1	1.5
	4.6	60	17.0	2.9
12AH	3.7	90	16.8	3.1
	9.1	200	6.0	9.6
12AI	2.7	40	18.0	2.5
	8.7	140	5.3	9.5
12AJ	1.8	20	18.8	1.1
	5.5	60	15.0	3.5
12AK	3.7	60	15.9	4.3
	9.1	220	5.4	7.8
12AL	0.9	40	18.6	1.8
	4.6	60	16.4	3.8
12AM	11.1	NS <sup>b</sup>	NS	NS
12AN	1.8	60	16.2	4.6
	5.2	90	12.6	7.9
	8.2	120	14.0	4.5
12AO	3.7	40	18.0	2.9
	9.1	460	2.5	11.2
12AP	2.7	40	18.5	2.4
	7.3	140	10.8	7.4
12AQ	2.7	40	18.4	2.7
	7.3	80	12.6	6.7
12AR	0.9	0	19.6	1.7
	4.6	60	16.8	4.2
12AT	9.4	NS	NS	NS
CONTROL	3.7	0	20.8	0.2
CONTROL	7.3	0	20.8	0.2

<sup>a</sup>By volume.

<sup>b</sup>Not sampled.

**TABLE 5.14 SOIL GAS CONSTITUENTS IN TUBING CLUSTERS**  
**16 NOVEMBER 1995**

Sample ID	Depth, m	P <sub>G</sub> , ppm <sup>a</sup>	P <sub>X</sub> , % <sup>a</sup>	P <sub>C</sub> , % <sup>a</sup>
12AA	7.3	100	11	7.2
12AB	0.9	40	18.7	2.1
	4.6	60	15	5.6
12AC	1.8	110	19.3	0.9
	5.5	140	15.5	1.9
12AD	3.7	40	17.8	2.0
	7.3	80	11.7	4.3
12AE	1.8	45	19.1	1.4
	5.3	80	16.4	2.8
12AF	1.8	40	19.4	0.9
	5	60	16.7	2.2
12AG	0.9	40	19.5	0.7
	4.6	80	18.2	1.8
12AH	3.7	10	17	3.5
	9.1	160	9.2	9.5
12AI	2.7	40	18.7	1.6
	8.7	100	7.3	7.3
12AJ	1.8	60	19.3	0.8
	5.5	60	14.4	4.2
12AK	3.7	80	16.1	3.0
	9.1	100	8	17.3
12AL	0.9	60	19	1.0
	4.6	80	16.2	2.7
12AM	11.1	80	6.9	7.0
12AN	1.8	80	17	3.5
	5.2	90	12.9	6.8
	8.2	100	10	6.0
12AO	3.7	60	17.7	2.2
	9.1	100	15.8	8.3
12AP	2.7	40	19	1.3
	7.3	60	11.3	5.7
12AQ	2.7	30	18.6	1.6
	7.3	80	12.6	3.9
12AR	0.9	20	19.8	0.7
	4.6	60	16.3	3.0
12AT	9.4	NS <sup>b</sup>	NS	NS
CONTROL	3.7	0	20.7	0.0
CONTROL	7.3	0	20.7	0.0

<sup>a</sup>By volume.

<sup>b</sup>Not sampled.

**TABLE 5.15 SOIL GAS CONSTITUENTS IN TUBING CLUSTERS**  
**16 JANUARY 1996**

Sample ID	Depth, m	P <sub>G</sub> , ppm <sup>a</sup>	P <sub>X</sub> , % <sup>a</sup>	P <sub>C</sub> , % <sup>a</sup>	P <sub>Y</sub> , ppm <sup>a</sup>
12AA	7.3	70	11	7	18
12AB	0.9	30	18	2	NS
	4.6	60	16	4	NS
12AC	1.8	20	19	1	NS
	5.5	50	16	3	2
12AD	3.7	40	19	2	NS
	7.3	100	11	7	19
12AE	1.8	20	19	1	NS
	5.3	60	17	3	2
12AF	1.8	20	20	1	NS
	5	40	18	2	NS
12AG	0.9	20	20	1	NS
	4.6	40	19	2	NS
12AH	3.7	40	18	2	NS
	9.1	100	8	9	20
12AI	2.7	20	19	4	NS
	8.7	100	7	10	6
12AJ	1.8	20	19	1	NS
	5.5	50	15	4	7
12AK	3.7	50	17	3	NS
	9.1	120	8	10	19
12AL	0.9	30	19	1	NS
	4.6	50	17	2	NS
12AM	11.1	120	5	11	23
12AN	1.8	50	18	2	NS
	5.2	80	14	5	NS
	8.2	110	8	10	1
12AO	3.7	20	18	2	NS
	9.1	100	5	11	11
12AP	2.7	10	20	1	NS
	7.3	70	12	6	NS
12AQ	2.7	20	19	1	NS
	7.3	70	13	4	16
12AR	0.9	NS <sup>b</sup>	NS	NS	NS
	4.6	40	18	2	6
12AT	9.4	220	4	12	1
CONTROL	3.7	0	21	0	NS
CONTROL	7.3	0	21	0	NS

<sup>a</sup>By volume.

<sup>b</sup>Not sampled.

**TABLE 5.16 SOIL GAS CONSTITUENTS IN TUBING CLUSTERS**  
**7 FEBRUARY 1996**

Sample ID	Depth, m	p <sub>G</sub> , ppm <sup>a</sup>	p <sub>X</sub> , % <sup>a</sup>	p <sub>C</sub> , % <sup>a</sup>	p <sub>Y</sub> , ppm <sup>a</sup>
12AA	7.3	80	10.7	7.0	51.8
12AB	0.9	30	17.5	2.3	4.2
	4.6	60	15.4	3.9	23.8
12AC	1.8	20	18.3	1.7	4.5
	5.5	40	15.8	3.5	19.9
12AD	3.7	30	17.8	2.0	12.8
	7.3	80	10.2	7.7	58.2
12AE	1.8	40	18	1.8	4.3
	5.3	60	16.4	3.3	18.2
12AF	1.8	40	18.8	1.5	3.5
	5	50	17.2	2.8	13.0
12AG	0.9	20	18.8	1.4	9.8
	4.6	20	17.9	2.2	13.0
12AH	3.7	40	17.1	2.7	16.8
	9.1	80	12.5	5.6	43.4
12AI	2.7	30	18	1.8	7.3
	8.7	110	6.6	9.4	68.4
12AJ	1.8	20	18.6	1.2	7.0
	5.5	80	15	4.1	22.7
12AK	3.7	60	15.8	3.1	13.8
	9.1	120	6.5	13.0	62.3
12AL	0.9	40	16.9	2.3	4.8
	4.6	60	16.5	3.1	12.5
12AO	3.7	20	17.8	3.6	9.5
	9.1	120	4.9	11.0	105.7
12AP	2.7	40	18.7	1.3	5.2
	7.3	80	10.8	6.8	34.4
12AQ	2.7	10	18.8	1.3	5.2
	7.3	70	12.7	5.0	51.6
12AR	0.9	0	19.3	0.9	0
	4.6	10	17	3.1	15.9

<sup>a</sup>By volume.

The hydrocarbon reaction rate  $\lambda$  zeros the mean error, while the oxygen flux at the ground surface  $J_{XO}$  minimizes the error standard deviation. The cluster 12AN, 12AT, and 12AX data yield the following calibrated values:

**TABLE 5.17 SOIL GAS CONSTITUENTS IN TUBING CLUSTERS**  
**13 FEBRUARY 1996**

Sample ID	Depth, m	p <sub>G</sub> , ppm <sup>a</sup>	p <sub>X</sub> , % <sup>a</sup>	p <sub>C</sub> , % <sup>a</sup>	p <sub>Y</sub> , ppm <sup>a</sup>
12AA	7.3	50	16.9	2.7	23
12AB	0.9	50	18.4	1.8	2
	4.6	50	19	1.1	8
12AC	1.8	0	18.2	1.5	4
	5.5	0	17.4	2.2	15
12AD	3.7	0	18	1.8	9
	7.3	50	13.6	5.5	54
12AE	1.8	50	17.9	1.8	4
	5.3	70	17.1	2.7	18
12AF	1.8	30	18.8	1.2	3
	5	50	17.7	2.0	14
12AG	0.9	0	18.7	1.4	2
	4.6	0	17.9	1.9	12
12AH	3.7	50	18.2	1.8	13
	9.1	80	19.7	0.8	6
12AI	2.7	50	18.6	1.4	4
	8.7	80	15	4.1	40
12AJ	1.8	30	19	1.0	3
	5.5	30	16.9	2.6	10
12AK	3.7	70	17.3	2.2	13
	9.1	100	13.5	5.4	44
12AL	0.9	30	17.7	2.0	3
	4.6	50	17.4	2.1	9
12AM	11.1	NS <sup>b</sup>	NS	NS	NS
12AN	1.8	20	18.6	1.4	1
	5.2	70	13.5	5.8	2
	8.2	40	17.1	2.7	2
12AO	3.7	0	18.6	1.2	5
	9.1	40	16.3	3.3	34
12AP	2.7	10	19.4	0.7	2
	7.3	50	16	3.6	14
12AQ	2.7	0	19	1.0	3
	7.3	40	15.5	3.5	32
12AR	0.9	0	19.7	0.7	1
	4.6	20	18.2	1.6	12
12AT	9.4	140	9.9	8.9	5
CONTROL	3.7	0	20.8	0.1	1
CONTROL	7.3	0	20.9	0.1	0

<sup>a</sup>By volume.

<sup>b</sup>Not sampled.

**TABLE 5.18 SOIL GAS CONSTITUENTS IN TUBING CLUSTERS**  
**7 MARCH 1996**

Sample ID	Depth, m	p <sub>G</sub> , ppm <sup>a</sup>	p <sub>X</sub> , % <sup>a</sup>	p <sub>C</sub> , % <sup>a</sup>	p <sub>Y</sub> , ppm <sup>a</sup>
12AA	7.3	30	18.7	1.4	15
12AB	0.9	20	18.2	1.8	3
	4.6	10	19	1.1	7
12AC	1.8	10	18.4	1.5	4
	5.5	20	18.4	1.8	16
12AD	3.7	10	17.9	1.6	9
	7.3	50	16	4.0	62
12AE	1.8	30	17.8	2.0	4
	5.3	40	17.5	2.2	18
12AF	1.8	40	18	1.8	2
	5	30	16.8	2.5	16
12AG	0.9	0	18.4	1.6	2
	4.6	20	17.8	2.2	11
12AH	3.7	40	18	1.7	7
	9.1	10	20.3	0.5	3
12AI	2.7	30	17.9	1.9	7
	8.7	70	14.7	4.0	57
12AJ	1.8	20	18.5	1.4	5
	5.5	60	15.4	3.3	23
12AK	3.7	20	17	2.6	15
	9.1	70	13.8	1.8	61
12AL	0.9	NS <sup>b</sup>	NS	NS	NS
	4.6	30	16.5	2.3	13
12AM	11.1	NS	NS	NS	NS
12AN	1.8	60	17.3	3.8	1
	5.2	70	14.7	7.1	3
	8.2	90	10.8	8.9	5
12AO	3.7	30	17.4	1.8	7
	9.1	50	17.4	2.2	34
12AP	2.7	20	18.4	1.4	4
	7.3	60	15.8	3.8	50
12AQ	2.7	20	18.4	0.1	4
	7.3	70	14.5	NS	47
12AR	0.9	10	19	0.8	1
	4.6	40	17.3	1.9	17
12AT	9.4	170	8	8.9	6
CONTROL	3.7	0	20.9	0.1	0
CONTROL	7.3	0	20.8	0.1	0

<sup>a</sup>By volume.

<sup>b</sup>Not sampled.

**TABLE 5.19 SOIL GAS CONSTITUENTS IN TUBING CLUSTERS**  
**17 MARCH 1996**

Sample ID	Depth, m	P <sub>G</sub> , ppm <sup>a</sup>	P <sub>X</sub> , % <sup>a</sup>	P <sub>C</sub> , % <sup>a</sup>	P <sub>V</sub> , ppm <sup>a</sup>
12AA	7.3	40	19.2	1.2	8
12AB	0.9	50	17.8	2.3	4
	4.6	50	18.8	1.2	7
12AC	1.8	40	18.3	1.6	5
	5.5	60	18.9	1.7	13
12AD	3.7	60	17.7	2.3	10
	7.3	90	16.9	3.8	47
12AE	1.8	50	17.5	2.0	6
	5.3	60	18	2.0	17
12AF	1.8	50	17.5	1.6	4
	5	60	16.2	2.8	16
12AG	0.9	50	17.7	1.8	4
	4.6	40	17.4	2.0	3
12AH	3.7	40	17.1	2.0	12
	9.1	10	20.4	0.2	3
12AI	2.7	60	17.5	2.2	7
	8.7	70	15.3	3.6	37
12AJ	1.8	50	17.7	1.8	6
	5.5	60	15.1	3.7	19
12AK	3.7	50	17	2.5	15
	9.1	60	13.8	5.0	45
12AL	0.9	50	18.8	1.3	9
	4.6	60	16.1	2.8	13
12AM	11.1	NS <sup>b</sup>	NS	NS	NS
12AN	1.8	30	16.3	2.5	1
	5.2	30	13.5	5.0	3
	8.2	60	9.3	8.1	5
12AO	3.7	50	16.9	2.5	8
	9.1	50	18	1.6	20
12AP	2.7	50	18	1.8	5
	7.3	50	16.8	3.2	34
12AQ	2.7	40	17.9	1.8	5
	7.3	70	14.9	4.4	44
12AR	0.9	30	18.2	1.2	3
	4.6	40	17.1	1.8	14
12AT	9.4	130	4.3	14.0	5
CONTROL	3.7	10	20.8	0.1	2
CONTROL	7.3	10	20.8	0.1	1

<sup>a</sup>By volume.

<sup>b</sup>Not sampled.



**TABLE 5.20 SOIL GAS CONSTITUENTS IN TUBING CLUSTERS**  
**4 APRIL 1996**

Sample ID	Depth, m	P <sub>G</sub> , ppm <sup>a</sup>	P <sub>X</sub> , % <sup>a</sup>	P <sub>C</sub> , % <sup>a</sup>	P <sub>Y</sub> , ppm <sup>a</sup>
12AA	7.3	0	19.8	0.7	6
12AB	0.9	10	19.3	0.9	5
	4.6	0	19.2	0.7	5
12AC	1.8	0	18.9	1.7	5
	5.5	0	18.9	1.3	11
12AD	3.7	20	18.1	1.9	9
	7.3	30	18.2	2.3	39
12AE	1.8	20	18.4	1.8	5
	5.3	30	17.8	2.4	5
12AF	1.8	20	18.1	2.2	3
	5	30	16.2	3.0	16
12AG	0.9	20	18.9	1.7	3
	4.6	40	17.8	2.2	14
12AH	3.7	20	18.3	2.0	9
	9.1	0	20.5	2.5	2
12AI	2.7	20	18.5	2.0	9
	8.7	40	16.3	4.0	29
12AJ	1.8	20	18.5	2.4	8
	5.5	30	15.4	4.8	21
12AK	3.7	40	17.4	1.8	13
	9.1	60	15	2.8	34
12AL	0.9	20	18.9	1.9	6
	4.6	30	16.5	2.0	13
12AM	11.1	NS <sup>b</sup>	NS	NS	NS
12AN	1.8	20	15.5	4.0	2
	5.2	50	12.3	6.4	3
	8.2	80	7.1	14.0	5
12AO	3.7	20	17.4	2.9	4
	9.1	20	18.8	2.0	17
12AP	2.7	10	18.8	2.2	6
	7.3	20	17.8	3.1	12
12AQ	2.7	20	18.5	2.5	7
	7.3	60	16.5	5.2	47
12AR	0.9	10	19.5	1.6	3
	4.6	30	17.7	3.3	16
12AT	9.4	200	3.9	20.0	8
CONTROL	3.7	0	20.8	0.2	0
CONTROL	7.3	0	20.8	0.2	0

<sup>a</sup>By volume.

<sup>b</sup>Not sampled.

**TABLE 5.21 SOIL GAS CONSTITUENTS IN TUBING CLUSTERS**  
**5 MAY 1996**

<b>Sample ID</b>	<b>Depth, m</b>	<b>p<sub>G</sub>, ppm<sup>a</sup></b>	<b>p<sub>X</sub>, %<sup>a</sup></b>	<b>p<sub>Y</sub>, ppm<sup>a</sup></b>
12AA	7.3	60	20.0	5
12AB	0.9	50	19.0	10
	4.6	40	19.0	5
12AC	1.8	60	19.0	7
	5.5	40	19.0	9
12AD	3.7	40	19.0	11
	7.3	60	19.0	32
12AE	1.8	50	19.0	6
	5.3	60	18.0	15
12AF	1.8	50	19.0	4
	5	60	17.0	17
12AG	0.9	40	20.0	5
	4.6	50	19.0	14
12AH	3.7	60	19.0	9
	9.1	70	21.0	0
12AI	2.7	60	19.0	11
	8.7	70	17.0	22
12AJ	1.8	60	19.0	9
	5.5	80	16.0	20
12AK	3.7	50	18.0	12
	9.1	80	15.0	31
12AL	0.9	50	19.0	9
	4.6	60	17.0	11
12AM	11.1	10	21.0	0
12AN	1.8	70	15.0	2
	5.2	80	12.0	3
	8.2	120	6.6	4
12AO	3.7	50	18.0	12
	9.1	40	19.0	14
12AP	2.7	50	19.0	6
	7.3	60	18.0	27
12AQ	2.7	60	19.0	8
	7.3	50	18.0	45
12AR	0.9	40	20.0	2
	4.6	60	18.0	16
12AT	9.4	250	2.6	7
CONTROL	3.7	20	20.9	0
CONTROL	7.3	20	20.9	0

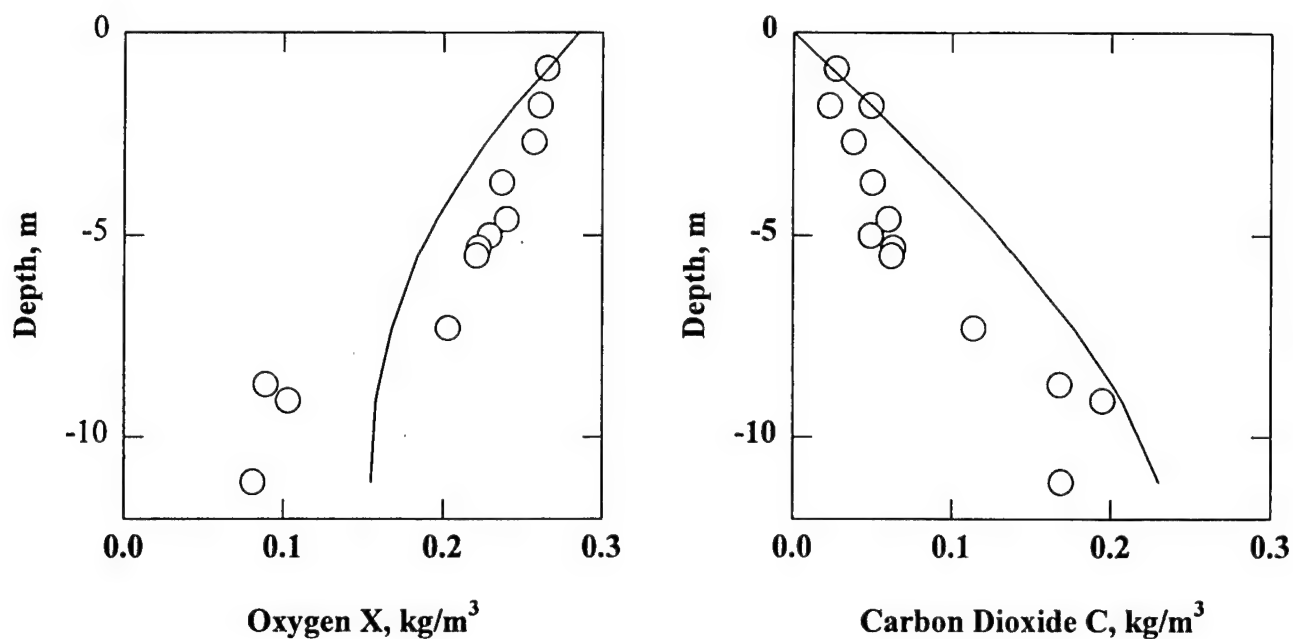
<sup>a</sup>By volume.

**TABLE 5.14 SOIL GAS CONSTITUENTS IN TUBING CLUSTERS**  
**16 NOVEMBER 1995**

Sample ID	Depth, m	p <sub>G</sub> , ppm <sup>a</sup>	p <sub>X</sub> , % <sup>a</sup>	p <sub>C</sub> , % <sup>a</sup>
12AA	7.3	100	11	7.2
12AB	0.9	40	18.7	2.1
	4.6	60	15	5.6
12AC	1.8	110	19.3	0.9
	5.5	140	15.5	1.9
12AD	3.7	40	17.8	2.0
	7.3	80	11.7	4.3
12AE	1.8	45	19.1	1.4
	5.3	80	16.4	2.8
12AF	1.8	40	19.4	0.9
	5	60	16.7	2.2
12AG	0.9	40	19.5	0.7
	4.6	80	18.2	1.8
12AH	3.7	10	17	3.5
	9.1	160	9.2	9.5
12AI	2.7	40	18.7	1.6
	8.7	100	7.3	7.3
12AJ	1.8	60	19.3	0.8
	5.5	60	14.4	4.2
12AK	3.7	80	16.1	3.0
	9.1	100	8	17.3
12AL	0.9	60	19	1.0
	4.6	80	16.2	2.7
12AM	11.1	80	6.9	7.0
12AN	1.8	80	17	3.5
	5.2	90	12.9	6.8
	8.2	100	10	6.0
12AO	3.7	60	17.7	2.2
	9.1	100	15.8	8.3
12AP	2.7	40	19	1.3
	7.3	60	11.3	5.7
12AQ	2.7	30	18.6	1.6
	7.3	80	12.6	3.9
12AR	0.9	20	19.8	0.7
	4.6	60	16.3	3.0
12AT	9.4	NS <sup>b</sup>	NS	NS
CONTROL	3.7	0	20.7	0.0
CONTROL	7.3	0	20.7	0.0

<sup>a</sup>By volume.

<sup>b</sup>Not sampled.



Note: Time averaged data.

**Figure 5.10 Observed (Symbols) and Calibrated (Curves) Ambient Soil Gas Oxygen and Carbon Dioxide in Clusters 12AN, 12AT, and 12AX**

**TABLE 5.22 (Continued) SOIL GAS CONSTITUENTS IN TUBING CLUSTERS  
15 JUNE 1996**

Sample ID	Depth, m	$p_G$ , ppm <sup>a</sup>	$p_X$ , % <sup>a</sup>	$p_Y$ , ppm <sup>a</sup>
12AU	11	NS <sup>b</sup>	NS	NS
12AV	10.9	0	20.9	0
12AW	10.8	0	20.9	0
12AX	3	80	15.0	2
	9.3	100	13.0	3
12AZ	10.7	120	20.9	4
12BA	11	120	20.9	12

<sup>a</sup>By volume.

<sup>b</sup>Not sampled.

$$\lambda = 3.34 \times 10^{-8} \text{ s}^{-1} \quad (\text{ambient}) \quad (5.31a)$$

$$J_{XO} = 6.62 \times 10^{-8} \frac{\text{kg}}{\text{m}^2 \cdot \text{s}} \quad (5.31b)$$

The combined error standard deviation is 15%, a reasonable accuracy in view of the scatter

**TABLE 5.24 SOIL GAS TRICHLOROETHYLENE IN TUBING CLUSTERS  
9 AUGUST 1996**

Sample ID	Depth, m	p <sub>y</sub> , ppm <sup>a</sup>	Sample ID	Depth, m	p <sub>y</sub> , ppm <sup>a</sup>
12AA	7.3	0	12AM	11.1	0
12AB	0.9	7	12AN	1.8	2
	4.6	0		5.5	1
12AC	1.8	4		9.1	0
	5.5	8	12AO	3.7	25
12AD	3.7	11		9.1	5
	7.3	27	12AP	2.7	11
12AE	1.8	1		7.3	43
	5.3	18	12AQ	2.7	25
12AF	1.8	6		7.3	126
	5	60	12AR	0.9	7
12AG	0.9	9		4.6	44
	4.6	8	12AT	9.4	5
12AH	3.7	8	12AU	11	0
	9.1	0	12AV	10.9	0
12AI	2.7	10	12AW	10.8	0
	8.7	10	12AX	3	0
12AJ	1.8	8		9.3	0
	5.5	51	12AZ	10.7	0
12AK	3.7	12	12BA	11	0
	9.1	52	CONTROL	3.7	0
12AL	0.9	8	CONTROL	7.3	0
	4.6	17			

<sup>a</sup>By volume.

$$\delta_{GM} = \frac{1}{N} \sum_N \delta_G \quad (5.32b)$$

$$\sigma_G = \sqrt{\frac{1}{N} \sum_N \delta_G^2 - \delta_{GM}^2} \quad (5.32c)$$

Figure 5.11 shows the results of the total hydrocarbon calibration at clusters 12AN, 12AT, and 12AX, based on the following parameter values:

$$G_F = 9.36 \times 10^{-4} \frac{\text{kg}}{\text{m}^3} \quad (\text{ambient}) \quad (5.33a)$$

$$b_F = 11.76 \text{m} \quad (12\text{AN}, 12\text{AT}, 12\text{AX}) \quad (5.33b)$$

TABLE 5.25 SOIL GAS CONSTITUENTS IN TUBING CLUSTERS

20 AUGUST 1996

Sample ID	Depth, m	p <sub>G</sub> , ppm <sup>a</sup>	p <sub>X</sub> , % <sup>a</sup>	p <sub>C</sub> , % <sup>a</sup>	p <sub>Y</sub> , ppm <sup>a</sup>
12AD	3.7	50	18.7	1.9	16
	7.3	50	19.0	1.0	19
12AH	9.1	350	18.6	0.3	133
12AI	2.7	20	18.8	1.8	0
	8.7	80	15.8	1.8	51
12AK	3.7	100	18.8	0.3	11
	9.1	120	18.6	0.2	31
12AM	11.1	500	18.5	0.2	120
12AQ	2.7	60	18.9	2.2	14
	7.3	60	18.7	1.4	34
12AR	0.9	40	19.1	1.4	5
	4.6	50	18.3	1.7	17
12AV	10.9	300	18.6	0.8	120
12AW	10.8	500	19.3	0.2	157
12AZ	10.7	220	18.9	0.19	104
12BA	11	320	19.1	0.21	115

<sup>a</sup>By volume.

We note considerable scatter in the fit, evidenced by the  $\sigma_G$  value of 45%. Nonetheless, the use of a common reaction rate across the oxygen, carbon dioxide, and total hydrocarbon ambient data sets endorses the physical validity of the calibration.

We test the calibrated steady ambient model reaction rate (Equation 5.31a) and oxygen flux (Equation 5.31b) against the ambient vapor probe data (VP1, VP2, and VP3), with the observations averaged at each depth. Figure 5.12 summarizes the results: the combined mean error is 12%, suggesting a modest overprediction of the probe data. The error standard deviation is 31%. We note a systematic overprediction with depth--an error that may be partially due to our use of fall probe data in a time averaged model. In this regard, the soil temperature is warmer than average in the fall (Figure 5.1), giving rise to higher diffusivities in this period. A flatter gradient would accordingly be needed to sustain the same flux. The ambient vapor probe hydrocarbon data are calibrated with a higher fringe concentration than the ambient cluster data, as suggested by Figure 5.13:

$$G_F = 3.66 \times 10^{-3} \frac{\text{kg}}{\text{m}^3} \quad (\text{ambient}) \quad (5.34a)$$

$$b_F = 13.15 \text{ m} \quad (\text{vapor probes}) \quad (5.32b)$$

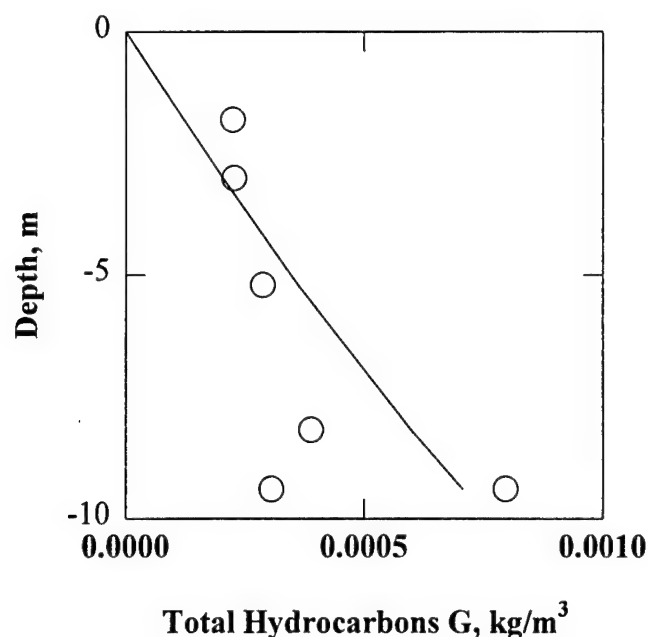
We sampled the clusters above the injection points on 26 October 1995, 16 November 1995, and

**TABLE 5.23 SOIL GAS CONSTITUENTS IN TUBING CLUSTERS**

**15 JULY 1996**

Sample ID	Depth, m	p <sub>G</sub> , ppm <sup>a</sup>	p <sub>X</sub> , % <sup>a</sup>	p <sub>Y</sub> , ppm <sup>a</sup>
12AA	7.3	0	20.0	0.1
12AB	0.9	20	19.0	6
	4.6	0	20.0	0.3
12AC	1.8	20	19.0	5
	5.5	40	17.0	7
12AD	3.7	20	19.0	21
	7.3	20	20.0	51
12AE	1.8	20	19.0	16
	5.3	20	19.0	23
12AF	1.8	40	19.0	7
	5	40	19.0	67
12AG	0.9	40	19.0	12
	4.6	40	19.0	54
12AH	3.7	40	19.0	9
	9.1	0	20.9	0
12AI	2.7	20	19.0	5
	8.7	20	17.0	10
12AJ	1.8	20	19.0	5
	5.5	40	16.0	22
12AK	3.7	40	18.0	8
	9.1	60	16.0	37
12AL	0.9	20	19.0	6
	4.6	40	17.0	20
12AM	11.1	0	20.9	0
12AN	1.8	40	17.0	1
	5.2	60	16.0	1
	8.2	60	15.0	1
12AO	3.7	40	18.0	15
	9.1	60	20.0	1
12AP	2.7	20	19.0	2
	7.3	10	19.0	15
12AQ	2.7	40	19.0	11
	7.3	40	19.0	95
12AR	0.9	50	18.0	2
	4.6	30	19.0	12
12AT	9.4	200	8.2	2
CONTROL	3.7	20	20.9	0
CONTROL	7.3	20	20.9	0

<sup>a</sup>By volume.



Note: Time averaged data.

**Figure 5.11 Observed (Symbols) and Calibrated (Curves) Ambient Soil Gas Total Hydrocarbons in Clusters 12AN, 12AT, and 12AX**

**TABLE 5.23 (Continued) SOIL GAS CONSTITUENTS IN TUBING CLUSTERS  
15 JULY 1996**

Sample ID	Depth, m	$p_G$ , ppm <sup>a</sup>	$p_X$ , % <sup>a</sup>	$p_Y$ , ppm <sup>a</sup>
12AU	11	0	20.9	0
12AV	10.9	0	20.9	0
12AW	10.8	0	20.9	0
12AX	3	40	16.0	0
	9.3	60	15.0	3
12AZ	10.7	40	19.0	0
12BA	11	0	20.9	0

<sup>a</sup>By volume.

inherent in field sampling under adverse conditions.

Since the degradation rate are specified, the total hydrocarbon profiles may be calibrated with the capillary fringe boundary concentration  $G_0$  and the depth  $z_0$  to the origin of clusters 12AN, 12AX, and 12AT. These two parameters drive a Fibonacci search designed to optimize the hydrocarbon vapor error statistics  $\delta_{GM}$  and  $\sigma_G$  defined in the usual fashion

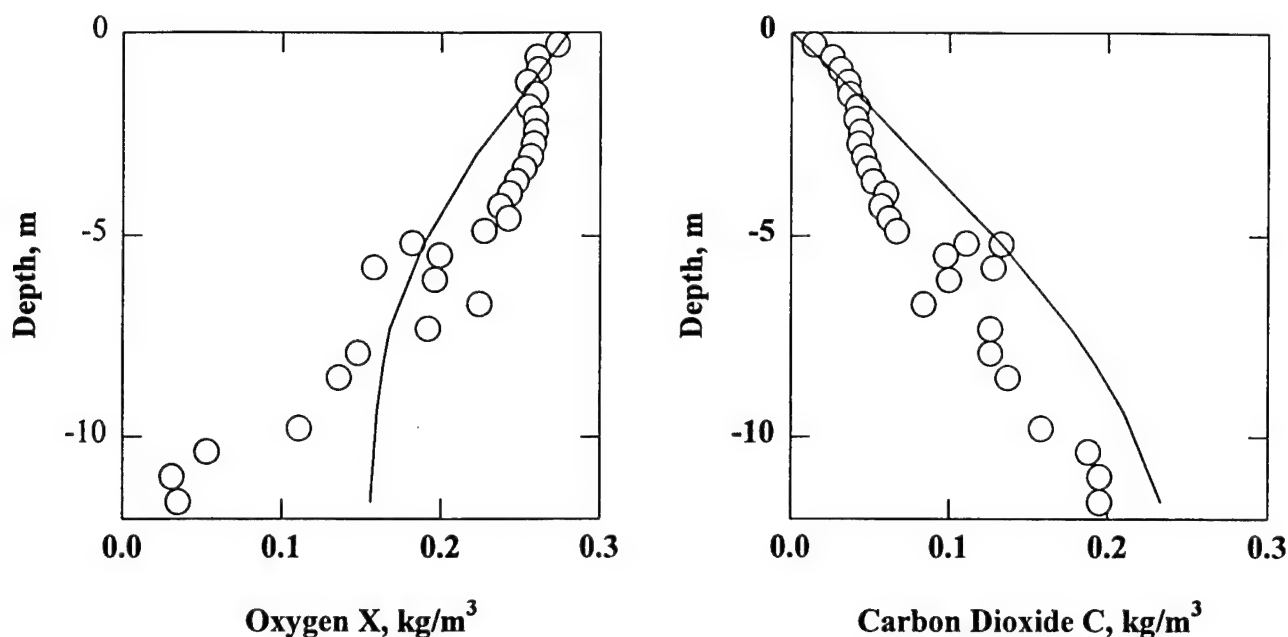
$$\delta_G = \frac{G(\text{measured}) - G(\text{predicted})}{G(\text{predicted})} \quad (5.32a)$$



**TABLE 5.26 SOIL GAS CONSTITUENTS IN TUBING CLUSTERS**  
**13 OCTOBER 1996**

Sample ID	Depth, m	p <sub>G</sub> , ppm <sup>a</sup>	p <sub>X</sub> , % <sup>a</sup>	p <sub>Y</sub> , ppm <sup>a</sup>
12AA	7.3	60	17.3	12.9
12AB	0.9	60	20	2.1
	4.6	60	18.7	7.8
12AC	1.8	40	19.8	1.5
	5.5	20	18.6	11.1
12AD	3.7	60	19.1	10.3
	7.3	60	17.9	17.8
12AE	1.8	60	19.7	3.4
	5.3	60	18.6	11.1
12AF	1.8	60	19.6	3.0
	5	60	18.3	13.2
12AG	0.9	60	19.8	2.9
	4.6	60	19	13.3
12AH	3.7	60	19.1	6.7
	9.1	40	16.1	10.3
12AI	2.7	60	19.6	4.3
	8.7	80	13.6	12.3
12AJ	1.8	60	19.9	2.0
	5.5	80	17	12.3
12AK	3.7	60	18.9	6.8
	9.1	80	14.9	13.4
12AL	0.9	40	20	0.0
	4.6	60	18.5	7.2
12AM	11.1	80	16	10.9
12AN	1.8	100	18.8	0.2
	5.2	100	16.7	2.0
	8.2	120	15.2	3.0
12AO	3.7	80	19.1	8.1
	9.1	60	15.4	11.2
12AP	2.7	60	19.4	3.4
	7.3	60	17.4	19.1
12AQ	2.7	80	19.2	7.7
	7.3	80	18.2	32.9
12AR	0.9	60	19.9	1.1
	4.6	60	18.9	14.0
12AT	9.4	200	12.4	6.4
CONTROL	3.7	20	20.7	0
CONTROL	7.3	20	20.7	0

<sup>a</sup>By volume.



Note: Vapor probe data are averaged at each depth.

**Figure 5.12 Observed (Symbols) and Calibrated (Curves) Ambient Soil Gas Oxygen and Carbon Dioxide in VP1, VP2, and VP3**

**TABLE 5.26 (Continued) SOIL GAS CONSTITUENTS IN TUBING CLUSTERS  
13 OCTOBER 1996**

Sample ID	Depth, m	$p_G$ , ppm <sup>a</sup>	$p_X$ , % <sup>a</sup>	$p_Y$ , ppm <sup>a</sup>
12AU	11	80	15.4	9.3
12AV	10.9	60	15.1	10.1
12AW	10.8	60	16.6	11.7
12AX	3	80	16.7	1.0
	9.3	100	14.5	1.5
12AZ	10.7	60	15.6	12.7
12BA	11	60	16.5	12.5

<sup>a</sup>By volume.

16 January 1996 before inducing an air flow in the subsurface. We average clusters over the three dates and at each depth to generate a third ambient data base for supplemental model testing and calibration:

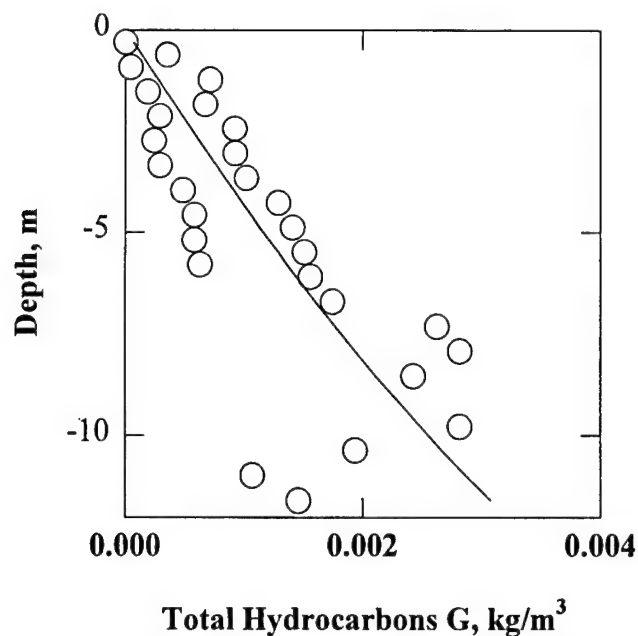
- Depth 0.9 m-12AB, 12AG, 12AL, and 12AR
- Depth 1.8 m-12AC, 12AE, 12AF, and 12AJ
- Depth 2.7 m-12AI, 12AP, and 12AQ
- Depth 3.7 m-12AD, 12AH, 12AK, and 12AO
- Depth 4.6 m-12AB, 12AG, 12AL and 12AR
- Depth 5.0 m-12AF

**TABLE 5.27 SOIL GAS CONSTITUENTS IN TUBING CLUSTERS  
7 NOVEMBER 1996**

Sample ID	Depth, m	p <sub>G</sub> , ppm <sup>a</sup>	p <sub>X</sub> , % <sup>a</sup>	p <sub>Y</sub> , ppm <sup>a</sup>
12AA	7.3	0	20.1	7
12AB	0.9	20	20.3	3
	4.6	0	20.0	9
12AC	1.8	0	20.0	4
	5.5	0	19.8	14
12AD	3.7	0	19.4	10
	7.3	0	19.1	21
12AE	1.8	0	20.1	0
	5.3	0	19.6	15
12AF	1.8	0	20.0	4
	5	10	19.2	16
12AG	0.9	0	20.0	3
	4.6	0	20.3	17
12AH	3.7	0	19.7	7
	9.1	0	20.6	7
12AI	2.7	0	20.3	3
	8.7	30	17.8	17
12AJ	1.8	0	20.4	1
	5.5	30	18.4	17
12AK	3.7	0	19.8	7
	9.1	20	18.7	2
12AL	0.9	0	20.4	2
	4.6	0	19.8	NS <sup>b</sup>
12AM	11.1	0	20.7	13
12AN	1.8	10	18.5	1
	5.2	10	18.5	2
	8.2	60	15.0	5
12AO	3.7	0	19.1	3
	9.1	0	18.3	17
12AP	2.7	0	19.7	NS
	7.3	10	18.7	21
12AQ	2.7	0	19.4	9
	7.3	30	18.3	40
12AR	0.9	0	20.0	2
	4.6	20	19.0	19
12AT	9.4	100	13.5	2
CONTROL	3.7	0	20.8	0
CONTROL	7.3	0	20.8	0

<sup>a</sup>By volume.

<sup>b</sup>Not sampled.



Note: Vapor probe data are averaged at each depth.

**Figure 5.13 Observed (Symbols) and Calibrated (Curves) Ambient Soil Gas Total Hydrocarbon in VP1 and VP3**

**TABLE 5.27 (Continued) SOIL GAS CONSTITUENTS IN TUBING CLUSTERS  
7 NOVEMBER 1996**

Sample ID	Depth, m	$p_G$ , ppm <sup>a</sup>	$p_X$ , % <sup>a</sup>	$p_Y$ , ppm <sup>a</sup>
12AU	11	20	20.7	13
12AV	10.9	260	20.7	93
12AW	10.8	0	20.7	8
12AX	3	NS <sup>b</sup>	NS	2
	9.3	60	14.5	4
12AZ	10.7	0	20.7	5
12BA	11	0	20.7	7

<sup>a</sup>By volume.

<sup>b</sup>Not sampled.

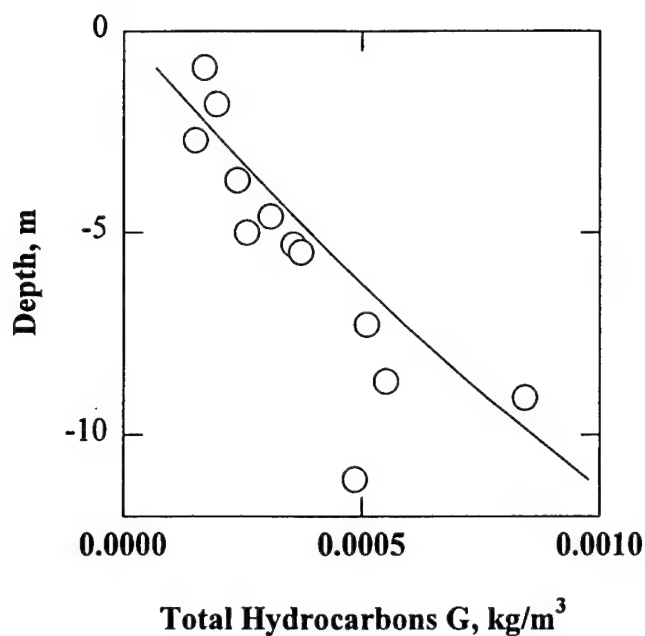
- Depth 5.3 m-12AE
- Depth 5.5m-12AC and 12AJ
- Depth 7.3 m-12AA, 12AD, 12AP, and 12AQ
- Depth 8.7 m-12AI
- Depth 9.1 m-12AH, 12AK, and 12AO
- Depth 11.1 m-12AM

**TABLE 5.29 SOIL GAS CONSTITUENTS IN TUBING CLUSTERS**  
**19 DECEMBER 1996**

Sample ID	Depth, m	p <sub>G</sub> , ppm <sup>a</sup>	p <sub>X</sub> , % <sup>a</sup>	p <sub>Y</sub> , ppm <sup>a</sup>
12AA	7.3	0	20.5	0.7
12AB	0.9	0	20.5	1
	4.6	0	20.3	0.7
12AC	1.8	0	20.5	0.5
	5.5	10	20.3	0.8
12AD	3.7	10	20.2	1.3
	7.3	20	20	1.5
12AE	1.8	10	20.4	0.5
	5.3	10	19.9	0.5
12AF	1.8	10	20.2	1.2
	5	10	19.3	1.8
12AG	0.9	0	20.6	0.6
	4.6	10	20.2	1.3
12AH	3.7	0	20	1.2
	9.1	0	20.8	0.3
12AI	2.7	0	20.2	1
	8.7	10	17.8	1.8
12AJ	1.8	0	20.1	0.7
	5.5	20	18.2	2.4
12AK	3.7	0	19.7	1
	9.1	10	18.3	1.8
12AL	0.9	0	20.2	0.3
	4.6	10	19.3	1.5
12AM	11.1	NS <sup>b</sup>	NS	NS
12AN	1.8	30	17.8	5.3
	5.2	20	17.9	4
	8.2	40	15.4	6.3
12AO	3.7	10	19.3	2.2
	9.1	20	19	2
12AP	2.7	0	20.3	1.3
	7.3	20	19.3	1.2
12AQ	2.7	0	20.1	1.3
	7.3	10	19.1	2.2
12AR	0.9	0	20.4	0.5
	4.6	20	19.7	1.6
12AT	9.4	110	13.6	8
CONTROL	3.7	0	20.8	0.2
CONTROL	7.3	NS	NS	NS

<sup>a</sup>By volume.

<sup>b</sup>Not sampled.



Note: Cluster data are averaged at each depth.

**Figure 5.15 Observed (Symbols) and Calibrated (Curves) Ambient Soil Gas Total Hydrocarbons in 12AA-12AM, 12AO-12AR, 12AU-12AW, 12AZ, and 12BA 26 October 1995-16 January 1996**

**TABLE 5.29 (Continued) SOIL GAS CONSTITUENTS IN TUBING CLUSTERS 19 DECEMBER 1996**

Sample ID	Depth, m	$p_G$ , ppm <sup>a</sup>	$p_X$ , % <sup>a</sup>	$p_Y$ , ppm <sup>a</sup>
12AU	11	0	20.8	0.4
12AV	10.9	0	20.9	0.2
12AW	10.8	10	20.8	0.4
12AX	3	10	18.5	3.5
	9.3	20	14.8	7.4
12AZ	10.7	0	20.9	0.2
12BA	11	NS <sup>b</sup>	NS	NS

<sup>a</sup>By volume.

<sup>b</sup>Not sampled.

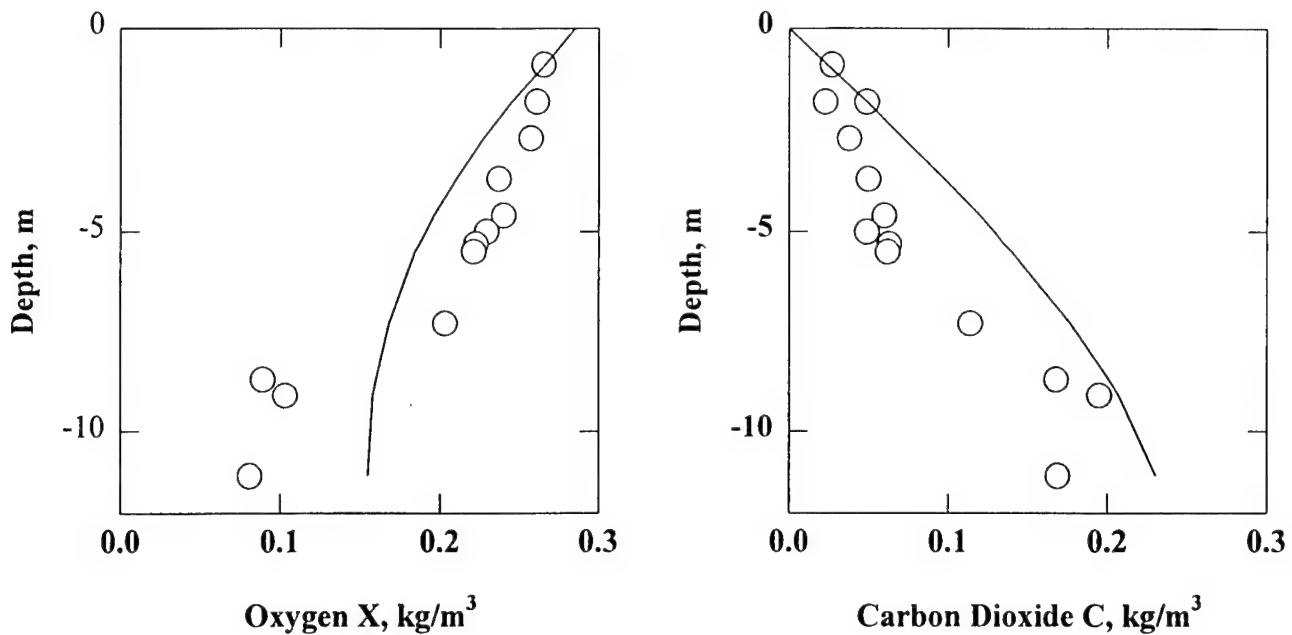
$$G_F = 1.39 \times 10^{-3} \frac{\text{kg}}{\text{m}^3} \quad (\text{ambient}) \quad (5.35a)$$

$$b_F = 14.29\text{m} \quad (\text{fall clusters}) \quad (5.35b)$$

**TABLE 5.28 SOIL GAS CONSTITUENTS IN TUBING CLUSTERS  
21 NOVEMBER 1996**

Sample ID	Depth, m	p <sub>G</sub> , ppm <sup>a</sup>	p <sub>X</sub> , % <sup>a</sup>	p <sub>Y</sub> , ppm <sup>a</sup>
12AA	7.3	0	20.7	3
12AB	0.9	0	20.5	2
	4.6	0	20.3	5
12AC	1.8	0	20.5	3
	5.5	0	20.3	10
12AD	3.7	10	20.1	11
	7.3	30	19.9	21
12AE	1.8	0	20.4	3
	5.3	10	20.1	12
12AF	1.8	20	20.9	1
	5	50	20.1	14
12AG	0.9	0	20.3	3
	4.6	20	19.8	11
12AH	3.7	0	20.9	6
	9.1	0	20.6	2
12AI	2.7	20	20.2	3
	8.7	40	18.8	10
12AJ	1.8	0	20.2	2
	5.5	40	19.4	11
12AK	3.7	20	20	6
	9.1	20	18.8	10
12AL	0.9	0	20.3	1
	4.6	0	19.9	6
12AM	11.1	10	20.8	11
12AN	1.8	20	18.3	2
	5.2	40	16.3	2
	8.2	60	15.7	3
12AO	3.7	20	19.3	9
	9.1	30	19.6	9
12AP	2.7	0	19.9	4
	7.3	20	19.9	19
12AQ	2.7	0	20	7
	7.3	40	19.5	32
12AR	0.9	0	20.4	1
	4.6	20	19.8	14
12AT	9.4	240	14.4	8
CONTROL	3.7	0	20.6	0
CONTROL	7.3	0	20.7	0

<sup>a</sup>By volume.



Note: Cluster data are averaged at each depth.

**Figure 5.14 Observed (Symbols) and Calibrated (Curves) Ambient Soil Gas Oxygen and Carbon Dioxide in 12AA-12AM, 12AO-12AR, 12AU-12AW, 12AZ, and 12BA  
26 October 1995-16 January 1996**

**TABLE 5.28 (Continued) SOIL GAS CONSTITUENTS IN TUBING CLUSTERS  
21 NOVEMBER 1996**

Sample ID	Depth, m	$p_G$ , ppm <sup>a</sup>	$p_X$ , % <sup>a</sup>	$p_Y$ , ppm <sup>a</sup>
12AU	11	0	20.8	5
12AV	10.9	40	20.7	19
12AW	10.8	0	20.6	8
12AX	3	60	15.8	1
	9.3	60	15.7	2
12AZ	10.7	0	20.6	4
12BA	11	0	20.7	8

<sup>a</sup>By volume.

Figure 5.14 displays the ambient tubing cluster data and calibration for oxygen and carbon dioxide, which feature a combined mean error of 20% and a combined error standard deviation of 28%. The figure is similar to its vapor probe counterpart in Figure 5.12--both data sets were taken in the fall only, subject to higher diffusivities and flatter gradients of vapor. The corresponding total hydrocarbon vapor concentration and water table depth are



**TABLE 5.30 HELIUM TRACER PRESSURES  $p_H$  IN TUBING CLUSTERS<sup>a</sup>**

Sample ID	Depth, m	13Feb96 6 days	21Feb96 14 days	7Nov96 14 days	20Nov96 27 days
12AA	7.3	NS <sup>b</sup>	1790	3355	4473
12AB	0.9	144	232	483	1234
	4.6	83	422	1839	3084
12AC	1.8	67	144	65	675
	5.5	138	568	1393	2693
12AD	3.7	39	148	523	1377
	7.3	219	948	2436	3896
12AE	1.8	48	146	109	905
	5.3	82	296	1121	2292
12AF	1.8	33	26	60	289
	5	22	59	181	643
12AG	0.9	17	64	85	376
	4.6	47	127	398	781
12AH	3.7	65	219	700	1499
	9.1	808	2433	307	5174
12AI	2.7	43	101	322	756
	8.7	391	1114	3447	4431
12AJ	1.8	22	59	145	415
	5.5	97	94	469	12041
12AK	3.7	88	332	1110	2151
	9.1	473	1416	148	4732
12AL	0.9	72	77	432	997
	4.6	53	134	NS	1113
12AM	11.1	NS	NS	5957	8962
12AO	3.7	18	35	470	533
	9.1	432	1263	3465	4831
12AP	2.7	66	54	179	454
	7.3	163	545	2346	3701
12AQ	2.7	0	31	NS	472
	7.3	48	213	1377	2780
12AR	0.9	13	73	64	288
	4.6	44	108	608	1766
12AU	9.4	NS	NS	5886	6940
12AV	11	NS	NS	2239	9726
12AW	10.9	NS	NS	5183	5493
12AZ	9.3	NS	NS	4974	5783
12BA	10.7	NS	NS	4968	5769

<sup>a</sup> ppm by volume.

<sup>b</sup> Not sampled.

TABLE 5.31 SOIL GAS CONSTITUENTS IN VAPOR PROBE VP1

Depth, m	p <sub>G</sub> , ppm <sup>a</sup>	p <sub>X</sub> , % <sup>a</sup>	p <sub>C</sub> , % <sup>a</sup>
0	40	20.8	0
0.61	150	19.4	1.5
1.22	240	18.5	2
1.83	260	18.3	2.4
2.44	320	18.2	2.4
3.05	320	18.1	2.5
3.66	340	18.1	2.6
4.27	420	17.6	2.9
4.88	480	16.8	3.8
5.49	500	16.3	3.8
6.10	500	16.2	3.9
6.71	360	14.8	4.5
7.32	540	11.3	6.7
7.93	580	11	6.7
8.54	500	10	7.3
9.76	580	8.1	8.4
10.37	400	3.9	10
10.98	220	2.3	10.4
11.59	300 <sup>b</sup>	2.6	10.4

<sup>a</sup>By volume.

<sup>b</sup>Dilution bag used.

Figure 5.15 summarizes the calibration, which has a zero mean and an error standard deviation of 50%.

### 5.3.2 Ambient Assimilative Capacity for Total Hydrocarbon Vapors

The ambient calibrated parameter values support an estimate of the assimilative capacity of the subsurface to degrade JP4 jet fuel vapors in the study area. The flux of oxygen entering the ground ( $J_{XO}$ , Equation 5.31b) is assumed to be consumed by aerobic degradation in the subsurface, a process that generates a stoichiometrically proportional flux of carbon dioxide entering the atmosphere. It is instructive to compare  $J_{XO}$  to the flux of total hydrocarbon vapors leaving the capillary fringe  $J_{GF}$

$$J_{GF} = -\theta D_{GS} \frac{dG_S}{dz} \quad (z=-b_F) \quad (5.36a)$$

$$J_{GF} = \theta G_O \sqrt{\lambda_G D_{GS}} \tanh(z_O \sqrt{\frac{\lambda_G}{D_{GS}}}) \quad (\text{ambient}) \quad (5.36b)$$

**TABLE 5.32 SOIL GAS CONSTITUENTS IN VAPOR PROBE VP2**

Depth, m	p <sub>G</sub> , ppm	p <sub>X</sub> , % <sup>a</sup>	p <sub>C</sub> , %
0	NS <sup>b</sup>	20.9	NS
0.61	NS	19.6	NS
1.22	NS	18.9	NS
1.83	NS	19	NS
2.44	NS	19.5	NS
3.05	NS	19.4	NS
3.66	NS	18	NS
4.27	NS	16.5	NS
4.88	NS	15.3	NS
5.49	NS	15.4	NS
6.10	NS	15.4	NS
6.71	NS	18	NS
7.32	NS	16.8	NS
7.93	NS	10.7	NS

<sup>a</sup>Downhole oxygen probe, % by volume.

<sup>b</sup>Not sampled.

**TABLE 5.33 SOIL GAS CONSTITUENTS IN VAPOR PROBE VP3**

Depth, m	p <sub>G</sub> , ppm <sup>a</sup>	p <sub>X</sub> , % <sup>a</sup>	p <sub>C</sub> , % <sup>a</sup>
0.30	0	20.7	0.8
0.61	0	19.9	1.4
0.91	10	19.6	1.7
1.22	60	19.4	1.9
1.52	40	19.2	2
1.83	20	19.2	2.1
2.13	60	19.1	2.2
2.44	60	19.4	2.3
2.74	50	18.9	2.3
3.05	60	18.7	2.4
3.35	60	18.4	2.6
3.66	80	18	3
3.96	100	17.8	3.2
4.27	110	17.8	3.2
4.57	120	17.7	3.3
4.88	100	17.7	3.3
5.18	120	13.3	5.9
5.49	120	12.1	6.6
5.79	130	11.6	6.8
6.10	140	11.4	6.8

<sup>a</sup>By volume.

**TABLE 5.34 SOIL GAS CONSTITUENTS IN VAPOR PROBE 12BC**

Depth, m	p <sub>G</sub> , ppm <sup>a</sup>	p <sub>X</sub> , % <sup>a</sup>	p <sub>C</sub> , % <sup>a</sup>	p <sub>Y</sub> , ppm <sup>a</sup>
10.06	0	21.7	1.5	49
10.37	260	18.7	1.2	107
10.52	280	18.8	1.1	118
10.67	340	18.7	1.2	144
10.82	450	18.6	1.1	181
10.98	620	18.6	1.2	226
10.98	740	18.6	1.2	273
11.12	800	18.5	1.2	299
11.28	820	21.6	0.0	80

<sup>a</sup>By volume.

<sup>b</sup>Not sampled.

**TABLE 5.35 SOIL GAS CONSTITUENTS IN VAPOR PROBE 12BE**

Depth, m	p <sub>G</sub> , ppm <sup>a</sup>	p <sub>X</sub> , % <sup>a</sup>	p <sub>C</sub> , % <sup>a</sup>	p <sub>Y</sub> , ppm <sup>a</sup>
9.5	200	18.0	0.66	54
9.6	200	18.0	0.72	48
9.8	220	18.0	0.72	48
9.9	320	18.0	0.6	52
10.1	320	18.0	0.57	49
10.2	300	18.0	0.58	49
10.4	300	18.0	0.52	34
10.7	280	18.1	0.65	54
10.8	300	18.1	0.66	52
11.0	300	18.1	0.67	50
11.1	280	18.1	0.67	50
11.3	280	18.1	0.67	46
11.4	300	18.0	0.62	56

<sup>a</sup>By volume.

<sup>b</sup>Not sampled.

We derive Equation 5.34b from the steady profile of Equation 4.26. We evaluate  $D_{GS}$  using Equations 4.28b and 4.29, adopt an ambient  $G_F$  value of  $0.001 \text{ kg/m}^3$ , set  $b_F$  equal to 13 m, and compute the steady, ambient hydrocarbon diffusion rate entering the unsaturated zone as

$$J_{GF} = 8.92 \times 10^{-11} \frac{\text{kg}}{\text{m}^2 - \text{s}} \quad (\text{ambient diffusion}) \quad (5.37a)$$

$$D_{GS} = 4.37 \times 10^{-6} \frac{\text{m}^2}{\text{s}} \quad (5.37b)$$

**TABLE 5.36 SOIL GAS CONSTITUENTS IN VAPOR PROBE 12BH**

Depth, m	$p_G$ , ppm <sup>a</sup>	$p_X$ , % <sup>a</sup>	$p_C$ , % <sup>a</sup>	$p_Y$ , ppm <sup>a</sup>
9.3	110	20.0	0.310	81
9.5	140	20.0	0.064	85
9.6	200	19.8	0.18	121
9.8	220	19.9	0.18	123
9.9	220	19.9	0.18	121
10.1	230	19.8	0.183	122
10.2	230	19.9	0.184	128
10.4	220	19.8	0.184	121
10.5	210	19.9	0.186	92
10.7	210	19.8	0.190	130
10.8	200	19.9	0.167	119
11.0	210	19.9	0.171	118

<sup>a</sup>By volume.

**TABLE 5.37 SOIL GAS CONSTITUENTS IN VAPOR PROBE 12BJ**

Depth, m	$p_G$ , ppm <sup>a</sup>	$p_X$ , % <sup>a</sup>	$p_C$ , % <sup>a</sup>	$p_Y$ , ppm <sup>a</sup>
9.3	160	19.5	0.222	140
9.8	150	19.6	0.234	141
9.9	140	19.5	0.262	139
10.1	140	19.6	0.267	145
10.2	140	19.4	0.290	144
10.4	140	19.6	0.287	146
10.5	140	19.5	0.292	147
10.7	120	19.9	0.471	132
10.8	120	20.1	0.491	129
11.0	100	20.1	1.00	38

<sup>a</sup>By volume.

We compare Eqs. 5.31b and 5.37a and conclude that the hydrocarbon vapor flux leaving the capillary fringe is far less than the oxygen and carbon dioxide fluxes entering the soil

$$J_{XO} \gg J_{GF} \quad (\text{ambient diffusion}) \quad (5.38)$$

The aerobic degradation responsible for oxygen consumption and carbon dioxide generation, must occur in the capillary fringe, reducing hydrocarbon vapor concentrations from values near saturation to the low levels found in the unsaturated zone.

We compute the natural attenuation rate  $\lambda_F$  in the capillary fringe by equating the oxygen supply rate to the product of the air volume in the fringe and the attenuation rate, adjusted for stoichiometry

**TABLE 5.38 SOIL GAS CONSTITUENTS IN VAPOR PROBE 12BK**

Depth, m	p <sub>G</sub> , ppm <sup>a</sup>	p <sub>X</sub> , % <sup>a</sup>	p <sub>C</sub> , % <sup>a</sup>	p <sub>Y</sub> , ppm <sup>a</sup>
9.30	100	13.2	3.3	35
9.45	100	13.5	3.6	31
9.60	100	13.3	3.6	33
9.76	100	13.3	3.6	33
9.91	100	13.4	3.1	29
10.06	110	14.1	2.3	18
10.21	240	17.0	1.4	78
10.37	300	16.8	1.2	82
10.52	340	16.6	1.3	85
10.67	420	16.5	1.3	84
10.82	460	16.9	1.3	83
10.98	540	16.9	1.3	85
11.13	700	16.9	1.3	88

<sup>a</sup>By volume.

**TABLE 5.39 SOIL GAS CONSTITUENTS IN VAPOR PROBE 12BM**

Depth, m	p <sub>G</sub> , ppm <sup>a</sup>	p <sub>X</sub> , % <sup>a</sup>	p <sub>C</sub> , % <sup>a</sup>	p <sub>Y</sub> , ppm <sup>a</sup>
9.30	120	16.0	1.5	48
9.45	110	16.2	1.5	53
9.60	110	15.7	1.5	50
9.76	110	16.8	1.3	47
9.91	110	16.7	1.3	45
10.06	180	17.5	1.1	84
10.21	180	17.2	1.0	90
10.37	190	17.3	1.1	96
10.52	200	17.1	1.1	107
10.67	230	17.2	1.1	NS <sup>b</sup>
10.82	240	17.1	1.1	157
10.98	280	17.1	1.1	190
11.13	340	16.9	1.2	202

<sup>a</sup>By volume.

$$J_{XO} \approx \lambda_F \zeta \theta G_{SAT} \gamma_X \quad (5.39a)$$

$$\lambda_F \approx 1.42 \times 10^{-6} \text{ s}^{-1} \quad (5.39b)$$

Equation 5.39b is predicated on a saturated hydrocarbon vapor pressure  $G_{SAT}$  of 0.05 kg/m<sup>3</sup> (10,000 ppm), an upper bound on the headspace vapor concentrations found during core

TABLE 5.40 SOIL GAS CONSTITUENTS IN VAPOR PROBE 12BN

Depth, m	$p_G$ , ppm <sup>a</sup>	$p_X$ , % <sup>a</sup>	$p_C$ , % <sup>a</sup>	$p_Y$ , ppm <sup>a</sup>
9.30	200	18.6	0.48	163
9.45	230	18.8	0.48	165
9.60	240	18.7	0.46	178
9.76	220	18.6	0.45	NS
9.76	NS <sup>b</sup>	NS	NS	NS
9.91	240	18.7	0.43	181
10.06	280	18.4	0.41	131
10.21	320	18.5	0.60	204
10.37	380	18.5	0.391	216
10.67	480	18.6	0.376	229
10.82	500	18.8	0.364	233
10.98	520	18.4	0.357	234

<sup>a</sup>By volume.

<sup>b</sup>Not sampled.

sampling (Figure 3.5). The capillary fringe thickness  $\zeta$  is assumed to be 1 m.

### 5.3.3 Helium Tracer Tests for Soil Venting and Air Sparging

We analyze the helium tracer data with the finite element model described in Section 4.4. A no (normal) flux boundary is imposed on the capillary fringe (as well as on the vertical axis), and zero concentrations are imposed at the ground surface and the radius of influence

$$H = 0 \quad (r=r_E) \quad (5.40a)$$

$$H = 0 \quad (z=0) \quad (5.40b)$$

$$\frac{\partial H}{\partial r} = 0 \quad (r=0, z > -b_F) \quad (5.40c)$$

$$\frac{\partial H}{\partial z} = 0 \quad (r > 0, z = -b_F) \quad (5.40d)$$

The model is run from a pure initial condition on the assumption of steady pneumatics.

We test the model by using measured or estimated parameter values for all input data. The volumetric discharge is set at its measured value cited in Equation 3.8, while the total and air porosities are given by independently observed data summarized in Equations 5.11b and 5.13. Soil temperature is specified by Equations 5.1 and 5.3, while the hydrocarbon diffusivity is

computed in accordance with Equation 4.33, yielding the steady helium diffusivity cited in Table 4.2. The radial coordinates  $r_p$  of the cluster points are computed from their surveyed positions (Table 3.1), using the injection point coordinates  $x_{INJ}$ ,  $y_{INJ}$  (in feet) as the origin

$$r_p = \sqrt{\frac{(x_p - x_{INJ})^2 + (y_p - y_{INJ})^2}{10.76}} \quad (5.41)$$

The sparge or venting injection point is set on the capillary fringe, and the radius of influence is set at 15 m for both tests

$$r_E = 15\text{m} \quad (5.42a)$$

$$b_F = 13\text{m} \quad (\text{venting and sparging}) \quad (5.42b)$$

We assess the accuracy of the model tests using statistics of the helium error  $\delta_H$  defined by

$$\delta_H = H_{\text{MEASURED}} - H_{\text{PREDICTED}} \quad (5.43a)$$

$$\delta_{HS} = \frac{1}{N} \sum \delta_H \quad (5.43b)$$

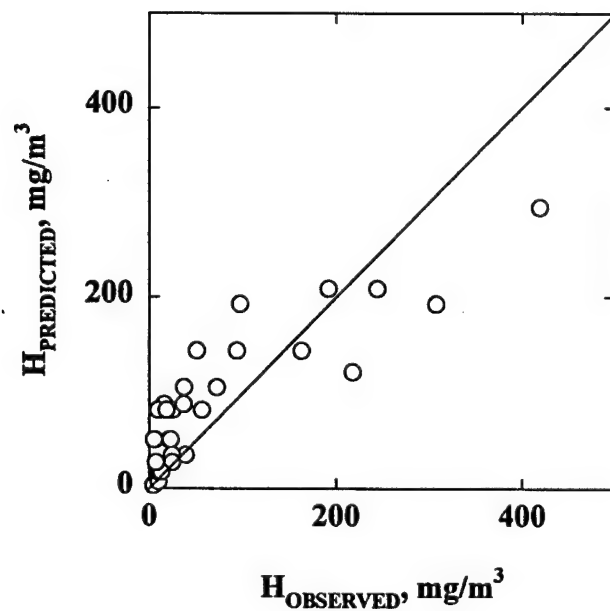
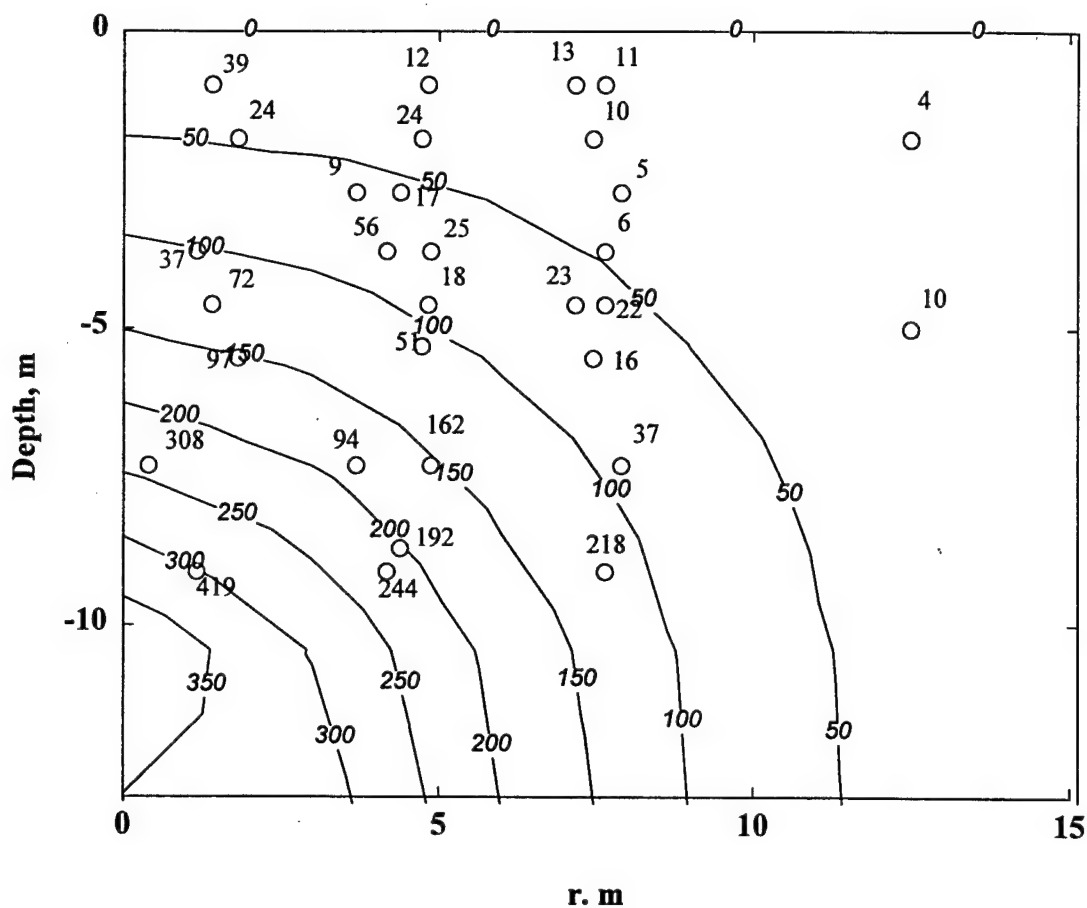
$$\sigma_H = \sqrt{\frac{1}{N} \delta_H^2 - \delta_{HM}^2} \quad (5.43c)$$

We predict the helium concentration  $H_p$  at an arbitrary point by interpolating adjacent nodal values  $H_i$ . Round 2 sampling data are used in both venting and sparging tests, to minimize effects of transient pneumatics on the theory.

Figure 5.16 summarizes Round 2 testing for soil venting. We note a mean helium model error  $\delta_{HS}$  of 18 mg/m<sup>3</sup>, and an error standard deviation  $\sigma_H$  of 53 mg/m<sup>3</sup>, which are an order of magnitude less than the injection concentration  $H_{INJ}$  of 347 mg/m<sup>3</sup> cited in Table 3.6. The data are predictions are plotted as a contour diagram, and a scatter plot on the figure--we tend to overpredict smaller, more distant, concentrations and underpredict larger concentrations near the origin. The former error may reflect transient pneumatics near the leading edge of the injection, while the latter error may be attributed in part to schematizing the venting injection as a single point. The test results are encouraging nonetheless, particularly in view of the scatter inherent in field sampling under the adverse weather conditions of upstate New York.

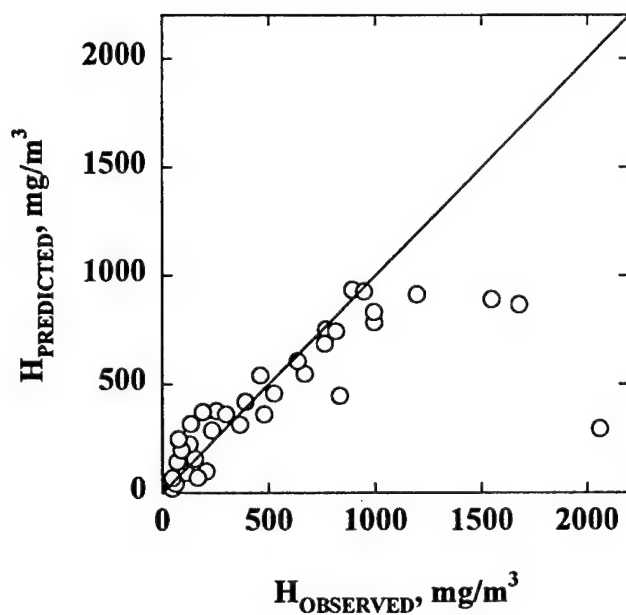
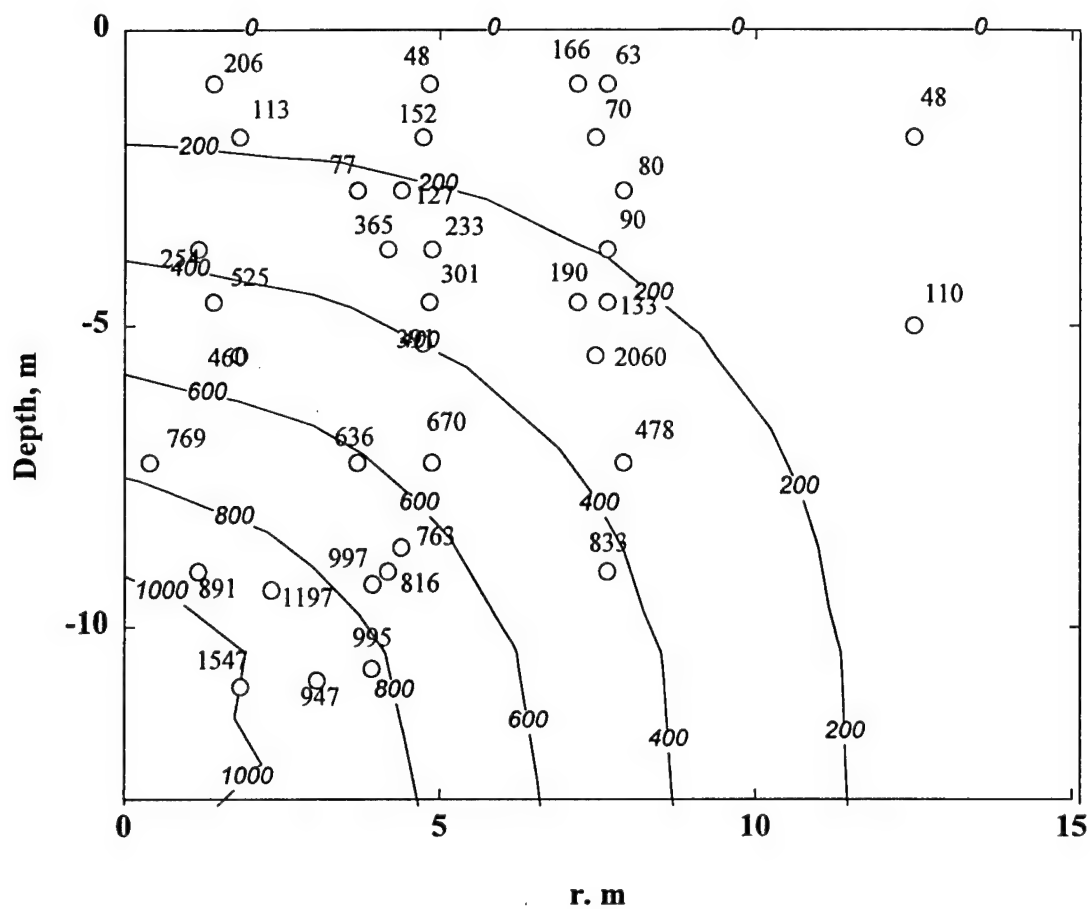
Figure 5.17 summarizes Round 2 testing for air sparging, based on an injection concentration of 1,010 mg/m<sup>3</sup> (Table 3.6). The mean model error of 105 mg/m<sup>3</sup> and the error standard deviation of 341 mg/m<sup>3</sup> are also an order of magnitude less than the injection concentration. As with the soil venting test, the strong concentrations are slightly overpredicted, while the distant, weaker data are somewhat underpredicted. Taken together, the consistent test





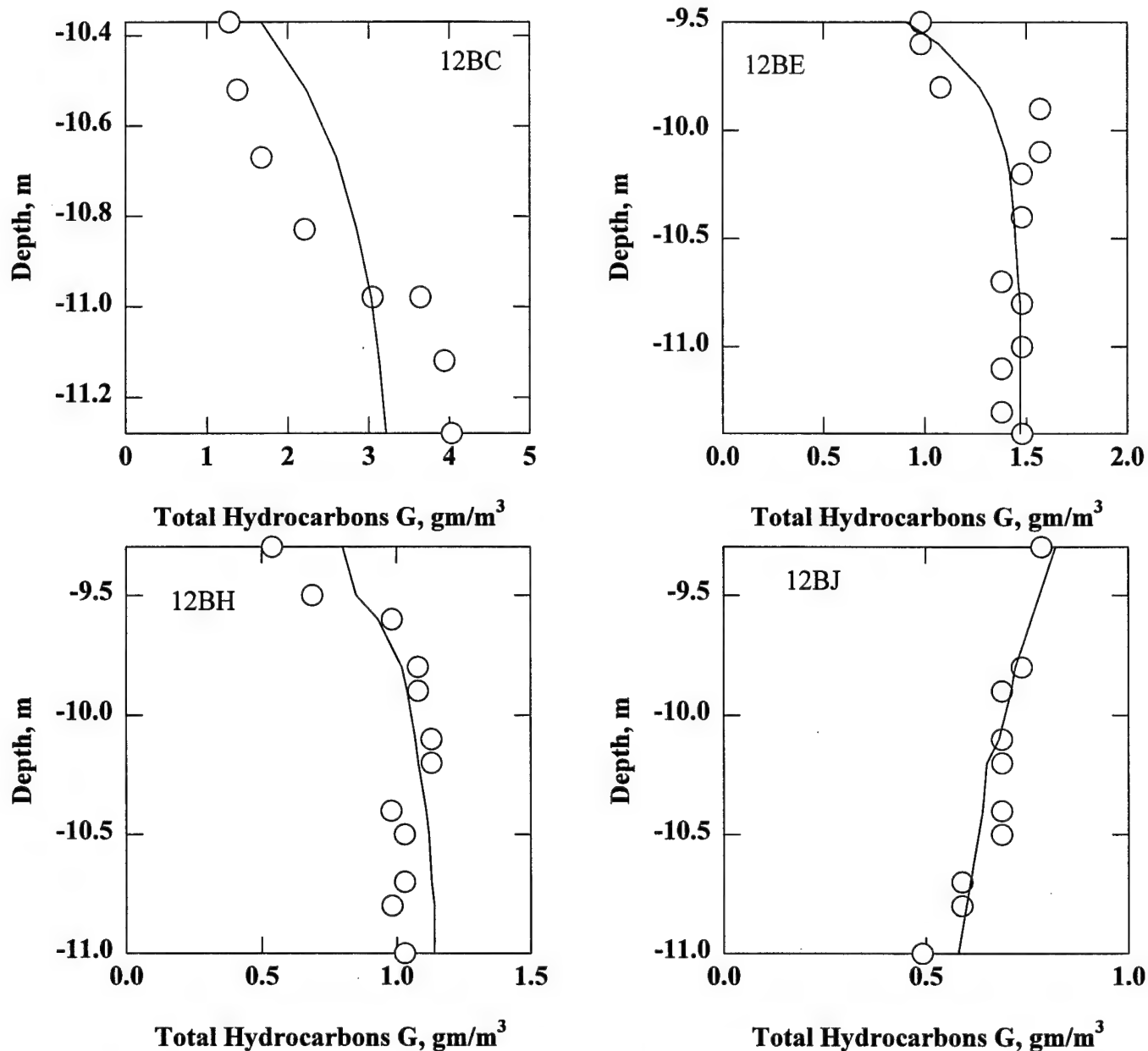
Note: Straight line is perfect model prediction.

**Figure 5.16 Observed and Predicted Helium Concentrations for Soil Venting (Round 2)**



Note: Straight line is perfect model prediction.

**Figure 5.17 Observed and Predicted Helium Concentrations for Air Sparging (Round 2)**



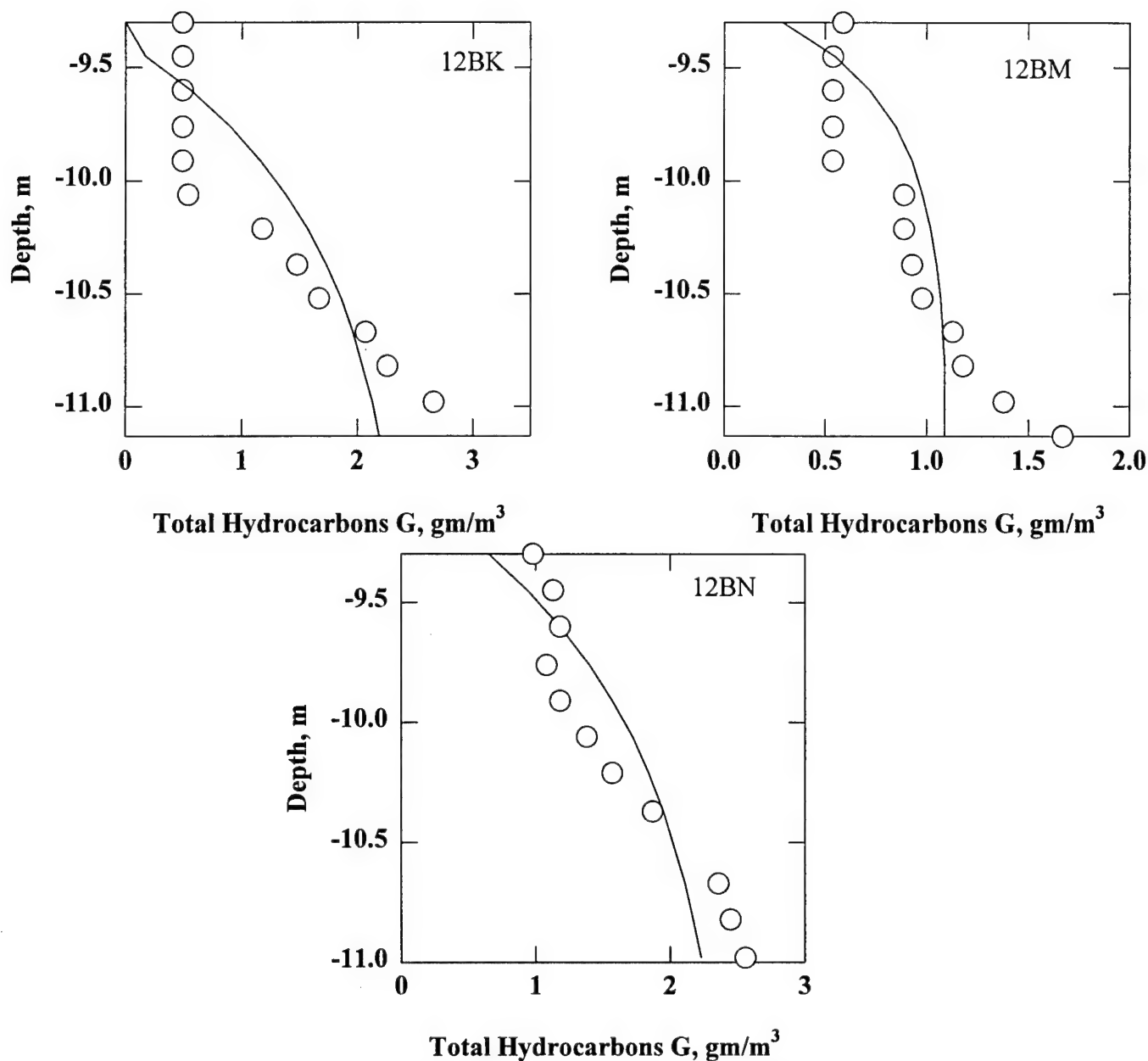
Note: Data Observed on 22 August 1996, after 12 days of air sparging

**Figure 5.18 Observed (Symbols) and Calibrated (Curves) Total Hydrocarbon Concentrations in Vapor Probe Boreholes**

accuracy endorses the physical validity of the model approach, the adequacy of field sampling methodology, and confirms the values of the advective and diffusive transport coefficients.

#### 5.3.4 Soil Venting and Air Sparging of Total Hydrocarbons

We documented the initial response of the study area to air sparging (9 August 1995 startup) with a round of stainless steel tubing cluster sampling (20 August 1996, Table 5.25) and



Note: Data Observed on 22 August 1996, after 12 days of air sparging

**Figure 5.18 (Continued) Observed (Symbols) and Calibrated (Curves) Total Hydrocarbon Concentrations in Vapor Probe Boreholes**

vapor probes (boreholes 12BC, 12BE, 12BH, 12BJ, 12BK, 12BM, and 12BN, Tables 5.34-5.40).

The vapor probes delineate the vertical profile near the capillary fringe in an attempt to quantify boundary conditions for the finite element grid. We calibrate the quasi steady vertical profile model for total hydrocarbons (Equation 4.59) with the results summarized in Figure 5.18 and Table 5.41. The fringe concentration  $G_F$  zeroed the mean hydrocarbon error  $\delta_{GM}$ , while the

**TABLE 5.41 TOTAL HYDROCARBON PROFILE CALIBRATION NEAR  
CAPILLARY FRINGE**

Borehole	$\sigma_G, \text{gm/m}^3$	$G_F, \text{gm/m}^3$	$J_{GF}, \mu\text{g/m}^2\text{-s}$	$r, \text{m}$	$w_F, \text{m/s}$
12BC	0.68	3.36	11.4	2.83	$3.38 \times 10^{-6}$
12BE	0.12	1.45	6.26	1.91	$4.29 \times 10^{-6}$
12BH	0.11	1.18	2.04	4.19	$1.73 \times 10^{-6}$
12BJ	0.04	0.465	0.26	7.22	$6.51 \times 10^{-7}$
12BK	0.56	2.45	3.79	4.53	$1.53 \times 10^{-6}$
12BM	0.25	1.10	3.46	2.62	$3.13 \times 10^{-6}$
12BN	0.28	2.48	3.55	4.75	$1.42 \times 10^{-6}$

fringe flux  $J_{GF}$  minimizes the error standard deviation  $\sigma_G$ , with the error  $\delta_G$  and statistics defined by Equation 5.32. The error standard deviation ranges from 0.04 to 0.68  $\text{gm/m}^3$ , while the calibrated fringe concentration is between 0.47 and 3.36  $\text{gm/m}^3$  in magnitude. The average of the seven fringe concentrations and fringe hydrocarbon fluxes induced by air sparging is given by

$$G_F = 1.78 \frac{\text{mg}}{\text{m}^3} \quad (\text{air sparging, vapor probes}) \quad (5.44a)$$

$$J_{GF} = 4.39 \frac{\mu\text{g}}{\text{m}^2\text{-s}} \quad (\text{air sparging, vapor probes}) \quad (5.44b)$$

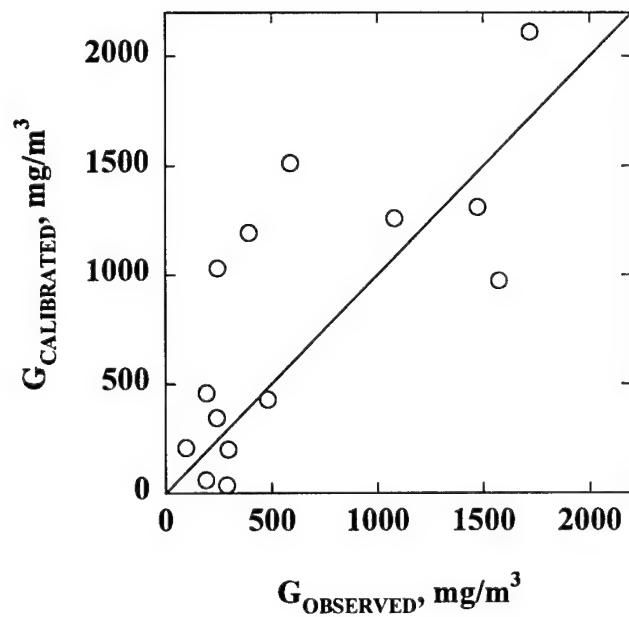
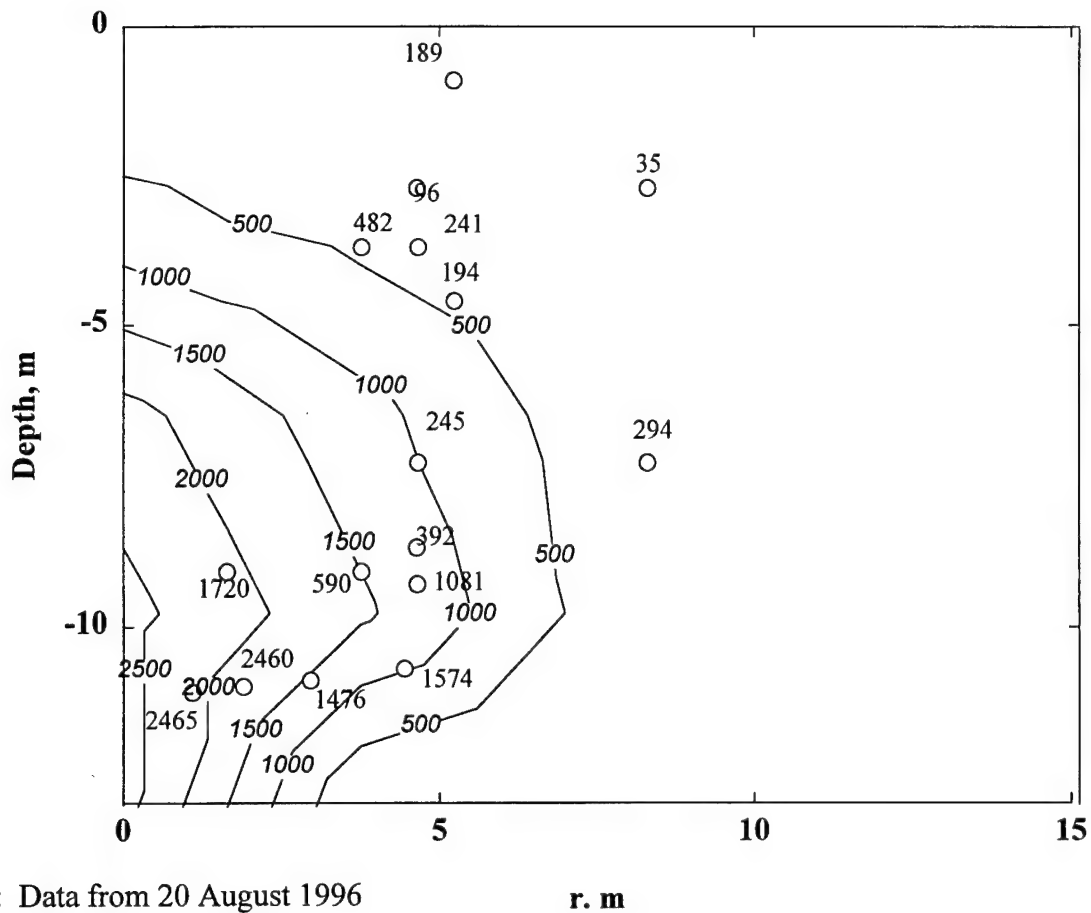
We note that sparging stimulates an initial hydrocarbon evaporation rate two orders of magnitude higher than ambient diffusion (Equation 5.37a).

The 20 August 1996 tubing cluster data are distributed over the entire study area, and are accordingly amenable to analysis by the finite element code. We impose a zero boundary condition on the capillary fringe in place of Equation 5.40d, input the reference diffusivity for total hydrocarbons (Table 4.2), and optimize the hydrocarbon model error with the injection concentration  $G_{INF}$ . Figure 5.19 displays the results of the calibration, based on the following parameter values

$$G_{INF} = 2.66 \frac{\text{gm}}{\text{m}^3} \quad (\text{air sparging, tubing cluster}) \quad (5.45a)$$

$$\delta_{GM} = 0.06 \frac{\text{gm}}{\text{m}^3} \quad (5.45b)$$

$$\sigma_G = 0.6 \frac{\text{gm}}{\text{m}^3} \quad (5.45c)$$



Note: Straight line is perfect model prediction, tubing cluster data.

**Figure 5.19 Observed and Calibrated Hydrocarbon Concentrations for Air Sparging**

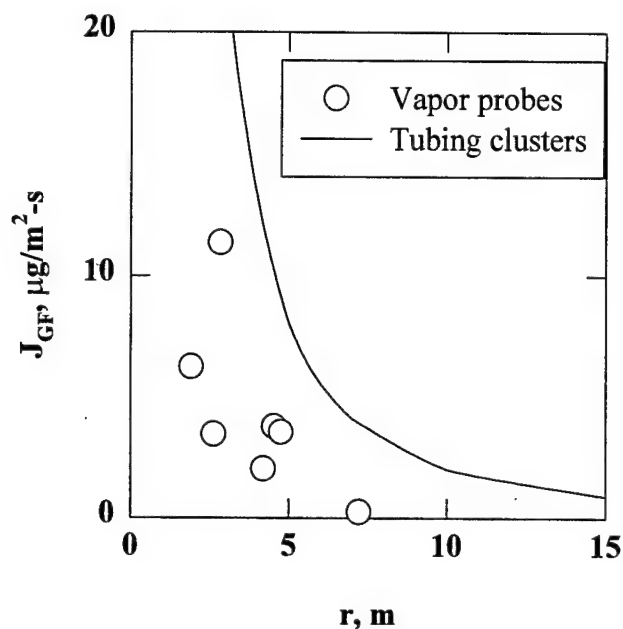


**Figure 5.20 Vertical Hydrocarbon Flux Estimates by Vapor Probe Profiles (Symbols) and Stainless Steel Tubing Clusters (Curve)**

We infer the sparged flux  $F_{\text{GSPARGE}}$  of total hydrocarbons by multiplying the calibrated injection concentration by the volumetric discharge with the result

$$F_{\text{GSPARGE}} = QG_{\text{INJ}} \quad (5.46a)$$

$$F_{\text{GSPARGE}} = 1.26 \times 10^{-6} \frac{\text{kg}}{\text{s}} \quad (5.46b)$$

This flux advects and diffuses radially (spherically) away from the sparge point. We derive a rough estimate of the vertical flux component near the capillary fringe by dividing the half of this flux by the projected area of the sphere on the horizontal plane with the result

$$J_{\text{GF}} \approx \frac{QG_{\text{INJ}}}{2\pi r^2} \quad (5.47)$$

We plot this radial variation on Figure 5.20, along with the calibrated values inferred from the vapor probe data. The decrease of flux with distance from the sparge point is apparent.

We monitored the soil venting of total hydrocarbon vapors with the stainless steel tubing clusters from startup of soil venting on 18 January 1996 to shutdown on 9 August 1996. Venting proceeded without interruption over this six month period, as documented by Tables 5.17-5.23. We fit the finite element model to the data by a Fibonacci search for  $G_{\text{INJ}}$ , with the results shown

**TABLE 5.42 SOIL VENTING OF TOTAL HYDROCARBONS  
CALIBRATION RESULTS**

Date	$\delta_{GM}, \text{gm/m}^3$	$\sigma_G, \text{gm/m}^3$	$G_{INF}, \text{gm/m}^3$	Points	$t, \text{s}^a$
7 Feb96	0.003	0.16	0.525	31	$1.73 \times 10^6$
13 Feb96	0.011	0.13	0.363	31	$2.25 \times 10^6$
7 Mar96	0.003	0.12	0.254	30	$4.24 \times 10^6$
17 Mar96	0.003	0.15	0.404	31	$5.10 \times 10^6$
4 Apr96	0.001	0.09	0.179	31	$6.66 \times 10^6$
5 May96	0.013	0.12	0.401	31	$9.34 \times 10^6$
15 Jun96	0.002	0.18	0.351	36	$1.29 \times 10^7$
15 July96	0.010	0.12	0.179	37	$1.55 \times 10^7$

<sup>a</sup>from start of soil venting.

in Table 5.42. The injection concentrations, which minimize the mean model error individual sampling trips, vary from 0.179 to 0.525 gm/m<sup>3</sup>, with an overall average of

$$G_{INJ} = 0.332 \frac{\text{gm}}{\text{m}^3} \quad (\text{soil venting}) \quad (5.48a)$$

$$F_{GVENT} = 1.56 \times 10^{-7} \frac{\text{kg}}{\text{s}} \quad (5.48b)$$

The error standard deviation ranges from 0.09 to 0.16 gm/m<sup>3</sup> in magnitude. The spherical flux of total hydrocarbons entering the unsaturated zone  $F_{GVENT}$  is an order of magnitude less than that initially induced by air sparging. The efflux varies with time, although a systematic decrease is not evinced by the data. Figure 5.21 displays the observed and calibrated total hydrocarbon vapor concentrations on 7 February 1996, after 20 days of soil venting.

## 5.4 Trichloroethylene Vapor Concentrations

### 5.4.1 Trichloroethylene venting and sparging data

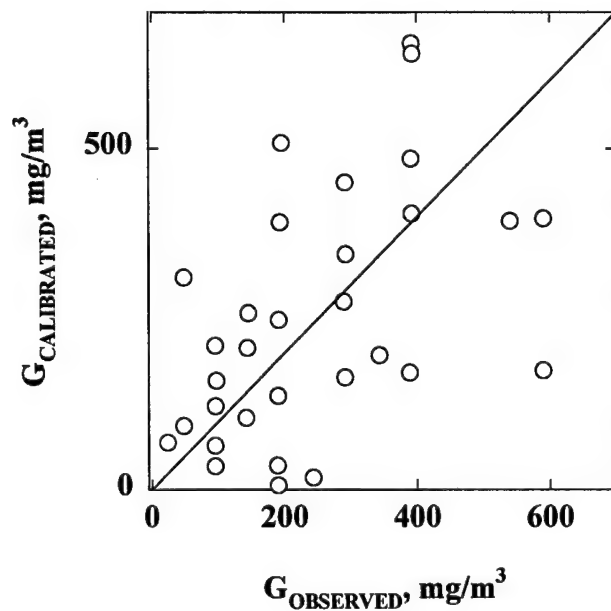
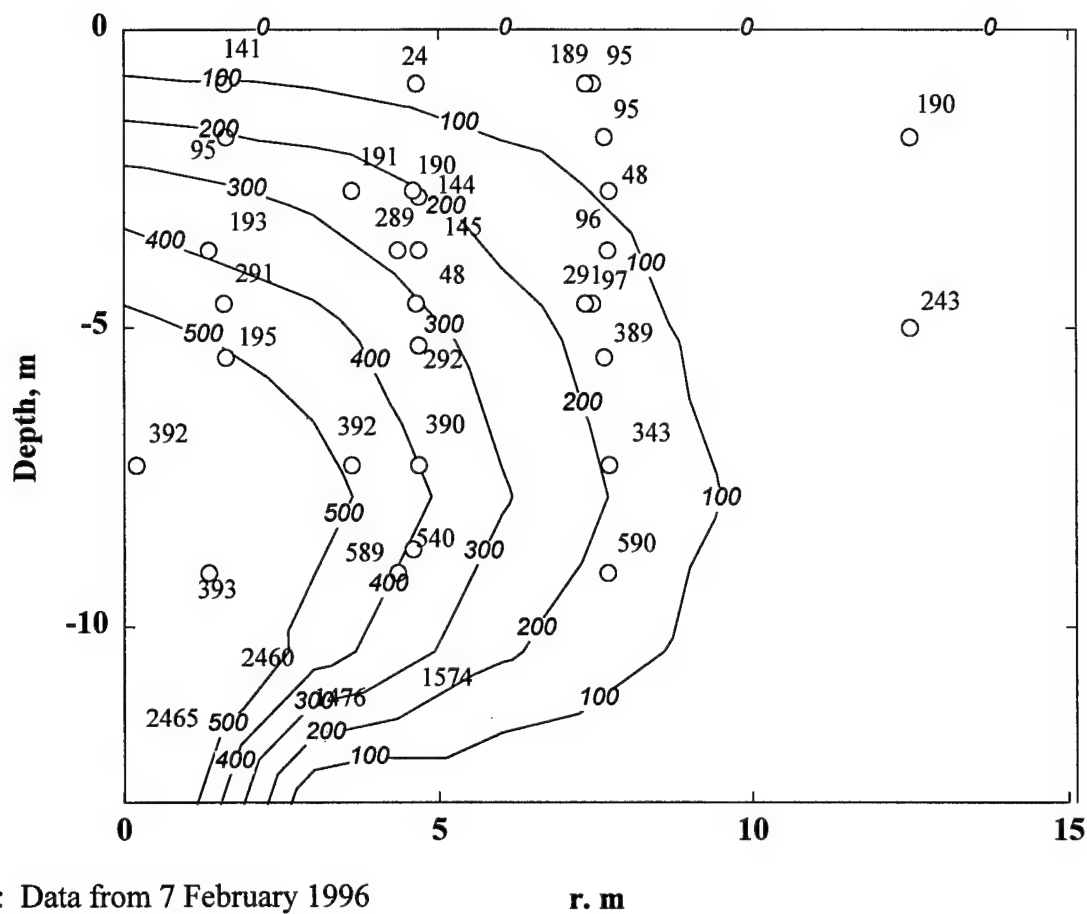
We analyze trichloroethylene soil gas concentrations in similar fashion to the total hydrocarbon data, based on the following parameter values:

$$D_{YS} = 4.07 \times 10^{-6} \frac{\text{m}^2}{\text{s}} \quad (5.49a)$$

$$\lambda_{TCE} = 0 \quad (\text{unsaturated zone}) \quad (5.49b)$$

Soil venting is considered first. Tables 5.17-5.24 list the data, which are input to the finite element model. We calibrate values for the injection concentration  $Y_{INJ}$  by minimizing the TCE model error mean  $\delta_{YM}$ , with the error  $\delta_Y$  and error standard deviation  $\sigma_Y$  defined by





Note: Straight line is perfect model prediction, tubing cluster data.

**Figure 5.21 Observed and Calibrated Hydrocarbon Concentrations for Soil Venting**

**TABLE 5.43 SOIL VENTING OF TRICHLOROETHYLENE  
CALIBRATION RESULTS**

Date	$\delta_{YM}$ , gm/m <sup>3</sup>	$\sigma_Y$ , gm/m <sup>3</sup>	$Y_{INF}$ , gm/m <sup>3</sup>	Points	t, s <sup>a</sup>
7 Feb96	0.002	0.11	0.231	31	1.73x10 <sup>6</sup>
13Feb96	0.037	0.07	0.181	31	2.25x10 <sup>6</sup>
7 Mar96	0.001	0.09	0.125	30	4.24x10 <sup>6</sup>
17Mar96	0.010	0.07	0.131	31	5.10x10 <sup>6</sup>
4Apr96	0.022	0.06	0.125	31	6.66x10 <sup>6</sup>
5May96	0.029	0.06	0.131	31	9.34x10 <sup>6</sup>
15Jun96	0.022	0.05	0.119	31	1.29x10 <sup>7</sup>
15July96	0.017	0.12	0.150	31	1.55x10 <sup>7</sup>
9Aug96	0.005	0.13	0.150	31	1.77x10 <sup>7</sup>

<sup>a</sup>from start of soil venting.

$$\delta_Y = Y_{MEASURED} - Y_{CALIBRATED} \quad (5.50a)$$

$$\delta_{YM} = \frac{1}{N} \sum \delta_Y \quad (5.50b)$$

$$\sigma_Y = \sqrt{\frac{1}{N} \delta_Y^2 - \delta_{YM}^2} \quad (5.50c)$$

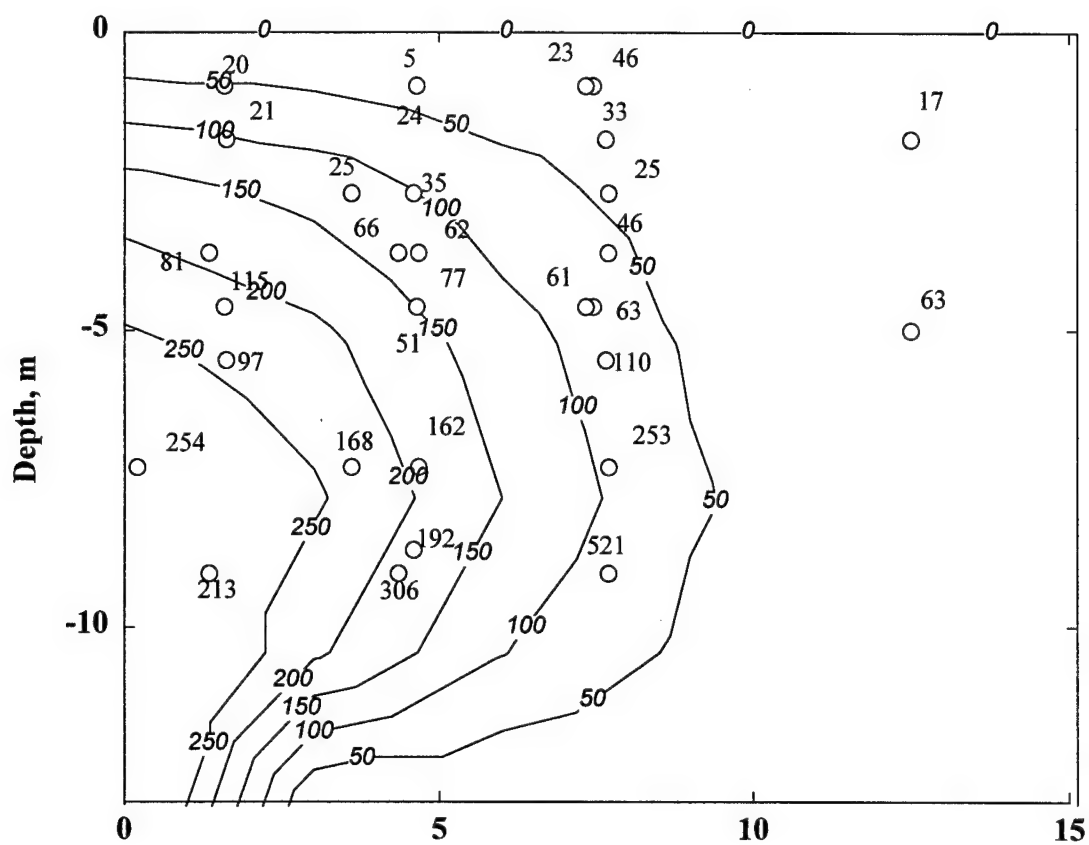
Table 5.43 summarizes the calibration results for trichloroethylene venting. Figure 5.22 displays typical TCE data and calibration for soil venting on 13 February 1996. The error standard deviation varies from 0.06 to 0.13 gm/m<sup>3</sup>, while the injection concentration ranges from 0.119 to 0.231 gm/m<sup>3</sup> over seven months of venting. The average of the nine calibrations is

$$Y_{INJ} = 0.149 \frac{\text{gm}}{\text{m}^3} \quad (\text{soil venting}) \quad (5.51a)$$

$$\frac{Y_{INJ}}{Y_{SAT}} \approx 0.16 \quad (5.51b)$$

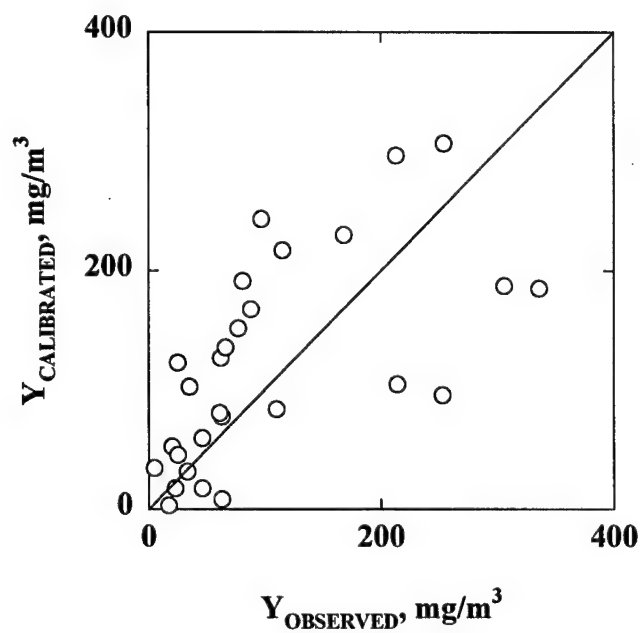
The calibrated injection concentration is one order of magnitude less than the (Equation 5.29a) value obtained by applying Raoult's law to the measured separate phase composition. This order of magnitude reduction is a typical gradient for the diffusive stripping of LNAPL vapors from separate phase contaminated soil by soil venting [Ostendorf et al. (1993b)]. This contrasts markedly with the corresponding ratio for total hydrocarbons implied by Equation 5.48 (with  $G_{SAT}$  estimated to be 0.05 kg/m<sup>3</sup>)

$$\frac{G_{INJ}}{G_{SAT}} \approx 0.007 \quad (\text{soil venting}) \quad (5.52)$$



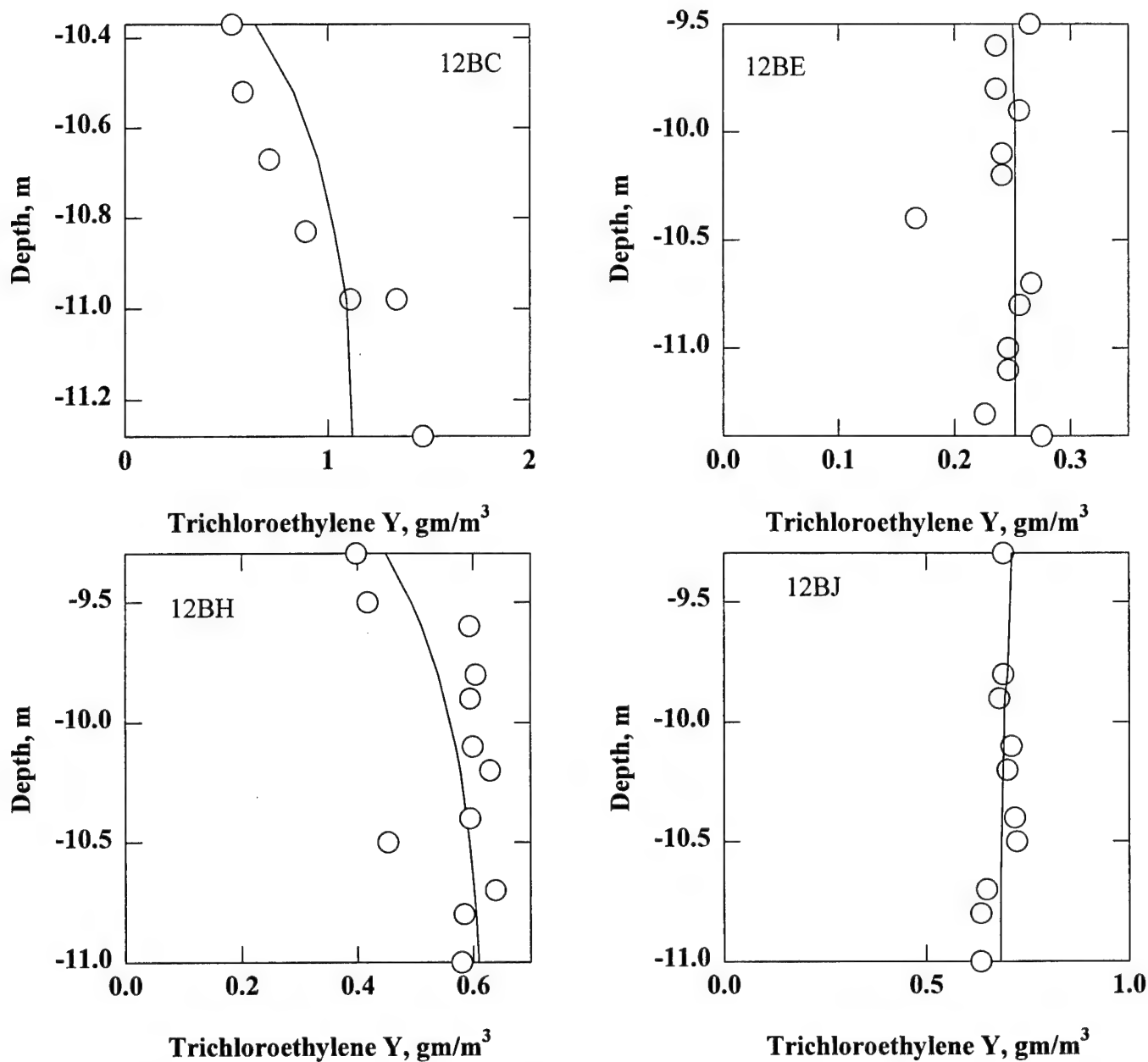
Note: Data from 7 February 1996

r. m



Note: Straight line is perfect model prediction, tubing cluster data.

**Figure 5.22 Observed and Calibrated Trichloroethylene Concentrations for Soil Venting**

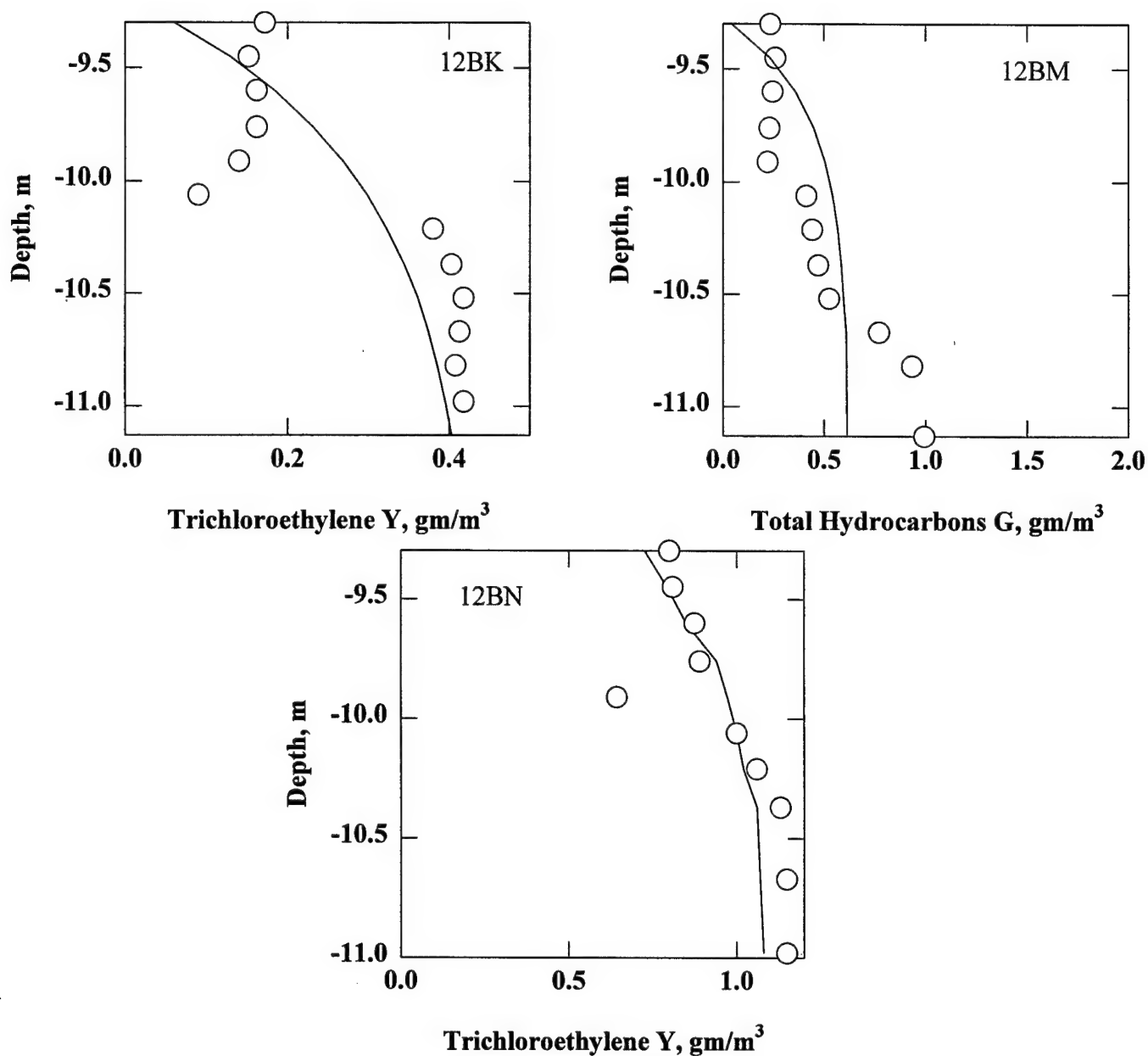


Note: Data observed on 22 August 1996, after 12 days of sparging

**Figure 5.23 Observed (Symbols) and Calibrated (Curves) Trichloroethylene Concentrations in Vapor Probe Boreholes**

We underscore the point by comparing the TCE to total hydrocarbon ratios for saturated conditions and for soil venting calibrations

$$\frac{Y_{\text{SAT}}}{G_{\text{SAT}}} \approx 0.019 \quad (\text{Raoult's law}) \quad (5.53a)$$



Note: Data observed on 22 August 1996, after 12 days of sparging

**Figure 5.23 (Continued) Observed (Symbols) and Calibrated (Curves) Trichloroethylene Concentrations in Vapor Probe Boreholes**

$$\frac{Y_{\text{INJ}}}{G_{\text{INJ}}} \approx 0.45 \quad (\text{soil venting}) \quad (5.53b)$$

Trichloroethylene accounts for nearly half of the vapors vented from the capillary fringe--a fraction 20 times greater than the ratio implied by Raoult's law.

**TABLE 5.44 TRICHLOROETHYLENE VAPOR PROFILE CALIBRATION  
NEAR CAPILLARY FRINGE**

Borehole	$\sigma_Y, \text{gm/m}^3$	$Y_F, \text{gm/m}^3$	$J_{YF}, \mu\text{g/m}^2\text{-s}$	$r, \text{m}$	$w_F, \text{m/s}$
12BC	0.21	1.18	4.00	2.83	$3.38 \times 10^{-6}$
12BE	0.03	0.252	1.08	1.91	$4.29 \times 10^{-6}$
12BH	0.06	0.623	1.08	4.19	$1.73 \times 10^{-6}$
12BJ	0.03	0.669	0.43	7.22	$6.51 \times 10^{-7}$
12BK	0.08	0.434	0.67	4.53	$1.53 \times 10^{-6}$
12BM	0.21	0.618	1.94	2.62	$3.13 \times 10^{-6}$
12BN	0.12	1.13	1.61	4.75	$1.42 \times 10^{-6}$

Table 5.44 and Figure 5.23 summarize the results of vapor probe trichloroethylene calibrations for air sparging on 22 August 1996. They are analogous to the total hydrocarbon vapor calibrations of Table 5.41 and Figure 5.18. The TCE concentration near the capillary fringe  $Y_F$  is chosen to zero the difference between the observed trichloroethylene and the constant flux layer prediction embodied by Equation 4.59. The error standard deviation varies between 0.03 and 0.21  $\text{gm/m}^3$ , while the fringe concentration implied by the vapor probe profiles ranges from 0.25 to 1.18  $\text{gm/m}^3$ , with an average value of

$$Y_F = 0.700 \frac{\text{gm}}{\text{m}^3} \quad (\text{air sparging, vapor probes}) \quad (5.54a)$$

$$\frac{Y_F}{G_F} \approx 0.39 \quad (\text{air sparging, vapor probes}) \quad (5.54b)$$

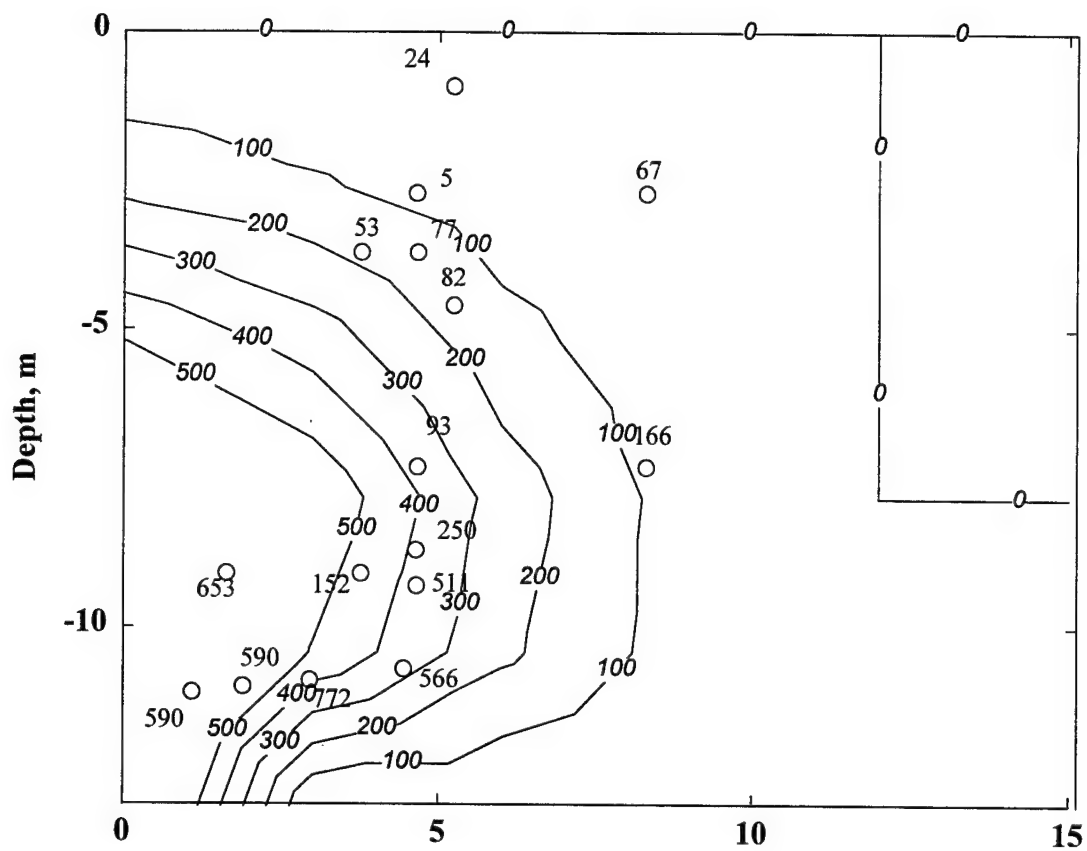
The ratio of the sparging induced trichloroethylene and total hydrocarbon (Equation 5.44a) concentrations near the fringe is quite similar to that exhibited by soil venting (Equation 5.53b). Total hydrocarbon vapors persist in the unsaturated zone, although trichloroethylene vapors do. In the latter regard, the average of the calibrated vertical TCE fluxes is

$$J_{YF} = 1.54 \frac{\mu\text{g}}{\text{m}^2\text{-s}} \quad (\text{air sparging, vapor probes}) \quad (5.55)$$

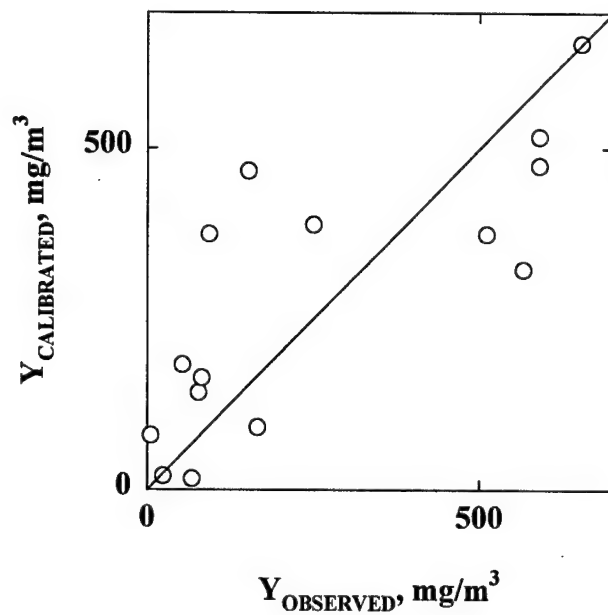
This is more than a third of the total hydrocarbon flux leaving the fringe (Equation 5.44b).

We calibrate the finite element model with the TCE sparging data of 22 August 1996 (Table 5.25). Figure 5.24 displays the results from a calibrated injection concentration of

$$Y_{\text{INJ}} = 0.550 \frac{\text{gm}}{\text{m}^3} \quad (\text{air sparging, tubing cluster}) \quad (5.56a)$$



Note: Data from 20 August 1996



Note: Straight line is perfect model prediction, tubing cluster data.

**Figure 5.24 Observed and Calibrated Trichloroethylene Concentrations for Air Sparging**

**TABLE 5.45 HELIUM AND TRICHLOROETHYLENE SOIL GAS  
CONCENTRATIONS IN NAW 20 NOVEMBER 1996**

Depth, m	p <sub>Y</sub> , ppb <sup>a</sup>	p <sub>H</sub> , ppm <sup>a</sup>	Depth, m	p <sub>Y</sub> , ppb <sup>a</sup>	p <sub>H</sub> , ppm <sup>a</sup>
0.051	98	68	0.407	277	408
0.102	138	414	0.458	54	47
0.153	217	103	0.509	517	630
0.204	241	296	0.509 <sup>b</sup>	666	500
0.254	234	384	0.636	605	481
0.254 <sup>b</sup>	432	327	0.763	285	628
0.305	287	486	0.891	701	257
0.356	406	544	1.02	888	53

<sup>a</sup>by volume.

<sup>b</sup>cluster point.

$$\delta_{GM} = 0.001 \frac{\text{gm}}{\text{m}^3} \quad (5.56b)$$

$$\sigma_G = 0.17 \frac{\text{gm}}{\text{m}^3} \quad (5.56c)$$

$$\frac{Y_{INJ}}{G_{INJ}} \approx 0.21 \quad (5.56d)$$

The calibration standard deviation is  $0.17 \text{ gm/m}^3$ , while the injection concentration is a significant fraction of the total hydrocarbon injection concentration (Equation 5.45a). The product of the volumetric discharge and the injection concentration is  $F_{YSPARGE}$  (Equation 5.46a), which for TCE is given by

$$F_{YSPARGE} = 2.60 \times 10^{-7} \frac{\text{kg}}{\text{s}} \quad (\text{air sparging, tubing cluster}) \quad (5.57)$$

#### 5.4.2 Trichloroethylene degradation in the root zone

We also measured helium and trichloroethylene concentrations in the near surface array on 20 November 1996, during the course of the air sparging experiment. Tables 5.45 and 5.46 summarize the data. We analyze these vertically resolved profiles with the quasi steady, one dimensional advection, diffusion model of Section 4.5.1. Helium is considered first by ignoring reactions in Equation 4.57 with the result



**TABLE 5.46 HELIUM AND TRICHLOROETHYLENE SOIL GAS  
CONCENTRATIONS IN NAE 20 NOVEMBER 1996**

Depth, m	p <sub>Y</sub> , ppb <sup>a</sup>	p <sub>H</sub> , ppm <sup>a</sup>	Depth, m	p <sub>Y</sub> , ppb <sup>a</sup>	p <sub>H</sub> , ppm <sup>a</sup>
0.051	51	31	0.407	379	219
0.102	140	36	0.458	360	171
0.153	141	39	0.509	288	214
0.204	150	109	0.636	463	51
0.254	259	62	0.763	540	132
0.305	243	138	0.891	734	259
0.356	291	139	1.02	745	231

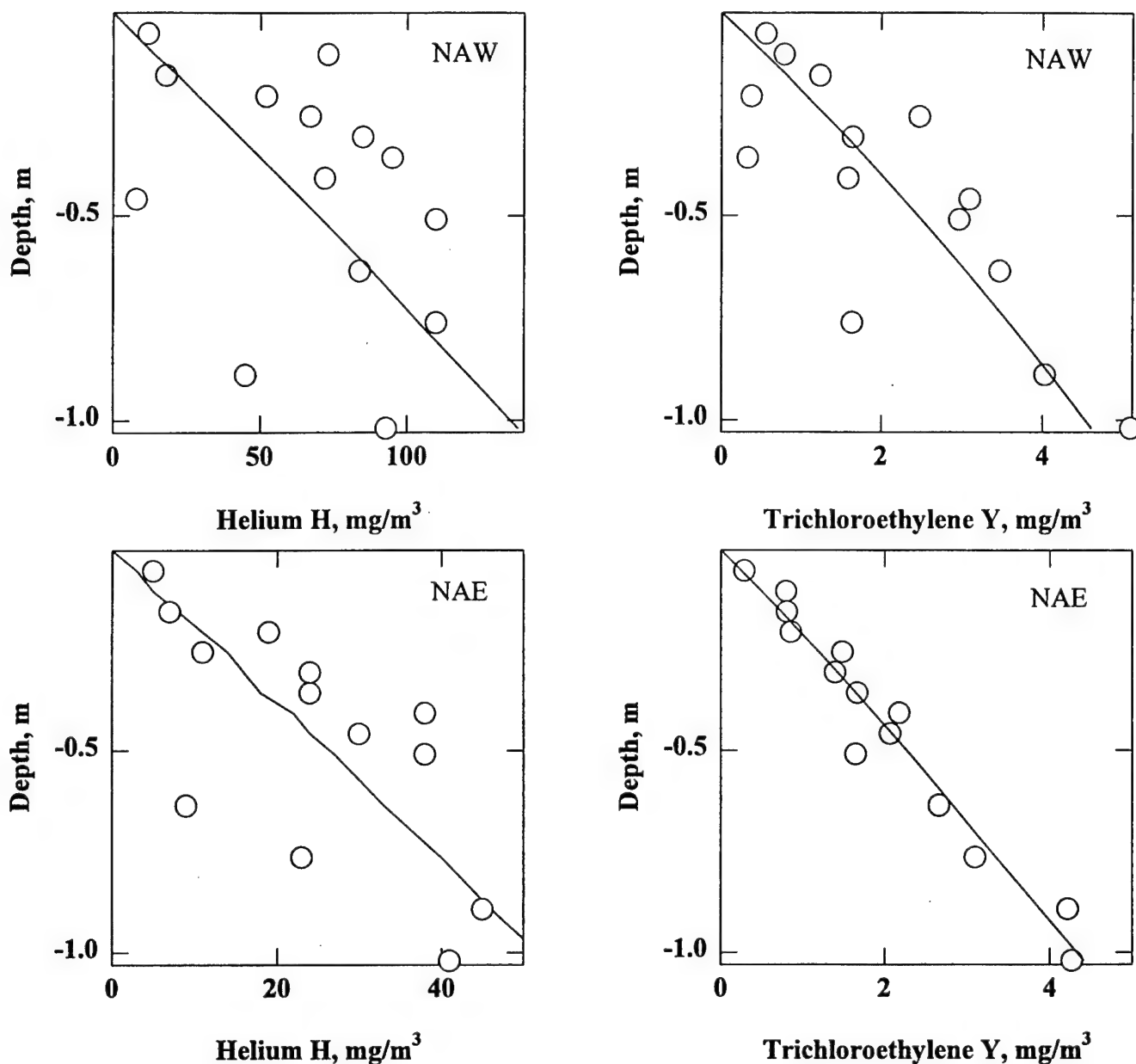
<sup>a</sup>by volume.

$$H = H_0 \exp\left[\frac{w_0(z + b_R)}{2\theta D_H}\right] \left[ \frac{\sinh\left(-\frac{w_0 z}{2\theta D_H}\right)}{\sinh\left(\frac{w_0 b_R}{2\theta D_H}\right)} \right] \quad (5.58)$$

We calibrate the theory with a ground surface temperature equal to 277.18°K, based on Equations 4.1c, 5.1, and 5.3b. The observed partial pressures are converted to concentrations with the ideal gas law (e.g. Equation 5.28), while the gaseous diffusivity is estimated at 2.25x10<sup>-5</sup> m<sup>2</sup>/s. The latter value reflects Equations 4.33, 5.11b, and 5.13. The coordinates of Table 3.1 yield radial distances of 7.66 and 6.00 m, respectively, from the sparge point to NAE and NAW, so that the vertical specific discharges (Equation 4.19b) are 5.68x10<sup>-7</sup> and 6.65x10<sup>-7</sup> m/s.

Table 5.47 and Figure 5.25 summarize the near surface array calibrations. We use the helium data to calibrate the root zone thickness at each array through a nested Fibonacci search. The approach concentration (H<sub>0</sub>) minimizes the mean helium model error, while b<sub>R</sub> minimizes the error standard deviation. We find approach helium concentrations of 284 and 91 mg/m<sup>3</sup> in NAW and NAE, which correspond to p<sub>H</sub> values of 1,600 and 520 ppm, respectively. These values are consistent with the 20 November 1996 tubing cluster data cited in Table 5.30. The helium error standard deviations are 51 and 11 mg/m<sup>3</sup> for the two arrays. The root zone thicknesses are then input to the trichloroethylene model (Equation 4.57), and we search for optimal Y<sub>0</sub> and degradation values. The TCE error standard deviations are 0.25 and 0.87 mg/m<sup>3</sup> in NAW and NAE. The approach concentrations of 8.08 and 9.76 mg/m<sup>3</sup> correspond to p<sub>Y</sub> values (1.4 and 1.6 ppm) in keeping with the 21 November 1996 tubing cluster observations cited in Table 5.28. The near surface array data are consistent with the stainless steel tubing cluster data.

The calibrated TCE degradation rates are 2.26x10<sup>-6</sup> s<sup>-1</sup> and 1.76x10<sup>-6</sup> s<sup>-1</sup> at arrays NAW and NAE. The average of these two values is



Note: data from 20 November 1996, after 27 days of sparging and helium injection.

**Figure 5.25 Observed (Symbols) and Calibrated (Curves) Helium and TCE Vapor Concentrations in Near Surface Arrays**

$$\lambda_{\text{TCE}} = 2.01 \times 10^{-6} \text{ s}^{-1} \quad (\text{root zone}) \quad (5.59)$$

These kinetics are consistent with the results of Anderson and Walton (1995), who observe radiolabeled TCE degradation in the rhizosphere of aerobic soil plant microcosms. The

**TABLE 5.47 NEAR SURFACE ARRAY CALIBRATION RESULTS**

	NAW	NAE
$w_O, \text{m/s}$	$6.65 \times 10^{-7}$	$5.68 \times 10^{-7}$
$H_O, \text{mg/m}^3$	284	91
$b_R, \text{m}$	2.24	1.83
$\sigma_H, \text{mg/m}^3$	51	11
$Y_O, \text{mg/m}^3$	8.08	9.76
$\lambda_{TCE}, \text{s}^{-1}$	$2.26 \times 10^{-6}$	$1.76 \times 10^{-6}$
$\sigma_Y, \text{mg/m}^3$	0.25	0.87

microcosms exhibit a TCE half life of about 5 days (corresponding to a first order decay coefficient of  $1.6 \times 10^{-6} \text{ s}^{-1}$ ).

## 5.5 Total Hydrocarbon Assimilation Capacity Estimates and Surface Emissions

### 5.5.1 Oxygen and Carbon Dioxide Concentrations for Soil Venting

Figure 5.26 plots the temporal variation of the spatially averaged soil gas oxygen and carbon dioxide partial pressures with time from the onset of soil venting. These data are taken from Tables 5.16 to 5.23 excluding clusters 12AN, 12AT, and 12AX, which lie outside the study area. Soil vapor pressures from the control cluster are also shown in the figure, along with atmospheric values. We note that the control soil gas pressures are quite close to atmospheric levels, so it is apparent that soil venting depresses oxygen and elevates carbon dioxide in the unsaturated zone. We attribute this oxygen depletion and carbon dioxide elevation to aerobic degradation, and approximate the process by considering the difference between the average partial pressures in the study area ( $p_{XM}, p_{CM}$ ) and control cluster ( $p_{XCONTROL}, p_{CCONTROL}$ )

$$\Delta X = \frac{1010(p_{XCONTROL} - p_{XM})m_X}{R_T \tau_\infty} \quad (p_{XM}=17.8\%) \quad (5.60a)$$

$$\Delta X = 0.0428 \frac{\text{kg}}{\text{m}^3} \quad (p_{XCONTROL}=20.9\%) \quad (5.60b)$$

$$\Delta C = \frac{1010(p_{CCONTROL} - p_{CM})m_C}{R_T \tau_\infty} \quad (p_{CM}=2.51\%) \quad (5.60c)$$

$$\Delta C = 0.0457 \frac{\text{kg}}{\text{m}^3} \quad (p_{CCONTROL}=0.1\%) \quad (5.60d)$$

Equation 4.22 details the stoichiometry assumed for complete mineralization of hydrocarbons by aerobic degradation. We accordingly convert the oxygen depletion  $\Delta X$  and

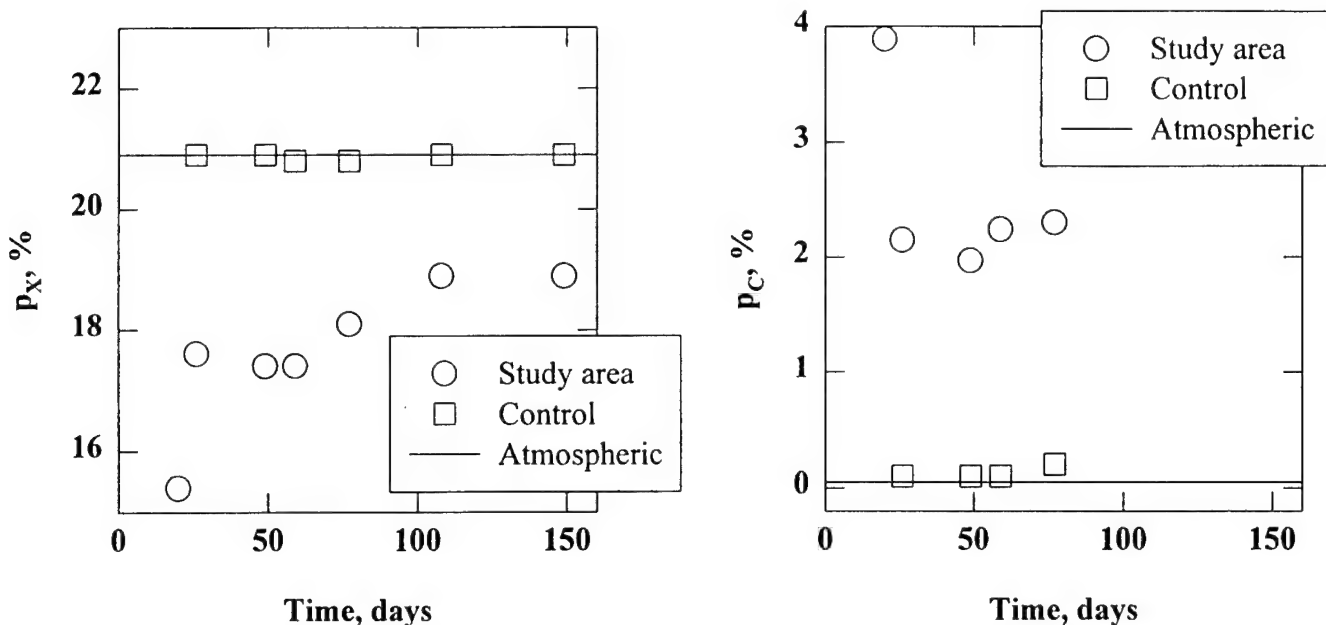


**Figure 5.26 Spatial Averaged Oxygen and Carbon Dioxide Partial Pressures for Soil Venting**

carbon dioxide generation  $\Delta C$  to hydrocarbons  $\Delta G$  degraded by soil venting. The oxygen depletion implies

$$\Delta G = \frac{\Delta X}{\gamma_X} \quad (\text{soil venting}) \quad (5.61a)$$

$$\Delta G = 0.0133 \frac{\text{kg}}{\text{m}^3} \quad (\text{oxygen depletion}) \quad (5.61b)$$

The carbon dioxide generation yields a similar estimate

$$\Delta G = \frac{\Delta C}{\gamma_C} \quad (\text{soil venting}) \quad (5.62a)$$

$$\Delta G = 0.0169 \frac{\text{kg}}{\text{m}^3} \quad (\text{carbon dioxide generation}) \quad (5.62b)$$

Our suggestion is that the hydrocarbons degrade near the capillary fringe, and so appear only at low levels in the unsaturated zone. We may add the  $\Delta G$  represented by Equations 5.61 and 5.62 to the calibrated  $G_{\text{INJ}}$  value of  $0.332 \text{ gm/m}^3$  to derive an estimate of the total hydrocarbons  $G_{\text{TOTAL}}$  stripped from the contaminated soil interval

$$G_{\text{TOTAL}} \approx G_{\text{INJ}} + \Delta G \quad (\text{soil venting}) \quad (5.63a)$$

$$G_{\text{TOTAL}} \approx 0.0154 \frac{\text{kg}}{\text{m}^3} \quad (\Delta G = 0.0151 \text{ kg/m}^3) \quad (5.63b)$$

The adopted  $\Delta G$  is the average of the oxygen and carbon dioxide based estimates. We note that 98% of the hydrocarbons are degraded. We use Raoult's law to check our calculations, since the trichloroethylene is assumed to be conserved in the capillary fringe. Comparing Equations 5.51a and 5.63b, then

$$\frac{Y_{\text{INJ}}}{G_{\text{TOTAL}}} \approx 0.0097 \quad (\text{soil venting}) \quad (5.64)$$

This ratio agrees reasonably well with the saturated vapor ratio (0.019) implied by the LNAPL composition (Equation 5.53a).

### 5.5.2 Assimilation Capacity for Total Hydrocarbons by Soil Venting

We approximate the kinetics of soil venting near the injection point in order to infer the assimilation capacity for total hydrocarbon vapors associated with this remedial measure from the foregoing  $\Delta G$  calculation. Hydrocarbon transport in the immediate vicinity of the venting wells is taken as a quasi steady balance of spherical advection and first order decay

$$Q \frac{dG}{dr'} = -2\pi r'^2 \theta \lambda G \quad (5.65a)$$

$$G = G_{\text{TOTAL}} \quad (r'=0) \quad (5.65b)$$

with constant volumetric discharge  $Q$ . We separate the variables in Equation 5.65, integrate, and solve for the first order decay constant with the result

$$\lambda = \frac{3Q}{2\pi r'^3} \ln\left(\frac{G_{\text{TOTAL}}}{G}\right) \quad (5.66)$$

The maximum assimilation capacity for hydrocarbons follows by substituting a 3 m value for  $r'$  along with  $G$  ( $0.332 \text{ gm/m}^3$ ) and  $G_{\text{TOTAL}}$  ( $15.4 \text{ gm/m}^3$ ) into Equation 5.66

$$\lambda = 3.2 \times 10^{-5} \text{ s}^{-1} \quad (\text{soil venting}) \quad (5.67)$$

These kinetics are an order of magnitude faster than the ambient rate cited in Equation 5.39b. The increase may be attributed in part to the direct introduction of oxygen into the capillary fringe, proximate to the separate phase contamination.

### 5.5.3 Surface Emissions

**TABLE 5.48 SURFACE EMISSIONS MEASUREMENTS  
1 DECEMBER 1996**

Location	$\tau$ , °C	North, ft	East, ft	ECD	Y	$J_{YO}$
Control	5	-200.00	0.00	78 <sup>a</sup>	BDL <sup>b</sup>	BDL
	5	-200.00	0.00	78	BDL	BDL
	5	-200.00	0.00	208	BDL	BDL
12AK (adjacent)	5	120.36	63.44	105	BDL	BDL
	5	120.36	63.44	73	BDL	BDL
	5	120.36	63.44	55	BDL	BDL
12AB (adjacent)	9	126.47	69.54	86	BDL	BDL
	9	126.47	69.54	0	BDL	BDL
	9	126.47	69.54	99	BDL	BDL
12AV (adjacent)	10	131.67	68.28	83	BDL	BDL
	10	131.67	68.28	0	BDL	BDL
	10	131.67	68.28	0	BDL	BDL
12AM (adjacent)	10	123.88	77.29	0	BDL	BDL
	10	123.88	77.29	0	BDL	BDL
	10	123.88	77.29	0	BDL	BDL

<sup>a</sup>Area units.

<sup>b</sup>Below detection limit.

We may estimate the flux  $J_{YO}$  of trichloroethylene vapors to the atmosphere by differentiating Equation 4.57 with the result

$$J_{YO} = w_O Y - \theta D_Y \frac{dY}{dz} \quad (z=0) \quad (5.68a)$$

$$J_{YO} = \frac{w_O Y_O}{2} \frac{\exp(\frac{w_O b_R}{2\theta D_Y})}{\sinh(\frac{w_O b_R}{2\theta D_Y} \sqrt{1 + \frac{4\lambda_{TCE}\theta^2 D_Y}{w_O^2}})} \quad (5.68b)$$

We substitute the NAW values of Table 5.47 into Equation 5.68b and estimate a TCE emissions rate of

$$J_{YO} = 1.8 \times 10^{-6} \frac{\text{mg}}{\text{m}^2 \cdot \text{s}} \quad (\text{air sparging}) \quad (5.69a)$$

$$J_{YO} = 0.11 \frac{\mu\text{g}}{\text{m}^2 \cdot \text{min}} \quad (5.69b)$$

We deployed a surface emissions flux chamber [Tehrany et al. (1996)] at the site on 1 December 1996 to verify low TCE emissions to the atmosphere from sparging, with the results cited in Table 5.48. We detected no emissions at the site, which, in view of Equation 3.13, implies that

$$J_{YO} < 0.9 \frac{\mu\text{g}}{\text{m}^2 - \text{min}} \quad (\text{flux chamber}) \quad (5.70)$$

The observed Equation 5.70 is consistent with the theoretical Equation 5.69b.

We assess this flux in light of surface emission standards of the Federal Clear Air Act Amendments of 1990, which specify a total discharge  $F_{YO}$  of 10 tons per year of individual hazardous air pollutants and 25 tons per year of a combination of hazardous air pollutants from industrial sources. The California Air Resources Board permits 1 kg day of trichloroethylene emissions. Parsons Engineering Science (1995) estimates that the separate phase is currently spread over an areal extent  $A_{SPILL}$  of 33,000  $\text{m}^2$ . Collecting these standards into an allowable surface emission per unit area, we find

$$J_{YO} < \frac{F_{YO}}{A_{SPILL}} \quad (5.71a)$$

$$J_{YO} < 520 \frac{\mu\text{g}}{\text{m}^2 - \text{min}} \quad (\text{individual HAP}) \quad (5.71b)$$

$$J_{YO} < 21 \frac{\mu\text{g}}{\text{m}^2 - \text{min}} \quad (\text{TCE CARB standard}) \quad (5.71c)$$

The detection limit of our surface isolation flux chamber is three orders of magnitude lower than the emissions standard for TCE. Trichloroethylene emissions are negligible.

## 6 SUMMARY AND CONCLUSIONS

### 6.1 Summary of Work

The Civil and Environmental Engineering Department of the University of Massachusetts at Amherst (UMASS) was contracted by the United States Air Force Center for Environmental Excellence (AFCEE) to conduct field research from 19 September 1995 to 30 September 1996 under Contract No. F41624-95-C-8012 "Surface Emissions from Jet Fuel Bioventing at Plattsburgh AFB". The work focused on bioventing of residual JP4 jet fuel and chlorinated solvents in the unsaturated zone and capillary fringe beneath Fire Training Area FT-002 at the Air Force Base in Plattsburgh, NY. **UMASS tested the hypothesis that natural attenuation processes, stimulated by injected air, reduce emissions of hydrocarbons and trichloroethylene vapors to acceptable air quality standards at the site.** Drs. David W. Ostendorf, Alan J. Lutenegger, and Sarina J. Ergas were the UMASS Principal Investigators, while Patrick Haas served as AFCEE Technical Representative for the contract.

The contract was performed in four tasks: unsaturated zone characterization, soil gas and solid core sampling, maximum assimilative capacity testing, and emissions testing.

#### 6.1.1 Unsaturated Zone Characterization

- Grain size distributions were measured at 108 depths from three boreholes. We determined moisture content profiles 785 samples from 24 boreholes completed during drilling trips on 9-13 October 1995, 30 November-1 December 1995, 5-7 June 1996, and 19-22 August 1996.
- We installed two thermocoupled arrays and measured soil temperature on 17 field sampling trips from 13 October 1995 to 19 December 1996, generating a data base of 377 observations.
- Stainless steel soil vapor probes were deployed in three boreholes on 11-13 October 1995 to determine ambient soil gas oxygen, total hydrocarbon, and carbon dioxide partial pressures across the unsaturated zone. Portable soil meters and a Tedlar bag sampling system were used to analyze the data from 38 depths in two of the boreholes, while a downhole oxygen sensor corroborated the profiles at 14 depths in the third borehole.
- We analyzed a separate phase sampled bailed from a recovery well by Base engineers to determine the composition of the residual JP4 jet fuel solvent liquid. A Hewlett Packard G1800A gas chromatograph with a mass spectrometer detector (GCD) was used to identify 84 alkanes, aromatics, and chlorinated hydrocarbons in the sample.
- UMASS personnel surveyed the plan location and mean sea level elevation of all probe profiles, clusters, arrays, and boreholes, for insertion into an AUTOCAD file for the project. Coordinates for all sample points are cited in Table 3.1.

#### 6.1.2 Soil Gas and Solid Core Sampling

- We constructed 26 stainless steel soil gas tubing clusters to document the fate and transport of vapors through the unsaturated zone. One cluster was a control positioned well outside underlying LNAPL. The clusters were multidepth, so that 45 depths were sampled.



- The soil gas tubing clusters were sampled with portable analyzers and field installed Hewlett Packard 5890 gas chromatographs equipped with flame ionization (FID) and electron capture (ECD) detectors. We sampled soil gas oxygen, carbon dioxide, total hydrocarbons, and trichloroethylene partial pressures in Tedlar bag samples from the clusters on 17 field trips from 26 October 1995 to 19 December 1996, generating 2,083 observations.
- The vertical distribution of separate phase contamination was estimated from gas chromatographic IFD analysis of methylene chloride extracts from 785 solid core samples from 24 boreholes sampled on 9-13 October 1995, 30 November-1 December 1995, 5-7 June 1996, and 19-22 August 1996.
- The headspace of the samples was analyzed in a nitrogen glove box on line, to direct sampling efforts and delineate the contaminated interval.
- Separate phase trichloroethylene content was determined at 66 depths in six of the boreholes, using the GCD.

#### 6.1.3 Maximum Assimilative Capacity Testing

- A soil venting system was installed in the center of the test area on 1 December 1995. The soil venting system injected heated air at a metered rate of 1 cfm into the capillary fringe, and included a helium tracer injection system. The soil was vented from 18 January 1996 to 9 August 1996, and a helium tracer was injected continuously from 7 February to 7 March 1996.
- We measured vented helium in 31 of the stainless steel tubing cluster sampling points on 13 February and 21 February 1996 to document the pneumatics of the soil venting. A field installed Hewlett Packard 5890 gas chromatograph with thermal conductivity detector (TCD) was used to measure the helium in Tedlar bag samples.
- An air sparging system was built in the center of the test area on 1 December 1995 as well. The air sparging system injected heated air 1.2 m below the water table from 9 August to 5 September 1996 and from 24 October to 19 December 1996. A helium tracer was injected continuously from 24 October to 24 November 1996.
- We measured helium in 35 of the stainless steel tubing cluster sampling points on 7 November and 29 November 1996, using the TCD gas chromatograph.
- A finite element model with supplemental analytical subroutines was used to model the stainless steel tubing cluster and vapor probe data. The model was tested with the helium tracer data, followed by soil gas data calibrations to determine the maximum assimilative capacity of the unsaturated zone for hydrocarbon and trichloroethylene vapor degradation. Air and total porosities were input from the moisture content data, and soil temperature was modeled with a constant diffusivity analysis.

#### 6.1.4 Emissions Testing

- We installed two near surface arrays to measure helium and TCE profiles through the root zone. The arrays were of stainless steel construction, with a low sample volume facilitating sampling on 5 cm vertical spacing. Fourteen depths were established at each array.
- We analyzed helium and trichloroethylene soil gas concentrations on 20 November 1996 using field installed gas chromatographs with TCD and ECD detectors.

- We measured soil gas oxygen, total hydrocarbons, carbon dioxide, and trichloroethylene partial pressures near the capillary fringe using a soil vapor probe during air sparging. Eighty one depths were sampled in seven boreholes on 21-22 August 1996, using portable meters and a field installed FID equipped gas chromatograph.
- The near surface array data were input to an analytical model of soil gas transport through the root zone. The helium data calibrated the pneumatics, while the TCE data were used to calibrate the capacity of the root zone to assimilate TCE vapors.
- A surface isolation flux chamber was designed, built, and deployed, to verify low levels of emissions from the site area.

## 6.2 Conclusions

This extensive field sampling, laboratory analysis, and mathematical modeling efforts tests the hypothesis with the following result: **natural attenuation processes reduce emissions of hydrocarbon and trichloroethylene vapors to acceptable air quality standards at the site.**

We support this general conclusion with particular results:

- **A significant mass of separate phase petroleum persists in and immediately below the capillary fringe.** We found total petroleum hydrocarbon levels as high as 26,400 mg TPH/kg dry soil (borehole 12AS), with contaminated intervals ranging from 1.1 to 2.54 m in extent (Table 5.6). The distribution is unimodal, and is reasonably described by capillary scaling theory (Figure 5.7). A significant fraction of the LNAPL is residually bound to the soil (as much as 7,000 mg TPH/kg dry soil). The separate phase is well correlated with the headspace concentrations.
- **Separate phase trichloroethylene occurs at levels as high as 59 mg TCE/kg dry soil immediately below the capillary fringe (Table 5.7).** The ratio of separate phase TCE to total LNAPL in 95 samples is 0.0025, yielding a separate phase mole fraction of 0.00222 and a saturated TCE vapor pressure of 170 ppm.
- **Soil gas oxygen and carbon dioxide concentrations suggest a maximum assimilative capacity of  $1.4 \times 10^{-6} \text{ s}^{-1}$  under ambient conditions near the capillary fringe (Equation 5.39b).** This capacity is based on high, stoichiometrically coupled fluxes of oxygen entering and carbon dioxide leaving the fringe by ambient diffusion.
- **Soil gas oxygen and carbon dioxide concentrations suggest that soil venting increases the maximum assimilative capacity near the capillary fringe to  $3.2 \times 10^{-5} \text{ s}^{-1}$  (Equation 5.67).** This capacity is based on a comparison of soil gas concentrations in study area with those observed at the control cluster.
- **We see little evidence of hydrocarbons or of hydrocarbon degradation in the unsaturated zone, although trichloroethylene exists at significant levels.** The finite element code, calibrated with tubing cluster data, suggests that trichloroethylene comprises a disproportionately high fraction of the hydrocarbon vapors found in the stainless steel tubing clusters under ambient, soil venting (Equation 5.53b), or air sparging (Equation 5.56b) conditions. The observed TCE concentrations are consistent with the saturated vapor pressure implied by Raoult's law, while the hydrocarbon pressures are two orders of magnitude lower than values expected in the absence of degradation. **These findings, together with the observed fluxes of**

oxygen and carbon dioxide, support the hypothesis that JP4 hydrocarbon vapors degrade aerobically near the capillary fringe.

- **Trichloroethylene vapors degrade in the root zone, at a maximum assimilative capacity of  $2.0 \times 10^{-6} \text{ s}^{-1}$  (Equation 5.59).** This conclusion reflects calibration of quasi steady vertical transport models for abiotic helium (Equation 5.58) and first order decaying trichloroethylene (Equation 4.57) with replicated near surface array data (Tables 5.46, 5.47 and Figure 5.25). These data were gathered late in the study period, after seven months of soil venting and two months of air sparging.
- **No detectable trichloroethylene was emitted to the atmosphere.** We base this conclusion on a computed flux rate of  $0.11 \text{ } \mu\text{g}/\text{m}^2\text{-min}$  (Equation 5.69b), confirmed by emissions testing at the site using the flux chamber.

## 7 REFERENCES

ABB Environmental Services, Inc. 1992. FT-002 Soil remedial investigation report: Plattsburgh Air Force Base, New York. *Draft Report*. Portland, ME.

ABB Environmental Services, Inc. 1993. FT-002 Soil remedial investigation report. *Final Draft*. Portland, ME.

Abramowitz, M. and I.A. Stegun. 1972. *Handbook of mathematical functions*. National Bureau of Standards, Washington, DC.

Abriola, L.M. and G.F. Pinder. 1985. A multiphase approach to the modeling of porous media contamination by organic compounds 1. equation development. *Water Resources Research*, Vol. 21: 11-18.

Air Force Center for Environmental Excellence. 1994. Using soil gas surveys to determine bioventing feasibility and natural attenuation potential. *Addendum One to Test Plan and Technical Protocol for a Field Treatability Test for Bioventing*, AFCEE, Brooks AFB, TX.

Alvarez-Cohen, L., and P.L. McCarty. 1991. A cometabolic biotransformation model for halogenated aliphatic compounds exhibiting product toxicity. *Environmental Science and Technology*, Vol. 25: 1381-1392.

American Academy of Environmental Engineers. 1994. Vacuum vapor extraction. *Innovative Site Remediation Technology*, Vol. 8, AAEE, Washington, DC.

American Society for Testing and Materials. 1992a. Standard method for penetration test and split barrel sampling of soils. *ASTM D-1586*, Vol. 4.08: 242-246.

American Society for Testing and Materials. 1992b. Standard test method for particle size analysis. *ASTM D-422*, Vol. 4.08: 94-100.

American Society for Testing and Materials. 1992c. Standard test method for laboratory determination of water content of soil and rock. *ASTM D-2216*, Vol. 4.08: 295-298.

Baehr, A.L. and R.J. Baker. 1995. Use of a Reactive Gas Transport Model to Determine Rates of Hydrocarbon Biodegradation in Unsaturated Porous Media. *Water Resources Research*. Vol. 31: 2877-2882.

Baehr, A.L., G.E. Hoag, and M.C. Marley. 1989. Removing volatile contaminants from the unsaturated zone by inducing advective air phase transport. *Journal of Contaminant Hydrology*, Vol. 13: 1-26.

Batterman, S.A., A. Kulshrestha, and H. Cheng. 1995. Hydrocarbon vapor transport in low moisture soils. *Environmental Science and Technology*, Vol. 29: 171-180.

Becker, E.B., G.F. Carey, and J.T. Oden. 1981. *Finite elements: An introduction*. Prentice Hall, Englewood Cliffs, NJ.

Beckett, G.D. and D. Huntley. 1994. Characterization of flow parameters controlling soil vapor extraction, *Ground Water*, Vol. 32: 239-247.

Benjamin, J.R. and Cornell, C.A. 1970. *Probability, statistics and decision for civil engineers*. McGraw-Hill, New York, NY.

Beveridge, G.S.G. and R.S. Schechter. 1970. *Optimization: Theory and practice*. McGraw-Hill, New York, NY.

Bourg, A.C.M., C. Mouvet and D.N. Lerner. 1992. A Review of the Attenuation of Trichloroethylene in Soils and Aquifers. *Quarterly Journal of Engineering Geography*, Vol. 25: 359-370.

Boyle, J.J. and J.R. Shann. 1995. Biodegradation of phenol, 2,4-DCP, 2,4-D, and 2,4,5-T in the field-collected rhizosphere and non-rhizosphere soils. *Journal of Environmental Quality*, Vol. 24: 782-785.

Brown, R. 1993. Treatment of petroleum hydrocarbons in groundwater by air sparging. In *Handbook of Bioremediation*. Lewis Publishers. Boca Raton. 61-83.

Bulman, T.L., M. Newland, A. Webster. 1993. In situ bioventing of a diesel fuel spill. *Hydrological Sciences Journal*, Vol. 38: 297-308.

Carslaw, H.S. and J.C. Jaeger. 1973. *Conduction of heat in solids*. Oxford Press, New York, NY.

Christy, T.M. and S.C. Spradlin. 1992. The use of small diameter probing equipment for contaminated site investigation. *Proceedings Sixth National Outdoor Action Conference*. NGWA, Dublin, OH, pp. 87-101.

Chrysikpoulos, C.V. 1995. Three-Dimensional Analytical Models of Contaminant Transport from Nonaqueous Phase Liquid Pool Dissolution in Saturated Subsurface Formations. *Water Resources Research*. Vol. 31: 1137-1145.

Chu, K.H. and L. Alvarez-Cohen. 1996. Trichloroethylene degradation by methane oxidizing cultures grown with various nitrogen sources. *Water Environment Research*, Vol. 68: 76-82.

Chu, K.H., J. Vernalia, and L. Alvarez-Cohen, 1995. Nitrogen sources for bioremediation of TCE in unsaturated porous media. In *Bioremediation of Chlorinated Solvents*, edited by R.E. Hincsee, Battelle Press, Columbus, Ohio.

Conrad, S.H., J.L. Wilson, W.R. Mason, and W.J. Peplinski. 1992. Visualization of residual organic liquid trapped in aquifers. *Water Resources Research*, Vol. 28: 467-478.

Corapcioglu, M.Y. and A.L. Baehr. 1987. A compositional multiphase model for groundwater contamination by petroleum products 1. theoretical considerations. *Water Resources Research*, Vol. 23: 191-200.

Deyo, B.G., G.A. Robbins, and G.K. Binkhorst. 1993. Use of portable oxygen and carbon dioxide detectors to screen soil gas for subsurface gasoline contamination. *Groundwater*, Vol. 31: 598-604.

Deutsch, J.J. and J.A. Smith. 1995. Effect of triton X-100 on the rate of trichloroethene desorption from soil to water. *Environmental Science and Technology*, Vol. 29: 1069-1080.

Downey, D.C. and P.H. Guest. 1991. Physical and biological treatment of deep diesel contaminated soils. *Proceedings Petroleum Hydrocarbons and Organic Chemicals in Groundwater*. NGWA/API, Dublin, OH, pp. 361-376.

Downey, D.C., P.R. Guest, and J.W. Ratz. 1995. Results of a two year in situ bioventing demonstration. *Environmental Progress*, Vol. 14: 121-125.

Dupont, R.R. 1993. Fundamentals of bioventing applied to fuel contaminated sites. *Environmental Progress*, Vol. 12: 45-52.

Eastman, R.H. 1975. *Essentials of modern chemistry*. Rinehart Press, San Francisco.

E.C. Jordan Co. 1989a. Installation restoration program (Remedial investigation/feasibility study) at Plattsburgh Air Force Base, New York. *Supplemental Field Investigation Technical Memorandum*. Portland, ME.

E.C. Jordan Co. 1989b. Installation restoration program (Remedial investigation/feasibility study) at Plattsburgh Air Force Base, New York. *Site Inspection Report*. Portland, ME.

E.C. Jordan Co. 1990. Installation restoration program (Engineering evaluation/cost analysis) at Plattsburgh Air Force Base, New York. *Site FT-002 Free-Product Removal Action*. Portland, ME.

E.C. Jordan Co. 1991a. Installation restoration program at Plattsburgh Air Force Base, New York. *Sampling and Analysis Plan*. Portland, ME.

E.C. Jordan Co. 1991b. Installation restoration program (Free product recovery pilot test) at Plattsburgh Air Force Base, New York. *Technical Memorandum*. Portland, ME.

Enzien, M.V. F. Picardal, T.C. Hazen-, R.G. Arnold and C.B. Fliermans. 1994. Reductive dechlorination of trichloroethylene and tetrachloroethylene under aerobic conditions in a sediment column. *Applied and Environmental Microbiology*, Vol. 60: 2200-2204.

Falta, R.W., I. Javandel, K. Pruess, and P.A. Witherspoon. 1989. Density driven flow of gas in the unsaturated zone due to the evaporation of volatile organic compounds. *Water Resources Research*, Vol. 25: 2159-2169.

Fan, S. and K.M. Scow, 1993. Biodegradation of trichloroethylene and toluene by indigenous microbial populations in soil. *Applied and Environmental Microbiology*, Vol. 59: 1911-1918.

Fitch, M.W., G.E. Speitel and G. Georgiou. 1996. Degradation of trichloroethylene by methanol grown cultures of methylosinus-trichosporium Ob3B Pp358. *Applied and Environmental Microbiology*, Vol. 62: 1124-1128.

Folkes, D.J., M.S. Bergman, and W.E. Herst. 1987. Detection and delineation of a fuel oil plume in a layered bed rock deposit. *Proceedings Petroleum Hydrocarbons and Organic Chemicals in Groundwater*. NGWA/API, Dublin, OH, pp. 279-304.

Freedman, D.L. and J.M. Gossett. 1989. Biological reductive dechlorination of tetrachloroethylene and trichloroethylene to ethylene under methanogenic conditions. *Applied and Environmental Microbiology*, Vol. 55: 2144-2151.

Furukawa, K., J. Hirose, S. Hayashida and K. Nakamura. 1994. Efficient degradation of trichloroethylene by a hybrid aromatic ring dioxygenase. *Journal of Bacteriology*, Vol. 176: 2121-2123.

Gates, D.D. and R.L. Siegrist. 1995. In situ chemical oxidation of trichloroethylene using hydrogen peroxide. *Journal of Environmental Engineering*, Vol. 121: 639-644.

Gierke, J.S., N.J. Hutzler, and D.B. McKenzie. 1992. Vapor transport in unsaturated soil columns: implications for vapor extraction. *Water Resources Research*, Vol. 28: 323-335.

Gomez-Lahoz, C., J.J. Rodriguez, J.M. Rodriguezmaroto, and D.J. Wilson. 1994. Biodegradation phenomena during soil vapor extraction: sensitivity studies for two substrates. *Separation Science and Technology*, Vol. 29: 1275-1291.

Grathwohl, P. and M. Reinhard. 1993. Desorption of trichloroethylene in aquifer material - rate limitation at the grain scale. *Environmental Science and Technology*, Vol. 27: 2360-2366.

Hatfield, K. and T.B. Stauffer. 1993. Transport in porous media containing residual hydrocarbon. I: Model. *Journal of Environmental Engineering*. Vol. 119: 540-558.



Hecht, V., D. Brebbermann, P. Bremer and W.D. Deckwer. 1995. Cometabolic degradation of trichloroethylene in a bubble column bioscrubber. *Biotechnology and Bioengineering*, Vol. 47: 461-469.

Hickey, W.J. 1995a. Soil ventilation - effects on microbial populations in gasoline contaminated subsurface soils. *Journal of Environmental Quality*. Vol. 24: 571-582.

Hickey, W.J. 1995b. In situ respirometry-field methods and implications for hydrocarbon biodegradation in subsurface soils. *Journal of Environmental Quality*, Vol. 24: 583-588.

Hillel, D. 1982. Introduction to soil physics. Academic Press, New York, NY.

Hinchee, R.E. 1994. *Air Sparging for Site Remediation*. Lewis Publishers, Ann Arbor, MI.

Hinchee, R.E. and S.K. Ong. 1992. A rapid in situ respiration test for measuring aerobic biodegradation rates of hydrocarbons in soil. *Journal Air and Waste Management Association*, Vol. 42: 1305-1312.

Hoag, G.E. and M.C. Marley. 1986. Gasoline residual saturation in unsaturated uniform aquifer materials. *Journal of Environmental Engineering*, Vol. 112: 586-604.

Hopkins, G.D., J. Munakata, L. Semprini and P.L. Mccarty. 1993. Trichloroethylene concentration effects on pilot field scale in-situ groundwater bioremediation by phenol oxidizing microorganisms. *Environmental Science and Technology*, Vol. 27: 2542-2547.

Jin, Y., T. Streck and W.A. Jury. 1994. Transport and biodegradation of toluene in unsaturated soil. *Journal of Contaminant Hydrology*, Vol. 17: 111-127.

Johnson, P.C., M.B. Hertz, and D.L. Byers. 1990a. Estimates for hydrocarbon vapor emissions resulting from service station remediations and buried gasoline contaminated soils. *Petroleum Contaminated Soils*. Kostecki, PT E.J. Calabrese. Lewis Publishers. 295-326.

Johnson, P.C., M.W. Kemblowski, and J.D. Colthart. 1990b. Quantitative analysis for the cleanup of hydrocarbon contaminated soils by in situ soil venting. *Ground Water*, Vol. 28: 413-429.

Kaluarachchi, J.J. and K.M. Mesbah-Ul Islam. 1995. Thermal venting to recover hydrocarbons from the unsaturated zone: theory. *Journal of Contaminant Hydrology*, Vol. 17: 293-311.

Kampbell, D.H., J.T. Wilson, H.W. Read, and T.T. Stocksdale. 1987. Removal of volatile aliphatic hydrocarbons in a soil bioreactor. *Journal Air Pollution Control Federation*, Vol. 37: 1236-1240.



Kampbell, D.H., J.T. Wilson, and D.W. Ostendorf. 1990. Simplified soil gas sensing techniques for plume mapping and remediation monitoring. *Proceedings Third National Conference on Petroleum Contaminated Soils*. Lewis Publishers, Chelsea, MI, pp. 125-139.

Kerfoot, H.B. 1987. Soil gas measurement for detection of groundwater contamination by volatile organic compounds. *Environmental Science and Technology*, Vol. 21: 1022-1024.

Kerfoot, H.B. 1990. Soil gas surveys for detection and delineation of groundwater contamination. *Traces and Trends in Analytical Chemistry*. Vol. 9: 157-163.

Kerfoot, H.B., C.L. Mayer, P.B. Durgin, and J.J. D'Lugosz. 1988. Measurement of carbon dioxide in soil gases for indication of subsurface hydrocarbon contamination. *Groundwater Monitoring Review*, Vol. 8: 67-71.

Kia, S.F. and A.S. Abdul. 1990. Retention of diesel fuel in aquifer material. *Journal of Hydraulic Engineering*, Vol. 116: 881-894.

Kittel, J.A., R.E. Hinchee, R.N. Miller, C.C. Vogel, and R. Hoeppel. 1993. In situ respiration testing: A field treatability test for bioventing. *Proceedings Petroleum Hydrocarbons and Organic Chemicals in Groundwater*, Houston, TX, NGWA/API, pp. 351-366.

Landa, A.S., E.M. Sipkema, J. Weijma, A.A.C.M. Beenackers, J. Dolfing and D.B. Janssen. 1994. Cometabolic degradation of trichloroethylene by pseudomonas-Cepacia G4 in a chemostat with toluene as the primary substrate. *Applied and Environmental Microbiology*, Vol. 60: 3368-3374.

Lanzarone, N.A. and P.L. McCarty. 1990. Column studies on methanotrophic degradation of trichloroethene and 1,2-dichloroethane. *Ground Water*, Vol. 28: 910-919.

Leach, L.E., F.P. Beck, J.T. Wilson, and D.H. Kampbell. 1988. Aseptic subsurface sampling techniques for hollow stem auger drilling. *Proceedings Second National Outdoor Action Conference*, Las Vegas, NV, NGWA, pp. 31-51.

Leahy, J.G., A.M. Byrne and R.H. Olsen. 1996. Comparison of factors influencing trichloroethylene degradation by toluene oxidizing bacteria. *Applied and Environmental Microbiology*, Vol. 62: 825-833.

Lee, M.D., and C.M. Swindoll. 1993. Bioventing for in situ remediation *Journal of Hydrological Sciences*, Vol. 38: 273-281.

Leeson, A, R.E. Hinchee, J. Kittel, G. Sayles, C.M. Vogel, and R.N. Miller. 1993. Optimizing bioventing in shallow vadose zones and cold climates *Journal of Hydrological Sciences*, Vol. 38: 283-295.

Lenhard, R.J. and J.C. Parker. 1987. Measurement and prediction of saturation-pressure relationships in three phase porous media systems. *Journal of Contaminant Hydrology*, Vol. 1, pp. 407-424.

Lenhard, R.J. and J.C. Parker. 1988. Experimental validation of the theory of extending two phase saturation-pressure relations to three fluid phase systems for monotonic drainage paths. *Water Resources Research*, Vol. 24: 373-380.

Lenhard, R.J. and J.C. Parker. 1990. Estimation of free hydrocarbon volume from fluid levels in monitoring wells. *Groundwater*, Vol. 28: 57-67.

Li, D.X. 1995. Bioventing feasibility assessment and system design using subsurface oxygen sensors. *Journal of the Air and Waste Management Association*, Vol. 45: 762-769.

Li, S.Y. and L.P. Wackett. 1992. Trichloroethylene oxidation by toluene dioxygenase. *Biochemical and Biophysical Research Communications*, Vol. 185: 443-451.

Long, G. 1992. Bioventing and vapor extraction: innovative technologies for contaminated site remediation. *Journal of the Air & Waste Management Association*, Vol. 42: 345-348.

Luu, P.P., C.W. Yung, A.K. Sun and T.K. Wood. 1995. Monitoring trichloroethylene mineralization by pseudomonas-cepacia G4 Pr1. *Applied Microbiology and Biotechnology*, Vol. 44: 259-264.

Malachowsky, K.J., T.J. Phelps, A.B. Teboli, D.E. Minnikin and D.C. White. 1994. Aerobic mineralization of trichloroethylene, vinyl chloride, and aromatic compounds by rhodococcus species. *Applied and Environmental Microbiology*, Vol. 60: 542-548.

Marrin, D.L. Soil Gas Sampling and Misinterpretation. 1988. *Groundwater Monitoring Review*, Vol. 8: 51-54.

Marrin, D.L. 1991. Subsurface biogenic gas ratios associated with hydrocarbon contamination. *Proceedings In Situ Bioreclamation*, San Diego, CA, Batelle, pp. 546-560.

Mars, A.E., J. Houwing, J. Dolfing and D.B. Janssen. 1996. Degradation of toluene and trichloroethylene by burkholderia-cepacia G4 in growth limited fed batch culture. *Applied and Environmental Microbiology*, Vol. 62: 886-891.

McCarthy, K.A., and R.L. Johnson. 1995. Measurement of trichloroethylene diffusion as a function of moisture content in sections of gravity drained soil columns. *Journal of Environmental Quality*, Vol. 24: 49-55.

Miller, R.N., C.C. Vogel, and R.E. Hinchee. 1991. A field scale investigation of petroleum hydrocarbon biodegradation in the vadose zone enhanced by soil venting at Tyndall AFB, Florida. *Proceedings In Situ Bioreclamation*, San Diego, CA, Batelle, pp. 283-302.

Millington, R.J. 1959. Gas diffusion in porous media. *Science*, Vol. 130: 100-102.

Mohr, D.H. and P.H. Merz. 1995. Application of a 2D air flow model to soil vapor extraction and bioventing case studies. *Ground Water*, Vol. 33: 433-444.

Moyer, E.E., D.W. Ostendorf, D.H. Kampbell, and Y.F. Xie. 1994. Field trapping of subsurface vapor phase petroleum hydrocarbons. *Groundwater Monitoring and Remediation*, Vol. 14: 110-119.

Mu, D.Y. and K.M. Scow. 1994. Effect of trichloroethylene and toluene Concentrations on TCE and toluene biodegradation and the population density of TCE and toluene degraders in soil. *Applied and Environmental Microbiology*, Vol. 60: 2661-2665.

Nelson, M.J.K., S.O. Montgomery and P.H. Prichard. 1988. Trichloroethylene metabolism by microorganisms that degrade aromatic compounds. *Applied and Environmental Microbiology*, Vol. 54: 602-604.

Nilson, R.H., E.W. Peterson, K.H. Lie, N.R. Burkhard, J.R. Hearst. 1991. Atmospheric pumping: a mechanism causing vertical transport of contaminated gases through fractured permeable media. *Journal of Geophysical Research*, Vol. 96: 21,933-21,948.

Ostendorf D.W. and D.H. Kampbell. 1991. Biodegradation of hydrocarbon vapors in the unsaturated zone. *Water Resources Research*. Vol. 27: 453-462.

Ostendorf, D.W., L.E. Leach, E.S. Hinlein, and Y.F. Xie. 1991. Field sampling of residual aviation gasoline in sandy soil. *Groundwater Monitoring Review*, Vol. 11: 107-120.

Ostendorf, D.W., E.E. Moyer, R.J. Richards, E.S. Hinlein, Y.F. Xie, and R.V. Rajan. 1992. LNAPL distribution and hydrocarbon vapor transport in the capillary fringe. Report No. 600-R-92-247, USEPA. Ada, OK.

Ostendorf, D.W., R.J. Richards, and F.P. Beck. 1993a. LNAPL retention in sandy soil. *Groundwater*, Vol. 31:285-292.

Ostendorf, D.W., E.E. Moyer, Y.F. Yie, and R.V. Rajan. 1993b. Hydrocarbon Vapor Diffusion in Intact Core Sleeves. *Groundwater Monitoring and Remediation*, Vol. 13: 139-150.

Ostendorf, D.W., A.J. Lutenegeger, and S.J. Pollock. 1995a. Soil gas sampling and analysis in a petroleum contaminated transportation department right of way. *Transportation Research Record*, Vol. 1475: 110-122.

Ostendorf, D.W., A.J. Lutenegeger, D.J. DeGroot, S.C. Long, E.S. Isaacson, P.J. Cheever, E.S. Hinlein, R.J. Suchana, J.P. Tehrany, T.H. Schoenberg, and J.Jordan. 1995c. Fate and transport of

petroleum hydrocarbons at a leaking storage tank site. *Report UMTC-95-4*, University of Massachusetts Transportation Center, Amherst, MA.

Ostendorf, D.W., A.J. Luttenegger, R.J. Suchana, P.S. Cheever, and S.J. Pollock. 1996. LNAPL detection, measurement, and distribution in the subsurface environment. *Proceedings NAPLS in the Subsurface Environment*, ASCE, Washington, DC: 91-102.

Ostendorf, D.W., D.J. DeGroot, S.J. Pollock, and L.J. Long. 1997a. Aerobic degradation potential assessment from oxygen and carbon dioxide soil gas concentrations in roadside soil. *Journal of Environmental Quality*, in press.

Ostendorf, D.W., D.J. DeGroot, A.J. Luttenegger, P.J. Gagnon, J.G. Panton, H.M. Vandewalker, M.P. Bonus, L.J. Long, C.S. Howell, and R.C. Glass. 1997b. Fate and transport of calcium magnesium acetate in the unsaturated zone of a roadside soil. *Research Report*, FHWA, in press.

Pantazidou, M. and N. Sitar. 1993. Emplacement of Nonaqueous Phase Liquids in the Vadose Zone. *Water Resources Research*. 29(3): 705-722.

Parker, J.C. and R.J. Lenhard. 1987. A model for hysteretic constitutive relations governing multiphase flow 1. Saturation pressure relations. *Water Resources Research*, Vol. 23: 2187-2196.

Parsons Engineering-Science, Inc. 1995. Intrinsic remediation-engineering evaluation/cost analysis for site FT-002-Plattsburgh Air Force Base-Plattsburgh, NY. *Final Draft*. Denver, CO.

Pavlostathis, S.G. and P. Zhuang. 1991. Transformation of trichloroethylene by sulfate reducing cultures enriched from a contaminated subsurface soil. *Applied Microbiology and Biotechnology*, Vol. 36: 416-420.

Pinder, G.F. and L.M. Abriola. 1986. On the simulation of nonaqueous phase organic compounds in the subsurface. *Water Resources Research*, Vol. 22: 109S-119S.

Pirkle, R.J., D.E. Wyatt, and B.P. Looney. 1992. Barometric pumping: the connection between the vadose zone and the atmosphere. *Presented at The Focus Eastern Regional Ground Water Issues Conference*. Newton, MA.

Potter, T.L. 1989. Analysis of petroleum contaminated soil and water: an overview. *Proceedings Second National Conference on Petroleum Contaminated Soils*. Lewis Publishers, Chelsea, MI, pp. 97-109.

Radian Corporation. 1985. *Installation restoration program-phase I: records search, Plattsburgh Air Force Base, Plattsburgh, New York*. Herndon, VA.

Rainville, E.D. and P.E. Bedient. 1969. *Elementary differential equations*. Macmillan, New York.

Rathfelder, K., J.R. Lang, and L.M. Abriola. 1995. Soil vapor extraction and bioventing-applications, limitations, and future research directions. *Reviews of Geophysics*, Vol. 33: 1067-1081.

Reible, D.D., T.H. Illangasekare, D.V. Doshi, and M.E. Malhiet. 1990. Infiltration of immiscible contaminants in the unsaturated zone. *Groundwater*, Vol. 28: 685-692.

Reid, R.C., J.M. Prausnitz, and B.E. Poling. 1987. The properties of gases and liquids. McGraw-Hill, New York.

Robbins, G.A., B.G. Deyo, M.R. Temple, J.D. Stuart, and M.J. Lacy. 1990. Soil gas surveying for subsurface gasoline contamination using total organic vapor detection instruments 1. Theory and laboratory experimentation. *Groundwater Monitoring Review*, Vol. 10: 122-131.

Roberts, L.A. and D.J. Wilson. 1993. Groundwater cleanup by in situ sparging: modeling of dense nonaqueous phase liquid droplet removal. *Separation Science and Technology*, Vol. 28: 1127-1143.

Russell, T.F. 1995. Modeling of multiphase multicontaminant transport in the subsurface. *Reviews of Geophysics*, Vol. 33: 1035-1047.

Schwille, F. 1967. Petroleum contamination of the subsoil--a hydrological problem. Joint Problems of the Oil and Water Industries, Institute of Petroleum Engineers, New York, NY.

Schwille, F. 1988. Dense chlorinated solvents in porous and fractured media. Lewis Publishers, Chelsea, MI.

Semprini, L., G.D. Hopkins, P.V. Roberts, D. Grbic-Galic, and P.L. McCarty. 1991. A field evaluation of in situ biodegradation of chlorinated ethenes: studies of competitive inhibition. *Ground Water*, Vol. 29: 239-250.

Shan, C. 1995. Analytical solutions for determining vertical air permeability in unsaturated soils. *Water Resources Research*. Vol. 31: 2193-2200.

Sleep, B.E. and J.F. Sykes. 1989. Modeling the transport of volatile organics in variably saturated media. *Water Resources Research*, Vol. 25: 81-92.

Sleep, B.E. and Sykes, J.F. 1993. Compositional simulation of groundwater contamination by organic compounds: model applications. *Water Resources Research*, Vol. 29: 1709-1718.

Speitel, G.E. Jr. and F.B. Cloosmann. 1991. Chlorinated solvent biodegradation by methanotrophs in unsaturated soils. *Journal of Environmental Engineering*, Vol. 117: 541-558.

Streeter, V.L. and E.B. Wylie. 1979. Fluid mechanics, McGraw Hill, New York, NY.

Stylianou, C. and B.A. DeVantier. 1995. Relative air permeability as function of saturation in soil venting. *Journal of Environmental Engineering*, Vol. 121: 337-347.

Taylor, J.K. 1987. Quality assurance of chemical measurements. Lewis Publishers, Chelsea, MI.

Tehrany, J.P., P.O. Reyes, S.J. Ergas, and D.W. Ostendorf. 1996. Evaluation of surface emissions from bioventing sites. *Proceedings 89th Annual Meeting*. AWMA, Nashville, TN, TP40.01, 12 pp.

Tillman, N. and L. Leonard. 1993. Vehicle mounted direct push systems, sampling tools, and case histories: an Overview of an emerging technology. *Proceedings Petroleum Hydrocarbons and Organic Chemicals in Groundwater*. NGWA/API, Dublin, OH, pp. 177-188.

Unger, A.J.A., E.A. Sudicky, and P.A. Forsyth. 1995. Mechanisms controlling vacuum extraction coupled with air sparging for remediation of heterogeneous formations contaminated by dense nonaqueous phase liquids. *Water Resources Research*, Vol. 31:1913-1925.

URS Consultants, Inc. 1993. Installation restoration program at Plattsburgh Air Force Base, New York. *Site FT-002 Groundwater Operable Unit Feasibility Study Report*. Buffalo, NY.

Vandegrift, S.A. and D.H. Kampbell. 1988. Gas chromatographic determination of aviation gasoline and JP4 jet fuel in subsurface core samples. *Journal Chromatographic Science*, Vol. 26: 566-569.

Van Genuchten, M.T. 1980. A closed form equation for predicting the hydraulic conductivity of unsaturated soils. *Soil Science Society of America Journal*, Vol. 44: 892-898.

Van Geel, P.J. and J.F. Sykes. 1994. Laboratory and model simulations of an LNAPL spill in a variably saturated sand. *Journal of Contaminant Hydrology*, Vol. 17: 27-53.

Van Vliet, D.J., N.R. Thomson, and J.F. Sykes. 1993. Seasonal concentration fluctuations of volatile organic compounds in the subsurface. *Proceedings Petroleum Hydrocarbons and Organic Chemicals in Groundwater*, Houston, TX. NGWA/API, pp. 577-591.

Vogel, T.M. and P.L. McCarty. 1985. Biotransformation of tetrachloroethylene to trichloroethylene, dichloroethylene, vinyl chloride, and carbon dioxide under methanogenic conditions. *Applied and Environmental Microbiology*. 49(5): 1080-1083.

Weast, R.C. 1967. Handbook of chemistry and physics. Chemical Rubber Co., Cleveland.

Weeks, E.P. 1979. Barometric fluctuations in wells tapping deep unconfined aquifers. *Water Resources Research*, Vol. 15: 1167-1175.

Wilcox, D.W., R.L. Autenrieth and J.S. Bonner. 1995. Propane induced biodegradation of vapor phase trichloroethylene. *Biotechnology and Bioengineering*, Vol. 46: 333-342.

Wilson, J.D., J.M. Rodriguez-Maroto, and C. Gomez-Lahoz. 1994. Soil cleanup by in situ aeration: effects of spill age on soil vapor extraction remediation rates. *Separation Science and Technology*, Vol. 29: 1645-1671.

Wilson, J.D., A.N. Clark, and R.D. Mutch Jr. 1989. Soil cleanup by in situ aeration: passive vent wells, recontamination and removal of underlying nonaqueous phase liquid. *Separation Science and Technology*, Vol. 24: 939-979.

Wilson, J.L. and S.H. Conrad. 1984. Is physical displacement of residual hydrocarbons a realistic possibility in aquifer restoration? Proceedings Petroleum Hydrocarbons and Organic Chemicals in Groundwater, NWWA/API, Houston, TX, pp. 274-298.

Wilson, R.D. and D.M. Mackay. 1993. The use of sulphur hexafluoride as a conservative tracer in saturated sandy media. *Ground Water*, Vol. 31: 719-724.

Wilson, J.T. and B.H. Wilson. 1985. Biotransformation of trichloroethylene in soil. *Applied and Environmental Microbiology*, Vol. 49: 242-243.

Wood, B.D. and T.R. Ginn. 1995. Effects of microbial metabolic lag in contaminant transport and biodegradation modeling. *Water Resources Research*. Vol. 31: 553-563.

Zaidell, J. and D. Russo. 1994. Diffusive transport of organic vapors in the unsaturated zone with kinetically controlled volatilization and dissolution: analytical model and analysis. *Journal of Contaminant Hydrology*, Vol. 17: 145-165.

Zwick, T., R. Hinchee, R. Hoeppl, C. Kyburg, and L. Bowling. 1994. Passive bioventing driven by natural air exchange. *Proceedings of the Petroleum Hydrocarbons and Organic Chemicals in Ground Water: Prevention, Detection and Remediation*. 305-315.

## **APPENDIX I BOREHOLE LOGS**



**3" Spoon Data**

Site Location:	Plattsburgh AFB				
Date:	10/09/95				
Personnel on site:	S.Kelley, C. Riccardi, T. Mitchell, A. Lutenegger, D. Ostendorf, P. Terrany, R. Suchana, E. Hinlein, M. McGrath, B. Chakow, P. Reyes, R. Miknis				
Drillers:	CTB - Steve, Johnny				
12AA					
Boring Information:	Semi-continuous sampling from surface (every 5')				
Rods used:	NWJ				
SPT Protocol:	Automatic 140 lb. hammer with a 30" drop height				
Location:	Center of transects				
Core #	Depth (ft)	Blows/6"	N-value	Recovery	notes
1	0-1.5	3-6-7	13	16	
2	5-6.5	4-4-5	9	16	dark brown sand
3	10.0-11.5	10-14-17	31	20.5	light brown sand
4	15.0-16.5	13-21-24	45	18.5	
5	20.0-21.5	5-8-8	16	19	light brown sand
6	25.0-26.5	6-8-10	18	18.5	
7	30.0-31.5	6-14-18	32	20	
8	35.0-36.5	9-12-12	24	19	
9	36.5-38.0	7-13-15	28	19	
10	38.0-39.5	8-12-13	25	18	
11	39.5-41.0	9-10-12	22	15	
12	41.0-42.5	4-9-11	20	17.5	
13	42.5-44.0	16-7-9	18	17	
14	44.0-45.5	11-9-16	25	13.5	
15	45.5-47.0	3-5-5	10	8	
16	47.0-48.5	9-10-14	24	13	Water used inside
17	48.5-50.0	4-6-9	15	11	augers to keep borehole open
18	50.0-51.5	4-4-8	12	0	

**3" Spoon Data**

Site Location:	Plattsburgh AFB				
Date:	10/09/95				
Personnel on site:	S.Kelley, C. Riccardi, T. Mitchell, A. Lutenegger, D. Ostendorf, P. Terrany, R. Suchana, E. Hinlein, M. McGrath, B. Chakow, P. Reyes, R. Miknis				
Drillers:	CTB - Steve, Johnny				
12AB					
Boring Information:	Auger to 35' and sample semi-continuous (every 5')				
Rods used:	NWJ				
SPT Protocol:	Automatic 140 lb. hammer with a 30" drop height				
Location:	5' south west of 12AA				
Core #	Depth (ft)	Blows/6"	N-value	Recovery	notes
1	35-36.5	11-14-15	29	18	
2	40-41.5	2-4-7	11	14	Water used inside
3	45-46.5	5-8-15	23	11.5	augers to keep borehole open
4	50-51.5	4-7-12	19	0	

**3" Spoon Data**

Site Location:	Plattsburgh AFB				
Date:	34982				
Personnel on site:	S.Kelley, C. Riccardi, T. Mitchell, A. Lutenegger, D. Ostendorf, S. Ergas, P. Terrany, R. Suchana, E. Hinlein, M. McGrath, B. Chakow, P. Reyes, R. Miknis, P.Cheever				
Drillers:	CTB - Steve, Johnny				
<div>12AD</div>					
Boring Information:	Semi-continuous sampling from surface (every 5'), Continuous sampling 35'-48'				
Rods used:	NWJ				
SPT Protocol:	Automatic 140 lb. hammer with a 30" drop height				
Location:	15' North of 12AA				
Core #	Depth (ft)	Blows/6"	N-value	Recovery	notes
1	0-1.5	3-3-5	8	18	
2	5-6.5	3-3-4	7	11	
3	10.0-11.5	10-13-15	28	19	
4	15.0-16.5	11-16-18	34	20	
5	20.0-21.5	8-11-11	22	19	
6	25.0-26.5	6-10-12	22	18	
7	30.0-31.5	9-13-16	29	18	
8	35.0-36.5	7-8-8	16	17	
9	36.5-38.0	6-6-8	14	17	
10	38.0-39.5	3-4-5	9	16	
11	39.5-41.0	30-9-5	14	16	
12	41.0-42.5	3-4-5	9	3	
13	42.5-44.0	3-5-6	11	0	Since no recovery changed to a 2" SS (24" long)
14	44.0-46.0	2-3-3-7	6	18	24" drive
15	46.0-48.0	2-3-5-6	8	14	24" drive
End of Boring					

**3" Spoon Data**

Site Location:	Plattsburgh AFB				
Date:	10/10/95				
Personnel on site:	S.Kelley, C. Riccardi, T. Mitchell, A. Lutenegger, D. Ostendorf, S. Ergas, P. Terrany, R. Suchana, E. Hinlein, M. McGrath, B. Chakow, P. Reyes, R. Miknis, P.Cheever				
Drillers:	CTB - Steve, Johnny				
12AG					
Boring Information:	Semi-continuous sampling from surface (every 5'), Continuous sampling 35'-48'				
Rods used:	NWJ				
SPT Protocol:	Automatic 140 lb. hammer with a 30" drop height				
Location:	25' North of 12AA				
Core #	Depth (ft)	Blows/6"	N-value	Recovery	notes
1	0-1.5	3-4-3	7	18	
2	5-6.5	WOH-1-1	2	7	
3	10.0-11.5	1-1-1	2	18	
4	15.0-16.5	6-10-11	21	18	
5	20.0-21.5	5-8-8	16	19	
6	25.0-26.5	5-12-13	25	18	
7	30.0-31.5	4-9-13	22	18	
8	35.0-36.5	5-8-9	17	18	
9	36.5-38.0	4-6-6	12	18	
10	38.0-39.5	5-5-6	11	16	
11	39.5-41.0	4-5-6	11	20	
12	41.0-42.5	5-7-7	14	18	
13	42.5-44.0	3-5-8	13	0	Since no recovery changed to a 2" SS (24" long)
14	44.0-46.0	3-4-5-8	9	9	24" drive
15	46.0-48.0	2-5-6-7	11	16	24" drive
End of Boring					

**3" Spoon Data**

Site Location:	Plattsburgh AFB				
Date:	10/11/95				
Personnel on site:	S.Kelley, C. Riccardi, T. Mitchell, D. Ostendorf, P. Terrany, R. Suchana, E. Hinlein, M. McGrath, P. Reyes, R. Miknis, P.Cheever				
Drillers:	CTB - Steve, Johnny				
<div>12AK</div>					
Boring Information:	Semi-continuous sampling from surface (every 5'), Continuous sampling 35'-48'				
Rods used:	NWJ				
SPT Protocol:	Automatic 140 lb. hammer with a 30" drop height				
Location:	15' Southwest of 12AA				
Core #	Depth (ft)	Blows/6"	N-value	Recovery	notes
1	0-1.5	4-5-6	11	16	
2	1.5-3.0	5-3-3	6	16	
3	5-6.5	3-8-7	15	15	
4	10.0-11.5	4-6-10	16	18	
5	15.0-16.5	11-18-20	38	19	
6	20.0-21.5	6-8-10	18	19	
7	25.0-26.5	7-10-11	21	19	
8	30.0-31.5	4-8-12	20	18	
9	35.0-36.5	11-15-16	31	19	
10	36.5-38.0	4-11-13	24	23	
11	38.0-39.5	5-7-10	17	18	
12	39.5-41.0	12-5-7	12	17	
13	41.0-43.0	2-5-6-8	11	20/24	24" drive with water as drilling fluid
14	43.0-45.0	3-5-6-7	11	20/24	24" drive with water as drilling fluid
15	45.0-47.0	1-3-5-7	8	21/24	24" drive with water as drilling fluid
End of Boring					

**3" Spoon Data**

Site Location:	Plattsburgh AFB
Date:	10/12/95
Personnel on site:	S.Kelley, C. Riccardi, T. Mitchell, P.Cheever R. Suchana, E. Hinlein, M. McGrath, P. Reyes, R. Miknis
Drillers:	CTB - Steve, Johnny

**12AM**

Boring Information:	Auger down to 35', Continuous sampling 35'-48'
Rods used:	NWJ
SPT Protocol:	Automatic 140 lb. hammer with a 30" drop height
Location:	5' Northwest of 12AA

Core #	Depth (ft)	Blows/6"	N-value	Recovery	notes
1	35.0-36.5	9-13-15	28	19	
2	36.5-38.0	12-13-16	29	19	
3	38.0-39.5	7-10-11	21	18	
4	39.5-41.0	7-5-8	13	21	
5	41.0-43.0	3-4-7-9	11	18/24	24" drive with water as drilling fluid
6	43.0-45.0	3-5-6-8	11	19/24	24" drive with water as drilling fluid
7	45.0-47.0	4-6-8-8	14	18/24	24" drive with water as drilling fluid

**End of Boring**

**3" Spoon Data**

Site Location:	Plattsburgh AFB				
Date:	34985				
Personnel on site:	S.Kelley, C. Riccardi, T. Mitchell, P.Cheever R. Suchana, E. Hinlein, M. McGrath, P. Reyes, R. Miknis				
Drillers:	CTB - Steve, Johnny				
<div>12AP</div>					
Boring Information:	Auger down to 35', Continuous sampling 35'-48'				
Rods used:	NWJ				
SPT Protocol:	Automatic 140 lb. hammer with a 30" drop height				
Location:	12' East of 12AA				
<b>Core #</b>	<b>Depth (ft)</b>	<b>Blows/6"</b>	<b>N-value</b>	<b>Recovery</b>	<b>notes</b>
1	35.0-36.5	7-13-11	24	19	
2	36.5-38.0	15-12-14	26	19	
3	38.0-39.5	10-13-15	28	19	
4	39.5-41.0	3-7-12	29	18	
5	41.0-43.0	7-9-13-13	22	17/24	24" drive with water as drilling fluid
6	43.0-45.0	2-7-10-12	17	17/24	24" drive with water as drilling fluid
End of Boring					

**3" Spoon Data**

Site Location:	Plattsburgh AFB
Date:	10/13/95
Personnel on site:	S.Kelley, C. Riccardi, T. Mitchell, P.Cheever R. Suchana, E. Hinlein, M. McGrath, P. Reyes, R. Miknis
Drillers:	CTB - Steve, Johnny

**12AR**

Boring Information:	Auger down to 35', Continuous sampling 35'-48'
Rods used:	NWJ
SPT Protocol:	Automatic 140 lb. hammer with a 30" drop height
Location:	15' Northeast of 12AA

Core #	Depth (ft)	Blows/6"	N-value	Recovery	notes
1	35.0-36.5	6-8-12	20	18	
2	36.5-38.0	7-8-8	16	16	
3	38.0-39.5	1-1-1	2	17	
4	39.5-41.0	12-5-4	9	16	
5	41.0-43.0	4-5-6-14	11	21/24	24" drive with water as drilling fluid
6	43.0-45.0	1-2-4-5	6	12/24	24" drive with water as drilling fluid
7	45.0-47.0	2-4-7-9	11	16/24	24" drive with water as drilling fluid

**End of Boring**



**3" Spoon Data**

Site Location:	Plattsburgh AFB				
Date:	12/2/95				
Personnel on site:	S.Kelley, Dr. Lutenegger, Dr. DeGroot, T. Mitchell, G. Costa R. Mikinis, R. Suchana, P.Reyes, B.Glass, Chris, B. Charkhow P. Tehrany, D. Ostendorf, E. Hinlein				
Drillers:	CTB - Steve and Johnny				
		12AS			
Boring Information:	Augered to 35' (with 3 1/4" augers) and sample continuous from 35' to 49.0'				
Rods used:	NWJ				
SPT Protocol:	Automatic 140 lb. hammer with a 30" height				
Location:	5' south of 12AA				
Core #	Depth (ft)	Blows/6"	N-value	Recovery	notes
1	35.0-36.5	9-10-14	24	18	
2	36.5-38.0	8-11-13	24	18	
3	38.0-39.5	10-8-7	15	18	water at 39.5'
4	39.5-41.0	16-7-9	16	18	
5	41.0-42.5	8-12-20	32	18	
6	42.5-44.0	12-16-19	35	14	pour 2 bkts H2O
7	44.0-45.5	9-12-15	27	12	
8	45.5-47.0	4-5-8	13	0	pour 2 bkts H2O
9	45.5-47.0	1-3-4	7	18	2" split spoon
10	47.0-49.0	4-7-10-30	17	24	pour 2 bkts H2O

**3" Spoon Data**

Site Location:	Plattsburgh AFB				
Date:	12/1/95				
Personnel on site:	S.Kelley, Dr. Lutenegger, Dr. DeGroot, T. Mitchell, G. Costa R. Mikinis, R. Suchana, P.Reyes, B.Glass, Chris, B. Charkhow P. Tehrany, D. Ostendorf, E. Hinlein				
Drillers:	CTB - Steve and Johnny				
	12AT				
Boring Information:	Augered to 25' (with 3 1/4" augers) and sample continuous from 35' to 40.5'				
Rods used:	NWJ				
SPT Protocol:	Automatic 140 lb. hammer with a 30" height				
Location:	200' south of 12AA				
Core #	Depth (ft)	Blows/6"	N-value	Recovery	notes
1	25.0-26.5	8-10-10	20	18	
2	30.0-31.5	6-12-11	23	18	
3	31.5-33.0	5-10-11	21	18	
4	33.0-34.5	5-8-12	20	18	
5	34.5-36.0	21-10-11	21	18	
6	36.0-37.5	6-16-19	35	18	
7	37.5-39.0	9-13-16	29	12.5	used water to keep
8	39.0-40.5	13-16-16	32	14	hole open

**3" Spoon Data**

Site Location:	Plattsburgh AFB
Date:	06/05/96
Personnel on site:	S.Kelley, Dr. Lutenegger, T.Mitchell, G.Costa, T.Thomson, M. Rodick, J. Clary E. Hinlein, B. Charkow, B. Glass, T. Scheonberg, DaveO.
Drillers:	CTB - Steve, Johnny

**12AU**

Boring Information:	Augered to 38' (with 3 1/4" augers) and sample continuous from 38' to 53'
Rods used:	NWJ
SPT Protocol:	3" Barrel sampler driven with an automatic 140 lb. hammer with a 30" drop height
Location:	8' in from 12AA perpendicular to fence.

Core #	Depth (ft)	Blows/6"	N-value	Recovery (in)	notes
1	38.0-39.5	5-5-6	11	17	
2	39.5-41.0	13-6-9	15	23.5	
3	41.0-42.5	9-9-11	20	0	Switched to a 2" SS with water.
4	42.5-44.0	2-4-6	10	0	
5	44.0-45.5	3-5-27	32	15.5	
6	45.5-47.0	3-4-6	10	13	
7	47.0-49.0	3-3-6-7	9	17.5	Driven 24"
8	49.0-53.0	2-3-3-7-11-12	N/A	34	Driven 4'

### 3" Spoon Data

Site Location:	Plattsburgh AFB				
Date:	06/05/96				
Personnel on site:	S.Kelley, Dr. Lutenegger, T.Mitchell, G.Costa, T.Thomson, M. Rodick E. Hinlein, B. Charkow, B. Glass, T. Scheonberg, DaveO.				
Drillers:	CTB - Steve, Johnny				
<b>12AV</b>					
Boring Information:	Augered to 35' (with 3 1/4" augers) and sample continuous from 35' to 49'				
Rods used:	NWJ				
SPT Protocol:	3" Barrel sampler driven 18" with an automatic 140 lb. hammer with a 30" drop height				
Location:	6' Southwest of AA				
Core #	Depth (ft)	Blows/6"	N-value	Recovery (in)	notes
3	35.0-36.5	4-7-6	13	20	3" core Drive 18"
4	36.5-38.0	3-4-4	8	18.5	
5	38.0-39.5	3-3-3	6	16	
6	39.5-41.0	12-4-4	8	13.5	
7	41.0-42.5	5-9-18	27	0	Add water in augers
8	43.0-45.0	2-3-3-14	17	19.5	2" split spoon Drive 24"
9	45.0-47.0	1-2-2-3	5	22	
10	47.0-49.0	1-1-2-2	4	17.5	

### 3" Spoon Data

Site Location:	Plattsburgh AFB				
Date:	06/05/96				
Personnel on site:	S.Kelley, Dr. Lutenegger, T.Mitchell, G.Costa, T.Thomson, M. Rodick E. Hinlein, B. Charkow, B. Glass, T. Scheonberg, DaveO.				
Drillers:	CTB - Steve, Johnny				
<div>12AW</div>					
Boring Information:	Augered to 35' (with 3 1/4" augers) and sample continuous from 35' to 48.5'				
Rods used:	NWJ				
SPT Protocol:	3" Barrel sampler driven 18" with an automatic 140 lb. hammer with a 30" drop height				
Location:	Midway between 12AC and 12AD				
Core #	Depth (ft)	Blows/6"	N-value	Recovery (in)	notes
1	35.0-36.5	5-11-14	25	18	3" barrel, Drive 18"
2	36.5-38.0	8-8-8	16	16	
3	38.0-39.5	5-4-6	10	16.5	
4	39.5-41.0	8-5-5	10	18	Used water to keep sand out
5	41.0-42.5	6-10-17	27	12	
6	42.5-44.5	2-2-4-5	9	17	Switched to a 2" Split Spoon,
7	44.6-46.5	1-2-4-6	10	16	Drive 24"
8	46.5-48.5	3-4-7-9	16	17	

### 3" Spoon Data

Site Location:	Plattsburgh AFB
Date:	06/06/96
Personnel on site:	S.Kelley, T.Mitchell, M. Rodick, J.Clary E. Hinlein, B. Charkow, B. Glass, T. Scheonberg, DaveO.
Drillers:	CTB - Steve, Johnny

12AX

Boring Information:	Augered to 35' (with 3 1/4" augers) and sample continuous from 5' to 37.0'
Rods used:	NWJ
SPT Protocol:	3" Barrel sampler driven 18" with an automatic 140 lb. hammer with a 30" drop height
Location:	6'10" South of Barometric well

Core #	Depth (ft)	Blows/6"	N-value	Recovery (in)	notes
1	5.0-6.5	5-6-5	11	17	3" barrel, Drive 18"
2	6.5-8.0	4-10-10	20	17	
3	8.0-9.5	6-8-11	19	18	
4	9.5-11.0	8-8-12	20	20	
5	11.0-12.5	6-8-7	15	16	
6	12.5-14.0	5-5-6	11	14	
7	14.0-15.5	5-8-7	15	17	
8	15.5-17.0	3-8-8	16	16	
9	17.0-18.5	6-8-10	18	20.5	
10	18.5-20.0	3-6-6	12	14	
11	20.0-21.5	5-5-9	14	18	
12	21.5-23.0	6-9-9	18	18	
13	23.0-24.5	4-6-8	14	18	
14	24.5-26.0	3-7-7	14	17	
15	26.0-27.5	7-10-11	21	20	
16	27.5-29.0	3-8-13	21	15.5	
17	29.0-30.5	7-10-10	20	19	
18	30.5-32.0	5-7-9	16	17	Sample is fairly wet.
19	32.0-33.5	7-7-6	13	17	Sample is wet.
20	33.5-35.0	4-6-10	16	16	Adding water.
21	35.0-36.5	3-5-8	13	12	
22	36.5-37.0	5-10-14	24	0	

**2" Spoon Data**

Site Location:	Plattsburgh AFB				
Date:	06/06/96				
Personnel on site:	S. Kelley, T. Mitchell, M. Rodick, J. Clary E. Hinlein, B. Charkhow, B. Glass, T. Schoenberg, Dave Ostendorf				
Drillers:	CTB - Steve, Johnny				
	<b>12AY</b>				
Boring Information:	Samples continuous from 0' to 45.0'				
Rods used:	NWJ				
SPT Protocol:	2" split spoon (unlined) sampler driven with an automatic 140 lb. hammer with a 30" drop height				
Location:	24' Southeast of SPK1				
Core #	Depth (ft)	Blows/6"	N-value	Recovery (in)	notes
1	0-2.0	1-2-2-2	4	23	
2	2.0-4.0	2-1-1-2	3	21.5	
3	4.0-6.0	5-5-6-8	14	24	
4	6.0-8.0	5-7-7-10	17	19	
5	8.0-10.0	7-10-14-13	27	14	
6	10.0-12.0	6-9-11-12	23	26	
7	12.0-14.0	8-10-11-13	24	24	
8	14.0-16.0	7-9-10-14	24	23	
9	16.0-18.0	6-6-8-12	20	23.5	
10	18.0-20.0	4-7-10-10	20	22.5	
11	20.0-22.0	5-8-8-10	18	25	
12	22.0-24.0	5-8-8-18	26	24	
13	24.0-26.0	6-6-8-8	16	23	
14	26.0-28.0	8-6-6-8	14	24	
15	28.0-30.0	6-7-7-8	15	26	
16	30.0-32.0	5-7-8-12	20	24	
17	32.0-34.0	10-14-18-19	37	23	
18	34.0-36.0	9-14-11-11	22	23	Switched to a 3" Core Sampler,
19	36.0-37.5	10-12-17	29	19	18" Drives.
20	37.5-39.0	4-10-14	24	18	
21	39.0-40.5	7-11-10	21	22	Switched to a 2" split spoon.
22	41.0-43.0	2-4-6-7	13	15	
23	43.0-45.0	6-6-9-10	19	12	

### 3" Spoon Data

Site Location:	Plattsburgh AFB				
Date:	06/07/96				
Personnel on site:	S.Kelley, T.Mitchell, M. Rodick E. Hinlein, B. Charkow, B. Glass, T. Scheonberg				
Drillers:	CTB - Steve, Johnny				
12AZ					
Boring Information:	Augered to 35' (with 3 1/4" augers) and sample continuous from 35' to 51.0'				
Rods used:	NWJ				
SPT Protocol:	3" Barrel sampler driven 18" with an automatic 140 lb. hammer with a 30" drop height				
Location:	5' Northwest of SPK1				
Core #	Depth (ft)	Blows/6"	N-value	Recovery (in)	notes
1	35.0-36.5	5-11-12	23	18	3" barrel, 18" drives
2	36.5-38.0	10-12-15	27	18	
3	38.0-39.5	5-5-8	13	18	
4	39.5-41.0	7-17-23	40	18	
5	41.0-43.0	5-6-7-9	13	18	2" spilt spoon, 24" drives
6	43.0-45.0	3-5-6-9	11	19	used water to keep static head
7	45.0-47.0	2-5-7-9	12	14	
8	47.0-49.0	3-5-8-8	13	18	
9	49.0-51.0	9-10-4-5	14	24	



**3" Spoon Data**

Site Location:	Plattsburgh AFB				
Date:	06/07/96				
Personnel on site:	S.Kelley, T.Mitchell, M. Rodick E. Hinlein, B. Charkow, B. Glass, T. Scheonberg				
Drillers:	CTB - Steve, Johnny				
12BA					
Boring Information:	Augered to 35' (with 3 1/4" augers) and sample continuous from 35' to 53.0'				
Rods used:	NWJ				
SPT Protocol:	3" Barrel sampler driven 18" with an automatic 140 lb. hammer with a 30" drop height				
Location:	4' Northwest of 12AP				
Core #	Depth (ft)	Blows/6"	N-value	Recovery (in)	notes
1	35.0-36.5	13-10-10	20	18	3" barrel, 18" drives
2	36.5-38.0	7-6-5	11	18	
3	38.0-39.5	4-5-5	10	18	
4	39.5-41.0	4-6-8	14	18	
5	41.0-43.0	3-2-3-5	5	13.5	2" spilt spoon, 24" drives
6	43.0-45.0	1-3-4-6	7	12	used water to keep static head
7	45.0-47.0	2-4-5-9	9	16	
8	47.0-49.0	6-13-15-17	28	20.5	
9	49.0-51.0	6-11-14-14	25	20	
10	51.0-53.0	4-7-12-15	19	24	

### 3" Spoon Data

Site Location:	Plattsburgh, AFB	
Date:	08/19/96	
Personnel on site:	S.Kelley, M.Mitchell, M. Rodick, AJL, M. Meyer, D. Ostendorf, R. Suchan B. Charkhow, B. Glass, C. Francis	
Drillers & Drill Rig:	CTB - Steve Butrej, Chad	CME 75
	12BB	
Boring Information:	Samples continuous from 0.0' to 20.0' , augered with 3 1/4" augers to 20.	
Rods used:	NWJ	
SPT Protocol:	3" Split Spoon sampler driven with a 140 lb. automatic hammer with a 30 Unlined split spoon with torque test.	
Torque Meas. Info.:	P-3500 strain indicator (UMA107640), Gage factor = 1.000	
Location:	6' West of 12AV	

Sample #	Depth (ft)	Blows/6"	N-value	Torque (ft-lb)	Recovery (in)
1	0-1.5	4-12-8	20	108.2	17
2	1.5-3.0	2-2-2	4	59.8	20
3	3.0-4.5	2-1-2	3	50.0	15
4	4.5-6.0	2-5-8	13	62.1	12
5	6.0-7.5	5-7-12	19	216.8	14
6	7.5-9.0	6-9-11	20	275.5	18
7	9.0-10.5	8-14-16	30	347.9	19
8	10.5-12.0	9-16-22	38	455.7	18
9	12.0-13.5	15-27-29	56	676.2	19
10	13.5-15.0	11-20-24	44	509.2	20
11	15.0-16.5	11-15-16	31	475.7	18
12	16.5-18.0	12-15-17	32	424.8	20
13	18.0-19.5	9-11-11	22	318.5	19.5

Solid 3" sampler	Sample #	Depth (ft)	Blows/6"	N-value	Recovery (in)
	1	34.0-35.5	7-8-9	17	18
	2	35.5-37.0	3-9-7	16	17
	3	37.0-38.5	4-4-5	9	18
	4	38.5-40.0	3-5-6	11	20
	5	40.0-41.5	3-6-7	13	0
	6	40.0-42.0	woh-2-4	2	12
	7	42.0-44.0	2-4-4-7	8	11
	8	44.0-46.0	3-4-4-7	8	15
	9	46.0-48.0	4-4-7-7	11	17

**2" Spoon Data**

Site Location:	Plattsburgh, AFB
Date:	08/20/96
Personnel on site:	S.Kelley, M.Mitchell, M. Rodick, AJL, M. Meyer, D. Ostendorf, R. Suchana, B. Charkhow, B. Glass, C. Francis
Drillers & Drill Rig:	CTB - Steve Butrej, Chad CME 75
	<b>12BF</b>
Boring Information:	Samples continuous from 1.5' to 20.0' , augered with 3 1/4" augers to 20.0' - 35.0', soil samples 35.0' - 47.
Rods used:	NWJ
SPT Protocol:	2" Split Spoon sampler driven with a 140 lb. safety hammer with a 30" drop height Unlined split spoon with torque test.
Torque Meas. Info.:	P-3500 strain indicator (UMA107640), Gage factor = 1.000
Location:	7' North of 12BE, 5 1/2' West 12AW

Sample #	Depth (ft)	Blows/6"	N-value	Torque (ft-lb)	Recovery (in)	notes
1	1.5-3.0	4-6-5	11	61.3	10	Brown sand with cobbles
2	3.0-4.5	5-3-5	8	12.4	8	"
3	4.5-6.0	4-6-6	12	64.2	12	Fine to med. yellow sand
4	6.0-7.5	4-5-6	11	83.6	14	fine to med. yellowish orange
5	7.5-9.0	5-8-11	19	106.6	14	fine tan sand
6	9.0-10.5	8-10-16	26	200.2	16	"
7	10.5-12.0	7-11-16	27	160.3	17	fine tan with some yellow fine
8	12.0-13.5	8-16-25	41	218.6	16	"
9	13.5-15.0	9-17-23	40	296.2	16	"
10	15.0-16.5	10-13-17	30	173.9	18	"
11	16.5-18.0	6-10-12	22	144.3	18	"
12	18.0-19.5	7-6-7	13	85.4	18	small silt layer

Solid 3" sampler	Sample #	Depth (ft)	Blows/6"	N-value	Recovery (in)	notes
	1	35.0-36.5	8-16-14	30	18	
	2	36.5-38.0	6-8-10	18	18	
	3	38.0-39.5	4-8-11	19	18	
	4	39.5-41.5	4-5-11	16	6	@ 40.0' started running water
	5	39.5-41.5	woh-6-7	6	22	switched to 2"ss
	6	41.5-43.5	1-2-5-7	7	18	
	7	43.5-45.5	3-6-8-7	14	19	
	8	45.5-47.5	3-5-5-8	10	12	

**4" Stainless Steel Solid Core Data**

Site Location:	Plattsburgh, AFB			
Date:	08/21/96			
Personnel on site:	S.Kelley, M.Mitchell, M. Rodick, AJL, M. Meyer, R. Suchana, B. Charkhow, B. Glass			
Drillers & Drill Rig:	CTB - Steve Butrej, Chad		CME 75	
	12BG			
Boring Information:	Augered with 4 1/2" augers, samples from root zone, capillary fringe, and contamination source			
Rods used:	NWJ			
SPT Protocol:	4" stainless steel solid core sampler driven with a 140 lb. automatic hammer with a 30" drop height			
Location:	n/a			
Sample #	Depth (ft)	Blows/6"	Recovery (in)	notes
1	0.0-3.0	7-10-8-4-4-6	27.5	
2	36.0-39.0	5-17-21-25-28-21	27.5	
3	39.0-42.0	6-9-10-15-16-17	36	

**Vapor Probe Data**

Site Location:	Plattsburgh, AFB		
Date:	08/21/96		
Personnel on site:	S.Kelley, M.Mitchell, M. Rodick, AJL, M. Meyer, R. Suchana, B. Charkhow, B. Glass		
Drillers & Drill Rig:	CTB - Steve Butrej, Chad	CME 75	
	12BH		
Boring Information:	Augered with 3 1/4" augers to 0.0' - 30.0', soil gas sampling 30.0' - 36.0'		
Rods used:	NWJ		
SPT Protocol:	Vapor probe sampler driven with a 140 lb. automatic hammer with a 30" drop height Exposed flush mounted sintered steel filter soil gas probe		
Location:	3' north 12AP, 3' south 12BA, 5' east of fence		
Sample #	Depth (ft)	Blows/6"	notes
1	30.0-30.5	6	
2	30.5-31.0	13	
3	31.0-31.5	14	
4	31.5-32.0	13	
5	32.0-32.5	22	
6	32.5-33.0	19	
7	33.0-33.5	15	
8	33.5-34.0	10	
9	34.0-34.5	8	
10	34.5-35.0	5	
11	35.0-35.5	5	
12	35.5-36.0	4	

**2" Spoon Data**

Site Location:	Plattsburgh, AFB	
Date:	08/21/96	
Personnel on site:	S.Kelley, M.Mitchell, M. Rodick, AJL, M. Meyer, R. Suchana, B. Charkhow, B. Glass	
Drillers & Drill Rig:	CTB - Steve Butrej, Chad	CME 75
	12BI	
Boring Information:	Samples every 5' from 5' to 35' , augered with 3 1/4" augers to 37.0', soil samples 37.0' - 47.5'	
Rods used:	NWJ	
SPT Protocol:	2" Split Spoon sample driven with an automatic 140 lb. hammer with a 30" drop height Unlined split spoon with torque test.	
Torque Meas. Info.:	P-3500 strain indicator (UMA107640), Gage factor = 1.000	
Location:	9' East of fence, 2' North of 12AH	

Sample #	Depth (ft)	Blows/6"	N-value	Torque (ft-lb)	Recovery (in)	notes
1	5.0-7.0	4-5-4-6	9	84.2	12	hit sand layer at bot. of spoon
2	10.0-12.0	9-9-11-13	20	159.4	12	tan fine-med. sand
3	15.0-17.0	15-24-20-21	44	159.4	12.5	"
4	20.0-22.0	3-7-6-8	13	130.1	22	fine tan sand
5	25.0-27.0	4-8-9-10	17	193.8	22	fine tan sand with 2" layer of silt
6	30.0-32.0	3-7-16-24	23	324.7	20	fine tan sand
7	35.0-37.0	4-5-5-8	10	92.9	17	fine to med moist tan sand

Solid 3" sampler	Sample #	Depth (ft)	Blows/6"	N-value	Recovery (in)	notes
	1	37.0-38.5	5-7-8	15	18	
	2	38.5-40.0	3-4-6	10	16	
	3	40.0-41.5	3-4-4	8	9.5	@ 40.0' started running water
	4	41.5-43.5	1-2-3-4	5	14	switched to 2"ss
	5	43.5-45.5	2-3-5-6	8	14	
	6	45.5-47.5	1-3-6-7	9	16	

**Vapor and Resistivity Probe Data**

Site Location:	Plattsburgh AFB	
Date:	08/21/96	
Personnel on site:	S.Kelley, M.Mitchell, M. Rodick, AJL, M. Meyer, R. Suchana, B. Charkhow, B. Glass	
Drillers & Drill Rig:	CTB - Steve Butrej, Chad	CME 75
		12BJ
Boring Information:	Augered with 3 1/4" augers down to 30.0', soil gas sampling 30.0' - 47.5'	
Rods used:	NWJ	
SPT Protocol:	Vapor probe sampler driven with a 140 lb. automatic hammer with a 30" drop height Exposed flush mounted sintered steel filter soil gas probe	
Location:	13.5' east of fence and 1' north from 12BA	

Sample #	Depth (ft)	Blows/6"	notes
1	30.0-30.5	8	
2	30.5-31.0	18	
3	31.0-31.5	21	
4	31.5-32.0	28	
5	32.0-32.5	29	
6	32.5-33.0	23	
7	33.0-33.5	22	
8	33.5-34.0	18	
9	34.0-34.5	11	
10	34.5-35.0	9	
11	35.0-35.5	7	
12	35.5-36.0	8	Hit capillary fringe
13	36.0-36.5	8	
14	36.5-37.0	8	
15	37.0-37.5	6	
16	37.5-38.0	8	
17	38.0-38.5	7	
18	38.5-39.0	6	
19	39.0-39.5	7	
20	39.5-40.0	7	
21	40.0-40.5	7	
22	40.5-41.0	7	
23	41.0-41.5	7	
24	41.5-42.0	8	
25	42.0-42.5	6	
26	42.5-43.0	8	
27	43.0-43.5	8	
28	43.5-44.0	8	
29	44.0-44.5	8	
30	44.5-45.0	11	
31	45.0-45.5	12	
32	45.5-46.0	13	
33	46.0-46.5	14	
34	46.5-47.0	16	
35	47.0-47.5	15	

**Vapor Probe Data**

Site Location:	Plattsburgh, AFB		
Date:	08/22/96		
Personnel on site:	S.Kelley, M.Mitchell, M. Rodick, M. Meyer, R. Suchana, B. Glass		
Drillers & Drill Rig:	CTB - Steve Butrej, Chad	CME 75	
	12BK		
Boring Information:	Augered with 3 1/4" augers to 0.0' - 30.0', soil gas sampling 30.0' - 37.0'		
Rods used:	NWJ		
SPT Protocol:	Vapor probe sampler driven with a 140 lb. automatic hammer with a 30" drop height Exposed flush mounted sintered steel filter soil gas probe		
Location:	6' west of 12AK and 4.5' south of dog house		
Sample #	Depth (ft)	Blows/6"	notes
1	30.0-30.5	8/8"	vac'm @ 5"Hg
2	30.5-31.0	11	Blank (TLV=100, O2=20.5, CO2=0.048)
3	31.0-31.5	10	
4	31.5-32.0	N/A	
5	32.0-32.5	11	vac'm @ 10"Hg
6	32.5-33.0	13	
7	33.0-33.5	15	TLV=240, O2=16.9, CO2=1.3
8	33.5-34.0	19	
9	34.0-34.5	17	
10	34.5-35.0	17	
11	35.0-35.5	15	
12	35.5-36.0	14	vac'm @ 11"Hg
13	36.0-36.5	14	TLV=540, O2=16.9, CO2=1.3
14	36.5-37.0	13	TLV=700, O2=16.9, CO2=1.3



**Vapor and Resistivity Probe Data**

Site Location:	Plattsburgh, AFB
Date:	08/22/96
Personnel on site:	S.Kelley, M.Mitchell, M. Rodi
Drillers & Drill Rig:	CTB - Steve Butrej, Chad
	<b>12BL</b>
Boring Information:	Augered with 3 1/4" augers
Rods used:	NWJ
SPT Protocol:	Vapor probe sampler driven Exposed flush mounted sinte
Location:	4.5' south of 12 BE, 7.5' east

Sample #	Depth (ft)	Blows/6"
1	30.0-30.5	4/8"
2	30.5-31.0	8
3	31.0-31.5	7
4	31.5-32.0	10
5	32.0-32.5	13
6	32.5-33.0	14
7	33.0-33.5	12
8	33.5-34.0	12
9	34.0-34.5	10
10	34.5-35.0	9
11	35.0-35.5	7
12	35.5-36.0	6
13	36.0-36.5	4
14	36.5-37.0	4
15	37.0-37.5	2
16	37.5-38.0	2
17	38.0-38.5	2
18	38.5-39.0	1
19	39.0-39.5	1
20	39.5-40.0	2
21	40.0-40.5	1
22	40.5-41.0	1
23	41.0-41.5	2
24	41.5-42.0	2
25	42.0-42.5	2
26	42.5-43.0	3

### Vapor Probe Data

Site Location:	Plattsburgh, AFB
Date:	08/22/96
Personnel on site:	S.Kelley, M.Mitchell, M. Ro
Drillers & Drill Rig:	CTB - Steve Butrej, Chad
	12BM
Boring Information:	Augered with 3 1/4" augers
Rods used:	NWJ
SPT Protocol:	Vapor probe sampler driven Exposed flush mounted sint
Location:	9' west of center of west sid

Sample #	Depth (ft)	Blows/6"
1	30.0-30.5	6/8"
2	30.5-31.0	9
3	31.0-31.5	13
4	31.5-32.0	11
5	32.0-32.5	11
6	32.5-33.0	16
7	33.0-33.5	18
8	33.5-34.0	17
9	34.0-34.5	17
10	34.5-35.0	14
11	35.0-35.5	10
12	35.5-36.0	10
13	36.0-36.5	9
14	36.5-37.0	10

**Vapor Probe Data**

Site Location:	Plattsburgh, AFB		
Date:	08/22/96		
Personnel on site:	S.Kelley, M.Mitchell, M. Rodick, M. Meyer, R. Suchana, B. Glass		
Drillers & Drill Rig:	CTB - Steve Butrej, Chad	CME 75	
	12BN		
Boring Information:	Augered with 3 1/4" augers down to 30.0', soil gas sampling 30.5' - 36.5'		
Rods used:	NWJ		
SPT Protocol:	Vapor probe sampler driven with a 140 lb. automatic hammer with a 30" drop height Exposed flush mounted sintered steel filter soil gas probe		
Location:	21.5' north NW corner side of dog house, 14.5' west of fence		
Sample #	Depth (ft)	Blows/6"	notes
1	30.0-30.5	6/8"	vac'm @ 10"Hg
2	30.5-31.0	13	vac'm @ 11"Hg
3	31.0-31.5	16	vac'm @ 11.5"Hg
4	31.5-32.0	21	vac'm @ 13" Hg
5	32.0-32.5	21	vac'm @ 13" Hg
6	32.5-33.0	28	vac'm @ 13" Hg
7	33.0-33.5	13	vac'm @ 13" Hg
8	33.5-34.0	14	vac'm @ 13.5" Hg
9	34.0-34.5	12	vac'm @ 13.5" Hg
10	34.5-35.0	11	vac'm @ 13.5" Hg
11	35.0-35.5	8	vac'm @ 14" Hg
12	35.5-36.0	9	vac'm @ 12" Hg
13	36.0-36.5	9	Hit capillary fringe Vac'm >23.0" Hg

## 2" Split Spoon Data

Site Location:	Plattsburgh AFB
Date:	08/22/96
Personnel on site:	S.Kelley, M.Mitchell, M. Rodic
Drillers:	CTB - Steve, Chad
<b>12BO</b>	
Boring Information:	Augered down to 30.0', soil g
Rods used:	NWJ
SPT Protocol:	2" Split Spoon sampler jacked
Torque Meas. Info.:	P-3500 strain indicator (UMA1
Thrust Meas. Info.:	P-3500 strain indicator (UMA1
Location:	4' east of fence, 8, north of 12

Sample #	Depth (ft)	Thrust (lbf)
1	0-1.5	
2	1.5-3.0	
3	3.0-4.5	
4	4.5-6.0	
5	6.5-8.0	
6	8.0-9.5	
7	9.5-11.0	
8	11.0-12.5	
9	12.5-14.0	
10	14.0-15.5	
11	15.5-17.0	
12	17.0-18.5	
13	18.5-20.0	

**2" Spoon Data**

Site Location:	Plattsburgh AFB
Date:	10/12/95
Personnel on site:	S.Kelley, C. Riccardi, T. Mitchell, P.Cheever R. Suchana, E. Hinlein, M. McGrath, P. Reyes, R. Miknis
Drillers:	CTB - Steve, Johnny

**SPK1**

Boring Information:	Continuous sampling from surface
Rods used:	NWJ
SPT Protocol:	Automatic 140 lb. hammer with a 30" drop height
Location:	15' Southeast from 12AA

Core #	Depth (ft)	Blows/6"	N-value	Recovery	notes
1	0-1.5	4-3-1	4	2	
2	1.5-3.0	WOH	2	0	
3	3.0-4.5	2-3-6	9	15	
4	4.5-6.0	5-5-6	11	14	
5	6.0-7.5	2-4-3	7	15	
6	7.5-9.0	4-6-9	15	14	
7	9.0-10.5	6-9-10	19	15	
8	10.5-12.0	7-11-12	23	17	
9	12.0-13.5	6-11-18	29	17	
10	13.5-15.0	13-20-21	41	17	
11	15.0-16.5	5-9-14	23	14	
12	16.5-18.0	6-12-14	26	16	
13	18.0-19.5	7-9-10	19	16	
14	19.5-21.0	4-6-6	12	17	
15	21.0-22.5	5-7-8	15	17	
16	22.5-24.0	5-6-7	13	16	
17	24.0-25.5	6-7-8	15	16	
18	25.5-27.0	4-5-7	12	17	
19	27.0-28.5	5-7-11	18	17	
20	28.5-30.0	9-17-15	32	19	
21	30.0-31.5	6-8-11	19	17	
22	31.5-33.0	8-15-18	33	17	
23	33.0-34.5	12-16-16	32	19	
24	34.5-36.0	8-11-13	24	18	
25	36.0-37.5	7-10-15	25	19	
26	37.5-39.0	4-6-8	14	18	Water used to keep hole open
27	39.0-40.5	3-7-11	18	16	
28	40.5-42.0	1-8-12	20	15	
29	42.0-43.5	5-9-10	19	13	
30	43.5-45.0	4-5-7	12	14	

**End of Boring**

**2" Spoon Data**

Site Location:	Plattsburgh AFB
Date:	12/2/95
Personnel on site:	S.Kelley, Dr. Lutenegeger, Dr. DeGroot, T. Mitchell, G. Costa R. Mikinis, R. Suchana, P.Reyes, B.Glass, Chris, B. Charkhow P. Tehrany, D. Ostendorf, E. Hinlein
Drillers:	CTB - Steve and Johnny

**SPK2**

Boring Information:	Augered with 3 1/4" augers and sampled continuous from surface to 40.5'
Rods used:	NWJ
SPT Protocol:	Automatic 140 lb. hammer with a 30" height
Location:	24' northwest of 12AA

Core #	Depth (ft)	Blows/6"	N-value	Recovery	notes
1	0-1.5	4-3-4	7	18	
2	1.5-3.0	2-1-2	3	17	
3	3.0-4.5	1-1-1	2	18	
4	4.5-6.0	WOH-1-1	2	2	
5	6.0-7.5	WOH-WOH-1	2	2	
6	7.5-9.0	2-2-4	6	10	
7	9.0-10.5	5-4-5	9	18	
8	10.5-12.0	5-5-6	11	18	
9	12.0-13.5	6-7-9	16	18	
10	13.5-15.0	6-8-10	18	18	
11	15.0-16.5	6-8-10	18	18	
12	16.5-18.0	7-8-9	17	18	
13	18.0-19.5	5-4-5	9	18	
14	19.5-21.0	3-3-5	8	18	
15	21.0-22.5	7-6-7	13	18	
16	22.5-24.0	4-5-6	11	18	
17	24.0-25.5	6-6-7	13	18	
18	25.5-27.0	5-6-10	16	19	
19	27.0-28.5	9-12-20	32	19	
20	28.5-30.0	15-17-19	36	19	
21	30.0-31.5	9-8-9	17	17	
22	31.5-33.0	7-12-14	26	17	
23	33.0-34.5	7-11-13	24	16	
24	34.5-36.0	8-11-11	22	18	
25	36.0-37.5	5-6-8	14	18	
26	37.5-39.0	3-5-7	12	17	Water used to keep hole open
27	39.0-40.5	5-6-7	13	20	

**End of Boring**

**3" Spoon Data**

Site Location:	Plattsburgh AFB				
Date:	11/30/95				
Personnel on site:	S.Kelley, Dr. Lutenegger, Dr. DeGroot, T. Mitchell, G. Costa R. Mikinis, R. Suchana, P.Reyes, B.Glass, Chris, B. Charkhow P. Tehrany, D. Ostendorf, E. Hinlein				
Drillers:	CTB - Steve and Johnny				
			Vent 1		
Boring Information:	Augered to 35' (with 6 1/4" augers) and sample continuous from 35' to 42.5'				
Rods used:	NWJ				
SPT Protocol:	Automatic 140 lb. hammer with a 30" height				
Location:	2.5' north of 12AA				
Core #	Depth (ft)	Blows/6"	N-value	Recovery	notes
1	35.0-36.5	4-10-10	20	18	
2	36.5-38.0	6-10-10	20	18	dark brown sand
3	38.0-39.5	4-4-7	11	18	water table at 39.5'
4	39.5-41.0	3-3-5	8	17	grey sand with odor
5	41.0-42.5	1-3-5	8	18	

**3" Spoon Data**

Site Location:	Plattsburgh AFB				
Date:	11/30/95				
Personnel on site:	S.Kelley, Dr. Lutenegger, Dr. DeGroot, T. Mitchell, G. Costa R. Mikinis, R. Suchana, P.Reyes, B.Glass, Chris, B. Charkhow P. Tehrany, D. Ostendorf, E. Hinlein				
Drillers:	CTB - Steve and Johnny				
		Vent 2			
Boring Information:	Augered to 35' (with 6 1/4" augers) and sample continuous from 35' to 43.0'				
Rods used:	NWJ				
SPT Protocol:	Automatic 140 lb. hammer with a 30" height				
Location:	2.5'south of 12AA				
Core #	Depth (ft)	Blows/6"	N-value	Recovery	notes
1	35.0-36.5	2-5-5	10	16	
2	36.5-38.0	1-4-5	9	17	dark brown sand
3	38.0-39.5	3-3-4	7	18	water table at 39.5'
4	39.5-41.0	3-4-4	8	18	grey sand with odor
5	41.0-43.0	2-3-4-5	7	0	SCSS
6	41.0-43.0	OH-WOH-WOH-	2	24	2" split spoon



**3" Spoon Data**

Site Location:	Plattsburgh AFB				
Date:	12/1/95				
Personnel on site:	S.Kelley, Dr. Lutenegger, Dr. DeGroot, T. Mitchell, G. Costa R. Mikinis, R. Suchana, P.Reyes, B.Glass, Chris, B. Charkhow P. Tehrany, D. Ostendorf, E. Hinlein				
Drillers:	CTB - Steve and Johnny				
			<b>Sparge 1</b>		
Boring Information:	Augered to 35' (with 6 1/4" augers) and sample continuous from 35' to 49.5'				
Rods used:	NWJ				
SPT Protocol:	Automatic 140 lb. hammer with a 30" height				
Location:	2.5' west of 12AA				
<b>Core #</b>	<b>Depth (ft)</b>	<b>Blows/6"</b>	<b>N-value</b>	<b>Recovery</b>	<b>notes</b>
1	35.0-36.5	7-8-7	15	18	
2	36.5-38.0	5-5-6	11	18	
3	38.0-39.5	4-5-5	10	18	water table at 39.5'
4	39.5-41.0	4-4-4	8	18	
5	41.0-42.5	2-2-4	6	16	
6	42.5-44	8-6-8	14	11	
7	44.0-45.5	4-4-7	11	9.5	
8	45.5-47.0	5-8-9	17	10.5	
9	47.0-49.5	11-16-13-13	29	8/24	2" split spoon

## **APPENDIX II TUBING CLUSTER DETAILS**

# Construction Details For Borehole/Soil Gas Cluster

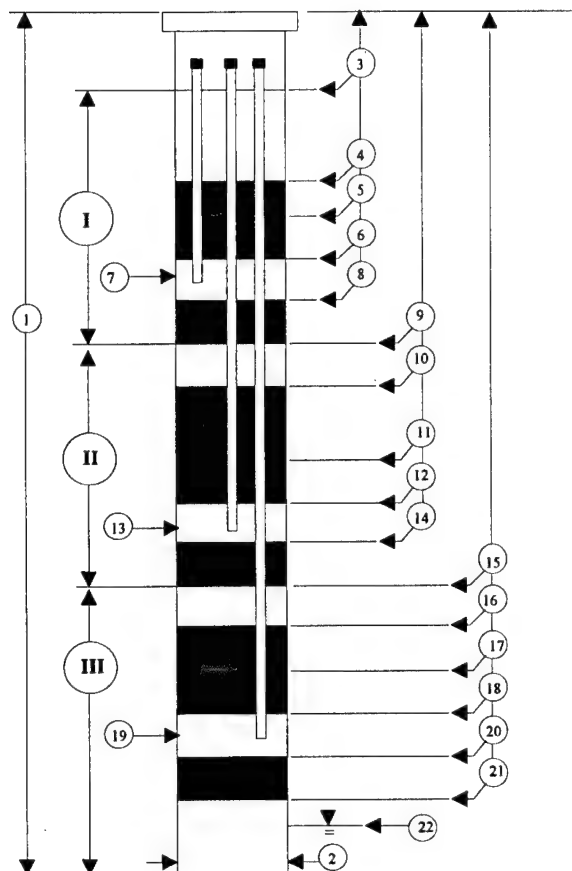
12AA

Data Entered by: ESH

Date Installed: 10/9/95

Date Entered: 2/18/97

Manhole Elevation: 256.26'




1.	Depth of Borehole	51.5
2.	Borehole Diameter (in)	6.75
3.	Depth to Top of Fill I	0.4
4.	Depth to Top of Slurry I	15.0
5.	Depth to Top of Upper Seal I	22.5
6.	Depth to Top of Sand I	23.5
7.	Depth of Cluster Point I	24.0
	Depth (ft MSL)	232.26'
8.	Depth to Top of Lower Seal I	27.0
9.	Depth to Top of Fill II	N/A
10.	Depth to Top of Slurry II	27.5
11.	Depth to Top of Upper Seal II	37.5
12.	Depth to Top of Sand II	38.5
13.	Depth of Cluster Point II	39.0
	Depth (ft MSL)	217.26'
14.	Depth to Top of Lower Seal II	N/A
15.	Depth to Top of Fill III	N/A
16.	Depth to Top of Slurry III	N/A
17.	Depth to Top of Upper Seal III	39.5
18.	Depth to Top of Sand III	44
19.	Depth of Cluster Point III	45
	Depth (ft MSL)	211.26'
20.	Depth to Top of Lower Seal III	N/A
	NOTE: CAVED IN FROM 29.0' TO 31.0'	
21.	Depth to Top Remaining Fill	47.5
22.	Depth to Water Table	40.0

All Dimensions in feet unless otherwise noted

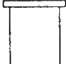
## Materials Legend

-  — Fill: Clean Native Fill
-  — Seal: Bentonite Pellets
-  — Sand: Pool sand
-  — Slurry: Bentonite Slurry

## Permanent Soil Gas Monitoring Point

-  - 1/4" Swagelok fitting @ top
- Riser, 1/4" SS tubing.
- Sintered SS intake filter @ bottom

## Manhole Specifications

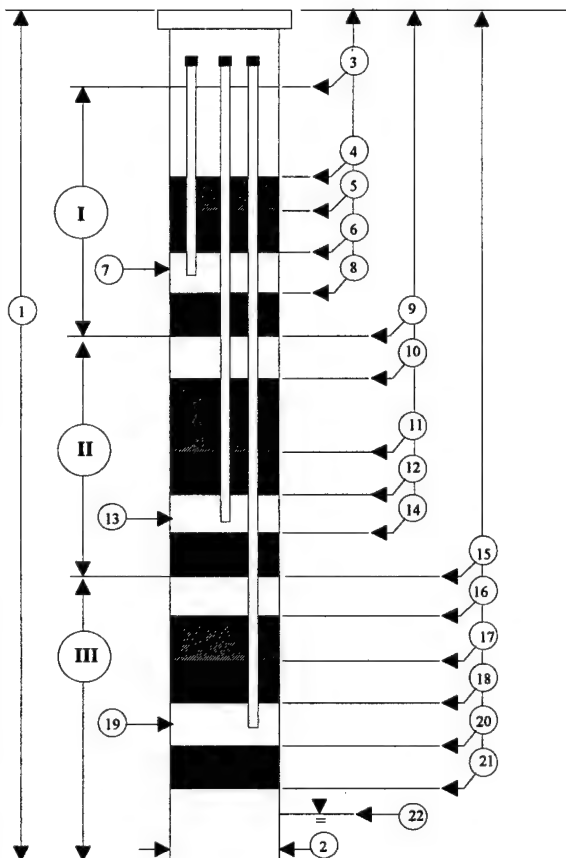
-  8" Cast iron manhole w/ galvanized steel, 8" diameter, 18" deep collar

# Construction Details For Borehole/Soil Gas Cluster

12AB

Data Entered by: ESH  
Date Entered: 2/18/97

Date Installed: 10/10/95  
Manhole Elevation: 256.33'



1.	Depth of Borehole	51.5
2.	Borehole Diameter (in)	6.75
3.	Depth to Top of Fill I	1.0
4.	Depth to Top of Slurry I	N/A
5.	Depth to Top of Upper Seal I	2.0
6.	Depth to Top of Sand I	3.0
7.	Depth of Cluster Point I Depth (ft MSL)	241.33'
8.	Depth to Top of Lower Seal I	4.0
9.	Depth to Top of Fill II	6.0
10.	Depth to Top of Slurry II	8.6
11.	Depth to Top of Upper Seal II	14.4
12.	Depth to Top of Sand II	15.4
13.	Depth of Cluster Point II Depth (ft MSL)	253.33'
14.	Depth to Top of Lower Seal II	16.4
15.	Depth to Top of Fill III	N/A
16.	Depth to Top of Slurry III	N/A
17.	Depth to Top of Upper Seal III	N/A
18.	Depth to Top of Sand III	N/A
19.	Depth of Cluster Point III Depth (ft MSL)	N/A
20.	Depth to Top of Lower Seal III	N/A
21.	Depth to Top Remaining Fill	18.6
22.	Depth to Water Table	40.0

All Dimensions in feet unless otherwise noted

## Materials Legend

- Fill: Clean Native Fill
- Seal: Bentonite Pellets
- Sand: Pool sand
- Slurry: Bentonite Slurry

## Permanent Soil Gas Monitoring Point.



- 1/4" Swagelok fitting @ top
- Riser, 1/4" SS tubing.
- Sintered SS intake filter @ bottom

## Manhole Specifications



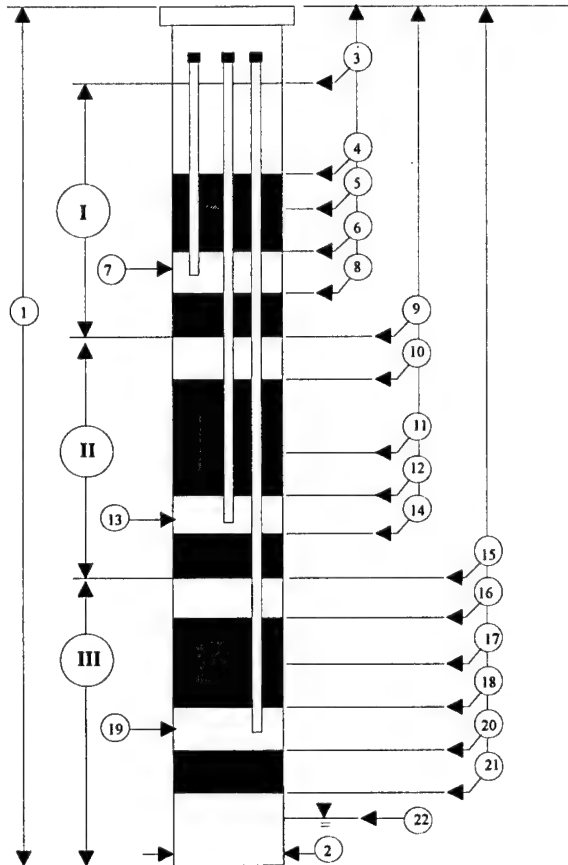
- 8" Cast iron manhole w/ galvanized steel, 8" diameter, 18" deep collar

# Construction Details For Borehole/Soil Gas Cluster

12AC

Data Entered by: ESH  
Date Entered: 2/18/97

Date Installed: 10/10/95  
Manhole Elevation: 256.50'



1.	Depth of Borehole	19.5
2.	Borehole Diameter (in)	6.75
3.	Depth to Top of Fill I	0.4
4.	Depth to Top of Slurry I	4.0
5.	Depth to Top of Upper Seal I	5.0
6.	Depth to Top of Sand I	6.0
7.	Depth of Cluster Point I	6.4
	Depth (ft MSL)	238.50'
8.	Depth to Top of Lower Seal I	7.2
9.	Depth to Top of Fill II	N/A
10.	Depth to Top of Slurry II	9.2
11.	Depth to Top of Upper Seal II	17.1
12.	Depth to Top of Sand II	18.2
13.	Depth of Cluster Point II	18.6
	Depth (ft MSL)	250.50'
14.	Depth to Top of Lower Seal II	19.2
15.	Depth to Top of Fill III	N/A
16.	Depth to Top of Slurry III	N/A
17.	Depth to Top of Upper Seal III	N/A
18.	Depth to Top of Sand III	N/A
19.	Depth of Cluster Point III	N/A
	Depth (ft MSL)	N/A
20.	Depth to Top of Lower Seal III	N/A
21.	Depth to Top Remaining Fill	N/A
22.	Depth to Water Table	N/A

All Dimensions in feet unless otherwise noted

## Materials Legend

- Fill: Clean Native Fill
- Seal: Bentonite Pellets
- Sand: Pool sand
- Slurry: Bentonite Slurry

## Permanent Soil Gas Monitoring Point.

- 1/4" Swagelok fitting @ top
- Riser, 1/4" SS tubing.
- Sintered SS intake filter @ bottom

## Manhole Specifications

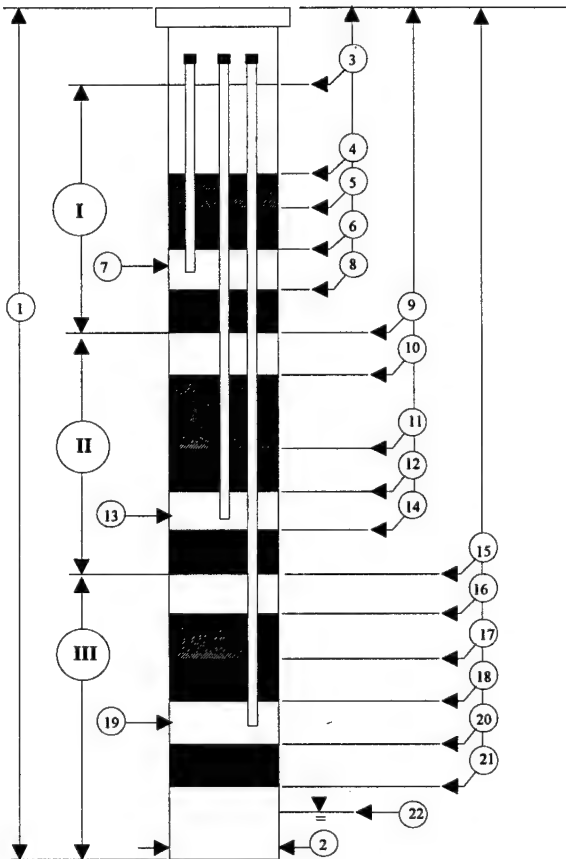
- 8" Cast iron manhole w/ galvanized steel, 8" diameter, 18" deep collar

# Construction Details For Borehole/Soil Gas Cluster

12AD

Data Entered by: ESH  
Date Entered: 2/18/97

Date Installed: 10/10/95  
Manhole Elevation: 256.34'



1.	Depth of Borehole	48.0
2.	Borehole Diameter (in)	6.75
3.	Depth to Top of Fill I	0.4
4.	Depth to Top of Slurry I	10.0
5.	Depth to Top of Upper Seal I	11.1
6.	Depth to Top of Sand I	12.0
7.	Depth of Cluster Point I Depth (ft MSL) 232.34'	12.5
8.	Depth to Top of Lower Seal I	12.8
9.	Depth to Top of Fill II	15.0
10.	Depth to Top of Slurry II	18.6
11.	Depth to Top of Upper Seal II	23.0
12.	Depth to Top of Sand II	24.0
13.	Depth of Cluster Point II Depth (ft MSL) 244.34'	24.4
14.	Depth to Top of Lower Seal II	24.8
15.	Depth to Top of Fill III	N/A
16.	Depth to Top of Slurry III	N/A
17.	Depth to Top of Upper Seal III	N/A
18.	Depth to Top of Sand III	N/A
19.	Depth of Cluster Point III Depth (ft MSL) N/A	N/A
20.	Depth to Top of Lower Seal III	N/A
21.	Depth to Top Remaining Fill	27.0
22.	Depth to Water Table	40.0

All Dimensions in feet unless otherwise noted

## Materials Legend

- Fill: Clean Native Fill
- Seal: Bentonite Pellets
- Sand: Pool sand
- Slurry: Bentonite Slurry

## Permanent Soil Gas Monitoring Point.

- 1/4" Swagelok fitting @ top
- Riser, 1/4" SS tubing.
- Sintered SS intake filter @ bottom

## Manhole Specifications

- 8" Cast iron manhole w/ galvanized steel, 8" diameter, 18" deep collar

# Construction Details For Borehole/Soil Gas Cluster

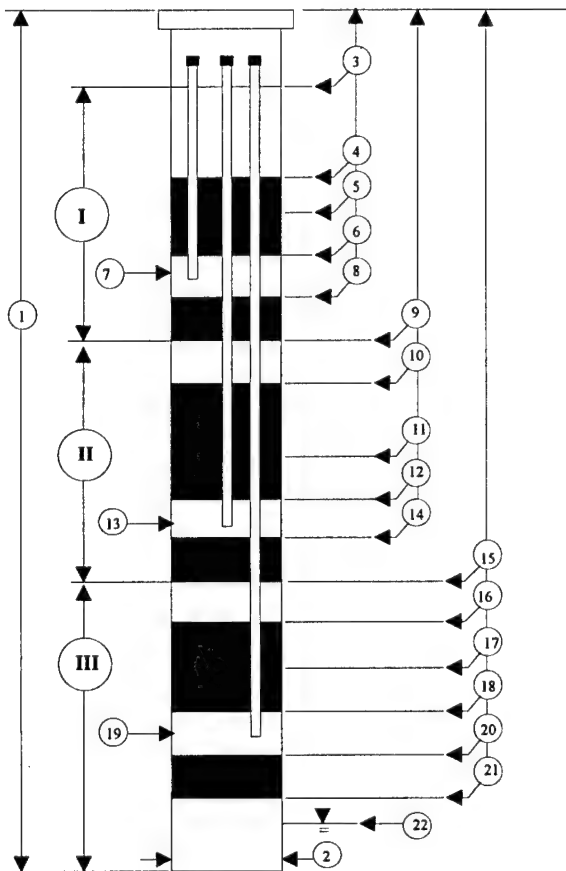
12AE

Data Entered by: ESH

Date Installed: 10/10/95

Date Entered: 2/18/97

Manhole Elevation: 256.70'



1.	Depth of Borehole	19.0
2.	Borehole Diameter (in)	6.75
3.	Depth to Top of Fill I	0.4
4.	Depth to Top of Slurry I	3.2
5.	Depth to Top of Upper Seal I	5.2
6.	Depth to Top of Sand I	6.4
7.	Depth of Cluster Point I	7.0
	Depth (ft MSL)	239.20'
8.	Depth to Top of Lower Seal I	7.4
9.	Depth to Top of Fill II	9.5
10.	Depth to Top of Slurry II	11.2
11.	Depth to Top of Upper Seal II	17.0
12.	Depth to Top of Sand II	18.6
13.	Depth of Cluster Point II	19.2
	Depth (ft MSL)	250.70'
14.	Depth to Top of Lower Seal II	19.8
15.	Depth to Top of Fill III	N/A
16.	Depth to Top of Slurry III	N/A
17.	Depth to Top of Upper Seal III	N/A
18.	Depth to Top of Sand III	N/A
19.	Depth of Cluster Point III	N/A
	Depth (ft MSL)	N/A
20.	Depth to Top of Lower Seal III	N/A
21.	Depth to Top Remaining Fill	N/A
22.	Depth to Water Table	N/A

All Dimensions in feet unless otherwise noted

## Materials Legend

- Fill: Clean Native Fill
- Seal: Bentonite Pellets
- Sand: Pool sand
- Slurry: Bentonite Slurry

## Permanent Soil Gas Monitoring Point.

- 1/4" Swagelok fitting @ top
- Riser, 1/4" SS tubing.
- Sintered SS intake filter @ bottom

## Manhole Specifications

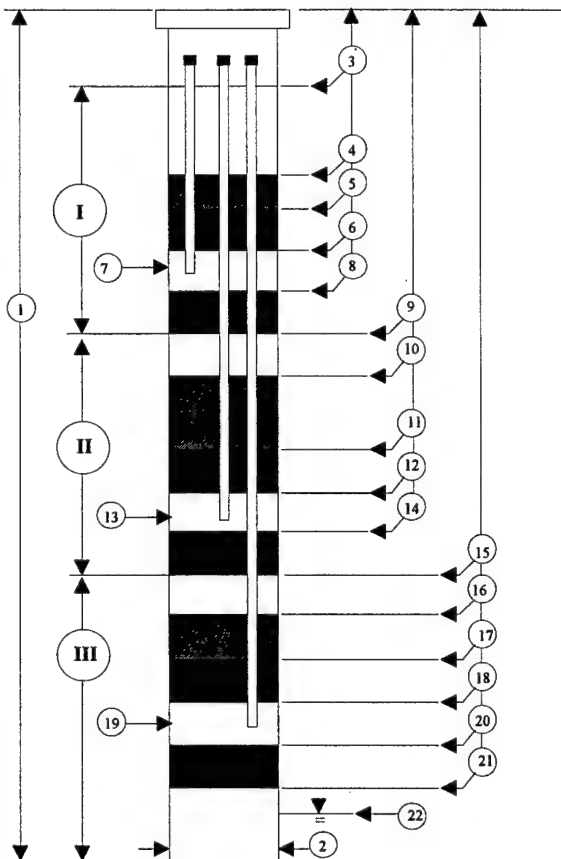
- 8" Cast iron manhole w/ galvanized steel, 8" diameter, 18" deep collar

# Construction Details For Borehole/Soil Gas Cluster

12AF

Data Entered by: ESH  
Date Entered: 2/18/97

Date Installed: 10/10/95  
Manhole Elevation: 257.28'



1.	Depth of Borehole	19.0
2.	Borehole Diameter (in)	6.75
3.	Depth to Top of Fill I	0.4
4.	Depth to Top of Slurry I	3.2
5.	Depth to Top of Upper Seal I	5.2
6.	Depth to Top of Sand I	6.2
7.	Depth of Cluster Point I	7.0
	Depth (ft MSL)	240.78'
8.	Depth to Top of Lower Seal I	7.4
9.	Depth to Top of Fill II	9.6
10.	Depth to Top of Slurry II	10.6
11.	Depth to Top of Upper Seal II	16.5
12.	Depth to Top of Sand II	17.6
13.	Depth of Cluster Point II	18.0
	Depth (ft MSL)	251.28'
14.	Depth to Top of Lower Seal II	18.6
15.	Depth to Top of Fill III	N/A
16.	Depth to Top of Slurry III	N/A
17.	Depth to Top of Upper Seal III	N/A
18.	Depth to Top of Sand III	N/A
19.	Depth of Cluster Point III	N/A
	Depth (ft MSL)	N/A
20.	Depth to Top of Lower Seal III	N/A
21.	Depth to Top Remaining Fill	N/A
22.	Depth to Water Table	N/A

All Dimensions in feet unless otherwise noted

## Materials Legend

- Fill: Clean Native Fill
- Seal: Bentonite Pellets
- Sand: Pool sand
- Slurry: Bentonite Slurry

## Permanent Soil Gas Monitoring Point.

- 1/4" Swagelok fitting @ top
- Riser, 1/4" SS tubing.
- Sintered SS intake filter @ bottom

## Manhole Specifications

- 8" Cast iron manhole w/ galvanized steel, 8" diameter, 18" deep collar



# Construction Details For Borehole/Soil Gas Cluster

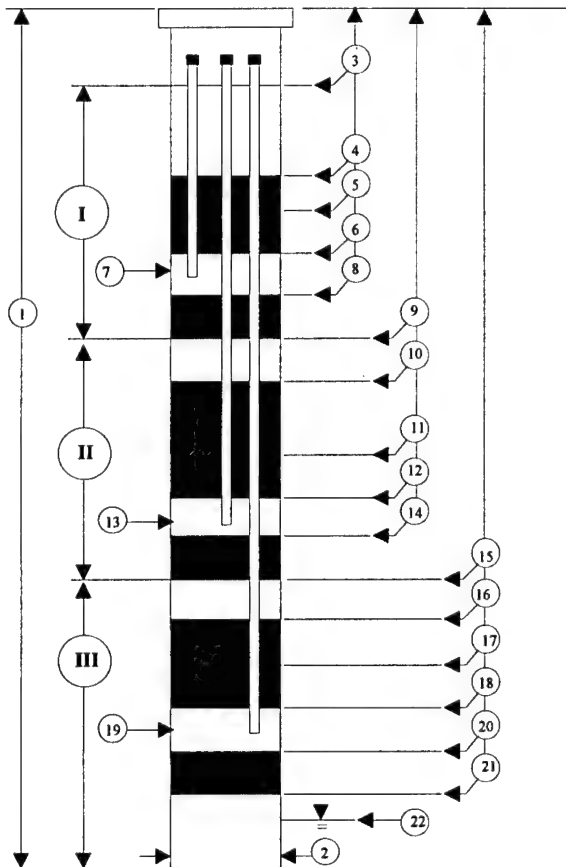
12AG

Data Entered by: ESH

Date Installed: 10/10/95

Date Entered: 2/18/97

Manhole Elevation: 256.42'



1.	Depth of Borehole	48.0
2.	Borehole Diameter (in)	6.75
3.	Depth to Top of Fill I	0.4
4.	Depth to Top of Slurry I	N/A
5.	Depth to Top of Upper Seal I	1.8
6.	Depth to Top of Sand I	3.0
7.	Depth of Cluster Point I	3.4
	Depth (ft MSL)	241.42'
8.	Depth to Top of Lower Seal I	4.0
9.	Depth to Top of Fill II	N/A
10.	Depth to Top of Slurry II	6.0
11.	Depth to Top of Upper Seal II	13.8
12.	Depth to Top of Sand II	14.9
13.	Depth of Cluster Point II	15.2
	Depth (ft MSL)	253.42'
14.	Depth to Top of Lower Seal II	15.8
15.	Depth to Top of Fill III	N/A
16.	Depth to Top of Slurry III	N/A
17.	Depth to Top of Upper Seal III	N/A
18.	Depth to Top of Sand III	N/A
19.	Depth of Cluster Point III	N/A
	Depth (ft MSL)	N/A
20.	Depth to Top of Lower Seal III	N/A
21.	Depth to Top Remaining Fill	16.8
22.	Depth to Water Table	40.0

All Dimensions in feet unless otherwise noted

## Materials Legend

- Fill: Clean Native Fill
- Seal: Bentonite Pellets
- Sand: Pool sand
- Slurry: Bentonite Slurry

## Permanent Soil Gas Monitoring Point.



- 1/4" Swagelok fitting @ top
- Riser, 1/4" SS tubing.
- Sintered SS intake filter @ bottom

## Manhole Specifications



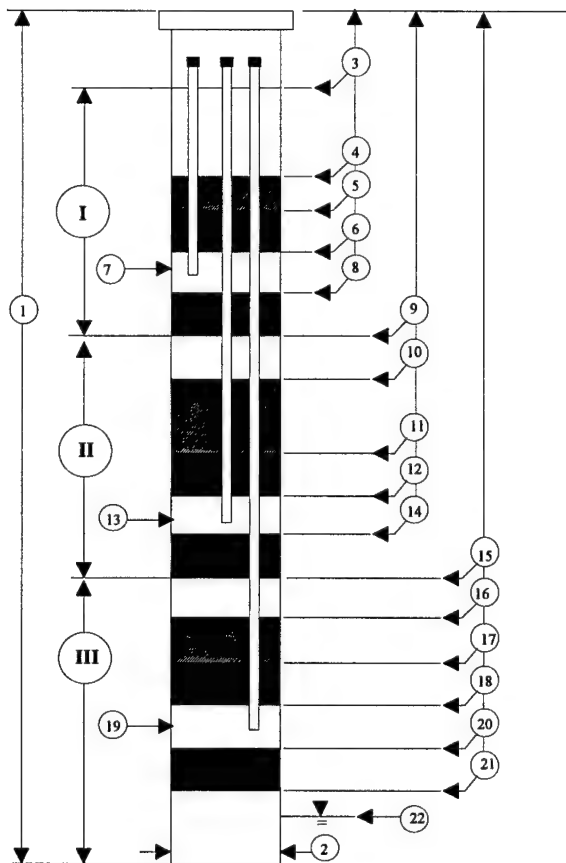
8" Cast iron manhole  
w/ galvanized steel, 8"  
diameter, 18" deep collar

# Construction Details For Borehole/Soil Gas Cluster

12AH

Data Entered by: ESH  
Date Entered: 2/18/97

Date Installed: 10/11/95  
Manhole Elevation: 256.28'



1.	Depth of Borehole	31.8
2.	Borehole Diameter (in)	6.75
3.	Depth to Top of Fill I	0.4
4.	Depth to Top of Slurry I	10.0
5.	Depth to Top of Upper Seal I	11.0
6.	Depth to Top of Sand I	3.0
7.	Depth of Cluster Point I	12.4
	Depth (ft MSL)	226.28'
8.	Depth to Top of Lower Seal I	13.0
9.	Depth to Top of Fill II	15.0
10.	Depth to Top of Slurry II	21.6
11.	Depth to Top of Upper Seal II	29.0
12.	Depth to Top of Sand II	30.2
13.	Depth of Cluster Point II	30.5
	Depth (ft MSL)	244.28'
14.	Depth to Top of Lower Seal II	31.0
15.	Depth to Top of Fill III	N/A
16.	Depth to Top of Slurry III	N/A
17.	Depth to Top of Upper Seal III	N/A
18.	Depth to Top of Sand III	N/A
19.	Depth of Cluster Point III	N/A
	Depth (ft MSL)	N/A
20.	Depth to Top of Lower Seal III	N/A
21.	Depth to Top Remaining Fill	N/A
22.	Depth to Water Table	N/A

All Dimensions in feet unless otherwise noted

## Materials Legend

- Fill: Clean Native Fill
- Seal: Bentonite Pellets
- Sand: Pool sand
- Slurry: Bentonite Slurry

## Permanent Soil Gas Monitoring Point.

- 1/4" Swagelok fitting @ top
- Riser, 1/4" SS tubing.
- Sintered SS intake filter @ bottom

## Manhole Specifications

- 8" Cast iron manhole w/ galvanized steel, 8" diameter, 18" deep collar

# Construction Details For Borehole/Soil Gas Cluster

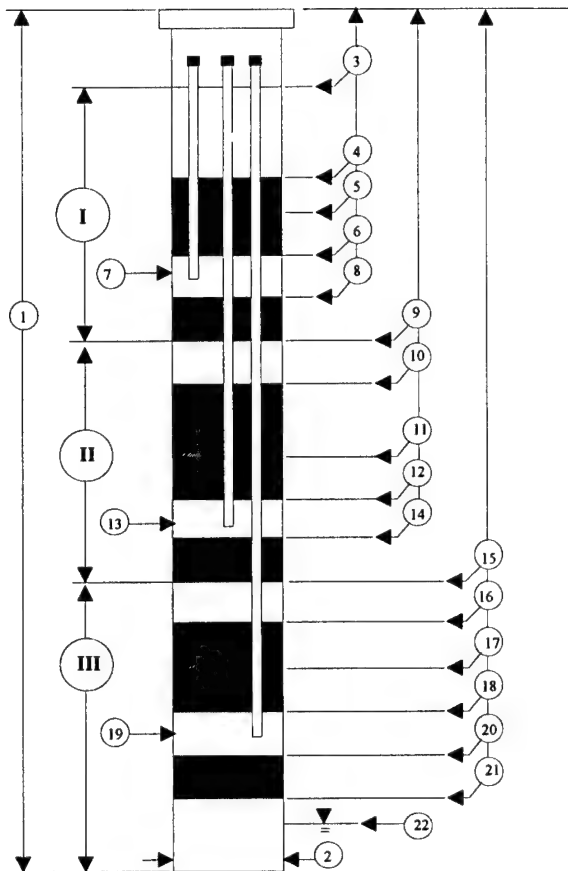
12AI

Data Entered by: ESH

Date Installed: 10/11/95

Date Entered: 2/18/97

Manhole Elevation: 256.20'



1.	Depth of Borehole	31.0
2.	Borehole Diameter (in)	6.75
3.	Depth to Top of Fill I	0.4
4.	Depth to Top of Slurry I	7.4
5.	Depth to Top of Upper Seal I	8.6
6.	Depth to Top of Sand I	9.6
7.	Depth of Cluster Point I	10.0
8.	Depth to Top of Lower Seal I	10.6
9.	Depth to Top of Fill II	12.6
10.	Depth to Top of Slurry II	20.8
11.	Depth to Top of Upper Seal II	29.2
12.	Depth to Top of Sand II	30.4
13.	Depth of Cluster Point II	31.0
14.	Depth to Top of Lower Seal II	31.6
15.	Depth to Top of Fill III	N/A
16.	Depth to Top of Slurry III	N/A
17.	Depth to Top of Upper Seal III	N/A
18.	Depth to Top of Sand III	N/A
19.	Depth of Cluster Point III	N/A
20.	Depth to Top of Lower Seal III	N/A
21.	Depth to Top Remaining Fill	N/A
22.	Depth to Water Table	N/A

All Dimensions in feet unless otherwise noted

## Materials Legend

- Fill: Clean Native Fill
- Seal: Bentonite Pellets
- Sand: Pool sand
- Slurry: Bentonite Slurry

## Permanent Soil Gas Monitoring Point.

- 1/4" Swagelok fitting @ top
- Riser, 1/4" SS tubing.
- Sintered SS intake filter @ bottom

## Manhole Specifications

- 8" Cast iron manhole w/ galvanized steel, 8" diameter, 18" deep collar

# Construction Details For Borehole/Soil Gas Cluster

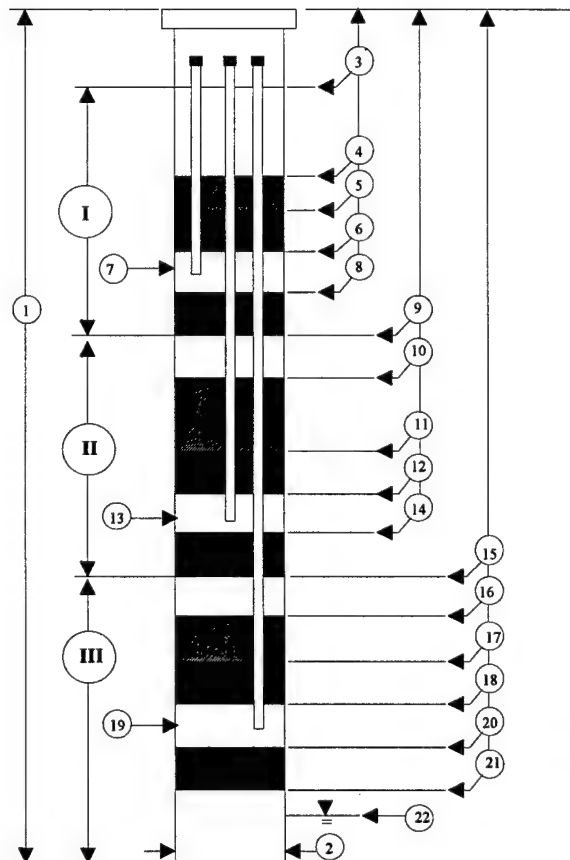
12AJ

Data Entered by: ESH

Date Installed: 10/11/95

Date Entered: 2/18/97

Manhole Elevation: 255.85'



1.	Depth of Borehole	20.5
2.	Borehole Diameter (in)	6.75
3.	Depth to Top of Fill I	0.4
4.	Depth to Top of Slurry I	3.6
5.	Depth to Top of Upper Seal I	5.0
6.	Depth to Top of Sand I	6.2
7.	Depth of Cluster Point I	6.7
	Depth (ft MSL)	237.85'
8.	Depth to Top of Lower Seal I	7.4
9.	Depth to Top of Fill II	9.4
10.	Depth to Top of Slurry II	10.0
11.	Depth to Top of Upper Seal II	17.8
12.	Depth to Top of Sand II	18.6
13.	Depth of Cluster Point II	19.2
	Depth (ft MSL)	249.85'
14.	Depth to Top of Lower Seal II	19.8
15.	Depth to Top of Fill III	N/A
16.	Depth to Top of Slurry III	N/A
17.	Depth to Top of Upper Seal III	N/A
18.	Depth to Top of Sand III	N/A
19.	Depth of Cluster Point III	N/A
	Depth (ft MSL)	N/A
20.	Depth to Top of Lower Seal III	N/A
21.	Depth to Top Remaining Fill	N/A
22.	Depth to Water Table	N/A

All Dimensions in feet unless otherwise noted

## Materials Legend

- Fill: Clean Native Fill
- Seal: Bentonite Pellets
- Sand: Pool sand
- Slurry: Bentonite Slurry

## Permanent Soil Gas Monitoring Point.

- 1/4" Swagelok fitting @ top
- Riser, 1/4" SS tubing.
- Sintered SS intake filter @ bottom

## Manhole Specifications

- 8" Cast iron manhole w/ galvanized steel, 8" diameter, 18" deep collar

# Construction Details For Borehole/Soil Gas Cluster

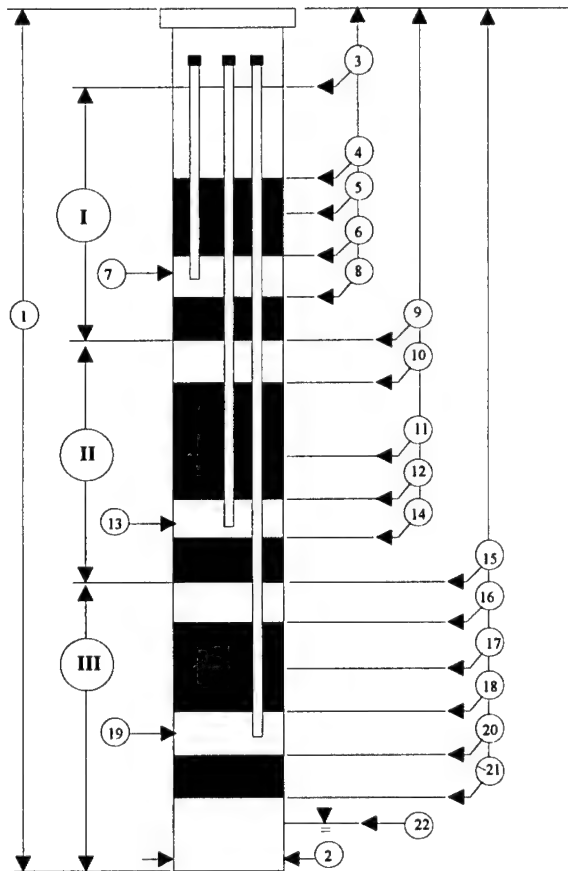
12AK

Data Entered by: ESH

Date Installed: 10/11/95

Date Entered: 2/18/97




Manhole Elevation: 256.49'




1.	Depth of Borehole	47.0
2.	Borehole Diameter (in)	6.75
3.	Depth to Top of Fill I	0.4
4.	Depth to Top of Slurry I	9.8
5.	Depth to Top of Upper Seal I	10.9
6.	Depth to Top of Sand I	12.0
7.	Depth of Cluster Point I	12.4
	Depth (ft MSL)	226.49'
8.	Depth to Top of Lower Seal I	12.8
9.	Depth to Top of Fill II	15.0
10.	Depth to Top of Slurry II	20.6
11.	Depth to Top of Upper Seal II	28.8
12.	Depth to Top of Sand II	29.6
13.	Depth of Cluster Point II	30.2
	Depth (ft MSL)	244.49'
14.	Depth to Top of Lower Seal II	30.7
15.	Depth to Top of Fill III	N/A
16.	Depth to Top of Slurry III	N/A
17.	Depth to Top of Upper Seal III	N/A
18.	Depth to Top of Sand III	N/A
19.	Depth of Cluster Point III	N/A
	Depth (ft MSL)	N/A
20.	Depth to Top of Lower Seal III	N/A
21.	Depth to Top Remaining Fill	32.7
22.	Depth to Water Table	40.0

All Dimensions in feet unless otherwise noted

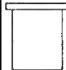
## Materials Legend

-  — Fill: Clean Native Fill
-  — Seal: Bentonite Pellets
-  — Sand: Pool sand
-  — Slurry: Bentonite Slurry

## Permanent Soil Gas Monitoring Point.

-  - 1/4" Swagelok fitting @ top
- Riser, 1/4" SS tubing.
- Sintered SS intake filter @ bottom

## Manhole Specifications

-  8" Cast iron manhole w/ galvanized steel, 8" diameter, 18" deep collar

# Construction Details For Borehole/Soil Gas Cluster

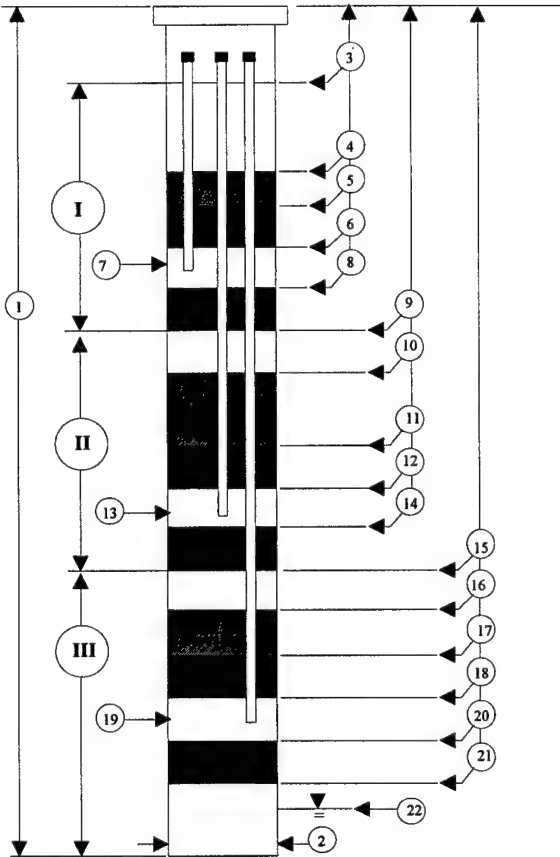
12AL

Data Entered by: ESH

Date Installed: 10/11/95

Date Entered: 2/18/97

Manhole Elevation: 257.55'



1.	Depth of Borehole	18.0
2.	Borehole Diameter (in)	6.75
3.	Depth to Top of Fill I	0.4
4.	Depth to Top of Slurry I	N/A
5.	Depth to Top of Upper Seal I	2.0
6.	Depth to Top of Sand I	2.9
7.	Depth of Cluster Point I	3.4
	Depth (ft MSL)	242.55'
8.	Depth to Top of Lower Seal I	4.0
9.	Depth to Top of Fill II	6.0
10.	Depth to Top of Slurry II	8.0
11.	Depth to Top of Upper Seal II	14.1
12.	Depth to Top of Sand II	15.2
13.	Depth of Cluster Point II	15.6
	Depth (ft MSL)	254.55'
14.	Depth to Top of Lower Seal II	16.2
15.	Depth to Top of Fill III	N/A
16.	Depth to Top of Slurry III	N/A
17.	Depth to Top of Upper Seal III	N/A
18.	Depth to Top of Sand III	N/A
19.	Depth of Cluster Point III	N/A
	Depth (ft MSL)	N/A
20.	Depth to Top of Lower Seal III	N/A
21.	Depth to Top Remaining Fill	18.2
22.	Depth to Water Table	N/A

All Dimensions in feet unless otherwise noted

## Materials Legend

- Fill: Clean Native Fill
- Seal: Bentonite Pellets
- Sand: Pool sand
- Slurry: Bentonite Slurry

## Permanent Soil Gas Monitoring Point.



- 1/4" Swagelok fitting @ top
- Riser, 1/4" SS tubing.
- Sintered SS intake filter @ bottom

## Manhole Specifications



- 8" Cast iron manhole w/ galvanized steel, 8" diameter, 18" deep collar

# Construction Details For Borehole/Soil Gas Cluster

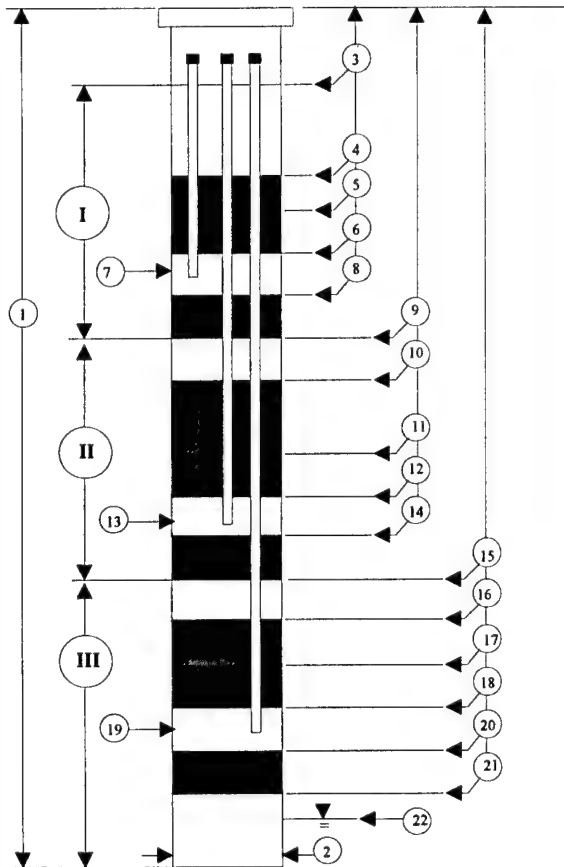
12AM

Data Entered by: ESH

Date Installed: 10/12/95

Date Entered: 2/18/97

Manhole Elevation: 256.49'



1.	Depth of Borehole	48.0
2.	Borehole Diameter (in)	6.75
3.	Depth to Top of Fill I	0.4
4.	Depth to Top of Slurry I	2.4
5.	Depth to Top of Upper Seal I	33.6
6.	Depth to Top of Sand I	34.6
7.	Depth of Cluster Point I	35.2
	Depth (ft MSL)	211.99'
8.	Depth to Top of Lower Seal I	36.2
9.	Depth to Top of Fill II	N/A
10.	Depth to Top of Slurry II	N/A
11.	Depth to Top of Upper Seal II	N/A
12.	Depth to Top of Sand II	42.4
13.	Depth of Cluster Point II	42.9
	Depth (ft MSL)	219.99'
14.	Depth to Top of Lower Seal II	43.6
15.	Depth to Top of Fill III	N/A
16.	Depth to Top of Slurry III	N/A
17.	Depth to Top of Upper Seal III	N/A
18.	Depth to Top of Sand III	N/A
19.	Depth of Cluster Point III	N/A
	Depth (ft MSL)	N/A
20.	Depth to Top of Lower Seal III	N/A
21.	Depth to Top Remaining Fill	N/A
22.	Depth to Water Table	40.0

All Dimensions in feet unless otherwise noted

## Materials Legend

- Fill: Clean Native Fill
- Seal: Bentonite Pellets
- Sand: Pool sand
- Slurry: Bentonite Slurry

## Permanent Soil Gas Monitoring Point.

- 1/4" Swagelok fitting @ top
- Riser, 1/4" SS tubing.
- Sintered SS intake filter @ bottom

## Manhole Specifications

- 8" Cast iron manhole w/ galvanized steel, 8" diameter, 18" deep collar

# Construction Details For Borehole/Soil Gas Cluster

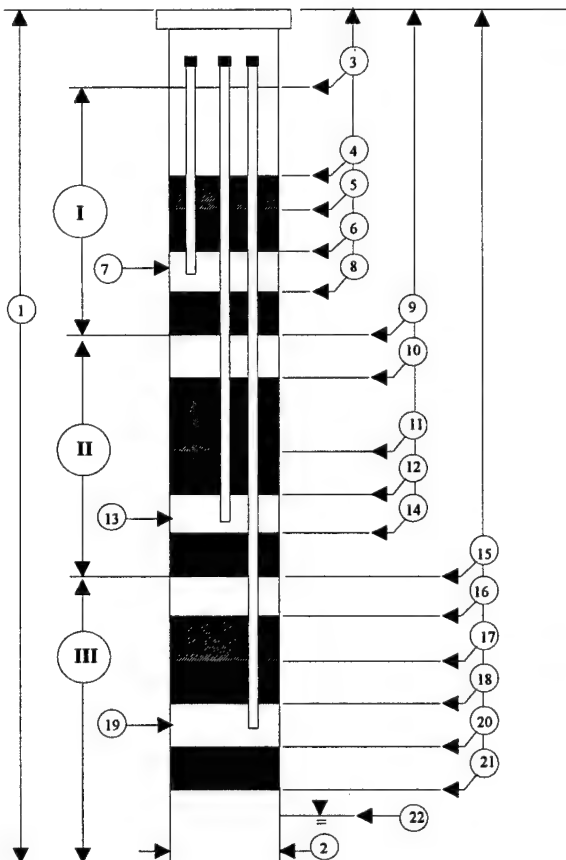
12AN

Data Entered by: ESH

Date Installed: 10/12/95

Date Entered: 2/18/97

Manhole Elevation: 251.29'



1.	Depth of Borehole	32.5
2.	Borehole Diameter (in)	6.75
3.	Depth to Top of Fill I	0.4
4.	Depth to Top of Slurry I	2.6
5.	Depth to Top of Upper Seal I	5.4
6.	Depth to Top of Sand I	6.2
7.	Depth of Cluster Point I Depth (ft MSL) 224.29'	6.7
8.	Depth to Top of Lower Seal I	7.4
9.	Depth to Top of Fill II	9.4
10.	Depth to Top of Slurry II	13.2
11.	Depth to Top of Upper Seal II	16.8
12.	Depth to Top of Sand II	17.7
13.	Depth of Cluster Point II Depth (ft MSL) 234.29'	18.4
14.	Depth to Top of Lower Seal II	19.6
15.	Depth to Top of Fill III	N/A
16.	Depth to Top of Slurry III	22.1
17.	Depth to Top of Upper Seal III	27.2
18.	Depth to Top of Sand III	28.4
19.	Depth of Cluster Point III Depth (ft MSL) 245.29'	29
20.	Depth to Top of Lower Seal III NOTE: CAVED IN FROM 29.0' TO 31.0'	29.6
21.	Depth to Top Remaining Fill	N/A
22.	Depth to Water Table	N/A

All Dimensions in feet unless otherwise noted

## Materials Legend

- Fill: Clean Native Fill
- Seal: Bentonite Pellets
- Sand: Pool sand
- Slurry: Bentonite Slurry

## Permanent Soil Gas Monitoring Point

- 1/4" Swagelok fitting @ top
- Riser, 1/4" SS tubing.
- Sintered SS intake filter @ bottom

## Manhole Specifications

- 8" Cast iron manhole w/ galvanized steel, 8" diameter, 18" deep collar



# Construction Details For Borehole/Soil Gas Cluster

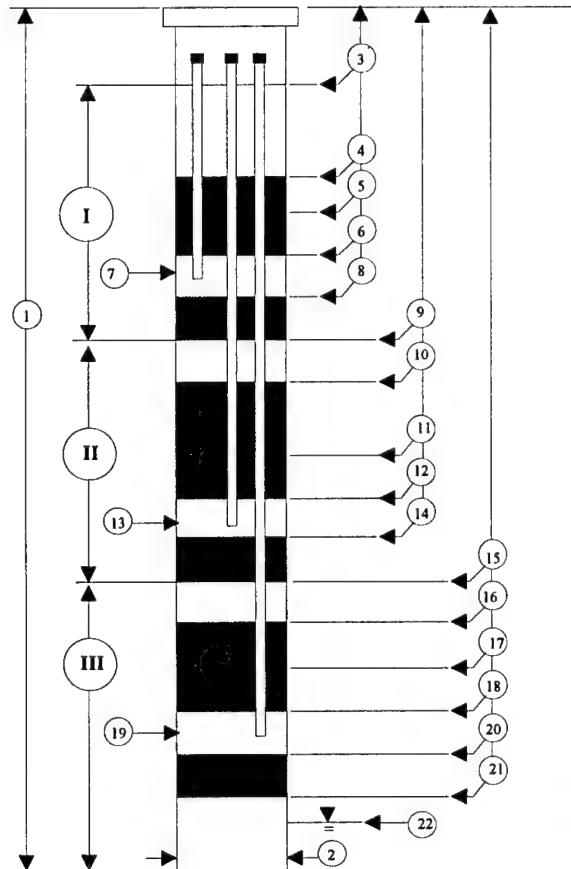
12AN

Data Entered by: ESH

Date Installed: 10/12/95

Date Entered: 2/18/97

Manhole Elevation: 251.29'




1.	Depth of Borehole	32.5
2.	Borehole Diameter (in)	6.75
3.	Depth to Top of Fill I	0.4
4.	Depth to Top of Slurry I	2.6
5.	Depth to Top of Upper Seal I	5.4
6.	Depth to Top of Sand I	6.2
7.	Depth of Cluster Point I	6.7
	Depth (ft MSL)	224.29'
8.	Depth to Top of Lower Seal I	7.4
9.	Depth to Top of Fill II	9.4
10.	Depth to Top of Slurry II	13.2
11.	Depth to Top of Upper Seal II	16.8
12.	Depth to Top of Sand II	17.7
13.	Depth of Cluster Point II	18.4
	Depth (ft MSL)	234.29'
14.	Depth to Top of Lower Seal II	19.6
15.	Depth to Top of Fill III	N/A
16.	Depth to Top of Slurry III	22.1
17.	Depth to Top of Upper Seal III	27.2
18.	Depth to Top of Sand III	28.4
19.	Depth of Cluster Point III	29
	Depth (ft MSL)	245.29'
20.	Depth to Top of Lower Seal III	29.6
	NOTE: CAVED IN FROM 29.0' TO 31.0'	
21.	Depth to Top Remaining Fill	N/A
22.	Depth to Water Table	N/A

All Dimensions in feet unless otherwise noted


## Materials Legend

-  — Fill: Clean Native Fill
-  — Seal: Bentonite Pellets
-  — Sand: Pool sand
-  — Slurry: Bentonite Slurry

## Permanent Soil Gas Monitoring Point

-  - 1/4" Swagelok fitting @ top
- Riser, 1/4" SS tubing.
- Sintered SS intake filter @ bottom

## Manhole Specifications

-  8" Cast iron manhole w/ galvanized steel, 8" diameter, 18" deep collar

# Construction Details For Borehole/Soil Gas Cluster

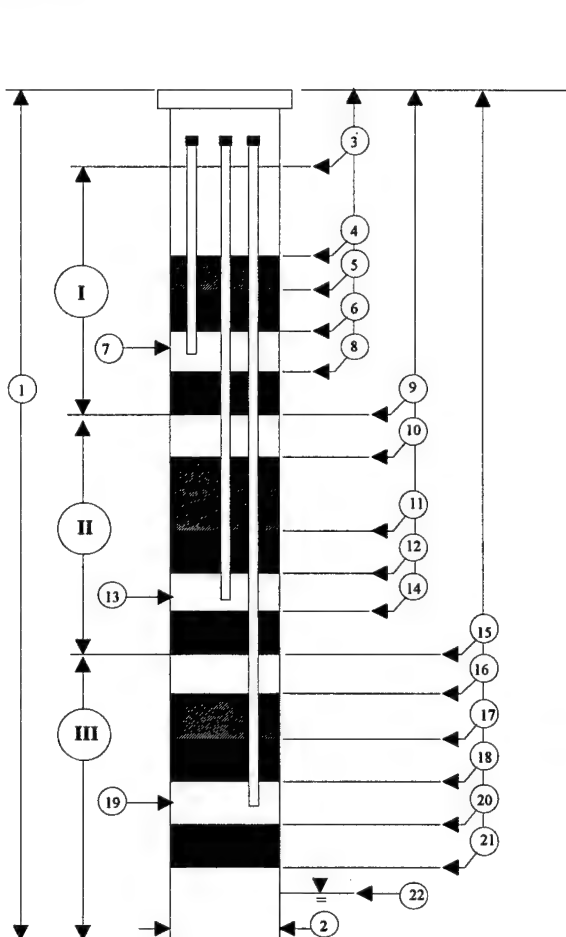
12AO

Data Entered by: ESH

Date Installed: 10/11/95

Date Entered: 2/18/97

Manhole Elevation: 255.58'



1.	Depth of Borehole	31.5
2.	Borehole Diameter (in)	6.75
3.	Depth to Top of Fill I	0.4
4.	Depth to Top of Slurry I	8.4
5.	Depth to Top of Upper Seal I	11.5
6.	Depth to Top of Sand I	12.8
7.	Depth of Cluster Point I	13.2
	Depth (ft MSL)	225.58'
8.	Depth to Top of Lower Seal I	13.6
9.	Depth to Top of Fill II	16.0
10.	Depth to Top of Slurry II	22.2
11.	Depth to Top of Upper Seal II	28.5
12.	Depth to Top of Sand II	29.5
13.	Depth of Cluster Point II	30.0
	Depth (ft MSL)	243.58'
14.	Depth to Top of Lower Seal II	30.4
15.	Depth to Top of Fill III	N/A
16.	Depth to Top of Slurry III	N/A
17.	Depth to Top of Upper Seal III	N/A
18.	Depth to Top of Sand III	N/A
19.	Depth of Cluster Point III	N/A
	Depth (ft MSL)	N/A
20.	Depth to Top of Lower Seal III	N/A
21.	Depth to Top Remaining Fill	18.2
22.	Depth to Water Table	N/A

All Dimensions in feet unless otherwise noted

## Materials Legend

- Fill: Clean Native Fill
- Seal: Bentonite Pellets
- Sand: Pool sand
- Slurry: Bentonite Slurry

## Permanent Soil Gas Monitoring Point.



- 1/4" Swagelok fitting @ top
- Riser, 1/4" SS tubing.
- Sintered SS intake filter @ bottom

## Manhole Specifications



- 8" Cast iron manhole w/ galvanized steel, 8" diameter, 18" deep collar

# Construction Details For Borehole/Soil Gas Cluster

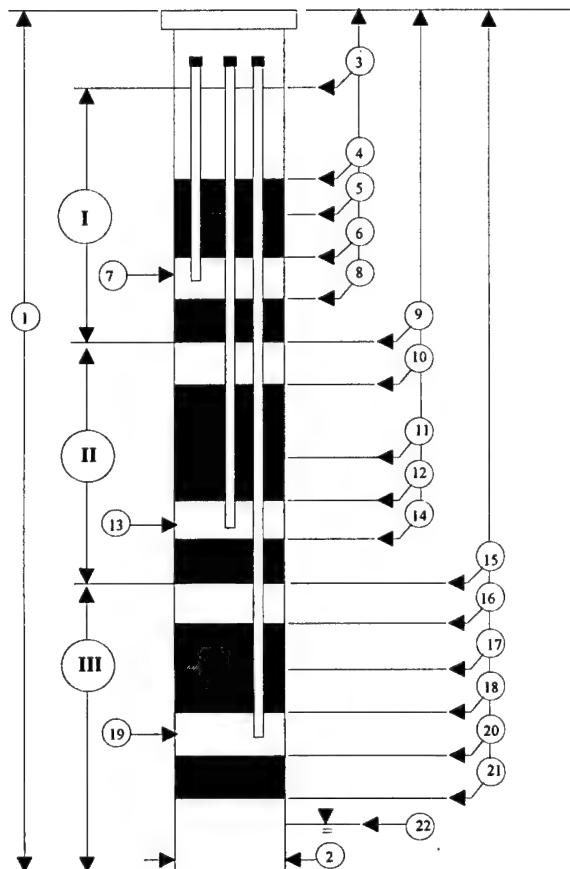
12AP

Data Entered by: ESH

Date Installed: 10/13/95

Date Entered: 2/18/97

Manhole Elevation: 255.98'



1.	Depth of Borehole	45.0
2.	Borehole Diameter (in)	6.75
3.	Depth to Top of Fill I	0.4
4.	Depth to Top of Slurry I	6.0
5.	Depth to Top of Upper Seal I	8.0
6.	Depth to Top of Sand I	9.0
7.	Depth of Cluster Point I	9.4
	Depth (ft MSL)	231.98'
8.	Depth to Top of Lower Seal I	10.0
9.	Depth to Top of Fill II	12.0
10.	Depth to Top of Slurry II	15.0
11.	Depth to Top of Upper Seal II	23.0
12.	Depth to Top of Sand II	24.0
13.	Depth of Cluster Point II	25.5
	Depth (ft MSL)	246.98'
14.	Depth to Top of Lower Seal II	24.8
15.	Depth to Top of Fill III	N/A
16.	Depth to Top of Slurry III	N/A
17.	Depth to Top of Upper Seal III	N/A
18.	Depth to Top of Sand III	N/A
19.	Depth of Cluster Point III	N/A
	Depth (ft MSL)	N/A
20.	Depth to Top of Lower Seal III	N/A
21.	Depth to Top Remaining Fill	27.0
22.	Depth to Water Table	40.0

All Dimensions in feet unless otherwise noted

## Materials Legend

- Fill: Clean Native Fill
- Seal: Bentonite Pellets
- Sand: Pool sand
- Slurry: Bentonite Slurry

## Permanent Soil Gas Monitoring Point.



- 1/4" Swagelok fitting @ top
- Riser, 1/4" SS tubing.
- Sintered SS intake filter @ bottom

## Manhole Specifications



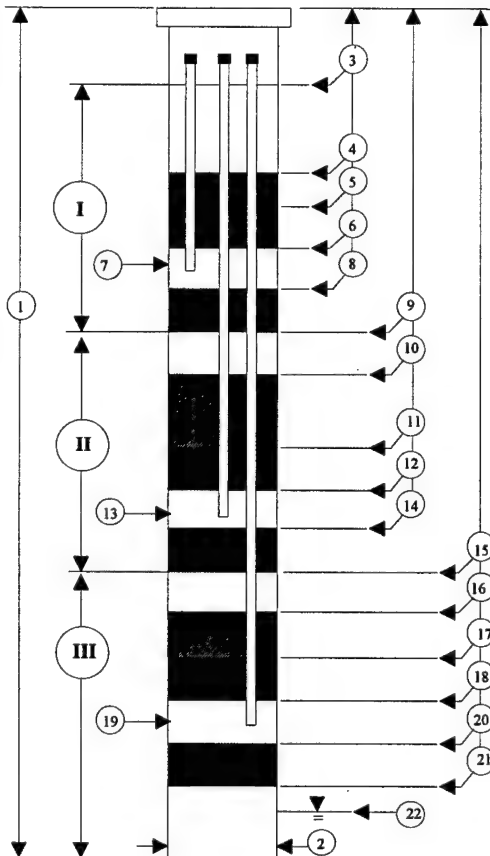
- 8" Cast iron manhole w/ galvanized steel, 8" diameter, 18" deep collar

# Construction Details For Borehole/Soil Gas Cluster

12AQ

Data Entered by: ESH  
Date Entered: 2/18/97

Date Installed: 10/13/95  
Manhole Elevation: 255.45'



1.	Depth of Borehole	28.0
2.	Borehole Diameter (in)	6.75
3.	Depth to Top of Fill I	0.4
4.	Depth to Top of Slurry I	N/A
5.	Depth to Top of Upper Seal I	7.7
6.	Depth to Top of Sand I	8.4
7.	Depth of Cluster Point I	9.0
	Depth (ft MSL)	231.45'
8.	Depth to Top of Lower Seal I	9.5
9.	Depth to Top of Fill II	11.4
10.	Depth to Top of Slurry II	14.3
11.	Depth to Top of Upper Seal II	22.0
12.	Depth to Top of Sand II	22.9
13.	Depth of Cluster Point II	23.2
	Depth (ft MSL)	246.45'
14.	Depth to Top of Lower Seal II	23.8
15.	Depth to Top of Fill III	N/A
16.	Depth to Top of Slurry III	N/A
17.	Depth to Top of Upper Seal III	N/A
18.	Depth to Top of Sand III	N/A
19.	Depth of Cluster Point III	N/A
	Depth (ft MSL)	N/A
20.	Depth to Top of Lower Seal III	N/A
21.	Depth to Top Remaining Fill	25.7
22.	Depth to Water Table	N/A

All Dimensions in feet unless otherwise noted

## Materials Legend

- Fill: Clean Native Fill
- Seal: Bentonite Pellets
- Sand: Pool sand
- Slurry: Bentonite Slurry

## Permanent Soil Gas Monitoring Point.



- 1/4" Swagelok fitting @ top
- Riser, 1/4" SS tubing.
- Sintered SS intake filter @ bottom

## Manhole Specifications



8" Cast iron manhole  
w/ galvanized steel, 8"  
diameter, 18" deep collar

# Construction Details For Borehole/Soil Gas Cluster

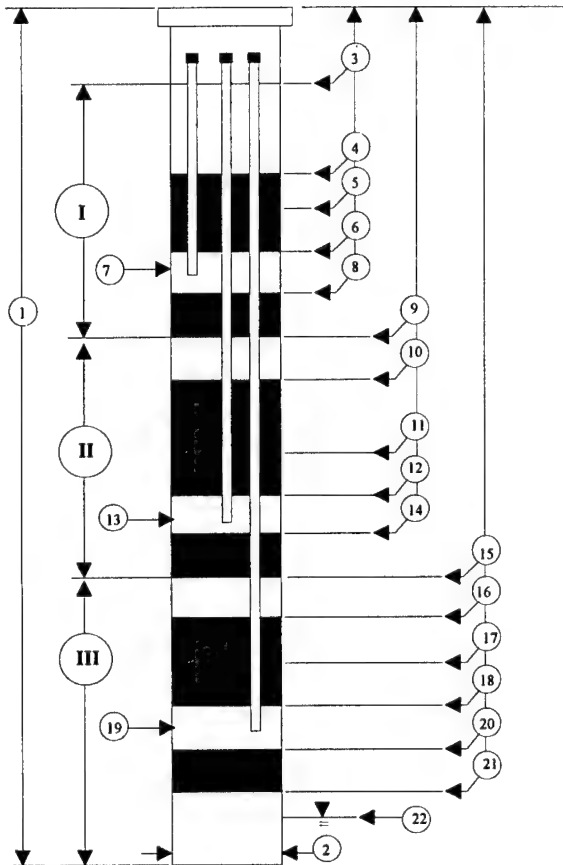
12AR

Data Entered by: ESH

Date Installed: 10/13/95

Date Entered: 2/18/97

Manhole Elevation: 255.58'



1.	Depth of Borehole	47.0
2.	Borehole Diameter (in)	6.75
3.	Depth to Top of Fill I	0.4
4.	Depth to Top of Slurry I	N/A
5.	Depth to Top of Upper Seal I	1.8
6.	Depth to Top of Sand I	3.0
7.	Depth of Cluster Point I	3.4
	Depth (ft MSL)	240.58'
8.	Depth to Top of Lower Seal I	4.0
9.	Depth to Top of Fill II	N/A
10.	Depth to Top of Slurry II	6.0
11.	Depth to Top of Upper Seal II	13.6
12.	Depth to Top of Sand II	14.6
13.	Depth of Cluster Point II	15.2
	Depth (ft MSL)	252.58'
14.	Depth to Top of Lower Seal II	15.6
15.	Depth to Top of Fill III	N/A
16.	Depth to Top of Slurry III	N/A
17.	Depth to Top of Upper Seal III	N/A
18.	Depth to Top of Sand III	N/A
19.	Depth of Cluster Point III	N/A
	Depth (ft MSL)	N/A
20.	Depth to Top of Lower Seal III	N/A
21.	Depth to Top Remaining Fill	17.6
22.	Depth to Water Table	40.0

All Dimensions in feet unless otherwise noted

## Materials Legend

- Fill: Clean Native Fill
- Seal: Bentonite Pellets
- Sand: Pool sand
- Slurry: Bentonite Slurry

## Permanent Soil Gas Monitoring Point.

- 1/4" Swagelok fitting @ top
- Riser, 1/4" SS tubing.
- Sintered SS intake filter @ bottom

## Manhole Specifications

- 8" Cast iron manhole w/ galvanized steel, 8" diameter, 18" deep collar

# Construction Details For Borehole/Soil Gas Cluster

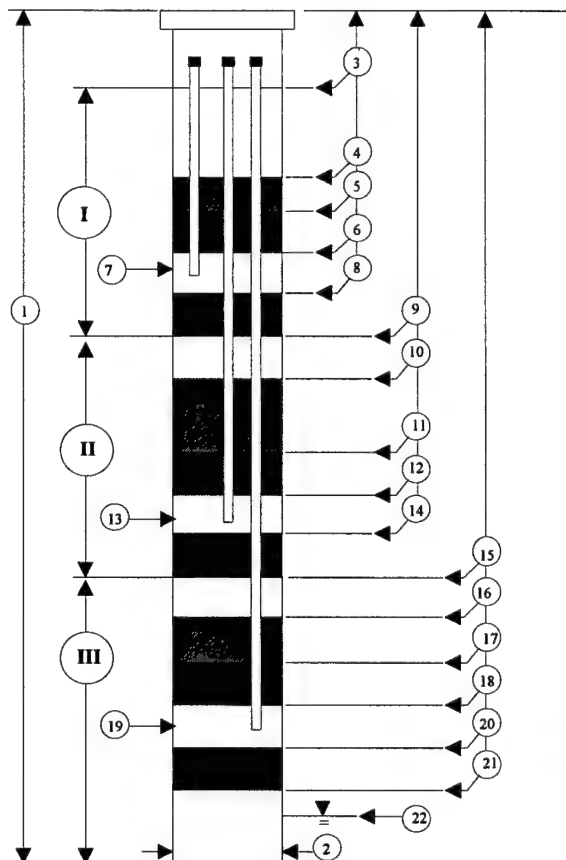
12AT

Data Entered by: ESH

Date Installed: 12/1/95

Date Entered: 2/18/97


Manhole Elevation: 250.18'






1.	Depth of Borehole	40.5
2.	Borehole Diameter (in)	6.75
3.	Depth to Top of Fill I	0.4
4.	Depth to Top of Slurry I	N/A
5.	Depth to Top of Upper Seal I	27.0
6.	Depth to Top of Sand I	30.5
7.	Depth of Cluster Point I	31.0
	Depth (ft MSL)	219.18'
8.	Depth to Top of Lower Seal I	N/A
9.	Depth to Top of Fill II	N/A
10.	Depth to Top of Slurry II	N/A
11.	Depth to Top of Upper Seal II	N/A
12.	Depth to Top of Sand II	N/A
13.	Depth of Cluster Point II	N/A
	Depth (ft MSL)	N/A
14.	Depth to Top of Lower Seal II	N/A
15.	Depth to Top of Fill III	N/A
16.	Depth to Top of Slurry III	N/A
17.	Depth to Top of Upper Seal III	N/A
18.	Depth to Top of Sand III	N/A
19.	Depth of Cluster Point III	N/A
	Depth (ft MSL)	N/A
20.	Depth to Top of Lower Seal III	N/A
21.	Depth to Top Remaining Fill	31.5
22.	Depth to Water Table	N/A

All Dimensions in feet unless otherwise noted

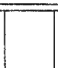
## Materials Legend

-  — Fill: Clean Native Fill
-  — Seal: Bentonite Pellets
-  — Sand: Pool sand
-  — Slurry: Bentonite Slurry

## Permanent Soil Gas Monitoring Point.

-  - 1/4" Swagelok fitting @ top
-  - Riser, 1/4" SS tubing.
-  - Sintered SS intake filter @ bottom

## Manhole Specifications

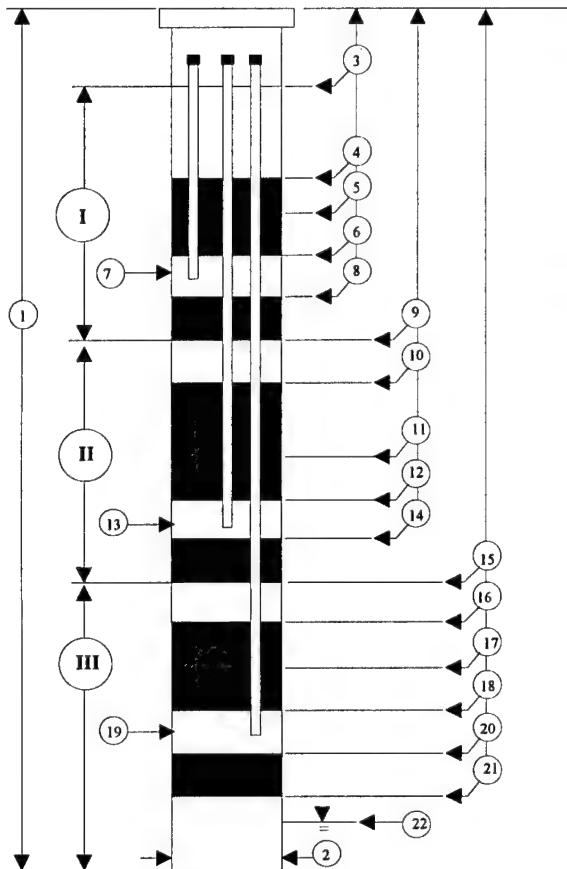
-  8" Cast iron manhole w/ galvanized steel, 8" diameter, 18" deep collar

# Construction Details For Borehole/Soil Gas Cluster

12AU

Data Entered by: ESH  
Date Entered: 2/18/97

Date Installed: 6/5/96  
Manhole Elevation: 256.53'



1.	Depth of Borehole	47.0
2.	Borehole Diameter (in)	6.75
3.	Depth to Top of Fill I	0.4
4.	Depth to Top of Slurry I	17.0
5.	Depth to Top of Upper Seal I	33.9
6.	Depth to Top of Sand I	33.5
7.	Depth of Cluster Point I	36.0
	Depth (ft MSL)	220.53'
8.	Depth to Top of Lower Seal I	36.3
9.	Depth to Top of Fill II	N/A
10.	Depth to Top of Slurry II	N/A
11.	Depth to Top of Upper Seal II	N/A
12.	Depth to Top of Sand II	N/A
13.	Depth of Cluster Point II	N/A
	Depth (ft MSL)	N/A
14.	Depth to Top of Lower Seal II	N/A
15.	Depth to Top of Fill III	N/A
16.	Depth to Top of Slurry III	N/A
17.	Depth to Top of Upper Seal III	N/A
18.	Depth to Top of Sand III	N/A
19.	Depth of Cluster Point III	N/A
	Depth (ft MSL)	N/A
20.	Depth to Top of Lower Seal III	N/A
21.	Depth to Top Remaining Fill	36.9
22.	Depth to Water Table	N/A

All Dimensions in feet unless otherwise noted

## Materials Legend

- Fill: Clean Native Fill
- Seal: Bentonite Pellets
- Sand: Pool sand
- Slurry: Bentonite Slurry

## Permanent Soil Gas Monitoring Point.



- 1/4" Swagelok fitting @ top
- Riser, 1/4" SS tubing.
- Sintered SS intake filter @ bottom

## Manhole Specifications



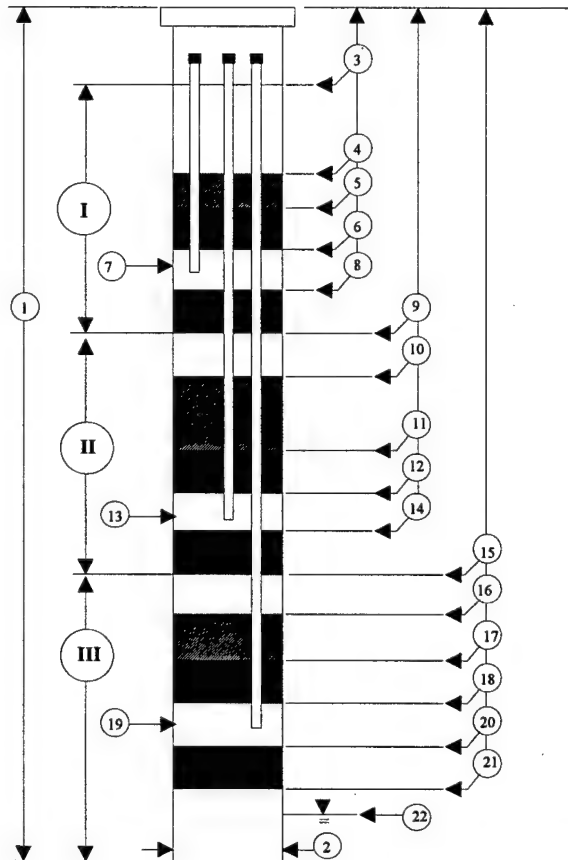
8" Cast iron manhole  
w/ galvanized steel, 8"  
diameter, 18" deep collar

# Construction Details For Borehole/Soil Gas Cluster

12AV

Data Entered by: ESH  
Date Entered: 2/18/97

Date Installed: 6/5/96  
Manhole Elevation: 256.36'



1.	Depth of Borehole	49.0
2.	Borehole Diameter (in)	6.75
3.	Depth to Top of Fill I	0.4
4.	Depth to Top of Slurry I	14.5
5.	Depth to Top of Upper Seal I	34.0
6.	Depth to Top of Sand I	35.0
7.	Depth of Cluster Point I	35.7
	Depth (ft MSL)	220.66'
8.	Depth to Top of Lower Seal I	N/A
9.	Depth to Top of Fill II	N/A
10.	Depth to Top of Slurry II	N/A
11.	Depth to Top of Upper Seal II	N/A
12.	Depth to Top of Sand II	N/A
13.	Depth of Cluster Point II	N/A
	Depth (ft MSL)	N/A
14.	Depth to Top of Lower Seal II	N/A
15.	Depth to Top of Fill III	N/A
16.	Depth to Top of Slurry III	N/A
17.	Depth to Top of Upper Seal III	N/A
18.	Depth to Top of Sand III	N/A
19.	Depth of Cluster Point III	N/A
	Depth (ft MSL)	N/A
20.	Depth to Top of Lower Seal III	N/A
21.	Depth to Top Remaining Fill	36.2
22.	Depth to Water Table	40.0

All Dimensions in feet unless otherwise noted

## Materials Legend

- Fill: Clean Native Fill
- Seal: Bentonite Pellets
- Sand: Pool sand
- Slurry: Bentonite Slurry

## Permanent Soil Gas Monitoring Point.

- 1/4" Swagelok fitting @ top
- Riser, 1/4" SS tubing.
- Sintered SS intake filter @ bottom

## Manhole Specifications

- 8" Cast iron manhole w/ galvanized steel, 8" diameter, 18" deep collar

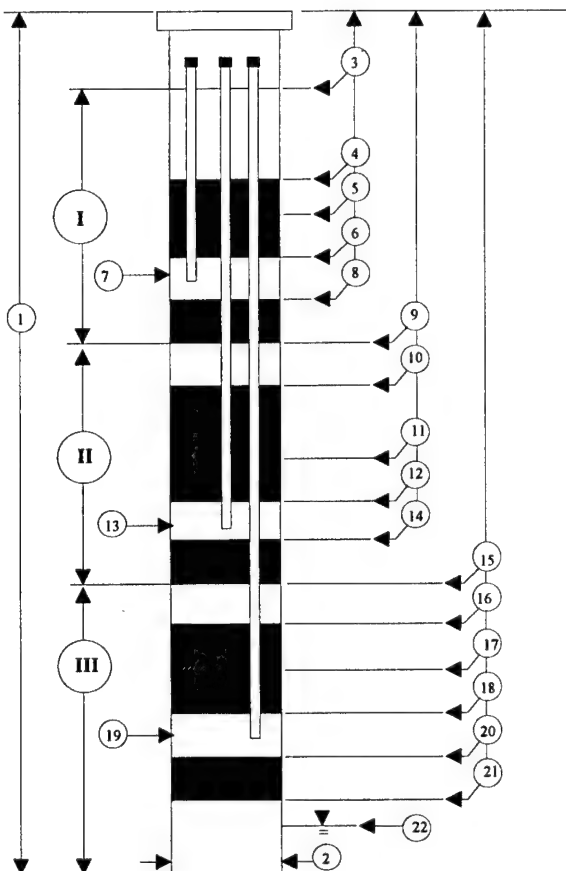


# Construction Details For Borehole/Soil Gas Cluster

12AW

Data Entered by: **ESH**  
Date Entered: **2/18/97**

Date Installed: **6/5/96**  
Manhole Elevation: **256.32**



1.	Depth of Borehole	48.5
2.	Borehole Diameter (in)	6.75
3.	Depth to Top of Fill I	0.4
4.	Depth to Top of Slurry I	4.0
5.	Depth to Top of Upper Seal I	33.7
6.	Depth to Top of Sand I	34.7
7.	Depth of Cluster Point I	35.5
	Depth (ft MSL)	220.82'
8.	Depth to Top of Lower Seal I	N/A
9.	Depth to Top of Fill II	N/A
10.	Depth to Top of Slurry II	N/A
11.	Depth to Top of Upper Seal II	N/A
12.	Depth to Top of Sand II	N/A
13.	Depth of Cluster Point II	N/A
	Depth (ft MSL)	N/A
14.	Depth to Top of Lower Seal II	N/A
15.	Depth to Top of Fill III	N/A
16.	Depth to Top of Slurry III	N/A
17.	Depth to Top of Upper Seal III	N/A
18.	Depth to Top of Sand III	N/A
19.	Depth of Cluster Point III	N/A
	Depth (ft MSL)	N/A
20.	Depth to Top of Lower Seal III	N/A
21.	Depth to Top Remaining Fill	36.2
22.	Depth to Water Table	40.0

All Dimensions in feet unless otherwise noted

## Materials Legend

- Fill: Clean Native Fill
- Seal: Bentonite Pellets
- Sand: Pool sand
- Slurry: Bentonite Slurry

## Permanent Soil Gas Monitoring Point.



- 1/4" Swagelok fitting @ top
- Riser, 1/4" SS tubing.
- Sintered SS intake filter @ bottom

## Manhole Specifications



8" Cast iron manhole  
w/ galvanized steel, 8"  
diameter, 18" deep collar

# Construction Details For Borehole/Soil Gas Cluster

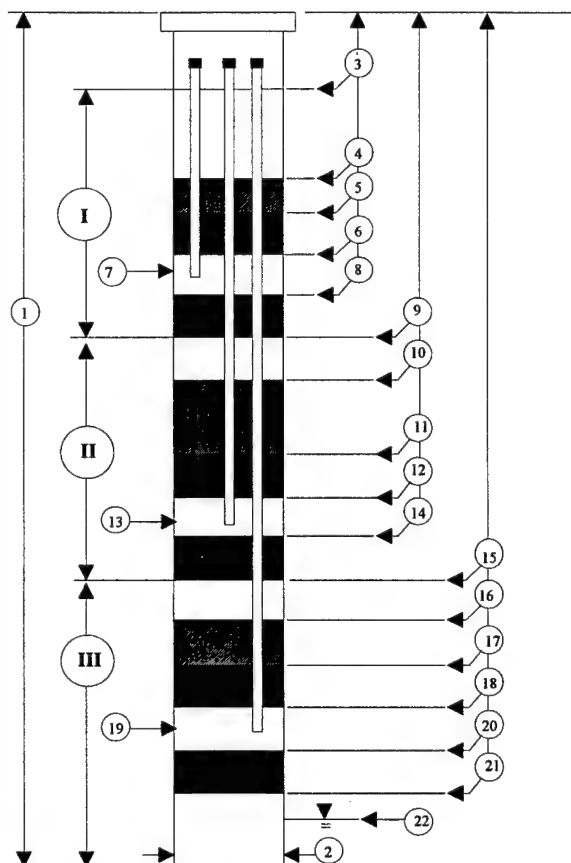
12AX

Data Entered by: ESH

Date Installed: 6/6/96

Date Entered: 2/18/97

Manhole Elevation: 249.97'



1.	Depth of Borehole	37.0
2.	Borehole Diameter (in)	6.75
3.	Depth to Top of Fill I	0.4
4.	Depth to Top of Slurry I	1.8
5.	Depth to Top of Upper Seal I	7.0
6.	Depth to Top of Sand I	9.0
7.	Depth of Cluster Point I	9.8
	Depth (ft MSL)	240.17'
8.	Depth to Top of Lower Seal I	10.3
9.	Depth to Top of Fill II	10.8
10.	Depth to Top of Slurry II	17.5
11.	Depth to Top of Upper Seal II	26.7
12.	Depth to Top of Sand II	29.7
13.	Depth of Cluster Point II	30.4
	Depth (ft MSL)	219.57'
14.	Depth to Top of Lower Seal II	N/A
15.	Depth to Top of Fill III	N/A
16.	Depth to Top of Slurry III	N/A
17.	Depth to Top of Upper Seal III	N/A
18.	Depth to Top of Sand III	N/A
19.	Depth of Cluster Point III	N/A
	Depth (ft MSL)	N/A
20.	Depth to Top of Lower Seal III	N/A
21.	Depth to Top Remaining Fill	32.0
22.	Depth to Water Table	31.5

All Dimensions in feet unless otherwise noted

## Materials Legend

- Fill: Clean Native Fill
- Seal: Bentonite Pellets
- Sand: Pool sand
- Slurry: Bentonite Slurry

## Permanent Soil Gas Monitoring Point.

- 1/4" Swagelok fitting @ top
- Riser, 1/4" SS tubing.
- Sintered SS intake filter @ bottom

## Manhole Specifications

- 8" Cast iron manhole w/ galvanized steel, 8" diameter, 18" deep collar

# Construction Details For Borehole/Well

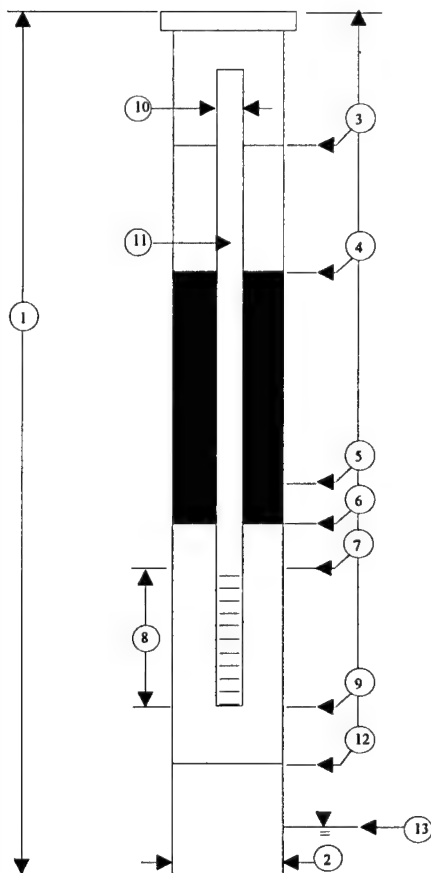
12AY

Data Entered by: ESH

Date Installed: 6/6/96

Date Entered: 2/18/97

Manhole Elevation: 255.46'



1.	Depth of Borehole	53
2.	Borehole Diameter (in)	6.75
3.	Depth to Top of Fill	0.5
4.	Depth to Top of Slurry	N/A
5.	Depth to Top of Upper Seal	31.0
6.	Depth to Top of Sand	35.0
8.	Depth to Top of Well Screen	37.0
	Depth (ft MSL)	218.46'
8.	Well Screen Length	15.0
7.	Depth of Well Bottom	52.0
9.	Diameter of Well (in)	2.0
10.	Well Material	PVC
21.	Depth to Top Remaining Fill	N/A
22.	Depth to Water Table	37.0

All Dimensions in feet unless otherwise noted

## Materials Legend

-  — Fill: Clean Native Fill
-  — Seal: Bentonite Pellets
-  — Sand: Pool sand
-  — Slurry: Bentonite Slurry

## Manhole Specifications



8" Cast iron manhole  
w/ galvanized steel, 8"  
diameter, 18" deep collar

# Construction Details For Borehole/Soil Gas Cluster

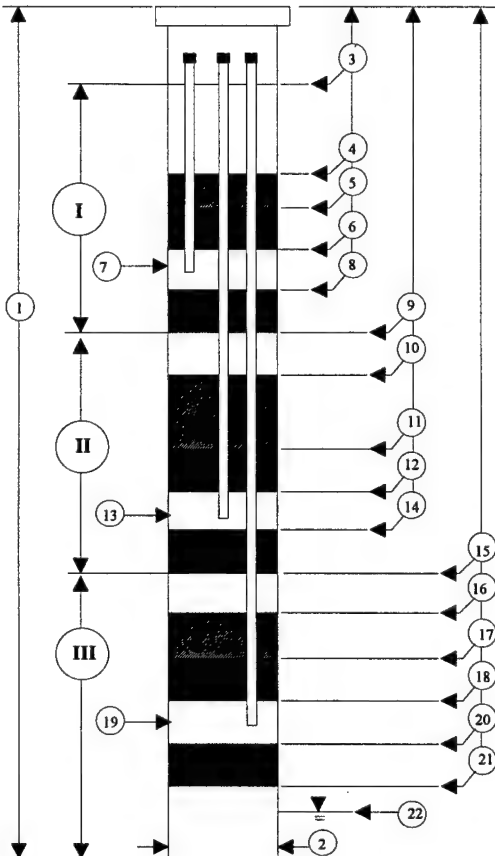
12AZ

Data Entered by: ESH

Date Installed: 6/7/96

Date Entered: 2/18/97

Manhole Elevation: 254.18




1.	Depth of Borehole	51.0
2.	Borehole Diameter (in)	6.75
3.	Depth to Top of Fill I	0.4
4.	Depth to Top of Slurry I NOTE: CAVED IN FROM 32.3' TO 8.5'	N/A
5.	Depth to Top of Upper Seal I	32.3
6.	Depth to Top of Sand I	34.3
7.	Depth of Cluster Point I Depth (ft MSL)	218.88
8.	Depth to Top of Lower Seal I	N/A
9.	Depth to Top of Fill II	N/A
10.	Depth to Top of Slurry II	N/A
11.	Depth to Top of Upper Seal II	N/A
12.	Depth to Top of Sand II	N/A
13.	Depth of Cluster Point II Depth (ft MSL)	N/A
14.	Depth to Top of Lower Seal II	N/A
15.	Depth to Top of Fill III	N/A
16.	Depth to Top of Slurry III	N/A
17.	Depth to Top of Upper Seal III	N/A
18.	Depth to Top of Sand III	N/A
19.	Depth of Cluster Point III Depth (ft MSL)	N/A
20.	Depth to Top of Lower Seal III	N/A
21.	Depth to Top Remaining Fill	35.5
22.	Depth to Water Table	40.0

All Dimensions in feet unless otherwise noted

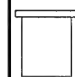
## Materials Legend

-  — Fill: Clean Native Fill
-  — Seal: Bentonite Pellets
-  — Sand: Pool sand
-  — Slurry: Bentonite Slurry

## Permanent Soil Gas Monitoring Point.

-  - 1/4" Swagelok fitting @ top
- Riser, 1/4" SS tubing.
- Sintered SS intake filter @ bottom

## Manhole Specifications

-  8" Cast iron manhole w/ galvanized steel, 8" diameter, 18" deep collar

# Construction Details For Borehole/Soil Gas Cluster

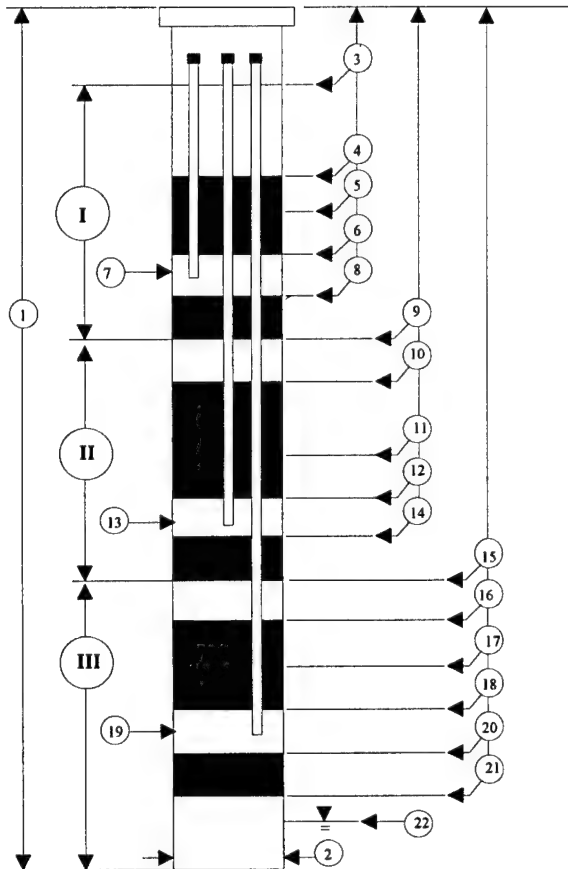
12BA

Data Entered by: ESH

Date Installed: 6/7/96

Date Entered: 2/18/97

Manhole Elevation: 255.86'



1.	Depth of Borehole	53.0
2.	Borehole Diameter (in)	6.75
3.	Depth to Top of Fill I	0.4
4.	Depth to Top of Slurry I	6.5
5.	Depth to Top of Upper Seal I	32.5
6.	Depth to Top of Sand I	35.1
7.	Depth of Cluster Point I	36.0
	Depth (ft MSL)	219.86
8.	Depth to Top of Lower Seal I	N/A
9.	Depth to Top of Fill II	N/A
10.	Depth to Top of Slurry II	N/A
11.	Depth to Top of Upper Seal II	N/A
12.	Depth to Top of Sand II	N/A
13.	Depth of Cluster Point II	N/A
	Depth (ft MSL)	N/A
14.	Depth to Top of Lower Seal II	N/A
15.	Depth to Top of Fill III	N/A
16.	Depth to Top of Slurry III	N/A
17.	Depth to Top of Upper Seal III	N/A
18.	Depth to Top of Sand III	N/A
19.	Depth of Cluster Point III	N/A
	Depth (ft MSL)	N/A
20.	Depth to Top of Lower Seal III	N/A
21.	Depth to Top Remaining Fill	36.2
22.	Depth to Water Table	40.0

All Dimensions in feet unless otherwise noted

## Materials Legend

- Fill: Clean Native Fill
- Seal: Bentonite Pellets
- Sand: Pool sand
- Slurry: Bentonite Slurry

## Permanent Soil Gas Monitoring Point.



- 1/4" Swagelok fitting @ top
- Riser, 1/4" SS tubing.
- Sintered SS intake filter @ bottom

## Manhole Specifications



8" Cast iron manhole  
w/ galvanized steel, 8"  
diameter, 18" deep collar

# Construction Details For Borehole/Well

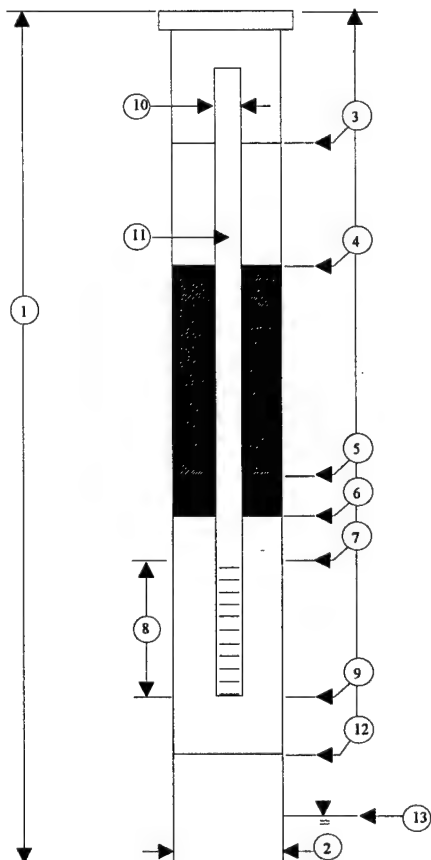
VENT 1

Data Entered by: ESH

Date Installed: 11/30/95

Date Entered: 2/18/97

Manhole Elevation: 256.26'



1.	Depth of Borehole	42.5
2.	Borehole Diameter (in)	9.9
3.	Depth to Top of Fill	N/A
4.	Depth to Top of Slurry	0.5
5.	Depth to Top of Upper Seal	34.5
6.	Depth to Top of Sand	37.5
7.	Depth to Top of Well Screen	37.0
	Depth (ft MSL)	219.26'
8.	Well Screen Length	5.0
9.	Depth of Well Bottom	42.0
10.	Diameter of Well (in)	3.0
11.	Well Material	PVC
12.	Depth to Top Remaining Fill	N/A
13.	Depth to Water Table	39.5

All Dimensions in feet unless otherwise noted

## Materials Legend

- Fill: Clean Native Fill
- Seal: Bentonite Pellets
- Sand: Pool sand
- Slurry: Bentonite Slurry

## Manhole Specifications



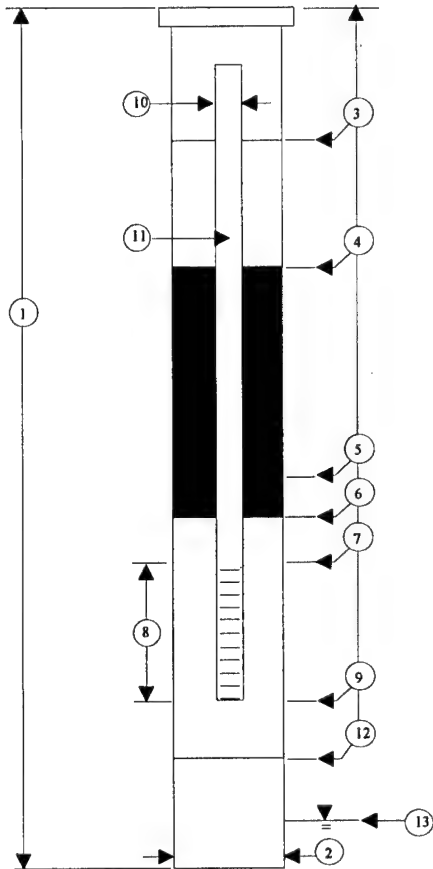
10" Cast iron manhole  
w/ galvanized steel, 10"  
diameter, 18" deep collar

# Construction Details For Borehole/Well

VENT 2

Data Entered by: ESH  
Date Entered: 2/18/97

Date Installed: 11/30/95  
Manhole Elevation: 256.30'



1.	Depth of Borehole	43
2.	Borehole Diameter (in)	9.9
3.	Depth to Top of Fill	N/A
4.	Depth to Top of Slurry	0.5
5.	Depth to Top of Upper Seal	34.5
6.	Depth to Top of Sand	37.5
7.	Depth to Top of Well Screen	37.0
	Depth (ft MSL)	219.30'
8.	Well Screen Length	5.0
9.	Depth of Well Bottom	42.0
10.	Diameter of Well (in)	3.0
11.	Well Material	PVC
12.	Depth to Top Remaining Fill	42.5
13.	Depth to Water Table	39.5

All Dimensions in feet unless otherwise noted

## Materials Legend

- Fill: Clean Native Fill
- Seal: Bentonite Pellets
- Sand: Pool sand
- Slurry: Bentonite Slurry

## Manhole Specifications



10" Cast iron manhole  
w/ galvanized steel, 10"  
diameter, 18" deep collar

# Construction Details For Borehole/Well

SPARGE 1

Data Entered by:

ESH

Date Installed:

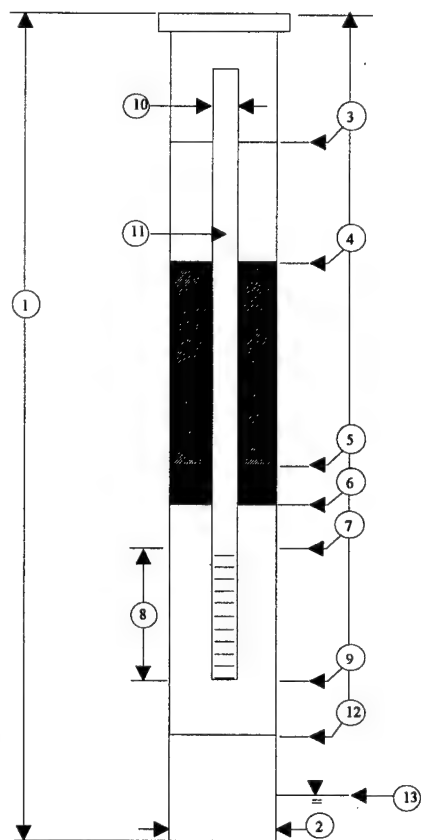
12/1/95

Date Entered:

2/18/97

Manhole Elevation:

256.30'



1.	Depth of Borehole	50
2.	Borehole Diameter (in)	9.9
3.	Depth to Top of Fill	0.5
4.	Depth to Top of Slurry	5.0
5.	Depth to Top of Upper Seal	36.0
6.	Depth to Top of Sand	43.0
7.	Depth to Top of Well Screen	43.1
	Depth (ft MSL)	213.20'
8.	Well Screen Length	0.7
9.	Depth of Well Bottom	43.8
10.	Diameter of Well (in)	0.8
11.	Well Material	PVC
12.	Depth to Top Remaining Fill	N/A
13.	Depth to Water Table	39.0

All Dimensions in feet unless otherwise noted

NOTE: SHARES COMMON HOLE W/ SPARGE 2

## Materials Legend

-  — Fill: Clean Native Fill
-  — Seal: Bentonite Pellets
-  — Sand: Pool sand
-  — Slurry: Bentonite Slurry

## Manhole Specifications



10" Cast iron manhole  
w/ galvanized steel, 10"  
diameter, 18" deep collar



# Construction Details For Borehole/Soil Gas Cluster

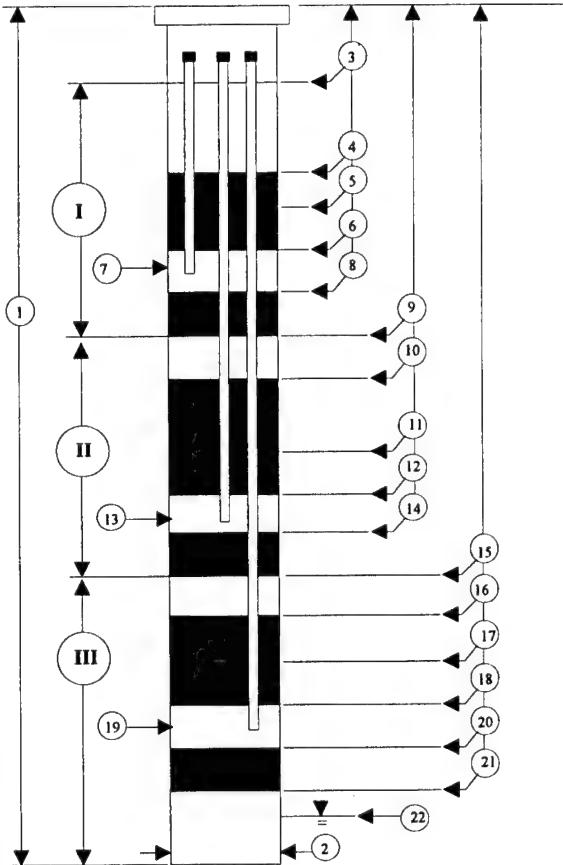
CONTROL

Data Entered by: ESH

Date Installed: 10/12/95

Date Entered: 2/18/97

Manhole Elevation: 244.12'



1.	Depth of Borehole	32.0
2.	Borehole Diameter (in)	6.75
3.	Depth to Top of Fill I	0.4
4.	Depth to Top of Slurry I	9.0
5.	Depth to Top of Upper Seal I	11.0
6.	Depth to Top of Sand I	12.0
7.	Depth of Cluster Point I	12.6
	Depth (ft MSL)	220.12'
8.	Depth to Top of Lower Seal I	13.2
9.	Depth to Top of Fill II	N/A
10.	Depth to Top of Slurry II	15.2
11.	Depth to Top of Upper Seal II	23.0
12.	Depth to Top of Sand II	24.2
13.	Depth of Cluster Point II	24.6
	Depth (ft MSL)	232.12'
14.	Depth to Top of Lower Seal II	25.3
15.	Depth to Top of Fill III	N/A
16.	Depth to Top of Slurry III	N/A
17.	Depth to Top of Upper Seal III	N/A
18.	Depth to Top of Sand III	N/A
19.	Depth of Cluster Point III	N/A
	Depth (ft MSL)	N/A
20.	Depth to Top of Lower Seal III	N/A
21.	Depth to Top Remaining Fill	27.2
22.	Depth to Water Table	N/A

All Dimensions in feet unless otherwise noted

## Materials Legend

- Fill: Clean Native Fill
- Seal: Bentonite Pellets
- Sand: Pool sand
- Slurry: Bentonite Slurry

## Permanent Soil Gas Monitoring Point.

- 1/4" Swagelok fitting @ top
- Riser, 1/4" SS tubing.
- Sintered SS intake filter @ bottom

## Manhole Specifications

- 8" Cast iron manhole w/ galvanized steel, 8" diameter, 18" deep collar

## **APPENDIX III GRAIN SIZE DATA**

Sieve Size	Boring		SPK1		Sample		133
	Depth (m)	0.0 - 0.46		Dry Wt. (g)			150.0
	Soil Wt. (g)	Retained	% Retained	% Retained	Accum.	% Finer	
3/8	27.1	18.1	66.8	18.1	18.1	81.9	
4	14.0	9.3	66.4	27.4	27.4	72.6	
10	10.8	7.2	66.7	34.6	34.6	65.4	
20	15.6	10.4	66.7	45.0	45.0	55.0	
40	32.0	21.3	66.6	66.3	66.3	33.7	
60	27.1	18.1	66.8	84.4	84.4	15.6	
80	9.7	6.5	66.9	90.9	90.9	9.1	
100	3.0	2.0	66.7	92.9	92.9	7.1	
200	7.2	4.8	66.7	97.7	97.7	2.3	
Pan	3.5	2.3	66.7	100.0	100.0	0.0	
Total	150.0						

Sieve Size	Boring		SPK1		Sample		136
	Depth (m)		1.37 - 1.83		Dry Wt. (g)		
	Soil Wt. (g)	Retained	% Retained	% Retained	Accum.	% Retained	
3/8	6.5	1.3	20.0	1.3	1.3	20.0	98.7
4	45.8	9.1	20.0	10.4	10.4	20.0	89.6
10	78.2	15.6	20.0	26.0	26.0	20.0	74.0
20	82.3	16.4	20.0	42.4	42.4	20.0	57.6
40	131.5	26.2	20.0	68.7	68.7	20.0	31.3
60	100.2	20.0	20.0	88.7	88.7	20.0	11.3
80	23.0	4.6	20.0	93.3	93.3	20.0	6.7
100	7.1	1.4	20.0	94.7	94.7	20.0	5.3
200	14.3	2.9	20.0	97.5	97.5	20.0	2.5
Pan	12.4	2.5	20.0	100.0	100.0	20.0	0.0
Total	501.3						

Sieve Size	Boring		SPK1		Sample		139
	Depth (m)		2.74 - 3.20		Dry Wt. (g)		
	Soil Wt. (g)	Retained	% Retained	% Retained	Accum.	% Retained	
3/8	0.0	0.0	0.0	0.0	0.0	0.0	100.0
4	6.4	1.3	2.5	1.3	1.3	3.8	98.7
10	12.2	2.5	2.5	3.8	3.8	3.8	96.2
20	53.5	10.8	10.8	14.6	14.6	14.6	85.4
40	194.0	39.3	39.3	53.9	53.9	53.9	46.1
60	143.2	29.0	29.0	82.9	82.9	82.9	17.1
80	39.5	8.0	8.0	90.9	90.9	90.9	9.1
100	13.9	2.8	2.8	93.7	93.7	93.7	6.3
200	19.3	3.9	3.9	97.6	97.6	97.6	2.4
Pan	11.8	2.4	2.4	100.0	100.0	100.0	0.0
Total	493.8						

Sieve Size	Boring		SPK1		Sample		134
	Depth (m)		0.46 - 0.91		Dry Wt. (g)		
	Soil Wt. (g)	Retained	% Retained	% Retained	Accum.	% Retained	
3/8	0.0	0.0	0.0	0.0	0.0	0.0	100.0
4	8.7	2.7	2.7	97.3	2.7	97.3	87.6
10	31.1	9.7	9.7	12.4	12.4	71.1	87.6
20	53.2	16.5	16.5	28.9	28.9	41.4	71.1
40	95.9	29.8	29.8	58.6	58.6	13.0	41.4
60	91.5	28.4	28.4	87.0	87.0	7.1	13.0
80	18.9	5.9	5.9	92.9	92.9	5.6	7.1
100	4.7	1.5	1.5	94.4	94.4	2.5	5.6
200	10.3	3.2	3.2	97.5	97.5	0.0	2.5
Pan	7.9	2.5	2.5	100.0	100.0	0.0	0.0
Total	322.2						

Sieve Size	Boring		SPK1		Sample		137
	Depth (m)		1.83 - 2.29		Dry Wt. (g)		
	Soil Wt. (g)	Retained	% Retained	% Retained	Accum.	% Retained	
3/8	6.6		1.3		1.3		98.7
4	5.8		1.2		2.5		97.5
10	8.8		1.6		4.2		95.8
20	53.2		10.6		14.8		85.2
40	220.2		43.8		58.6		41.4
60	137.9		27.4		86.0		14.0
80	34.6		6.9		92.9		7.1
100	12.4		2.5		95.4		4.6
200	16.5		3.3		98.6		1.4
Pan	6.8		1.4		100.0		0.0
Total	502.8						

Sieve Size	Boring		SPK1		Sample		140
	Depth (m)	Soil Wt. (g) Retained	3.20 - 3.66		Dry Wt. (g) Accum.	% Retained	
			% Retained	% Retained			
3/8		0.0	0.0	0.0	0.0	100.0	
4		8.6	1.7	1.7	5.0	98.3	
10		16.2	3.3	3.3	17.4	95.0	
20		61.1	12.4	12.4	52.8	82.6	
40		175.0	35.4	35.4	80.7	47.2	
60		138.2	28.0	28.0	89.2	19.3	
80		41.7	8.4	8.4	92.3	10.8	
100		15.6	3.2	3.2	97.3	7.7	
200		24.8	5.0	5.0	100.0	2.7	
Pan		13.2	2.7	2.7		0.0	
Total		494.4					

Sieve Size	Boring		SPK1		Sample		135
	Depth (m)	Soil Wt. (g)	0.91 - 1.37		Dry Wt. (g)		
	Retained		% Retained	% Retained	Accum.		
3/8	20.6	20.6	8.4	8.4	8.4	91.6	% Finer
4	6.1	6.1	2.5	2.5	10.9	89.1	
10	11.4	11.4	4.7	4.7	15.6	84.4	
20	27.9	27.9	11.4	11.4	27.0	73.0	
40	72.6	72.6	29.7	29.7	56.7	43.3	
60	63.9	63.9	26.2	26.2	82.9	17.1	
80	17.6	17.6	7.2	7.2	90.1	9.9	
100	7.3	7.3	3.0	3.0	93.1	6.9	
200	9.8	9.8	4.0	4.0	97.1	2.9	
Pan	7.1	7.1	2.9	2.9	100.0	0.0	
Total	244.3						

Sieve Size	Boring		SPK1		Sample		138
	Depth (m)		2.29 - 2.74		Dry Wt. (g)		
	Soil Wt. (g)	Retained	% Retained	% Retained	Accum.	% Retained	
3/8	7.5		1.5		1.5		98.5
4	14.0		2.8		4.3		95.7
10	16.0		3.2		7.6		92.4
20	35.1		7.1		14.7		85.3
40	177.4		35.9		50.5		49.5
60	156.1		31.6		82.1		17.9
80	42.6		8.6		90.7		9.3
100	14.8		3.0		93.7		6.3
200	20.7		4.2		97.9		2.1
Pan	10.4		2.1		100.0		0.0
Total	494.6						

Sieve Size	Boring		SPK1		Sample		141
	Depth (m)	3.66 - 4.11		Dry Wt. (g)			
	Soil Wt. (g)	% Retained		% Retained		% Finer	
3/8	0.0	0.0	0.0	0.0	0.0	100.0	
4	3.7	0.7	0.7	0.7	0.7	99.3	
10	7.3	1.5	1.5	2.2	2.2	97.8	
20	24.8	5.0	5.0	7.2	7.2	92.8	
40	103.7	20.9	20.9	28.1	28.1	71.9	
60	147.4	29.7	29.7	57.8	57.8	42.2	
80	72.8	14.7	14.7	72.5	72.5	27.5	
100	33.7	6.8	6.8	79.3	79.3	20.7	
200	63.0	12.7	12.7	91.9	91.9	8.1	
Pan	40.0	8.1	8.1	100.0	100.0	0.0	
Total	496.4						

Sieve Size	Boring		SPK1		Sample		142
	Depth (m)	Soil Wt. (g)	% Retained	% Retained	Dry Wt. (g)	Accum.	% Finer
3/8	0.0	0.0	0.0	0.0	0.0	0.0	100.0
4	0.7	4	0.1	0.1	0.1	0.1	99.9
10	5.9	12	1.2	1.3	1.3	1.3	98.7
20	33.0	6.6	6.6	7.9	7.9	7.9	92.1
40	136.2	27.2	30.5	35.1	35.1	35.1	64.9
60	152.4	30.5	30.5	65.6	65.6	65.6	34.4
80	60.4	12.1	12.1	77.7	77.7	77.7	22.3
100	28.3	5.7	5.7	83.3	83.3	83.3	16.7
200	55.4	11.1	11.1	94.4	94.4	94.4	5.6
Pan	27.9	5.6	5.6	100.0	100.0	100.0	0.0
Total	500.2						

Sieve Size	Boring		SPK1		Sample		145
	Depth (m)	Soil Wt. (g)	% Retained	% Retained	Dry Wt. (g)	Accum.	% Finer
3/8	0.0	0.0	0.0	0.0	0.0	0.0	100.0
4	7.0	1.4	1.4	1.4	1.4	1.4	98.6
10	6.7	1.4	1.4	2.8	2.8	2.8	97.2
20	8.3	1.7	1.7	4.5	4.5	4.5	95.5
40	15.4	3.1	3.1	7.6	7.6	7.6	92.4
60	68.0	13.8	13.8	21.4	21.4	21.4	78.6
80	131.2	26.6	26.6	48.0	48.0	48.0	52.0
100	66.6	13.5	13.5	61.5	61.5	61.5	38.5
200	156.9	31.8	31.8	93.3	93.3	93.3	6.7
Pan	32.8	6.7	6.7	100.0	100.0	100.0	0.0
Total	492.9						

Sieve Size	Boring		SPK1		Sample		148
	Depth (m)	Soil Wt. (g)	% Retained	% Retained	Dry Wt. (g)	Accum.	% Finer
3/8	0.0	0.0	0.0	0.0	0.0	0.0	100.0
4	0.0	0.0	0.0	0.0	0.0	0.0	100.0
10	0.0	0.0	0.0	0.0	0.0	0.0	100.0
20	0.4	0.1	0.1	0.1	0.1	0.1	99.9
40	13.5	2.7	2.7	2.8	2.8	2.8	97.2
60	150.6	30.2	30.2	33.0	33.0	33.0	67.0
80	148.7	29.9	29.9	62.9	62.9	62.9	37.1
100	61.1	12.3	12.3	75.2	75.2	75.2	24.8
200	91.4	18.4	18.4	93.5	93.5	93.5	6.5
Pan	32.2	6.5	6.5	100.0	100.0	100.0	0.0
Total	497.9						

Sieve Size	Boring		SPK1		Sample		143
	Depth (m)	Soil Wt. (g)	% Retained	% Retained	Dry Wt. (g)	Accum.	% Finer
3/8	0.0	0.0	0.0	0.0	0.0	0.0	100.0
4	0.7	0.1	0.1	0.1	0.1	0.1	99.9
10	3.9	0.8	0.8	0.9	0.9	0.9	99.1
20	22.0	4.5	4.5	5.4	5.4	5.4	94.6
40	77.8	15.8	15.8	21.3	21.3	21.3	78.7
60	88.4	18.0	18.0	39.3	39.3	39.3	60.7
80	58.5	11.9	11.9	51.2	51.2	51.2	48.8
100	36.3	7.4	7.4	58.6	58.6	58.6	41.4
200	122.0	24.9	24.9	83.4	83.4	83.4	16.6
Pan	81.3	16.6	16.6	100.0	100.0	100.0	0.0
Total	490.9						

Sieve Size	Boring		SPK1		Sample		146
	Depth (m)	Soil Wt. (g)	% Retained	% Retained	Dry Wt. (g)	Accum.	% Finer
3/8	0.0	0.0	0.0	0.0	0.0	0.0	100.0
4	0.0	0.0	0.0	0.0	0.0	0.0	100.0
10	0.6	0.1	0.1	0.1	0.1	0.1	99.9
20	1.1	0.2	0.2	0.3	0.3	0.3	99.7
40	4.1	0.8	0.8	1.2	1.2	1.2	98.8
60	41.4	8.3	8.3	9.4	9.4	9.4	90.6
80	96.4	19.2	19.2	28.6	28.6	28.6	71.4
100	93.0	18.5	18.5	47.2	47.2	47.2	52.8
200	196.2	39.1	39.1	86.3	86.3	86.3	13.7
Pan	68.6	13.7	13.7	100.0	100.0	100.0	0.0
Total	501.4						

Sieve Size	Boring		SPK1		Sample		149
	Depth (m)	Soil Wt. (g)	% Retained	% Retained	Dry Wt. (g)	Accum.	% Finer
3/8	0.0	0.0	0.0	0.0	0.0	0.0	100.0
4	0.0	0.0	0.0	0.0	0.0	0.0	100.0
10	0.0	0.0	0.0	0.0	0.0	0.0	100.0
20	0.6	0.1	0.1	0.1	0.1	0.1	99.9
40	14.4	2.9	2.9	3.0	3.0	3.0	97.0
60	141.7	28.4	28.4	31.4	31.4	31.4	68.6
80	171.0	34.3	34.3	65.8	65.8	65.8	34.2
100	61.8	12.4	12.4	78.2	78.2	78.2	21.8
200	85.7	17.2	17.2	95.3	95.3	95.3	4.7
Pan	23.2	4.7	4.7	100.0	100.0	100.0	0.0
Total	498.4						

Sieve Size	Boring		SPK1		Sample		144
	Depth (m)	Soil Wt. (g)	% Retained	% Retained	Dry Wt. (g)	Accum.	% Finer
3/8	0.0	0.0	0.0	0.0	0.0	0.0	100.0
4	2.4	0.5	0.5	0.5	0.5	0.5	99.5
10	4.0	0.8	0.8	1.3	1.3	1.3	98.7
20	12.1	2.5	2.5	3.8	3.8	3.8	96.2
40	54.9	11.1	11.1	14.9	14.9	14.9	85.1
60	144.5	29.3	29.3	44.2	44.2	44.2	55.8
80	98.4	20.0	20.0	64.2	64.2	64.2	35.8
100	48.7	9.9	9.9	74.1	74.1	74.1	25.9
200	97.9	19.9	19.9	93.9	93.9	93.9	6.1
Pan	29.9	6.1	6.1	100.0	100.0	100.0	0.0
Total	492.8						

Sieve Size	Boring		SPK1		Sample		147
	Depth (m)	Soil Wt. (g)	% Retained	% Retained	Dry Wt. (g)	Accum.	% Finer
3/8	0.0	0.0	0.0	0.0	0.0	0.0	100.0
4	0.0	0.0	0.0	0.0	0.0	0.0	100.0
10	0.1	0.0	0.0	0.0	0.0	0.0	100.0
20	1.1	0.2	0.2	0.2	0.2	0.2	99.8
40	4.0	0.8	0.8	1.0	1.0	1.0	99.0
60	26.4	5.3	5.3	6.3	6.3	6.3	93.7
80	92.4	18.6	18.6	24.9	24.9	24.9	75.1
100	65.3	13.1	13.1	38.0	38.0	38.0	62.0
200	234.7	47.1	47.1	85.1	85.1	85.1	14.9
Pan	74.1	14.9	14.9	100.0	100.0	100.0	0.0
Total	498.1						

Sieve Size	Boring		SPK1		Sample		150
	Depth (m)	Soil Wt. (g)	% Retained	% Retained	Dry Wt. (g)	Accum.	% Finer
3/8	0.0	0.0	0.0	0.0	0.0	0.0	100.0
4	0.3	0.1	0.1	0.1	0.1	0.1	99.9
10	0.1	0.0	0.0	0.1	0.1	0.1	99.9
20	0.6	0.1	0.1	0.2	0.2	0.2	99.8
40	6.2	1.3	1.3	1.5	1.5	1.5	98.5
60	61.8	12.5	12.5	14.0	14.0	14.0	86.0
80	83.7	17.0	17.0	30.9	30.9	30.9	69.1
100	53.9	10.9	10.9	41.8	41.8	41.8	58.2
200	177.0	35.9	35.9	77.7	77.7	77.7	22.3
Pan	110.1	22.3	22.3	100.0	100.0	100.0	0.0
Total	493.7						

Sieve Size	Boring		SPK1		Sample		151
	Depth (m)	Soil Wt. (g)	8.23 - 8.69	9.14 - 9.60	Dry Wt. (g)	Accum.	
	Retained	% Retained	% Retained	% Retained	% Retained	% Retained	
3/8	0.0	0.0	0.0	0.0	0.0	0.0	100.0
4	0.0	0.0	0.0	0.0	0.0	0.0	100.0
10	0.0	0.0	0.0	0.0	0.0	0.0	100.0
20	0.1	0.0	0.0	0.0	0.0	0.0	100.0
40	1.2	0.2	0.2	0.3	0.3	0.3	99.7
60	14.7	3.0	3.0	3.2	3.2	3.2	96.8
80	81.6	16.5	16.5	19.8	19.8	19.8	80.2
100	69.9	14.2	14.2	34.0	34.0	34.0	66.0
200	265.6	53.9	53.9	87.8	87.8	87.8	12.2
Pan	60.0	12.2	12.2	100.0	100.0	100.0	0.0
Total	493.1						

Sieve Size	Boring		SPK1		Sample		152
	Depth (m)	Soil Wt. (g)	8.69 - 9.14	9.14 - 9.60	Dry Wt. (g)	Accum.	
	Retained	% Retained	% Retained	% Retained	% Retained	% Retained	
3/8	0.0	0.0	0.0	0.0	0.0	0.0	100.0
4	0.0	0.0	0.0	0.0	0.0	0.0	100.0
10	0.0	0.0	0.0	0.0	0.0	0.0	100.0
20	0.2	0.0	0.0	0.0	0.0	0.0	100.0
40	7.3	1.5	1.5	1.5	1.5	1.5	98.5
60	88.6	17.9	17.9	19.5	19.5	19.5	80.5
80	134.3	27.2	27.2	46.7	46.7	46.7	53.3
100	81.3	16.5	16.5	63.1	63.1	63.1	36.9
200	140.9	28.5	28.5	91.7	91.7	91.7	8.3
Pan	41.2	8.3	8.3	100.0	100.0	100.0	0.0
Total	493.8						

Sieve Size	Boring		SPK1		Sample		153
	Depth (m)	Soil Wt. (g)	9.14 - 9.60	9.60 - 10.00	Dry Wt. (g)	Accum.	
	Retained	% Retained	% Retained	% Retained	% Retained	% Retained	
3/8	0.0	0.0	0.0	0.0	0.0	0.0	100.0
4	0.0	0.0	0.0	0.0	0.0	0.0	100.0
10	0.2	0.0	0.0	0.0	0.0	0.0	100.0
20	1.9	0.4	0.4	0.4	0.4	0.4	99.6
40	42.1	8.5	8.5	9.0	9.0	9.0	91.0
60	172.6	35.0	35.0	43.9	43.9	43.9	56.1
80	93.5	18.9	18.9	62.8	62.8	62.8	37.2
100	34.4	7.0	7.0	69.8	69.8	69.8	30.2
200	101.4	20.5	20.5	90.3	90.3	90.3	9.7
Pan	47.7	9.7	9.7	100.0	100.0	100.0	0.0
Total	493.8						

Sieve Size	Boring		SPK1		Sample		154
	Depth (m)	Soil Wt. (g)	9.60 - 10.06	10.06 - 10.52	Dry Wt. (g)	Accum.	
	Retained	% Retained	% Retained	% Retained	% Retained	% Retained	
3/8	0.0	0.0	0.0	0.0	0.0	0.0	100.0
4	0.0	0.0	0.0	0.0	0.0	0.0	100.0
10	0.3	0.1	0.1	0.1	0.1	0.1	99.9
20	5.5	1.1	1.1	1.2	1.2	1.2	98.8
40	176.6	35.9	35.9	37.0	37.0	37.0	63.0
60	230.4	46.8	46.8	83.8	83.8	83.8	16.2
80	46.1	9.4	9.4	93.2	93.2	93.2	6.8
100	10.8	2.2	2.2	95.4	95.4	95.4	4.6
200	13.5	2.7	2.7	98.1	98.1	98.1	1.9
Pan	9.2	1.9	1.9	100.0	100.0	100.0	0.0
Total	492.4						

Sieve Size	Boring		SPK1		Sample		155
	Depth (m)	Soil Wt. (g)	10.06 - 10.52	10.52 - 11.00	Dry Wt. (g)	Accum.	
	Retained	% Retained	% Retained	% Retained	% Retained	% Retained	
3/8	0.0	0.0	0.0	0.0	0.0	0.0	100.0
4	0.2	0.0	0.0	0.0	0.0	0.0	100.0
10	1.1	0.2	0.2	0.3	0.3	0.3	99.7
20	18.1	3.7	3.7	3.9	3.9	3.9	96.1
40	191.8	38.8	38.8	42.7	42.7	42.7	57.3
60	211.7	42.8	42.8	85.6	85.6	85.6	14.4
80	35.0	7.1	7.1	92.7	92.7	92.7	7.3
100	9.8	2.0	2.0	94.7	94.7	94.7	5.3
200	14.0	2.8	2.8	97.5	97.5	97.5	2.5
Pan	12.4	2.5	2.5	100.0	100.0	100.0	0.0
Total	494.1						

Sieve Size	Boring		SPK1		Sample		156
	Depth (m)	Soil Wt. (g)	10.52 - 10.97	10.97 - 11.43	Dry Wt. (g)	Accum.	
	Retained	% Retained	% Retained	% Retained	% Retained	% Retained	
3/8	6.5	1.3	1.3	1.3	1.3	1.3	98.7
4	4.3	0.9	0.9	2.2	2.2	2.2	97.8
10	10.7	2.1	2.1	4.3	4.3	4.3	95.7
20	29.1	5.8	5.8	10.2	10.2	10.2	89.8
40	191.0	38.3	38.3	48.5	48.5	48.5	51.5
60	191.7	38.5	38.5	87.0	87.0	87.0	13.0
80	29.4	5.9	5.9	92.9	92.9	92.9	7.1
100	7.2	1.4	1.4	94.3	94.3	94.3	5.7
200	12.0	2.4	2.4	96.7	96.7	96.7	3.3
Pan	16.4	3.3	3.3	100.0	100.0	100.0	0.0
Total	498.3						

Sieve Size	Boring		SPK1		Sample		157
	Depth (m)	Soil Wt. (g)	10.97 - 11.43	11.43 - 11.89	Dry Wt. (g)	Accum.	
	Retained	% Retained	% Retained	% Retained	% Retained	% Retained	
3/8	0.0	0.0	0.0	0.0	0.0	0.0	100.0
4	0.0	0.0	0.0	0.0	0.0	0.0	100.0
10	0.1	0.0	0.0	0.0	0.0	0.0	100.0
20	5.3	1.5	1.5	1.6	1.6	1.6	98.4
40	98.2	28.3	28.3	29.8	29.8	29.8	70.2
60	178.9	51.5	51.5	81.3	81.3	81.3	18.7
80	42.1	12.1	12.1	93.4	93.4	93.4	6.6
100	8.0	2.3	2.3	95.7	95.7	95.7	4.3
200	8.6	2.5	2.5	98.2	98.2	98.2	1.8
Pan	6.3	1.8	1.8	100.0	100.0	100.0	0.0
Total	347.5						

Sieve Size	Boring		SPK1		Sample		158
	Depth (m)	Soil Wt. (g)	11.43 - 11.89	11.89 - 12.34	Dry Wt. (g)	Accum.	
	Retained	% Retained	% Retained	% Retained	% Retained	% Retained	
3/8	4.1	1.0	1.0	1.0	1.0	1.0	99.0
4	1.2	0.3	0.3	1.3	1.3	1.3	98.7
10	3.6	0.9	0.9	2.2	2.2	2.2	97.8
20	19.8	4.9	4.9	7.1	7.1	7.1	92.9
40	151.7	37.7	37.7	44.8	44.8	44.8	55.2
60	150.3	37.3	37.3	82.2	82.2	82.2	17.8
80	26.8	6.7	6.7	88.8	88.8	88.8	11.2
100	8.3	2.1	2.1	90.9	90.9	90.9	9.1
200	17.7	4.4	4.4	95.3	95.3	95.3	4.7
Pan	19.0	4.7	4.7	100.0	100.0	100.0	0.0
Total	402.5						

Sieve Size	Boring		SPK1		Sample		159
	Depth (m)	Soil Wt. (g)	11.89 - 12.34	12.34 - 12.80	Dry Wt. (g)	Accum.	
	Retained	% Retained	% Retained	% Retained	% Retained	% Retained	
3/8	0.0	0.0	0.0	0.0	0.0	0.0	100.0
4	0.0	0.0	0.0	0.0	0.0	0.0	100.0
10	0.1	0.0	0.0	0.0	0.0	0.0	100.0
20	11.4	4.2	4.2	4.3	4.3	4.3	95.7
40	129.1	48.0	48.0	52.2	52.2	52.2	47.8
60	104.8	38.9	38.9	91.2	91.2	91.2	8.8
80	14.8	5.5	5.5	96.7	96.7	96.7	3.3
100	3.0	1.1	1.1	97.8	97.8	97.8	2.2
200	3.8	1.4	1.4	99.2	99.2	99.2	0.8
Pan	2.2	0.8	0.8	100.0	100.0	100.0	0.0
Total	269.2						

Sieve Size	Boring		SPK1		Sample		160
	Depth (m)	Soil Wt. (g)	12.34 - 12.80	13.72 - 14.17	Dry Wt. (g)	Accum.	
		Retained	% Retained	% Retained	% Retained	% Retained	% Finer
3/8	0.0	0.0	0.0	0.0	0.0	0.0	100.0
4	0.0	0.0	0.0	0.0	0.0	0.0	100.0
10	0.1	0.0	0.0	0.0	0.0	0.0	100.0
20	13.3	4.2	4.2	4.2	4.2	4.2	95.8
40	156.5	49.6	49.6	53.9	53.9	53.9	46.1
60	119.0	37.7	37.7	91.6	91.6	91.6	8.4
80	17.1	5.4	5.4	97.0	97.0	97.0	3.0
100	3.4	1.1	1.1	98.1	98.1	98.1	1.9
200	4.1	1.3	1.3	99.4	99.4	99.4	0.6
Pan	1.9	0.6	0.6	100.0	100.0	100.0	0.0
Total	315.4						

Sieve Size	Boring		SPK1		Sample		161
	Depth (m)	Soil Wt. (g)	12.80 - 13.26	14.63 - 15.09	Dry Wt. (g)	Accum.	
		Retained	% Retained	% Retained	% Retained	% Retained	% Finer
3/8	0.0	0.0	0.0	0.0	0.0	0.0	100.0
4	0.0	0.0	0.0	0.0	0.0	0.0	100.0
10	0.1	0.0	0.0	0.0	0.0	0.0	100.0
20	4.7	2.1	2.1	2.1	2.1	2.1	97.9
40	83.3	36.8	36.8	38.9	38.9	38.9	61.1
60	104.7	46.2	46.2	85.1	85.1	85.1	14.9
80	20.8	9.2	9.2	94.3	94.3	94.3	5.7
100	4.4	1.9	1.9	96.2	96.2	96.2	3.8
200	5.3	2.3	2.3	98.6	98.6	98.6	1.4
Pan	3.2	1.4	1.4	100.0	100.0	100.0	0.0
Total	226.5						

Sieve Size	Boring		SPK1		Sample		162
	Depth (m)	Soil Wt. (g)	13.26 - 13.72	14.63 - 15.09	Dry Wt. (g)	Accum.	
		Retained	% Retained	% Retained	% Retained	% Retained	% Finer
3/8	0.0	0.0	0.0	0.0	0.0	0.0	100.0
4	0.0	0.0	0.0	0.0	0.0	0.0	100.0
10	0.0	0.0	0.0	0.0	0.0	0.0	100.0
20	9.7	2.6	2.6	2.6	2.6	2.6	97.4
40	136.7	36.5	36.5	39.1	39.1	39.1	60.9
60	164.6	43.9	43.9	83.0	83.0	83.0	17.0
80	35.5	9.5	9.5	92.5	92.5	92.5	7.5
100	8.9	2.4	2.4	94.8	94.8	94.8	5.2
200	12.2	3.3	3.3	98.1	98.1	98.1	1.9
Pan	7.1	1.9	1.9	100.0	100.0	100.0	0.0
Total	374.7						

Sieve Size	Boring		SPK1		Sample		163
	Depth (m)	Soil Wt. (g)	13.72 - 14.17	15.09 - 15.54	Dry Wt. (g)	Accum.	
		Retained	% Retained	% Retained	% Retained	% Retained	% Finer
3/8	0.0	0.0	0.0	0.0	0.0	0.0	100.0
4	0.0	0.0	0.0	0.0	0.0	0.0	100.0
10	0.0	0.0	0.0	0.0	0.0	0.0	100.0
20	3.0	1.2	1.2	1.2	1.2	1.2	98.8
40	78.0	30.0	30.0	31.2	31.2	31.2	68.8
60	132.1	50.8	50.8	82.0	82.0	82.0	18.0
80	29.1	11.2	11.2	93.2	93.2	93.2	6.8
100	6.3	2.4	2.4	95.6	95.6	95.6	4.4
200	7.2	2.8	2.8	98.3	98.3	98.3	1.7
Pan	4.3	1.7	1.7	100.0	100.0	100.0	0.0
Total	260.0						

Sieve Size	Boring		SPK1		Sample		164
	Depth (m)	Soil Wt. (g)	14.17 - 14.63	15.54 - 16.00	Dry Wt. (g)	Accum.	
		Retained	% Retained	% Retained	% Retained	% Retained	% Finer
3/8	0.0	0.0	0.0	0.0	0.0	0.0	100.0
4	0.0	0.0	0.0	0.0	0.0	0.0	100.0
10	0.0	0.0	0.0	0.0	0.0	0.0	100.0
20	6.0	1.7	1.7	1.7	1.7	1.7	98.3
40	111.4	32.3	32.3	34.0	34.0	34.0	66.0
60	152.0	44.0	44.0	78.0	78.0	78.0	22.0
80	35.9	10.4	10.4	88.4	88.4	88.4	11.6
100	9.6	2.8	2.8	91.2	91.2	91.2	8.8
200	16.6	4.8	4.8	96.0	96.0	96.0	4.0
Pan	13.8	4.0	4.0	100.0	100.0	100.0	0.0
Total	345.3						

Sieve Size	Boring		SPK1		Sample		165
	Depth (m)	Soil Wt. (g)	14.63 - 15.09	15.54 - 16.00	Dry Wt. (g)	Accum.	
		Retained	% Retained	% Retained	% Retained	% Retained	% Finer
3/8	0.0	0.0	0.0	0.0	0.0	0.0	100.0
4	0.0	0.0	0.0	0.0	0.0	0.0	100.0
10	0.0	0.0	0.0	0.0	0.0	0.0	100.0
20	8.2	1.8	1.8	1.8	1.8	1.8	98.2
40	151.1	33.0	33.0	34.8	34.8	34.8	65.2
60	223.5	48.8	48.8	83.6	83.6	83.6	16.4
80	45.5	9.9	9.9	93.5	93.5	93.5	6.5
100	10.2	2.2	2.2	95.7	95.7	95.7	4.3
200	11.4	2.5	2.5	98.2	98.2	98.2	1.8
Pan	8.2	1.8	1.8	100.0	100.0	100.0	0.0
Total	458.1						

Sieve Size	Boring		SPK1		Sample		166
	Depth (m)	Soil Wt. (g)	15.09 - 15.54	16.00 - 16.46	Dry Wt. (g)	Accum.	
		Retained	% Retained	% Retained	% Retained	% Retained	% Finer
3/8	0.0	0.0	0.0	0.0	0.0	0.0	100.0
4	0.0	0.0	0.0	0.0	0.0	0.0	100.0
10	1.3	0.3	0.3	0.3	0.3	0.3	99.7
20	24.3	4.9	4.9	5.1	5.1	5.1	94.9
40	175.3	35.1	35.1	40.2	40.2	40.2	59.8
60	217.0	43.5	43.5	83.7	83.7	83.7	16.3
80	51.2	10.3	10.3	94.0	94.0	94.0	6.0
100	11.5	2.3	2.3	96.3	96.3	96.3	3.7
200	12.6	2.5	2.5	98.8	98.8	98.8	1.2
Pan	6.1	1.2	1.2	100.0	100.0	100.0	0.0
Total	499.3						

Sieve Size	Boring		SPK2		Sample		3
	Depth (m)	Soil Wt (g)	% Retained	% Retained	Dry Wt. (g)	Accum.	
3/4	0.0	0.0	0.0	0.0	0.0	0.0	263.4
3/8	0.0	0.0	0.0	0.0	0.0	0.0	100.0
4	1.9	1.9	0.7	0.7	0.7	0.7	99.3
10	5.0	5.0	1.9	1.9	2.6	2.6	97.4
20	33.4	33.4	12.7	12.7	15.3	15.3	84.7
40	114.7	43.6	43.6	43.6	58.9	58.9	41.1
60	65.1	24.7	83.6	83.6	83.6	83.6	16.4
100	23.0	8.7	92.4	92.4	92.4	92.4	7.6
200	11.7	4.4	96.8	96.8	96.8	96.8	3.2
Pan	8.4	3.2	100.0	100.0	100.0	100.0	0.0
Total	263.2						

Sieve Size	Boring		SPK2		Sample		6
	Depth (m)	Soil Wt. (g)	2.29 - 2.74	% Retained	Dry Wt. (g)	Accum. % Retained	
3/4	0.0	0.0	0.0	0.0	0.0	0.0	100.0
3/8	0.0	0.0	0.0	0.0	0.0	0.0	100.0
4	0.2	0.2	0.2	0.2	0.2	0.2	99.8
10	1.9	1.9	2.3	2.3	2.6	2.6	97.4
20	6.9	8.4	8.4	8.4	11.0	11.0	89.0
40	20.8	25.5	25.5	25.5	36.5	36.5	63.5
60	22.2	27.2	27.2	27.2	63.6	63.6	36.4
100	17.1	20.9	20.9	20.9	84.6	84.6	15.4
200	9.2	11.3	11.3	11.3	95.8	95.8	4.2
Pan	3.4	4.2	4.2	4.2	100.0	100.0	0.0
Total	81.7						

Sieve Size	Boring		SPK2		Sample		9
	Depth (m)	Soil Wt. (g)	% Retained	3.66 - 4.11	Dry Wt. (g)	Accum. % Retained	
3/4	0.0	0.0	0.0	0.0	0.0	0.0	100.0
3/8	0.0	0.0	0.0	0.0	0.0	0.0	100.0
4	1.0	0.2	0.2	0.2	0.2	0.2	99.8
10	1.8	0.4	0.4	0.7	0.7	0.7	99.3
20	2.8	0.7	0.7	1.3	1.3	1.3	98.7
40	33.5	8.1	8.1	9.4	9.4	9.4	90.6
60	195.0	46.9	46.9	56.3	56.3	56.3	43.7
100	143.4	34.5	34.5	90.8	90.8	90.8	9.2
200	32.1	7.7	7.7	98.6	98.6	98.6	1.4
Pan	6.0	1.4	1.4	100.0	100.0	100.0	0.0
Total	415.6						

Sieve Size	Boring		SPK2 0.46 - 0.91		Sample		2
	Depth (m)	Soil Wt. (g) Retained	% Retained	Dry Wt. (g) Accum.	% Retained	% Finer	
3/4		0.0	0.0	0.0	0.0	100.0	
3/8		4.4	1.6	1.6	1.6	98.4	
4		8.9	3.2	4.8	4.8	95.2	
10		9.3	3.4	8.2	8.2	91.8	
20		29.8	10.8	18.9	18.9	81.1	
40		76.5	27.6	46.5	46.5	53.5	
60			22.7	69.2	69.2	30.8	
100		48.3	17.4	86.6	86.6	13.4	
200		27.8	10.0	96.6	96.6	3.4	
Pan			3.4	100.0	100.0	0.0	
Total		277.1					

Sieve Size	Boring		SPK2		Sample		5
	Depth (m)	Soil Wt. (g)	% Retained	% Retained	Dry Wt. (g)	Accum. % Retained	
3/4	0.0	0.0	0.0	0.0	0.0	0.0	100.0
3/8	0.0	0.0	0.0	0.0	0.0	0.0	100.0
4	0.0	0.0	0.0	0.0	0.0	0.0	100.0
10	0.6	0.6	1.7	1.7	1.7	1.7	98.3
20	3.8	3.8	11.0	11.0	12.8	12.8	87.2
40	10.7	10.7	31.1	31.1	43.9	43.9	56.1
60	9.5	9.5	27.6	27.6	71.5	71.5	28.5
100	5.7	5.7	16.6	16.6	88.1	88.1	11.9
200	2.7	2.7	7.8	7.8	95.9	95.9	4.1
Pan	1.4	1.4	4.1	4.1	100.0	100.0	0.0
Total	34.4						

Sieve Size	Boring		SPK2		Sample		8
	Depth (m)	Soil Wt. (g)	% Retained	3.20 - 3.66	Dry Wt. (g)	Accum.	
3/4	0.0	0.0	0.0	0.0	0.0	0.0	100.0
3/8	0.0	0.0	0.0	0.0	0.0	0.0	100.0
4	1.7	0.4	0.4	0.4	0.4	0.4	99.6
10	8.6	2.0	2.0	2.0	2.4	2.4	97.6
20	15.6	3.6	3.6	3.6	6.0	6.0	94.0
40	42.6	9.9	9.9	9.9	16.0	16.0	84.0
60	92.9	21.7	21.7	21.7	37.7	37.7	62.3
100	92.6	21.6	21.6	21.6	59.3	59.3	40.7
200	157.9	36.8	36.8	36.8	96.1	96.1	3.9
Pan	16.6	3.9	3.9	3.9	100.0	100.0	0.0
Total	428.5						

Sieve Size	Boring		SPK2		Sample		1
	Depth (m)	Soil Wt. (g)	% Retained	% Retained	Dry Wt. (g)	Accum.	
3/4	0.0	0.0	0.0	0.0	0.0	0.0	299.9
3/8	0.0	0.0	0.0	0.0	0.0	0.0	100.0
4	2.7	0.9	0.9	0.9	0.9	0.9	99.1
10	9.7	3.2	3.2	4.1	4.1	4.1	95.9
20	23.9	8.0	8.0	12.1	12.1	12.1	87.9
40	85.7	28.6	28.6	40.7	40.7	40.7	59.3
60	105.0	35.0	35.0	75.7	75.7	75.7	24.3
100	42.3	14.1	14.1	89.8	89.8	89.8	10.2
200	18.3	6.1	6.1	95.9	95.9	95.9	4.1
Pan	12.3	4.1	4.1	100.0	100.0	100.0	0.0
Total	299.9						

Sieve Size	Boring		SPK2		Sample		4
	Depth (m)	Soil Wt. (g)	% Retained	% Retained	Dry Wt. (g)	Accum.	
3/4	0.0	0.0	0.0	0.0	0.0	0.0	100.0
3/8	0.0	0.0	0.0	0.0	0.0	0.0	100.0
4	0.6	0.6	1.9	1.9	1.9	1.9	98.1
10	0.5	0.5	1.6	1.6	3.4	3.4	96.6
20	2.7	2.7	8.4	8.4	11.8	11.8	88.2
40	9.1	9.1	28.3	28.3	40.2	40.2	59.8
60	9.7	9.7	30.2	30.2	70.4	70.4	29.6
100	5.4	5.4	16.8	16.8	87.2	87.2	12.8
200	2.6	2.6	8.1	8.1	95.3	95.3	4.7
Pan	1.5	1.5	4.7	4.7	100.0	100.0	0.0
Total	32.1	32.1					

Sieve Size	Boring		SPK2		Sample		7
	Depth (m)	Soil Wt. (g)	2.74 - 3.20	% Retained	Dry Wt. (g)	Accum.	
3/4	0.0	0.0	0.0	0.0	0.0	0.0	100.0
3/8	0.0	0.0	0.0	0.0	0.0	0.0	100.0
4	0.3	0.3	0.1	0.1	0.1	0.1	99.9
10	2.5	2.5	0.8	0.8	0.9	0.9	99.1
20	19.1	19.1	6.0	6.0	6.9	6.9	93.1
40	66.3	66.3	21.0	21.0	27.9	27.9	72.1
60	56.6	56.6	17.9	17.9	45.8	45.8	54.2
100	54.2	54.2	17.1	17.1	62.9	62.9	37.1
200	90.4	90.4	28.6	28.6	91.5	91.5	8.5
Pan	27.0	27.0	8.5	8.5	100.0	100.0	0.0



Sieve Size	Boring		SPK2		Sample		10	
	Depth (m)	Soil Wt. (g)	Depth (m)	Soil Wt. (g)	Dry Wt. (g)	Accum.	Dry Wt. (g)	396.5
	Retained	% Retained	Retained	% Retained	% Retained	% Retained	% Retained	% Finer
3/4	0.0	0.0	0.0	0.0	0.0	0.0	0.0	100.0
3/8	0.0	0.0	0.0	0.0	0.0	0.0	0.0	100.0
4	0.0	0.0	0.0	0.0	0.0	0.0	0.0	100.0
10	1.0	0.3	0.3	0.3	0.3	0.3	0.3	99.7
20	4.6	1.2	1.4	1.4	1.4	1.4	1.4	98.6
40	36.8	9.3	10.7	10.7	10.7	10.7	10.7	89.3
60	91.8	23.2	33.8	33.8	33.8	33.8	33.8	66.2
100	132.1	33.3	67.2	67.2	67.2	67.2	67.2	32.8
200	104.8	26.4	93.6	93.6	93.6	93.6	93.6	6.4
Pan	25.4	6.4	100.0	100.0	100.0	100.0	100.0	0.0
Total	396.5							

Sieve Size	Boring		SPK2		Sample		13	
	Depth (m)	Soil Wt. (g)	Depth (m)	Soil Wt. (g)	Dry Wt. (g)	Accum.	Dry Wt. (g)	405.9
	Retained	% Retained	Retained	% Retained	% Retained	% Retained	% Retained	% Finer
3/4	0.0	0.0	0.0	0.0	0.0	0.0	0.0	100.0
3/8	0.0	0.0	0.0	0.0	0.0	0.0	0.0	100.0
4	0.0	0.0	0.0	0.0	0.0	0.0	0.0	100.0
10	0.1	0.0	0.0	0.0	0.0	0.0	0.0	100.0
20	0.1	0.0	0.0	0.0	0.0	0.0	0.0	100.0
40	0.9	0.2	0.3	0.3	0.3	0.3	0.3	99.7
60	34.7	8.6	8.8	8.8	8.8	8.8	8.8	91.2
100	119.3	29.4	38.2	38.2	38.2	38.2	38.2	61.8
200	177.1	43.7	81.9	81.9	81.9	81.9	81.9	18.1
Pan	73.4	18.1	100.0	100.0	100.0	100.0	100.0	0.0
Total	405.6							

Sieve Size	Boring		SPK2		Sample		16	
	Depth (m)	Soil Wt. (g)	Depth (m)	Soil Wt. (g)	Dry Wt. (g)	Accum.	Dry Wt. (g)	358.5
	Retained	% Retained	Retained	% Retained	% Retained	% Retained	% Retained	% Finer
3/4	0.0	0.0	0.0	0.0	0.0	0.0	0.0	100.0
3/8	0.0	0.0	0.0	0.0	0.0	0.0	0.0	100.0
4	0.0	0.0	0.0	0.0	0.0	0.0	0.0	100.0
10	0.0	0.0	0.0	0.0	0.0	0.0	0.0	100.0
20	0.3	0.1	0.1	0.1	0.1	0.1	0.1	99.9
40	19.7	5.5	5.6	5.6	5.6	5.6	5.6	94.4
60	163.4	45.6	51.2	51.2	51.2	51.2	51.2	48.8
100	135.5	37.8	89.0	89.0	89.0	89.0	89.0	11.0
200	31.9	8.9	97.9	97.9	97.9	97.9	97.9	2.1
Pan	7.5	2.1	100.0	100.0	100.0	100.0	100.0	0.0
Total	358.3							

Sieve Size	Boring		SPK2		Sample		11	
	Depth (m)	Soil Wt. (g)	Depth (m)	Soil Wt. (g)	Dry Wt. (g)	Accum.	Dry Wt. (g)	427.0
	Retained	% Retained	Retained	% Retained	% Retained	% Retained	% Retained	% Finer
3/4	0.0	0.0	0.0	0.0	0.0	0.0	0.0	100.0
3/8	0.0	0.0	0.0	0.0	0.0	0.0	0.0	100.0
4	0.0	0.0	0.0	0.0	0.0	0.0	0.0	100.0
10	3.7	0.9	0.9	0.9	0.9	0.9	0.9	99.1
20	6.3	1.5	2.3	2.3	2.3	2.3	2.3	97.7
40	21.6	5.1	7.4	7.4	7.4	7.4	7.4	92.6
60	119.7	28.0	35.4	35.4	35.4	35.4	35.4	64.6
100	183.6	43.0	78.4	78.4	78.4	78.4	78.4	21.6
200	78.5	18.4	96.8	96.8	96.8	96.8	96.8	3.2
Pan	13.5	3.2	100.0	100.0	100.0	100.0	100.0	0.0
Total	426.9							

Sieve Size	Boring		SPK2		Sample		14	
	Depth (m)	Soil Wt. (g)	Depth (m)	Soil Wt. (g)	Dry Wt. (g)	Accum.	Dry Wt. (g)	359.7
	Retained	% Retained	Retained	% Retained	% Retained	% Retained	% Retained	% Finer
3/4	0.0	0.0	0.0	0.0	0.0	0.0	0.0	100.0
3/8	0.0	0.0	0.0	0.0	0.0	0.0	0.0	100.0
4	0.0	0.0	0.0	0.0	0.0	0.0	0.0	100.0
10	0.1	0.0	0.0	0.0	0.0	0.0	0.0	100.0
20	0.1	0.0	0.1	0.1	0.1	0.1	0.1	99.9
40	0.2	0.1	0.1	0.1	0.1	0.1	0.1	99.9
60	18.9	5.3	5.4	5.4	5.4	5.4	5.4	94.6
100	101.6	28.3	33.6	33.6	33.6	33.6	33.6	66.4
200	168.4	46.9	80.5	80.5	80.5	80.5	80.5	19.5
Pan	70.0	19.5	100.0	100.0	100.0	100.0	100.0	0.0
Total	359.3							

Sieve Size	Boring		SPK2		Sample		17	
	Depth (m)	Soil Wt. (g)	Depth (m)	Soil Wt. (g)	Dry Wt. (g)	Accum.	Dry Wt. (g)	379.1
	Retained	% Retained	Retained	% Retained	% Retained	% Retained	% Retained	% Finer
3/4	0.0	0.0	0.0	0.0	0.0	0.0	0.0	100.0
3/8	0.0	0.0	0.0	0.0	0.0	0.0	0.0	100.0
4	0.0	0.0	0.0	0.0	0.0	0.0	0.0	100.0
10	0.0	0.0	0.0	0.0	0.0	0.0	0.0	100.0
20	0.4	0.1	0.1	0.1	0.1	0.1	0.1	99.9
40	0.6	0.2	0.3	0.3	0.3	0.3	0.3	99.7
60	3.0	0.8	1.1	1.1	1.1	1.1	1.1	98.9
100	91.5	24.2	25.2	25.2	25.2	25.2	25.2	74.8
200	198.4	52.4	77.6	77.6	77.6	77.6	77.6	22.4
Pan	84.7	22.4	100.0	100.0	100.0	100.0	100.0	0.0
Total	378.6							

Sieve Size	Boring		SPK2		Sample		12	
	Depth (m)	Soil Wt. (g)	Depth (m)	Soil Wt. (g)	Dry Wt. (g)	Accum.	Dry Wt. (g)	402.2
	Retained	% Retained	Retained	% Retained	% Retained	% Retained	% Retained	% Finer
3/4	0.0	0.0	0.0	0.0	0.0	0.0	0.0	100.0
3/8	0.0	0.0	0.0	0.0	0.0	0.0	0.0	100.0
4	0.0	0.0	0.0	0.0	0.0	0.0	0.0	100.0
10	0.2	0.0	0.0	0.0	0.0	0.0	0.0	100.0
20	0.2	0.0	0.0	0.0	0.1	0.1	0.1	99.9
40	0.6	0.1	0.2	0.2	0.2	0.2	0.2	99.8
60	27.1	6.7	7.0	7.0	7.0	7.0	7.0	93.0
100	180.5	44.9	51.9	51.9	51.9	51.9	51.9	48.1
200	165.5	41.2	93.1	93.1	93.1	93.1	93.1	6.9
Pan	27.7	6.9	100.0	100.0	100.0	100.0	100.0	0.0
Total	401.8							

Sieve Size	Boring		SPK2		Sample		15	
	Depth (m)	Soil Wt. (g)	Depth (m)	Soil Wt. (g)	Dry Wt. (g)	Accum.	Dry Wt. (g)	380.1
	Retained	% Retained	Retained	% Retained	% Retained	% Retained	% Retained	% Finer
3/4	0.0	0.0	0.0	0.0	0.0	0.0	0.0	100.0
3/8	0.0	0.0	0.0	0.0	0.0	0.0	0.0	100.0
4	0.1	0.0	0.0	0.0	0.0	0.0	0.0	100.0
10	0.5	0.1	0.2	0.2	0.2	0.2	0.2	99.8
20	1.8	0.5	0.6	0.6	0.6	0.6	0.6	99.4
40	9.7	2.6	3.2	3.2	3.2	3.2	3.2	96.8
60	61.9	16.3	19.5	19.5	19.5	19.5	19.5	80.5
100	164.7	43.4	62.8	62.8	62.8	62.8	62.8	37.2
200	114.0	30.0	92.8	92.8	92.8	92.8	92.8	7.2
Pan	27.2	7.2	100.0	100.0	100.0	100.0	100.0	0.0
Total	379.9							

Sieve Size	Boring		SPK2		Sample		18	
	Depth (m)	Soil Wt. (g)	Depth (m)	Soil Wt. (g)	Dry Wt. (g)	Accum.	Dry Wt. (g)	412.4
	Retained	% Retained	Retained	% Retained	% Retained	% Retained	% Retained	% Finer
3/4	0.0	0.0	0.0	0.0	0.0	0.0	0.0	100.0
3/8	0.0	0.0	0.0	0.0	0.0	0.0	0.0	100.0
4	0.0	0.0	0.0	0.0	0.0	0.0	0.0	100.0
10	0.1	0.0	0.0	0.0	0.0	0.0	0.0	100.0
20	0.4	0.1	0.1	0.1	0.1	0.1	0.1	99.9
40	2.1	0.5	0.6	0.6	0.6	0.6	0.6	99.4
60	39.6	9.6	10.2	10.2	10.2	10.2	10.2	89.8
100	162.1	39.3	49.5	49.5	49.5	49.5	49.5	50.5
200	134.1	32.5	82.1	82.1	82.1	82.1	82.1	17.9
Pan	74.0	17.9	100.0	100.0	100.0	100.0	100.0	0.0
Total	412.4							



Sieve Size	Boring		SPK2		Sample	
	Depth (m)	Soil Wt. (g)	9.14 - 9.60	% Retained	Dry Wt. (g)	% Finer
3/4	0.0	0.0	0.0	0.0	0.0	100.0
3/8	0.0	0.0	0.0	0.0	0.0	100.0
4	0.0	0.0	0.0	0.0	0.0	100.0
10	0.0	0.4	0.1	0.1	0.1	99.9
20	1.0	1.0	0.2	0.2	0.3	99.7
40	1.5	1.5	3.1	3.1	3.4	96.6
60	155.4	32.2	32.2	32.2	35.6	64.4
100	186.4	38.6	38.6	38.6	74.2	25.8
200	91.6	19.0	19.0	19.0	93.2	6.8
Pan	32.8	6.8	6.8	6.8	100.0	0.0
Total	482.7					

Sieve Size	Boring		SPK2		Sample	
	Depth (m)	Soil Wt. (g)	10.52 - 10.97	% Retained	Dry Wt. (g)	% Finer
3/4	0.0	0.0	0.0	0.0	0.0	100.0
3/8	0.0	0.0	0.0	0.0	0.0	100.0
4	8.7	1.7	1.7	1.7	1.7	98.3
10	25.0	4.8	4.8	4.8	6.5	93.5
20	70.6	13.6	13.6	13.6	20.1	79.9
40	197.7	38.1	38.1	38.1	58.1	41.9
60	168.2	32.4	32.4	32.4	90.5	9.5
100	27.9	5.4	5.4	5.4	95.9	4.1
200	10.2	2.0	2.0	2.0	97.9	2.1
Pan	11.1	2.1	2.1	2.1	100.0	0.0
Total	519.4					

Sieve Size	Boring		SPK2		Sample	
	Depth (m)	Soil Wt. (g)	11.89 - 12.34	% Retained	Dry Wt. (g)	% Finer
3/4	0.0	0.0	0.0	0.0	0.0	100.0
3/8	0.0	0.0	0.0	0.0	0.0	100.0
4	0.0	0.0	0.0	0.0	0.0	100.0
10	0.4	0.1	0.1	0.1	0.1	99.9
20	8.1	1.5	1.5	1.5	1.6	98.4
40	238.6	44.7	44.7	44.7	46.3	53.7
60	230.6	43.2	43.2	43.2	89.6	10.4
100	44.7	8.4	8.4	8.4	98.0	2.0
200	9.0	1.7	1.7	1.7	99.6	0.4
Pan	1.9	0.4	0.4	0.4	100.0	0.0
Total	533.3					

Sieve Size	Boring		SPK2		Sample	
	Depth (m)	Soil Wt. (g)	8.69 - 9.14	% Retained	Dry Wt. (g)	% Finer
3/4	0.0	0.0	0.0	0.0	0.0	100.0
3/8	0.0	0.0	0.0	0.0	0.0	100.0
4	0.0	0.0	0.0	0.0	0.0	100.0
10	0.0	0.0	0.0	0.0	0.0	100.0
20	0.2	0.0	0.0	0.0	0.0	100.0
40	10.6	2.1	2.1	2.1	2.2	97.8
60	149.1	29.9	29.9	29.9	32.0	68.0
100	217.6	43.6	43.6	43.6	75.7	24.3
200	102.1	20.5	20.5	20.5	96.1	3.9
Pan	19.4	3.9	3.9	3.9	100.0	0.0
Total	499.0					

Sieve Size	Boring		SPK2		Sample	
	Depth (m)	Soil Wt. (g)	10.06 - 10.52	% Retained	Dry Wt. (g)	% Finer
3/4	0.0	0.0	0.0	0.0	0.0	100.0
3/8	0.0	0.0	0.0	0.0	0.0	100.0
4	0.0	0.0	0.0	0.0	0.0	100.0
10	0.1	0.0	0.0	0.0	0.0	100.0
20	8.4	2.1	2.1	2.1	2.1	97.9
40	169.7	41.8	41.8	41.8	43.9	56.1
60	183.2	45.1	45.1	45.1	89.0	11.0
100	31.1	7.7	7.7	7.7	96.6	3.4
200	7.6	1.9	1.9	1.9	98.5	1.5
Pan	6.1	1.5	1.5	1.5	100.0	0.0
Total	406.2					

Sieve Size	Boring		SPK2		Sample	
	Depth (m)	Soil Wt. (g)	11.43 - 11.89	% Retained	Dry Wt. (g)	% Finer
3/4	0.0	0.0	0.0	0.0	0.0	100.0
3/8	0.0	0.0	0.0	0.0	0.0	100.0
4	0.0	0.0	0.0	0.0	0.0	100.0
10	0.0	0.0	0.0	0.0	0.0	100.0
20	7.4	1.6	1.6	1.6	1.6	98.4
40	190.9	41.1	41.1	41.1	42.7	57.3
60	208.2	44.9	44.9	44.9	87.6	12.4
100	41.4	8.9	8.9	8.9	96.5	3.5
200	9.3	2.0	2.0	2.0	98.5	1.5
Pan	7.0	1.5	1.5	1.5	100.0	0.0
Total	464.2					

Sieve Size	Boring		SPK2		Sample	
	Depth (m)	Soil Wt. (g)	8.23 - 8.69	% Retained	Dry Wt. (g)	% Finer
3/4	0.0	0.0	0.0	0.0	0.0	100.0
3/8	0.0	0.0	0.0	0.0	0.0	100.0
4	0.0	0.0	0.0	0.0	0.0	100.0
10	0.0	0.0	0.0	0.0	0.0	100.0
20	0.1	0.0	0.0	0.0	0.0	100.0
40	0.4	0.1	0.1	0.1	0.1	99.9
60	27.2	5.8	5.8	5.8	5.9	94.1
100	150.6	32.2	32.2	32.2	38.2	61.8
200	230.4	49.3	49.3	49.3	87.5	12.5
Pan	58.6	12.5	12.5	12.5	100.0	0.0
Total	467.3					

Sieve Size	Boring		SPK2		Sample	
	Depth (m)	Soil Wt. (g)	9.60 - 10.06	% Retained	Dry Wt. (g)	% Finer
3/4	0.0	0.0	0.0	0.0	0.0	100.0
3/8	0.0	0.0	0.0	0.0	0.0	100.0
4	0.7	0.1	0.1	0.1	0.1	99.9
10	1.1	0.2	0.2	0.2	0.4	99.6
20	24.9	5.0	5.0	5.0	5.4	94.6
40	182.5	36.8	36.8	36.8	42.2	57.8
60	203.9	41.1	41.1	41.1	83.3	16.7
100	57.2	11.5	11.5	11.5	94.8	5.2
200	16.6	3.3	3.3	3.3	98.1	1.9
Pan	9.3	1.9	1.9	1.9	100.0	0.0
Total	496.2					

Sieve Size	Boring		SPK2		Sample	
	Depth (m)	Soil Wt. (g)	10.97 - 11.43	% Retained	Dry Wt. (g)	% Finer
3/4	0.0	0.0	0.0	0.0	0.0	100.0
3/8	0.0	0.0	0.0	0.0	0.0	100.0
4	0.0	0.0	0.0	0.0	0.0	100.0
10	0.0	0.0	0.0	0.0	0.0	100.0
20	4.2	0.9	0.9	0.9	0.9	99.1
40	138.1	28.0	28.0	28.0	28.9	71.1
60	273.3	55.4	55.4	55.4	84.3	15.7
100	60.2	12.2	12.2	12.2	96.5	3.5
200	10.5	2.1	2.1	2.1	98.6	1.4
Pan	6.8	1.4	1.4	1.4	100.0	0.0
Total	493.1					

		Boring	12-AY	Sample	1	
Sieve	Size	Depth (m)	Soil Wt. (g)	Dry Wt. (g)	Accum.	% Finer
		Retained	% Retained	% Retained	% Retained	% Finer
3/8	3/8	18.1	6.6	6.6	6.6	93.4
4	4	6.6	2.4	9.0	9.0	91.0
10	10	11.2	4.1	13.0	13.0	87.0
20	20	26.5	9.6	22.6	22.6	77.4
40	40	76.9	27.9	50.5	50.5	49.5
60	60	72.5	26.3	76.8	76.8	23.2
80	80	26.3	9.5	86.4	86.4	13.6
100	100	9.9	3.6	90.0	90.0	10.0
200	200	18.4	6.7	96.6	96.6	3.4
Pan	Pan	9.3	3.4	100.0	100.0	0.0
Total	Total	275.7				

		Boring	12-AY	Sample	4	
Sieve	Size	Depth (m)	Soil Wt. (g)	Dry Wt. (g)	Accum.	% Finer
		Retained	% Retained	% Retained	% Retained	% Finer
3/8	3/8	8.8	2.6	2.6	2.6	97.4
4	4	12.6	3.7	6.3	6.3	93.7
10	10	22.7	6.7	13.1	13.1	86.9
20	20	39.3	11.7	24.7	24.7	75.3
40	40	107.0	31.7	56.5	56.5	43.5
60	60	83.0	24.6	81.1	81.1	18.9
80	80	27.0	8.0	89.1	89.1	10.9
100	100	9.5	2.8	91.9	91.9	8.1
200	200	16.7	5.0	96.9	96.9	3.1
Pan	Pan	10.6	3.1	100.0	100.0	0.0
Total	Total	337.2				

		Boring	12-AY	Sample	7	
Sieve	Size	Depth (m)	Soil Wt. (g)	Dry Wt. (g)	Accum.	% Finer
		Retained	% Retained	% Retained	% Retained	% Finer
3/8	3/8	25.6	7.1	7.1	7.1	92.9
4	4	33.6	9.3	16.4	16.4	83.6
10	10	47.4	13.1	29.5	29.5	70.5
20	20	53.3	14.7	44.2	44.2	55.8
40	40	113.5	31.4	75.6	75.6	24.4
60	60	59.4	16.4	92.0	92.0	8.0
80	80	9.8	2.7	94.7	94.7	5.3
100	100	3.2	0.9	95.6	95.6	4.4
200	200	7.0	1.9	97.6	97.6	2.4
Pan	Pan	8.8	2.4	100.0	100.0	0.0
Total	Total	361.6				

		Boring	12-AY	Sample	2	
Sieve	Size	Depth (m)	Soil Wt. (g)	Dry Wt. (g)	Accum.	% Finer
		Retained	% Retained	% Retained	% Retained	% Finer
3/8	3/8	0.0	0.0	0.0	0.0	100.0
4	4	2.7	0.9	0.9	0.9	99.1
10	10	19.9	6.6	7.5	7.5	92.5
20	20	37.8	12.6	20.1	20.1	79.9
40	40	80.6	26.8	46.9	46.9	53.1
60	60	77.2	25.7	72.6	72.6	27.4
80	80	31.9	10.6	83.2	83.2	16.8
100	100	13.8	4.6	87.8	87.8	12.2
200	200	23.6	7.9	95.7	95.7	4.3
Pan	Pan	13.0	4.3	100.0	100.0	0.0
Total	Total	300.5				

		Boring	12-AY	Sample	5	
Sieve	Size	Depth (m)	Soil Wt. (g)	Dry Wt. (g)	Accum.	% Finer
		Retained	% Retained	% Retained	% Retained	% Finer
3/8	3/8	14.3	4.9	4.9	4.9	95.1
4	4	2.5	0.9	5.8	5.8	94.2
10	10	7.0	2.4	8.2	8.2	91.8
20	20	27.6	9.5	17.6	17.6	82.4
40	40	104.7	35.9	53.5	53.5	46.5
60	60	84.9	29.1	82.6	82.6	17.4
80	80	23.0	7.9	90.5	90.5	9.5
100	100	7.7	2.6	93.2	93.2	6.8
200	200	10.7	3.7	96.8	96.8	3.2
Pan	Pan	9.2	3.2	100.0	100.0	0.0
Total	Total	291.6				

		Boring	12-AY	Sample	8	
Sieve	Size	Depth (m)	Soil Wt. (g)	Dry Wt. (g)	Accum.	% Finer
		Retained	% Retained	% Retained	% Retained	% Finer
3/8	3/8	10.2	3.2	3.2	3.2	96.8
4	4	10.8	3.3	6.5	6.5	93.5
10	10	10.8	3.3	9.8	9.8	90.2
20	20	22.6	7.0	16.8	16.8	83.2
40	40	97.9	30.3	47.1	47.1	52.9
60	60	84.0	26.0	73.0	73.0	27.0
80	80	39.9	12.3	85.4	85.4	14.6
100	100	18.0	5.6	90.9	90.9	9.1
200	200	21.6	6.7	97.6	97.6	2.4
Pan	Pan	7.8	2.4	100.0	100.0	0.0
Total	Total	323.6				

		Boring	12-AY	Sample	3	
Sieve	Size	Depth (m)	Soil Wt. (g)	Dry Wt. (g)	Accum.	% Finer
		Retained	% Retained	% Retained	% Retained	% Finer
3/8	3/8	2.7	0.9	0.9	0.9	99.1
4	4	5.0	1.6	2.5	2.5	97.5
10	10	22.6	7.3	9.8	9.8	90.2
20	20	33.9	11.0	20.8	20.8	79.2
40	40	80.3	26.0	46.8	46.8	53.2
60	60	79.4	25.7	72.6	72.6	27.4
80	80	34.0	11.0	83.6	83.6	16.4
100	100	13.8	4.5	88.1	88.1	11.9
200	200	25.9	8.4	96.5	96.5	3.5
Pan	Pan	10.9	3.5	100.0	100.0	0.0
Total	Total	308.5				

		Boring	12-AY	Sample	6	
Sieve	Size	Depth (m)	Soil Wt. (g)	Dry Wt. (g)	Accum.	% Finer
		Retained	% Retained	% Retained	% Retained	% Finer
3/8	3/8	50.5	13.6	13.6	13.6	86.4
4	4	15.0	4.1	17.7	17.7	82.3
10	10	19.9	5.4	23.1	23.1	76.9
20	20	41.8	11.3	34.4	34.4	65.6
40	40	121.5	32.8	67.2	67.2	32.8
60	60	85.8	23.2	90.3	90.3	9.7
80	80	17.3	4.7	95.0	95.0	5.0
100	100	4.7	1.3	96.3	96.3	3.7
200	200	6.7	1.8	98.1	98.1	1.9
Pan	Pan	7.1	1.9	100.0	100.0	0.0
Total	Total	370.3				

		Boring	12-AY	Sample	9	
Sieve	Size	Depth (m)	Soil Wt. (g)	Dry Wt. (g)	Accum.	% Finer
		Retained	% Retained	% Retained	% Retained	% Finer
3/8	3/8	22.3	10.0	10.0	10.0	90.0
4	4	15.7	7.1	17.1	17.1	82.9
10	10	16.1	7.2	24.3	24.3	75.7
20	20	32.2	14.5	38.8	38.8	61.2
40	40	72.0	32.3	71.1	71.1	28.9
60	60	41.7	18.7	89.8	89.8	10.2
80	80	8.3	3.7	93.6	93.6	6.4
100	100	2.8	1.3	94.8	94.8	5.2
200	200	5.2	2.3	97.2	97.2	2.8
Pan	Pan	6.3	2.8	100.0	100.0	0.0
Total	Total	222.6				

Sieve Size	Boring		12-AY		Sample		10
	Depth (m)	Soil Wt. (g)	% Retained	% Retained	Dry Wt. (g)	Accum.	
3/8	62.4	80.3	19.7	19.7	19.7	0.0	316.8
4	6.6	2.1	21.8	21.8	21.8	0.0	78.2
10	3.9	1.2	23.0	23.0	23.0	0.0	77.0
20	2.8	0.9	23.9	23.9	23.9	0.0	76.1
40	20.0	6.3	30.2	30.2	30.2	0.0	69.8
60	88.5	27.9	58.1	58.1	58.1	0.0	41.9
80	57.9	18.3	76.4	76.4	76.4	0.0	23.6
100	23.7	7.5	83.9	83.9	83.9	0.0	16.1
200	35.2	11.1	95.0	95.0	95.0	0.0	5.0
Pan	15.8	5.0	100.0	100.0	100.0	0.0	0.0
Total	316.8						

Sieve Size	Boring		12-AY		Sample		13
	Depth (m)	Soil Wt. (g)	% Retained	% Retained	Dry Wt. (g)	Accum.	
3/8	0.0	0.0	0.0	0.0	0.0	0.0	226.2
4	0.0	0.0	0.0	0.0	0.0	0.0	100.0
10	1.6	0.7	0.7	0.7	0.7	0.0	99.3
20	23.6	10.4	11.1	11.1	11.1	0.0	88.9
40	82.1	36.3	47.4	47.4	47.4	0.0	52.6
60	69.3	30.6	78.1	78.1	78.1	0.0	21.9
80	21.6	9.5	87.6	87.6	87.6	0.0	12.4
100	7.6	3.4	91.0	91.0	91.0	0.0	9.0
200	11.1	4.9	95.9	95.9	95.9	0.0	4.1
Pan	9.3	4.1	100.0	100.0	100.0	0.0	0.0
Total	226.2						

Sieve Size	Boring		12-AY		Sample		16
	Depth (m)	Soil Wt. (g)	% Retained	% Retained	Dry Wt. (g)	Accum.	
3/8	0.0	0.0	0.0	0.0	0.0	0.0	314.4
4	1.0	0.3	0.3	0.3	0.3	0.0	99.7
10	1.5	0.5	0.8	0.8	0.8	0.0	99.2
20	12.4	3.9	4.7	4.7	4.7	0.0	95.3
40	92.4	29.4	34.1	34.1	34.1	0.0	65.9
60	130.7	41.6	75.7	75.7	75.7	0.0	24.3
80	42.5	13.5	89.2	89.2	89.2	0.0	10.8
100	12.7	4.0	93.3	93.3	93.3	0.0	6.7
200	14.8	4.7	98.0	98.0	98.0	0.0	2.0
Pan	6.4	2.0	100.0	100.0	100.0	0.0	0.0
Total	314.4						

Sieve Size	Boring		12-AY		Sample		11
	Depth (m)	Soil Wt. (g)	% Retained	% Retained	Dry Wt. (g)	Accum.	
3/8	0.0	0.0	0.0	0.0	0.0	0.0	353.5
4	0.0	0.0	0.0	0.0	0.0	0.0	100.0
10	0.4	0.1	0.1	0.1	0.1	0.0	99.9
20	3.9	1.1	1.2	1.2	1.2	0.0	98.8
40	109.8	31.1	32.3	32.3	32.3	0.0	67.7
60	153.7	43.5	75.8	75.8	75.8	0.0	24.2
80	46.7	13.2	89.0	89.0	89.0	0.0	11.0
100	15.4	4.4	93.3	93.3	93.3	0.0	6.7
200	17.5	5.0	98.3	98.3	98.3	0.0	1.7
Pan	6.1	1.7	100.0	100.0	100.0	0.0	0.0
Total	353.5						

Sieve Size	Boring		12-AY		Sample		14
	Depth (m)	Soil Wt. (g)	% Retained	% Retained	Dry Wt. (g)	Accum.	
3/8	0.0	0.0	0.0	0.0	0.0	0.0	365.7
4	0.9	0.2	0.2	0.2	0.2	0.0	99.8
10	9.7	2.7	2.9	2.9	2.9	0.0	97.1
20	61.3	16.8	19.7	19.7	19.7	0.0	80.3
40	146.3	40.0	59.7	59.7	59.7	0.0	40.3
60	92.0	25.2	84.8	84.8	84.8	0.0	15.2
80	27.6	7.5	92.4	92.4	92.4	0.0	7.6
100	8.5	2.3	94.7	94.7	94.7	0.0	5.3
200	12.9	3.5	98.2	98.2	98.2	0.0	1.8
Pan	6.5	1.8	100.0	100.0	100.0	0.0	0.0
Total	365.7						

Sieve Size	Boring		12-AY		Sample		17
	Depth (m)	Soil Wt. (g)	% Retained	% Retained	Dry Wt. (g)	Accum.	
3/8	0.0	0.0	0.0	0.0	0.0	0.0	243.9
4	0.0	0.0	0.0	0.0	0.0	0.0	100.0
10	0.3	0.1	0.1	0.1	0.1	0.0	99.9
20	4.0	1.6	1.8	1.8	1.8	0.0	98.2
40	53.4	21.9	23.7	23.7	23.7	0.0	76.3
60	97.8	40.1	63.8	63.8	63.8	0.0	36.2
80	34.4	14.1	77.9	77.9	77.9	0.0	22.1
100	12.2	5.0	82.9	82.9	82.9	0.0	17.1
200	27.2	11.2	94.0	94.0	94.0	0.0	6.0
Pan	14.6	6.0	100.0	100.0	100.0	0.0	0.0
Total	243.9						

Sieve Size	Boring		12-AY		Sample		12
	Depth (m)	Soil Wt. (g)	% Retained	% Retained	Dry Wt. (g)	Accum.	
3/8	0.0	0.0	0.0	0.0	0.0	0.0	260.0
4	0.0	0.0	0.0	0.0	0.0	0.0	100.0
10	0.6	0.2	0.2	0.2	0.2	0.0	99.8
20	22.5	8.7	8.9	8.9	8.9	0.0	91.1
40	105.6	40.6	49.5	49.5	49.5	0.0	50.5
60	84.1	32.3	81.8	81.8	81.8	0.0	18.2
80	22.5	8.7	90.5	90.5	90.5	0.0	9.5
100	7.2	2.8	93.3	93.3	93.3	0.0	6.7
200	10.1	3.9	97.2	97.2	97.2	0.0	2.8
Pan	7.4	2.8	100.0	100.0	100.0	0.0	0.0
Total	260.0						

Sieve Size	Boring		12-AY		Sample		15
	Depth (m)	Soil Wt. (g)	% Retained	% Retained	Dry Wt. (g)	Accum.	
3/8	0.0	0.0	0.0	0.0	0.0	0.0	268.8
4	0.2	0.1	0.1	0.1	0.1	0.0	99.9
10	1.9	0.7	0.8	0.8	0.8	0.0	99.2
20	18.2	6.8	7.6	7.6	7.6	0.0	92.4
40	98.8	36.8	44.3	44.3	44.3	0.0	55.7
60	90.8	33.8	78.1	78.1	78.1	0.0	21.9
80	28.1	10.5	88.5	88.5	88.5	0.0	11.5
100	8.4	3.1	91.7	91.7	91.7	0.0	8.3
200	13.7	5.1	96.8	96.8	96.8	0.0	3.2
Pan	8.7	3.2	100.0	100.0	100.0	0.0	0.0
Total	268.8						

Sieve Size	Boring		12-AY		Sample		18
	Depth (m)	Soil Wt. (g)	% Retained	% Retained	Dry Wt. (g)	Accum.	
3/8	0.0	0.0	0.0	0.0	0.0	0.0	299.5
4	0.0	0.0	0.0	0.0	0.0	0.0	100.0
10	0.4	0.1	0.1	0.1	0.1	0.0	99.9
20	2.6	0.9	1.0	1.0	1.0	0.0	99.0
40	15.8	5.3	6.3	6.3	6.3	0.0	93.7
60	37.2	12.4	18.7	18.7	18.7	0.0	81.3
80	33.5	11.2	29.9	29.9	29.9	0.0	70.1
100	24.8	8.3	38.2	38.2	38.2	0.0	61.8
200	105.1	35.1	73.3	73.3	73.3	0.0	26.7
Pan	80.1	26.7	100.0	100.0	100.0	0.0	0.0
Total	299.5						

Sieve Size	Boring		12-AY		Sample		19
	Depth (m)	Soil Wt. (g)	% Retained	% Retained	Dry Wt. (g)	Accum.	250.3
3/8	1.5	1.5	0.6	0.6	0.6	0.6	99.4
4	2.0	2.0	0.8	1.4	1.4	1.4	98.6
10	1.7	0.7	2.1	2.1	2.1	2.1	97.9
20	8.6	3.4	5.5	5.5	5.5	5.5	94.5
40	43.5	17.4	22.9	22.9	22.9	22.9	77.1
60	89.4	35.7	58.6	58.6	58.6	58.6	41.4
80	61.4	24.5	83.1	83.1	83.1	83.1	16.9
100	19.8	7.9	91.1	91.1	91.1	91.1	8.9
200	17.0	6.8	97.8	97.8	97.8	97.8	2.2
Pan	5.4	2.2	100.0	100.0	100.0	100.0	0.0
Total		250.3					

Sieve Size	Boring		12-AY		Sample		22
	Depth (m)	Soil Wt. (g)	% Retained	% Retained	Dry Wt. (g)	Accum.	306.1
3/8	0.0	0.0	0.0	0.0	0.0	0.0	100.0
4	0.0	0.0	0.0	0.0	0.0	0.0	100.0
10	0.0	0.0	0.0	0.0	0.0	0.0	100.0
20	0.0	0.0	0.0	0.0	0.0	0.0	100.0
40	0.4	0.1	0.1	0.1	0.1	0.1	99.9
60	20.0	6.5	6.7	6.7	6.7	6.7	93.3
80	60.7	19.8	26.5	26.5	26.5	26.5	73.5
100	51.3	16.8	43.3	43.3	43.3	43.3	56.7
200	139.4	45.5	88.8	88.8	88.8	88.8	11.2
Pan	34.3	11.2	100.0	100.0	100.0	100.0	0.0
Total		306.1					

Sieve Size	Boring		12-AY		Sample		25
	Depth (m)	Soil Wt. (g)	% Retained	% Retained	Dry Wt. (g)	Accum.	301.8
3/8	0.0	0.0	0.0	0.0	0.0	0.0	100.0
4	0.0	0.0	0.0	0.0	0.0	0.0	100.0
10	0.0	0.0	0.0	0.0	0.0	0.0	100.0
20	0.2	0.1	0.1	0.1	0.1	0.1	99.9
40	6.0	2.0	2.1	2.1	2.1	2.1	97.9
60	85.9	28.5	30.5	30.5	30.5	30.5	69.5
80	106.3	35.2	65.7	65.7	65.7	65.7	34.3
100	42.5	14.1	79.8	79.8	79.8	79.8	20.2
200	47.2	15.6	95.5	95.5	95.5	95.5	4.5
Pan	13.7	4.5	100.0	100.0	100.0	100.0	0.0
Total		301.8					

Sieve Size	Boring		12-AY		Sample		20
	Depth (m)	Soil Wt. (g)	% Retained	% Retained	Dry Wt. (g)	Accum.	326.8
3/8	0.0	0.0	0.0	0.0	0.0	0.0	100.0
4	0.0	0.0	0.0	0.0	0.0	0.0	100.0
10	0.2	0.1	0.1	0.1	0.1	0.1	99.9
20	1.5	0.5	0.5	0.5	0.5	0.5	99.5
40	7.1	2.2	2.7	2.7	2.7	2.7	97.3
60	35.1	10.7	13.4	13.4	13.4	13.4	86.6
80	79.9	24.4	37.9	37.9	37.9	37.9	62.1
100	58.7	18.0	55.8	55.8	55.8	55.8	44.2
200	120.3	36.8	92.7	92.7	92.7	92.7	7.3
Pan	24.0	7.3	100.0	100.0	100.0	100.0	0.0
Total		326.8					

Sieve Size	Boring		12-AY		Sample		23
	Depth (m)	Soil Wt. (g)	% Retained	% Retained	Dry Wt. (g)	Accum.	312.1
3/8	0.0	0.0	0.0	0.0	0.0	0.0	100.0
4	0.0	0.0	0.0	0.0	0.0	0.0	100.0
10	0.0	0.0	0.0	0.0	0.0	0.0	100.0
20	0.1	0.0	0.0	0.0	0.0	0.0	100.0
40	0.4	0.1	0.2	0.2	0.2	0.2	99.8
60	18.0	5.8	5.9	5.9	5.9	5.9	94.1
80	45.3	14.5	20.4	20.4	20.4	20.4	79.6
100	44.5	14.3	34.7	34.7	34.7	34.7	65.3
200	140.6	45.0	79.8	79.8	79.8	79.8	20.2
Pan	63.2	20.2	100.0	100.0	100.0	100.0	0.0
Total		312.1					

Sieve Size	Boring		12-AY		Sample		26
	Depth (m)	Soil Wt. (g)	% Retained	% Retained	Dry Wt. (g)	Accum.	308.8
3/8	0.0	0.0	0.0	0.0	0.0	0.0	100.0
4	0.0	0.0	0.0	0.0	0.0	0.0	100.0
10	0.0	0.0	0.0	0.0	0.0	0.0	100.0
20	0.4	0.1	0.1	0.1	0.1	0.1	99.9
40	11.5	3.7	3.9	3.9	3.9	3.9	96.1
60	71.3	23.1	26.9	26.9	26.9	26.9	73.1
80	75.0	24.3	51.2	51.2	51.2	51.2	48.8
100	43.1	14.0	65.2	65.2	65.2	65.2	34.8
200	79.0	25.6	90.8	90.8	90.8	90.8	9.2
Pan	28.5	9.2	100.0	100.0	100.0	100.0	0.0
Total		308.8					

Sieve Size	Boring		12-AY		Sample		21
	Depth (m)	Soil Wt. (g)	% Retained	% Retained	Dry Wt. (g)	Accum.	308.9
3/8	0.0	0.0	0.0	0.0	0.0	0.0	100.0
4	0.2	0.1	0.1	0.1	0.1	0.1	99.9
10	0.4	0.1	0.2	0.2	0.2	0.2	99.8
20	1.5	0.5	0.5	0.5	0.5	0.5	99.3
40	8.2	2.7	3.3	3.3	3.3	3.3	96.7
60	31.0	10.0	13.4	13.4	13.4	13.4	86.6
80	72.6	23.5	36.9	36.9	36.9	36.9	63.1
100	51.5	16.7	53.5	53.5	53.5	53.5	46.5
200	118.9	38.5	92.0	92.0	92.0	92.0	8.0
Pan	24.6	8.0	100.0	100.0	100.0	100.0	0.0
Total		308.9					

Sieve Size	Boring		12-AY		Sample		24
	Depth (m)	Soil Wt. (g)	% Retained	% Retained	Dry Wt. (g)	Accum.	328.6
3/8	0.0	0.0	0.0	0.0	0.0	0.0	100.0
4	0.0	0.0	0.0	0.0	0.0	0.0	100.0
10	0.0	0.0	0.0	0.0	0.0	0.0	100.0
20	0.0	0.0	0.0	0.0	0.0	0.0	100.0
40	0.8	0.2	0.2	0.2	0.2	0.2	99.8
60	27.0	8.2	8.5	8.5	8.5	8.5	91.5
80	103.4	31.5	39.9	39.9	39.9	39.9	60.1
100	64.8	19.7	59.6	59.6	59.6	59.6	40.4
200	109.5	33.3	93.0	93.0	93.0	93.0	7.0
Pan	23.1	7.0	100.0	100.0	100.0	100.0	0.0
Total		328.6					

Sieve Size	Boring		12-AY		Sample		27
	Depth (m)	Soil Wt. (g)	% Retained	% Retained	Dry Wt. (g)	Accum.	300.0
3/8	0.0	0.0	0.0	0.0	0.0	0.0	100.0
4	0.0	0.0	0.0	0.0	0.0	0.0	100.0
10	0.1	0.0	0.0	0.0	0.0	0.0	100.0
20	0.7	0.2	0.3	0.3	0.3	0.3	99.7
40	9.5	3.2	3.4	3.4	3.4	3.4	96.6
60	62.3	20.8	24.2	24.2	24.2	24.2	75.8
80	67.3	22.4	46.5	46.5	46.5	46.5	53.4
100	30.7	10.2	56.9	56.9	56.9	56.9	43.1
200	80.9	27.0	83.8	83.8	83.8	83.8	16.2
Pan	48.5	16.2	100.0	100.0	100.0	100.0	0.0
Total		300.0					

Sieve Size	Boring		12-AY		Sample		28
	Depth (m)	Soil Wt. (g)	% Retained	% Retained	Dry Wt. (g)	Accum.	
3/8	0.0	0.0	0.0	0.0	0.0	0.0	302.7
4	0.0	0.0	0.0	0.0	0.0	0.0	100.0
10	0.0	0.0	0.0	0.0	0.0	0.0	100.0
20	0.1	0.0	0.0	0.0	0.0	0.0	100.0
40	0.1	0.0	0.0	0.1	0.1	0.1	99.9
60	6.7	2.2	2.3	2.3	97.7		
80	40.3	13.3	15.6		84.4		
100	34.9	11.5	27.1		72.9		
200	128.7	42.5	69.6		30.4		
Pan	91.9	30.4	100.0		0.0		
Total	302.7						

Sieve Size	Boring		12-AY		Sample		31
	Depth (m)	Soil Wt. (g)	% Retained	% Retained	Dry Wt. (g)	Accum.	
3/8	0.0	0.0	0.0	0.0	0.0	0.0	100.0
4	0.0	0.0	0.0	0.0	0.0	0.0	100.0
10	0.0	0.0	0.0	0.0	0.0	0.0	100.0
20	0.0	0.0	0.0	0.0	0.0	0.0	100.0
40	5.3	1.7	1.7		98.3		
60	70.4	22.9	24.6		75.4		
80	95.3	31.0	55.6		44.4		
100	42.5	13.8	69.4		30.6		
200	77.7	25.3	94.6		5.4		
Pan	16.5	5.4	100.0		0.0		
Total	307.7						

Sieve Size	Boring		12-AY		Sample		34
	Depth (m)	Soil Wt. (g)	% Retained	% Retained	Dry Wt. (g)	Accum.	
3/8	0.0	0.0	0.0	0.0	0.0	0.0	324.1
4	0.0	0.0	0.0	0.0	0.0	0.0	100.0
10	0.4	0.1	0.1		99.9		
20	14.4	4.4	4.6		95.4		
40	144.8	44.7	49.2		50.8		
60	121.1	37.4	86.6		13.4		
80	22.5	6.9	93.6		6.4		
100	5.7	1.8	95.3		4.7		
200	7.2	2.2	97.5		2.5		
Pan	8.0	2.5	100.0		0.0		
Total	324.1						

Sieve Size	Boring		12-AY		Sample		29
	Depth (m)	Soil Wt. (g)	% Retained	% Retained	Dry Wt. (g)	Accum.	
3/8	0.0	0.0	0.0	0.0	0.0	0.0	329.9
4	0.0	0.0	0.0	0.0	0.0	0.0	100.0
10	0.0	0.0	0.0	0.0	0.0	0.0	100.0
20	0.2	0.1	0.1		99.9		
40	2.6	0.8	0.8		99.2		
60	19.3	5.9	6.7		93.3		
80	34.8	10.5	17.2		82.8		
100	33.4	10.1	27.4		72.6		
200	165.1	50.0	77.4		22.6		
Pan	74.5	22.6	100.0		0.0		
Total	329.9						

Sieve Size	Boring		12-AY		Sample		32
	Depth (m)	Soil Wt. (g)	% Retained	% Retained	Dry Wt. (g)	Accum.	
3/8	0.0	0.0	0.0	0.0	0.0	0.0	334.2
4	0.0	0.0	0.0	0.0	0.0	0.0	100.0
10	0.0	0.0	0.0	0.0	0.0	0.0	100.0
20	0.1	0.0	0.0	0.0	0.0	0.0	100.0
40	16.6	5.0	5.0		95.0		
60	118.5	35.5	40.5		59.5		
80	81.8	24.5	64.9		35.1		
100	29.6	8.9	73.8		26.2		
200	61.9	18.5	92.3		7.7		
Pan	25.7	7.7	100.0		0.0		
Total	334.2						

Sieve Size	Boring		12-AY		Sample		35
	Depth (m)	Soil Wt. (g)	% Retained	% Retained	Dry Wt. (g)	Accum.	
3/8	0.0	0.0	0.0	0.0	0.0	0.0	346.9
4	2.7	0.8	0.8		99.2		
10	5.5	1.6	2.4		97.6		
20	17.3	5.0	7.4		92.6		
40	137.1	39.5	46.9		53.1		
60	122.2	35.2	82.1		17.9		
80	28.3	8.2	90.3		9.7		
100	8.8	2.5	92.8		7.2		
200	14.4	4.2	96.9		3.1		
Pan	10.6	3.1	100.0		0.0		
Total	346.9						

Sieve Size	Boring		12-AY		Sample		30
	Depth (m)	Soil Wt. (g)	% Retained	% Retained	Dry Wt. (g)	Accum.	
3/8	0.0	0.0	0.0	0.0	0.0	0.0	328.9
4	0.0	0.0	0.0	0.0	0.0	0.0	100.0
10	0.0	0.0	0.0	0.0	0.0	0.0	100.0
20	0.2	0.1	0.1		99.9		
40	5.0	1.5	1.5		98.4		
60	45.0	13.7	15.3		84.7		
80	76.4	23.2	38.5		61.5		
100	50.8	15.4	53.9		46.1		
200	113.2	34.4	88.4		11.6		
Pan	38.3	11.6	100.0		0.0		
Total	328.9						

Sieve Size	Boring		12-AY		Sample		33
	Depth (m)	Soil Wt. (g)	% Retained	% Retained	Dry Wt. (g)	Accum.	
3/8	0.0	0.0	0.0	0.0	0.0	0.0	224.3
4	0.0	0.0	0.0	0.0	0.0	0.0	100.0
10	0.3	0.1	0.1		99.9		
20	13.2	5.9	6.0		94.0		
40	93.2	41.6	47.6		52.4		
60	85.7	38.2	85.8		14.2		
80	17.7	7.9	93.7		6.3		
100	4.7	2.1	95.8		4.2		
200	6.0	2.7	98.4		1.6		
Pan	3.5	1.6	100.0		0.0		
Total	224.3						

Sieve Size	Boring		12-AY		Sample		36
	Depth (m)	Soil Wt. (g)	% Retained	% Retained	Dry Wt. (g)	Accum.	
3/8	4.6	1.5	1.5		98.5		
4	11.8	3.7	5.2		94.8		
10	15.8	5.0	10.2		89.8		
20	23.6	7.5	17.6		82.4		
40	108.6	34.3	52.0		48.0		
60	116.2	36.7	88.7		11.3		
80	19.1	6.0	94.7		5.3		
100	3.5	1.1	95.8		4.2		
200	5.5	1.7	97.6		2.4		
Pan	7.7	2.4	100.0		0.0		
Total	316.4						



Sieve Size	Boring		12-AY		Sample		213
	Depth (m)	Soil Wt. (g) Retained	11.35		Dry Wt. (g)		
			% Retained	% Retained	Accum. % Retained	% Finer	
3/8	0.0	0.0	0.0	0.0	0.0	0.0	100.0
4	0.0	0.0	0.0	0.0	0.0	0.0	100.0
10	0.3	0.1	0.1	0.1	0.1	0.1	99.9
20	11.4	2.8	2.8	2.8	2.8	2.8	97.2
40	140.6	34.2	34.2	37.1	37.1	37.1	62.9
60	198.7	48.4	48.4	85.5	85.5	85.5	14.5
80	41.2	10.0	10.0	95.5	95.5	95.5	4.5
100	7.5	1.8	1.8	97.3	97.3	97.3	2.7
200	6.3	1.5	1.5	98.9	98.9	98.9	1.1
Pan	4.6	1.1	1.1	100.0	100.0	100.0	0.0
Total	410.6						

Sieve Size	Boring		12-AY		Sample		216
	Depth (m)	Soil Wt. (g) Retained	11.81	% Retained	Dry Wt. (g) Accum. % Retained	% Finer	
3/8		0.0		0.0		0.0	100.0
4		0.0		0.0		0.0	100.0
10		0.0		0.0		0.0	100.0
20		2.0		0.5		0.5	99.5
40		123.3		33.4		33.9	66.1
60		184.9		50.1		84.0	16.0
80		37.0		10.0		94.0	6.0
100		8.0		2.2		96.2	3.8
200		8.1		2.2		98.4	1.6
Pan		5.9		1.6		100.0	0.0
Total		369.2					

Sieve Size	Boring		12-AY		Sample		66
	Depth (m)	12.19	Dry Wt. (g)	66			
	Soil Wt. (g)	% Retained	Soil Wt. (g)	% Retained			
3/8	0.0	0.0	0.0	0.0	100.0		
4	0.0	0.0	0.0	0.0	100.0		
10	0.0	0.0	0.0	0.0	100.0		
20	1.7	1.1	1.1	1.1	98.9		
40	65.7	41.1	42.2	42.2	57.8		
60	73.5	46.0	88.2	88.2	11.8		
80	11.9	7.5	95.7	95.7	4.3		
100	2.2	1.4	97.1	97.1	2.9		
200	2.7	1.7	98.7	98.7	1.3		
Pan	2.0	1.3	100.0	100.0	0.0		
Total	159.7						

Sieve Size	Boring		12-AY		Sample		214
	Depth (m)	11.20	Dry Wt. (g)	Accum.	% Retained	% Finer	
	Soil Wt. (g) Retained	% Retained	% Retained	% Retained	% Retained	% Finer	
3/8	4.7	1.3	1.3	1.3	98.7	98.7	
4	0.7	0.2	1.5	1.5	98.5	98.5	
10	1.1	0.3	1.8	1.8	98.2	98.2	
20	9.6	2.6	4.3	4.3	95.7	95.7	
40	110.0	29.7	34.0	34.0	66.0	66.0	
60	180.4	48.7	82.7	82.7	17.3	17.3	
80	37.3	10.1	92.7	92.7	7.3	7.3	
100	7.0	1.9	94.6	94.6	5.4	5.4	
200	8.6	2.3	96.9	96.9	3.1	3.1	
Pan	11.4	3.1	100.0	100.0	0.0	0.0	
Total	370.8						

Sieve Size	Boring		12-AY		Sample		217
	Depth (m)		11.66		Dry Wt. (g)		
	Soil Wt. (g)	% Retained	Soil Wt. (g)	% Retained	Accum. % Retained	% Finer	
3/8	0.0	0.0	0.0	0.0	0.0	100.0	
4	0.2	0.1	0.1	0.1	0.1	99.9	
10	0.0	0.0	0.0	0.1	0.1	99.9	
20	3.1	1.0	1.0	1.0	1.0	99.0	
40	94.0	29.8	30.9	30.9	30.9	69.1	
60	148.7	47.2	78.0	78.0	78.0	22.0	
80	35.7	11.3	89.3	89.3	89.3	~ 10.7	
100	7.6	2.4	91.8	91.8	91.8	8.2	
200	10.9	3.5	95.2	95.2	95.2	4.8	
Pan	15.1	4.8	100.0	100.0	100.0	0.0	
Total	315.3						

Sieve Size	Boring		12-AY		Sample		67
	Depth (m)	12.07	Dry Wt. (g)	146.5			
	Soil Wt. (g)	% Retained	% Retained	% Finer			
3/8	0.0	0.0	0.0	100.0			
4	0.0	0.0	0.0	100.0			
10	0.0	0.0	0.0	100.0			
20	4.3	2.9	2.9	97.1			
40	65.9	45.0	47.9	52.1			
60	61.9	42.3	90.2	9.8			
80	10.0	6.8	97.0	3.0			
100	2.0	1.4	98.4	1.6			
200	1.7	1.2	99.5	0.5			
Pan	0.7	0.5	100.0	0.0			
Total	146.5						

Sieve Size	Boring		12-AY		Sample		215
	Depth (m)	11.05	Dry Wt. (g)	220.4			
	Soil Wt. (g)	% Retained	% Retained	% Finer			
3/8	0.0	0.0	0.0	100.0			
4	0.0	0.0	0.0	100.0			
10	2.7	1.2	1.2	98.8			
20	10.1	4.6	5.8	94.2			
40	71.1	32.3	38.1	61.9			
60	75.4	34.2	72.3	27.7			
80	24.0	10.9	83.2	16.8			
100	8.8	4.0	87.2	12.8			
200	18.0	8.2	95.3	4.7			
Pan	10.3	4.7	100.0	0.0			
Total	220.4						

Sieve Size	Boring		12-AY		Sample		218
	Depth (m)		11.51		Dry Wt. (g)		
	Soil Wt. (g)	% Retained	% Retained	% Retained	Accum.	% Retained	
3/8	0.0	0.0	0.0	0.0	0.0	0.0	100.0
4	0.0	0.0	0.0	0.0	0.0	0.0	100.0
10	0.5	0.1	0.1	0.1	0.1	0.1	99.9
20	9.6	2.8	2.8	2.9	2.9	97.1	97.1
40	94.2	27.2	27.2	30.1	30.1	69.9	69.9
60	164.2	47.4	47.4	77.5	77.5	22.5	22.5
80	44.4	12.8	12.8	90.4	90.4	9.6	9.6
100	10.3	3.0	3.0	93.3	93.3	6.7	6.7
200	13.1	3.8	3.8	97.1	97.1	2.9	2.9
Pan	10.0	2.9	2.9	100.0	100.0	0.0	0.0
Total	346.3						

Sieve Size	Boring		12-AY		Sample		68
	Depth (m)	Soil Wt. (g)	11.95		Dry Wt. (g)		
			% Retained	% Retained	Accum.	% Retained	
3/8	0.0	0.0	0.0	0.0	0.0	0.0	100.0
4	0.0	0.0	0.0	0.0	0.0	0.0	100.0
10	0.0	0.0	0.0	0.0	0.0	0.0	100.0
20	3.2	3.2	1.8	1.8	1.8	1.8	98.2
40	80.0	80.0	44.9	46.7	46.7	46.7	53.3
60	75.2	75.2	42.2	88.8	88.8	88.8	11.2
80	12.8	12.8	7.2	96.0	96.0	96.0	4.0
100	2.6	2.6	1.5	97.5	97.5	97.5	2.5
200	3.2	3.2	1.8	99.3	99.3	99.3	0.7
Pan	1.3	1.3	0.7	100.0	100.0	100.0	0.0
Total	178.3	178.3					

Sieve Size	Boring		12-AY		Sample		65
	Depth (m)	Soil Wt. (g) Retained	12.37		Dry Wt. (g) Accum.		
			% Retained	% Retained	% Retained		
3/8	0.0	0.0	0.0	0.0	0.0	100.0	
4	0.0	0.0	0.0	0.0	0.0	100.0	
10	0.0	0.0	0.0	0.0	0.0	100.0	
20	3.6	3.6	2.4	2.4	2.4	97.6	
40	62.8	41.6	41.6	44.0	44.0	56.0	
60	62.1	41.2	41.2	85.2	85.2	14.8	
80	11.2	7.4	7.4	92.6	92.6	7.4	
100	2.4	1.6	1.6	94.2	94.2	5.8	
200	4.6	3.0	3.0	97.2	97.2	2.8	
Pan	4.2	2.8	2.8	100.0	100.0	0.0	
Total	150.9						

Sieve Size	Boring		12-AY		Sample		70
	Depth (m)		12.77		Dry Wt. (g)		
	Soil Wt. (g)	Retained	% Retained	% Retained	Accum.	% Retained	
3/8	0.0	0.0	0.0	0.0	0.0	0.0	100.0
4	0.0	0.0	0.0	0.0	0.0	0.0	100.0
10	0.0	0.0	0.0	0.0	0.0	0.0	100.0
20	0.8	0.6	0.6	0.6	0.6	99.4	99.4
40	41.7	32.4	32.4	33.0	33.0	67.0	67.0
60	64.8	50.4	50.4	83.4	83.4	16.6	16.6
80	14.5	11.3	11.3	94.7	94.7	5.3	5.3
100	3.0	2.3	2.3	97.0	97.0	3.0	3.0
200	2.6	2.0	2.0	99.1	99.1	0.9	0.9
Pan	1.2	0.9	0.9	100.0	100.0	0.0	0.0
Total	128.6						

Sieve Size	Boring		12-AY		Sample		73
	Depth (m)		13.38		Dry Wt. (g)		
	Soil Wt. (g)	Retained	% Retained	% Retained	Accum.	% Retained	
3/8	0.0	0.0	0.0	0.0	0.0	0.0	100.0
4	0.0	0.0	0.0	0.0	0.0	0.0	100.0
10	0.0	0.0	0.0	0.0	0.0	0.0	100.0
20	0.4	0.5	0.5	0.5	0.5	99.5	99.5
40	20.7	27.1	27.1	27.7	27.7	72.3	72.3
60	40.3	52.8	52.8	80.5	80.5	19.5	19.5
80	10.3	13.5	13.5	94.0	94.0	6.0	6.0
100	1.9	2.5	2.5	96.5	96.5	3.5	3.5
200	2.0	2.6	2.6	99.1	99.1	0.9	0.9
Pan	0.7	0.9	0.9	100.0	100.0	0.0	0.0
Total	76.3						

Sieve Size	Boring		12-AY		Sample		64
	Depth (m)		12.44		Dry Wt. (g)		
	Soil Wt. (g)	Retained	% Retained	% Retained	Accum.	% Finer	
3/8	0.0	0.0	0.0	0.0	0.0	100.0	
4	0.0	0.0	0.0	0.0	0.0	100.0	
10	0.0	0.0	0.0	0.0	0.0	100.0	
20	2.4	3.3	3.3	3.3	96.7	96.7	
40	28.8	39.3	42.6	42.6	57.4	57.4	
60	30.7	41.9	84.6	84.6	15.4	15.4	
80	6.0	8.2	92.8	92.8	7.2	7.2	
100	1.5	2.0	94.8	94.8	5.2	5.2	
200	1.9	2.6	97.4	97.4	2.6	2.6	
Pan	1.9	2.6	100.0	100.0	0.0	0.0	
Total	73.2						

Sieve Size	Boring		12-AY		Sample		69
	Depth (m)		12.95		Dry Wt. (g)		
	Soil Wt. (g)	Retained	% Retained	% Retained	Accum.	% Finer	
3/8	0.0	0.0	0.0	0.0	0.0	100.0	
4	0.0	0.0	0.0	0.0	0.0	100.0	
10	0.0	0.0	0.0	0.0	0.0	100.0	
20	0.5	0.4	0.4	0.4	0.4	99.6	
40	41.0	29.4	29.7	29.7	70.3	70.3	
60	72.2	51.8	81.5	81.5	18.5	18.5	
80	16.4	11.8	93.3	93.3	6.7	6.7	
100	3.7	2.7	95.9	95.9	4.1	4.1	
200	3.3	2.4	98.3	98.3	1.7	1.7	
Pan	2.4	1.7	100.0	100.0	0.0	0.0	
Total	139.5						

Sieve Size	Boring		12-AY		Sample		72
	Depth (m)		13.56		Dry Wt. (g)		
	Soil Wt. (g)	Retained	% Retained	% Retained	Accum.	% Finer	
3/8	0.0	0.0	0.0	0.0	0.0	100.0	
4	0.0	0.0	0.0	0.0	0.0	100.0	
10	0.0	0.0	0.0	0.0	0.0	100.0	
20	0.6	0.7	0.7	0.7	99.3	99.3	
40	23.8	26.6	27.3	27.3	72.7	72.7	
60	46.0	51.5	78.7	78.7	21.3	21.3	
80	12.4	13.9	92.6	92.6	7.4	7.4	
100	2.4	2.7	95.3	95.3	4.7	4.7	
200	2.9	3.2	98.5	98.5	1.5	1.5	
Pan	1.3	1.5	100.0	100.0	0.0	0.0	
Total	89.4						

Sieve Size	Boring		12-AY		Sample		71
	Depth (m)		12.59		Dry Wt. (g)		
	Soil Wt. (g)	% Retained	% Retained	% Retained	Accum.	% Finer	
3/8	0.0	0.0	0.0	0.0	0.0	0.0	100.0
4	0.0	0.0	0.0	0.0	0.0	0.0	100.0
10	0.0	0.0	0.0	0.0	0.0	0.0	100.0
20	7.5	3.9	3.9	3.9	96.1	96.1	96.1
40	78.7	40.5	40.5	44.4	55.6	55.6	55.6
60	83.0	42.7	42.7	87.1	87.1	12.9	12.9
80	16.7	8.6	8.6	95.7	95.7	4.3	4.3
100	3.7	1.9	1.9	97.6	97.6	2.4	2.4
200	3.1	1.6	1.6	99.2	99.2	0.8	0.8
Pan	1.6	0.8	0.8	100.0	100.0	0.0	0.0
Total	194.3						

Sieve Size	Boring		12-AY		Sample		74
	Depth (m)		13.20		Dry Wt. (g)		
	Soil Wt. (g)	% Retained	% Retained	% Retained	Accum.	% Finer	
3/8	0.0	0.0	0.0	0.0	0.0	0.0	100.0
4	0.0	0.0	0.0	0.0	0.0	0.0	100.0
10	0.0	0.0	0.0	0.0	0.0	0.0	100.0
20	1.8	1.1	1.1	1.1	1.1	1.1	98.9
40	49.6	31.0	31.0	32.1	32.1	32.1	67.9
60	81.6	51.0	51.0	83.1	83.1	83.1	16.9
80	18.1	11.3	11.3	94.4	94.4	94.4	5.6
100	3.8	2.4	2.4	96.8	96.8	96.8	3.2
200	3.6	2.2	2.2	99.0	99.0	99.0	1.0
Pan	1.6	1.0	1.0	100.0	100.0	100.0	0.0
Total	160.1						

## **APPENDIX IV SOLID CORE SAMPLING ANALYSES**



Plattsburgh Solid Soil Core Data - October 9-13, 1995  
Separate Phase Analysis

Borehole ID	Depth Below Surface (in)	Sample ID	Area	Replicate Area	Mass of Wet Soil (kg)	Mass Moisture Mass Dry Soil (%)	TLV (ppm)	Conc of Sep Phase in Dry Soil (mg/kg)
12-AA	7.5	2	0		0.012	4.66	0	0
	14.5	1	0		0.012	7.45	0	0
	70.5	4	0		0.012	6.43	0	0
	130.5	5	0		0.011	5.41	0	0
	190.5	6	0		0.013	5.43	0	0
	250.5	7	0		0.011	10.98	0	0
	310.5	8	0		0.011	10.30	0	0
	370.5	9	0		0.014	2.68	0	0
	422.0	13	0		0.012	5.95	0	0
	427.0	12	0		0.014	3.86	20	0
	434.0	10	0	0	0.012	2.67	50	0
	434.0	11	0		0.013	2.86	50	0
	441.0	16	0		0.012	3.57	20	0
	447.0	15	0		0.012	3.60	20	0
	453.0	14	0		0.013	3.93	30	0
	459.0	19	0		0.012	4.62	100	0
	465.0	18	1305642		0.015	10.88	1400	6122
	471.0	17	4338019		0.017	14.15	4000	18369
	478.5	21	1550233		0.016	16.93	3800	7217
	478.5	22	1450785		0.013	16.77	3800	7843
	487.5	20	242953	619189	0.015	20.67	2800	1204
	494.5	25	783977		0.018	19.24	3100	3226
	500.5	24	1180143		0.012	18.80	4200	7589
	507.0	23	1522689		0.015	21.63	5200	7602
	514.5	27	615181		0.016	19.85	2600	2937
	523.5	26	390167		0.017	20.89	3400	1695
	532.0	29	182323		0.018	23.30	1400	797
	541.0	28	174523		0.016	21.07	1800	853
	555.0	30	60965	64073	0.019	21.37	820	260
	569.0	32	236495		0.016	19.48	600	1095
	569.0	33	127894		0.012	22.70	600	867
	578.0	31	16325		0.017	21.28	340	89
	586.5	35	0		0.012	23.29	60	0
	595.5	34	0		0.015	22.28	70	0
12-AB	424.0	37	0		0.013	2.29	0	0
	433.0	36	0		0.012	3.60	20	0
	484.0	39	38057		0.019	22.15	660	163
	493.0	38	295690		0.014	23.81	820	1593
	544.5	41	1108724		0.017	23.42	4400	5020
	553.5	40	82442	81577	0.017	24.70	1700	383

Plattsburgh Solid Soil Core Data - October 9-13, 1995  
Separate Phase Analysis

Borehole ID	Depth Below Surface (in)	Sample ID	Area	Replicate Area	Mass of Wet Soil (kg)	Mass Moisture Mass Dry Soil (%)	TLV (ppm)	Conc of Sep Phase in Dry Soil (mg/kg)
12-AD	4.5	43	0		0.012	5.93	0	0
	4.5	44	0		0.010	6.90	0	0
	13.5	42	0		0.015	6.86	30	0
	74.5	196	0		0.011	11.21	0	0
	134.5	46	0		0.014	2.46	10	0
	194.5	197	0		0.012	5.41	0	0
	252.5	48	0		0.014	5.86	0	0
	314.5	49	0		0.013	8.03	0	0
	374.5	50	0	0	0.012	2.35	0	0
	435.0	51	0		0.014	2.14	10	0
	442.5	53	2854		0.011	2.22	10	38
	458.0	57	9318		0.011	5.52	100	78
	463.5	56	467547		0.015	12.69	340	2154
	470.5	54	3746236		0.014	20.77	2600	19535
	470.5	55	3877073		0.017	20.87	2600	16679
	476.0	60	1074210	19769352	0.013	12.96	1600	5795
	481.5	59	2169205		0.017	14.03	4000	9333
	488.5	58	2586528		0.017	19.69	3400	11423
	501.0	61	1997565		0.016	23.14	3000	9580
	514.0	64	0		0.014	17.92	120	0
	522.0	63	0		0.015	21.00	60	0
	530.0	62	0		0.018	20.34	120	0
	541.0	67	0		0.017	22.21	40	0
	553.0	65	3941		0.018	17.92	40	32
	553.0	66	0		0.013	20.77	40	0
12-AG	2.0	70	0	0	0.009	4.73	50	0
	7.5	69	0		0.015	5.99	50	0
	14.5	68	0		0.014	7.40	40	0
	75.0	71	0		0.013	5.98	60	0
	134.5	72	0		0.014	3.70	40	0
	194.5	73	0		0.013	7.54	50	0
	252.5	74	0		0.013	4.03	60	0
	315.0	75	0		0.013	5.55	50	0
	375.0	76	0		0.012	1.05	50	0
	375.0	77	0		0.014	1.18	50	0
	435.0	78	0		0.013	2.75	50	0
	440.0	81	0		0.014	5.34	40	0
	445.5	80	0	0	0.014	2.54	50	0
	452.5	79	0		0.012	2.65	50	0
	463.5	83	4237		0.012	4.11	80	42
	470.5	82	374789		0.016	14.66	520	1716
	477.0	88	2006547		0.018	15.58	2900	8243
	477.0	87	1756838		0.016	15.27	2900	7701
	483.0	86	2276692		0.014	18.51	5800	12226
	489.0	85	2199815		0.016	20.90	4600	10184
	494.5	91	2544488		0.017	18.64	5600	11092
	501.0	90	4051521	3562875	0.018	19.91	5400	16364
	507.5	89	2572653		0.017	22.41	4700	11444
	508.0	84	0		0.013	3.42	60	0
	522.0	92	10439		0.018	23.46	270	62
	539.0	94	0		0.014	19.38	50	0
	551.0	93	0		0.016	18.94	90	0

Plattsburgh Solid Soil Core Data - October 9-13, 1995  
Separate Phase Analysis

Borehole ID	Depth Below Surface (in)	Sample ID	Area	Replicate Area	Mass of Wet Soil (kg)	Mass Moisture Mass Dry Soil (%)	TLV (ppm)	Conc of Sep Phase in Dry Soil (mg/kg)
12-AK	3.0	199	0		0.007	6.39	0	0
	9.0	198	0		0.013	4.35	0	0
	15.0	95	0		0.014	5.60	20	0
	27.0	98	0		0.015	5.27	20	0
	74.5	99	0		0.012	8.68	40	0
	74.5	100	0	0	0.017	6.13	40	0
	134.5	101	0		0.017	6.53	40	0
	194.0	102	0		0.013	1.40	0	0
	253.0	103	0		0.014	8.18	0	0
	309.0	104	0		0.013	2.03	70	0
	375.0	105	0		0.013	4.26	60	0
	435.0	106	1433		0.011	1.33	270	30
	442.5	108	483935		0.014	1.82	800	2230
	451.5	107	598974		0.012	1.86	660	3212
	461.5	110	387540	411463	0.014	2.69	1100	1796
	470.5	109	191709		0.015	11.10	1200	882
	477.0	114	1538525		0.016	16.74	3400	7083
	483.0	112	3076818		0.016	18.10	5000	14186
	483.0	113	2982004		0.018	18.64	5000	12191
	489.0	111	1546875		0.016	22.94	5500	7337
	495.0	118	1859796		0.018	22.46	4800	7933
	501.0	117	2718315		0.018	11.85	3400	10467
	507.0	116	40996		0.015	21.01	560	223
	513.0	115	6743		0.015	21.70	500	52
	519.0	122	9903		0.017	20.69	320	59
	525.0	121	0		0.018	20.65	110	0
	531.0	120	0	0	0.016	20.73	140	0
	537.0	119	0		0.017	22.83	220	0
	544.0	126	0		0.014	18.77	120	0
	552.0	125	0		0.017	19.99	60	0
	560.0	123	0		0.017	22.40	80	0
	560.0	124	0		0.017	22.54	80	0
12-AM	422.0	129	0		0.013	2.03	10	0
	427.5	128	0		0.011	2.54	10	0
	434.5	127	0		0.013	1.74	20	0
	442.0	132	0		0.015	2.58	20	0
	448.5	131	0		0.014	2.91	20	0
	453.5	130	0	0	0.014	3.46	20	0
	458.0	136	28943		0.013	5.02	190	161
	464.0	134	353042		0.016	9.68	930	1498
	464.0	135	380821		0.016	13.05	930	1689
	471.0	133	3755490		0.016	16.52	3000	16795
	477.0	139	837336		0.016	15.13	3600	3683
	483.0	138	2572739		0.018	16.59	4600	10651
	489.0	137	2266576		0.016	20.30	3600	10434
	496.0	142	1555272		0.016	20.74	5400	7529
	504.0	141	2937909		0.016	19.07	5800	13615
	512.0	140	275492	392204	0.017	20.08	2200	1253
	520.0	145	755908		0.016	20.85	2200	3463
	520.0	146	166516		0.007	22.57	2200	1780
	528.0	144	2839		0.017	20.27	320	29
	536.0	143	0		0.016	21.27	120	0
	546.0	148	2048		0.014	22.60	70	33
	558.0	147	0		0.016	20.88	10	0

Plattsburgh Solid Soil Core Data - October 9-13, 1995  
Separate Phase Analysis

Borehole ID	Depth Below Surface (in)	Sample ID	Area	Replicate Area	Mass of Wet Soil (kg)	Mass Moisture Mass Dry Soil (%)	TLV (ppm)	Conc of Sep Phase in Dry Soil (mg/kg)
Control	15.0	200	0	0	0.010	2.74	0	0
	75.0	202	0		0.014	7.46	0	0
	75.0	151	0		0.012	6.89	0	0
	134.5	203	0		0.013	5.17	0	0
	194.5	204	0		0.012	3.47	0	0
	252.5	154	0		0.013	1.22	0	0
	309.0	155	0		0.013	15.27	10	0
	322.5	157	0		0.011	22.90	10	0
	331.5	156	0		0.016	20.28	0	0
12-AR	422.0	160	0	0	0.012	2.14	30	0
	427.5	159	0		0.010	2.05	40	0
	434.5	158	0		0.013	2.60	40	0
	440.0	164	0		0.012	2.82	280	0
	445.5	163	46308		0.013	7.66	600	250
	452.5	162	826529		0.011	15.79	1900	5648
	452.5	161	618958		0.014	16.06	1900	3168
	459.0	167	626508		0.012	10.11	4000	3699
	465.0	166	2453906		0.018	19.53	6000	10427
	471.0	165	2137463		0.016	19.40	5200	9672
	477.0	170	3375813	3082126	0.017	18.03	5200	14864
	483.0	169	1740299		0.017	18.17	4900	7571
	489.0	168	2226897		0.018	19.32	4700	9330
	496.0	174	805140		0.015	17.81	4200	3834
	504.0	172	19664		0.015	14.45	380	109
	504.0	173	5877		0.014	13.51	380	47
	512.0	171	1574		0.014	19.86	280	28
	522.0	176	15375		0.014	18.33	1000	99
	528.0	175	2199		0.015	21.34	100	29
	546.0	178	0		0.015	19.45	800	0
	558.0	177	0		0.016	21.50	60	0

Plattsburgh Solid Soil Core Data - October 9-13, 1995  
Separate Phase Analysis

Borehole ID	Depth Below	Sample ID	Area	Replicate Area	Mass of Wet Soil (kg)	Mass Moisture	TLV (ppm)	Conc of Sep
	Surface (in)					Mass Dry Soil (%)		Phase in Dry Soil (mg/kg)
12-A_P	423.0	181	0	0	0.011	4.46	100	0
	428.5	180	0		0.013	2.10	60	0
	434.5	179	0		0.013	2.26	100	0
	440.0	185	0		0.011	3.59	50	0
	446.0	183	0		0.014	2.26	100	0
	453.0	182	0		0.011	3.00	180	0
	459.0	188	0		0.012	4.19	420	0
	471.0	184	0		0.015	2.95	100	0
	477.0	191	1461446	2676938	0.015	16.19	6400	7121
	480.0	186	2302759		0.017	17.04	4400	9750
	483.0	190	2574952		0.015	16.93	5300	12131
	483.0	187	654569		0.015	13.70	1500	3102
	489.0	189	2135038		0.017	21.05	5400	9345
	498.0	193	112929		0.007	18.29	3600	1168
	510.0	192	5749		0.014	17.28	460	48
	522.0	195	11913		0.012	16.72	1600	98
	534.0	194	0		0.011	17.99	220	0
Field Spikes								
12-AD	74.5	45	698788					
12-AD	194.5	47	1552176					
12-AK	9.0	96	2660374					
12-AK	3.0	97	2142122					
Control	15.0	149	758642					
Control	75.0	150	1298716					
Control	134.5	152	2188391					
Control	194.5	153	2631153					

Plattsburgh Solid Soil Core Data - Nov. 30 - Dec. 2, 1995  
Separate Phase Analysis

Borehole ID	Depth Below Surface (in)	Sample ID	Area	Replicate Area	Mass of Wet Soil (kg)	Mass Moisture Mass Dry Soil (%)	TLV (ppm)	Conc of Sep Phase in Dry Soil (mg/kg)
VENT 1	420.5	10	0	0	0.013	5.16	10	0
	420.5	11	0		0.013	4.81	10	0
	421.5	9	0		0.011	7.59	0	0
	423	8	0		0.012	2.97	10	0
	425	7	0		0.012	3.20	0	0
	427	6	0		0.014	3.40	0	0
	429	5	0		0.012	2.62	0	0
	431	4	0		0.010	2.93	0	0
	433	3	0		0.010	2.70	0	0
	435	2	0		0.016	2.73	0	0
	437	1	0		0.013	2.56	0	0
	438.5	23	0		0.011	3.80	0	0
	439.5	22	0		0.014	3.15	0	0
	439.5	21	0		0.013	3.17	0	0
	440.5	20	0	0	0.014	2.81	10	0
	441.5	19	0		0.014	2.77	0	0
	443	18	0		0.014	2.65	10	0
	445	17	0		0.014	2.65	0	0
	447	16	0		0.014	2.52	10	0
	449	15	0		0.010	2.66	0	0
	451	14	0		0.011	3.03	0	0
	453	13	0		0.014	2.97	0	0
	455	12	0		0.010	3.32	20	0
	457	32	0		0.012	3.56	10	0
	457	33	0		0.011	3.19	10	0
	459	31	0		0.012	1.62	10	0
	461	30	0	0	0.014	2.44	10	0
	463	29	0		0.016	3.25	0	0
	465	28	0		0.008	2.64	0	0
	467	27	0		0.013	7.13	0	0
	469	26	0		0.015	11.28	10	0
	471	25	0		0.013	13.87	10	0
	473	24	11592		0.014	14.79	10	165
	475	41	0		0.012	18.71	30	0
	477.5	40	0	0	0.016	17.90	60	0
	480	39	0		0.017	19.52	100	0
	482	38	59997		0.018	18.65	3400	345
	484	37	2414821		0.013	19.02	2900	14184
	486	36	5054119		0.031	20.55	2800	12895
	488	35	3378201		0.018	21.23	2600	15166
	490.5	34	2991441		0.015	20.50	2200	15613
	493	49	9943		0.019	19.79	70	120
	498	48	46106		0.014	18.70	900	374
	500	47	2321683		0.019	18.49	1800	9714
	502	46	1800893		0.018	19.95	2700	7738
	504	45	3404974		0.018	20.11	2700	14496
	506	43	3190930		0.019	19.94	2500	13262
	506	44	2226882		0.017	19.84	2500	10219
	508.5	42	2367055		0.017	22.00	3200	10944

Plattsburgh Solid Soil Core Data - Nov. 30 - Dec. 2, 1995  
 Separate Phase Analysis

Borehole ID	Depth Below Surface (in)	Sample ID	Area	Replicate Area	Mass of Wet Soil (kg)	Mass Moisture Mass Dry Soil (%)	TLV (ppm)	Conc of Sep Phase in Dry Soil (mg/kg)
VENT 2	422	276	0	0	0.013	10.69	0	0
	427.5	275	0		0.013	5.82	0	0
	434.5	50	0		0.011	3.25	0	0
	440	56	0		0.013	10.02	0	0
	445.5	55	0		0.014	5.37	0	0
	452.5	53	0		0.014	3.51	0	0
	452.5	54	0		0.013	3.51	0	0
	457	65	0		0.015	5.92	0	0
	457	64	0		0.013	6.30	0	0
	459.5	63	0		0.012	4.02	0	0
	462	62	0		0.012	4.06	0	0
	464	61	0		0.009	4.31	0	0
	466	60	321411	171744	0.016	16.32	80	1611
	468	59	605845		0.015	18.64	900	3193
	470	58	2374633		0.017	18.40	1000	10811
	472.5	57	2348668		0.018	18.25	1800	10352
	475	74	6288		0.013	11.89	80	147
	477	73	0	2423035	0.017	14.11	80	0
	479	72	0		0.017	16.52	80	0
	481	71	547965		0.017	17.39	200	2554
	483	70	2975112		0.018	17.48	2200	12823
	485	69	1552542		0.016	17.00	1800	7550
	487	68	96366		0.016	20.06	1800	551
	489	67	22379		0.015	20.88	300	220
	491	66	27730		0.018	20.60	800	206
	496	78	326369		0.018	22.86	800	1505
	504	77	1836054		0.018	21.77	2000	8362
	512	75	26420		0.016	22.79	200	225
	512	76	25673		0.019	22.84	200	195

Plattsburgh Solid Soil Core Data - Nov. 30 - Dec. 2, 1995  
Separate Phase Analysis

Borehole ID	Depth Below Surface (in)	Sample ID	Area	Replicate Area	Mass of Wet Soil (kg)	Mass Moisture Mass Dry Soil (%)	TLV (ppm)	Conc of Sep Phase In Dry Soil (mg/kg)
SPARGE 1	421	86	0		0.013	7.44	0	0
	423.5	85	0		0.014	7.67	0	0
	426	84	0		0.014	3.61	0	0
	428	278	0		0.010	4.91	0	0
	430	277	0		0.011	2.63	0	0
	432	81	0		0.014	2.65	0	0
	434	80	0	0	0.013	3.03	0	0
	436.5	79	0		0.013	2.23	0	0
	438.5	97	0		0.010	10.71	0	0
	439.5	96	0		0.015	9.82	0	0
	441	95	0		0.015	7.40	0	0
	443	94	0		0.013	5.92	0	0
	445	93	0		0.015	4.61	0	0
	447	92	0		0.013	3.02	0	0
	449	91	0		0.014	2.84	0	0
	451	90	0	0	0.014	3.01	0	0
	453	89	0		0.013	3.69	0	0
	453	88	0		0.014	3.70	0	0
	455	87	0		0.015	3.43	0	0
	457	107	0		0.014	9.77	0	0
	459	106	0		0.015	6.94	0	0
	461	105	0		0.014	4.66	0	0
	463	104	0		0.015	2.89	20	0
	465	103	11044		0.015	6.44	20	144
	467	102	518556		0.017	17.04	60	2459
	469	101	243701		0.017	17.56	100	1191
	471	100	278967	252516	0.016	18.68	1000	1425
	471	99	275022		0.017	18.24	1000	1358
	473	98	2168262		0.018	18.15	2000	9464
	475	117	0		0.014	10.12	60	0
	477	116	0		0.019	14.24	120	0
	479	115	0		0.017	18.04	100	0
	481	114	7188		0.016	19.05	240	127
	483	113	453374		0.017	17.50	1200	2112
	485	112	2836379		0.020	19.25	3800	11213
	487	111	465789		0.017	20.73	2800	2210
	487	110	718797	735451	0.017	22.62	2800	3475
	489	109	959133		0.016	21.06	1700	4712
	491	108	1634453		0.019	21.47	1800	6829
	493	125	51125		0.023	21.88	120	242
	495	124	71574		0.018	20.07	190	395
	497	122	70085		0.017	19.94	400	401
	497	123	149420		0.017	19.10	400	770
	499.5	121	1436937		0.017	20.00	620	6713
	502.5	120	2604494	2791875	0.018	21.13	1500	11431
	505.5	119	3255408		0.017	21.94	2200	15623
	508.5	118	2332817		0.019	21.86	2400	10032
	511.5	130	72387	31135	0.017	19.71	0	422
	514.5	129	92864		0.018	18.53	30	473
	518	128	90162		0.018	18.51	30	466
	522	127	113198		0.018	21.03	120	572
	526	126	0		0.017	22.38	20	0
	530	135	46892		0.016	20.06	0	334
	534	134	10899		0.015	18.34	0	155
	538.5	133	46430		0.018	18.29	0	275
	538.5	132	31359		0.017	78.87	0	340
	543.5	131	140536		0.017	21.02	80	722
	547.5	141	33794		0.013	25.02	10	329
	550.5	140	24249	22559	0.017	18.28	90	194
	553.5	139	26031		0.016	18.09	60	214
	556.5	138	87594		0.018	20.91	150	463
	559.5	137	23128		0.013	21.77	20	265
	562.5	136	1498		0.019	23.79	0	89
	566	147	47928		0.016	19.65	280	322
	566	148	15169		0.016	19.55	280	166
	570	146	151189		0.015	18.15	340	880
	574	145	186173		0.017	20.10	180	953
	578	144	23253		0.011	23.12	280	310
	582	143	3178		0.019	31.93	180	102
	586	142	0		0.014	31.93	20	0



Plattsburgh Solid Soil Core Data - Nov. 30 - Dec. 2, 1995  
Separate Phase Analysis

Borehole ID	Depth Below Surface (in)	Sample ID	Area	Replicate Area	Mass of Wet Soil (kg)	Mass Moisture Mass Dry Soil (%)	TLV (ppm)	Conc of Sep Phase In Dry Soil (mg/kg)
12-AS	421.5	282	0		0.018	14.99	0	0
	427	281	0		0.015	7.01	0	0
	429	213	0		0.014	2.08	0	0
	431	280	0	0	0.012	2.20	0	0
	433	211	0		0.013	2.29	0	0
	435	279	0		0.011	2.65	0	0
	437	209	0		0.014	3.13	0	0
	439	225	0		0.016	7.71	0	0
	441	224	0		0.014	3.25	0	0
	443	223	0		0.015	6.40	10	0
	445	222	0		0.014	3.14	0	0
	447	221	0		0.013	2.64	20	0
	449	220	0	0	0.011	2.77	30	0
	451.5	218	102594		0.014	7.98	100	602
	454.5	217	244410		0.014	14.58	100	1420
	457	235	0		0.017	6.22	40	0
	459	234	0		0.016	6.04	60	0
	461	233	174407		0.018	15.70	120	824
	463	232	361357		0.017	18.22	240	1703
	465	230	250611	236535	0.017	19.64	300	1220
	465	231	308302		0.016	18.26	300	1618
	467	229	2114501		0.016	17.84	1400	10284
	469	228	5920009		0.017	18.10	2600	26335
	471	227	3851366		0.017	19.67	2200	17593
	473	226	3050885		0.017	17.98	2000	14021
	475	245	3387306		0.018	17.77	2800	14241
	477	244	1130388		0.018	15.15	2200	4917
	479	243	1257685		0.017	14.55	1800	5586
	481	241	3385903		0.016	15.86	3200	15796
	481	242	2527829		0.017	15.76	3200	11226
	483	240	2851620	3168876	0.018	17.64	2000	12536
	485	239	2596824		0.017	19.79	2600	12087
	487	238	2235215		0.017	20.63	3200	10514
	489	237	3351756		0.018	22.16	3000	15078
	491	236	2433956		0.018	23.69	3200	11086
	493	254	849273		0.017	21.32	2200	4032
	495.5	253	929003		0.017	18.83	1500	4311
	495.5	252	1313418		0.018	19.91	1500	5689
	498	251	895440		0.012	19.15	2600	5739
	500	250	1498019	1198899	0.015	19.98	4000	7697
	502	249	2708365		0.018	20.64	2600	12228
	504	248	947555		0.017	21.99	1600	4414
	506	247	259762		0.013	24.08	200	1694
	508.5	246	517489		0.019	22.94	700	2285
	511.5	259	1312746		0.019	22.03	200	5644
	514	258	289127		0.018	20.79	650	1360
	518	257	1296582		0.018	22.38	900	5701
	522	256	373117		0.019	24.03	380	1678
	526	255	0		0.018	22.59	250	0
	531	262	244596		0.019	24.64	80	1129
	537	261	136006		0.018	24.71	150	688
	543	260	98368	102537	0.017	24.04	180	572
	549	267	57614		0.016	20.72	40	383
	555	266	77864		0.017	20.55	220	458
	561	265	69725		0.017	20.81	340	418
	567	264	12626		0.016	22.30	60	165
	567	263	13294		0.017	21.96	60	153
	572	273	5666		0.017	22.09	40	116
	572	274	0		0.013	22.09	40	0
	580	271	2250		0.017	19.75	40	100
	584	270	0	0	0.012	20.18	10	0
	588	269	0		0.016	20.41	20	0
	592	268	0		0.016	20.76	20	0

Plattsburgh Solid Soil Core Data - Nov. 30 - Dec. 2, 1995  
Separate Phase Analysis

Borehole ID	Depth Below Surface (in)	Sample ID	Area	Replicate Area	Mass of Wet Soil (kg)	Mass Moisture Mass Dry Soil (%)	TLV (ppm)	Conc of Sep Phase in Dry Soil (mg/kg)
12-AT	300.5	159	0		0.016	15.28	0	0
	300.5	158	0		0.016	15.70	0	0
	301.5	157	0		0.015	15.19	0	0
	303	156	0		0.014	19.56	0	0
	305	155	0		0.014	19.11	0	0
	307	154	0		0.018	17.64	0	0
	309	153	0		0.012	9.02	0	0
	311	152	0		0.016	20.38	0	0
	313	151	0		0.012	19.00	0	0
	315	150	0	0	0.013	6.53	0	0
	317	149	0		0.011	2.88	0	0
	360.5	169	0		0.014	16.64	0	0
	361.5	168	0		0.016	15.95	0	0
	363	167	0		0.016	20.26	0	0
	365	166	0		0.015	18.42	0	0
	367	165	0		0.014	12.31	0	0
	369	164	0		0.012	7.56	0	0
	371	163	0		0.016	15.56	0	0
	373	162	0		0.008	7.55	0	0
	375	161	0		0.015	13.31	0	0
	377	160	0	0	0.010	14.35	0	0
	379	178	0		0.011	15.38	10	0
	381	177	0		0.016	10.68	10	0
	383	176	0		0.015	7.06	0	0
	385	175	0		0.016	16.31	0	0
	387	174	0		0.013	11.26	0	0
	389.5	173	0		0.016	13.46	0	0
	392	172	0		0.016	18.07	0	0
	394.5	171	0		0.015	16.96	0	0
	394.5	170	0	0	0.015	16.34	0	0
	397	186	0		0.018	24.50	130	0
	399.5	185	0		0.018	18.07	120	0
	402.5	184	0		0.018	17.70	20	0
	405	183	0		0.016	16.91	0	0
	407	182	0		0.017	21.00	0	0
	407	181	0		0.017	20.60	0	0
	409.5	180	0	0	0.018	23.01	10	0
	412.5	179	0		0.019	23.16	0	0
	415	196	0		0.018	21.20	0	0
	417	195	0		0.017	19.44	0	0
	418.5	194	0		0.016	17.57	30	0
	419.5	193	0		0.018	19.23	20	0
	420.5	192	0		0.018	18.25	20	0
	422	191	0		0.016	20.33	20	0
	424	190	0	0	0.016	19.27	20	0
	426	189	0		0.018	19.73	0	0
	428	188	0		0.017	22.04	0	0
	430.5	187	0		0.019	21.40	0	0
	432.5	207	0		0.017	24.06	0	0
	433.5	206	0		0.011	21.23	0	0
	435	205	0		0.016	21.12	0	0
	437	204	0		0.018	21.47	0	0
	439	203	0		0.018	22.02	0	0
	441	202	0		0.018	21.23	0	0
	441	201	0		0.013	21.74	0	0
	443	200	0		0.013	21.12	0	0
	445	199	0		0.018	21.84	0	0
	447	198	0		0.019	21.36	0	0
	449	197	0		0.020	21.99	0	0
	467	208	0		0.019	22.03	0	0

Plattsburgh Solid Core Data-June5-7, 1996

Separate Phase Analysis-12AU

Barrel Depth (ft)	Sample Depth (in)	Sample Depth (m)	Jar Number	Vial Number	TLV (ppm)	Moisture Content (%)	HC conc (mg sep. ph./ kg dry soil)	Rep HC Conc (mg/kg)
38.0-39.5	456-462	459	11.7	171	72	0	11.1%	0
	462-468	465	11.8	170	71	80	15.6%	0
	468-474	471	12.0	169	70	480	19.3%	1037
39.5-41.0	474-480	477	12.1	174	75	1200	16.8%	4196
	480-486	483	12.3	173	74	1800	15.7%	1990
	486-492	489	12.4	172	73	3400	22.0%	15976
41.0-42.5	492-510							
42.5-44.0	510-513	511	13.0	4	4	450	21.2%	196
	513-518	515	13.1	3	3	950	20.7%	1756
	518-523	520	13.2	2	2	180	21.0%	49
44.0-45.5	523-528	526	13.4	1	1	60	23.0%	21
	528-531	530	13.5	8	8	680	20.1%	360
	531-536	534	13.6	7	7	1200	19.9%	1227
45.5-47.0	536-541	538	13.7	6	6	200	20.2%	58
	541-546	544	13.8	5	5	140	21.6%	72
	546-552	549	13.9	11	12	220	21.6%	218
R	552-558	555	14.1	10	10	100	21.9%	30
	552-558	555	14.1	10	11	100	20.6%	29
	558-564	561	14.2	9	9	60	22.9%	7
47.0-49.0	564-570	567	14.4	15	16	200	19.5%	66
	570-576	573	14.6	14	15	40	19.4%	1
	576-582	579	14.7	13	14	20	21.2%	1
	582-588	585	14.9	12	13	30	22.4%	0

Plattsburgh Solid Core Data-June5-7, 1996  
 Separate Phase Analysis-12AV

Barrel Depth (ft)	Sample Depth (in)	Sample Depth (m)	Jar Number	Vial Number	TLV (ppm)	Moisture Content (%)	HC conc (mg sep. ph./ kg dry soil)	Rep HC Conc (mg/kg)
35.0-36.5	420-422	420	177	79	20	4.7%	0	0
	422-430	426	176	77	60	2.6%	0	0
R	422-430	426	176	78	60	2.4%	0	0
	430-438	434	175	76	60	3.4%	0	0
36.5-38.0	438-440	441	18	19	80	5.5%	1	1
	442-445	443	17	18	60	4.2%	5	5
	454-456	455	16	17	260	20.6%	4754	4754
38.0-39.5	456-464	459	179	81	260	14.6%	231	231
	464-472	467	178	80	1500	17.7%	7324	7324
39.5-41.0	474-478	476	23	25	1200	20.0%	1669	1669
	478-482	480	22	24	720	17.5%	3947	3947
	482-486	484	21	23	1200	16.8%	13814	13814
	486-490	488	20	21	4400	19.6%	13156	13156
R	486-490	488	20	22	4400	19.7%	7732	7732
	490-492	490	19	20	3200	22.0%	4558	4558
41.0-43.0	492-498	495	27	29	880	21.6%	679	679
	498-504	501	26	28	600	19.1%	340	340
	504-510	507	25	27	1200	18.5%	1594	1594
	510-516	513	24	26	1800	20%	3312	3312
43.0-45.0	516-521	518	32	35	520	20.0%	816	816
	521-526	523	31	34	1200	19.2%	1691	1691
	526-531	528	30	32	1600	19.6%	1394	1394
R	526-531	528	30	33	1600	19.4%	1293	1293
	531-536	533	29	31	280	19.5%	89	89
	536-540	538	28	30	280	19.7%	161	161
45.0-47.0	540-545	542	37	40	340	21.9%	412	412
	545-550	547	36	39	320	18.9%	210	210
	550-555	552	35	38	140	20.9%	42	42
	555-560	557	34	37	80	20.6%	2	2
	560-564	562	33	36	100	22.7%	3	3
47.0-49.0	564-570	567	41	45	180	24.3%	259	259
	570-576	573	40	43	120	21.6%	4	4
R	570-576	573	40	44	120	22.3%	4	4
	576-582	579	39	42	60	21.3%	0	0
	582-588	585	38	41	80	22.3%	0	0

Plattsburgh Solid Core Data-June5-7, 1996  
 Separate Phase Analysis-12AW

Barrel Depth (ft)	Sample Depth (in)	Sample Depth (in)	Sample Depth (m)	Jar Number	Vial Number	TLV (ppm)	Moisture Content (%)	HC conc (mg sep. ph./ kg dry soil)	Rep HC Conc (mg/kg)
35.0-36.5	420-424	422	10.7	182	84	40	5.4%	0	
	424-431	428	10.9	181	83	40	2.0%	0	
	431-438	434	11.0	180	82	50	1.9%	0	
36.5-38.0	438-444	441	11.2	184	86	60	3.1%	0	
	444-450	447	11.4	183	85	80	16.1%	0	
	456-464	460	11.7	186	88	200	15.9%	0	
38.0-39.5 R	456-464	460	11.7	186	89	200	15.4%	0	
	464-472	468	11.9	185	87	500	20.6%	402	
	474-476	475	12.1	187	90	2800	17.0%	4528	4852
39.5-41.0	476-478	477	12.1	48	52	480	16.9%	200	
	478-480	479	12.2	47	51	380	16.8%	58	
	481-483	482	12.2	46	50	1000	17.0%	2104	1994
	483-485	484	12.3	45	49	1100	15.7%	4616	
	485-487	486	12.3	44	48	2000	17.1%	15615	
	488-490	489	12.4	43	47	2400	18.3%	7268	
41.0-42.5	490-492	491	12.5	42	46	2000	18.5%	4435	
	492-495	493	12.5	53	58	680	25.0%	6021	
	495-498	496	12.6	52	57	760	22.5%	1438	
	498-501	499	12.7	51	56	560	21.4%	853	
	501-504	502	12.8	50	54	660	21.6%	706	
	501-504	502	12.8	50	55	660	20.9%	1141	
42.5-44.5 R	504-507	505	12.8	49	53	2000	20.5%	11667	
	510-516	513	13.0	56	61	100	20.4%	0	
	518-524	521	13.2	55	60	100	19.3%	0	
44.5-46.5	526-532	529	13.4	54	59	100	21.1%	0	0
	534-540	537	13.6	60	65	80	18.5%	0	
	534-540	537	13.6	60	66	80	19.5%	0	
R	540-546	543	13.8	59	64	100	19.8%	0	
	546-551	549	13.9	58	63	60	19.2%	0	
	551-556	554	14.1	57	62	80	19.9%	0	
46.5-48.5	558-566	562	14.3	63	69	50	18.4%	0	
	566-574	570	14.5	62	68	60	19.7%	0	
	574-580	578	14.7	61	67	40	19.3%	0	

Plattsburgh Solid Core Data-June5-7, 1996  
Separate Phase Analysis-12AX

Barrel Depth (ft)	Sample Depth (in)	Sample Depth (in)	Sample Depth (m)	Jar Number	Vial Number	TLV (ppm)	Moisture Content (%)	HC conc (mg sep. ph./ kg dry soil)	Rep HC Conc (mg/kg)
5.0-6.5	60-66	63	1.6	190	93	0	4.3%	0	0
	66-72	69	1.8	189	92	0	3.9%	0	0
	72-78	75	1.9	188	91	0	7.3%	0	0
6.5-8.0	78-84	81	2.1	193	96	20	4.9%	0	0
	84-90	87	2.2	192	95	20	3.5%	0	0
	90-96	93	2.4	191	94	0	4.4%	0	0
8.0-9.5	108-114	111	2.8	194	97	20	7.7%	0	0
9.5-11.0	126-132	129	3.3	195	98	20	4.5%	0	0
11.0-12.5	144-150	147	3.7	196	99	20	5.9%	0	0
12.5-14.0	162-168	165	4.2	197	100	40	6.1%	0	0
	162-168	165	4.2	197	101	40	6.2%	0	0
14.0-15.5	180-186	183	4.6	198	102	20	8.0%	0	0
15.5-17.0	198-204	201	5.1	199	103	40	5.3%	0	0
17.0-18.5	216-222	219	5.6	200	104	0	10.8%	0	0
18.5-20.0	234-240	237	6.0	201	105	40	10.5%	0	0
20.0-21.5	252-258	255	6.5	202	106	20	5.0%	0	0
21.5-23.0	270-276	273	6.9	203	107	60	10.1%	0	0
23.0-24.5	288-294	291	7.4	204	108	60	5.7%	0	0
24.5-26.0	306-312	309	7.8	205	109	50	6.9%	0	0
26.0-27.5	324-330	327	8.3	206	110	60	5.7%	0	0
27.5-29.0	342-348	345	8.8	207	111	60	15.1%	0	0
29.0-30.5	360-366	363	9.2	208	112	60	11.0%	0	0
	360-366	363	9.2	208	113	60	11.4%	0	0
30.5-32.0	378-384	381	9.7	209	114	80	22.0%	0	0
32.0-33.5	396-402	399	10.1	210	115	90	22.9%	0	0
33.5-35.0	414-420	417	10.6	211	116	80	24.6%	1	1
35.0-36.5	432-438	435	11.0	212	117	100	25.5%	2	2

Plattsburgh Solid Core Data-June5-7, 1996  
 Separate Phase Analysis-12AY

Barrel Depth (ft)	Sample Depth (in)	Sample Depth (in)	Sample Depth (m)	Jar Number	Vial Number	TLV (ppm)	Moisture Content (%)	HC conc (mg sep. ph./ kg dry soil)	Rep HC Conc (mg/kg)
36.0-37.5	432-438	435	11.0	215	132	40	4.5%	0	
	438-444	441	11.2	214	131	40	7.0%	0	
	444-450	447	11.4	213	130	40	17.6%	0	0
37.5-39.0	450-456	453	11.5	218	135	200	16.7%	0	
	456-462	459	11.7	217	134	760	16.0%	2	
	462-468	465	11.8	216	133	2600	23.7%	3237	
39.0-41.0	468-473	470	11.9	68	122	380	20.6%	1106	
	473-478	475	12.1	67	121	1200	19.8%	733	
	478-483	480	12.2	66	120	2800	19.8%	5013	5527
41.0-43.0	483-488	485	12.3	65	119	3600	17.9%	18152	
	488-492	490	12.4	64	118	3600	19.0%	9316	
	492-499	495	12.6	71	125	160	20.6%	0	
43.0-45.0	499-506	502	12.8	70	124	60	21.7%	0	
	506-513	509	12.9	69	123	60	21.5%	0	
	516-523	519	13.2	74	129	280	19.7%	51	
R	523-530	526	13.4	73	127	140	20.4%	8	
	523-530	526	13.4	73	128	140	21.1%	4	
	530-537	533	13.5	72	126	140	21.5%	2	

Plattsburgh Solid Core Data-June5-7, 1996

Separate Phase Analysis-12AZ

Barrel	Sample	Sample	Jar	Vial	TLV	Moisture	HC conc	Rep
Depth	Depth	Depth	Number	Number	(ppm)	Content	(mg sep. ph./	HC Conc
(ft)	(in)	(in)				(%)	kg dry soil)	(mg/kg)
35.0-36.5	420-422	421	10.7	221	174	0	4.7%	7
	422-430	426	10.8	220	173	0	6.1%	12
	430-438	434	11.0	219	172	0	2.9%	0
36.5-38.0	438-444	441	11.2	224	177	20	8.1%	0
	444-450	447	11.4	223	176	20	12.1%	0
	450-456	453	11.5	222	175	100	16.5%	0
38.0-39.5	456-462	459	11.7	227	181	1600	16.4%	2087
	462-468	465	11.8	226	179	1800	14.9%	299
R	462-468	465	11.8	226	180	1800	14.8%	403
	468-472	471	12.0	225	178	3800	18.0%	4613
39.5-41.0	472-474	473	12.0	84	147	2200	15.9%	4305
	474-476	475	12.1	83	145	2800	14.9%	12853
R	474-476	475	12.1	83	146	2800	14.9%	8342
	476-478	477	12.1	82	144	2400	16.7%	8801
	478-480	479	12.2	81	143	4400	17.6%	12382
	480-482	481	12.2	80	142	1400	18.6%	3114
	482-484	483	12.3	79	141	1600	20.1%	3693
	484-486	485	12.3	78	139	1400	22.9%	3061
	486-488	487	12.4	77	138	1800	23.1%	7687
	488-490	489	12.4	76	137	3000	22.7%	10362
41.0-43.0	490-492	491	12.5	75	136	2800	23.0%	9403
	492-498	495	12.6	88	151	3800	19.2%	10136
	498-504	501	12.7	87	150	2600	19.2%	902
	504-510	507	12.9	86	149	400	20.9%	35
	510-516	513	13.0	85	148	200	21.2%	54
43.0-45.0	516-522	519	13.2	92	155	2000	19.3%	1506
	522-528	525	13.3	91	154	360	20.7%	78
	528-534	531	13.5	90	153	280	20.4%	13
	534-540	537	13.6	89	152	280	21.0%	12
45.0-47.0	540-550	545	13.8	94	157	480	18.8%	23
R	540-550	545	13.8	94	158	480	19.7%	5
	552-562	557	14.1	93	156	200	21.4%	1
47.0-49.0	564-570	567	14.4	99	162	1400	18.4%	230
	570-576	573	14.6	98	161	100	19.9%	1
	576-582	579	14.7	97	160	100	19.5%	0
	582-588	585	14.9	95	159	140	20.0%	0
49.0-51.0	588-594	591	15.0	103	166	220	21.3%	0
	594-600	597	15.2	102	165	80	21.0%	0
	600-606	603	15.3	101	164	100	20.8%	0
	606-612	609	15.5	100	163	160	21.6%	0
51.0-53.0	612-617	615	15.6	108	171	80	21.1%	0
	617-622	619	15.7	107	140	40	21.3%	2
	622-627	624	15.8	106	170	40	23.0%	0
	627-632	629	16.0	105	168	60	22.5%	1
R	627-632	629	16.0	105	169	60	22.6%	0
	632-636	634	16.1	104	167	60	25.2%	0



Plattsburgh Solid Core Data-June 5-7, 1996

Separate Phase Analysis-12BA

Barrel Depth (ft)	Sample Depth (in)	Sample Depth (m)	Jar Number	Vial Number	TLV (ppm)	Moisture Content (%)	HC conc (mg sep. ph./ kg dry soil)	Rep HC Conc (mg/kg)
35.0-36.5	420-428	424	229	210	40	9.9%	0	0
	428-436	432	228	209	0	3.3%	0	
36.5-38.0	438-446	442	231	212	0	13.4%	0	
	446-454	450	230	211	80	19.1%	37	36
38.0-39.5	456-464	460	233	213	3400	14.7%	5920	
	464-472	468	232	214	4400	22.9%	14908	
39.5-41.0	474-479	476	236	218	2800	18.7%	5080	
	479-484	481	235	216	4700	16.5%	5818	
R	479-484	481	235	217	4700	16.7%	6848	
	484-489	486	234	215	4200	22.5%	12134	
41.0-43.0	492-499	495	111	184	2000	19.8%	13713	
	499-506	502	110	183	2400	18.9%	5128	
	506-513	509	109	182	560	20.8%	605	
43.0-45.0	516-523	519	115	188	1600	21.0%	2944	
	523-530	527	114	187	1800	21.5%	662	
	530-537	533	113	186	580	23.0%	236	
45.0-47.0	540-547	543	117	190	120	20.8%	15	16
	547-554	550	116	189	80	21.2%	2172 *Field Spike	
	554-561	557	112	185	140	21.0%	0	
47.0-49.0	564-570	567	121	195	220	19.6%	11	
	570-576	573	120	194	60	20.4%	0	
	576-582	579	119	193	40	18.4%	0	
	582-588	585	118	191	60	19.2%	8905 *Field Spike	
	582-588	585	118	192	60	19.3%	0	
49.0-51.0	588-594	591	125	201	200	19.7%	63	
	594-600	597	124	198	660	18.1%	73	74
	600-606	603	123	197	30	19.1%	2	
	606-612	609	122	196	40	20.2%	0	
51.0-53.0	612-616	615	131	208	30	19.9%	6	
	616-620	618	130	207	80	19.5%	2	
	620-624	622	129	206	20	21.1%	0	
	624-628	626	128	204	20	22.4%	0	
R	624-628	626	128	205	20	22.9%	0	
	628-632	630	127	203	20	20.6%	0	
	632-636	634	126	202	40	25.2%	0	

Separate Phase

Plattsburgh Solid Soil Core Data - August 19-23, 1996																		
Separate Phase Analysis-12BB																		
Borehole	Depth Below		Avg Depth		TLV	Jar	Moisture	Area	Replicate	Mass of	Phase in							
	Surface	(in)	Below Surface	(ft)								Content	Units	Wet Soil	Dry Soil			
ID	(in)	(in)	(ft)	(ppm)	ID	(%)	ID	Units	Units	(kg)	(mg/kg)							
12BB	408-417	412.5	34.38	80	2	6.1	202	0		0.01446	0							
12BB	417-426	421.5	35.13	0	1	2.2	201	0		0.01302	0							
12BB	426-432	429	35.75	0	5	2.0	205	0		0.01423	0							
12BB	432-438	435	36.25	0	4	2.4	204	0		0.01524	0							
12BB	438-444	441	36.75	0	3	4.5	203	0		0.01334	0							
12BB	444-450	447	37.25	50	8	16.3	208	24398		0.01566	185							
12BB	450-456	453	37.75	40	7	18.4	207	137931		0.01603	1039							
12BB	456-462	459	38.25	0	6	18.0	206	88376		0.01827	582							
12BB	464-466	465	38.75	280	10	15.9	215	53042		0.01828	343							
12BB	466-468	467	38.92	100	136	15.9	214	49595		0.01854	316							
12BB	468-470	469	39.08	160	135	16.6	213	124296		0.01738	850							
12BB	470-472	471	39.25	480	134	17.2	212	68100		0.01634	498							
12BB	472-474	473	39.42	1200	133	17.8	312	768026		0.01713	5388							
12BB	472-474	473	39.42	1200	133	17.8	211	246200	237889	0.01576	1877							
12BB	477-480	478.5	39.88	4300	9	19.4	209	2312252		0.01743	16164							
12BB	480-486	483	40.25	160	139	18.8	218	0		0.01724	0							
12BB	480-488	484	40.33	860	142	17.6	313	134087		0.01764	912							
12BB	480-488	484	40.33	860	142	17.6	221	98801		0.01772	669							
12BB	488-496	492	41.00	1000	141	18.2	220	110133	114765	0.01641	809							
12BB	492-498	495	41.25	720	137	20.9	217	67750		0.0151	553							
12BB	496-504	500	41.67	1000	140	18.0	219	433915		0.01741	3000							
12BB	504-516	510	42.50	200	144	18.7	223	2531		0.01812	17							
12BB	504-516	510	42.50	200	144	18.7	224	2398		0.01781	16							
12BB	516-528	522	43.50	260	143	19.3	222	3191		0.01876	21							
12BB	528-536	532	44.33	210	147	15.4	227	0		0.01701	0							
12BB	536-544	540	45.00	80	146	16.8	226	0		0.01569	0							
12BB	544-552	548	45.67	100	145	17.9	225	0		0.01703	0							
12BB	552-564	558	46.50	80	150	17.6	314	0		0.01805	0							
12BB	552-564	558	46.50	80	150	17.6	230	0	0	0.01678	0							
12BB	564-576	570	47.50	80	148	18.5	228	0		0.01825	0							

Separate Phase

Plattsburgh Solid Soil Core Data - August 19-23, 1996												
Separate Phase Analysis-12BF												
Borehole	Depth Below		Avg Depth		TLV	Jar	Moisture	Sample	Area	Replicate	Mass of	Phase In
	Surface	(in)	Below Surface	(ft)								
ID	(in)		(in)	(ft)	(ppm)	ID	(%)	ID	Units	Units	(kg)	(mg/kg)
12BF	420-426	423	35.25	0	13	2.1	233	0			0.01405	0
12BF	426-432	429	35.75	0	12	1.6	232	0			0.01371	0
12BF	432-438	435	36.25	0	11	1.5	231	0			0.01445	0
12BF	438-444	441	36.75	0	16	11.9	236	0			0.01459	0
12BF	444-450	447	37.25	0	15	16.1	235	0			0.01631	0
12BF	450-456	453	37.75	0	14	16.1	234	0			0.01625	0
12BF	456-459	457.5	38.13	100	158	36.5	244	0			0.00964	0
12BF	459-462	460.5	38.38	100	157	28.0	243	0			0.0159	0
12BF	462-464	463	38.58	60	156	19.4	242	0			0.01397	0
12BF	464-466	465	38.75	80	155	14.8	241	0			0.01481	0
12BF	466-468	467	38.92	110	154	15.9	315	0			0.01731	0
12BF	466-468	467	38.92	110	154	15.9	240	0	0		0.01708	0
12BF	468-470	469	39.08	440	153	17.5	239	68624			0.01538	535
12BF	470-472	471	39.25	850	152	17.5	238	439909			0.01775	2970
12BF	472-474	473	39.42	1200	151	18.7	237	548563			0.01759	3778
12BF	474-480	477	39.75	580	161	24.6	247	310930			0.01763	2241
12BF	474-480	477	39.75	1000	165	16.2	301	209700			0.01739	1429
12BF	480-486	483	40.25	860	164	15.6	316	280984			0.01761	1882
12BF	480-486	483	40.25	1000	160	17.6	246	754450			0.01523	5944
12BF	480-486	483	40.25	860	164	15.6	250	284523	150370		0.01633	2054
12BF	486-492	489	40.75	1000	159	14.6	245	648088			0.01751	4328
12BF	486-492	489	40.75	3000	163	15.1	249	1172797			0.01671	8242
12BF	492-498	495	41.25	2800	162	10.3	248	1878938			0.01753	12061
12BF	498-506	502	41.83	1000	170	17.7	304	804157			0.01751	5516
12BF	506-514	510	42.50	5000	169	15.8	303	2868427			0.0176	19253
12BF	514-522	518	43.17	1200	166	16.7	302	225395			0.01824	1471
12BF	522-528	525	43.75	480	172	16.5	308	65503			0.01758	443
12BF	528-534	531	44.25	120	171	15.4	307	3182			0.01698	22
12BF	534-540	537	44.75	120	168	18.9	306	0			0.01689	0
12BF	540-546	543	45.25	180	167	17.3	305	0			0.01715	0

Separate Phase

12BF	546-554	550	45.83	80	175	19.9	311	0		0.01687	0
12BF	554-562	558	46.50	60	174	16.3	310	0	0	0.01624	0
12BF	562-570	566	47.17	80	173	19.3	309	0		0.01569	0

Separate Phase

Plattsburgh Solid Soil Core Data - August 19-23, 1996											
Separate Phase Analysis-12BI											
Borehole	Depth Below Surface		Avg Depth	TLV	Jar	Moisture	Sample	Replicate		Mass of	Phase in
	Surface	Below Surface	Below Surface					Area	Area		
ID	(in)	(in)	(ft)	(ppm)	ID	(%)	ID	Units	Units	(kg)	(mg/kg)
12BI	445-447	446	37.17	100	181	13.3	323	0		0.01617	0
12BI	447-450	448.5	37.38	50	180	15.7	322	0		0.01776	0
12BI	450-453	451.5	37.63	60	179	16.6	321	0		0.01796	0
12BI	453-456	454.5	37.88	80	178	16.1	320	0	0	0.01752	0
12BI	456-459	457.5	38.13	100	177	17.2	319	71368		0.01281	666
12BI	459-462	460.5	38.38	450	176	18.2	318	145359		0.01762	994
12BI	462-463	462.5	38.54	880	189	16.2	331	211921		0.01356	1853
12BI	463-465	464	38.67	1800	188	16.2	330	212538		0.01458	1727
12BI	465-468	466.5	38.88	1800	187	15.0	329	137576		0.01558	1035
12BI	468-471	469.5	39.13	740	186	16.5	328	41615		0.01659	298
12BI	471-474	472.5	39.38	1400	185	15.6	327	106152		0.0168	745
12BI	471-474	472.5	39.38	1400	185	15.6	343	108115		0.01584	805
12BI	474-477	475.5	39.63	4000	184	16.7	326	1345667		0.01757	9119
12BI	477-480	478.5	39.88	3600	183	19.2	325	1138417		0.01517	9123
12BI	480-489	484.5	40.38	1600	17	18.8	339	840889		0.01904	5350
12BI	489-492	490.5	40.88	1600	192	16.7	334	230329		0.01468	1867
12BI	492-495	493.5	41.13	2000	191	16.8	333	318181	288559	0.01462	2592
12BI	495-498	496.5	41.38	2800	190	17.2	332	829414		0.01726	5748
12BI	498-506	502	41.83	4200	195	16.5	337	433128		0.01507	3416
12BI	506-514	510	42.50	400	194	17.4	336	38193		0.01589	288
12BI	506-514	510	42.50	400	194	17.4	344	30136		0.01813	199
12BI	514-522	518	43.17	320	193	18.3	335	61806		0.01716	435
12BI	522-530	526	43.83	100	202	16.0	342	24955		0.01539	192
12BI	538-546	542	45.17	180	200	18.8	340	10997		0.01586	84
12BI	546-570	558	46.50	1400	196	17.0	338	107004		0.01776	719

[illegible]

## **APPENDIX V COMPUTER PROGRAM LISTINGS**

```

1 OPEN "datf" FOR OUTPUT AS #1
2 DIM we(12), ve(12), wf(12), vf(12), vs(12), ws(12), canal(100), delta(100)
3 DIM cj(100), ck(100), kk(100, 100), ast(100, 100), b(100), bst(100), func(15)
4 DIM d(100), bvec(100), abl(100), fk(100, 100), wai(100), vai(100), coz(15)
5 PRINT #1, "Advection, Diffusion and Transience"
6 PRINT #1, "Finite Element-Finite Difference Solution"
7 PRINT #1, "Constant Concentration on Capillary Fringe"
8 PRINT #1, "Ostendorf et al. 1997 Uniform Grid"
9 PRINT #1,
10 REM Read in and Display Arrays
11 READ goo, ree
12 READ nn, zf, re, q, dref, cam, det, theta, lam, coo, tmax, tave, omeg, phase,
13 nnn = (nn + 2) ^ .5
14 PRINT "nodes="; nn; "zf="; zf; "re="; re; "q="; q; "det="; det; "dref="; dref;
15 PRINT "cam="; cam; "theta="; theta; "lam="; lam; "coo="; coo; "tmax="; tmax;
17 PRINT "goo="; goo; "ree="; ree
20 lamp = lam + 1 / det
27 dz = zf / (nnn + 1)
29 dr = re / nnn
35 REM Initialize Terms and compute flow vector
37 GOSUB 1300
41 REM Solve and Print the Time Steps
43 GOSUB 1500
95 END
98 DATA .00,15,47,13,15,1e-10,4.37e-6,.001,30.25e5,.288,5e-7
99 DATA 0,12,282,1.99e-7,0,1.74e-6
1000 REM Subroutine to find cj(n)
1005 FOR i10 = 1 TO n - 1
1008 m = n - i10
1010 ab = kk(1, 1)
1011 bb = b(1)
1012 FOR j10 = 2 TO m + 1
1014 abl(j10) = kk(1, j10)
1016 NEXT j10
1018 FOR k10 = 1 TO m
1020 FOR l10 = 1 TO m
1025 kk(k10, l10) = kk(k10 + 1, l10 + 1) - kk(k10 + 1, 1) * abl(l10 + 1) / ab
1030 NEXT l10
1035 b(k10) = b(k10 + 1) - kk(k10 + 1, 1) * bb / ab
1040 NEXT k10, i10
1050 cj(n) = b(1) / kk(1, 1)
1052 RETURN
1100 REM Gauss Elimination nn by nn Array
1105 FOR i11 = 1 TO nn
1110 n = nn - i11 + 1
1115 ns = n
1118 REM Store the n by n Array
1120 GOSUB 1200
1125 GOSUB 1000
1140 REM Reset the n-1 by n-1 Array with c(n) Known
1145 FOR j11 = 1 TO n - 1
1150 b(j11) = bst(j11) - ast(j11, n) * cj(n)
1152 FOR k11 = 1 TO n - 1
1154 kk(j11, k11) = ast(j11, k11)
1156 NEXT k11, j11, i11
1170 RETURN
1200 REM Store the Array Subroutine
1205 FOR i12 = 1 TO ns
1210 bst(i12) = b(i12)
1220 FOR j12 = 1 TO ns

```



```

225 ast(i12, j12) = kk(i12, j12)
1230 NEXT j12, i12
240 RETURN
300 REM Initialize, compute the flow vectors and radial boundary concentration
1301 REM Compute the interior flow vector
1302 REM find the radius and elevation
1303 bstar = EXP(zf * SQR(lam / dref)) - EXP(-zf * SQR(lam / dref))
1304 k13 = 0
1305 zref = dz
1306 func(1) = cam * (EXP((zf - zref) * SQR(lam / dref)) - EXP(-(zf - zref) * SQ
1307 rref = dr
1308 FOR i13 = 1 TO nnn - 2
1309 rref = rref + dr
1310 k13 = k13 + 1
1311 coz(i13) = cam
1312 vai(k13) = q * rref / (2 * 3.14 * (rref ^ 2 + zref ^ 2) ^ 1.5)
1313 wai(k13) = q * zref / (2 * 3.14 * (rref ^ 2 + zref ^ 2) ^ 1.5)
1323 canal(k13) = goo * (1 - EXP(q / (2 * 3.14 * theta * dref) * (1 / ree - 1 /
1325 NEXT i13
1326 FOR j13 = 2 TO nnn
1328 rref = -dr
1329 zref = zref + dz
1331 func(j13) = cam * (EXP((zf - zref) * SQR(lam / dref)) - EXP(-(zf - zref) *
1332 FOR l13 = 1 TO nnn
1333 k13 = k13 + 1
1334 rref = rref + dr
1336 vai(k13) = q * rref / (2 * 3.14 * (rref ^ 2 + zref ^ 2) ^ 1.5)
1337 wai(k13) = q * zref / (2 * 3.14 * (rref ^ 2 + zref ^ 2) ^ 1.5)
1339 canal(k13) = goo * (1 - EXP(q / (2 * 3.14 * theta * dref) * (1 / ree - 1 /
1340 NEXT l13, j13
1341 REM Boundary Vector Velocities
1342 FOR m13 = 1 TO nnn + 1
1343 we(m13) = q * dz * m13 / (2 * 3.14 * (re ^ 2 + (dz * m13) ^ 2) ^ 1.5)
1345 ve(m13) = q * re / (2 * 3.14 * (re ^ 2 + (dz * m13) ^ 2) ^ 1.5)
1347 ws(m13) = q * zf / (2 * 3.14 * ((dr * (m13 - 1)) ^ 2 + zf ^ 2) ^ 1.5)
1348 vs(m13) = q * (m13 - 1) * dr / (2 * 3.14 * ((dr * (m13 - 1)) ^ 2 + zf ^ 2)
1350 IF m > 3 GOTO 1360
1351 wf(1) = q / (2 * 3.14 * dz ^ 2)
1352 vf(1) = 0
1353 wf(2) = q * dz / (2 * 3.14 * (dr ^ 2 + dz ^ 2) ^ 1.5)
1354 vf(2) = q * dr / (2 * 3.14 * (dr ^ 2 + dz ^ 2) ^ 1.5)
1355 vf(3) = q / (2 * 3.14 * dr ^ 2)
1358 wf(3) = 0
1359 GOTO 1375
1360 vf(m13) = q / (2 * 3.14 * ((m13 - 2) * dr) ^ 2)
1361 wf(m13) = 0
1375 NEXT m13
1380 wfe = 0
1382 vfe = q / (2 * 3.14 * re ^ 2)
1384 wse = q * zf / (2 * 3.14 * (re ^ 2 + zf ^ 2))
1386 vse = q * re / (2 * 3.14 * (re ^ 2 + zf ^ 2))
1387 REM initialize ck
1389 FOR n13 = 1 TO nn
1390 ck(n13) = 0!
1392 NEXT n13
1394 ff = 4 * dr * dz / (9 * det)
1395 RETURN
1400 REM Initialize the Arrays
1401 FOR j14 = 1 TO nn
1402 FOR k14 = 1 TO nn

```

```

1403 di = (d(j14) + d(k14)) / 2
1404 vi = (vai(k14) + vai(j14)) / 2
1405 wi = (wai(k14) + wai(j14)) / 2
1406 REM Compute the k generics
1407 GOSUB 1700
1409 IF j14 = k14 GOTO 1448
1410 IF (j14 - k14) = 1 GOTO 1444
1411 IF (j14 - k14) = -1 GOTO 1441
1412 IF (j14 - k14) = nnn GOTO 1438
1413 IF (j14 - k14) = -nnn GOTO 1435
1414 IF (j14 - k14) = (nnn + 1) GOTO 1430
1415 IF (j14 - k14) = -(nnn + 1) GOTO 1427
1416 IF (j14 - k14) = (nnn - 1) GOTO 1424
1417 IF (j14 - k14) = -(nnn - 1) GOTO 1421
1418 kk(j14, k14) = 0
1419 fk(j14, k14) = 0
1420 GOTO 1451
1421 kk(j14, k14) = kul
1422 fk(j14, k14) = ff / 16
1423 GOTO 1451
1424 kk(j14, k14) = kdr
1425 fk(j14, k14) = ff / 16
1426 GOTO 1451
1427 kk(j14, k14) = kur
1428 fk(j14, k14) = ff / 16
1429 GOTO 1451
1430 kk(j14, k14) = kdl
1431 fk(j14, k14) = ff / 16
1434 GOTO 1451
1435 kk(j14, k14) = kvu
1436 fk(j14, k14) = ff / 4
1437 GOTO 1451
1438 kk(j14, k14) = kvd
1439 fk(j14, k14) = ff / 4
1440 GOTO 1451
1441 kk(j14, k14) = krr
1442 fk(j14, k14) = ff / 4
1443 GOTO 1451
1444 kk(j14, k14) = krl
1445 fk(j14, k14) = ff / 4
1446 GOTO 1451
1448 kk(j14, k14) = kf
1449 fk(j14, k14) = ff
1451 NEXT k14, j14
1453 REM Zero the Row Elements and Adjust the No Flux KII
1454 FOR l14 = 1 TO nnn
1455 vi = vai(l14 * nnn - 1)
1456 wi = wai(l14 * nnn - 1)
1457 di = d(l14 * nnn - 1)
1458 GOSUB 1700
1459 kk(l14 * nnn - 1, l14 * nnn - 1) = kfo
1460 fk(l14 * nnn - 1, l14 * nnn - 1) = ff / 2
1461 vi = (vai(l14 * nnn - 1) + vai((l14 + 1) * nnn - 1)) / 2
1462 wi = (wai(l14 * nnn - 1) + wai((l14 + 1) * nnn - 1)) / 2
1463 di = (d(l14 * nnn - 1) + d((l14 + 1) * nnn - 1)) / 2
1464 GOSUB 1700
1468 kk(l14 * nnn - 1, (l14 + 1) * nnn - 1) = kvuo
1469 fk(l14 * nnn - 1, (l14 + 1) * nnn - 1) = ff / 8
1476 kk((l14 + 1) * nnn - 1, l14 * nnn - 1) = kvdo
1481 fk((l14 + 1) * nnn - 1, l14 * nnn - 1) = ff / 8

```

```

1 OPEN "datf" FOR OUTPUT AS #1
2 DIM canal(90), delta(90), rr(100), zz(100), alg(6), rig(6)
3 DIM cj(100), ck(100), kk(90, 90), ast(90, 90), b(100), bst(100), func(15)
4 DIM d(102), bvec(100), ab1(100), fk(90, 90), wai(90), vai(90)
5 PRINT #1, "Advection, Diffusion and Transience"
6 PRINT #1, "Finite Element-Finite Difference Solution with 6 Point Gauss Quadra
7 PRINT #1, "No Flux on Capillary Fringe"
8 PRINT #1, "Ostendorf et al. 1997 Uniform Grid"
9 PRINT #1, "Advection and Diffusion Test"
10 REM Read in and Display Arrays
11 READ ginf
12 READ nn, zf, re, q, dref, cam, theta, lam, tmax, tave, omeg, phase, dt
13 FOR im = 1 TO 6
14 READ alg(im), rig(im)
16 NEXT im
23 nnn = nn ^ .5
24 PRINT #1, "nodes="; nn; "zf="; zf; "re="; re; "q="; q; "dref="; dref; "omeg="
25 PRINT #1, "cam="; cam; "theta="; theta; "lam="; lam; "tmax="; tmax; "tave=";
27 PRINT #1, "ginf="; ginf
29 dz = zf / (nnn - 1)
30 dr = re / (nnn - 1)
31 det = 605000!
32 lamp = lam + 1 / det
34 REM Initialize Arrays
35 GOSUB 1300
37 PRINT #1, "dz="; dz; "dr="; dr; "det="; det
38 REM Solve and Print the Time Steps
39 GOSUB 1500
95 END
98 DATA .01,49,13,15,1.00e-4,2.33e-5,0.0,.288,5e-12
99 DATA 12,282,1.99e-7,0,1.74e-6
100 DATA .46791,.23862,.46791,-.23862,.36076,.66120,.36076,-.66120
101 DATA .17132,.93246,.17132,-.93246
1000 REM Subroutine to find cj(n)
1001 FOR i10 = 1 TO n - 1
1002 m = n - i10
1004 ab = kk(1, 1)
1005 BB = b(1)
1012 FOR j10 = 2 TO m + 1
1014 ab1(j10) = kk(1, j10)
1016 NEXT j10
1018 FOR k10 = 1 TO m
1020 FOR l10 = 1 TO m
1021 IF ab = 0 GOTO 1028
1025 kk(k10, l10) = kk(k10 + 1, l10 + 1) - kk(k10 + 1, 1) * ab1(l10 + 1) / ab
1026 GOTO 1030
1028 kk(k10, l10) = kk(k10 + 1, l10 + 1)
1030 NEXT l10
1031 IF ab = 0 GOTO 1038
1035 b(k10) = b(k10 + 1) - kk(k10 + 1, 1) * BB / ab
1036 GOTO 1040
1038 b(k10) = b(k10 + 1)
1040 NEXT k10, i10
1044 IF kk(1, 1) = 0 GOTO 1052
1046 cj(n) = b(1) / kk(1, 1)
1047 delta(n) = (cj(n) - canal(n)) / canal(n)
1051 PRINT n; cj(n); canal(n); delta(n)
1052 PRINT #1, n; cj(n); canal(n); delta(n)
1053 RETURN
1100 REM Gauss Elimination nn by nn Array

```

```

1105 FOR I11 = 1 TO nn - nnn - 1
1110 n = nn - nnn - 1 - I11 + 1
1115 ns = n
1118 REM Store the n by n Array
1120 GOSUB 1200
1125 GOSUB 1000
1140 REM Reset the n-1 by n-1 Array with c(n) Known
1145 FOR j11 = 1 TO n - 1
1150 b(j11) = bst(j11) - ast(j11, n) * cj(n)
1152 FOR k11 = 1 TO n - 1
1154 kk(j11, k11) = ast(j11, k11)
1156 NEXT k11, j11, I11
1170 RETURN
1200 REM Store the Array Subroutine
1205 FOR i12 = 1 TO ns
1210 bst(i12) = b(i12)
1220 FOR j12 = 1 TO ns
1225 ast(i12, j12) = kk(i12, j12)
1230 NEXT j12, i12
1240 RETURN
1300 REM Initialize, compute the flow vectors and radial boundary concentration
1302 REM find the radius and elevation
1303 bstar = EXP(zf * SQR(lam / dref)) - EXP(-zf * SQR(lam / dref))
1304 k13 = 0
1305 zref = -dz
1306 FOR i13 = 1 TO nnn
1307 zref = zref + dz
1308 func(i13) = cam * (EXP((zf - zref) * SQR(lam / dref)) - EXP(-(zf - zref) *
1317 rref = -dr
1318 FOR j13 = 1 TO nnn
1320 rref = rref + dr
1321 k13 = k13 + 1
1322 rr(k13) = rref
1323 zz(k13) = zref
1326 IF k13 = 1 GOTO 1329
1328 canal(k13) = ginf * (1 - EXP(-q / (2 * 3.14 * theta * dref * SQR(rref ^ 2 +
1329 NEXT j13, i13
1387 REM initialize ck
1389 FOR l13 = 1 TO nn
1390 ck(l13) = 0!
1392 NEXT l13
1394 ff = 4 * theta * dr * dz / (9 * det)
1395 RETURN
1400 REM Initialize the Interior Arrays
1401 FOR i14 = 1 TO nn
1402 FOR j14 = 1 TO nn
1404 REM Zero the Boundary Elements
1405 vi = (vai(i14) + vai(j14)) / 2
1406 wi = (wai(i14) + wai(j14)) / 2
1407 di = (d(i14) + d(j14)) / 2
1408 GOSUB 3000
1409 IF kk(i14, j14) = 0 GOTO 1485
1410 GOSUB 1700
1413 IF i14 = j14 GOTO 1480
1415 IF (i14 - j14) = 1 GOTO 1474
1417 IF (i14 - j14) = -1 GOTO 1461
1418 IF (i14 - j14) = nnn GOTO 1455
1419 IF (i14 - j14) = -nnn GOTO 1450
1420 IF (i14 - j14) = (nnn + 1) GOTO 1445
1421 IF (i14 - j14) = -(nnn + 1) GOTO 1440

```

```

1721 kdl = theta * di * (-dz / dr - dr / dz) / 6 - vi * dz / 12 - wi * dr / 12 +
1722 kul = theta * di * (-dz / dr - dr / dz) / 6 - vi * dz / 12 + wi * dr / 12 +
1723 kdr = theta * di * (-dz / dr - dr / dz) / 6 + vi * dz / 12 - wi * dr / 12 +
1730 RETURN
1800 REM Load the Bottom Vector and Corners
1801 go1 = func(1)
1802 go2 = func(1)
1803 go3 = cam
1804 wi = (wai(1) + wf(3)) / 2
1805 vi = (vai(1) + vf(3)) / 2
1806 di = d(1)
1807 GOSUB 1700
1808 bvec(1) = go3 * (ff / 16 - kdl)
1809 wi = (wai(1) + wf(2)) / 2
1810 vi = (vai(1) + vf(2)) / 2
1811 GOSUB 1700
1812 bvec(1) = bvec(1) + go2 * (ff / 4 - krl)
1813 wi = (wai(1) + wf(4)) / 2
1814 vi = (vai(1) + vf(4)) / 2
1815 GOSUB 1700
1816 bvec(1) = bvec(1) + cam * (ff / 4 - kvd)
1817 wi = (wai(1) + wf(5)) / 2
1818 vi = (vai(1) + vf(5)) / 2
1819 GOSUB 1700
1820 bvec(1) = bvec(1) + cam * (ff / 16 - kdr)
1821 wi = (wai(nnn - 1) + wf(1)) / 2
1822 vi = (vai(nnn - 1) + vf(1)) / 2
1823 di = d(nnn - 1)
1824 GOSUB 1700
1825 bvec(nnn - 1) = go1 * (ff / 8 - kvdo)
1826 wi = (wai(nnn - 1) + wf(2)) / 2
1827 vi = (vai(nnn - 1) + vf(2)) / 2
1828 GOSUB 1700
1830 bvec(nnn - 1) = bvec(nnn - 1) + go2 * (ff / 16 - kdr)
1832 wi = (wai(nnn) + wf(1)) / 2
1834 vi = (vai(nnn) + vf(1)) / 2
1836 di = d(nnn)
1838 GOSUB 1700
1840 bvec(nnn) = go1 * (ff / 16 - kdl)
1842 wi = (wai(nnn) + wf(2)) / 2
1844 vi = (vai(nnn) + vf(2)) / 2
1848 GOSUB 1700
1850 bvec(nnn) = bvec(nnn) + go2 * (ff / 4 - kvd)
1852 wi = (wai(nnn + 1) + wf(2)) / 2
1854 vi = (vai(nnn + 1) + vf(2)) / 2
1855 di = d(nnn + 1)
1858 GOSUB 1700
1860 bvec(nnn + 1) = go2 * (ff / 16 - kdl)
1861 FOR i18 = 2 TO nnn - 3
1862 wi = (wai(i18) + wf(i18 + 2)) / 2
1863 vi = (vai(i18) + vf(i18 + 2)) / 2
1864 di = d(i18)
1865 GOSUB 1700
1866 bvec(i18) = bvec(i18) + cam * (ff / 16 - kdl)
1867 wi = (wai(i18) + wf(i18 + 3)) / 2
1868 vi = (vai(i18) + vf(i18 + 3)) / 2
1869 GOSUB 1700
1870 bvec(i18) = bvec(i18) + cam * (ff / 4 - kvd)
1871 wi = (wai(i18) + wf(i18 + 4)) / 2
1872 vi = (vai(i18) + vf(i18 + 4)) / 2

```

```

1874 GOSUB 1700
1875 bvec(i18) = bvec(i18) + cam * (ff / 16 - kdr)
1878 NEXT i18
1885 RETURN
1900 REM Diffusivity vector
1902 k19 = 0
1908 zref = 0
1910 FOR i19 = 1 TO nnn
1911 zref = zref + dz
1912 rref = -dr
1913 FOR j19 = 1 TO nnn
1915 k19 = k19 + 1
1917 rref = rref + dr
1925 temp = tave + tmax * EXP((zref - zf) * SQR(omeg / (2 * dt))) * SIN(omeg *
1930 d(k19) = dref * (temp / tave) ^ 1.75
1935 NEXT j19, i19
1940 RETURN

```

```

1482 kk(l14 * nnn - 2, l14 * nnn - 1) = 0
1483 fk(l14 * nnn - 2, l14 * nnn - 1) = 0
1485 kk(l14 * nnn - 1, l14 * nnn - 2) = 0
1486 fk(l14 * nnn - 1, l14 * nnn - 2) = 0
1488 kk(l14 * nnn - 2, (l14 + 1) * nnn - 1) = 0
1489 fk(l14 * nnn - 2, (l14 + 1) * nnn - 1) = 0
1491 kk((l14 + 1) * nnn - 1, l14 * nnn - 2) = 0
1492 fk((l14 + 1) * nnn - 1, l14 * nnn - 2) = 0
1493 kk(l14 * nnn - 1, (l14 + 1) * nnn - 2) = 0
1494 fk(l14 * nnn - 1, (l14 + 1) * nnn - 2) = 0
1495 kk((l14 + 1) * nnn - 2, l14 * nnn - 1) = 0
1496 fk((l14 + 1) * nnn - 1, l14 * nnn - 1) = 0
1498 NEXT l14
1499 RETURN
1500 REM Solve the Time Step
1501 t = 0
1502 REM Time Step
1503 FOR i15 = 1 TO 10
1504 t = t + det
1505 REM Compute the diffusivity vector for the time step
1507 GOSUB 1900
1516 REM Compute the KK array
1517 GOSUB 1400
1518 REM Load the bvec vectors
1519 GOSUB 1600
1520 REM run the time step and display
1532 GOSUB 1100
1533 PRINT #1, "time="; t
1534 PRINT "time="; t
1535 FOR l15 = 1 TO nn
1537 ck(l15) = cj(l15)
1565 NEXT l15
1567 PRINT #1, cj(1); cj(1 + nnn); cj(1 + 2 * nnn); cj(1 + 3 * nnn); cj(1 + 4 *
1585 NEXT i15
1587 RETURN
1600 REM Set the B and bvec Vectors for the time step
1601 FOR i16 = 1 TO nn
1602 bvec(i16) = 0
1604 NEXT i16
1606 REM Load the Bottom Vector and Corners
1607 GOSUB 1800
1608 REM load the radial concentration vector
1609 FOR j16 = 2 TO nnn - 1
1610 REM Outside Vector
1612 wi = (wai(j16 * nnn - 2) + we(j16)) / 2
1615 vi = (vai(j16 * nnn - 2) + ve(j16)) / 2
1616 di = d(j16 * nnn - 2)
1617 GOSUB 1700
1618 bvec(j16 * nnn - 2) = func(j16) * (ff / 4 - krr)
1619 wi = (wai(j16 * nnn - 2) + we(j16 - 1)) / 2
1620 vi = (vai(j16 * nnn - 2) + ve(j16 - 1)) / 2
1621 GOSUB 1700
1626 bvec(j16 * nnn - 2) = bvec(j16 * nnn - 2) + func(j16 - 1) * (ff / 16 - kdl)
1628 wi = (wai(j16 * nnn - 2) + we(j16 + 1)) / 2
1630 vi = (vai(j16 * nnn - 2) + ve(j16 + 1)) / 2
1632 GOSUB 1700
1634 bvec(j16 * nnn - 2) = bvec(j16 * nnn - 2) + func(j16 + 1) * (ff / 16 - kul)
1635 NEXT j16
1636 REM Lower Corner
1637 wi = (wai(nnn - 2) + wf(nnn)) / 2

```

```

1638 vi = (vai(nnn - 2) + vf(nnn)) / 2
1639 di = d(nnn - 2)
1640 GOSUB 1700
1641 bvec(nnn - 2) = cam * (ff / 16 - kdl)
1643 wi = (wai(nnn - 2) + wf(nnn + 1)) / 2
1644 vi = (vai(nnn - 2) + vf(nnn + 1)) / 2
1645 GOSUB 1700
1646 bvec(nnn - 2) = bvec(nnn - 2) + cam * (ff / 4 - kvd)
1647 wi = (wai(nnn - 2) + wfe) / 2
1648 vi = (vai(nnn - 2) + vfe) / 2
1650 GOSUB 1700
1652 bvec(nnn - 2) = bvec(nnn - 2) + cam * (ff / 16 - kdr)
1654 wi = (wai(nnn - 2) + we(1)) / 2
1655 vi = (vai(nnn - 2) + ve(1)) / 2
1657 GOSUB 1700
1658 bvec(nnn - 2) = bvec(nnn - 2) + func(1) * (ff / 4 - krr)
1660 wi = (wai(nnn - 2) + we(2)) / 2
1661 vi = (vai(nnn - 2) + ve(2)) / 2
1662 GOSUB 1700
1663 bvec(nnn - 2) = bvec(nnn - 2) + func(2) * (ff / 16 - kur)
1664 REM Upper Corner
1665 wi = (wai(nn) + ws(nnn - 1)) / 2
1666 vi = (vai(nn) + vs(nnn - 1)) / 2
1667 di = d(nn)
1668 GOSUB 1700
1669 bvec(nn) = coo * (ff / 16 - kul)
1670 wi = (wai(nn) + ws(nnn)) / 2
1671 vi = (vai(nn) + vs(nnn)) / 2
1672 GOSUB 1700
1673 bvec(nn) = bvec(nn) + coo * (ff / 4 - kvu)
1674 wi = (wai(nn) + wse) / 2
1675 vi = (vai(nn) + vse) / 2
1676 GOSUB 1700
1677 bvec(nn) = bvec(nn) + coo * (ff / 16 - kur)
1678 wi = (wai(nn) + we(nnn)) / 2
1679 vi = (vai(nn) + ve(nnn)) / 2
1680 GOSUB 1700
1681 bvec(nn) = bvec(nn) + func(nnn) * (ff / 4 - krr)
1683 wi = (wai(nn) + we(nnn - 1)) / 2
1684 vi = (vai(nn) + ve(nnn - 1)) / 2
1686 GOSUB 1700
1688 bvec(nn) = bvec(nn) + func(nnn - 1) * (ff / 16 - kdr)
1692 REM set the bvector
1693 FOR l16 = 1 TO nn
1694 b(l16) = bvec(l16)
1695 FOR m16 = 1 TO nn
1696 b(l16) = b(l16) + ck(m16) * fk(l16, m16)
1697 NEXT m16
1698 NEXT l16
1699 RETURN
1700 REM k generic
1742 kf = 4 * theta * di * (dz / dr + dr / dz) / 3 + 4 * lamp * dr * dz / 9
1713 kfo = 2 * theta * di * (dz / dr + dr / dz) / 3 + vi * dz / 3 + 2 * lamp *
1714 krl = theta * di * (-2 * dz / dr + dr / dz) / 3 - vi * dz / 3 + lamp * dr
1715 krr = theta * di * (-2 * dz / dr + dr / dz) / 3 + vi * dz / 3 + lamp * dr
1716 kvd = theta * di * (dz / dr - 2 * dr / dz) / 3 - wi * dr / 3 + lamp * dr
1717 kvu = theta * di * (dz / dr - 2 * dr / dz) / 3 + wi * dr / 3 + lamp * dr
1718 kvdo = theta * di * (dz / dr - 2 * dr / dz) / 6 + vi * dz / 12 - wi * dr /
1719 kvuo = theta * di * (dz / dr - 2 * dr / dz) / 6 + vi * dz / 12 + wi * dr /
1720 kur = theta * di * (-dz / dr - dr / dz) / 6 + vi * dz / 12 + wi * dr / 12

```



```

1422 IF (i14 - j14) = (nnn - 1) GOTO 1435
1423 IF (i14 - j14) = -(nnn - 1) GOTO 1430
1424 kk(i14, j14) = 0
1425 xx = 0
1426 fk(i14, j14) = 0
1427 yy = 0
1428 GOTO 1485
1430 GOSUB 3700
1434 GOTO 1485
1435 GOSUB 4700
1438 GOTO 1485
1440 GOSUB 4600
1444 GOTO 1485
1445 GOSUB 3500
1448 GOTO 1485
1450 GOSUB 3400
1453 GOTO 1485
1455 GOSUB 3300
1460 GOTO 1485
1461 GOSUB 3600
1465 GOTO 1485
1474 GOSUB 3200
1478 GOTO 1485
1480 GOSUB 3100
1485 NEXT j14, i14
1498 RETURN
1500 REM Solve the Time Step
1501 t = 0
1506 FOR j15 = 1 TO nn
1508 FOR k15 = 1 TO nn
1510 kk(j15, k15) = 1
1512 NEXT k15, j15
1517 REM Compute the diffusivity vector for the time step
1518 GOSUB 1900
1519 REM Compute the KK array
1520 GOSUB 1400
1521 FOR i15 = 1 TO 30
1522 t = t + det
1523 PRINT #1, "time="; t
1524 REM Load the bvector
1525 GOSUB 1600
1526 PRINT "time="; t
1528 REM run the time step and display
1532 GOSUB 1100
1535 FOR l15 = 1 TO nn
1537 ck(l15) = cj(l15)
1565 NEXT l15
1566 PRINT "time="; t
1585 NEXT i15
1587 RETURN
1600 REM Set the B and bvec Vectors for the time step
1601 FOR i16 = 1 TO nn
1602 bvec(i16) = 0
1604 NEXT i16
1605 REM Load the Bottom Inside Corner, and Surface Vectors
1606 GOSUB 2000
1607 GOSUB 1800
1608 REM load the radial vector and Outside Corner
1609 REM Outside Interiors
1611 FOR j16 = 2 TO nnn - 2

```

```

1612 k16 = j16 * nnn - 1
1613 bvec(k16) = canal(k16 - nnn + 1) * (fk(k16, k16 - nnn + 1) - kk(k16, k16 -
1619 bvec(k16) = bvec(k16) + canal(k16 + 1) * (fk(k16, k16 + 1) - kk(k16, k16 +
1628 bvec(k16) = bvec(k16) + canal(k16 + nnn + 1) * (fk(k16, k16 + nnn + 1) - k
1635 NEXT j16
1636 REM Lower Outside Corner
1637 bvec(nnn - 1) = canal(nnn) * (fk(nnn - 1, nnn) - kk(nnn - 1, nnn)) + canal
1650 REM Load the b
1652 FOR l16 = 1 TO nn
1654 b(l16) = bvec(l16)
1655 FOR m16 = 1 TO nn
1657 b(l16) = b(l16) + ck(m16) * fk(l16, m16)
1660 NEXT m16, l16
1699 RETURN
1700 REM k generic
1712 kf = 4 * theta * di * (dz / dr + dr / dz) / 3 + 4 * theta * lamp * dr * dz
1713 kfo = 2 * theta * di * (dz / dr + dr / dz) / 3 + vi * dz / 3 + 2 * theta *
1714 krl = theta * di * (-2 * dz / dr + dr / dz) / 3 - vi * dz / 3 + theta * lam
1715 krr = theta * di * (-2 * dz / dr + dr / dz) / 3 + vi * dz / 3 + theta * lam
1716 kvd = theta * di * (dz / dr - 2 * dr / dz) / 3 - wi * dr / 3 + theta * lam
1717 kvu = theta * di * (dz / dr - 2 * dr / dz) / 3 + wi * dr / 3 + theta * lam
1718 kvdo = theta * di * (dz / dr - 2 * dr / dz) / 6 + vi * dz / 12 - wi * dr /
1719 kvuo = theta * di * (dz / dr - 2 * dr / dz) / 6 + vi * dz / 12 + wi * dr /
1720 kur = theta * di * (-dz / dr - dr / dz) / 6 + vi * dz / 12 + wi * dr / 12
1721 kdl = theta * di * (-dz / dr - dr / dz) / 6 - vi * dz / 12 - wi * dr / 12 +
1722 kul = theta * di * (-dz / dr - dr / dz) / 6 - vi * dz / 12 + wi * dr / 12 +
1723 kdr = theta * di * (-dz / dr - dr / dz) / 6 + vi * dz / 12 - wi * dr / 12
1724 kfod = 2 * theta * di * (dz / dr + dr / dz) / 3 - wi * dz / 3 + 2 * theta
1726 krro = theta * di * (-2 * dz / dr + dr / dz) / 6 + vi * dz / 6 + wi * dr /
1728 krlo = theta * di * (-2 * dz / dr + dr / dz) / 6 - vi * dz / 6 + wi * dr /
1730 RETURN
1800 REM Load the Bottom Inside Corner
1805 bvec(2) = ginf * (fk(2, 1) - kk(2, 1))
1809 bvec(nnn + 1) = ginf * (fk(nnn + 1, 1) - kk(nnn + 1, 1))
1814 bvec(nnn + 2) = ginf * (fk(nnn + 2, 1) - kk(nnn + 2, 1))
1885 RETURN
1900 REM Diffusivity vector
1902 k19 = 0
1908 zref = -dz
1910 FOR i19 = 1 TO nnn
1911 zref = zref + dz
1912 rref = -dr
1913 FOR j19 = 1 TO nnn
1915 k19 = k19 + 1
1917 rref = rref + dr
1925 temp = tave + tmax * EXP((zref - zf) * SQR(omeg / (2 * dt))) * SIN(omeg * t
1930 d(k19) = dref * (temp / tave) ^ 1.75
1935 NEXT j19, i19
1940 RETURN
2000 REM Surface Boundary Vector
2002 REM Upper Surface
2004 FOR i20 = 2 TO nnn - 2
2005 j20 = nnn * (nnn - 2) + i20
2009 bvec(j20) = canal(j20 + nnn - 1) * (fk(j20, j20 + nnn - 1) - kk(j20, j20 +
2012 bvec(j20) = bvec(j20) + canal(j20 + nnn) * (fk(j20, j20 + nnn) - kk(j20, j
2016 bvec(j20) = bvec(j20) + canal(j20 + nnn + 1) * (fk(j20, j20 + nnn + 1) - kk
2017 NEXT i20
2018 REM Upper Outside Corner
2032 k20 = nn - nnn - 1
2034 bvec(k20) = canal(k20 + nnn - 1) * (fk(k20, k20 + nnn - 1) - kk(k20, k20 +

```

```

2042 bvec(k20) = bvec(k20) + canal(k20 + nnn) * (fk(k20, k20 + nnn) - kk(k20, k2
2052 bvec(k20) = bvec(k20) + canal(k20 + nnn + 1) * (fk(k20, k20 + nnn + 1) - kk
2055 bvec(k20) = bvec(k20) + canal(k20 + 1) * (fk(k20, k20 + 1) - kk(k20, k20 +
2060 bvec(k20) = bvec(k20) + canal(k20 - nnn + 1) * (fk(k20, k20 - nnn + 1) - kk
2070 REM Upper Inside Corner
2072 l20 = nn - 2 * nnn + 1
2074 bvec(l20) = canal(l20 + nnn) * (fk(l20, l20 + nnn) - kk(l20, l20 + nnn)) +
2092 RETURN
2700 REM k generic by 6 point Gauss Quadrature
2701 kaaaa = 0
2702 faaaa = 0
2703 kbaba = 0
2704 fbaba = 0
2705 kbbbb = 0
2706 fbbbb = 0
2707 kabab = 0
2708 fabab = 0
2709 kaaba = 0
2710 faaba = 0
2711 kabbb = 0
2712 fabbb = 0
2713 kbaaa = 0
2714 fbaaa = 0
2715 kbbab = 0
2716 fbbab = 0
2717 kaaab = 0
2718 faaab = 0
2719 kbabb = 0
2720 fbabb = 0
2721 kabaa = 0
2722 fabaa = 0
2723 kbbba = 0
2724 fbbba = 0
2725 kaabb = 0
2726 faabb = 0
2727 kbaab = 0
2728 fbaab = 0
2729 kbbaa = 0
2730 fbbaa = 0
2731 kabba = 0
2732 fabba = 0
2733 rb = ra + dr
2734 zb = za + dz
2735 FOR i27 = 1 TO 6
2736 rri = (ra + rb) / 2 + dr * rig(i27) / 2
2737 wri = dr * alg(i27) / 2
2741 zkaaaa = 0
2742 zfaaaa = 0
2743 zkbaba = 0
2744 zfbaba = 0
2745 zkbbbb = 0
2746 zfbbbb = 0
2747 zkabab = 0
2748 zfabab = 0
2749 zkaaba = 0
2750 zfaaba = 0
2751 zkabbb = 0
2752 zfabbb = 0
2753 zkbaaa = 0
2754 zfbaaa = 0

```

```

2755 zkbabb = 0
2756 zfbabb = 0
2757 zkaaab = 0
2758 zfaaab = 0
2759 zkbabb = 0
2760 zfbabb = 0
2761 zkabaa = 0
2762 zfabaa = 0
2763 zkbbaa = 0
2764 zfbbaa = 0
2765 zkaabb = 0
2766 zfaabb = 0
2767 zkbaab = 0
2768 zfbaab = 0
2769 zkbbaa = 0
2770 zfbbaa = 0
2771 zkabba = 0
2772 zfabba = 0
2776 FOR j27 = 1 TO 6
2777 zzi = (za + zb) / 2 + dz * rig(j27) / 2
2778 wzi = dz * alg(j27) / 2
2779 vvi = q * rri / (2 * 3.14 * (rri ^ 2 + zzi ^ 2) ^ 1.5)
2780 wwi = q * zzi / (2 * 3.14 * (rri ^ 2 + zzi ^ 2) ^ 1.5)
2781 GOSUB 2900
2801 zkaaaa = zkaaaa + wzi * fkaaaa
2802 zfaaaa = zfaaaa + wzi * ffaaaa
2803 zkbaba = zkbaba + wzi * fkbaba
2804 zfbaba = zfbaba + wzi * ffbaba
2805 zkbbaa = zkbbaa + wzi * fkbbaa
2806 zfbbaa = zfbbaa + wzi * ffbbaa
2807 zkabab = zkabab + wzi * fkabab
2808 zfabab = zfabab + wzi * ffabab
2809 zkaaba = zkaaba + wzi * fkaaba
2810 zfaaba = zfaaba + wzi * ffaaba
2811 zkabbb = zkabbb + wzi * fkabbb
2812 zfabbb = zfabbb + wzi * ffabbb
2813 zkbbaa = zkbbaa + wzi * fkbbaa
2814 zfbbaa = zfbbaa + wzi * ffbbaa
2815 zkbabb = zkbabb + wzi * fkbabb
2816 zfbabb = zfbabb + wzi * ffbabb
2817 zkaaab = zkaaab + wzi * fkaaab
2818 zfaaab = zfaaab + wzi * ffaaab
2819 zkbabb = zkbabb + wzi * fkbabb
2820 zfbabb = zfbabb + wzi * ffbabb
2821 zkabaa = zkabaa + wzi * fkabaa
2822 zfabaa = zfabaa + wzi * ffabaa
2823 zkbbaa = zkbbaa + wzi * fkbbaa
2824 zfbbaa = zfbbaa + wzi * ffbbaa
2825 zkaabb = zkaabb + wzi * fkaabb
2826 zfaabb = zfaabb + wzi * ffaabb
2827 zkbaab = zkbaab + wzi * fkbaab
2828 zfbaab = zfbaab + wzi * ffbaab
2829 zkbbaa = zkbbaa + wzi * fkbbaa
2830 zfbbaa = zfbbaa + wzi * ffbbaa
2831 zkabba = zkabba + wzi * fkabba
2832 zfabba = zfabba + wzi * ffabba
2850 NEXT j27
2851 kaaaa = kaaaa + wri * zkaaaa
2852 faaaa = faaaa + wri * zfaaaa
2853 kbaba = kbaba + wri * zkbaba

```

```

854 fbaba = fbaba + wri * zfbaba
2855 kbbbbb = kbbbbb + wri * zkbbbbb
856 fbbbbb = fbbbbb + wri * zfbbbbbb
857 kabab = kabab + wri * zkabab
2858 fabab = fabab + wri * zfabab
2859 kaaba = kaaba + wri * zkaaba
860 faaba = faaba + wri * zfaaba
861 kabbb = kabbb + wri * zkabbb
2862 fabbb = fabbb + wri * zfabbb
863 kbaaa = kbaaa + wri * zkbaaa
864 fbaaa = fbaaa + wri * zfbaaa
2865 kbbab = kbbab + wri * zkbbab
2866 fbbab = fbbab + wri * zfbbab
867 kaaab = kaaab + wri * zkaaab
2868 faaab = faaab + wri * zfaaab
2869 kbabb = kbabb + wri * zkbabb
870 fbabb = fbabb + wri * zfbabb
871 kabaa = kabaa + wri * zkabaa
2872 fabaa = fabaa + wri * zfabaa
873 kbbba = kbbba + wri * zkbbba
874 fbbba = fbbba + wri * zfbbaa
2875 kaabb = kaabb + wri * zkaabb
2876 faabb = faabb + wri * zfaabb
877 kbaab = kbaab + wri * zkbaab
2878 fbaab = fbaab + wri * zfbaab
2879 kbbaa = kbbaa + wri * zkbbaa
880 fbbaa = fbbaa + wri * zfbbaa
881 kabba = kabba + wri * zkabba
2882 fabba = fabba + wri * zfabba

```

```

897 NEXT i27

```

```

899 RETURN

```

```

2900 REM Individual Arguments

```

```

2911 fkaaaa = rri * (theta * di * ((zzi - zb) ^ 2 + (rri - rb) ^ 2) + vvi * (rb
2912 ffaaaa = rri * theta * ((rb - rri) * (zb - zzi)) ^ 2 / (det * (dz * dr) ^ 2
2913 fkbaba = rri * (theta * di * ((zb - zzi) ^ 2 + (ra - rri) ^ 2) - vvi * (rri
2914 ffbaba = rri * theta * ((ra - rri) * (zb - zzi)) ^ 2 / (det * (dr * dz) ^ 2
2915 fkbbbb = rri * (theta * di * ((zzi - za) ^ 2 + (rri - ra) ^ 2) - vvi * (rri
2916 ffbbbb = rri * theta * ((ra - rri) * (za - zzi)) ^ 2 / (det * (dr * dz) ^ 2
2917 fkabab = rri * (theta * di * ((za - zzi) ^ 2 + (rb - rri) ^ 2) + vvi * (rb
2918 ffabab = rri * theta * ((rb - rri) * (za - zzi)) ^ 2 / (det * (dr * dz) ^ 2
2919 fkaaba = rri * (theta * di * (-(zzi - zb) ^ 2 + (rri - rb) * (ra - rri)) +
2920 ffaaba = rri * theta * (rb - rri) * (zb - zzi) ^ 2 * (rri - ra) / (det * (d
2921 fkabbb = rri * (theta * di * (-(zzi - za) ^ 2 + (rb - rri) * (rri - ra)) +
2922 ffabbb = rri * theta * (rb - rri) * (zzi - za) ^ 2 * (rri - ra) / (det * (d
2923 fkbaaa = rri * (theta * di * (-(zzi - zb) ^ 2 + (rri - rb) * (ra - rri)) -
2924 ffbaaa = rri * theta * (rb - rri) * (zb - zzi) ^ 2 * (rri - ra) / (det * (d
2925 fkbbab = rri * (theta * di * (-(za - zzi) ^ 2 + (rb - rri) * (rri - ra)) -
2926 ffbbab = rri * theta * (rb - rri) * (zzi - za) ^ 2 * (rri - ra) / (det * (d
2927 fkaaab = rri * (theta * di * ((zzi - zb) * (za - zzi) - (rri - rb) ^ 2) - v
2928 ffaaab = rri * theta * (rb - rri) ^ 2 * (zb - zzi) * (zzi - za) / (det * (d
2929 fkbabb = rri * (theta * di * ((zb - zzi) * (zzi - za) - (ra - rri) ^ 2) - v
2930 ffbabb = rri * theta * (rri - ra) ^ 2 * (zb - zzi) * (zzi - za) / (det * (d
2931 fkabaa = rri * (theta * di * ((zzi - zb) * (za - zzi) - (rri - rb) ^ 2) - v
2932 ffabaa = rri * theta * (rb - rri) ^ 2 * (zb - zzi) * (zzi - za) / (det * (d
2933 fkbbaa = rri * (theta * di * ((zb - zzi) * (zzi - za) - (ra - rri) ^ 2) - v
2934 ffbbaa = rri * theta * (rri - ra) ^ 2 * (zb - zzi) * (zzi - za) / (det * (d
2935 fkaabb = rri * (theta * di * ((zzi - zb) * (zzi - za) + (rri - rb) * (rri -
2936 ffaabb = rri * theta * (rb - rri) * (zb - zzi) * (rri - ra) * (zzi - za) /
2937 fkbaab = rri * (theta * di * ((zb - zzi) * (za - zzi) + (ra - rri) * (rb -
2938 ffbaab = rri * theta * (rb - rri) * (zb - zzi) * (rri - ra) * (zzi - za) /

```

```

2939 fkbbaa = rri * (theta * di * ((zzi - zb) * (zzi - za) + (rri - rb) * (rri
2940 ffbbaa = rri * theta * (rb - rri) * (zb - zzi) * (rri - ra) * (zzi - za) /
2941 fkabba = rri * (theta * di * ((zb - zzi) * (za - zzi) + (ra - rri) * (rb
2942 ffabba = rri * theta * (rb - rri) * (zb - zzi) * (zzi - za) * (rri - ra) /
2950 RETURN
3000 REM Zero the Surface
3001 IF i14 > (nn - nnn) GOTO 3025
3002 REM Zero the Outside
3003 FOR i30 = 1 TO nnn
3005 IF i14 = (i30 * nnn) GOTO 3025
3007 NEXT i30
3010 REM Zero the Lower Corner
3014 IF i14 = 1 GOTO 3025
3020 GOTO 3035
3025 kk(i14, j14) = 0
3026 xx = 0
3027 fk(i14, j14) = 0
3028 yy = 0
3035 RETURN
3100 REM Kf and kfos
3104 IF i14 < nnn GOTO 3130
3105 REM kfo
3107 FOR i31 = 1 TO nnn - 2
3108 IF i14 = (nnn * i31 + 1) GOTO 3111
3110 GOTO 3126
3111 REM Interior Full
3112 ra = rr(i14)
3114 za = zz(i14)
3115 GOSUB 2700
3116 kkk = kaaaa
3117 fff = faaaa
3118 za = zz(i14) - dz
3119 GOSUB 2700
3120 kk(i14, j14) = kkk + kabab
3121 xx = kfo * (rr(i14) + rr(j14)) / 2
3122 fk(i14, j14) = fff + fabab
3123 yy = ff / 2 * (rr(i14) + rr(j14)) / 2
3125 GOTO 3195
3126 NEXT i31
3127 GOTO 3150
3130 REM kfod
3135 ra = rr(i14)
3136 za = zz(i14)
3138 GOSUB 2700
3140 kkk = kaaaa
3142 fff = faaaa
3143 ra = rr(i14) - dr
3144 GOSUB 2700
3145 kk(i14, j14) = kkk + kbaba
3146 xx = kfod * (rr(i14) + rr(j14)) / 2
3147 fk(i14, j14) = fff + fbaba
3148 yy = ff / 2 * (rr(i14) + rr(j14)) / 2
3149 GOTO 3195
3150 REM kf
3152 ra = rr(i14)
3156 za = zz(i14)
3157 GOSUB 2700
3158 kkk = kaaaa
3162 fff = faaaa
3165 ra = rr(i14) - dr

```

```

166 za = zz(i14) - dz
3167 GOSUB 2700
170 kkk = kkk + kbbbbb
172 fff = fff + fbbbbb
3175 ra = rr(i14)
3180 GOSUB 2700
181 kkk = kkk + kabab
182 fff = fff + fabab
3183 ra = rr(i14) - dr
185 za = zz(i14)
187 GOSUB 2700
3188 kk(i14, j14) = kkk + kbaba
189 xx = kf * (rr(i14) + rr(j14)) / 2
190 fk(i14, j14) = fff + fbaba
3192 yy = ff * (rr(i14) + rr(j14)) / 2
3195 RETURN
200 REM krl and Noninteractors
205 FOR I32 = 1 TO nnn - 2
3210 IF i14 = (nnn * I32 + 1) GOTO 3223
212 GOTO 3229
223 kk(i14, j14) = 0
3224 xx = 0
225 fk(i14, j14) = 0
226 yy = 0
3228 GOTO 3285
3229 NEXT I32
230 FOR J32 = 2 TO nnn - 1
232 IF i14 = J32 GOTO 3235
3233 GOTO 3252
235 REM krlo
240 ra = rr(i14) - dr
3242 za = zz(i14)
245 GOSUB 2700
246 kk(i14, j14) = kbaaa
247 xx = krlo * (rr(i14) + rr(j14)) / 2
3248 fk(i14, j14) = fbaaa
249 yy = ff / 8 * (rr(i14) + rr(j14)) / 2
250 GOTO 3285
3252 NEXT J32
254 REM krl
256 ra = rr(i14) - dr
3258 za = zz(i14)
3260 GOSUB 2700
262 kkk = kbaaa
264 fff = fbaaa
3265 za = zz(i14) - dz
268 GOSUB 2700
270 kk(i14, j14) = kkk + kbbab
3271 xx = krl * (rr(i14) + rr(j14)) / 2
272 fk(i14, j14) = fff + fbbab
273 yy = ff / 4 * (rr(i14) + rr(j14)) / 2
3285 RETURN
3300 REM kvd on Inside
305 FOR i33 = 1 TO nnn - 1
330 IF i14 = (i33 * nnn + 1) GOTO 3335
3332 GOTO 3350
335 REM kvdo
336 ra = rr(i14)
3338 za = zz(i14) - dz
3340 GOSUB 2700

```

```

3341 kk(i14, j14) = kabaa
3342 xx = kvdo * (rr(i14) + rr(j14)) / 2
3343 fk(i14, j14) = fabaa
3344 yy = ff / 8 * (rr(i14) + rr(j14)) / 2
3345 GOTO 3385
3350 NEXT i33
3352 REM kvd
3354 ra = rr(i14)
3356 za = zz(i14) - dz
3358 GOSUB 2700
3360 kkk = kabaa
3362 fff = fabaa
3364 ra = rr(i14) - dr
3368 GOSUB 2700
3370 kk(i14, j14) = kkk + kbbba
3371 xx = kvd * (rr(i14) + rr(j14)) / 2
3372 fk(i14, j14) = fff + fbbba
3373 yy = ff / 4 * (rr(i14) + rr(j14)) / 2
3385 RETURN
3400 REM kvu on Inside and Noninteractors
3405 FOR i34 = 1 TO nnn - 2
3430 IF i14 = (i34 * nnn + 1) GOTO 3435
3432 GOTO 3452
3435 REM kvuo
3440 ra = rr(i14)
3442 za = zz(i14)
3444 GOSUB 2700
3446 kk(i14, j14) = kaaab
3447 xx = kvuo * (rr(i14) + rr(j14)) / 2
3448 fk(i14, j14) = faaab
3449 yy = ff / 8 * (rr(i14) + rr(j14)) / 2
3450 GOTO 3485
3452 NEXT i34
3454 REM kvu
3456 ra = rr(i14)
3458 za = zz(i14)
3460 GOSUB 2700
3462 kkk = kaaab
3464 fff = faaab
3466 ra = rr(i14) - dr
3468 GOSUB 2700
3470 kk(i14, j14) = kkk + kbabb
3471 xx = kvu * (rr(i14) + rr(j14)) / 2
3472 fk(i14, j14) = fff + fbabb
3474 yy = ff / 4 * (rr(i14) + rr(j14)) / 2
3485 RETURN
3500 REM Zero the kdl Elements on Inside Boundary
3505 FOR i35 = 1 TO nnn - 2
3510 IF i14 = (i35 * nnn + 1) GOTO 3520
3515 GOTO 3550
3520 kk(i14, j14) = 0
3521 xx = 0
3522 fk(i14, j14) = 0
3523 yy = 0
3525 GOTO 3585
3550 NEXT i35
3552 REM kdl
3554 ra = rr(i14) - dr
3556 za = zz(i14) - dz
3558 GOSUB 2700

```



```

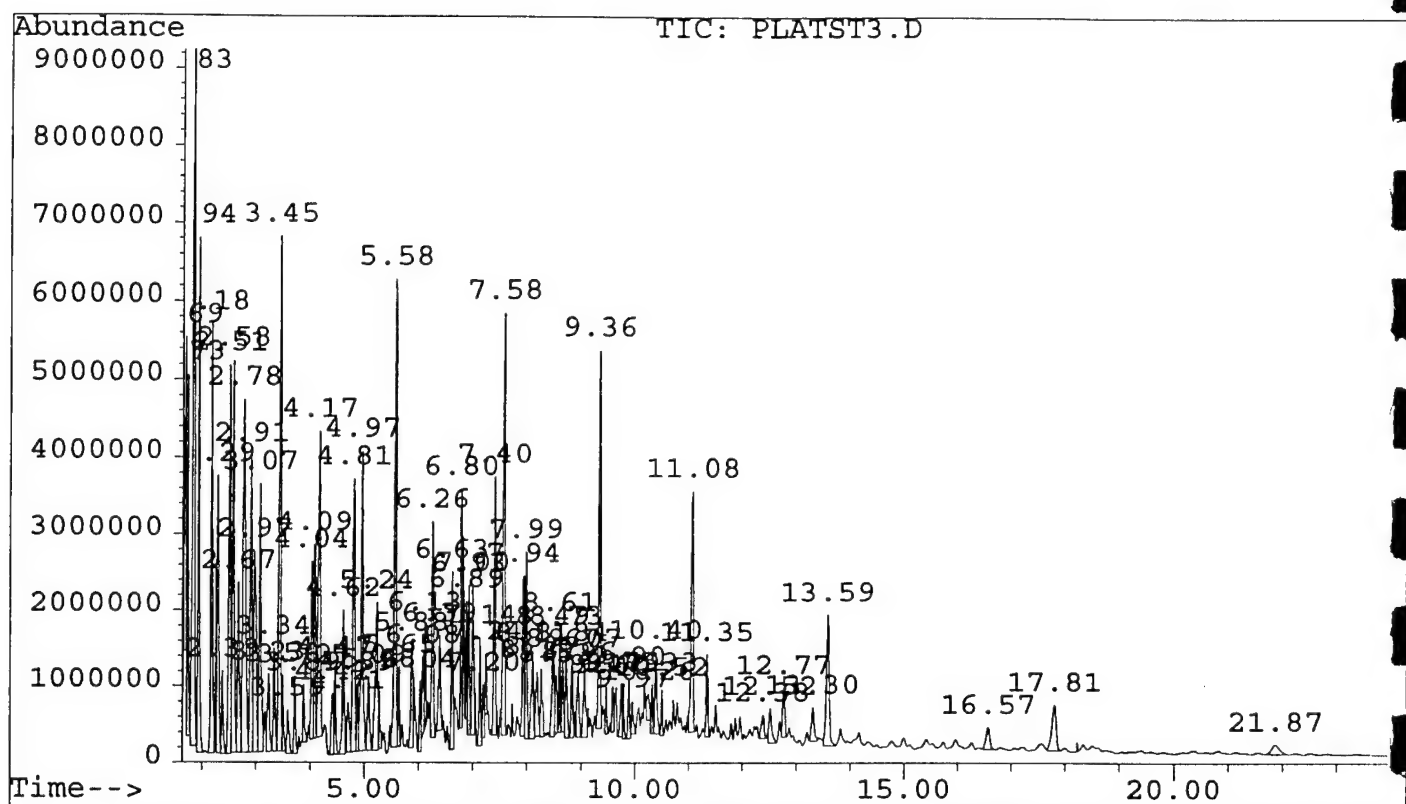
560 kk(i14, j14) = kbbaa
3561 xx = kdl * (rr(i14) + rr(j14)) / 2
562 fk(i14, j14) = fbbaa
563 yy = ff / 16 * (rr(i14) + rr(j14)) / 2
3585 RETURN
3600 REM krr on Bottom
605 FOR I36 = 2 TO nnn - 1
610 IF i14 = I36 GOTO 3635
3633 GOTO 3650
635 REM krro
636 ra = rr(i14)
3638 za = zz(i14)
640 GOSUB 2700
642 kk(i14, j14) = kaaba
643 xx = krro * (rr(i14) + rr(j14)) / 2
644 fk(i14, j14) = faaba
645 yy = ff / 8 * (rr(i14) + rr(j14)) / 2
648 GOTO 3695
3650 NEXT I36
653 REM krr
654 ra = rr(i14)
3656 za = zz(i14)
657 GOSUB 2700
658 kkk = kaaba
660 fff = faaba
3661 ra = rr(i14)
664 za = zz(i14) - dz
665 GOSUB 2700
3666 kk(i14, j14) = kkk + kabbb
668 xx = krr * (rr(i14) + rr(j14)) / 2
670 fk(i14, j14) = fff + fabbb
3672 yy = ff / 4 * (rr(i14) + rr(j14)) / 2
3695 RETURN
700 REM Zero the kul Elements on Inside Boundary
705 FOR i37 = 1 TO nnn - 1
3710 IF i14 = (i37 * nnn + 1) GOTO 3720
715 GOTO 3750
720 kk(i14, j14) = 0
3721 xx = 0
722 fk(i14, j14) = 0
723 yy = 0
3725 GOTO 3785
3750 NEXT i37
752 REM kul
755 ra = rr(i14) - dr
3756 za = zz(i14)
757 GOSUB 2700
759 kk(i14, j14) = kbaab
3760 xx = kul * (rr(i14) + rr(j14)) / 2
761 fk(i14, j14) = fbaab
762 yy = ff / 16 * (rr(i14) + rr(j14)) / 2
3785 RETURN
4600 REM kur
605 ra = rr(i14)
610 za = zz(i14)
4615 GOSUB 2700
620 kk(i14, j14) = kaabb
625 xx = kur * (rr(i14) + rr(j14)) / 2
4650 fk(i14, j14) = faabb
4652 yy = ff / 16 * (rr(i14) + rr(j14)) / 2

```

```
4685 RETURN
4700 REM kdr
4705 ra = rr(i14)
4710 za = zz(i14) - dz
4715 GOSUB 2700
4720 kk(i14, j14) = kabba
4725 xx = kdr * (rr(i14) + rr(j14)) / 2
4750 fk(i14, j14) = fabba
4755 yy = ff / 16 * (rr(i14) + rr(j14)) / 2
4752 RETURN
```

## **APPENDIX VI GCD OUTPUT FOR SEPARATE PHASE ANALYSIS**

File : C:\HPCHEM\1\DATA\PLATST3.D  
Operator :  
Acquired : 13 Dec 95 1:48 pm using AcqMethod PLATFAZE  
Instrument : GCD  
Sample Name:  
Misc Info :  
Vial Number: 1



## Summary Library Search Report

## Information from Data File:

File: C:\HPCHEM\1\DATA\PLATST3.D  
Acquired: 13 Dec 95 1:48 pm using AcqMethod PLATFAZE  
Sample Name:  
Info:  
Number: 1

Search Libraries: C:\DATABASE\NBS75K.L Minimum Quality: 0

Own Spectrum: Apex minus start of peak  
Integration Params: current RTEINT parameters

RT	Area%	Library/ID	Ref#	CAS#	Qual
1.69	1.83	C:\DATABASE\NBS75K.L			
		Pentane, 2,3-dimethyl-	63429	000565-59-3	87
		Heptane	1600	000142-82-5	64
		1-Pentanol, 2,3-dimethyl-	3343	010143-23-4	59
1.73	1.72	C:\DATABASE\NBS75K.L			
		Hexane, 3-methyl-	63421	000589-34-4	87
		Pentane, 3-ethyl-	1595	000617-78-7	87
		Hexane, 2,3-dimethyl-	3097	000584-94-1	64
1.83	4.99	C:\DATABASE\NBS75K.L			
		Butane, 2,2,3,3-tetramethyl-	64215	000594-82-1	78
		Hexane, 2,2-dimethyl-	64217	000590-73-8	78
		Heptane, 2,2,4-trimethyl-	8105	014720-74-2	72
1.94	3.14	C:\DATABASE\NBS75K.L			
		Heptane	63440	000142-82-5	93
		Hexane, 3-methyl-	1593	000589-34-4	62
		Pentane, 3-ethyl-	63426	000617-78-7	38
2.18	2.91	C:\DATABASE\NBS75K.L			
		Cyclohexane, methyl-	1326	000108-87-2	96
		2-Pentene, 4,4-dimethyl-, (E)-	1344	000690-08-4	70
		2-Pentene, 2,4-dimethyl-	63270	000625-65-0	70

2.29	2.07	C:\DATABASE\NBS75K.L			
		Hexane, 3,4-dimethyl-	64210	000583-48-2	78
		Butane, 2,2,3-trimethyl-	63437	000464-06-2	53
		Hexane, 2,4-dimethyl-	3089	000589-43-5	50
2.39	0.52	C:\DATABASE\NBS75K.L			
		Cyclopentane, 1,2,4-trimethyl-	2680	002815-58-9	78
		Cyclopentane, 1,2,4-trimethyl-, (1.al	2684	004850-28-6	74
		Undecane, 3-methylene-	14736	071138-64-2	72
2.51	3.00	C:\DATABASE\NBS75K.L			
		Pentane, 2,3,4-trimethyl-	3100	000565-75-3	90
		Hexane, 2,3-dimethyl-	3097	000584-94-1	87
		Heptane, 4-methyl-	3096	000589-53-7	74
2.58	2.79	C:\DATABASE\NBS75K.L			
		Pentane, 2,3,3-trimethyl-	3088	000560-21-4	90
		Hexane, 2,3,4-trimethyl-	5147	000921-47-1	64
		Hexane, 3-methyl-	1593	000589-34-4	64
2.67	1.41	C:\DATABASE\NBS75K.L			
		Hexane, 2,3-dimethyl-	64226	000584-94-1	78
		Heptane, 4-methyl-	64224	000589-53-7	64
		Pentane, 3-ethyl-	1595	000617-78-7	64
2.78	3.79	C:\DATABASE\NBS75K.L			
		Heptane, 2-methyl-	64219	000592-27-8	95
		Hexane, 2,5-dimethyl-	64204	000592-13-2	53
		Pentane, 2-methyl-	62863	000107-83-5	50
2.91	2.39	C:\DATABASE\NBS75K.L			
		Heptane, 3-methyl-	64227	000589-81-1	91
		Octane, 3,4-dimethyl-	8107	015869-92-8	72
		Hexane, 2,4-dimethyl-	64213	000589-43-5	68
2.97	1.91	C:\DATABASE\NBS75K.L			
		Cyclohexane, 1,3-dimethyl-, cis-	64018	000638-04-0	95
		Cyclohexane, 1,3-dimethyl-	2687	000591-21-9	94
		Cyclohexane, 1,4-dimethyl-, trans-	2668	002207-04-7	91
3.07	2.16	C:\DATABASE\NBS75K.L			

		Hexane, 2,2,5-trimethyl-	65126	003522-94-9	83
		Hexane, 2,2,4-trimethyl-	5131	016747-26-5	78
		Hexane, 2,2,5,5-tetramethyl-	66226	001071-81-4	72
3.23	0.73	C:\DATABASE\NBS75K.L			
		Cyclopentane, 1-ethyl-2-methyl-, cis-	2670	000930-89-2	93
		Cyclopentane, 1-ethyl-3-methyl-, tran	2698	002613-65-2	90
		Cyclopentane, 1-ethyl-3-methyl-	2696	003726-47-4	90
3.34	0.76	C:\DATABASE\NBS75K.L			
		Cyclohexane, 1,3-dimethyl-, trans-	64001	002207-03-6	94
		Cyclohexane, 1,2-dimethyl-, trans-	64014	006876-23-9	94
		Cyclohexane, 1,4-dimethyl-	64013	000589-90-2	91
3.45	4.10	C:\DATABASE\NBS75K.L			
		Octane	3084	000111-65-9	90
		Hexane, 2,4-dimethyl-	3089	000589-43-5	64
		Ether, hexyl pentyl	15858	032357-83-8	59
3.50	0.43	C:\DATABASE\NBS75K.L			
		Cyclohexane, 1,3-dimethyl-, cis-	64018	000638-04-0	95
		Cyclohexane, 1,3-dimethyl-, trans-	2661	002207-03-6	91
		Cyclohexane, 1,4-dimethyl-, cis-	2704	000624-29-3	91
3.59	0.37	C:\DATABASE\NBS75K.L			
		Tetrachloroethylene	13222	000127-18-4	99
		Pyrimidine, 5-fluoro-2,4-dichloro-	13787	002927-71-1	16
		2-Chloroquinoxaline	13329	001448-87-9	16
3.72	0.53	C:\DATABASE\NBS75K.L			
		Hexane, 2,3,5-trimethyl-	65140	001069-53-0	90
		Heptane, 2,4-dimethyl-	65120	002213-23-2	81
		Pentane, 3-ethyl-2,4-dimethyl-	5138	001068-87-7	78
3.89	0.38	C:\DATABASE\NBS75K.L			
		Heptane, 2,4-dimethyl-	65120	002213-23-2	91
		Dodecane, 5-methyl-	19034	017453-93-9	59
		Hexane, 2,4-dimethyl-	3089	000589-43-5	59
4.04	1.48	C:\DATABASE\NBS75K.L			
		Heptane, 2,6-dimethyl-	5156	001072-05-5	94
		Octane, 2-methyl-	65117	003221-61-2	90

	Dodecane	68249	000112-40-3	64
4.09	1.23 C:\DATABASE\NBS75K.L			
	Cyclohexane, ethyl-	64006	001678-91-7	90
	Cyclohexane, undecyl-	31654	054105-66-7	64
	Cyclohexane, octyl-	21971	001795-15-9	56
4.17	2.57 C:\DATABASE\NBS75K.L			
	Cyclohexane, 1,1,3-trimethyl-	64942	003073-66-3	50
	Cyclohexane, 1,3,5-trimethyl-, (1.alp	4669	001795-27-3	47
	Cyclooctane, butyl-	14729	016538-93-5	43
4.42	0.59 C:\DATABASE\NBS75K.L			
	1-Nonene	64956	000124-11-8	43
	1-Heptanol, 4-methyl-	5564	000817-91-4	43
	Cyclopentane, 1,3-dimethyl-, trans-	1329	001759-58-6	43
4.47	0.58 C:\DATABASE\NBS75K.L			
	Cyclohexane, 1,3,5-trimethyl-, (1.alp	64953	001795-27-3	91
	Cyclohexane, 1,3,5-trimethyl-	64930	001839-63-0	91
	Cyclohexane, 1,1,3-trimethyl-	4647	003073-66-3	64
4.62	1.15 C:\DATABASE\NBS75K.L			
	Heptane, 2,3-dimethyl-	65133	003074-71-3	86
	Hexane, 3-ethyl-2-methyl-	5160	016789-46-1	80
	Decane, 5,6-dimethyl-	15355	001636-43-7	72
4.71	0.47 C:\DATABASE\NBS75K.L			
	Ethylbenzene	63691	000100-41-4	91
	p-Xylene	63700	000106-42-3	50
	Benzene, 1,3-dimethyl-	2027	000108-38-3	43
4.81	2.57 C:\DATABASE\NBS75K.L			
	Octane, 2-methyl-	5142	003221-61-2	91
	Heptane, 2,6-dimethyl-	65137	001072-05-5	90
	Decane, 2,9-dimethyl-	15361	001002-17-1	72
4.89	0.43 C:\DATABASE\NBS75K.L			
	Benzene, 1,3-dimethyl-	63695	000108-38-3	97
	Benzene, 1,2-dimethyl-	63707	000095-47-6	97
	p-Xylene	63702	000106-42-3	97



4.97	2.46	C:\DATABASE\NBS75K.L			
		Octane, 3-methyl-	65130	002216-33-3	87
		Decane, 5-methyl-	11605	013151-35-4	53
		Heptane, 2,5-dimethyl-	5143	002216-30-0	53
5.09	0.66	C:\DATABASE\NBS75K.L			
		2-Pyrrolidinone, 1-ethenyl-	63902	000088-12-0	50
		Pentane, 3-ethyl-2,2-dimethyl-	5136	016747-32-3	47
		Cyclohexane, 1,1,2-trimethyl-	64970	007094-26-0	46
5.24	1.68	C:\DATABASE\NBS75K.L			
		1-Ethyl-3-methylcyclohexane (c,t)	4658	003728-55-0	81
		cis-1-Ethyl-3-methyl-cyclohexane	4636	019489-10-2	81
		Cyclohexane, 1-ethyl-2-methyl-, trans	4650	004923-78-8	70
5.28	0.33	C:\DATABASE\NBS75K.L			
		Cyclohexane, 1-ethyl-4-methyl-, trans	64955	006236-88-0	83
		Cyclohexane, 1-methyl-4-(1-methylethy	66078	006069-98-3	78
		Cyclohexane, 1-ethyl-4-methyl-, cis-	64934	004926-78-7	64
5.58	4.01	C:\DATABASE\NBS75K.L			
		Nonane	65142	000111-84-2	87
		1-Octanol, 2-butyl-	69110	003913-02-8	59
		Octane	64207	000111-65-9	59
5.65	0.41	C:\DATABASE\NBS75K.L			
		Cyclohexane, 1-bromo-3-methyl-	16582	013905-48-1	64
		Cyclohexane, 1-bromo-4-methyl-	16585	006294-40-2	64
		cis-1-Ethyl-3-methyl-cyclohexane	4636	019489-10-2	52
5.88	0.83	C:\DATABASE\NBS75K.L			
		Bicyclo[3.3.1]nonane	64809	000280-65-9	76
		Pentalene, octahydro-2-methyl-	4274	003868-64-2	64
		Bicyclo[4.1.0]heptane	63134	000286-08-8	58
6.04	0.45	C:\DATABASE\NBS75K.L			
		Benzene, (1-methylethyl)-	64555	000098-82-8	93
		Benzene, 1,2,3-trimethyl-	3773	000526-73-8	80
		Benzene, 1-ethyl-2-methyl-	64558	000611-14-3	72
6.08	0.47	C:\DATABASE\NBS75K.L			
		1-Decanol, 2-ethyl-	19527	021078-65-9	59

		Octane, 3,5-dimethyl-	66229	015869-93-9	49
		Hexane, 3-ethyl-4-methyl-	5162	003074-77-9	47
6.13	0.55	C:\DATABASE\NBS75K.L			
		Cyclohexane, (1-methylethyl)-	4682	000696-29-7	91
		Cyclohexane, propyl-	4637	001678-92-8	90
		Cyclohexane, hexyl-	68123	004292-75-5	72
6.26	1.43	C:\DATABASE\NBS75K.L			
		Octane, 3,6-dimethyl-	8109	015869-94-0	90
		Nonane, 3-methyl-	66200	005911-04-6	90
		Octane, 2,6-dimethyl-	8103	002051-30-1	80
6.39	0.78	C:\DATABASE\NBS75K.L			
		Heptane, 3-ethyl-2-methyl-	8080	014676-29-0	72
		Heptane, 4-(1-methylethyl)-	8084	052896-87-4	47
		Undecane, 5,6-dimethyl-	19004	017615-91-7	47
6.63	1.16	C:\DATABASE\NBS75K.L			
		Benzene, propyl-	3781	000103-65-1	83
		1,2-Ethanediamine, N,N'-bis(phenylmet	32052	000140-28-3	25
		Propanenitrile, 3-[(phenylmethyl)amin	12493	000706-03-6	25
6.80	1.67	C:\DATABASE\NBS75K.L			
		Benzene, 1-ethyl-3-methyl-	64563	000620-14-4	93
		Benzene, 1-ethyl-2-methyl-	64559	000611-14-3	93
		Benzene, 1-ethyl-4-methyl-	3770	000622-96-8	93
6.89	0.56	C:\DATABASE\NBS75K.L			
		Nonane, 2-methyl-	66220	000871-83-0	91
		Octane, 2,7-dimethyl-	66209	001072-16-8	78
		Decane	66205	000124-18-5	72
6.93	0.82	C:\DATABASE\NBS75K.L			
		Benzene, 1,2,3-trimethyl-	64573	000526-73-8	95
		1,2,4-Trimethylbenzene	3771	000095-36-3	95
		Benzene, 1,3,5-trimethyl-	64569	000108-67-8	94
7.00	0.96	C:\DATABASE\NBS75K.L			
		Nonane, 3-methyl-	66200	005911-04-6	70
		Octane, 4,5-dimethyl-	8076	015869-96-2	38
		Octane, 2,3,7-trimethyl-	11603	062016-34-6	38

7.14	0.67	C:\DATABASE\NBS75K.L			
		Benzene, 1-ethyl-2-methyl-	3765	000611-14-3	94
		Benzene, 1,3,5-trimethyl-	64570	000108-67-8	91
		Benzene, (1-methylethyl)-	64553	000098-82-8	91
7.20	0.31	C:\DATABASE\NBS75K.L			
		Cyclohexane, 1-methyl-4-(1-methylethyl)-	7600	001678-82-6	74
		Cyclohexane, 1-methyl-3-propyl-	7596	004291-80-9	72
		Cyclohexane, 1-methyl-2-propyl-	7590	004291-79-6	72
7.24	0.32	C:\DATABASE\NBS75K.L			
		1-Methyl-4-(1-methylethyl)-cyclohexan	66083	000099-82-1	45
		Cyclohexane, 1-methyl-4-(1-methylethyl)-	66079	001678-82-6	43
		Cyclohexane, 1-methyl-4-(1-methylethyl)-	66077	006069-98-3	41
7.40	1.67	C:\DATABASE\NBS75K.L			
		Benzene, 1,2,3-trimethyl-	64573	000526-73-8	94
		Benzene, 1,3,5-trimethyl-	64569	000108-67-8	94
		Benzene, 1,2,4-trimethyl-	64577	000095-63-6	94
7.58	2.87	C:\DATABASE\NBS75K.L			
		Decane	66205	000124-18-5	97
		Undecane	67317	001120-21-4	86
		Heneicosane	72684	000629-94-7	83
7.94	1.14	C:\DATABASE\NBS75K.L			
		1,2,4-Trimethylbenzene	3771	000095-36-3	94
		Benzene, 1,2,3-trimethyl-	64576	000526-73-8	93
		Benzene, 1,2,4-trimethyl-	3775	000095-63-6	93
7.99	1.21	C:\DATABASE\NBS75K.L			
		Decane, 4-methyl-	67323	002847-72-5	94
		Nonane, 2,6-dimethyl-	11598	017302-28-2	91
		Octane, 2,3,6-trimethyl-	11602	062016-33-5	78
8.11	0.73	C:\DATABASE\NBS75K.L			
		Cyclohexane, butyl-	66057	001678-93-9	93
		Cyclohexane, ethyl-	64006	001678-91-7	83
		Cyclohexane, propyl-	64935	001678-92-8	80
8.19	0.69	C:\DATABASE\NBS75K.L			

		Decane, 3-methyl-	67315	013151-34-3	70
		Hexadecane	70787	000544-76-3	49
		Dotriacontane	74490	000544-85-4	47
8.27	0.53	C:\DATABASE\NBS75K.L			
		Decane, 3-methyl-	67315	013151-34-3	87
		Nonane, 3,7-dimethyl-	11601	017302-32-8	59
		Nonane, 3-methyl-	66203	005911-04-6	47
8.49	0.85	C:\DATABASE\NBS75K.L			
		Benzene, 1-methyl-3-propyl-	6195	001074-43-7	90
		Benzene, 1-methyl-2-propyl-	6230	001074-17-5	55
		Benzene, (1-methylpropyl)-	65543	000135-98-8	50
8.53	0.46	C:\DATABASE\NBS75K.L			
		Benzene, 1-methyl-2-propyl-	65584	001074-17-5	92
		Benzene, 1-methyl-4-propyl-	6216	001074-55-1	70
		Benzene, (1-methylpropyl)-	65543	000135-98-8	62
8.61	0.52	C:\DATABASE\NBS75K.L			
		Decane, 5-methyl-	11605	013151-35-4	70
		Benzene, 1-methyl-4-(1-methylethyl)-	6201	000099-87-6	64
		Benzene, 4-ethyl-1,2-dimethyl-	65568	000934-80-5	64
8.67	0.41	C:\DATABASE\NBS75K.L			
		Decane, 4-methyl-	11615	002847-72-5	97
		Decane, 2,6,7-trimethyl-	19027	062108-25-2	78
		1,2-Cyclohexanediol, 1-methyl-, trans	5409	019534-08-8	72
8.73	0.75	C:\DATABASE\NBS75K.L			
		Decane, 2-methyl-	67320	006975-98-0	93
		Undecane, 5-methyl-	15363	001632-70-8	72
		Tridecane	69019	000629-50-5	64
8.84	0.47	C:\DATABASE\NBS75K.L			
		Decane, 3-methyl-	67314	013151-34-3	97
		Nonane, 3,7-dimethyl-	11601	017302-32-8	83
		Nonane, 5-(2-methylpropyl)-	19015	062185-53-9	64
8.96	0.62	C:\DATABASE\NBS75K.L			
		Benzene, 4-ethyl-1,2-dimethyl-	65568	000934-80-5	91
		Benzene, 1,2,3,5-tetramethyl-	6220	000527-53-7	91

Benzene, 1-methyl-4-(1-methylethyl)- 65534 000099-87-6 91

9.07 0.75 C:\DATABASE\NBS75K.L  
 Benzene, 1,2,3,4-tetramethyl- 65540 000488-23-3 83  
 Benzene, 1,2,4,5-tetramethyl- 65575 000095-93-2 83  
 Benzene, 1-methyl-4-(1-methylethyl)- 65534 000099-87-6 81

9.36 2.39 C:\DATABASE\NBS75K.L  
 Undecane 67317 001120-21-4 96  
 Tridecane 69020 000629-50-5 90  
 Undecane, 2,3-dimethyl- 18990 017312-77-5 83

9.47 0.28 C:\DATABASE\NBS75K.L  
 Naphthalene, decahydro-2-methyl- 67009 002958-76-1 90  
 Cyclohexanone, 5-methyl-2-(1-methylethyl)- 10356 015932-80-6 76  
 1-Dodecyne 68014 000765-03-7 74

9.60 0.34 C:\DATABASE\NBS75K.L  
 Benzene, 1-methyl-4-(1-methylethyl)- 65535 000099-87-6 91  
 Benzene, 1,2,4,5-tetramethyl- 65576 000095-93-2 91  
 Benzene, 2-ethyl-1,4-dimethyl- 65570 001758-88-9 70

9.75 0.36 C:\DATABASE\NBS75K.L  
 Naphthalene, decahydro-2-methyl- 67008 002958-76-1 90  
 Bicyclo[4.1.0]heptan-3-one, 4,7,7-tri 10380 004176-04-9 60  
 Bicyclo[2.2.1]heptan-2-one, 1,7,7-tri 66961 000464-48-2 58

9.79 0.31 C:\DATABASE\NBS75K.L  
 Undecane, 3,8-dimethyl- 19009 017301-30-3 83  
 Undecane, 4,7-dimethyl- 19020 017301-32-5 78  
 Undecane, 4-methyl- 15354 002980-69-0 68

9.90 0.34 C:\DATABASE\NBS75K.L  
 n-Amylcyclohexane 11054 029949-27-7 90  
 Cyclohexane, pentyl- 11044 004292-92-6 87  
 Cyclohexane, (1-methylethyl)- 64963 000696-29-7 74

9.97 0.25 C:\DATABASE\NBS75K.L  
 Cyclopentane, pentyl- 7536 003741-00-2 38  
 Cyclopentane, butyl- 64938 002040-95-1 35  
 Cyclopentane, (1-methylethyl)- 2707 003875-51-2 30

10.26	0.26	C:\DATABASE\NBS75K.L			
		Decane, 3,6-dimethyl-	15348	017312-53-7	52
		1-Iodo-2-methylnonane	37255	000000-00-0	49
		Octane, 3-ethyl-2,7-dimethyl-	15359	062183-55-5	47
10.33	0.29	C:\DATABASE\NBS75K.L			
		Undecane, 4-methyl-	15354	002980-69-0	58
		Undecane, 4,8-dimethyl-	19026	017301-33-6	47
		Dodecane, 2,6,10-trimethyl-	25995	003891-98-3	38
10.40	0.60	C:\DATABASE\NBS75K.L			
		Undecane, 2-methyl-	15356	007045-71-8	95
		Decane, 2,9-dimethyl-	15361	001002-17-1	72
		Undecane, 5-methyl-	15363	001632-70-8	58
10.52	0.28	C:\DATABASE\NBS75K.L			
		Undecane, 3-methyl-	15362	001002-43-3	78
		Decane, 3,8-dimethyl-	68255	017312-55-9	76
		Undecane, 5-methyl-	15363	001632-70-8	64
11.08	1.91	C:\DATABASE\NBS75K.L			
		Dodecane	68254	000112-40-3	95
		Tridecane	69019	000629-50-5	91
		Hexadecane	70787	000544-76-3	90
11.35	0.62	C:\DATABASE\NBS75K.L			
		Undecane, 2,6-dimethyl-	69033	017301-23-4	96
		Dodecane, 6-methyl-	19006	006044-71-9	94
		Undecane, 3,6-dimethyl-	19000	017301-28-9	90
12.38	0.28	C:\DATABASE\NBS75K.L			
		Dodecane, 4-methyl-	19025	006117-97-1	95
		3-Octen-2-one, 7-methyl-	7459	033046-81-0	53
		Pentane, 2,3,4-trimethyl-	3100	000565-75-3	30
12.52	0.41	C:\DATABASE\NBS75K.L			
		Dodecane, 2-methyl-	19039	001560-97-0	72
		Tetradecane, 2-methyl-	70279	001560-95-8	64
		Decane, 2-methyl-	67320	006975-98-0	59
12.77	0.42	C:\DATABASE\NBS75K.L			
		Dodecane, 4,6-dimethyl-	69666	061141-72-8	83

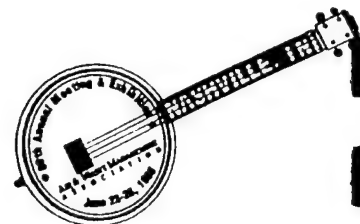
		Tridecane, 4-methyl-	69665	026730-12-1	72
		Octane, 2,3,7-trimethyl-	11603	062016-34-6	72
13.30	0.37	C:\DATABASE\NBS75K.L			
		Naphthalene, 2-methyl-	66236	000091-57-6	94
		Naphthalene, 1-methyl-	66231	000090-12-0	91
		Benzocycloheptatriene	8114	000264-09-5	90
13.59	1.55	C:\DATABASE\NBS75K.L			
		Tridecane	69019	000629-50-5	97
		Hexadecane	70789	000544-76-3	90
		Dodecane	68249	000112-40-3	90
16.57	0.35	C:\DATABASE\NBS75K.L			
		Dodecane, 2,6,11-trimethyl-	25998	031295-56-4	86
		Dodecane, 2,7,10-trimethyl-	26005	074645-98-0	80
		Dodecane, 2,6,10-trimethyl-	25995	003891-98-3	80
17.81	0.86	C:\DATABASE\NBS75K.L			
		Tetradecane	69658	000629-59-4	91
		Tridecane	69019	000629-50-5	91
		Hexadecane	70789	000544-76-3	90
21.87	0.31	C:\DATABASE\NBS75K.L			
		Tetradecane	69661	000629-59-4	80
		Decane, 5-propyl-	19035	017312-62-8	72
		Dodecane, 2,6,10-trimethyl-	70270	003891-98-3	72

Wed Dec 13 14:21:49 1995

**APPENDIX VII EMISSIONS ISOLATION FLUX  
CHAMBER**



# 1996 Annual Meeting Abstract Form



Paper No. 96-TP40.01

Paper Title Evaluation of Surface Emissions from Bioventing Sites

Citation: Tehrany, J.P., P.O. Reyes, S.J. Ergas, and D.W. Ostendorf (1996) "Evaluation of Surface Emissions from Bioventing Sites" Proceedings of the 89th Annual Meeting of the Air and Waste Management Assoc., Nashville, TN.

Author(s)

1. J. Pierre Tehrany

5. \_\_\_\_\_

2. Paul O. Reyes

6. \_\_\_\_\_

3. Sarina J. Ergas

7. \_\_\_\_\_

4. David W. Ostendorf

8. \_\_\_\_\_

Speaker Paul O. Reyes

Type brief description ...300 words or less. Use boxed area below.

Bioventing has become a popular means of remediating hazardous waste sites contaminated with aerobically biodegradable volatile organic compounds (VOCs). Bioventing systems can operate under positive or negative pressure. Positive pressure systems may have advantages with regard to treatment efficiency by forcing VOCs and oxygen through the microbially active rhizosphere. Emissions from positive pressure bioventing systems, however, can pose health and regulatory concerns and may also overstate the effectiveness of the process.

This paper investigates two proposed methods of quantifying air impacts from a bioventing site at a former air force base in Plattsburgh, New York, contaminated with VOCs. The first method uses a modified version of an enclosed isolation flux chamber (EIFC) design developed for the EPA. The EIFC is placed over the soil to be sampled, allowing a direct measurement of VOC flux from the soil. For this study, the EIFC collection method was modified from the EPA design to compensate for advective flux.

The second method utilizes a low volume soil gas probe which is used to obtain a vertically resolved profile of vapor phase contaminant concentrations in the near surface soil zone. The soil gas profiler (SGP) permits the extraction of small volume samples of soil gas at regular intervals from ground level to 45 cm below the surface. The resolved vertical profiles of such soil gas constituents as VOCs, oxygen, carbon dioxide, and conservative tracers document biotic and abiotic transport processes through the rhizosphere. The contaminant flux can be calculated from these profiles when combined with mathematical models of fate and transport of gases and vapors in porous media.

A laboratory evaluation of the EIFC and SGP methods was conducted under controlled conditions using a mesoscale bioventing system and helium as a conservative tracer. Mixing characteristics of the EIFC were evaluated and sweep gas flow rate and sampling times were optimized. A calibrated flux was determined using resolved vertical profiles obtained with the SGP and a simple transport model. Helium flux was also measured directly using the EIFC. Results indicate a slight underprediction of mass flux but consistent agreement between EIFC and SGP methods.

Evaluation of Surface Emissions from Bioventing Sites

J. Pierre Tehrany  
Paul O. Reyes  
Sarina J. Ergas  
David W. Ostendorf

Department of Civil and Environmental Engineering  
University of Massachusetts at Amherst  
Amherst, MA 01003

## INTRODUCTION

Bioventing is an attractive means of remediating hazardous waste sites contaminated with volatile organic compounds (VOCs). For aerobically biodegradable VOCs, advantages of bioventing include low cost and the ability to degrade contaminants to carbon dioxide and water.

Bioventing systems can operate under either negative or positive pressure. In negative pressure systems, a vacuum is applied to the subsurface to induce air and contaminant vapor flow toward an extraction well. The extraction well becomes a point source for off-gases, which can either be vented to the atmosphere or treated. In positive pressure systems, air is injected into the subsurface to induce air flow toward the soil surface. Positive pressure systems may have advantages with regard to treatment efficiency by moving VOCs and oxygen through the microbially active rhizosphere. Fugitive VOC emissions from positive pressure bioventing systems, however, may pose health and regulatory concerns and can overstate the effectiveness of the bioventing process. Air emissions can result from incomplete mineralization of biodegradable compounds or from volatilization of compounds such as tetrachloroethene (PCE) which are not degraded under the given conditions.

The fate of VOCs was considered during a bioventing treatability study conducted at the former Plattsburgh Air Force Base (PAFB)<sup>1</sup>. Over a period of four decades, fire training exercises were conducted at PAFB. During these exercises, bermed fire training pits were filled with water, jet fuel and spent solvents. The mixture was then ignited and extinguished. Unburned fuel migrated into the subsurface resulting in soil and groundwater contamination. The site is currently being remediated as part of the base closure process.<sup>1</sup>

Methods of measuring surface emissions from hazardous waste remediation sites include: 1) an inversion algorithm that relies on downwind measurements;<sup>2</sup> 2) remote sensing methods that utilize differential absorption Light Detection and Ranging (LIDAR), Fourier Transform Infrared (FTIR), and ultraviolet (UV) sensors to quantify emissions; and 3) an emission isolation flux chamber (EIFC) method.<sup>3</sup> The inversion algorithm method relies on downwind measurements of contaminants in order to back calculate total emissions. While this method can be accurate, it only works under steady wind and near neutral atmospheric conditions. Since meteorological conditions can not be known beforehand at the site, this method was not considered further in this project. Remote sensing methods, while accurate under most atmospheric conditions, are expensive and were therefore discounted.

The method that was considered to be the most applicable to the site given the budgetary constraints, site conditions and the scope of the proposed research was the EIFC method. In addition, a second method which uses a soil gas profile of the rhizosphere was developed by the authors to calculate emissions. This paper presents the results of an evaluation of the proposed methods for determining soil surface flux of VOCs. Specific objectives include: 1) evaluation and modification of EIFC for direct measurement of surface emissions; 2) development of a soil gas profiler (SGP) for near surface soil gas sampling; 3) testing of the EIFC and the SGP in a mesoscale bioventing system (MBS) using a conservative tracer; and 4) application of a mathematical model of contaminant transport and surface flux to the mesoscale system.

The EIFC method uses a modified version of a design developed for the EPA.<sup>3</sup> The EIFC allows a direct measurement of VOC flux from the soil. Sampling is performed at randomly selected points on a grid superimposed over the contaminated zone. The EIFC method was previously used to monitor

emissions at the site, however, data obtained showed a high degree of variability. The high variability may have been due to spatial variation in the emissions or to the inappropriate use of the EIFC, which was developed to measure emissions caused by diffusion (passive flow) and not by advection (forced flow) as in bioventing. For this study, the EIFC collection method was modified from the EPA design to compensate for advective flow.

The SGP permits the extraction of small volume samples of soil gas at regular intervals from ground level to 45 cm below the surface. Soil gas profiler data is used to calibrate a model of contaminant fate and transport. An estimation of contaminant flux at the soil/atmosphere interface is calculated from the calibrated model.

## THEORETICAL DEVELOPMENT

A simple analytical model of the transport of a conservative tracer through a soil column is presented in this section. In addition, a mass balance over an EIFC is presented.

### Transport Model

A simple analytical model of transport was used to describe the flux of a conservative tracer through a mesoscale bioventing system (MBS). The porous media was assumed to be homogeneous and isotropic and the mass flux was assumed to be constant. Sorption and chemical and biological reactions were also assumed to be insignificant. A balance of mass flux, diffusion, and advection yields the differential equation shown as Equation 1.

$$J = vC_z - \theta_A D^* \frac{dC_z}{dz} \quad (1)$$

where

- $J$  = Tracer flux ( $\mu\text{g m}^{-2} \text{s}^{-1}$ )
- $C_z$  = Tracer concentration ( $\mu\text{g m}^{-3}$ )
- $v$  = Specific discharge ( $\text{m s}^{-1}$ )
- $D^*$  = Effective diffusion coefficient, constant ( $\text{m}^2 \text{s}^{-1}$ )
- $\theta_A$  = Air-filled porosity, constant (dimensionless)
- $z$  = Vertical distance (m)

A schematic of the MBS, indicating the direction of tracer flow, is shown in Figure 1. Imposing the boundary condition of  $C = 0$  at  $z = 0$  (assuming the tracer is swept away from the surface), Equation 1 can be solved analytically to yield  $C$  as a function of  $z$ . The analytical solution is shown as Equation 2.

$$C_z = \frac{J}{v} \left[ 1 - \exp\left(\frac{vz}{\theta_A D^*}\right) \right] \quad (2)$$

Equation 2 can be calibrated using measured concentration profiles to yield a mass flux if the specific discharge and air-filled porosity are known and an effective diffusion coefficient is assumed. Solving for flux at the plenum ( $z = -L$ ), a contaminant flux based on plenum concentration can be obtained as shown in Equation 3.

$$J_p = \frac{vC_p}{1 - \exp\left(-vL/\theta_A D^*\right)} \quad (3)$$

where

- $C_p$  = Tracer concentration in plenum ( $\mu\text{g m}^{-3}$ )  
 $J_p$  = Mass flux estimation based on plenum concentration ( $\mu\text{g m}^{-2} \text{s}^{-1}$ )

The effective diffusion coefficient,  $D^*$ , describes the diffusive mass transport of a compound through a porous matrix. Millington<sup>4</sup> developed a model to describe the effects of a multiphase porous media (solid-liquid-gas) on a compound's theoretical binary diffusion coefficient<sup>5</sup>. The Millington model, which yields an effective diffusion coefficient, is shown as Equation 4.

$$D^* = D_{AB} \frac{\theta_A^{7/3}}{n^2} \quad (4)$$

where

- $D_{AB}$  = Theoretical binary diffusion coefficient  
 $n$  = Soil porosity

An estimate of  $D_{AB}$ <sup>6,7</sup> (helium into air) was used in conjunction with the Millington model for  $D^*$ . This predicted diffusion coefficient was used in calibrating the transport model (Equation 2).

### Emission Isolation Flux Chamber

A schematic of the EIFC is shown in Figure 2. The EIFC approach to the measurement of soil gas emissions is dependent upon the mixing characteristics of the isolation chamber.<sup>3</sup> A clean sweep air is introduced to the chamber of the EIFC which causes it to behave like a continuous flow stirred tank reactor (CFSTR), meaning that the concentration of trace gases in the chamber equals the concentration at the outlet. By measuring the exit gas concentration, the surface emissions can be calculated from a simple mass balance. The mass balance is given by Equation 5.

$$V \frac{dC}{dt} = Q_{sg} C_{sg} + JA_E - (Q_{sg} + vA_E)C \quad (5)$$

where

- $C$  = Measured concentration of contaminant at the outlet ( $\mu\text{g m}^{-3}$ )  
 $Q_{sg}$  = Sweep gas flow rate ( $\text{m}^3 \text{s}^{-1}$ )  
 $C_{sg}$  = Concentration of contaminant in sweep gas ( $\mu\text{g m}^{-3}$ )  
 $A_E$  = Surface area enclosed by the flux chamber ( $\text{m}^2$ )  
 $V$  = Volume of the EIFC ( $\text{m}^3$ )  
 $v$  = Specific discharge of contaminant ( $\text{m s}^{-1}$ )  
 $J$  = Surface flux of contaminant ( $\mu\text{g m}^{-2} \text{s}^{-1}$ )

Imposing the boundary conditions of  $C = 0$  at  $t = 0$ , Equation 5 can be solved to yield the concentration in the chamber as a function of time. This solution is shown as Equation 6.

$$C = C_{ss} \left[ 1 - \exp\left(-t/\tau\right) \right] \quad (6)$$

where

$C_{ss}$  = Steady-state contaminant concentration in EIFC ( $t \rightarrow \infty$ )

$t$  = Time

$\tau$  =  $V/Q_{sg}$

Assuming pure sweep gas ( $C_{sg} = 0$ ) and steady-state conditions, Equation 5 can be solved for the surface flux:

$$J = (Q_{sg} + vA_E)C_{ss}/A_E \quad (7)$$

## MATERIALS AND METHODS

Experiments were performed at the University of Massachusetts, Amherst, Environmental Engineering laboratories. All experiments were conducted using helium as a conservative tracer. Future work will include mesoscale evaluation of VOC emissions from an actively biodegrading system.

### Mesoscale Bioventing System

The MBS, shown in Figure 1, consisted of an anodized aluminum box (61 cm by 61cm by 46 cm high) packed with soil. Underlying the 25.4 cm of soil were 2.5 cm of pea gravel, a perforated plate and plenum chamber which together allowed for the introduction of air and an inert tracer gas at a known concentration. Air was supplied by an oilless compressor, and flow rates of both the air and tracer were controlled with flow meters. Air entering the MBS was humidified to maintain a constant soil moisture content.

Soil in the MBS was a uniform sand packed to a bulk density of approximately  $1.6 \text{ g cm}^{-3}$ . A porosity of 0.39 was calculated from the bulk density, a measured moisture content of 2.6% by weight, and a grain density of  $2.65 \text{ g cm}^{-3}$ .

### Soil Gas Profiler

The soil gas profiler (SGP), shown in Figure 3 was designed to extract 250 $\mu\text{L}$  soil gas samples while minimizing impact to the soil and adjacent soil gas. The SGP was constructed using narrow bore stainless steel tubing (24 in x 0.0625 in OD, 0.010 in ID). Total probe dead volume was 36  $\mu\text{L}$ . A 40  $\mu\text{m}$  sintered stainless steel filter element (Mott Metallurgical Corp.) was attached at the gas inlet end and a zero dead volume union (Valco) acted as a sampling port. The narrow bore tubing was inserted into 0.25 inch ID stainless steel tubing for structural rigidity. The narrow bore tubing and protective sheath were joined with brass compression fittings (Swagelok®). The filter element was crimped on to the narrow bore tubing and sealed to the stainless steel sheath with silicone caulking, ensuring that the gas was pulled only from the surrounding soil. A Teflon™ faced septa (0.125 in OD) was pressed against the ferrule inside the union to provide a sampling port for a syringe needle.

The SGP was hand-pushed into the soil to the desired sampling depth. A gas-tight syringe (Hamilton) was used to purge 50 $\mu\text{L}$  of gas from the probe before a 250 $\mu\text{L}$  sample was taken. The septum on the SGP sampling port was replaced after every three samples.

## Emission Isolation Flux Chamber

The EIFC built for this research was based on an EPA design, and was modified for the purpose of this project. All of the EIFC materials which come in contact with either the sweep gas or ground emissions are either stainless steel or Teflon™, except for the acrylic dome. The base of the EIFC consisted of an 18 cm high, 41 cm internal diameter stainless steel cylinder. A 51 cm outside diameter stainless steel flange was welded to the top of the cylinder. The dome was attached to the flange by 20 bolts, and it was held in place by a 51 cm OD aluminum flange. A Gore-tex™ gasket was used to make an air tight seal between the dome and the steel flange.

Five stainless steel ports were provided through the base of the EIFC. One port was used to provide access for a temperature probe, one for a pressure gauge, one as an inlet port to provide sweep air, one as an outlet port, and the last one was reserved as an auxiliary port.

The main EIFC modifications for this study were similar to those made by Dupont<sup>8</sup> and consisted of the addition of a gas sampling pump (SKC) at the EIFC outlet port and a magnehelic pressure gauge (Dwyer, -0.05 to + 0.20 inches wc). This allowed for fine control over pressure drop (maintained at zero in wc) across the EIFC.

## Soil Gas Sample Analysis

All gas samples from the MBS, the EIFC, and the SGP were analyzed isothermally (50 °C) using a Varian 3700 gas chromatograph (GC) equipped with a 3.05 m, 0.6 cm Porapak-Q packed column, a thermal conductivity detector (TCD) and a Varian 4270 integrator. The TCD was operated at a temperature of 220° C with a current at 78 mA, and a filament temperature of 290° C. Nitrogen was used as a carrier gas at a flow rate of 25 mL min<sup>-1</sup>. Quality control included standards during each sampling period and duplicates of EIFC and plenum samples. Duplicates of SGP samples could not be obtained. All gas samples (250 mL) were collected with gas-tight syringes.

## Experimental Program

A set of experiments was conducted to determine EIFC performance. Initial tests were performed with the bottom of the chamber sealed by an acrylic sheet and a gasket. An inert tracer or smoke was introduced into the EIFC. A vacuum pump (SKC) was attached to the EIFC outlet port to maintain zero gauge pressure in the chamber.

EIFC emission sensitivity to benzene was also evaluated. With the bottom of the EIFC sealed, benzene was introduced to maintain a 10 ppb<sub>v</sub> concentration in the EIFC. Benzene contaminated EIFC gas (160 mL) was pulled across adsorbent tubes (packed with Carbotrap™ B and Carbosieve™ S-III). The tubes were desorbed with an Envirochem Unacon Series 810 capillary inletting system and analyzed with a Varian 3300 GC equipped with a flame ionization detector.

Experiments to determine helium flux from the MBS were conducted at three different specific discharges (0.0020, 0.0052, and 0.0067 cm s<sup>-1</sup>), with  $n = 0.39$ ,  $\theta_A = 0.35$ , and  $L = 0.29$  m. Plenum helium concentration was maintained at approximately 10,000 ppm<sub>v</sub> throughout the experiments. Immediately prior to soil gas sampling, the plenum concentration and gas flow rates were measured three times to establish a mass flux. Plenum concentrations were also measured several times during the sampling period to ensure that mass flux remained constant.

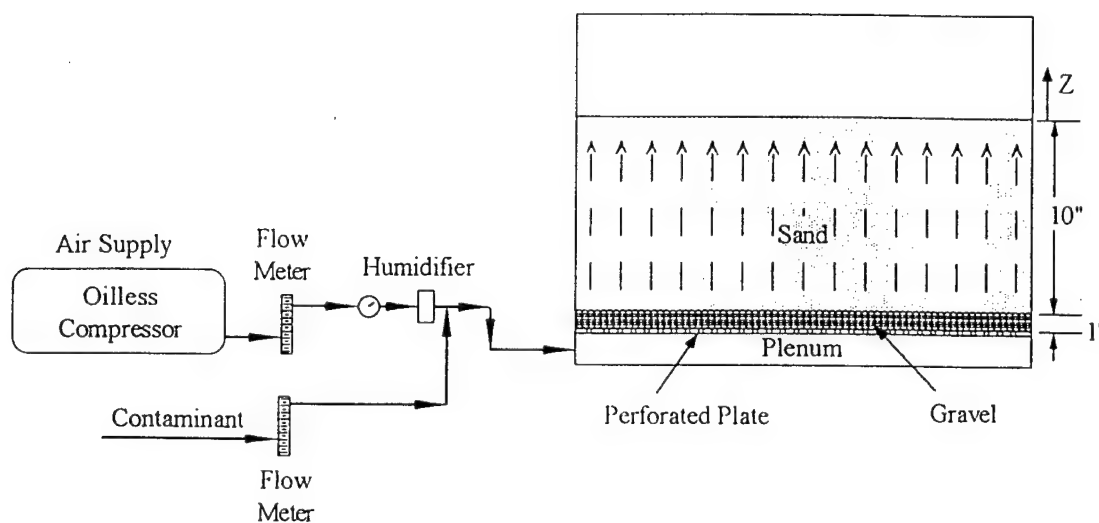


Figure 1: Mesoscale Bioventing System

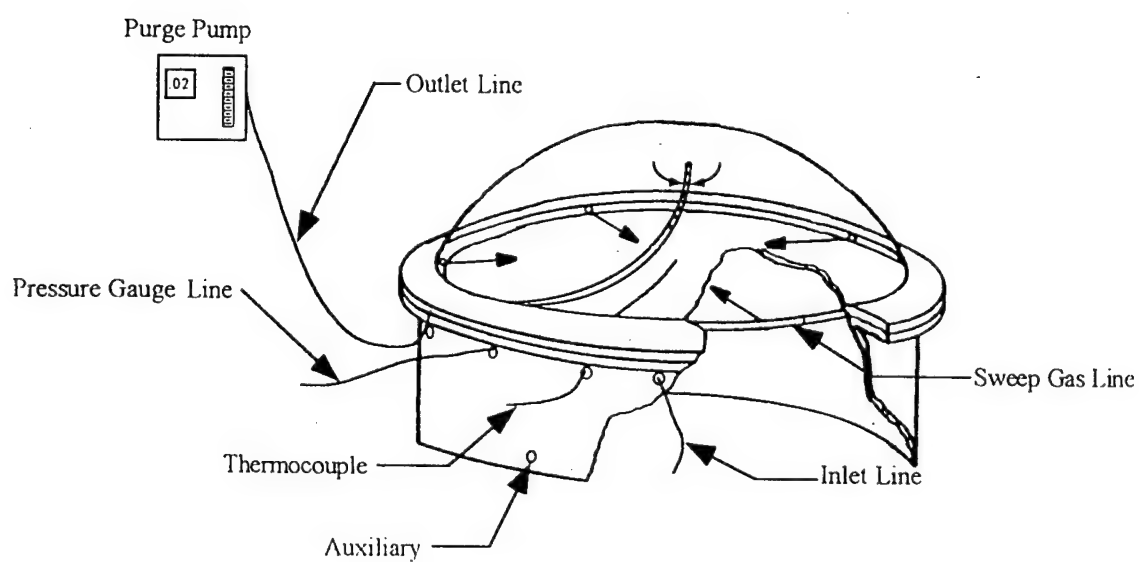


Figure 2: Isolation Flux Chamber



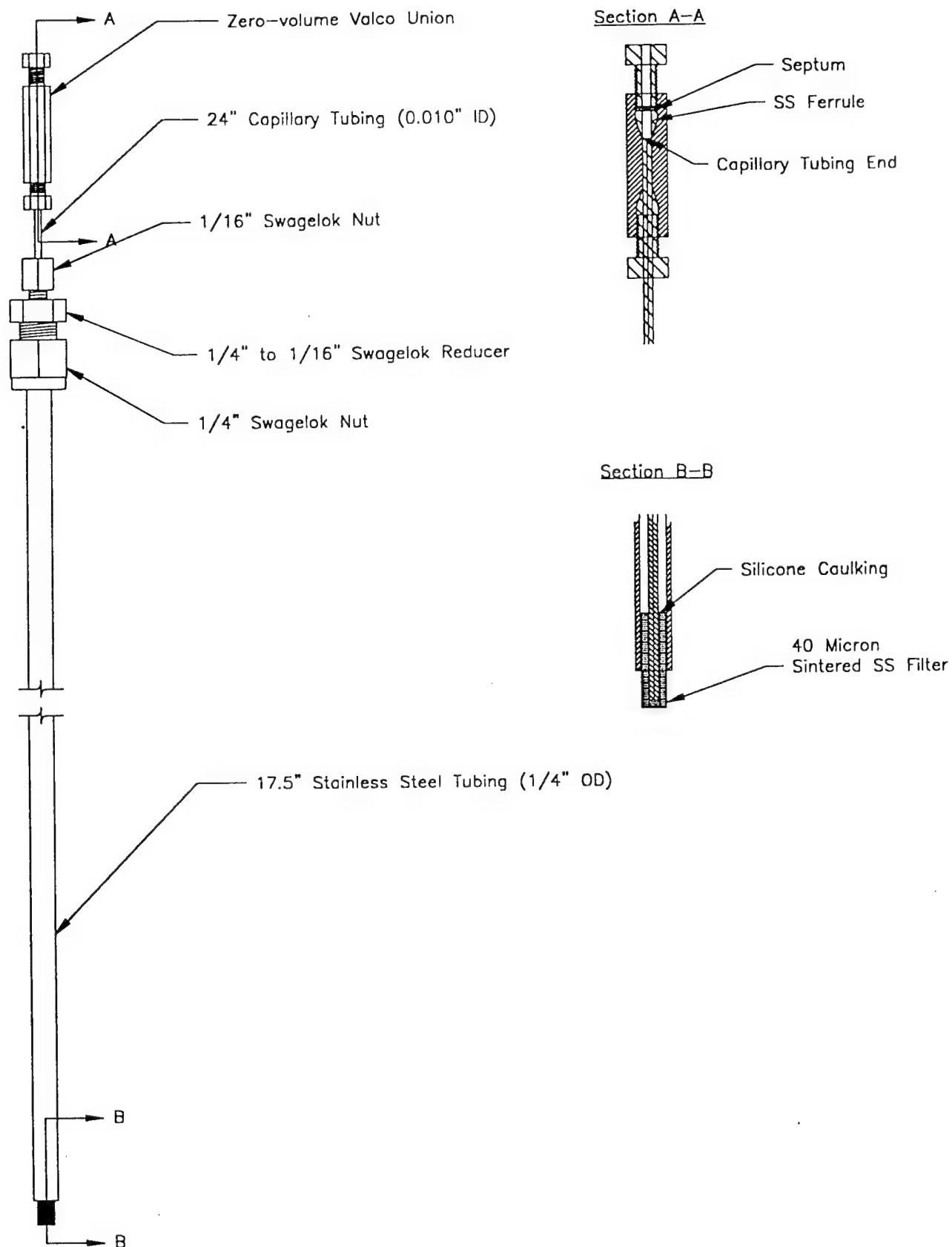


Figure 3: Soil Gas Profiler

## REFERENCES

1. R. B. Carpenter, FT-002 Bioventing Work Plan and Preliminary Air Emission Results, Department of the Air Force, Plattsburgh, 1993, 1-16.
2. M. Lehning, D. P. Y. Chang, D. R. Shonard, and R. L. Bell, "An Inversion Algorithm for Determining Area-Source Emissions from Downwind Concentration Measurements," Journal Air and Waste Management Assoc., 44(10): 1204 (1994).
3. M. R. Kienbusch, Measurement of Gaseous Emission Rates from Land Surfaces Using an Emission Isolation Flux Chamber: User's Guide, EPA/600/8-86/008, U. S. Environmental Protection Agency, Las Vegas, 1986.
4. R. J. Millington, "Gas diffusion in porous media," Science, 100 (1959).
5. E. H. Isaacson, Master's Thesis: The Use of Soil Gas Tracers in Intact Soil Core and Field Biodegradation Studies, University of Massachusetts, Amherst, Department of Civil and Environmental Engineering, 1995, pp. 6.
6. R. B. Bird, W. E. Stewart, and E. N. Lightfoot, Transport Phenomena, 1st ed., John Wiley & Sons, New York, 1960, pp. 510-513.
7. R. C. Reid, J. M. Prausnitz, and B. E. Poling, The Properties of Gases and Liquids, 4th ed., McGraw Hill Book Co., New York, 1987, pp. 581-589.
8. R. R. Dupont, "Measurement of Volatile Hazardous Organic Emissions," Journal Air Pollution Control Association, 37(2):168 (1987).
9. Reinhart, D.R., D.C. Cooper, B.L. Walker, "Flux Chamber Design and Operation for the Measurement of Municipal Solid Waste Landfill Gas Emission Rates," Journal Air and Waste Management Assoc., 42(8): 1607 (1992).
10. E. N. Fuller, P. D. Schettler, and J. C. Giddins, "A New Method for Prediction of Binary Gas-Phase Diffusion Coefficients," Industrial and Engineering Chemistry, 58: 19 (1966).
11. Chapman, S. and T.G. Cowling, Mathematical Theory of Non-Uniform Gases. Cambridge University Press, New York, 1939.

Table 1: Comparison of EIFC Measured and SGP Calibrated Mass Flux.

	$v = 0.0020 \text{ cm/s}$	$v = 0.0052 \text{ cm/s}$	$v = 0.0067 \text{ cm/s}$
	J	J	J
	$(\mu\text{g}/\text{m}^2 \text{ s})$	$(\mu\text{g}/\text{m}^2 \text{ s})$	$(\mu\text{g}/\text{m}^2 \text{ s})$
Plenum-Based Flux ( $J_P$ ) <sup>a</sup>	96	126	185
EIFC Measured Flux	74	99	151
SGP Calibrated Flux <sup>a</sup>	72	116	177

a.  $D^* = 0.36 \text{ cm}^2/\text{s}$  obtained using Millington<sup>4</sup> prediction and the Fuller *et al.*<sup>10</sup> estimate of  $D_{AB}$

Table 2: Minimum Detectable Emission Rate for Benzene

	SGP Method	Modified EIFC Method	EIFC Method <sup>a</sup>
Minimum Detectable Flux $(\mu\text{g}/\text{m}^2 \text{ min})$	4 <sup>b</sup>	1.3 <sup>c</sup>	1.2 <sup>c</sup>

a. Kienbusch<sup>3</sup>

b. Estimation based on 250  $\mu\text{L}$  sample (100 ppb<sub>v</sub> benzene detection limit)

c. Estimation based on 10 ppb<sub>v</sub> benzene concentration in EIFC

Surface emissions from the MBS were measured with the EIFC at various times throughout each sampling session. Helium concentrations were allowed to reach steady-state inside of the EIFC before sampling. A sweep gas flow of  $3.8 \text{ L min}^{-1}$  and a chamber pressure of zero gage in the EIFC were maintained in all experiments. Soil gas profiles were obtained at 3-5 random locations with the SGP for each mass flux. Soil, EIFC, and ambient temperatures were monitored with thermocouples. EIFC and soil temperatures were used to convert concentrations from a volumetric to a mass basis using the ideal gas law.

## RESULTS

### Emission Isolation Flux Chamber Evaluation

A smoke test was performed to visually observe mixing characteristics inside the chamber. For this experiment, a 1 L syringe was used to draw smoke from a smoke source. The smoke was then injected through the bottom of the chamber. This test allowed for visual verification of uniform mixing throughout the chamber.

A second test consisted of a tracer study to determine the time required to achieve steady state conditions in the EIFC and to quantitatively determine its mixing characteristics. Zero grade helium was injected through the bottom of the chamber. Samples were taken starting at the time the tracer was introduced into the chamber and at three minute intervals until steady state was achieved. Steady state was determined to be achieved when the concentration of helium inside the EIFC was 90 percent of the expected steady state concentration.

EIFC mixing characteristics were determined by comparing chamber concentration as a function of time to the theoretical values (Equation 6) expected in a CSTR. A comparison of the measured concentrations at various times inside the EIFC to those predicted for an ideal CFSTR is shown in Figure 4.

Experiments were performed at sweep gas flows from 1 to  $5 \text{ L min}^{-1}$ . The recovery at all flow rates was greater than 90% after steady state was achieved. However, as sweep gas flow decreased, the time required to achieve steady state increased from less than 20 min at a flow rate of  $5 \text{ L min}^{-1}$  to greater than 90 min at a flow rate of  $1 \text{ L min}^{-1}$ . The longer times are impractical for field work because of the large number of samples that must be taken. Low sweep gas flows also had a negative impact on the mixing regime.

Based on the time to steady state and on mixing characteristics, a working flow rate of between 3.5 and  $4 \text{ L min}^{-1}$  was chosen. This flow range provided a compromise between sampling time (under 27 minutes) and sample dilution. Low sweep gas flows are attractive because of sample dilution at higher flows, especially in the field where gas concentrations are usually low.

### Tracer Flux Evaluation

To evaluate the performance of the EIFC and SGP, both methods were used to measure three known tracer fluxes through the MBS. The tracer concentration profiles were used to calibrate the transport model by using mass flux as the calibrating parameter. A single parameter Fibonacci iterative search program was used to minimize the mean absolute error between measured and calibrated concentrations. Tracer concentration profiles for the three mass fluxes tested and model calibrations are shown in Figures

5 through 7. Model calibrations fit the profile data well for all fluxes tested with a mean normalized error ranging from 3.9 to 6.3% for each data set.

Flux calibrations and flux measurements derived from the EIFC results are compared to the plenum-based estimation of mass flux in Table 1. The results show that the SGP data and calibration underestimated  $J_p$  by 4 to 25%. The EIFC underestimations ranged from 18 to 23%. For both methods there is a trend toward under estimating mass flux at low MBS flux. A possible explanation of this trend is the non-linear response of the thermal conductivity detector at low helium concentrations. Calibration curves used in analyzing gas samples may not have been applicable to the concentrations in the MBS at the lowest flux. This may have led to the underestimation of flux.

A comparison between minimum emission rates of the methods under investigation is shown in Table 2. The SGP method was estimated to measure a minimum benzene flux of  $4 \mu\text{g m}^{-2} \text{min}^{-1}$ . This estimation assumes benzene vapor transport by diffusion with an effective diffusion coefficient  $D^* = 0.043 \text{ cm}^2 \text{s}^{-1}$ .  $D^*$  was calculated using the Fuller *et al.*<sup>10</sup> estimation of  $D_{AB}$  and a conservative Millington<sup>4</sup> correction of 0.5 for diffusion through porous media. The SGP estimation also assumes that the 250  $\mu\text{L}$  sample was taken at 2.5 cm below the surface. The emission sensitivities of the modified EIFC method and the EIFC method presented by Kienbusch<sup>3</sup> are 1.2 and  $1.3 \mu\text{g m}^{-2} \text{min}^{-1}$ , respectively. These values compare favorably to the  $4 \mu\text{g m}^{-2} \text{min}^{-1}$  calculated for the SGP method.

## CONCLUSIONS

Both the EIFC and the SGP methods are useful for calculating the flux of VOCs at bioventing sites. The EIFC had to be modified by the addition of a vacuum pump and a pressure gauge when monitoring advective flow systems to minimize negative biasing<sup>9</sup>. Optimum sweep gas flow rate was determined to be between 3.5 and 4  $\text{L min}^{-1}$  to balance time to steady state and sample dilution.

The SGP method was found to give comparable flux estimates to those given by the EIFC method. The SGP was also found to have some advantages over the EIFC. These include faster sampling time and the ability to obtain real time results without cryogenics or carbon tube trapping. However, the SGP is limited to small sample volumes to avoid disturbing adjacent soil gas.

Another drawback to the SGP method is its dependence on effective diffusivity and the assumptions of the model (e.g. zero gas concentration at the surface). Both methods were limited by GC detection limits, but the EIFC method can overcome this limitation by cryogenic or sorbent tube trapping methods.

## FUTURE WORK

Future work will consist of fine tuning both methods, especially in regard to method detection limits, and repeating the work with VOCs in a biologically active MBS.

## ACKNOWLEDGMENTS

The authors would like to acknowledge Mr. Erich Hinlein for analytical and technical support, and Mr. Benjamin Charkow for design of the mesoscale bioventing system. This research was supported by a grant from the Air Force Center for Environmental Excellence under Contract No. F41624-95-C-8012.

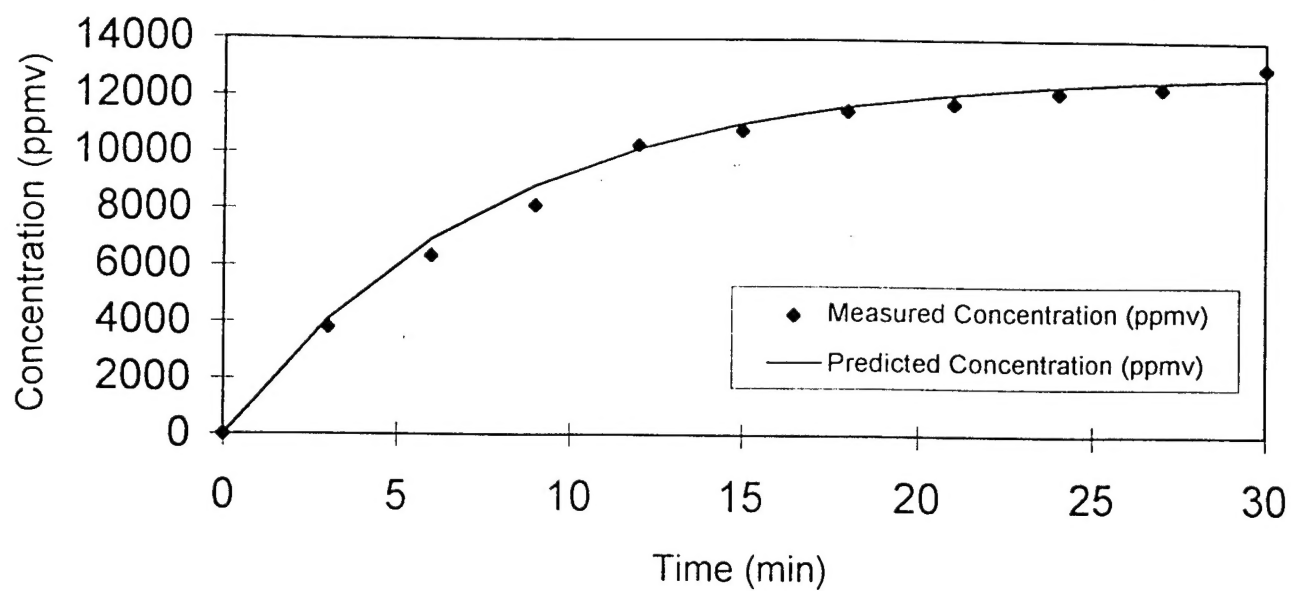


Figure 4: Comparison of Predicted to Measured Concentrations

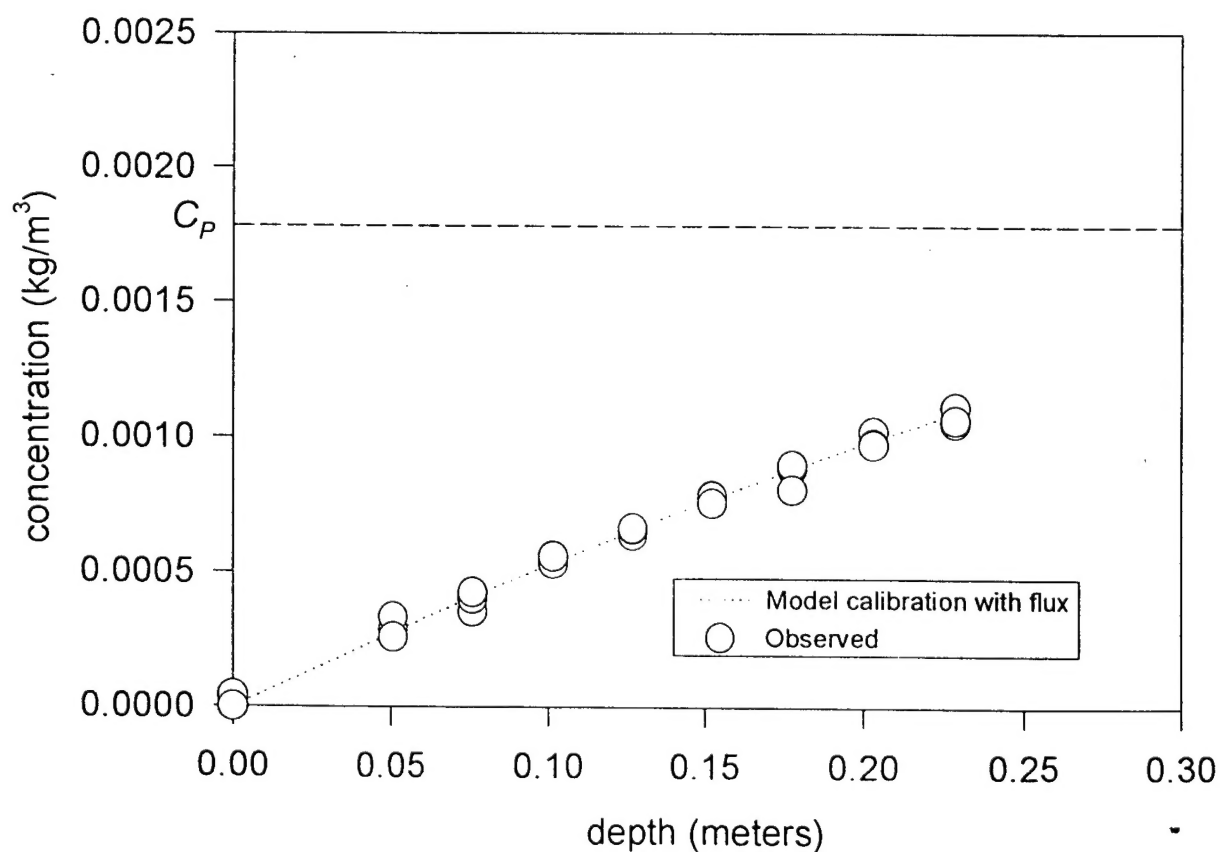


Figure 5: Concentration Profile For Mesoscale Bioventing System,  $v = 0.0020$  cm/s.

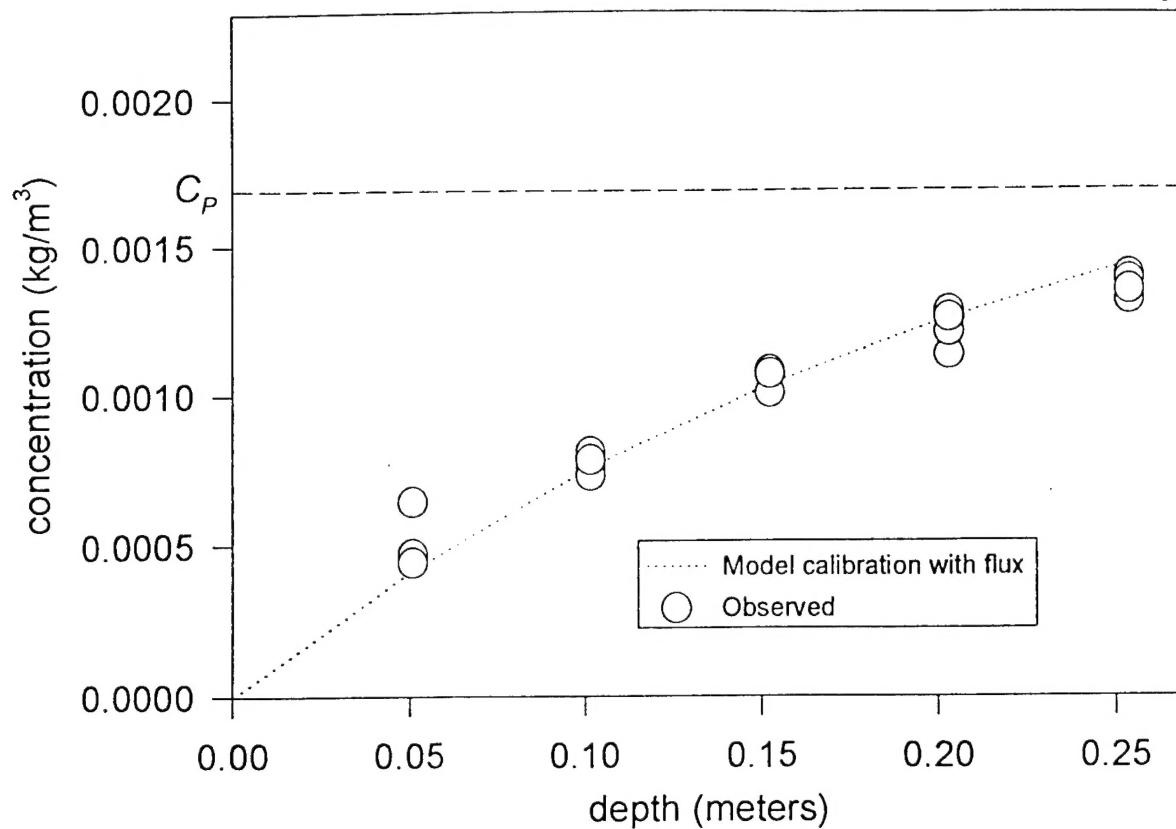


Figure 6: Concentration Profile For Mesoscale Bioventing System,  $v = 0.0052$  cm/s.

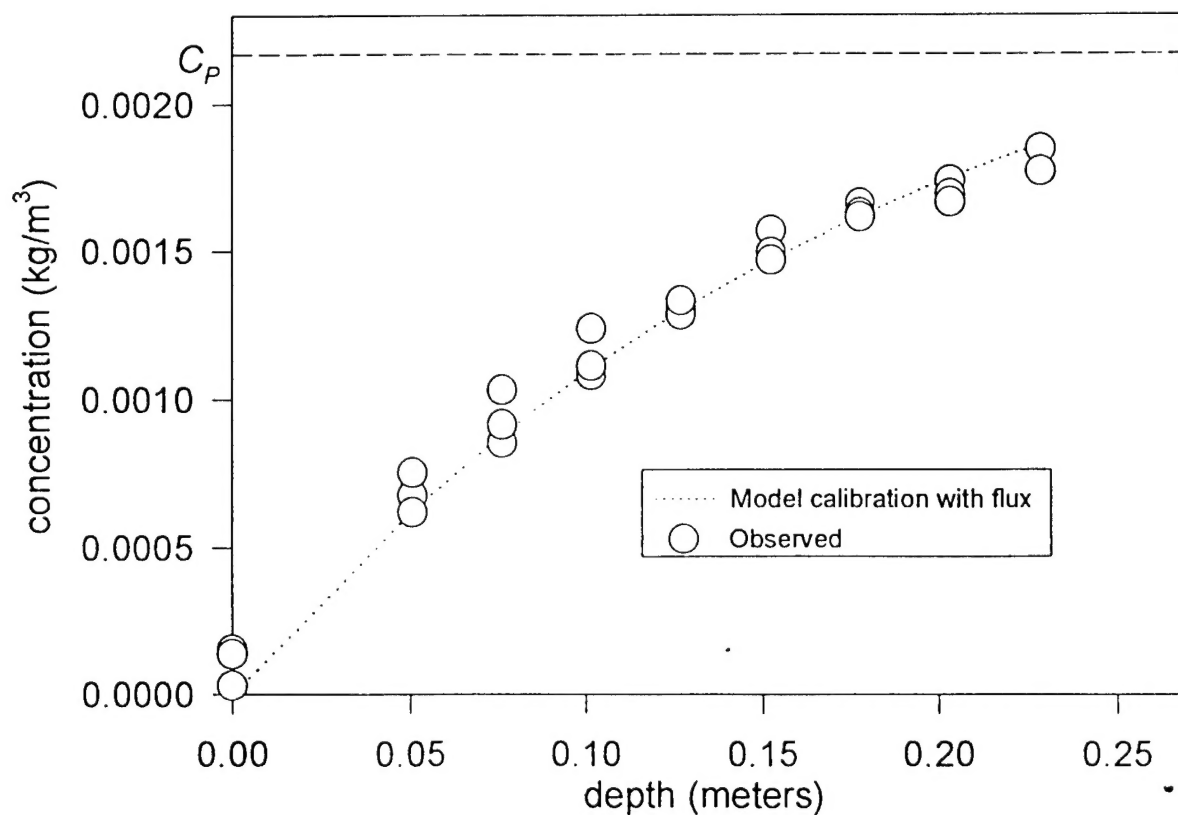


Figure 7: Concentration Profile For Mesoscale Bioventing System,  $v = 0.0067$  cm/s.